FUNDAMENTAL INVESTIGATIONS ON VIBRATIONAL AND AERODYNAMIC CHARACTERISTICS OF LONG-SPANNED SUSPENSION BRIDGE

Naruhito SHIRAISHI

Department of Civil Engineering
Kyoto University

August, 1970

FUNDAMENTAL INVESTIGATIONS ON VIBRATIONAL AND AERODYNAMIC CHARACTERISTICS OF LONG-SPANNED SUSPENSION BRIDGE

by

Naruhito SHIRAISHI

Department of Civil Engineering
Kyoto University

August, 1970

SUMMARY

This thesis presents the vibrational characteristics and the aerodynamic behaviours of suspension bridges. The oscillatory characteristics of suspension bridge are effectively influential factors to analyze the earthquake and the wind resistant behaviours. The coupling terms of vibrational modes for an ordinary type of suspension bridge with vertical hanger system are theoretically studied and disclosed to be a non-linear form. The fundamental equations for the inclined hanger system are derived and it is shown that the theoretically simplified solutions satisfactorily accord with the experimental results. As for aerodynamic behaviours associate with suspension bridges the flutter phenomena for various types of fundamental forms of stiffening girders are investigated experimentally. Also the statistical responses of plate-like structures due to fluctuating gusts are analyzed for which the aerodynamic coupling effect, the aerodynamic magnification factors and the frequency response functions for two dimensional system are illustrated from theoretical considerations.

CONTENTS

PREFACE

This thesis is concerned with oscillatory behaviours and aerodynamic responses of long-spanned suspension bridges. Since 1965 the laboratory of Bridge Engineering, Dep't of Civil Engineering, Kyoto University is engaged with the research project on the aerodynamic problems of bridge structures. Main theme of the project is to disclose the aerodynamic instability problems of long-spanned suspension bridge which is also closely related with free vibrational behaviours of the structure. In progress with the governmental work for the Honshu-Shikoku Connecting Bridge Plan in Japan the technical approach for its possibility is greatly emphasized in which the aerodynamic and the earthquake resistant design methods are considered of the primary importance. Our investigations intend to contribute to the above national project and, on the other hand, intend to disclose the related engineering problems from various points of views.

The present paper is prepared from the author's research work for five years, supported by the scientific research funds of the ministry of education and the research funds of the Japan Railway Construction Corporation.

The author is greatly indebted for a number of persons in the Bridge Engineering Laboratory and particularly for Messers. H. Utsunomiya, M. Noguchi, Y. Iida, S. Takita, M. Matsumoto, K. Tsuji and H. Asamuma for their enduring calculations and experimental works. Without their cooperation the project could not be achieved to the present stage. To Professor Ichiro Konishi the author should be to express his special thanks for his encouragement and critism on this investigations. Finally the writer is indebted to Prefessors T. Ishihara, Y. Niwa and the senior staffs in Dep't of Civil Engineering for their understanding and kind support by which the author is privileged to plan the Wind Tunnel to engage with the present research work.

CAHPTER 1 VIBRATIONAL CHARACTERISTICS OF SUSPENSION BRIDGE WITH VERTICAL AND INCLINED HANGERS

Part 1

ON THE COUPLED FREE VIBRATIONS OF SUSPENSION BRIDGE WITH VERTICAL HANGERS

1.1 INTRODUCTION

We present general vibrational characteristics of suspension bridge in the vertical direction as well as in the horizontal direction including the torsional rotation of stiffening floor system. Recent results of investigations to increase the dynamic stability of so flexible structures as long-spanned suspension bridge indicate possibilities of a number of newly developed types of stiffening girders, hanging systems, etc.[1), 2), 3)] In order to clarify the restraint effect in new type of suspension bridge an attention is placed on the vibrational behaviour of ordinary type of suspension bridge with vertical hangers. Though our consideration is restricted to linear elastic response of various structural members, it is easily expected that a set of fundamental equations is eventually of coupled form of expressions because of complexity in structural conjunctions of suspension bridges. For the sake of brevity the suspension bridge considered here is assumed to consist merely of two extensional cables, stiffening floor and vertical hangers distributed uniformly along the spanwise direction (Fig. 1.1). A set of fundamental equations is obtained by the aid of the variational principle and classified into two classes of modes, the first of which can be termed as deflectional modes, while the second can be termed as the torsional modes. Numerical illustrations are demonstrated for the proposed dimensions of the main span of the 1st plan of the Akashi Strait Bridge in Japan. The natural frequencies of the lower orders and the corresponding vibrational modes are determined by employing the Rayleigh-Ritz method.

1.2 DERIVATION OF FUNDAMENTAL DIFFERENTIAL EQUATIONS[4)]

In this paragraph we shall consider derivation of a set of fundametal differential equations of free vibrations of suspension bridge as shown in Fig. 1.1. The deformed configuration can be signified, as Fig. 1.2, by three components of displacements u_0 , v_0 , w_0 , which are longitudinal (horizontal), lateral (horizontal) and lateral (vertical) of stiffening girder and three components of displacements of cables for which ℓ , r are attached in order to distinguish the configurations of two cables. In addition to these the angle of rotation θ with respect to the center line, which varies with the coordinate x only, is considered so that torsional motions of the floor can be described simultaneously with horizontal and vertical modes of deformations. By the assumption that initial plane remains plane after deformation, we have, for stiffening floor,

$$\begin{aligned} u(x,y,z) &= u_0(x) - \frac{\partial w_0}{\partial x} z - \frac{\partial v_0}{\partial x} y \\ v(x,y,z) &= v_0(x) - \theta(x) z \\ w(x,y,z) &= w_0(x) + \theta(x) y \end{aligned} \qquad (1\cdot2\cdot1)$$

In order to obtain the fundamental equations, the strain and kinetic energies, U and T , stored in cables and stiffening floor system can be evaluated in terms of the displacements specified by eq's (1·2·1). Let W be the workdone by the dead weight and let w_f and w_c be the dead load per unit length of stiffening floor and a cable, respectively. Then we have, by virtue of the variational principle,

$$\delta (T - U + W - \lambda_1 f_1 - \lambda_2 f_2) = 0 \qquad (1\cdot2\cdot2)$$

where

$$T=\frac{1}{2}\int_0^{\ell}\frac{w_f}{gA}\left\{I_y\left(\frac{\partial^2 w_0}{\partial t\partial x}\right)^2+I_z\left(\frac{\partial^2 v_0}{\partial x\partial t}\right)^2+(I_y+I_z)\left(\frac{\partial\theta}{\partial t}\right)^2+A\left(\frac{\partial v_0}{\partial t}\right)^2+A\left(\frac{\partial w_0}{\partial t}\right)^2\right\}dx$$

$$+\frac{1}{2}\int_0^{\ell}\frac{w_c}{g}(1+h'^2)^{\frac{1}{2}}\left\{\left(\frac{\partial u_\ell}{\partial t}\right)^2+\left(\frac{\partial v_\ell}{\partial t}\right)^2+\left(\frac{\partial w_\ell}{\partial t}\right)^2+\left(\frac{\partial u_r}{\partial t}\right)^2+\left(\frac{\partial v_r}{\partial t}\right)^2+\left(\frac{\partial w_r}{\partial t}\right)^2\right\}dx \qquad (1\cdot2\cdot3)$$

$$U=\frac{1}{2}\int_0^{\ell}\left[E\left\{I_y\left(\frac{\partial^2 w_0}{\partial x^2}\right)^2+I_z\left(\frac{\partial^2 v_0}{\partial x^2}\right)^2\right\}+\mu\left(I_y+I_z\right)\left(\frac{\partial\theta}{\partial x}\right)^2\right]dx$$

$$+\frac{1}{2}\int_0^{\ell}E_cA_c\left\{\left(\frac{u'_\ell-h'w'_\ell}{1+h'^2}\right)^2+\left(\frac{u'_r-h'w'_r}{1+h'^2}\right)^2\right\}\sqrt{1+h'^2}\;dx$$

$$+\int_0^{\ell}H_W\left\{u'_\ell-h'w'_\ell+\frac{1}{2}\left(\frac{w'^2_\ell+2h'w'_\ell u'_\ell+h'^2u'^2_\ell}{1+h'^2}\right)+\frac{1}{2}v'^2_\ell\right\}dx$$

$$+\int_0^{\ell}H_W\left\{u'_r-h'w'_r+\frac{1}{2}\left(\frac{w'^2_r+2h'w'_ru'_r+h'^2u'^2_r}{1+h'^2}\right)+\frac{1}{2}v'^2_r\right\}dx \qquad (1\cdot2\cdot4)$$

$$W=\int_0^{\ell}\left\{w_f w_0+w_c\sqrt{1+h'^2}\;(w_\ell+w_r)\right\}dx$$

$$f_1=\int_0^{\ell}\left\{\left(\frac{b}{2}\frac{\partial v_0}{\partial x}-u_\ell\right)^2+(v_0-v_\ell)^2+\left(h+w_0-\frac{b\theta}{2}-w_\ell\right)^2-h^2\right\}dx$$

$$\Big\} \qquad (1\cdot2\cdot5)$$

$$f_2=\int_0^{\ell}\left\{\left(\frac{b}{2}\frac{\partial v_0}{\partial x}+u_r\right)^2+(v_0-v_r)^2+\left(h+w_0-\frac{b\theta}{2}-w_r\right)^2-h^2\right\}dx$$

λ_1 , λ_2 : Lagrange's multipliers

The expressions f_1 and f_2 indicate that hangers are inextensible throughout spanlength. Using the ordinary method of calculus of variation, eq. (1·2·2) yields to a following set of differential equations,

namely,

$$\frac{w_f}{g}\ddot{u} - \rho_f \frac{\partial^2}{\partial x \partial t}\left(I_y \frac{\partial^2 w_0}{\partial x \partial t} \right) + \frac{\partial^2}{\partial x^2}\left(EI_y \frac{\partial^2 w_0}{\partial x^2} \right) + 2\lambda_1 \left(h + w_0 + \frac{b\theta}{2} - w_\ell \right) + 2\lambda_2 \left(h + w_0 - \frac{b\theta}{2} - w_r \right) = w_f \tag{1·2·6}$$

$$\frac{w_f}{g}\ddot{v}_0 - \rho_f \frac{\partial^2}{\partial x \partial t}\left(I_z \frac{\partial^2 v_0}{\partial x \partial t} \right) + \frac{\partial^2}{\partial x^2}\left(EI_z \frac{\partial^2 v_0}{\partial x^2} \right) - \frac{\partial}{\partial x}\left\{ b\lambda_1 \left(\frac{b}{2}\frac{\partial v_0}{\partial x} - u_\ell \right) - b\lambda_2 \left(\frac{b}{2}\frac{\partial v_0}{\partial x} + u_r \right) \right\}$$

$$+ 2\lambda_1 \left(v_0 - v_\ell \right) + 2\lambda_2 \left(v_0 - v_r \right) = 0 \tag{1·2·7}$$

$$\frac{w_f}{gA}\left(I_y + I_z \right)\ddot{\theta} - \frac{\partial}{\partial x}\left\{ \mu \left(I_y + I_z \right)\frac{\partial \theta}{\partial x} \right\} + b\lambda_1 \left(h + w_0 + \frac{b\theta}{2} - w_\ell \right) - b\lambda_2 \left(h + w_0 - \frac{b\theta}{2} - w_r \right) = 0 \tag{1·2·8}$$

$$\frac{w_c}{g}\sqrt{1+h'^2}\,\ddot{u}_\ell - \frac{\partial}{\partial x}\left\{ E_c A_c \left(\frac{u'_\ell - h' w'_\ell}{(1+h'^2)^{\frac{3}{2}}} \right) \right\} - H_W \frac{\partial}{\partial x}\left\{ \frac{h'\left(w'_\ell + h' u'_\ell \right)}{1+h'^2} \right\} - 2\lambda_1 \left\{ \frac{b}{2}\frac{\partial v_0}{\partial x} - u_\ell \right\} = 0 \tag{1·2·9}$$

$$\frac{w_c}{g}\sqrt{1+h'^2}\,\ddot{u}_r - \frac{\partial}{\partial x}\left\{ E_c A_c \left(\frac{u'_r - h' w'_r}{(1+h'^2)^{\frac{3}{2}}} \right) - H_W \frac{\partial}{\partial x}\left\{ \frac{h'\left(w'_r + h' u'_r \right)}{1+h'^2} \right\} + 2\lambda_2 \left\{ \frac{b}{2}\frac{\partial v_0}{\partial x} + u_r \right\} = 0 \right. \tag{1·2·10}$$

$$\frac{w_c}{g}\sqrt{1+h'^2}\,\ddot{v}_\ell - H_W \frac{\partial^2 v_\ell}{\partial x^2} - 2\lambda_1 \left(v_0 - v_\ell \right) = 0 \tag{1·2·11}$$

$$\frac{w_c}{g}\sqrt{1+h'^2}\,\ddot{v}_r - H_W \frac{\partial^2 v_r}{\partial x^2} - 2\lambda_2 \left(v_0 - v_r \right) = 0 \tag{1·2·12}$$

$$\frac{w_c}{g}\sqrt{1+h'^2}\,\ddot{w}_\ell + \frac{\partial}{\partial x}\left\{ E_c A_c \frac{h'\left(u'_\ell - h' w'_\ell \right)}{(1+h'^2)^{\frac{3}{2}}} \right\} + H_W h'' - H_W \frac{\partial}{\partial x}\left(\frac{w'_\ell + h' u'_\ell}{1+h'^2} \right)$$

$$- 2\lambda_1 \left(h + w_0 + \frac{b\theta}{2} - w_\ell \right) = w_c \sqrt{1+h'^2} \tag{1·2·13}$$

$$\frac{w_c}{g}\sqrt{1+h'^2}\,\ddot{w}_r + \frac{\partial}{\partial x}\left\{ E_c A_c \frac{h'\left(u'_r - h' w'_r \right)}{(1+h'^2)^{\frac{3}{2}}} \right\} + H_W h'' - H_W \frac{\partial}{\partial x}\left(\frac{w'_r + h' u'_r}{1+h'^2} \right)$$

$$- 2\lambda_2 \left(h + w_0 - \frac{b\theta}{2} - w_r \right) = w_c \sqrt{1+h'^2} \tag{1·2·14}$$

The above nine equations contain eleven unknown dependent variables, w_0 , v_0 , θ , u_ℓ , v_ℓ , w_ℓ , u_r , v_r , w_r , λ_1 and λ_2 to be determined

by the eq's (1·2·6) through (1·2·14) plus two constraint conditions,

$$\left(\frac{b}{2}\frac{\partial v_0}{\partial x} - u\ell\right)^2 + \left(v_0 - v_\ell\right)^2 + \left(h + w_0 + \frac{b\theta}{2} - w_\ell\right)^2 = h^2 \qquad (1\cdot2\cdot15)$$

$$\left(\frac{b}{2}\frac{\partial v_0}{\partial x} - u_r\right)^2 + \left(v_0 - v_r\right)^2 + \left(h + w_0 + \frac{b\theta}{2} - w_r\right)^2 = h^2 \qquad (1\cdot2\cdot16)$$

Physically the Lagrange's multipliers λ_1, λ_2 correspond to mutual reactions for cables and floor as the results of constraint conditions. The eq's (1·2·6) through (1·2·14) are of the general form of expressions for dynamic behaviours of suspension bridge.

From above nine equations, the free vibrations of suspension bridge are classified into two types of modes, the first of which can be termed as the deflectional modes, while the second of which as the torsional modes. The former modes of vibrations indicate that neither lateral (horizontal) displacement nor rotation of floor with respect to the center line of bridge contributes to the oscillations. The second type of modes termed as the torsional modes consists of all displacement components and none of them can vanish. One should thus recognize the coupling of torsional and lateral displacements as a characteristic of this type of free vibrations.

1.3 REMARKS ON THE DEFLECTIONAL MODES OF FREE VIBRATIONS

As previously considered the deflectional modes of free vibrations of suspension bridge are given by the following set of expressions annihilating torsional, lateral (horizontal) displacements of stiffening floor and cables, viz.,

$$\frac{w_f}{g}\ddot{w}_0 - \frac{w_f}{gA}\frac{\partial^2}{\partial x \partial t}\left(I_y\frac{\partial^2 w_0}{\partial x \partial t}\right) + \frac{\partial^2}{\partial x^2}\left(EI_y\frac{\partial^2 w_0}{\partial x^2}\right) + 4\bar{\lambda}\left(h + w_0 - w\right) = w_f \qquad (1\cdot3\cdot1)$$

$$\frac{w_c}{g}\sqrt{1+h'^2}\,\ddot{u}+\frac{\partial}{\partial x}\left\{E_cA_c\frac{h'w'-u'}{(1+h'^2)^{3/2}}\right\}-H_W\frac{\partial}{\partial x}\left\{\frac{h'(w'+h'u')}{1+h'^2}\right\}+2\bar{\lambda}u=0 \qquad (1\cdot3\cdot2)$$

$$\frac{w_c}{g}\sqrt{1+h'^2}\,\ddot{w}+\frac{\partial}{\partial x}\left\{E_cA_c\frac{h'(h'w'-u')}{(1+h'^2)^{3/2}}\right\}+H_Wh''-H_W\frac{\partial}{\partial x}\left(\frac{w'+h'u'}{1+h'^2}\right)$$

$$-2\bar{\lambda}(h+w_0-w)=w_c\sqrt{1+h'^2} \qquad (1\cdot3\cdot3)$$

$$u^2+(h+w_0-w)^2=h^2 \qquad (1\cdot3\cdot4)$$

Note that $w_\ell=w_r\equiv w$, $u_\ell=u_r\equiv u$, and $\lambda_1=\lambda_2\equiv\lambda$. Eq's (1·3·1) through (1·3·4) provide obviously the non-linear form of solutions because of the constraint condition, eq.(1·3·4). To linearize the solutions let us find the Lagrange's multiplier λ in above expressions by vanishing all displacements, then eq. (1·3·1) and eq. (1·3·3) give us

$$\begin{aligned}4\lambda h&=w_f\\ 2H_Wh''&=w_f+2w_c\sqrt{1+h'^2}\end{aligned} \qquad (1\cdot3\cdot5)$$

Though the approximation may yield to $4\bar{\lambda}=w_f/h$, let us assume

$$4\bar{\lambda}=\frac{2H_Wh''}{h}=\frac{w_f+2w_c}{h} \qquad (1\cdot3\cdot6)$$

for this problem; this assumption reaches to the same form of the fundamental equations of the lateral vibrations of suspension bridge obtained by M. Ito.[5] Substituting eq. (1·3·6) into eq's (1·3·1) through (1·3·4) and defining w_0 , w , u as vibrational modes independent of time and ω as the circular frequency, we have

$$\frac{d^2}{dx}\left(EI_y\frac{d^2w_0}{dx^2}\right)+2H_W\frac{h''}{h}(w_0-w)-\omega^2\left\{\frac{w_f}{g}w_0-\frac{w_f}{gA}\frac{d}{dx}\left(I_y\frac{dw_0}{dx}\right)\right\}=0$$

$$\frac{d}{dx}\left\{E_cA_c\frac{h'w'-u'}{(1+h'^2)^{3/2}}\right\}-H_W\frac{d}{dx}\left\{\frac{h'(w'+h'u')}{1+h'^2}\right\}+H_W\frac{h''}{h}u-\omega^2\frac{w_f}{g}\sqrt{1+h'^2}\;u=0 \qquad (1\cdot3\cdot7)$$

$$-\frac{d}{dx}\left\{E_cA_c\frac{h'(h'w'-u')}{(1+h'^2)^{3/2}}\right\}-H_W\frac{d}{dx}\left(\frac{w'+h'u'}{1+h'^2}\right)-H_W\frac{h''}{h}(w_0-w)-\omega^2\frac{w_f}{g}\sqrt{1+h'^2}\;w=0$$

The above set of expressions, eq's (1·3·7), is considered as the general form of deflectional modes. It should be noted that eq's (1·3·7) are classified into cases depending on whether the equations are associated with singular point, in other words, $h=0$ at midspan or not. The center-diagonal stays, commonly adopted to modern types of suspension bridges, constrain horizontal displacement of cable at the midspan and consequently augment remarkably the deflectional stiffness of a suspension bridge. Thus, mathematically, installment of diagonal stays is conceived as singularity at the midspan of the bridge. Classically F. Bleich and others [6] give the fundamental equations of free vibrations of suspension bridge under the assumption that vertical displacements of cables and stiffening floor are identical and the horizontal increment of cable tension is introduced by the cable equation.

From the constraint condition for hangers, eq. (1·3·4), we have the following set of fundamental equations alternatively by assuming that

$$u=h\sin\varphi \qquad w=w_0+h(1-\cos\varphi)$$

so as to satisfy eq. (1·3·4). Substituting above expressions into eq's (1·3·7) and taking only linear terms into an account in terms of u and w, we have

$$\frac{d^2}{dx^2}\left(EI_y\frac{d^2w_0}{dx^2}\right)-2H_W\frac{d}{dx}\left(\frac{w_0'}{1+h'^2}\right)+\frac{d}{dx}\left\{\frac{2E_cA_ch'^2w_0'}{(1+h'^2)^{3/2}}\right\}+\frac{d}{dx}\left\{\left(\frac{2E_cA_ch'}{(1+h'^2)^{3/2}}+\frac{2H_Wh'}{1+h'^2}\right)u'\right\}$$

$$+\left(\frac{w_f}{g}+\frac{2w_c}{g}\sqrt{1+h'^2}\right)w_0=0$$

$$\frac{2w_c}{g}\sqrt{1+h'^2}\,hu''-\frac{d}{dx}\left\{\frac{2E_cA_ch\,u'}{(1+h'^2)^{3/2}}\right\}+2H_W\frac{d}{dx}(h'u)-\frac{d}{dx}\left\{\frac{2H_Whh'^2u'}{1+h'^2}\right\}-\frac{2E_cA_c\,h'\,u'}{(1+h'^2)^{3/2}}$$

$$-\frac{2H_Wh'u'}{1+h'^2}-2w_c\sqrt{1+h'^2}\,u+\frac{d}{dx}\left\{\left(\frac{2E_cA_c}{(1+h'^2)^{3/2}}-\frac{2H_W}{1+h'^2}\right)hh'w_0\right\}-\left\{\frac{2E_cA_c}{(1+h'^2)^{3/2}}-\frac{2H_W}{1+h'^2}\right\}h'^2w_0'=0 \qquad (1\cdot3\cdot8)$$

The numerical illustrations for above consideration are described in 1.5.

1.4 REMARKS ON THE TORSIONAL MODES OF FREE VIBRATIONS

The torsional modes defined previouly comprise all components of displacements of stiffening floor and cables, which means that all displacement modes are eventually of so coupled form as eq. (1·2·6) through (1·2·14). However the lateral horizontal modes, v_0 , v_ℓ , v_r , are given by eq's (1·2·7), (1·2·11) and (1·2·12) in which other modes of displacements do not appear explicitly if the horizontal longitudinal displacements u_ℓ , u_r , are neglected throughout the spanlength. Thus we may subdivide the torsional modes into the lateral horizontal modes and the purely torsional modes. The former can be written as

$$\frac{w_f}{g}\ddot{v}_0+\frac{\partial^2}{\partial x^2}\left(EI_z\frac{\partial^2v_0}{\partial x^2}\right)+\frac{2H_Wh''}{h}(v_0-v)=0$$

$$\frac{w_c}{g}\sqrt{1+h'^2}\,\ddot{v}-H_W\frac{\partial^2v}{\partial x^2}-\frac{H_Wh''}{h}(v_0-v)=0 \qquad (1\cdot4\cdot1)$$

where $\lambda_1=\lambda_2=H_Wh''/2h$ and $v_r=v_\ell\equiv v$. The latter, purely torsional, is expressed for the lowest approximation as

$$\left\{\frac{w_f}{gA_f}(I_y+I_z)+\frac{w_c}{2g}b^2\sqrt{1+h'^2}\right\}\ddot{\theta}+\frac{\partial^2}{\partial x^2}\left(EI_{ym}b\frac{\partial^2\theta}{\partial x^2}\right)-\mu(I_y+I_z)\frac{\partial^2\theta}{\partial x^2}$$

$$-\frac{\partial}{\partial x}\left\{\frac{E_cA_c}{2}\left(\frac{b^2h'^2}{1+h'^2}\right)\frac{\partial\theta}{\partial x}\right\}-\frac{\partial}{\partial x}\left\{\frac{H_Wb^2}{2(1+h'^2)}\frac{\partial\theta}{\partial x}\right\}=0 \qquad (1\cdot4\cdot2)$$

where I_{ym} is the moment of inertia of main girders of the floor system.

In order to examine the above consideration on subdivision of torsional modes, an attention is placed on the constraint conditions(1·2·5) which are satisfied, ignoring the first terms, if

$$\left.\begin{aligned} w_\ell &= w_0 + \frac{b\theta}{2} + h\,(1-\cos\alpha) \\ v_\ell &= v_0 - h\sin\alpha \end{aligned}\right\} \qquad (1\cdot4\cdot3)$$

$$\left.\begin{aligned} w_r &= w_0 - \frac{b\theta}{2} + h\,(1-\cos\beta) \\ v_r &= v_0 - h\sin\beta \end{aligned}\right\} \qquad (1\cdot4\cdot4)$$

Substituting eq's (1·4·3) and (1·4·4) into the energy expression and taking an account into consideration up to the cubic terms of displacements, we have

$$\left(EI_y w_0''\right)'' - 2H_W\left(\frac{w_0'}{1+h'^2}\right)' - 2\left\{\frac{E_c A_c h'^2 w_0'}{(1+h'^2)^{3/2}}\right\}' + \left(\frac{w_f}{g} + \frac{2w_c}{g}\sqrt{1+h'^2}\right)w_0'' - \frac{1}{2}L_{xt}\left\{\frac{(v_0-v_\ell)^2}{h} + \frac{(v_0-v_r)^2}{h}\right\} = 0 \qquad (1\cdot4\cdot5)$$

$$-\left(EI_{ym}b\theta''\right)'' + \left\{\mu(I_y+I_z)\theta'\right\}' + \frac{b^2}{2}\left\{\frac{E_c A_c h'^2\theta'}{(1+h'^2)^{3/2}}\right\}' + \frac{b^2}{2}\left(\frac{H_W\theta'}{1+h'^2}\right)' - \left(\frac{w_f(I_y+I_z)}{gA} + \frac{w_c b^2}{2g}\sqrt{1+h'^2}\right)\theta'' + \frac{1}{2}L_{xt}\left\{\frac{(v_0-v_\ell)^2}{h} - \frac{(v_0-v_r)^2}{h}\right\} = 0 \qquad (1\cdot4\cdot6)$$

$$\frac{w_c}{g}\sqrt{1+h'^2}\,h\ddot{v}_\ell - H_W h v_\ell'' - H_W h''\,(v_0 - v_\ell) + (v_0 - v_\ell)\,L_{xt}\left(w_0 + \frac{b\theta}{2}\right) = 0 \qquad (1\cdot4\cdot7)$$

$$\frac{w_c}{g}\sqrt{1+h'^2}\,h\ddot{v}_r - H_W h v_r'' - H_W h''\,(v_0 - v_r) + (v_0 - v_r)\,L_{xt}\left(w_0 - \frac{b\theta}{2}\right) = 0 \qquad (1\cdot4\cdot8)$$

$$\left(EI_z v_0''\right)'' + \frac{w_f}{g}\ddot{v}_0 - H_W\,(v_\ell'' + v_r'') + \frac{w_c}{g}\sqrt{1+h'^2}\,(\ddot{v}_\ell + \ddot{v}_r) = 0 \qquad (1\cdot4\cdot9)$$

where the operator L_{xt} is of the form

$$L_{xt} = \frac{\partial}{\partial x}\left\{\left(\frac{E_c A_c h'}{(1+h'^2)^{3/2}} + \frac{H_W}{1+h'^2}\right)\frac{\partial}{\partial x}\right\} - \frac{w_c}{g}\sqrt{1+h'^2}\,\frac{\partial^2}{\partial t^2}$$

From eq's (1.4.5) through (1·4·9) the displacement modes are considered to couple with other by means of non-linear terms as above expressions. It is worthwhile to note that on an account of eq's (1.4.5) through (1·4·9) the vertical deflectional modes w_0 exert no lateral (horizontal) modes, v_0 or v , when there exists no lateral displacement initially, while the lateral (horizontal) modes can exert the vertical deflection of stiffening floor when non-linear terms are taken into an account.

1.5 NUMERICAL ILLUSTRATIONS

Numerical calculations for above fundamental equations are performed for the main span of the 1st plan of proposed Akashi-Strait Bridge in Japan, which dimensions are as follows;

l(spanlength) = 1,300 m

f(sag) = 108 m

E_c(Young's modulus) = 2.1 x 10^7 t/m^2

A_c(cross sectional area) = 1.232 m^2/cable

H_w(horizontal component of cable tension) = 5.841 x 10^4 t/cable

W(total dead weight) = 30 t/cable

I_y(moment of inertia wrt lateral axis) = 5 m^4/one stiff. truss

I_z(moment of inertia wrt vertical axis) = 20.25 m^4

In calculation of the deflectional modes of free vibrations, two cases are considered depending on the singular points of fundamental equations at the mid-span, which correspond to whether we have the center diagonal stays or not.

(i) Without center diagonal stay

Since we consider simply supported stiffening girder, the deflectional modes are assumed as

$$\left.\begin{aligned} w_0 &= \sum_{k=1}^{\alpha} A_k \sin\frac{k\pi x}{\ell} \\ w &= \sum_{k=1}^{\beta} B_k \sin\frac{k\pi x}{\ell} \\ u &= \sum_{k=1}^{\gamma} C_k \sin\frac{k\pi x}{\ell} \end{aligned}\right\} \qquad (1\cdot5\cdot1)$$

which yields to the energy expression of the following form

$$\delta\Big[\sum_k\sum_j\Big\{D^{(1)}_{kj}A_kA_j+D^{(2)}_{kj}A_kB_j+D^{(3)}_{kj}B_kB_j+D^{(4)}_{kj}B_kC_j+D^{(5)}_{kj}C_kC_j\Big\}\Big]=0$$

from which the frequency equation is written as

$$\begin{vmatrix} D^{(1)}_{kj}+D^{(1)}_{jk} & D^{(2)}_{mj} & 0 \\ D^{(2)}_{j\ell} & D^{(3)}_{\ell m}+D^{(3)}_{m\ell} & D^{(4)}_{\ell n} \\ 0 & D^{(4)}_{mr} & D^{(5)}_{rn}+D^{(5)}_{nr} \end{vmatrix} = 0 \qquad (1\cdot5\cdot2)$$

where $j,k=1,\ \cdots\cdots\alpha$, $m,\ell=1,\ \cdots\cdots\beta$, $n,r=1,\ \cdots\cdots\gamma$

(ii) With center diagonal stays

For this case the additional mechanical constraint to the above case is given as $w_0(\ell/2)=w(\ell/2)$ and $u(\ell/2)=0$. Then the deflectional modes are assumed as

$$\left.\begin{aligned} w_0 &= \sum_i A_i \sin\frac{i\pi x}{\ell} \\ w &= \sum_i \left(A_i + B_i \frac{h}{\ell}\right)\sin\frac{i\pi x}{\ell} \\ u &= \sum_i C_i \frac{h}{\ell} \sin\frac{i\pi x}{\ell} \end{aligned}\right\} \qquad (1\cdot5\cdot3)$$

Similarly the characteristic equation is obtained as

$$\begin{vmatrix} \bar{D}^{(1)}_{2i+1,2\ell+1}+\bar{D}^{(1)}_{2\ell+1,2i+1} & \bar{D}^{(4)}_{2i+1,2m+1} & \bar{D}^{(6)}_{2i+1,2m} \\ \bar{D}^{(4)}_{2\ell+1,2j+1} & \bar{D}^{(2)}_{2j+1,2m+1}+\bar{D}^{(2)}_{2m+1,2j+1} & \bar{D}^{(5)}_{2j+1,2n} \\ \bar{D}^{(6)}_{2\ell+1,2k} & \bar{D}^{(5)}_{2m+1,2k} & \bar{D}^{(3)}_{2n,2k}+\bar{D}^{(3)}_{2k,2n} \end{vmatrix} = 0$$

For the torsional modes of free vibrations the purely torsional modes of stiffening floor with center diagonal stays are calculated in this study under the assumption for modes as

(a)

$$\left.\begin{aligned} \theta &= \frac{2w}{b} = \sum_k A_k \sin\frac{k\pi x}{\ell} \\ u &= \sum_k \frac{h}{\ell} C_k \sin\frac{k\pi x}{\ell} \end{aligned}\right\} \qquad (1\cdot5\cdot4)$$

(b)

$$\left.\begin{aligned} \theta &= \sum_k A_k \sin\frac{k\pi x}{\ell} \\ w &= \sum_k \left(\frac{b}{2} A_k + \frac{h}{\ell} B_k\right) \sin\frac{k\pi x}{\ell} \\ u &= \sum_k C_k \sin\frac{k\pi x}{\ell} \end{aligned}\right\} \qquad (1\cdot5\cdot5)$$

The characteristic equations are obtained in exactly same manner as the deflectional modes. The natural frequencies of first symmetric and anti-symmetric modes are given in Tables 1·1 , 1·2 and the modes are shown in Fig's 1·3, 1·4 , 1·5 , 1·6 for deflectional and torsional cases. The results are compared with those calculated by means of fundamental equations given by F. Bleich and others.

The numerical results indicate quantitatively the increasement of stiffness of the structure when we have center diagonal stays; that is, the natural frequencies increase approximately 10 to 20 % for the case with center stays and more than 50 % for the case without center stays to compare the results of assumption of identical vertical deformation with those of the assumption of unequal vertical deformation of cables and stiffening floor. Though the calculation seems to be rather complex the results can be obtained within short time when the electronic computor is used.

Part II
ON THE FREE VIBRATIONS OF A SUSPENSION BRIDGE WITH INCLINED HANGERS

1.6 INTRODUCTION

A theoretical consideration is performed on the free vibrations of

a long-spanned suspension bridge with customary vertical hanger system. However, recent results of investigations indicate possibilities of effective increasement of dynamic stability of suspension bridge by means of (i) increasement of flexural and torsional rigidities, (ii) increasement of structural damping, (iii) improved cross sectional shapes of stiffening girders. In this investigation the stress is placed on experimental analysis to clarify the discrepancy of stiffness of suspension bridge from the structural point of views, namely, the effect due to inclination of hangers. Because of complexity of structural conjunction of suspension bridge with inclined hangers a model of suspension bridge (3,250 + 6,500 + 3,250) is made based on the 1st plan of the proposed Akashi Strait Bridge with both vertical and inclined hangers (Fig. 1.7). The static and dynamic tests are performed and compared with two cases.

1.7 STATIC TESTS AND RESULTS

In order to clarify the mechanical response of a suspension bridge with vertical and inclined hangers the static tests are performed, in which the deflections are measured by telescope under 18 different loading conditions (Fig 1.8) for the cases of (a) inflexible towers and (b) flexible towers under the uniform load (i.e., 615.6 gr/6.25 cm/one side). The results are as follows;

(1) For the case of inclined hangers the maximum static deflections are obtained under fully loaded case on the main span, which corresponds to 1/165 of span length; for the case of the vertical hangers the maximum deflection to span length reaches to 1/154 under the corresponding load conditions. The decrease of deflections due to inclination of hangers tends to become remarkable when loaded asymmetrically or concentrated.

(2) When the tops of towers are fixed so as to be inflexible, the deflections of stiffening girders are about 35 % less than the case of flexible towers.

1.8 DYNAMIC TESTS AND RESULTS

This investigation intends to disclose the free vibrational characteristics of a suspension bridge with inclined hangers. (Fig. 1.9) The deflections of stiffening girders are obtained by use of the differential transformers (Type M1-6W-13, Shinkou Electric Co.) and the strains are measured by the wire strain gauges amplified by the DS6-MTH (Shinkou Communication Co.) and recorded by the electromagnetic oscillograph (Type FR-101, San-ei Sokki Co.). To have the steady state response the electrodynamic vibration exciter (Type VS-VVE-3202 As, IMV Co.) is used, the vibrator of which varies from 1 to 100 cps in frequency and up to 26 mm in amplitude, exerting the sinusoidal external forces up to 125 kg at the maximum. In this test, the natural frequencies, the corresponding modes, and the logarithmic decrement are obtained by measuring delfections and strains of stiffening girders and cables in free vibrations and under the steady state excitations for models with vertical and inclined hangers. In order to estimate the effect on the deflection of stiffening girders due to flexibility of towers, the tests are performed when the tops of towers move freely and when completely fixed by additional supports. The results are obtained as follows;

(1) For flexible towers, the vibrational modes seem to remain of similar form for vertical and inclined hangers, while the frequencies become N_c(calculated) = 1.17 cps, N_v(vertical hanger) = 1.23 cps, N_i (inclined hanger) = 1.45 cps for the fundamental modes, and N_c = 1.54 cps, N_v = 1.58 cps, N_i = 2.00 cps for the first asymmetric modes.

(2) The logarithmic decrements for models with vertical and inclined hangers are obtained and compared in Fig. 1.10. The relation between the decrements and amplitude can not be clearly found at the present but decrements tend to increase when the amplitudes decrease. In generally speaking, the damping effect for the case of inclined hangers is considered to be larger than the case of vertical hangers.

(3) With fixed tops of towers the natural frequencies for the case of inclined hangers seem to increase about 10 % to compare with those for

the case of vertical hangers.

1.9 CONCLUSIONS

In this investigation the free vibrations of suspension bridge are considered experimentally to disclose the characteristics for the cases of vertical and inclined hangers. The static loading tests indicate the discrepancy of responses due to hangers system, namely less flexibility when loaded asymmetrically and partly distributed for inclined hangers. The difference of static deflections for inclined and vertical hangers reaches approximately 10 %, while dynamically there appear remarkable differences on the natural frequencies for two cases and the damping seems to increase significantly for the case of inclined hangers.

In Part I a theoretical consideration is given on free vibrations to clarify the coupling of displacement modes and the effect of such stiffening as center diagonal stays for the case of vertical hangers. Recently various kinds of new types of suspension bridges are proposed, increasing dynamic stability, by means of improved cross sectional shapes of stiffening floor and improved hanger systems. To have analytical continuation the experimental investigation is performed to clarify the dynamic characteristics of free vibrations of suspension bridge with inclined hangers in Part II. This investigation obviously calls for thoroughful theoretical investigations on free vibrations for the case of inclined hangers so as to make such structural improvement properly justified.

REFERENCES

1.1) R. A. Frazer & C. Scruton: "A summarized amount of the Severn Bridge aerodynamic investigation", NPL/Aero/222, 1952

1.2) F. Leonhardt: "Aerodynamisch stabile Hänge-brücke für grosse Spannweiten", Proc. IABSE at Rio de Janairo Tb6, 1964

1.3) D. B. Steinman: "Suspension bridges; the aerodynamic problem and its solution", Sciencè in Progress, 9th Series, Yale Univ. Press, p 248 - 250

1.4) N. Shiraishi: "On the coupled free vibrations of a suspension bridge - I", Mem. Fac. Eng., Kyoto Univ., Vol. XXV, Part 2, '63

1.5) M. Ito: Trans. JSCE, No. 81, May, 1962

1.6) Bleich, McCullough, Rosecrans, Vincent: "The mathematical theory of vibrations in suspension bridge", Dep't of Commerce, 1950

Table 1.1

Vertical Deflectional Vibration

Symmetric Mode $W \neq W_o$ $\omega = 1.083$

$W = (0.7930 + 8.235h/L) \sin \pi x/L - (0.0655 + 3.535\ h/L) \sin 3\pi x/L + (0.0578 - 4.586h/L) \sin 5\pi x/L$

$W_o = 0.7930 \sin \pi x/L - 0.0655 \sin 3\pi x/L + 0.0578 \sin 5\pi x/L$

$U = 0.274\ h/L \sin 2\pi x/L - 0.414h/L \sin 4\pi x/L + h/L \sin 6\pi x/L$

Symmetric Mode $W = W_o$ $\omega = 1.330$

$W = W_o = 0.69885 \sin \pi x/L - 0.1514 \sin 3\pi x/L + 0.0382 \sin 5\pi x/L$

$U = -5.0570h/L \sin 2\pi x/L + 2.781h/L \sin 4\pi x/L - h/L \sin 6\pi x/L$

Anti-symmetric Mode $W \neq W_o$ $\omega = 1.549$

$W = (0.8526 + 0.9858h/L) \sin 2\pi x/L - (0.0384 + 12.809h/L) \sin 4\pi x/L - (0.0091 + 3.281h/L) \sin 6\pi x/L$

$W_o = 0.8526 \sin 2\pi x/L - 0.0384 \sin 4\pi x/L - 0.0091 \sin 6\pi x/L$

$U = -0.5996h/L \sin \pi x/L - 0.5858h/L \sin 3\pi x/L + h/L \sin 5\pi x/L$

Anti-symmetric Mode $W = W_o$ $\omega = 2.266$

$W = W_o = 0.7192 \sin 2\pi x/L - 0.1258 \sin 4\pi x/L - 0.0414 \sin 6\pi x/L$

$U = -0.0328h/L \sin \pi x/L - 1.4838h/L \sin 3\pi x/L + h/L \sin 5\pi x/L$

Torsional Vibration

Symmetric Mode $W \neq W_o$ $\omega = 1.433$

$\theta = 0.4772 \sin \pi x/L - 0.0479 \sin 3\pi x/L - 0.0171 \sin 5\pi x/L$

$W = b/2\theta - 5.717h/L \sin \pi x/L - 0.4169h/L \sin 3\pi x/L - 1.477h/L \sin 5\pi x/L$

$U = -4.439h/L \sin 2\pi x/L + 11.820h/L \sin 4\pi x/L + h/L \sin 6\pi x/L$

Symmetric Mode $W = W_o$ $\omega = 1.561$

$\theta = 2/b\ W = 1.142 \sin \pi x/L - 0.106 \sin 3\pi x/L - 0.0876 \sin 5\pi x/L$

$U = -2.950h/L \sin 2\pi x/L + 4.726 \sin 4\pi x/L - h/L \sin 6\pi x/L$

Anti-symmetric Mode $W \neq W_o$ $\omega = 3.020$

$\theta = 1.783 \sin 2\pi x/L - 0.5601 \sin 4\pi x/L = 0.5780 \sin 6\pi x/L$

$W = b/2\ \theta - 132h/L \sin 2\pi x/L - 156h/L \sin 4\pi x/L + 174h/L \sin 6\pi x/L$

$U = -8.014h/L \sin \pi x/L - 0.3758h/L \sin 3\pi x/L - 10h/L \sin 5\pi x/L$

Anti-symmetric Mode $W = W_o$ $\omega = 2.680$

$\theta = 7.102 \sin 2\pi x/L - 0.537 \sin 4\pi x/L + 0.0285 \sin 6\pi x/L$

$U = -2.950h/L \sin \pi x/L - 1.827h/L \sin 3\pi x/L + h/L \sin 5\pi x/L$

Table 1.2 Comparison of Circular Frequencies

Methods presented			Bleich's Eq.
Vertical Deflectional Vibrations			
Symmetric modes	1.083	$(w \neq w_o)$	1.343
	1.330	$(w = w_o)$	
Antisymmetric modes	1.549	$(w \neq w_o)$	1.810
	2.266	$(w = w_o)$	
Torsional Vibrations			
Symmetric modes	1.433	$(w \neq w_o)$	1.408
	1.561	$(w = w_o)$	
Antisymmetric modes	3.020	$(w \neq w_o)$	2.395
	2.680	$(w = w_o)$	

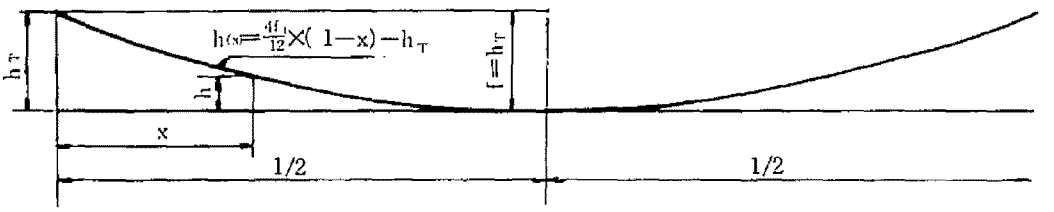

Fig. 1.1

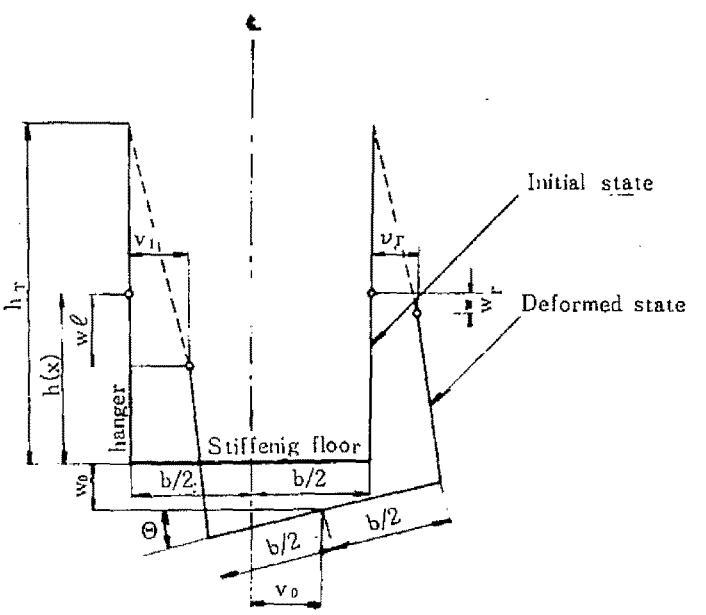

Fig. 1.2 Deformations at typical cross section of stiffening floor

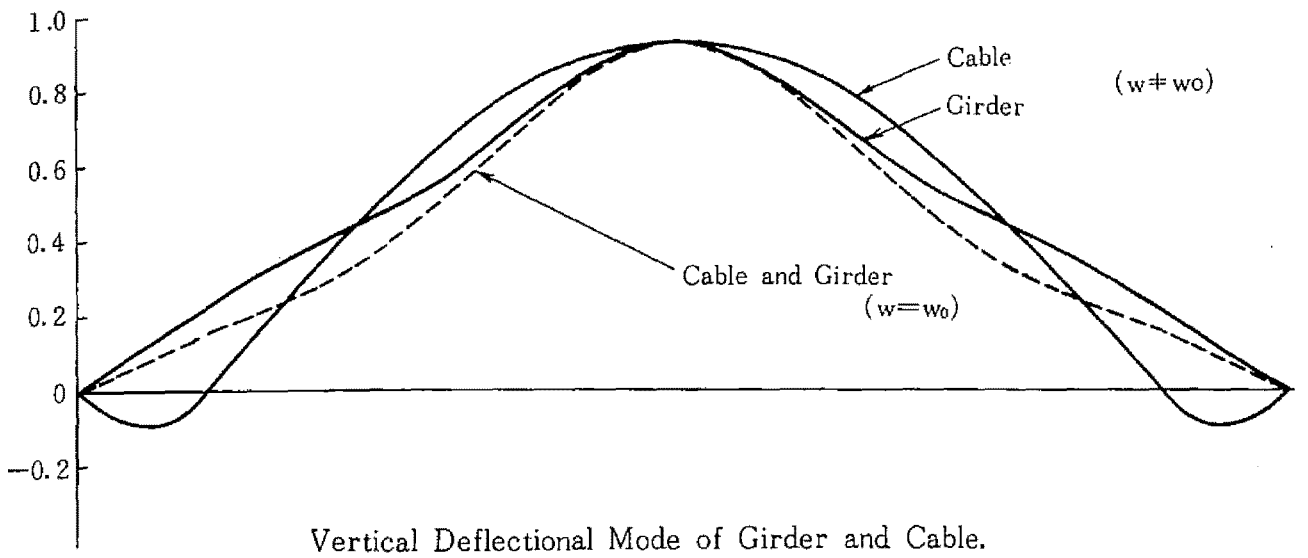

Vertical Deflectional Mode of Girder and Cable.

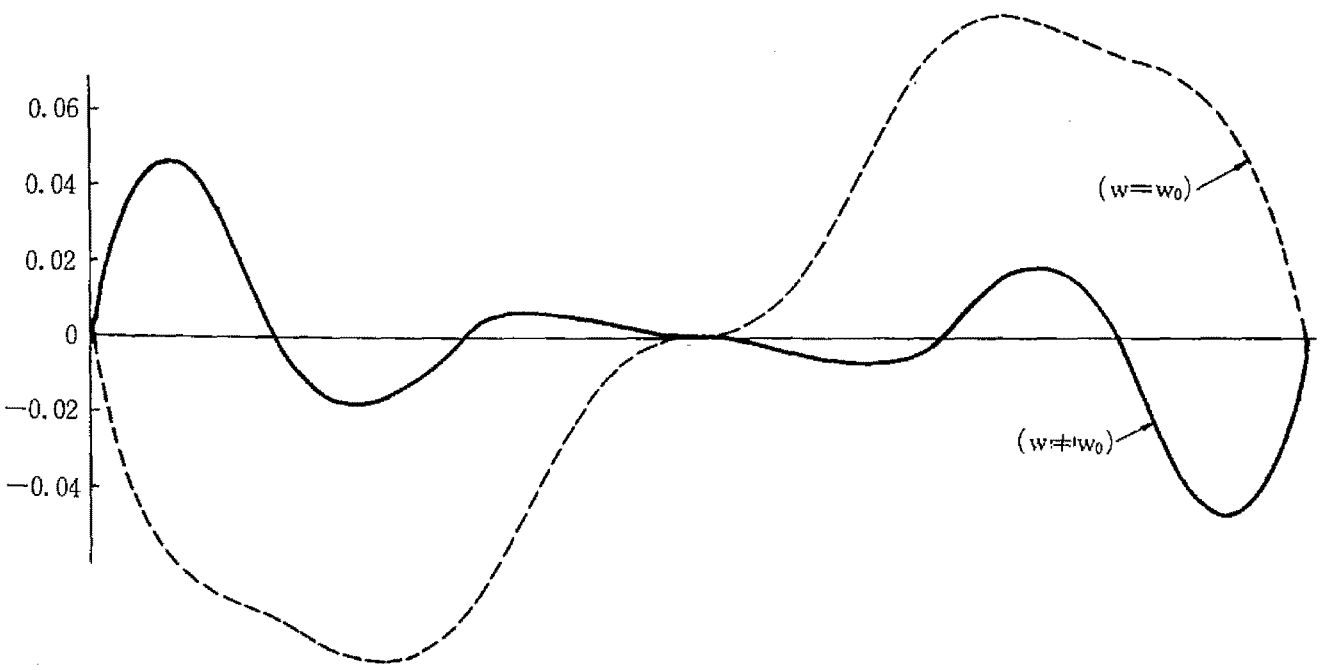

Horizontal Mode of Cable in Vertical Deflectional Vibration

Fig. 1.3

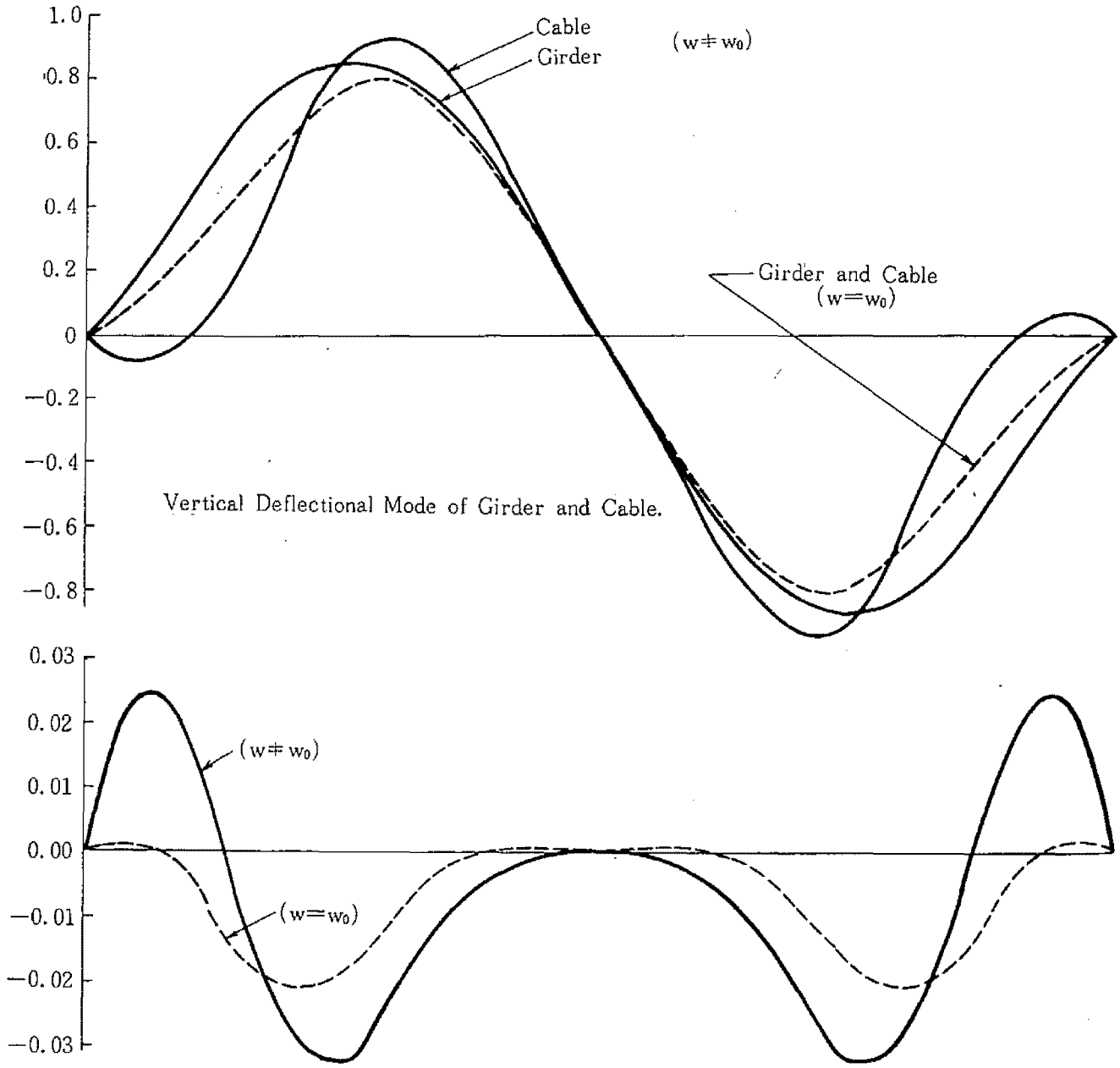

Horizontal Mode of Cable in Vertical Deflectional Vibration .

Fig. 1.4

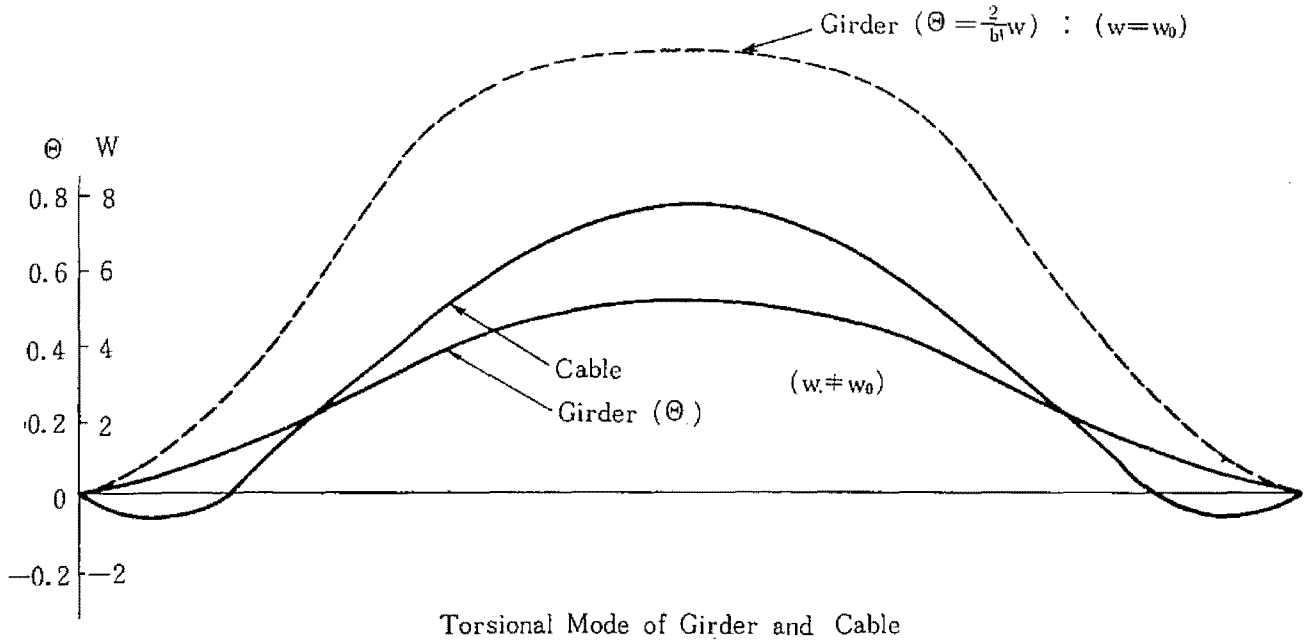

Torsional Mode of Girder and Cable

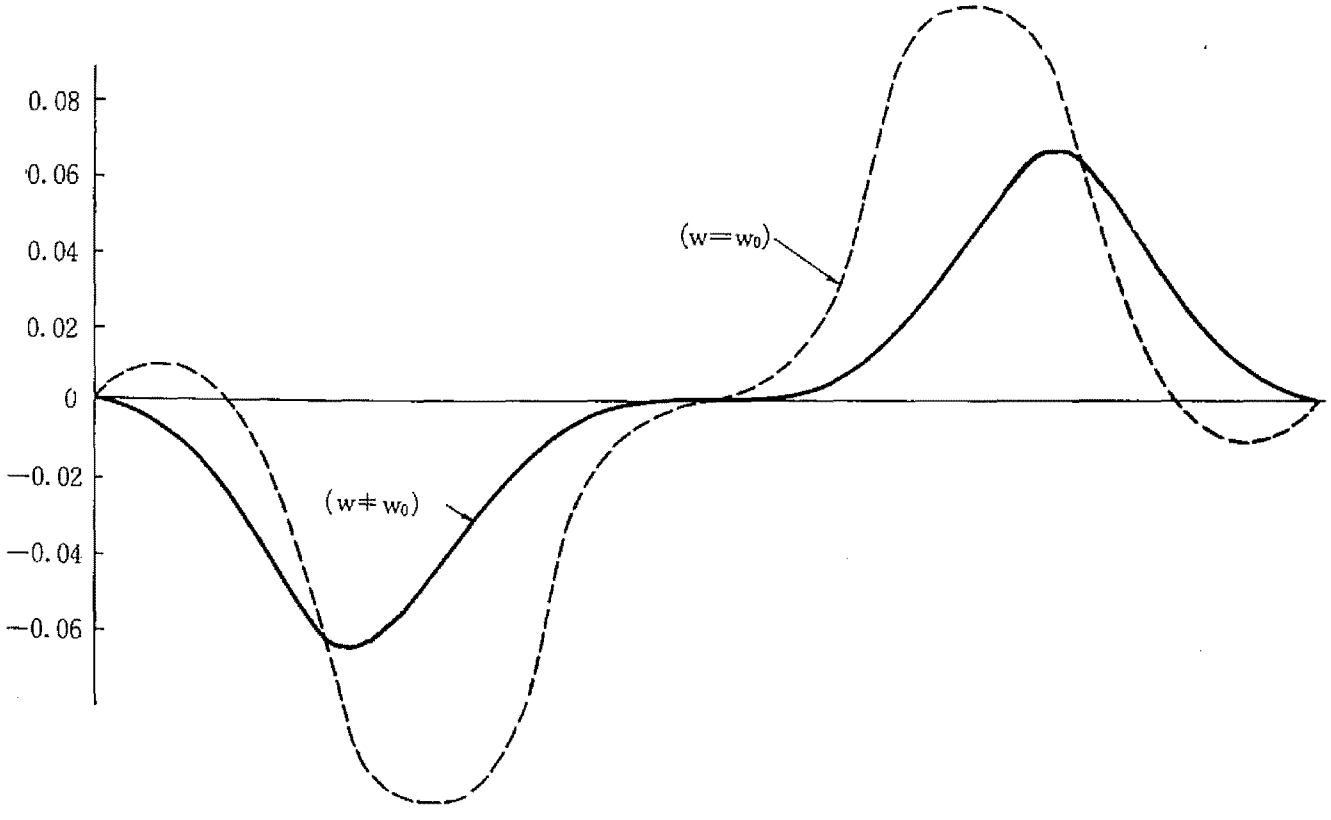

Horizontal Mode of Cable in Torsional Vibration

Fig. 1.5

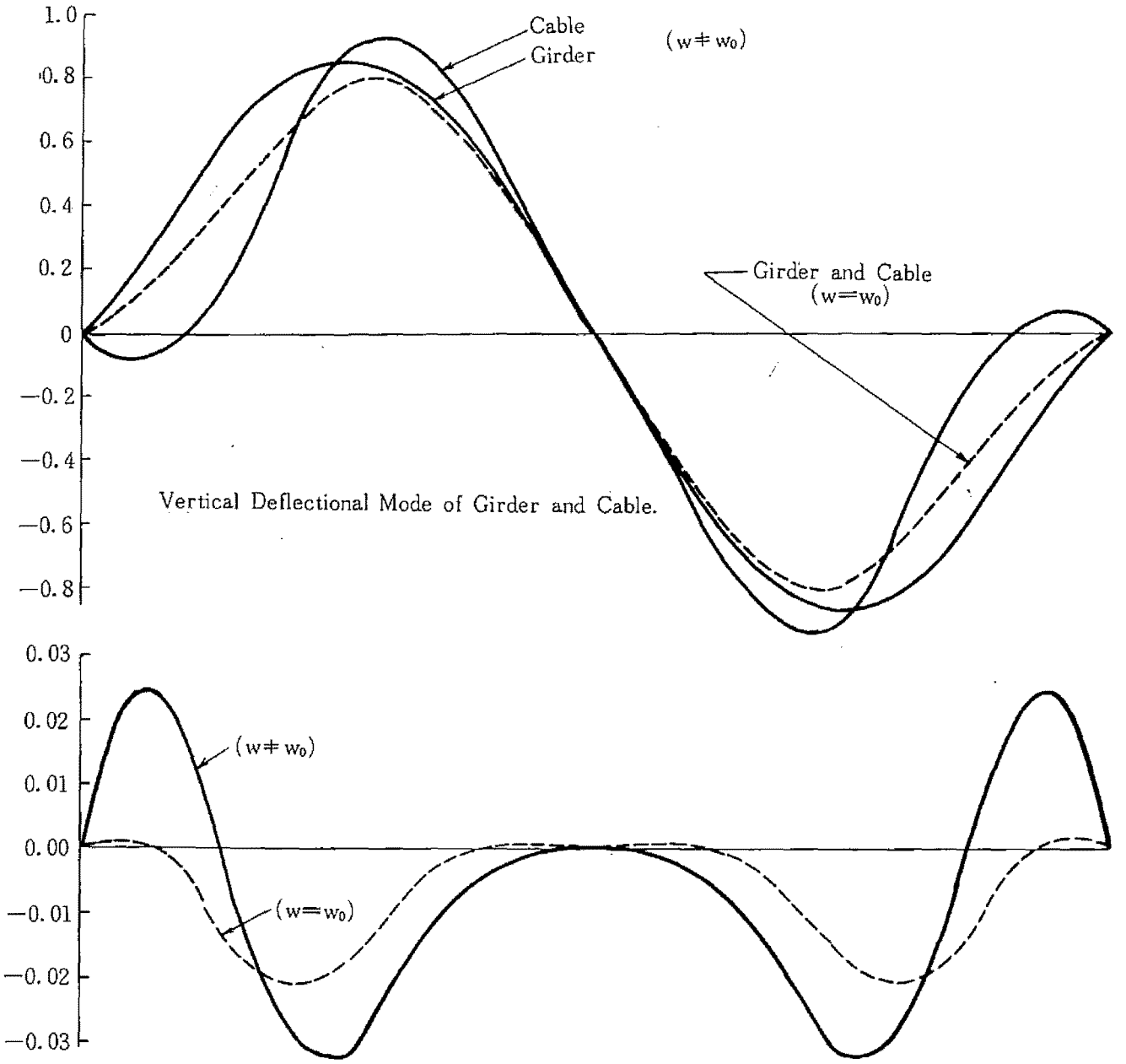

Horizontal Mode of Cable in Vertical Deflectional Vibration .

Fig. 1.4

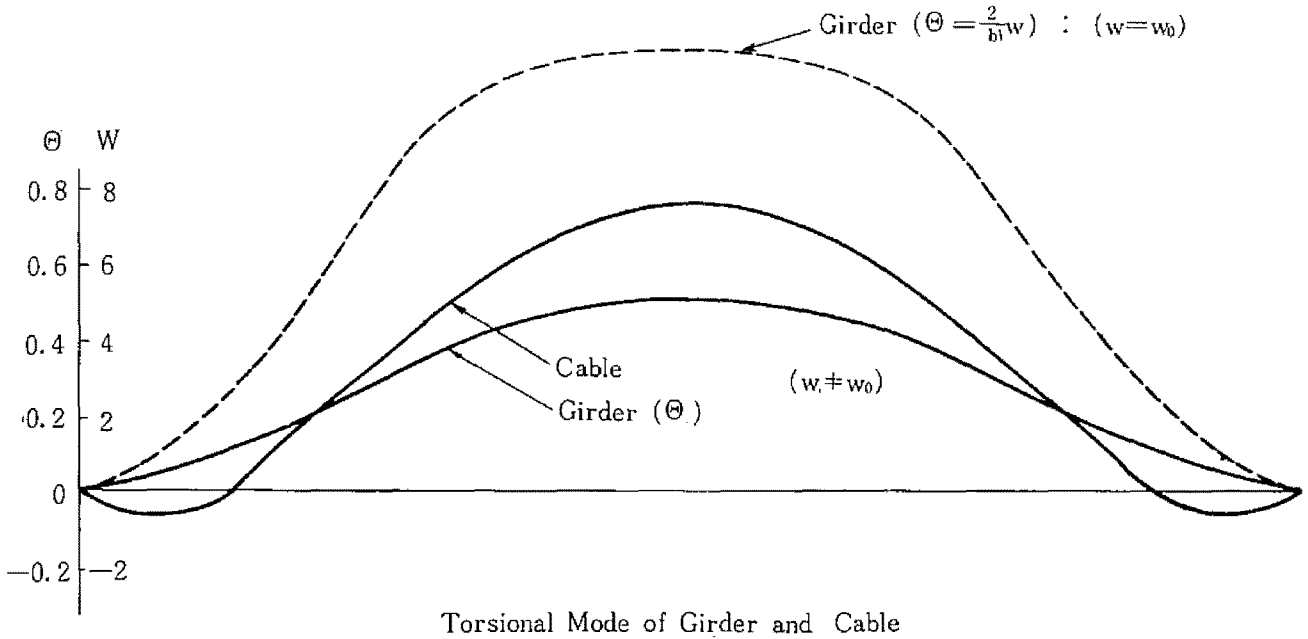

Torsional Mode of Girder and Cable

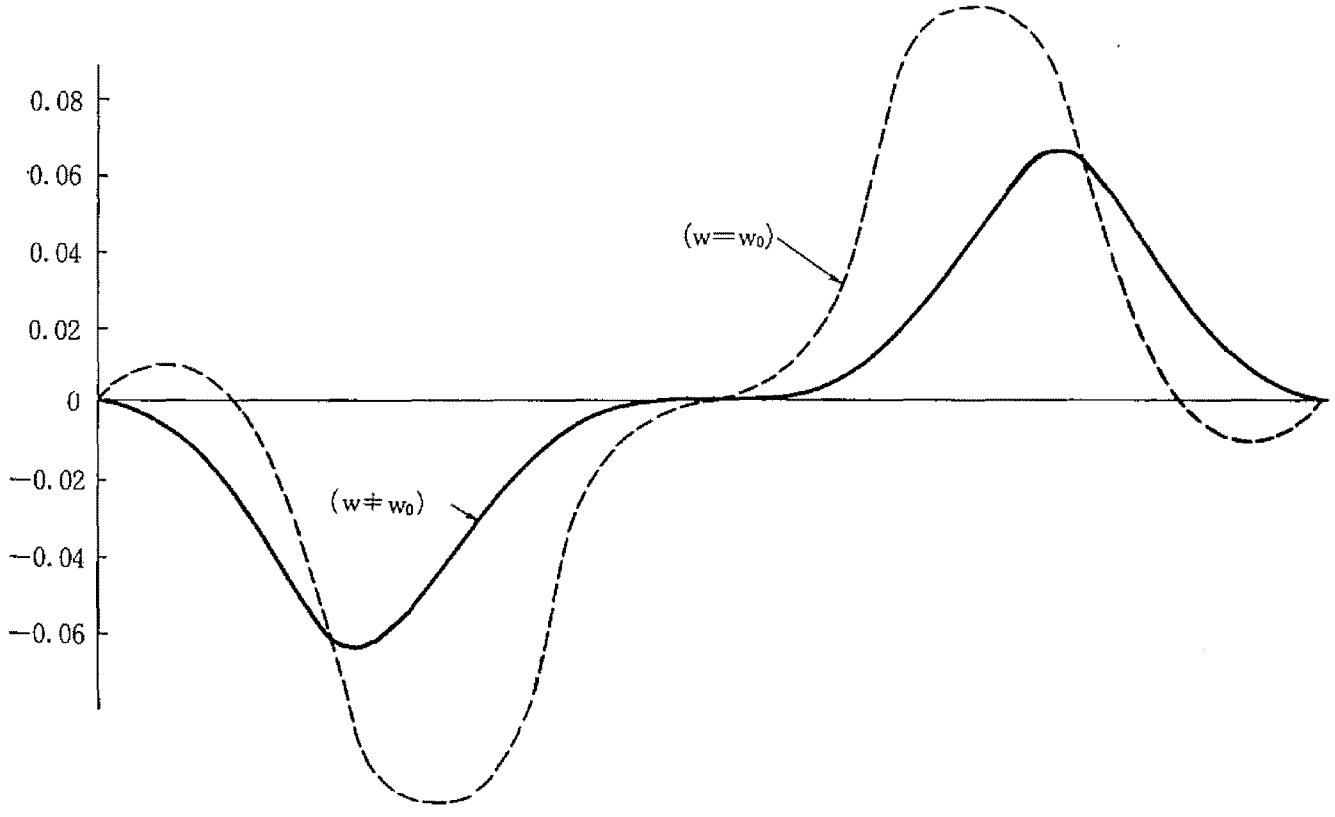

Horizontal Mode of Cable in Torsional Vibration

Fig. 1.5

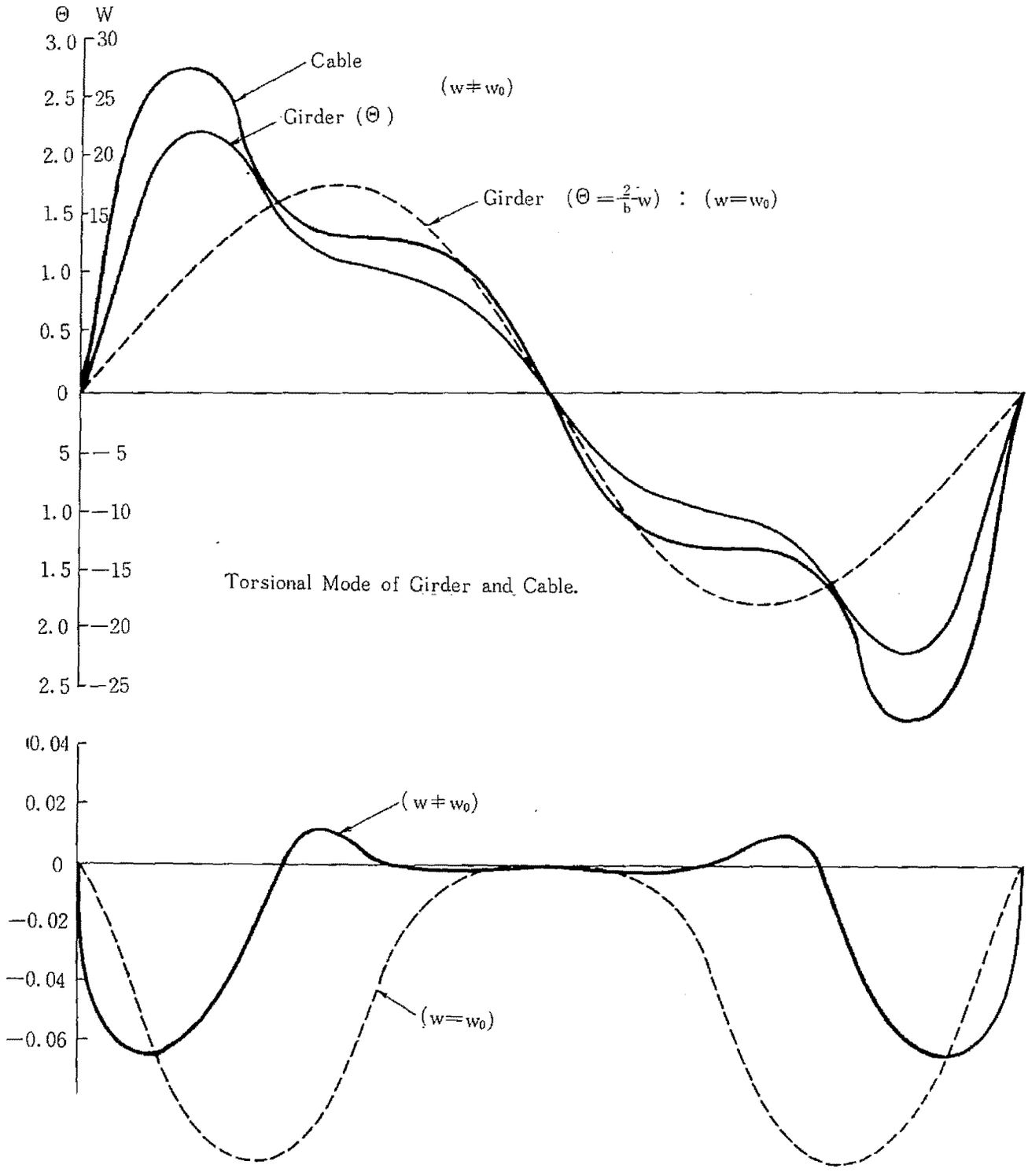

Horizontal Mode of Cable in Torsional Vibration.

Fig. 1.6

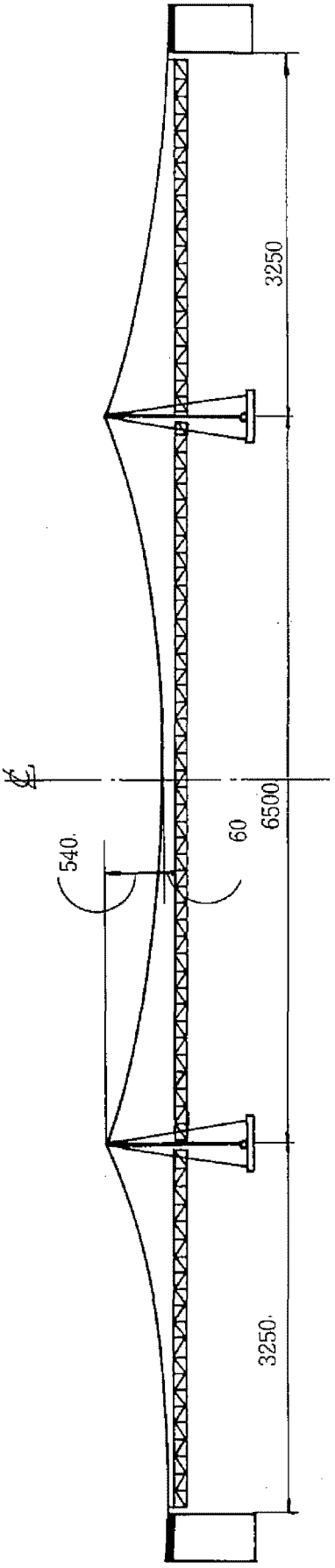

Fig. 1—7 General View of Full Model(Scale 1/100)

Static load conditions

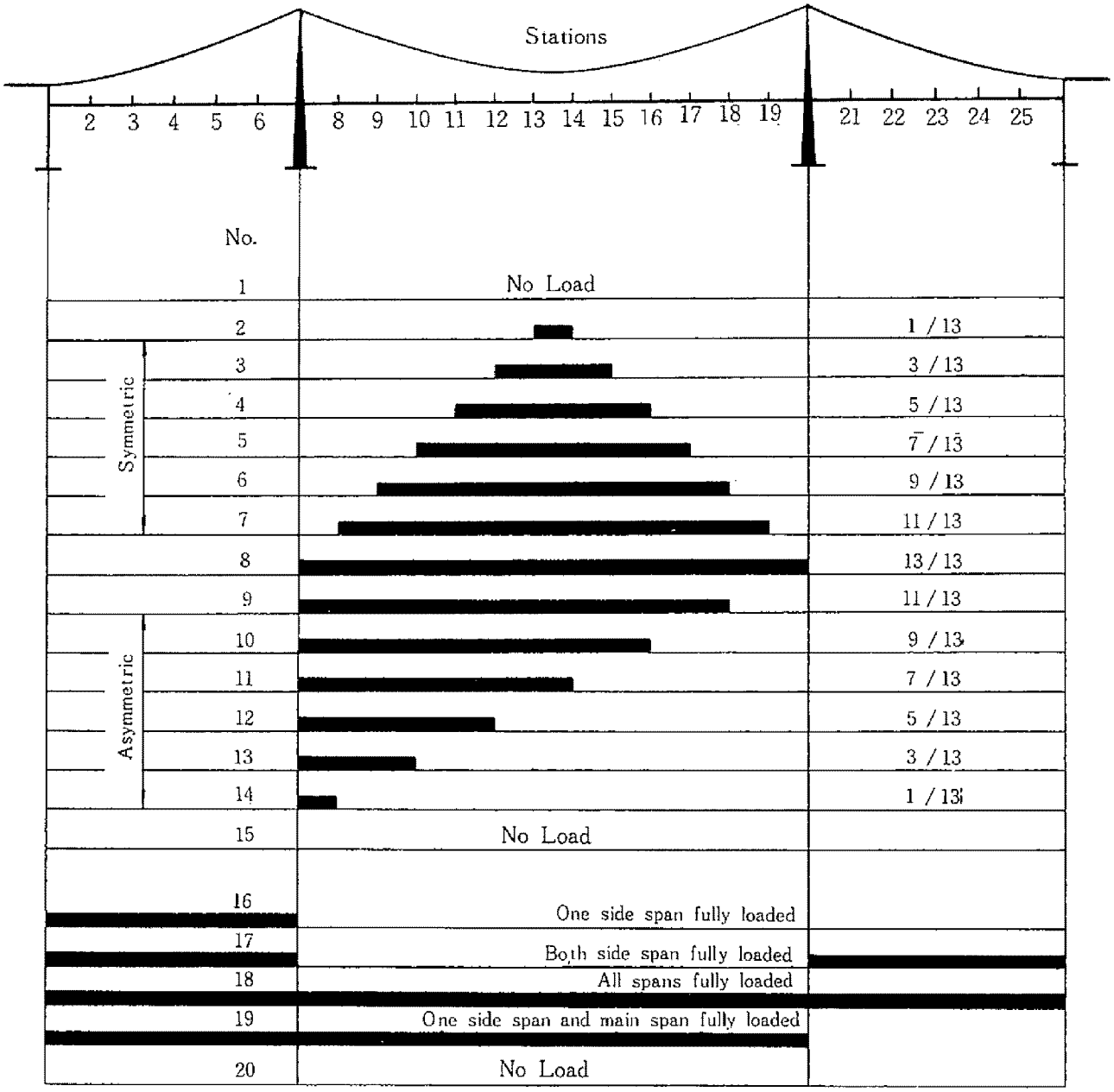

Fig. 1.8

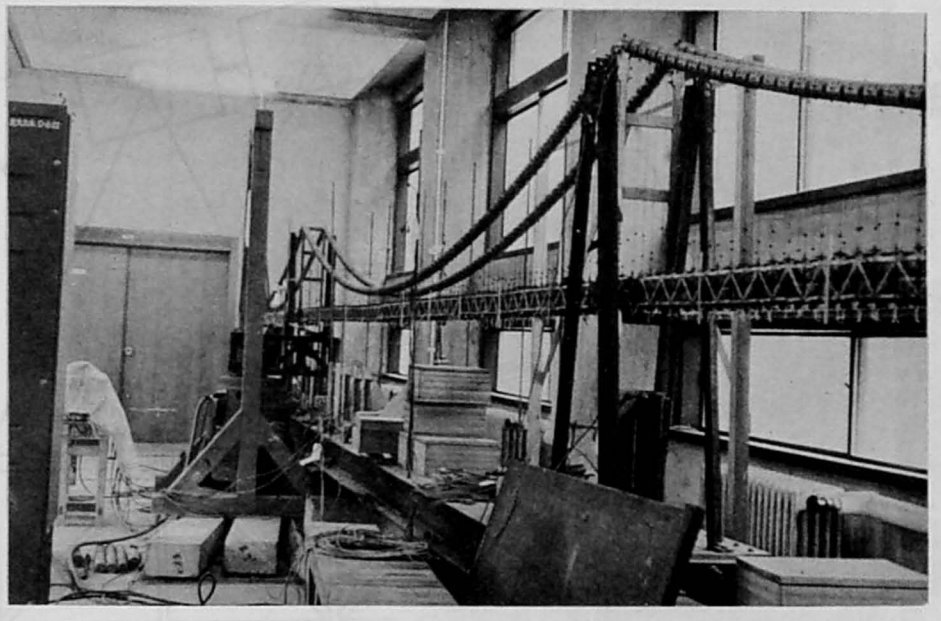

Photo 1.1 General Views of Model

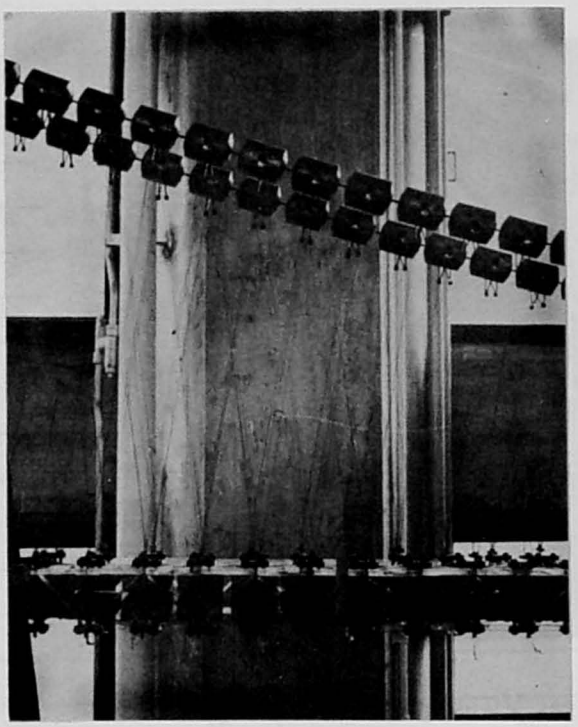

Photo 1.2 Inclined Hanger System

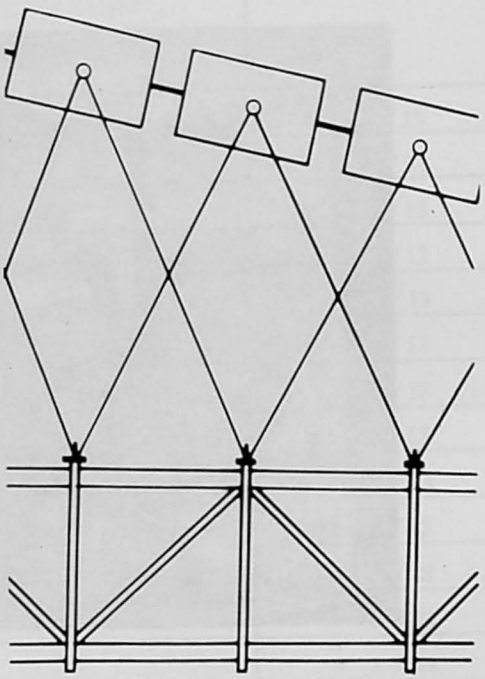

Fig 1.9

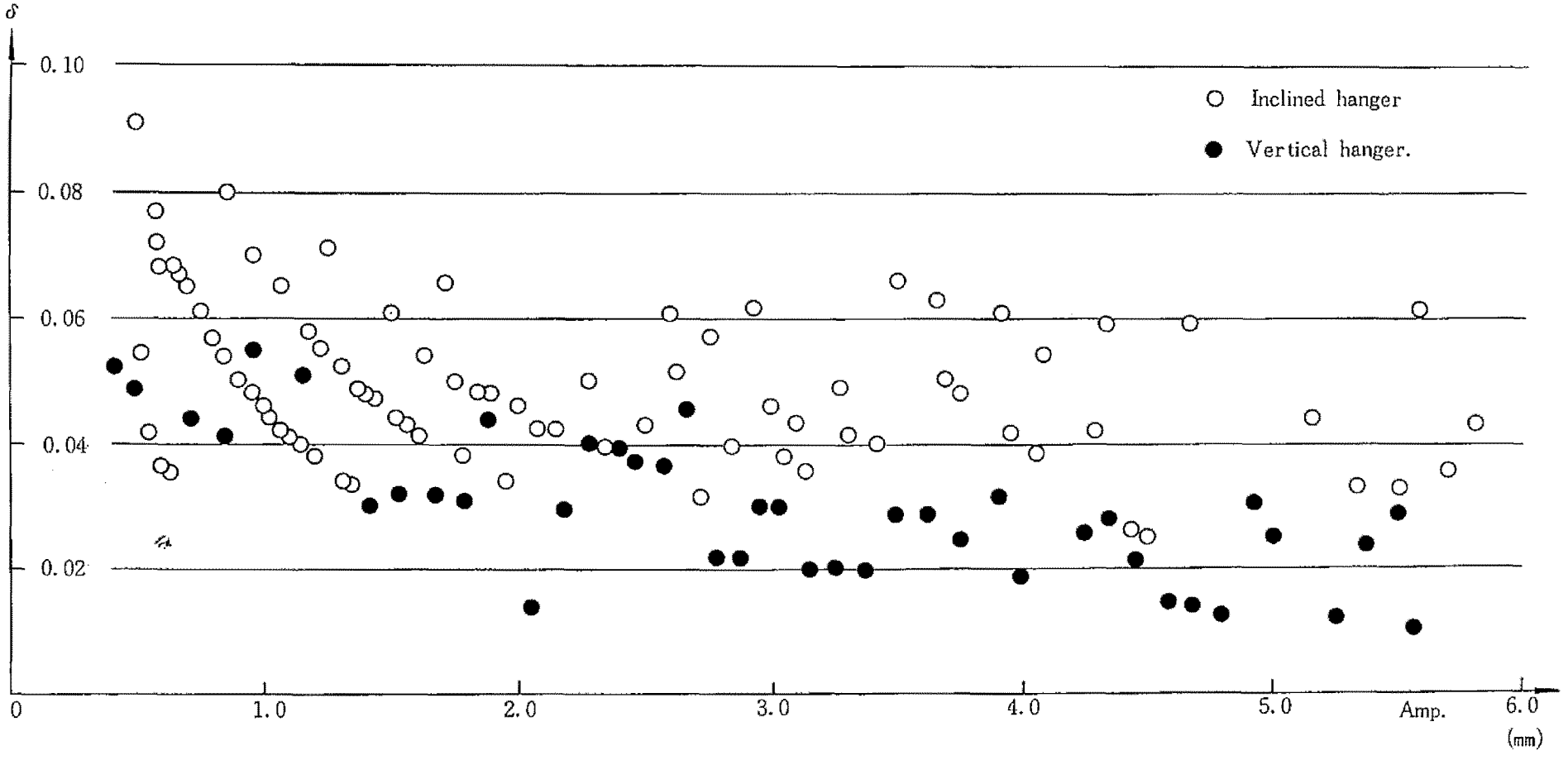

Fig. 1.10 Logarithmic Decrement of lst Symmetric Mode of Vertical Deflectional Vibration.

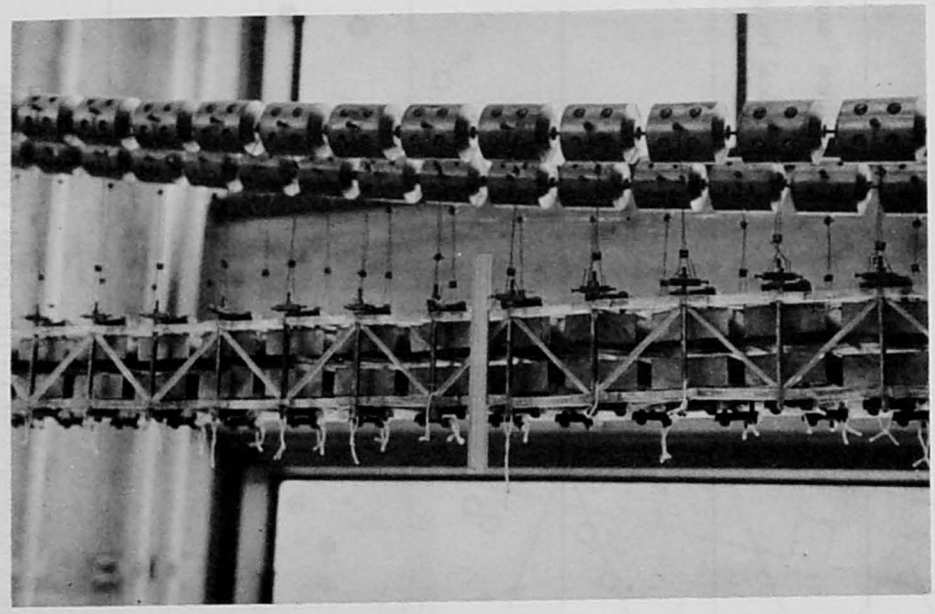

Photo 1.3 Vertical Hanger System

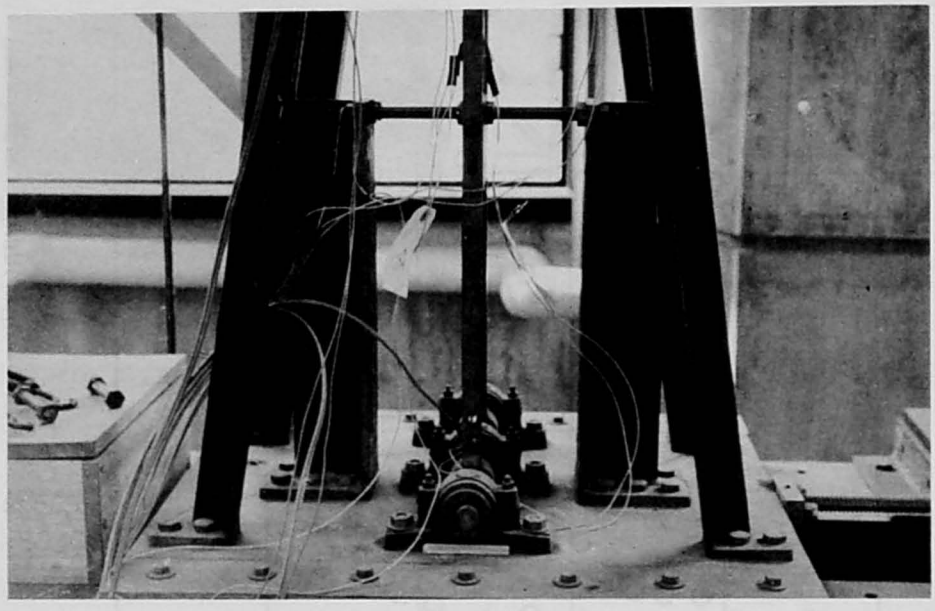

Photo 1.4 Detalis of Tower End.

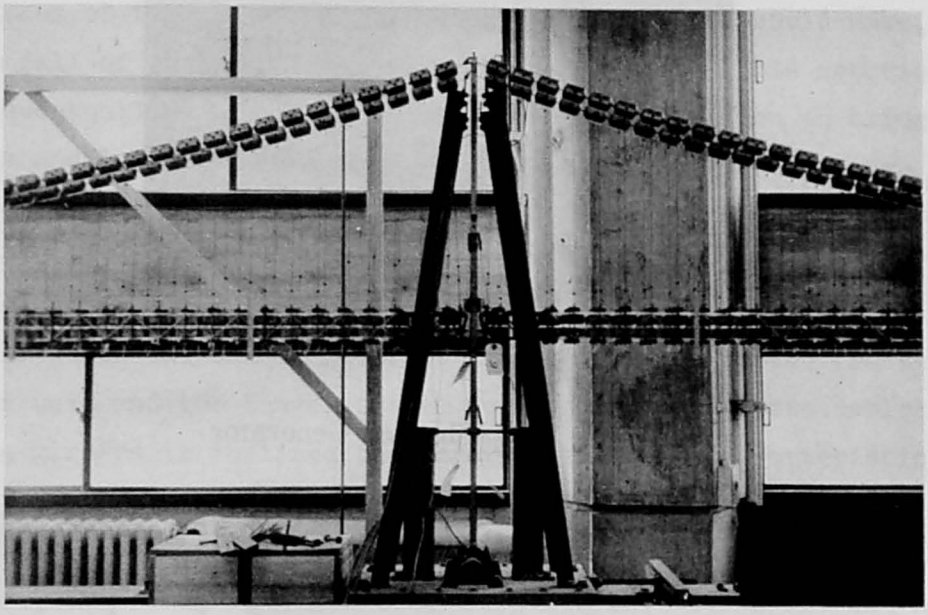

Photo 1.5 Fixing Angles for Top Movement of Tower

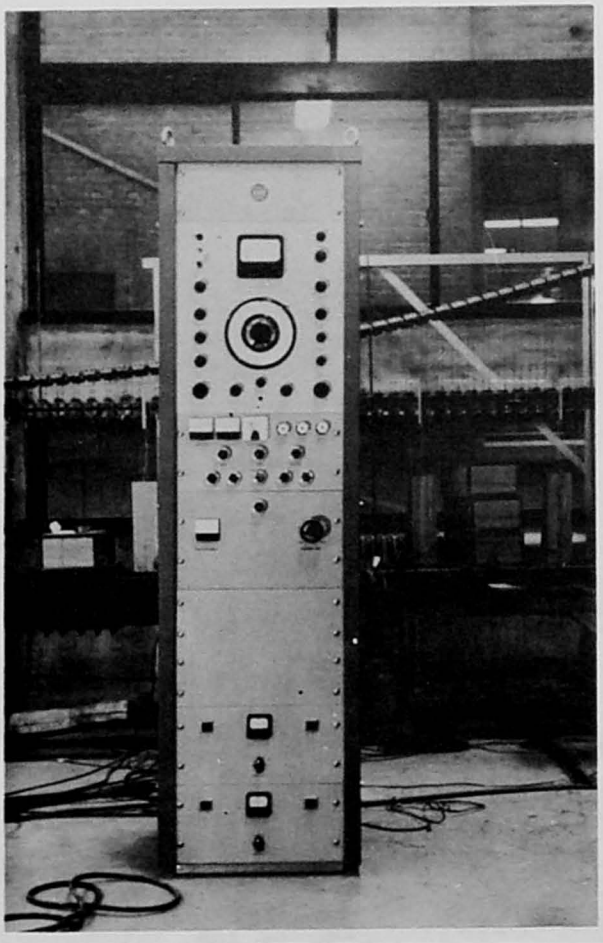

Photo 1.6 Vibration Generator

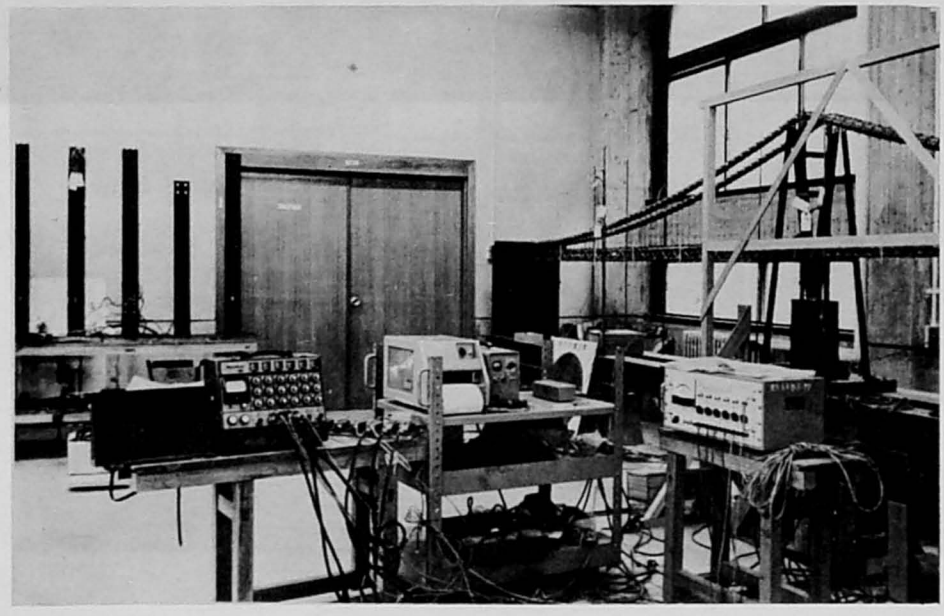

Photo 1.7 Instruments for Measurements.

CHAPTER 2 STRUCTURAL CHARACTERISTICS OF SUSPENSION BRIDGE WITH INCLINED HANGERS

2.1 INTRODUCTION

As mentioned in the previous chapter the suspension bridges, as one of the Man's oldest means of bridging a gap, have been investigated by number of researchers and were reported successful in designs and constructions of the largest steel structures which man could make, until the fall of the Tacoma Narrows Bridge in 1940. This notorious accident eventually revealed the importance of wind action on bridge structures and leaded to thoroughful researches on the stiffening systems of suspension bridges, which resulted in wide adoption of the truss-type stiffening girder instead of the plate girder type. [1),2)] Recently an attention is placed on the newly made Severn Bridge in Britain for which the unique reversed trapozoidal and closed cross section is used and the Hanger system for connection between cables and stiffening girders is inclined to improve structural characteristics.[3)] As well known, main parts of suspension bridge consists of the cables as the tensile members and the stiffening girder as the flexural members and the changes of individual rigidities effect on the estimation of the overall rigidity of bridges, which, however, also depend on and are largely influenced by the connection configuration between cables and stiffening girder, i.e., the Hanger System. D. B. Steinman[4)] suggested this effect of inclination of hangers and applied it for the Deer Isle Bridge in order to stiffen the structure sufficiently for wind action. Similar feature also is found in the mono-cable suspension bridge studied by F. Leonhardt.[5)]

Such structural progress in suspension bridge as mentioned above is considered closely related with recent development of structural engineering and particularly with the positive tendency to utilize the

suspension structures for huge spatial buildings.

It thus necessitates more detailed and exact analysis on the flexural behaviour of cables and also indicates a wide range of possibility to develop the new structural system. C. Thornton and C. Birnstiel[6] investigates, in the most unified sense, the mechanical characteristics of suspension structures by using the incremental load method as well as the method of continuity, which is considered to be based on the same priciple of analysis of the suspension bridge with inclined hangers by T. Fujino and K. Ohsaka.[7] The so called dual cable system is studied by D. Jawerth for various cases and clarified its characters for the system with the inclined stiffening members.[8] For the Barbara Bridge the dual cable system is used rigidly enough to stiffen the system without any inclined hanger system.[9] Z. Hiba investigated another structural feature of suspension bridge due to the inclination of hanger system, for which the plane enclosing cable and hangers tilts with respect to the vertical plane, for the lateral horizontal wind action.[10] Additionally it is noticed that several types of bridge structures such as the cable stayed beam bridge and the Nielsen system bridge increase the rigidity by inclined connections of main structural members.

For the Severn Bridge the inclined hanger system is used to increase its damping capacity, which mechanism is however analytically unsolved for actual bridges.[11),12] However T. Yamaguchi, K. Siraki, R. Nakagawa[13] performed the experimental study on the damping effect due to the inclined hanger system for the Severn type bridge and compared the result with the vertical hanger system, which the Bleich's theory[14] is applied for, to confirm the increasement of damping capacity in comparison with the former case.

It is easily expected that the dynamic and static characteristics of suspension bridge with inclined hangers exhibit a coupled form of various structural features. Of the most importance is thus the problem how one can acquires with sufficient accuracy the basic features of suspension bridge with inclined hangers. In order to clarify this

characteristics we investigate for the first place the coupling of displacements in the ordinary type of suspension bridge theoretically, [15),16)] as mentioned in the previous chapter, and performed an experimental study on the suspension bridge with inclined hangers.[17)] The results indicate that the inclination of hangers increases the damping capacity, remarkably different from the vertical hanger system, and the static flexural rigidity and also the natural frequencies. However, since the deformational characteristics for both cases seem to be similar and their coupling of deformations to be of the same order, it is possibly considered that the fundamental equations for the inclined hanger suspension bridge can be derived by the modification of the ordinary deflection theory of suspension bridge with vertical hangers.

In this chapter, the general structural features of the inclined hanger suspension bridge are illustrated; firstly the fundamental equations are derived for the Warren type hanger system in 2.2 and modified for the Double Warren type hanger system in 2.3. An analytical methods for static and free vibrational problems for three spanned suspension bridge are presented in 2.4 and 2.5. In 2.6 the numerical example is illustrated and compared in 2.7 with the experimental results of model tests.

2.2 DERIVATION OF FUNDAMENTAL EQUATIONS-I

2.2.1 INCREMENTAL HANGER TENSIONS FOR WARREN TYPE INCLINED HANGER SYSTEM

Let us consider the kinematical conditions for the cable-stiffening girder - hanger system as shown in Fig. 2.1. Let the triangle composed by the stiffening girders and two hangers be isosceles and let its base, the height, the vertex distance be $2e(x)$, $h(x)$ and $\bar{e}(x)$, respectively. And let the deflections of cables and those of stiffening girders be $\eta_c(x)$ and $\eta_b(x)$, then the induced incremental hanger tensions $\triangle T_+, \triangle T_-$

as shown in Fig. 2.1, for the small deflections are written of the form

$$\triangle T_{+} = \frac{E_1 A_1 \, h}{d^2} \left\{ \triangle h + \eta_c' \, e + \triangle h' \, e \right\}$$

$$\triangle T_{-} = \frac{E_1 A_1 \, h}{d^2} \left\{ -\triangle h + \eta_c' \, e + \triangle h' \, e \right\} \qquad (2 \cdot 2 \cdot 1)$$

where $d = (h^2 + e^2)^{1/2}$

Let Q_c and P_c be the horizontal and vertical components of the resultant hanger tensions at the vertex, then we have

$$Q_c = \frac{2 E_1 A_1}{d^3} \, h e^2 \left\{ \eta_c' + \triangle h' \right\}$$

$$P_c = \frac{2 E_1 A_1}{d^3} \, h^2 \triangle h \qquad (2 \cdot 2 \cdot 2)$$

where $E_1 A_1$ indicates the extensional rigidity of hanger.

Note that Q_c tends to zero in eq. (2.2.2) when e(x) tends to zero, which corresponds to the vertical hanger system.

And also we have

$$\lim_{e \to 0} P_c = \lim_{d \to h} \frac{2 E_1 A_1}{d^3} h^2 \triangle h = 2 E_1 A_1 \frac{\triangle h}{h}$$

which indicates that at the limiting case of vertical hanger system P_c tends to the hanger tension identically.

As shown in Fig. 2.2 the induced hanger tensions produce the resultant forces Q_c and P_c for the cable, while for stiffening girder the horizontal and vertical components of resultant force as well as the resultant moment $Q_c h$ are produced.

2.2.2 EQUILIBRIUM EQUATION FOR CABLE

In order to obtain the equilibrium equation of cable let the result-

ant forces distrubute along the cable as shown in Fig. 2.3 and let the intensity be denoted by p_c and q, then we have the resultant horizontal component of induced cable tension as the sum of H_g, the one due to the ownweight per unit length, Hpv, the one induced vertical load P_c, and H_{pq}, the one due to the horizontal load q. Since H_g and H_{pv} remain constant, the equlibrium conditions for cables in horizontal and vertical directions yield to

$$\frac{dH_{pq}}{dx} + q = 0 \qquad (2\cdot2\cdot3)$$

$$\frac{dH_{pq}}{dx}(y+\eta)' + (H_{pv}+H_{pq})y'' + (H_g+H_{pv}+H_{pq})\eta'' + (p_c - g_b) = 0 \qquad (2\cdot2\cdot4)$$

where y is the initial funicular curve of cable, which is determined by

$$H_g y'' + (g_c + g_b) = 0 \qquad (2\cdot2\cdot5)$$

in which g_c and g_b denote the own weight of cable per unit length and the one of stiffening girder.

Integrating eq. (2.2.3) with respect to x, it yields to

$$H_{pq} = -\int_0^x q(u)\,du + C \qquad (2\cdot2\cdot6)$$

Substituting eq. (2.2.6) into eq. (2.2.4) and neglecting the higher order terms, the equilibrium equation for cable is reduced to

$$-q(y'+\eta') + (H_{pv} + C - \int_0^x q\,du)y'' + (H_g + H_{pv} + C - \int_0^x q\,du)\eta''$$

$$+ P_c - g_b = 0 \qquad (2\cdot2\cdot7)$$

2.2.3 EQUILIBRIUM EQUATION FOR STIFFENING GIRDER

As in Fig. 2.4 let the sectional forces of stiffening girder be N, V and M and in same manner as mentioned previously let them

distribute within the length $\bar{e}(x)$ of the stiffening girder to be $q(x)$, (horizontal intensity), $-P_c$ (vertical intensity) and $m(x)$ (moment intensity). Then for the action of distributed live load p, we have

$$\frac{dN}{dx} = q \qquad \text{by the equilibrium in horizontal direction}$$

$$\frac{dV}{dx} = -(p + g_b + p_c) \qquad \text{by the equilibrium in vertical direction}$$

$$\frac{dM}{dx} = -m - N\eta' + V \qquad \text{by the equilibrium for moment}$$

which are therefore reduced to

$$\frac{d^2M}{dx^2} = -\frac{dm}{dx} - \left(\frac{dN}{dx}\eta' + N\eta''\right) + \frac{dV}{dx}$$

$$= -m' - (q\eta' + N\eta'') - (p + g_b - p_c)$$

$$(EI\eta'')'' - m' - (N\eta') + (p_c - g_b) = p \qquad (2\cdot2\cdot8)$$

2.2.4 FUNDAMENTAL EQUATIONS FOR SUSPENSION BRIDGE WITH INCLINED HANGERS

From the above mentioned eq's (2.2.7) and (2.2.8) one obtains the fundamental equations for suspension bridge with inclined hangers by eliminating the term $p_c - g_b$ from both equations equilibrium for cable

and for stiffening girder, as follows

$$(EI\eta'')'' - m' - (N\eta')' + q\,(y' + \eta') - (H_{pv} + C - \int_0^x q\,du)\,y''$$

$$- (H_g + H_{pv} + C - \int_0^x q(u)\,du)\,\eta'' = p \qquad (2\cdot2\cdot9)$$

for which m(x) and q(x) are rewritten by use of eq. (2.2.2) as

$$q(x) = \frac{Q_c}{\bar{e}} = \frac{2E_1A_1}{d^3\,\bar{e}}\,he^2\eta' \equiv \Lambda\eta' \qquad (2\cdot2\cdot10)$$

$$m(x) = \frac{Q_c\,h}{\bar{e}} = \frac{2E_1A_1\,he^2}{d^3\,\bar{e}}\,h\eta' \equiv \Lambda h\eta' \qquad (2\cdot2\cdot11)$$

assuming that the deflections of cable through the vertices of the triangles composed by hangers and stiffening girder coinside with those of stiffening girder; namely $\triangle h = 0$.

The horizontal equilibrium of force yields to

$$N = \int_0^x q(u)\,du \qquad (2\cdot2\cdot12)$$

Also the initial funicular curve of cable y is written by

$$y = h_T - h \qquad \therefore\ y'' = -h'' \qquad (2\cdot2\cdot13)$$

where h_T is the height of tower top from the stiffening girder. Substitution of eq's (2.2.10), (2.2.11), (2.2.12), (2.2.13) into eq. (2.2.9) yields to

$$(EI\eta'')'' - (\Lambda h\eta')' - \left\{\eta' \int_0^x \Lambda\eta'\,du\right\}' - \Lambda\eta'(h' - \eta') + (H_{pv} + C - \int_0^x \eta'\,\Lambda\,du)\,h''$$

$$- (H_g + H_{pv} + C - \int_0^x \Lambda\eta'\,du)\,\eta'' = p \qquad (2\cdot2\cdot14)$$

which is reduced to

$$(EI\eta'')'' - (H_g + H_p - \int_0^x \Lambda\,\eta'\,du)\,\eta'' + (H_p - \int_0^x \Lambda\,\eta'\,du)\,h''$$

$$- (\Lambda h\eta')' - \Lambda h'\eta' = p \qquad (2\cdot2\cdot15)$$

and

$$\Lambda = \frac{2E_1A_1}{d^3\,\bar{e}}\,he^2 \qquad (2\cdot2\cdot15')$$

if one annihilates the higher order terms of deformation and one introduces the relation $H_p = H_{pv} + C$. In eq's (2.2.15) and (2.2.15'), E_1A_1 denotes the extensional rigidity of hanger, h and e the vertical and horizontal projection of hanger length, d and $\bar{e}$ the distance of vertices. When e tends to zero in eq. (2.2.15), Λ also tends to zero and eq. (2.2.15 eventually yields to the form of fundamental equation of deflection theory for an ordinary type of suspension bridge.[18] Thus, the fundamental equation of equilibrium for a suspension bridge with inclined hangers (Warren type) is derived as a modified form of the ordinary deflection theory by introducing the parameter Λ.

The undetermined quantity H_p in eq. (2.2.15) is determined by the so called cable equation which is obtained in exactly same consideration as the case of vertical hanger system as follows

$$\int_L d\xi = \int_L \frac{H_p - \int_0^x \Lambda\eta'\,du}{E_cA_c}\left(\frac{ds}{dx}\right)^3 dx \pm \alpha_t T \int_L \left(\frac{ds}{dx}\right)^2 dx - h'' \int_L \eta\,dx \qquad (2\cdot2\cdot16)$$

where ξ denotes the longitudinal displacement cable, ds the infinitesimal curve length of cable, α_t the thermal expansion coefficient and T the temperature change.

2.2.5 SIMPLIFICATION OF THE FUNDAMENTAL EQUATION OF EQUILIBRIUM

As discussed in the previous sections eq's (2.2.16) and (2.2.16)

are the fundamental equations for suspension bridge with inclined hangers (Warren type), which can be greatly simplified if the vertical angles of hangers 2β and the distance $\bar{e}$ remain constant, as following,

$$\Lambda = \frac{2E_1A_1}{d^3\,\bar{e}}\,he^2 = \frac{2E_1A_1}{\bar{e}}\cos\beta\sin^2\beta = const \equiv \Lambda_0$$

$$\int_0^x \Lambda\eta'\,du = \Lambda_0\eta$$

for which $\bar{e} \geqq 2e$, $E_1A_1 = const$

So eq's (2.15) and (2.16) yield to

$$(EI\eta'')'' - \{(H_g + H_p + \Lambda_0 h)\eta\}'' + H_p h'' = p \qquad (2\cdot2\cdot17)$$

$$\int_L d\xi = \frac{H_p}{E_cA_c}\int_L \left(\frac{ds}{dx}\right)^3 dx \pm \alpha_t T \int_L \left(\frac{ds}{dx}\right)^2 dx$$

$$- \int_L \left\{ h'' + \frac{\Lambda_0}{E_cA_c}\left(\frac{ds}{dx}\right)^3 \right\} \eta\,dx \qquad (2\cdot2\cdot18)$$

These equations are of the most simplified form of equilibrium equations for the case of inclined hangers, signifying that the inclination of hangers is tantamount to the increase of horizontal component of cable tension induced by the own weight by the amount of $\Lambda_0 h$ from eq. (2.17) and to the decrease of sag ratio by the amount of $(l^2/8)(\Lambda_0/E_cA_c)\times (ds/dx)^3$ if the initial curve of cable is assumed as a parabola. The two effects therefore indicate the increase of the overwhole flexural rigidity for the case of inclined hanger.

2.3 DERIVATION OF FUNDAMENTAL EQUATION - II

In the previous paragraph the fundamental equations for the Warren type hanger system are considered and the same method applied is here used for the case of the Double Warren type hanger system as shown in Fig. 2.5. The relation of induced hanger tensions and flexural deflection within the distance 2e in Fig. 2.6 are obtained in exactly same manner as

$$\triangle \hat{T}_{+} = \frac{E_1 A_1}{d} \left\{ \eta_b (x+e) - \eta_c (x) \right\} \frac{h}{d}$$

$$\triangle \hat{T}_{-} = \frac{E_1 A_1}{d} \left\{ \eta_c (x) - \eta_b (x-e) \right\} \frac{h}{d}$$

$$\triangle \overset{\vee}{T}_{+} = \frac{E_1 A_1}{\sqrt{e^2 + h^2 (x+e)}} \left\{ \eta_c (x+e) - \eta_b (x) \right\} \frac{h (x+e)}{\sqrt{h^2 (x+e) + e^2}}$$

$$\triangle \overset{\vee}{T}_{-} = \frac{E_1 A_1}{\sqrt{e^2 + h^2 (x-e)}} \left\{ \eta_b (x) - \eta_c (x-e) \right\} \frac{h (x-e)}{\sqrt{h^2 (x-e) + e^2}}$$

Expanding terms, $\eta_b (x+e)$, $\eta_c (x+e)$, $h (x+e)$, $h (x-e)$, etc., with respect to x into a Taylor's series and assuming that $1 \gg k'(1-2h^2/d^2)(e/h)$ then we have $\beta_{i+1} \doteq \beta_i \doteq \beta_i - 1$ and above four equations are reduced to

$$\left.\begin{aligned} \triangle \hat{T}_{+} \doteq \triangle \overset{\vee}{T}_{-} &= \frac{E_1 A_1 h}{d^2} \left\{ e \eta_c' + \triangle h \right\} \\ \triangle \hat{T}_{-} \doteq \triangle \overset{\vee}{T}_{+} &= \frac{E_1 A_1 h}{d^2} \left\{ e \eta_c' - \triangle h \right\} \end{aligned}\right\} \qquad (2\cdot3\cdot1)$$

Eq. (2.3.1) indicates that the stiffening effect due to the Double Warren type hanger system is expected to be similar as the Warren type

hanger system except that the horizontal and vertical components of equivalent reactions q, p_c are doubled, while the equivalent moment m(x) remains same as the previous case.

The equilibrium equation is thus written by subsituting the relations,

$$\left.\begin{aligned} q &= \frac{(2\,Q_c)}{2e} = \frac{2E_1 A_1}{d^3} h e \eta' \equiv 2\tilde{\Lambda}\eta' \\ N &= \int_0^x q(u)\,du \\ m &= \frac{Q_c h}{2e} = \frac{E_1 A_1 h e}{d^3} h\eta' = \tilde{\Lambda} h \eta' \end{aligned}\right\} \qquad (2\cdot3\cdot2)$$

into eq. (2.2.9) and neglecting higher order terms, as follows;

$$(EI\eta'')'' - (H_g + H_p)\eta'' + H_p h'' - \left\{\tilde{\Lambda} h \eta' + 2h' \int_0^x \tilde{\Lambda}\eta'\,du\right\}' = p \qquad (2\cdot3\cdot3)$$

The cable equation yields, in exactly same consideration as before, to

$$\int_L d\xi = \int_L \frac{H_p - 2\int_0^x \tilde{\Lambda}\eta' du}{E_c A_c} \left(\frac{ds}{dx}\right)^3 dx \pm \alpha_t T \int_L \left(\frac{ds}{dx}\right)^2 dx - h'' \int_L \eta\, dx \qquad (2\cdot3\cdot4)$$

where

$$\tilde{\Lambda} = \frac{E_1 A_1 h e}{d^3} \qquad (2\cdot3\cdot5)$$

Note that eq. (2.3.5) can coincide with eq. (2.2.15') if one has $\bar{e} = 2e$ in eq. (2.3.5). Eq. (2.3.4) is also rewritten as

$$(EI\eta'')'' - \left\{(H_g + H_p + \tilde{\Lambda} h)\eta'\right\}' + \left\{(H_p - 2\int_0^x \tilde{\Lambda}\eta'\,du)h'\right\}' = p \qquad (2\cdot3\cdot6)$$

which is easily reduced to the fundamental equation of the deflection

theory for an ordinary type of suspension bridge since $\tilde{\Lambda}$ approaches to zero when e tends to zero. The stiffening effects due to inclination of hangers may therefore attribute to the second term correction $m(x)=\tilde{\Lambda} h \eta'$ and the third term correction $N=2\int_0^x \tilde{\Lambda}\eta' du$, the former of which signifies the corrective term for flexural deformation of stiffening girder and the latter of which signifies the one for deflection of cable.

2.4 STATIC ANALYSIS OF THREE SPANS SUSPENSION BRIDGES WITH INCLINED HANGERS

2.4.1 FORMULATION FOR WARREN TYPE HANGER SYSTEM

In this paragraph the static analysis of three spans suspension bridge with inclined hanger system in Fig. 2.7 is presented by using the simplified form of fundamental equation; namely eq. (2.2.17) is the equilibrium equation and eq. (2.2.18) the cable equation provided that the vertical angle 2β and the vertex distance $\bar{e}$ remains constant through the span length. Thus the difference equations for deflections excluding boundary points are given as

$$EI\eta_{i-2} - \left\{ 4EI + a^2 (H_g + H_p + \Lambda_0 h_{i-1}) \right\} \eta_{i-1} + \left\{ 6EI + 2a^2 (H_g + H_p + \Lambda_0 h_i) \right\} \eta_i$$

$$- \left\{ 4EI + a^2 (H_g + H_p + \Lambda_0 h_{i+1}) \right\} \eta_{i+1} + EI\eta_{i+2} + a^4 H_p h'' = a^4 p_i \qquad (2\cdot4\cdot1)$$

When the side and the main spans are equally divided into ten and twenty parts, respectively, we have

$$\mathbb{K} \cdot \eta = \mathbb{P} \qquad (2\cdot4\cdot2)$$

where

$$\mathbb{K} = \begin{vmatrix} \mathbb{K}_s & 0 \\ 0 & \mathbb{K}_m \end{vmatrix} \qquad \eta = \begin{vmatrix} \eta_s \\ \eta_m \end{vmatrix} \qquad \mathbb{P} = \begin{vmatrix} \mathbb{P}_s \\ \mathbb{P}_m \end{vmatrix}$$

and

$$\eta_s^T = | \eta_1 , \eta_2 , \cdots\cdots \eta_9 | \qquad \eta_m^T = | \eta_{11} , \eta_{12} , \cdots\cdots \eta_{20} |$$

$$P_s = (a^*)^4 \begin{vmatrix} p_1 - H_p h^{*''} \\ p_2 - H_p h^{*''} \\ - - - - - \\ - - - - - \\ p_9 - H_p h^{*''} \end{vmatrix} \qquad P_m = a^4 \begin{vmatrix} p_{11} - H_p h'' \\ p_{12} - H_p h'' \\ - - - - - \\ - - - - - \\ p_{20} - H_p h'' \end{vmatrix}$$

in which η_s and η_m denote column vectors for side and main spans deflections and P_s and P_m denote load terms obtained from the difference equation, eq. (2.4.1). Note that

$$K_s = \begin{vmatrix} G_1 - EI^* & F_2 & EI^* & 0 & 0 & 0 & 0 & 0 & 0 \\ F_1 & G_2 & F_3 & EI^* & 0 & 0 & 0 & 0 & 0 \\ EI^* & F_2 & G_3 & F_4 & EI^* & 0 & 0 & 0 & 0 \\ 0 & EI^* & F_3 & G_4 & F_5 & EI^* & 0 & 0 & 0 \\ 0 & 0 & EI^* & F_4 & G_5 & F_6 & EI^* & 0 & 0 \\ 0 & 0 & 0 & EI^* & F_5 & G_6 & F_7 & EI^* & 0 \\ 0 & 0 & 0 & 0 & EI^* & F_6 & G_7 & F_8 & EI^* \\ 0 & 0 & 0 & 0 & 0 & EI^* & F_7 & G_8 & F_9 \\ 0 & 0 & 0 & 0 & 0 & 0 & EI^* & F_8 & G_9 - EI^* \end{vmatrix}$$

$$
[K_m] = \begin{vmatrix}
G_{11}-EI & F_{12} & EI & & & & & & \\
F_{11} & G_{12} & F_{13} & EI & & & & & \\
EI & F_{12} & G_{13} & F_{14} & EI & & & 0 & \\
 & EI & F_{14} & G_{15} & F_{16} & EI & & & \\
 & & EI & F_{14} & G_{15} & F_{16} & EI & & \\
 & & & EI & F_{15} & G_{16} & F_{17} & EI & \\
 & & & & EI & F_{16} & G_{17} & F_{18} & EI \\
 & & & & & EI & F_{17} & G_{18} & F_{19} \\
 & & 0 & & & & EI & F_{18} & \begin{Bmatrix} G_{19}+EI \\ G_{19}-EI \end{Bmatrix} \\
 & & & & & & & \begin{Bmatrix} 2EI \\ 0 \end{Bmatrix} & \begin{Bmatrix} 2F_{19} \\ 0 \end{Bmatrix}
\end{vmatrix}
\begin{Bmatrix} EI \\ 0 \end{Bmatrix}
\begin{Bmatrix} F_{20} \\ 0 \end{Bmatrix}
\begin{Bmatrix} G_{20} \\ 0 \end{Bmatrix}
$$

in which the upper and lower terms correspond to the terms for symmetric and anti-symmetric live loads, respectively and

EI* flexural rigidity for side span

EI flexural rigidity for main span

a* one tenth of side span length

a one twentieth of main span length

$$
\begin{aligned}
F_K &= -4EI^* - (a^*)^2(H_g + H_p + \Lambda_0 h_k) \\
G_k &= 6EI^* + 2(a^*)^2(H_g + H_p + \Lambda_0 h_k) \qquad k = 1 \cdots\cdots 9 \\
h_k &= 0.1\, h_T\, k - 0.04\, f_1\, k(10 - k)
\end{aligned}
$$

h_T = height of tower top above stiffening girder

f_1 = sag for side span

$$F_k = -4EI - (a)^2(H_g + H_p + \Lambda_0 h_k)$$
$$G_k = 6EI + 2a^2(H_g + H_p + \Lambda_0 h_k) \qquad k = 11, \cdots\cdots 20$$
$$h_k = h_T - 0.01 f (k - 10)(30 - k)$$

f = sag for main span

With no temperature change the cable equation (2.2.18) is expressed by use of the Simpson's formula as follows

$$H_p = \frac{1}{L_E} \int_L \left(h'' + \frac{\Lambda_0}{E_c A_c} \left(\frac{ds}{dx}\right)^3 \right) \eta \, dx \qquad (2\cdot4\cdot3)$$

$$H_p = \frac{1}{10}\left[H_1 \eta_1 + 2 \sum_{j=2}^{8} H_j \eta_j + H_9 \eta_9\right] + \frac{1}{10}\left[H_{11} \eta_{11} + 2 \sum_{j=12}^{19} H_j \eta_j + H_{20} \eta_{20}\right]$$

where

$$H_j = \frac{1}{L_E}\left[\frac{8 f_1}{\ell_1^2} + \frac{\Lambda_0}{E_c A_c}\left\{\frac{h_T}{\ell_1} - \frac{4 f_1}{\ell_1}(1 - 0.2 j)^2 + 1\right\}^{\frac{3}{2}}\right] \quad j = 1, \cdots\cdots 9$$
$$(2\cdot4\cdot4)$$
$$H_j = \frac{1}{L_E}\left[\frac{8 f}{\ell^2} + \frac{\Lambda_0}{E_c A_c}\left\{1 + \frac{16 f^2}{\ell^2}(2 - 0.1 j)^2\right\}^{\frac{3}{2}}\right] \quad j = 11, \cdots\cdots 20$$

It should be mentioned that eq. (2.4.3) is valid only for symmetric live load and for the anti-symmetric load it vanishes identically.

Solving eq. (2.4.2) and eq. (2.4.3) simultaneously the deflections and sectional forces are given as follows:

For main span

1. Deflection : η_i
2. Slope : $\eta_i' = (1/2a)(\eta_{i+1} - \eta_{i-1})$ (2·4·5)
3. Shearing Force : $Q_i = (-EI/2a^3)(\eta_{i+2} - 2\eta_{i+1} + 2\eta_{i-1} - \eta_{i-2})$ (2·4·6)

4. Bending Moment : $M_L = (-EI/a^2)(\eta_{i+1} - 2\eta_i + \eta_{i-1})$ (2·4·7)

5. Increment of Induced Hanger Tension

$$\left.\begin{aligned} \triangle T_+^{\,i} &= \frac{1}{2}\frac{P_c{}^i}{\cos\beta} + \frac{1}{2}E_1A_1\sin\beta\ \frac{1}{2a}(\eta_{i+1} - \eta_{i-1}) \\ \triangle T_-^{\,i} &= -\frac{1}{2}\frac{P_c{}^i}{\cos\beta} + \frac{1}{2}E_1A_1\sin 2\beta\ \frac{1}{2a}(\eta_{i+1} - \eta_{i-1}) \end{aligned}\right\} \quad (2\cdot4\cdot8)$$

$$P_c{}^i = P_i - \frac{EI}{a^4}(\eta_{i+2} - 4\eta_{i+1} + 6\eta_i - 4\eta_{i-1} + \eta_{i-2})\,\bar{e}$$

where P_i is the love load acting at the panel point i.

For side span above relations are also valid except that EI and (a) are replaced by EI* and a* respectively.

2.4.2 FORMULATION FOR DOUBLE WARREN TYPE HANGER SYSTEM

For the Double Warren type inclined hanger system as shown in Fig. 2.5, the fundamental and cable equations are given by eq's (2.3.6) and (2.3.4), for which no simplification is made. The approximate characteristics can be analytically obtained by assumption that the parameter $\tilde{\Lambda}$ remains constant. It is physically exemplified by the case that the vertical angle 2β geometrically remains constant and the extentional rigidity of hanger E_1A_1/d are also constant, which differs from the case for the Warren type inclined hanger system.

Since the corrective terms in eq. (2.3.6) are written

$$-\tilde{\Lambda}\{(h\eta')' + 2(\eta h')'\} = -\tilde{\Lambda}\{(h\eta)'' + (h'\eta)'\}$$

so we have

$$(EI\eta'')'' - \{(H_g + H_p + \tilde{\Lambda}h)\eta\}'' + \{(H_p - \tilde{\Lambda}\eta)h'\}' = p \quad (2\cdot4\cdot9)$$

The difference equation for equilibrium is thus written as

$$EI\eta_{i-2}-\left\{4EI+a^2\left(H_g+H_p+\widetilde{\Lambda}h_{i-1}\right)-\frac{1}{2a}\widetilde{\Lambda}h'_{i-1}\right\}\eta_{i-1}+\left\{6EI+2a^2\left(H_g+H_p+\widetilde{\Lambda}h_i\right)\right\}\eta_i$$

$$-\left\{4EI+a^2\left(H_g+H_p+\widetilde{\Lambda}h_{i+1}\right)+\frac{1}{2a}\widetilde{\Lambda}h'_{i+1}\right\}\eta_{i+1}+EI\eta_{i+2}+a^4H_pk''$$

$$=a^4P_i \qquad (2\cdot4\cdot10)$$

and the cable equation with no temperature change is written as

$$H_p=\frac{1}{L_E}\int_L\left(k''+\frac{2\widetilde{\Lambda}}{E_cA_c}\left(\frac{ds}{dx}\right)^3\right)\eta\,dx \qquad L_E=\frac{1}{E_cA_c}\int_L\left(\frac{ds}{dx}\right)^3dx \qquad (2\cdot4\cdot11)$$

for which eq. (2.4.3) is valid except that

$$\left.\begin{aligned}H_j&=\frac{1}{L_E}\left[\frac{8f_1}{\ell_1^2}+\frac{2\widetilde{\Lambda}}{E_cA_c}\left\{1+\left(\frac{h_T}{\ell_1}-\frac{4f_1}{\ell_1}(1-0.2j)\right)^2\right\}^{\frac{3}{2}}\right]\quad j=1,\ \cdots\cdots,\ 9\\ H_j&=\frac{1}{L_E}\left[\frac{8f}{\ell^2}+\frac{2\widetilde{\Lambda}}{E_cA_c}\left\{1+\frac{16f^2}{\ell^2}(2-0.1j)^2\right\}^{\frac{3}{2}}\right]\quad j=11,\cdots\cdots,\ 20\end{aligned}\right\}\qquad (2\cdot4\cdot12)$$

Note that eq. (2.4.12) is simply obtained by substituting $2\widetilde{\Lambda}$ for Λ_0 in eq. (2.4.4).

Therefore the basic equation is obtained by substituting eq. (2.4.10) into eq. (2.4.9) to be

$$\begin{vmatrix}\widetilde{K}_s & 0\\ 0 & \widetilde{K}_m\end{vmatrix}\begin{vmatrix}\eta_s\\ \eta_m\end{vmatrix}=\begin{vmatrix}P_s\\ P_m\end{vmatrix}$$

All matrice defined above are exactly same as those in eq. (2.4.2) except that the terms F_k are replaced by the following terms F_k^u and F_k^l for upper off-diagonal and lower off-diagonal terms, viz.,

$$\begin{vmatrix} F_k^u \\ F_k^\ell \end{vmatrix} = \begin{vmatrix} F_k - \frac{\tilde{A}}{2a^*}\left\{\frac{h_r}{\ell_1} - \frac{4f_1}{\ell_1}(1-0.2k)\right\} \\ F_k + \frac{\tilde{A}}{2a^*}\left\{\frac{h_r}{\ell_1} - \frac{4f_1}{\ell_1}(1-0.2k)\right\} \end{vmatrix} \qquad k=1,\cdots,9$$

$$\begin{vmatrix} F_k^u \\ F_k^\ell \end{vmatrix} = \begin{vmatrix} F_k + \frac{4f}{\ell}\frac{\tilde{A}}{2a}(2-0.1k) \\ F_k - \frac{4f}{\ell}\frac{\tilde{A}}{2a}(2-0.1k) \end{vmatrix} \qquad k=1,\cdots,20$$

With above expressions and some modifications if necessary the three spans suspension bridge with the Double Warren type inclined hanger system is analytically solved for any loading conditions.

2.5.1 FREE VIBRATIONS OF SUSPENSION BRIDGE WITH INCLINED HANGER

2.5.1 CHARACTERISTICS OF WARREN TYPE HANGER SYSTEM

In the first place the free vibrational problem for the suspension bridge with inclined hangers is illustrated for the simplified case here. Let m and ω be the mass per unit length and the circular natural frequency, then we have the following variational equations in the place of eq. (2.2.17).

$$\delta \int_L \left\{ EI(\eta'')^2 - (H_g + \Lambda_0 h)\eta\eta'' + h'' H_p \eta - m\omega^2\eta^2 \right\} dx = 0 \qquad (2\cdot5\cdot1)$$

with

$$H_p = \frac{1}{L_E}\int_L \left\{ h'' + \frac{\Lambda_0}{E_c A_c}\left(\frac{ds}{dx}\right)^3 \right\} \eta \, dx$$

For a single span bridge, the natural frequency ω , is approximated by assuming that $\eta = \sin \pi x/\ell$ as the fundamental vibrational mode, as

$$\omega_1^2 = \frac{\pi^4 EI}{m\ell^4}\left(1+\frac{H_g \ell^2}{\pi^2 EI}\right) + \frac{512 f^2}{\pi^2 m \ell^3 L_E} + \Lambda_0 \left\{ \frac{2\pi^2}{m\ell^3}\int_0^\ell h \sin\frac{\pi x}{\ell}\,dx + \frac{32f}{\pi m \ell^2}\,\frac{\int_0^\ell \left(\frac{ds}{dx}\right)^3 \sin\frac{\pi x}{\ell}\,dx}{\int_0^\ell \left(\frac{ds}{dx}\right)^3 dx} \right\}$$

and also we have approximately (2·5·2)

$$\omega_2^2 = \frac{16\pi^4 EI}{m\ell^4}\left(1+\frac{H_g \ell^2}{8\pi^2 EI}\right) + \Lambda_0 \frac{8\pi^2}{m\ell^3}\int_0^\ell h \sin^2\frac{2\pi x}{\ell}\,dx \qquad (2\cdot5\cdot3)$$

for the first anti-symmetric mode by assuming that $\eta = \sin 2\pi x/\ell$.
In both expressions eq's (2.5.2) and (2.5.3.), the terms multiplied by the parameter Λ_0 indicate the stiffening effect due to the inclined hangers.

Generally the vibrational modes for a simply supported single span suspension bridge can be expressed as

$$\eta = \sum_{n=1}^{\infty} C_n \sin\frac{n\pi x}{\ell}$$

by use of which an application of the Rayleigh-Ritz method yields to the following characteristic equation to determine a set of approximate natural frequencies,

$$\left| \left(\frac{\pi^4 n^4 EI}{\ell^3} - m\omega^2 \ell\right)\delta_{ij} - \frac{(i^2+j^2)\pi^2}{\ell^2}\int_0^\ell (H_g + \Lambda_0 h)\sin\frac{i\pi x}{l}\sin\frac{j\pi x}{l}\,dx \right.$$

$$-\frac{1}{L_E}\left[\int_0^\ell \left(h'' + \frac{\Lambda_0}{E_c A_c}\left(\frac{ds}{dx}\right)^3\right)\sin\frac{i\pi x}{\ell}\,dx \int_0^\ell h''\sin\frac{j\pi x}{\ell}\,dx \right.$$

$$\left. \left. + \int_0^\ell \left(h'' + \frac{\Lambda_0}{E_c A_c}\left(\frac{ds}{dx}\right)^3\right)\sin\frac{i\pi x}{\ell}\,dx \int_0^\ell h''\sin\frac{j\pi x}{l}\,dx \right] \right| = 0 \qquad (2\cdot5\cdot4)$$

Since eq.(2.5.4) forms a symmmetric determinant, one may obtain a real set of characteristic values from it.

2.5.2 CHARACTERISTICS OF DOUBLE WARREN TYPE HANGER SYSTEM

In exactly same manner the free vibrational problem for the Double Warren type hanger system is solved by the equation

$$(EI\eta'')'' - (H_g+H_p+\tilde{\lambda}h)\,\eta'' + \{(H_p - 2\tilde{\lambda}\eta)\,h'\}' - m\omega^2\eta = 0 \qquad (2\cdot5\cdot5)$$

where $\tilde{\lambda}$ is assumed constant. When one approximates the first symmetric vibrational mode by $\eta = \sin \pi x/\ell$, the corresponding circular frequency ω_1 is written for single span suspension bridge as

$$\omega_1^2 = \frac{\pi^2 EI}{ml^4}\left(1+\frac{H_g\ell^2}{\pi^2 EI}\right) + \frac{512 f^2}{\pi^2 m\ell^3 L_E} + \tilde{\lambda}\left\{\frac{2\pi^2}{m\ell^2}\int_0^\ell h \sin^2\frac{\pi x}{\ell}\,dx + \frac{2\pi^3}{m\ell^2}\int_0^\ell h' \sin\frac{\pi x}{\ell}\,dx\right\}$$
$$+ \tilde{\lambda}\frac{64 f}{\pi m\ell^2}\left\{\frac{\int_0^\ell \left(\frac{ds}{dx}\right)^3 \sin\frac{\pi x}{\ell}\,dx}{\int_0^\ell \left(\frac{ds}{dx}\right)^3 dx}\right\} \qquad (2\cdot5\cdot6)$$

The natural frequencies for higher modes are obtained by the same manner as before, assuming the Fourier sine series for the deflectional curves.

2.5.3 FREE VIBRATIONAL ANALYSIS BY THE DIFFERENCE EQUATION

In above paragraphs the Rayleigh Ritz method is applied for free vibrations defined by eq's (2.5.1) and (2.5.2). It is also possible to obtain natural frequencies and the corresponding modes by use of the difference equation defined as eq. (2.5.2).

$$\begin{vmatrix} K_s & 0 \\ 0 & K_m \end{vmatrix} \begin{vmatrix} \eta_s \\ \eta_m \end{vmatrix} = \begin{vmatrix} P_s \\ P_m \end{vmatrix} \qquad (2\cdot5\cdot7)$$

where the right hand side terms are given as

$$P_s = -(a^*)^4 \begin{vmatrix} m\omega^2\eta_1 + H_p(h^*)'' \\ m\omega^2\eta_2 + H_p(h^*)'' \\ \cdots\cdots\cdots\cdots \\ \cdots\cdots\cdots\cdots \\ m\omega^2\eta_9 + H_p(h^*)'' \end{vmatrix} \qquad P_m = -a^4 \begin{vmatrix} m\omega^2\eta_{11} + H_p h'' \\ m\omega^2\eta_{12} + H_p h'' \\ \cdots\cdots\cdots\cdots \\ \cdots\cdots\cdots\cdots \\ m\omega^2\eta_{20} + H_p h'' \end{vmatrix}$$

and the cable equation is considered simultaneously for the symmetric modes. For anti-symmetric modes we have $H_p = 0$, so eq. (2.5.7) is solved independently from the cable equation.

2.6 NUMERICAL ILLUSTRATIONS

The fundamental equations for a suspension bridge with inclined hangers are numerically evaluated for the below mentioned model bridge, for which static and dynamic tests are performed. Various dimensions for the model are shown in Table 2.1 and its general view is shown in the Photos*. Since the stiffening girder of model forms a Warren truss of equal pannel length, eq. (2.4.2) is rearranged for the eight and twenty four partitioned deflectional points for side and main spans, respectively. Numerically eq. (2.4.2) is solved by use of the Kyoto University Digital Computer, KDC II (HITAC 5020).

The results are shown in Fig's 2.8 to 2.13, the first two cases of which are for symmetric loads, while the latter two cases of which are for asymmetric loads. For sake of brevity the influence due to the parameter Λ, Table 2.2, is evaluated for various number of

*pp 99 - 101

cases assuming it to be constant in each span lengths. It is noted from above figures that deflections in general decrease when the parameter Λ increases and the tendency seems to be remarkable particularly for asymmetric loading or locally concentrated loading. And deflectional slope at supports of spans decreases when the parameter Λ decreases. From the deflectional point of views the effect of inclination of hangers is characterized to decrease the deflections and distribute them spanwisely. As far as the present result is concerned the sectional forces vary their amounts little but distribute differently from each other depending on the value of parameter Λ . It should be mentioned that the hanger tensions differ remarkably from those for vertical hanger system and tend to be the maximum in the neighbourhood of the point where loads discontinuously change. However the spanwise distribution of hanger tension seems insensible with variation of the parameter Λ to be in the similar form.

The natural frequencies and the corresponding vibrational modes are given in Table 2.3 and illustrated in Fig's 2.12 and 2.13. The frequencies may increase by 10 to 20 % due to the parameter Λ in comparison with the vertical hanger system, while the vibrational modes of lower order bear resemblance to the vertical hanger system. Thus the parameter Λ rather effects on the higher order vibrational modes. As shown in Fig. 2.13 the first to third antisymmetric modes are considered in the same phase even when Λ increases but the fourth mode in the main and side spans can be out of the phase when the parameter exceeds the certain value of Λ .

2. 7 MODEL TESTS AND DISCUSSIONS

In order to clarify and confirm the deflectional behaviours of a suspension bridge with vertical and inclined hangers, static loading tests and free vibrations tests are performed for a model of the three spans suspension bridge in plan (300m + 860m + 300m), which dimensions are given in Table 2.1.

The model is so designed that the scale is 1/100 with the slicing factor 9.2757 and two cables (ϕ 2.6mm steel wire), the stiffening girder of Warren Truss (Methacrylic Acids) and the hangers (ϕ 0.6mm copper wire) are used.

In the static experiments the strains in cables are measured by the wire strain gauges affixed directly on cable surface and vertical and horizontal deflections are measured by the optical level, which is also used for measurement of deflections of stiffening girders. The induced hanger tensions are measured by a gauge device of trial production which responses proportionally to the applied hanger load.

In the free vibration tests the deflections of stiffening girders are obtained by use of the differential transformers, (Type 150 BL, Shinkou Electric Co.) and the amplifier (Type M1-6W-13, Shinkou Electric Co.) and strains in cables and stiffening girders are measured by the wire strain gauges amplified by the DS6-MTH amplifier (Shinkou Communication Co.) and recorded by the electromagnetic oscillograph (Type FR-101, San-ei Sokki Co.)

This experimental investigation is performed for four hanger systems; vertical, three members, Warren type, and Double Warren type hanger systems, Fig. 2.15. In the static tests deflections and strains of stiffening girders and cables are obtained and compared with the theoretical values evaluated by above described equations and in the dynamic tests the natural frequencies of lower orders, the corresponding modes and the logarithmic decrements are obtianed by measuring deflections and strains of stiffening girders and cables in free vibrations.

The results are summarized as follows:

(1) The cables and stiffening girders displace spanwisely for an arbitrary loaded state and the deflections differ dependent on the type of hanger system to become smaller in due order of the vertical, the three members, the Warren type, and the Double Warren type hanger

systems. The inclination of hangers are considered to stiffen the flexural rigidity of suspension bridge particularly effective for concentrated loads or asymmetric loads.

(2) Cable deformations are in generally decisive on the deformed configurations and furthermore the longitudinal deformations tend to be of singificant amount for local or asymmetric loads. As for cable deformations the effect due to the gravitational change is more dominate than the effect to the elongation of cables for the lowest or lower orders of deformed states.

(3) The deformational characteristics of a suspension bridge are considered to be sensitively dependent on the hanger system, while geometrical configurations and extensional rigidity should be therefore specified for analysis. Since the amount of elongation of hanger is comparatively small to the deflections of stiffening girder, it is considered more reasonable to evaluate the stiffening effect in terms of its constraint forces than in terms of its deformation configuration.

(4) For the vertical hanger system the hanger tension remains approximately constant in the spanwise direction, while positive and negative hanger tensions are induced alternatively for the inclined hanger systems, the envelope of which is approximately proportional to the deflectional slope of stiffening girder. As far as this experiment is concerned it is observed that no hanger receives compensative compression to relax for any loading case.

(5) In free vibrational tests the first symmetric modes is observed but the second or more higher symmetric and the anti-symmetric modes are not excited in a stable form. The results obtained are shown in Table 2.3, from which the natural frequencies are known to be varied for different types of hanger system. The corresponding mode however varies less sensitively and remains almost in similar form. The inclined hanger system is customarily characterized by its damping capacity,

which is hardly investigated analytically by the mechanical model used in this experiment. However the result we have is considered to some extent to indicate that the inclined hanger system reserves more damping capacity than the vertical hanger system , as illustrated in Fig. 2.16. The logarithmic decrement for the first symmetric mode seems to be independent from the amplitude so that the viscous damping may be doninant. In this experiment the inclined hanger system is considered to reserve a significant portion of structural damping in the region of more than 2 mm amplitudes but there are some cases we obtained in the previous tests that the Coulomb damping appears in the small amplitudes.

Compared the above experimental results with the fundamental equations in this investigations we have the following results; Fig's 2.17 - 2.26 indicate the deflections of stiffening girder and the induced hanger tensions obtained by the experiment and those evaluated theoretically. For the deflections the fundamental equations are considered well describing the experimental results when the parameters take $\lambda = \lambda_1 =$ 5.2763 kg/cm which correspond to the smallest values in the each spans. Since the stiffening girder of Warren Truss type is equally partitioned for a panel length, the parameter λ does vary from a point to other, so that the calculations are performed by use of the simplified equation for the parameters λ corresponding to 1/4, 1/8, 1/16 th points from the end support. These deflections obtained are smaller than the experimental results. Generally speaking such a long spanned flexible structure as suspension bridge is considered to response rather uniformly and to decentralize its deflections for live loads.

As for cable deformations the longitudinal components are apparently observed for locally concentrated or asymmetric loads, which magnitudes are comparatively small to the vertical component. Theoretically it is considered that the longitudinal deformation of cable tends to decrease the stiffening effect due to inclination of hangers. If this effect of stiffening decrease is taken into an account, the exact evaluation is necessary to obtain the precise deflections of stiffening girder.

Experimentally the deflections are sufficiently approximated by the simplified form of fundamental equations using the smallest value of parameter Λ to know the effect of inclination of hangers. Note that the longitudinal displacement of cable takes an important role in evaluation of induced hanger tensions and indirectly effects on the deflections of stiffening girder. The details are given in the appendix.

For the vertical hanger system the natural frequencies obtained are 9.32 rad/sec theoretically and 9.68 rad/sec experimentally with the 3.9 % difference and 10.7 rad/sec theoretically and 11.2 rad/sec experimentally for the Warren type inclined hanger system with the 4.7 % difference. In order to obtain the dynamic character of inclined hanger system the forced vibration tests are performed by use of the vibrator which is made specially for this purpose to be capable to apply the constant amplitude of sinusoidally time varing force. Results are illustrated in Fig. 2.27 through Fig. 2.31, which is summarized in Table 2.4. From these theoretical values are considered satisfactorily to accord with the experimental ones. So far the theoretical and the experimental investigations for suspension bridge with inclined hangers are considered to result in the fact that the fundamental equations obtained can characterize statically and dynamically the flexural behaviour of structure considered here.

As shown in 2.5 the stiffening effect due to inclination of hangers is characterize by the parameter Λ in the form $\Lambda h = EA\,(2h/\bar{e})\cos\beta \times \sin^2\beta$ $(\bar{e} \geqq 2e)$. Thus the maximum effect is obtained by setting $\bar{e} = 2e$, viz., $\Lambda h = E_1 A_1 \sin\beta \cos^2\beta$. The non-dimensional quantity $\Lambda h / E_1 A_1$ and β (the half of vertical angle) are related as shown in Fig. 2.34, in which the full line corresponds to the relation $\Lambda h = E_1 A_1 (2h/\bar{e}) \cos\beta \sin^2\beta$ and the dashed line to the relation $\Lambda h = E_1 A_1 \sin\beta \cos^2\beta$.
From these the intersecting point for a given value of $2h/\bar{e}$ gives the most effective vertical angle. For the Severn Bridge the vertical angle vary spanwisely as in Fig. 2.35. Based on Fig. 2.27 we have $2h/\bar{e} = 5$ to 6 so that the most effective vertical angle will be $\beta = 10^{\circ}$.

CONCLUSIONS

In this investigations the fundamental equations of equilibrium for a long-spanned suspension bridge with inclined hangers are derived and confirmed by the model tests performed. The equations can be solved comparatively easily by the aid of the digital computer with sufficient accuracy for the design purpose. Structurally the inclination of hangers is featured by the parameter λ to stiffen the flexural rigidity of structure, which can be assumed constant for an ordinary type of inclined hanger system, greatly simplifying the equations to be in a compact form. The effective geometrical configuration for inclined hanger system is obtained by illustrating the relation of the $\lambda h - \beta$ curve, which is independently determined from the flexural dimensions of cables and stiffening girders as the first approximation. More exactly the structural features for this system considered will be analyzed by taking into an account the longitudinal displacement of cable, which is considered less effective on the flexural deflections but important on evaluation of induced hanger tensions.

Dynamically the inclined hager system increases the natural frequencies up to 10 to 20 % without any significant variation of vibrational modes as far as the modes of lower orders are concerned. It is, however, noticed that the damping characteristics for the inclined hanger system remains analytically unsolved in spite of the fact that it apparently increases in our experimental study. The investigation for dynamic behaviour for suspension bridge with inclined hanger is therefore called for in order to characterize the system.

APPENDIX THE ANALYSIS OF SUSPENSION BRIDGE WITH INCLINED HANGER TAKING INTO AN ACCOUNT THE LONGITUDINAL DISPLACEMENTS OF CABLES

In this appendix the longitudinal displacement of cable is taken into an account for derivation of the fundamental equations. Using the similar notations in above study, the longitudinal displacement of cables ξ can be obtained as

$$d\xi = \frac{H_p - A\eta}{E_c A_c}\left(\frac{ds}{dx}\right)^2 dx \pm \alpha_t T\left(\frac{ds}{dx}\right) ds - y' d\eta - \frac{1}{2}\eta d\eta$$

$$\xi = \int_0^x \frac{H_p}{E_c A_c}\left(\frac{ds}{dx}\right)^3 dx \pm \alpha_t T \int_0^x \left(\frac{ds}{dx}\right)^2 dx + h'\eta - \int_0^x \left\{h'' + \frac{A}{E_c A_c}\left(\frac{ds}{dx}\right)^3\right\}\eta\, dx$$

Note that the integration of above expression yields to the cable equation.

The longitudinal displacement of cable may vary the induced cable tension, so that we have

$$\triangle T_+ = E_1 A_1 \frac{h}{d^2}\left\{\triangle h + e\left(\eta' - \frac{\xi}{h}\right)\right\}$$

$$\triangle T_- = E_1 A_1 \frac{h}{d^2}\left\{-\triangle h + e\left(\eta' - \frac{\xi}{h}\right)\right\}$$

In the exactly same manner as before the resultant force at the vertex can be written as

$$Q_c = \triangle T_+ \sin\beta + \triangle T_- \sin\beta = 2E_1 A_1 \frac{h e^2}{d^3} (\eta' - \frac{\xi}{h})$$

$$P_c = \triangle T_+ \cos\beta + \triangle T_- \cos\beta = 2E_1 A_1 \frac{h^2}{d^3} \triangle h$$

Let us define q(x) and m(x) as

$$q(x) = \frac{Q_c}{\bar{e}} = \frac{2E_1 A_1}{d^3 \bar{e}} h e^2 (\eta' - \frac{\xi}{h}) = \Lambda (\eta' - \frac{\xi}{h})$$

$$m(x) = \frac{Q_c h}{\bar{e}} = \Lambda h (\eta' - \frac{\xi}{h})$$

and substituting these into equilibrium conditions of stiffening girders and cables, one obtains

$$(EI\eta'')'' - (H_g + H_p)\eta'' + H_p = p + \{ \Lambda h (\eta' - \frac{\xi}{h})' + \Lambda h' (\eta' - \frac{\xi}{h}) \} \qquad (A \cdot 1)$$

wich can be simplified if Λ is assumed to be constant as follows

$$(EI\eta'') - \{ (H_g + H_p)\eta + \Lambda h \int_0^x (\eta' - \frac{\xi}{h}) du \} + h'' H_p = p \qquad (A \cdot 2)$$

More precisely the additional corrective term for moment is written as

$$m(x)\bar{e} = Q_c h + P_c \xi$$

$$m(x) = \Lambda h (\eta' - \frac{\xi}{h}) + p\xi$$

Thus eq. (A.1) can be of the form

$$(EI\eta'')'' - \left\{ (H_g + H_p)\eta + \Lambda h \int_0^x \left(\eta' - \frac{\xi}{h} \right) du \right\} + h'' H_p = p \ (1 + \xi') \qquad (A \cdot 3)$$

when p demotes the density of live load per unit length.

Therefore the exact form of fundamental equations are coupled consisting of three equations for three unknowns of the vertical deflections of stiffening girder η , the longitudinal displacement of cable ξ and the horizontal component of cable tension H_p.

$$(EI\eta'')'' - \left\{ (H_g + H_p + \Lambda_0 h)\eta - \Lambda_0 h \int_0^x \frac{\xi}{h} du \right\}'' + h'' H_p = p \ (1 + \xi')$$

$$\xi = \int_0^x \frac{H_p}{E_c A_c} \left(\frac{ds}{dx} \right)^3 dx + h' \eta - \int_0^x \left\{ h'' + \frac{\Lambda}{E_c A_c} \left(\frac{ds}{dx} \right)^3 \right\} \eta \, dx \pm \alpha_t T \int_0^x \left(\frac{ds}{dx} \right)^2 dx$$

$$H_p = \frac{\int_0^x \left\{ \left(h'' + \frac{\Lambda}{E_c A_c} \left(\frac{ds}{dx} \right)^3 \right) \eta \pm \alpha_t T \left(\frac{ds}{dx} \right)^2 \right\} dx}{\int_0^x \frac{1}{E_c A_c} \left(\frac{ds}{dx} \right)^3 dx}$$

REFERENCES

2.1) F. B. Fauquharson; Aerodynamic Stability of Suspension Bridges, Part 1 - 5, Univ. of Washington, 1954

2.2) Aerodynamic Stability of Suspension Bridge: 1952 Report of Advisory Board on the Investigation of Suspension Bridges, Trans. ASCE, Vol. 120, 1955, pp 721 - 781

2.3) D. E. Walshe; A Resume of the Aerodynamic Investigations for the Forth Road and the Severn Bridges, Proc. Inst. Civ. Eng., Vol. 37, May, 1967

2.4) D. B. Steinman; Suspension Bridge; The Aerodynamic Problem and its Solution, American Scientists, Vol. 42, No. 3, July, 1954

2.5) F. Leonhardt; Aerodynamisch stabile Haengebruecke fuer grosse Spannweiten, Proc. IABSE, Rio de Janeiro, Ib 6, 1964

2.6) C. Thornton & C. Birnstiel; Three-dimensional Suspension Structures, Proc. ASCE, ST2, 1962, pp 247 - 270

2.7) T. Fujino & K. Ohsaka; Static Structural Analysis of Suspension Bridges, Mitsubishi Heavy Industries Technical Review, Vol. 3, No. 6, 1966, pp 17 - 23

2.8) D. Jawerth; Vorgespannte Haengekonstruktion aus gegensinnig-gekrummten Seilen mit Diagonalverspannung, Stahlbau, 28, Heft 5, 1959, S. 126 - 131

2.9) F. Masanz; Die Barbarabruecke ueber die Donau, Stahlbau 28, Heft 8, 1959, S. 212 - 222

2.10) Z. Hiba; Winddruck auf Haengebruecken mit schraegliegenden Tragkabeln, Stahlbau, 28, Heft 4, 1959, S. 98 - 101

2.11) A. Selberg; Damping Effect in Suspension Bridges, IABSE, Vol. 10, 1950, pp 183 - 196

2.12) M. Ito & T. Katayama; Damping of Bridge Structures, Trans. JSCE, No. 117, May, 1965, pp 12 - 22

2.13) T. Yamaguchi, K. Siraki & R. Nakagawa; Study on the Damping Capacity of Suspension Bridge Hanger, Mitsubishi Heavy Industries Technical Review, Vol. 3, No. 6, 1966, pp 68 - 77

2.14) F. Bleich et al, The Mathmatical Theory of Vibrations in Suspension Bridges, Dep't of Commerce, 1950, pp 211 - 240

2.15) N. Shiraishi; On the Coupled Free Vibrations of a Suspension Bridge - I, Mem. Fac. Eng., Kyoto Univ., Vol. XXV, Part 2, 1963, pp 217 - 232

———————— ; On the Coupled Free Vibrations of a Suspension Bridge - II, Mem. Fac. Eng., Kyoto Univ., Vol. XXVI, Part 2, 1964, pp 75 - 84

2.16) I. Konishi & N. Shiraishi; On the Free Vibrational Characteristics of a Long-spanned Suspension Bridge, Sym. on Suspension Bridges/ Lisbon, Nov., 1966, Paper No. 23

2.17) ———————————— ; Experimental Studies on Free Vibrations of a Long-spanned Suspension Bridge, Mem. Fac. Eng., Kyoto Univ., Vol. XXVIII, Part 4, 1966, pp 351 - 366

2.18) A. Hawranek u. O. Steinhardt; Berechnung und Theorie der Stahlbruecken, Springer-Verlag, 1958

Table 2.1 Dimensions of Model

	Main Span	Side Span
Span Length	$l_m = 860$ Cm	$l_s = 300$ Cm
Cable Sag	$f_m = 71.5$ Cm	$f_s = 8.969$ Cm
Cross Section of Cable	$A_{cm} = 5.309$ mm^2	5.309 mm^2
Weight of Cable	$W_{cm} = 47.015$ g/Cm	$W_{cs} = 50.045$ g/Cm
Moment of Inertia of Stiffenig Girder	$I_{fm} = 28.753$ Cm^4	28.753 Cm^4
Weight of Stiff Girder	$W_{gm} = 126.70$ g/Cm	$W_{gs} = 128.02$ g/Cm
Panel Length	10 Cm	10 Cm
Distance of Cables (ctc)	$b_m = 33$ Cm	33 Cm
Height of Towers	$h_T = 143.7$ Cm	
Moment of Inertia of Tower	$I_{pm} = 0.8849$ Cm^4	
Live Load	$W_m = 62$ g/Cm	
Diameter of Hangers	ϕ 0.6	

Table 2.2 Parameter Λ

Main Span	
$\frac{1}{4}$ point	Λ_m = 30.311 Kg/Cm
$\frac{1}{8}$ point	15.156
$\frac{1}{16}$ point	8.6878
near tower	5.2763
Side Span	
near tower	Λ_s = 5.2763 Kg/Cm
$\frac{1}{8}$ point	7.6036

Table 2.3

Calculated Natural Frequencies

Mode \ Type		Vert. Hang. Sys.	Inclined Hanger Sys.	
			Warren Type	Double Warren Type
Sym.	1st	9.319	10.70	11.66
	2nd	14.760	18.29	21.12
	3rd	19.560	22.36	24.88
	4th	31.000	35.90	40.07
Anti-Sym.	1st	9.015	11.41	13.28
	2nd	13.950	17.87	20.98
	3rd	22.170	26.50	30.03
	4th	37.670	46.30	49.07
Hanger Parameter		$\Lambda m = 0$ $\Lambda s = 0$	$\Lambda m = \Lambda s$ $= 5.2763 Kg/Cm$	$\Lambda m = \Lambda s$ $= 10.553 Kg/Cm$

(rad/sec)

Experimental Natural Frequencies (Free Vibration Test)

	1st Sym Mode	2nd Sym Mode
Vertical Hanger	9.68	16.30
3 member type	10.8	——
Warren type	11.2	——
Double Warren type	11.5	——

Table 2.4

Comparison of the calculated Natural Frequencies with the Experimentally Obtained Frequencies (Forced Vibrations)

		Vertical Hanger Sys. $\Lambda m = \Lambda s = 0$		Inclined Hanger Sys. $\Lambda m = \Lambda s = 10.553$ Kg/Cm	
		Calculated	Experimental	Calculated	Experimental
Sym.	1st	9.32	9.43	11.66	11.78
	2nd	14.76	15.17	21.12	21.39
	3rd	19.56	19.90	24.88	25.16
	4th	31.0	——	40.07	——
Antisym.	1st	9.02	9.27	13.28	12.95
	2nd	13.95	13.35	20.98	18.86
	3rd	22.17	——	30.03	——
	4th	37.67	——	49.07	——

(rad/sec)

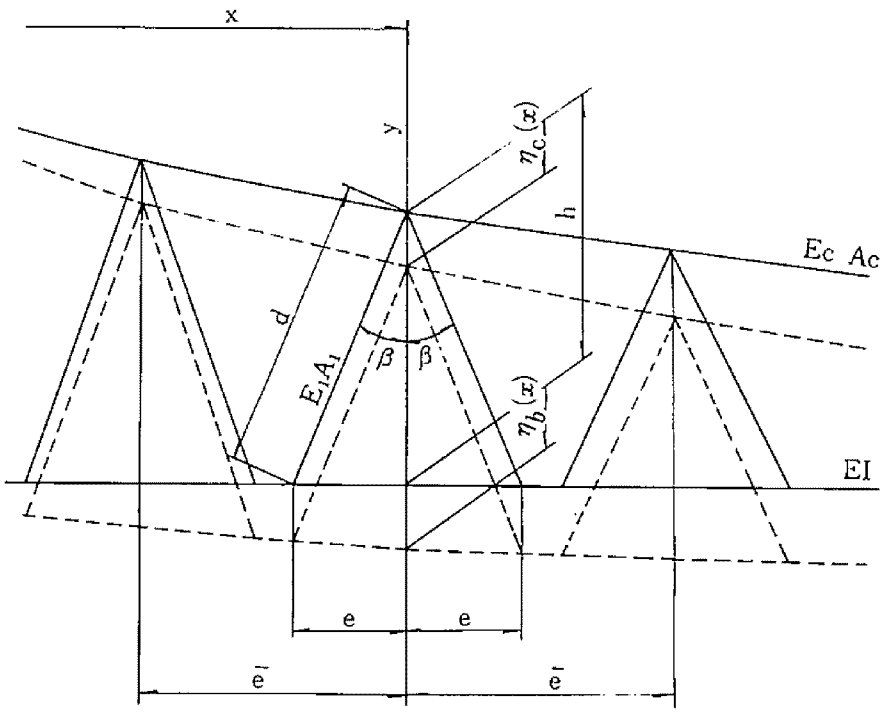

Fig 2·1 Inclined Hanger System

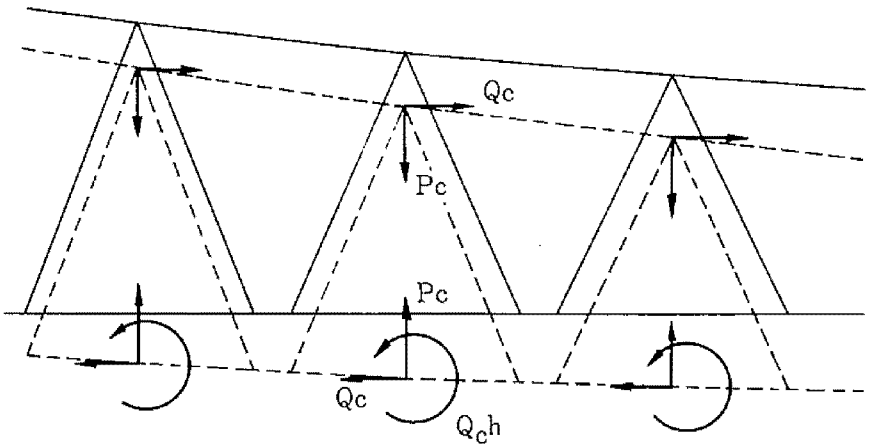

Fig 2·2 Additional Sectional Forces

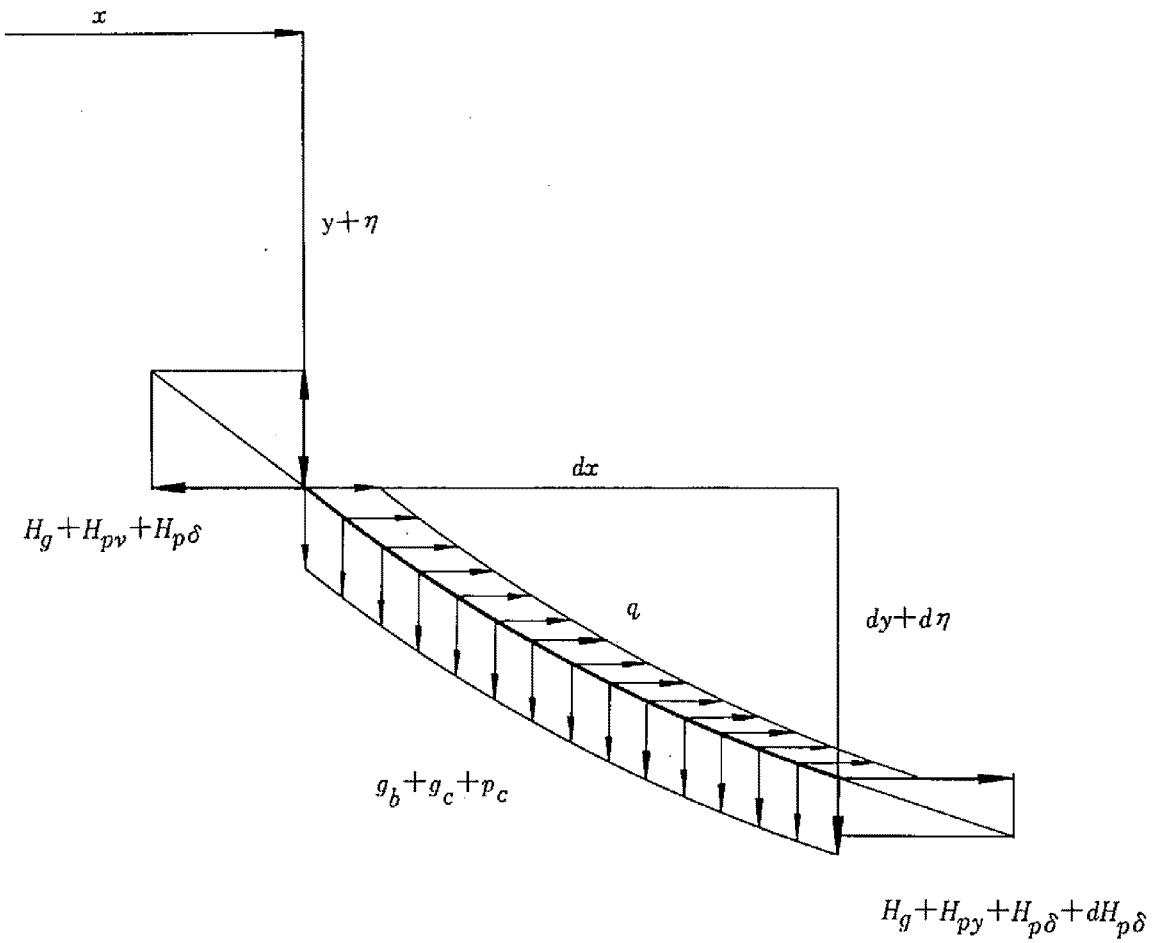

Fig. 2.3 Equilibrium of Cable Element

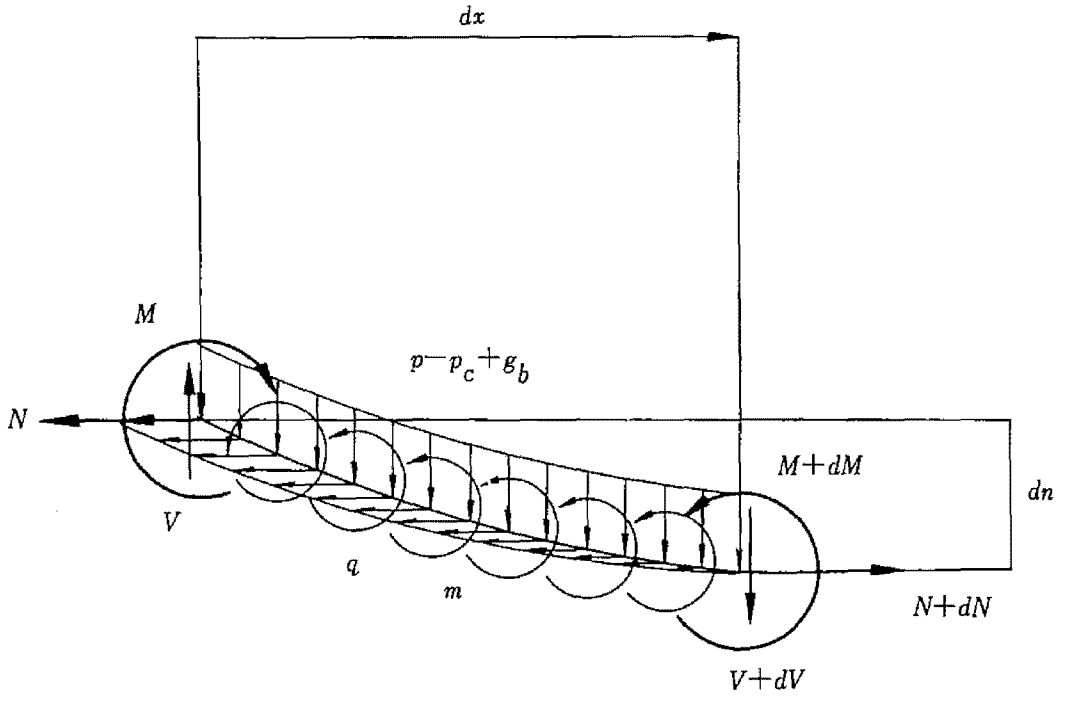

Fig. 2.4 Equilibrium of Stiffening Girder Element

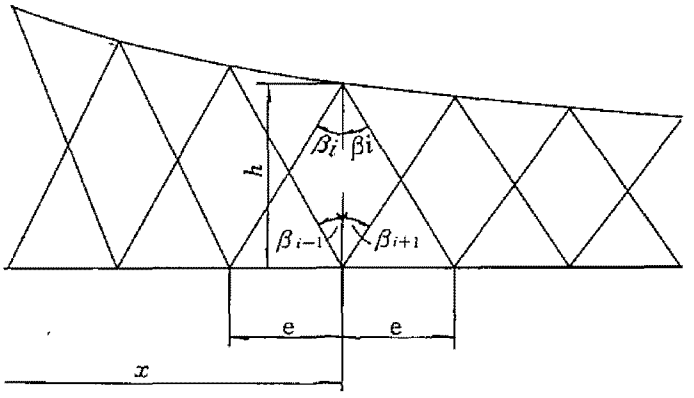
h
β_i
β_{i-1}
β_{i+1}
e
e
x

Fig. 2.5

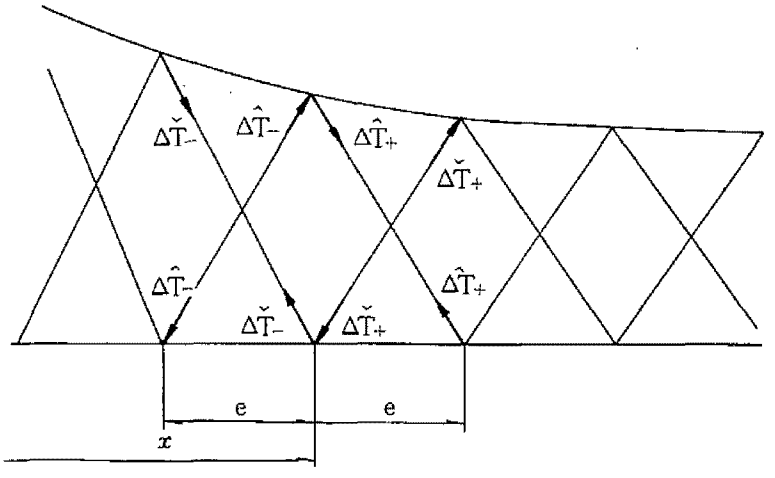
$\Delta\check{T}_-$
$\Delta\hat{T}_-$
$\Delta\hat{T}_+$
$\Delta\check{T}_+$
$\Delta\hat{T}_-$
$\Delta\check{T}_-$
$\Delta\check{T}_+$
$\Delta\hat{T}_+$
e
e
x

Fig. 2.6

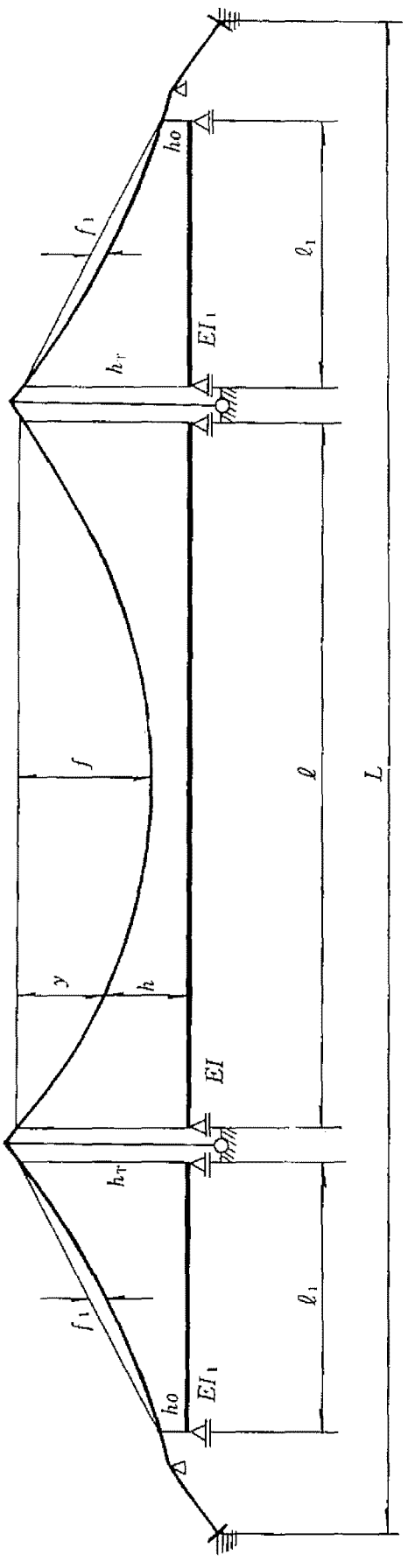

Fig. 2.7 Configurations for Three Spans Suspension Bridge

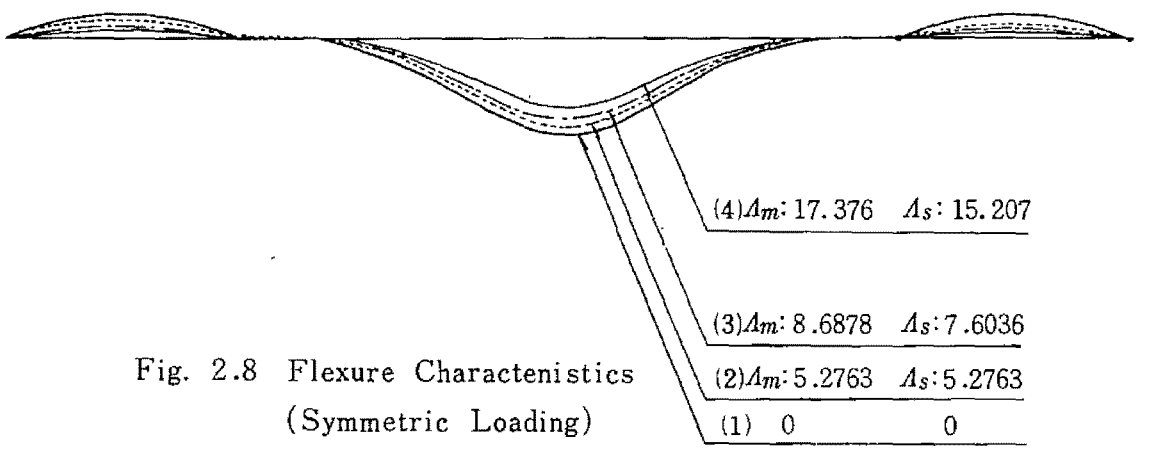

Fig. 2.8 Flexure Charactenistics
(Symmetric Loading)

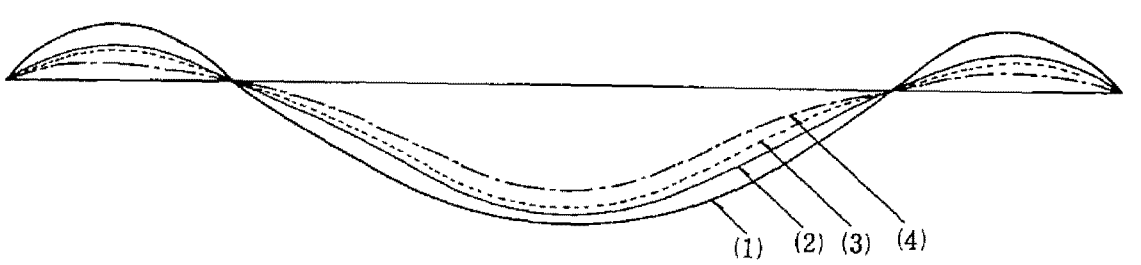

Fig 2.9 Flexure Characteristics
(Symmetric Loading)

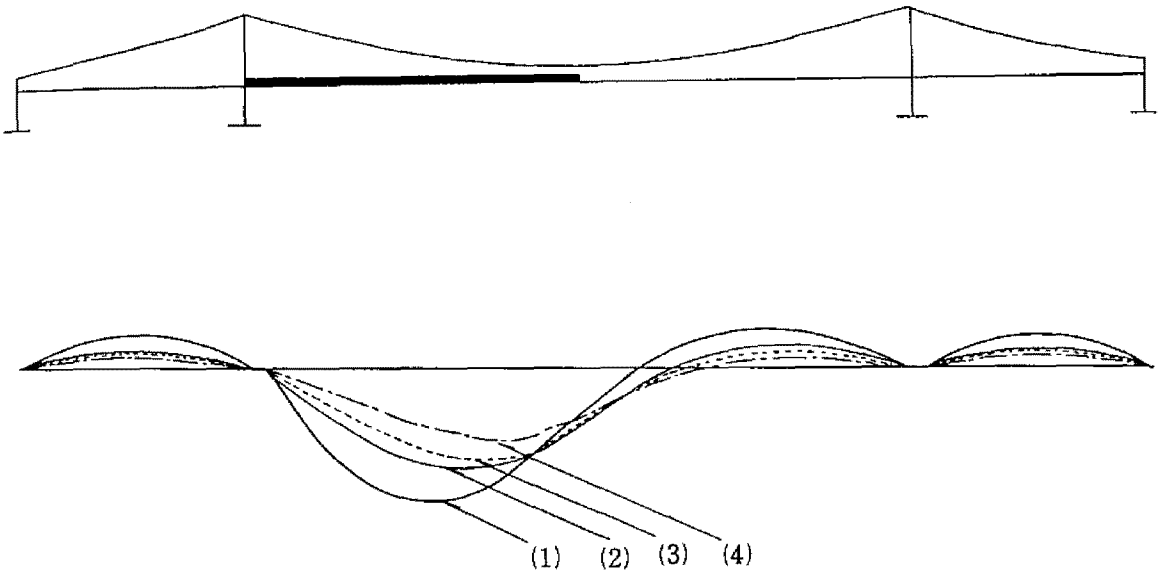

Fig 2.10 Flexure Characteristics
(Asymmetric Loading)

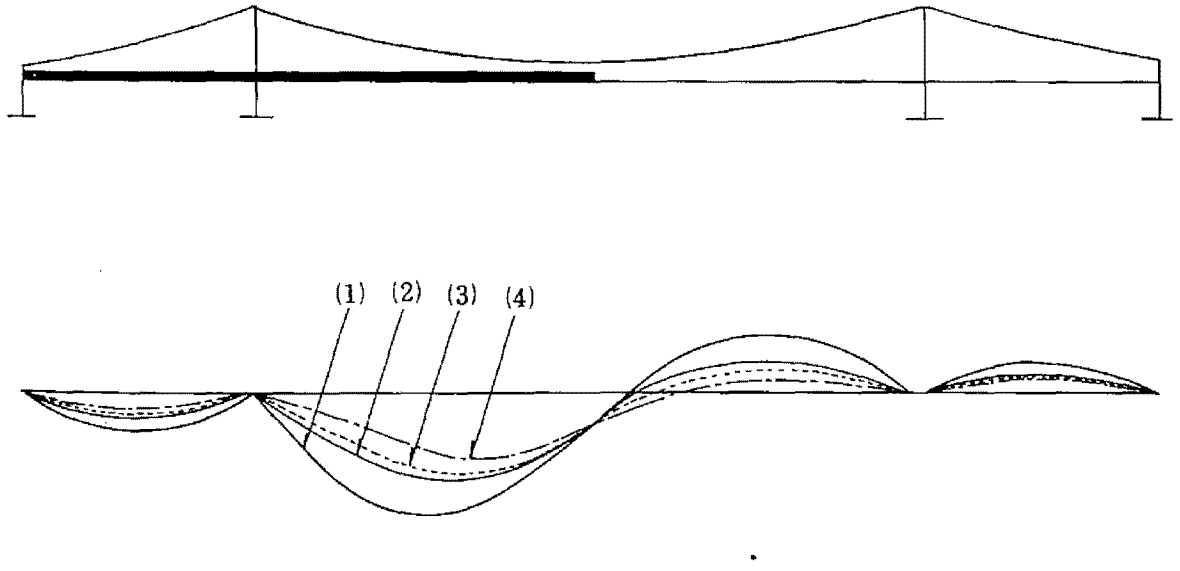

Fig 2.11 Flexure Characteristics
(Asymmetric Loading)

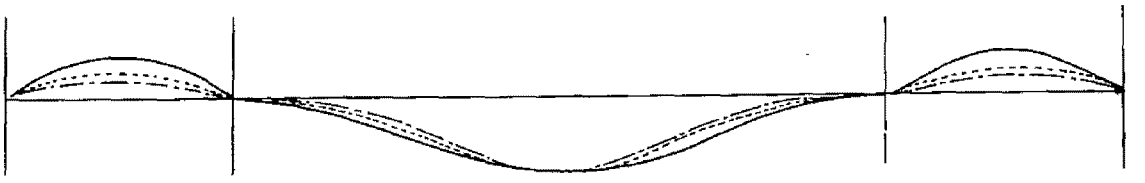

1st Symmetric Mode

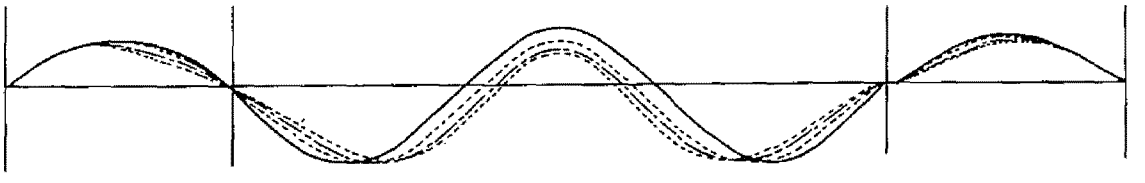

2nd Mode

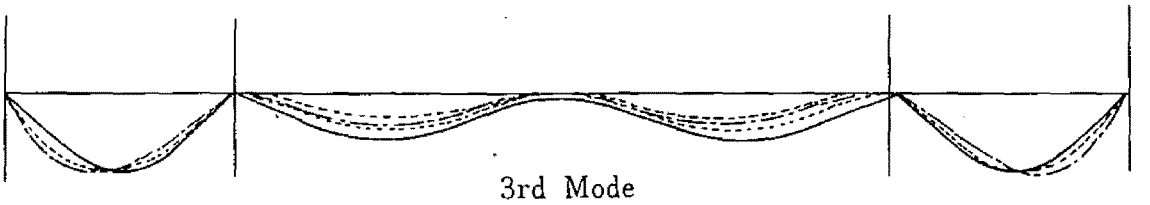

3rd Mode

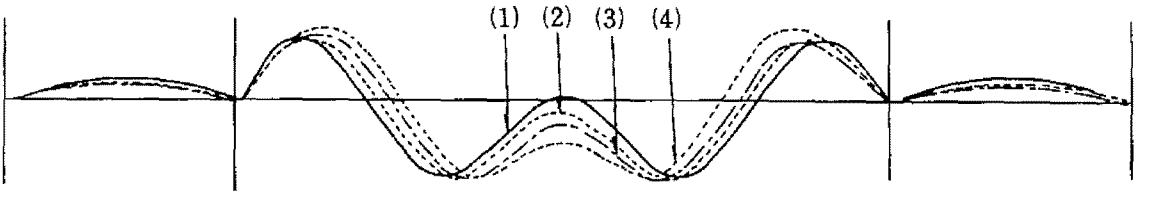

4th Mode

Fig 2.12 Symmertic Modes of Free Vibration

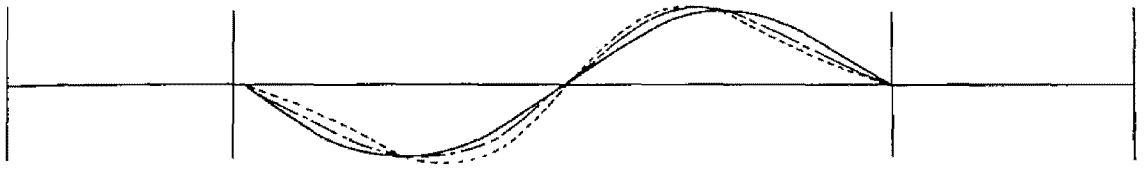

1st Anti-symmetric Mode

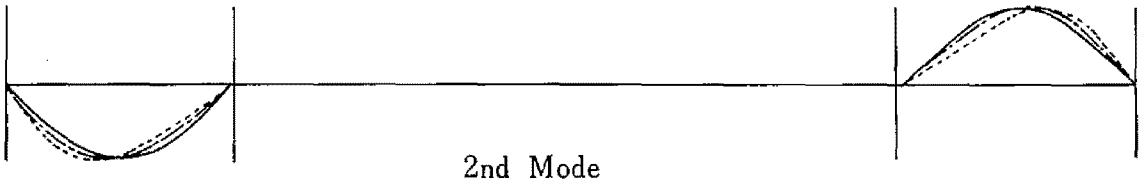

2nd Mode

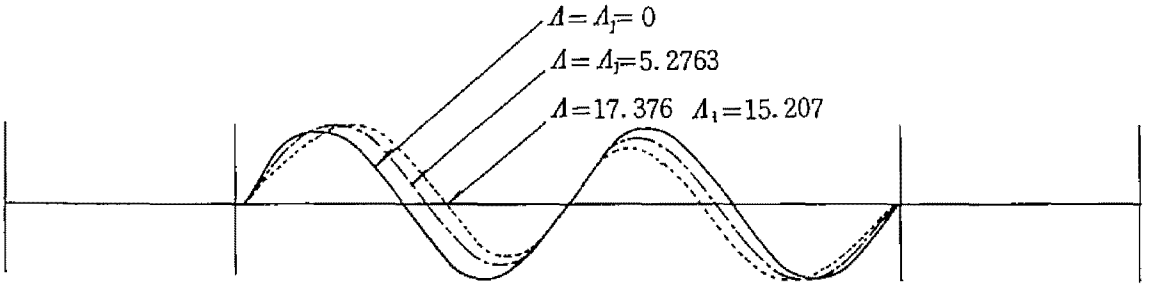

3rd Mode

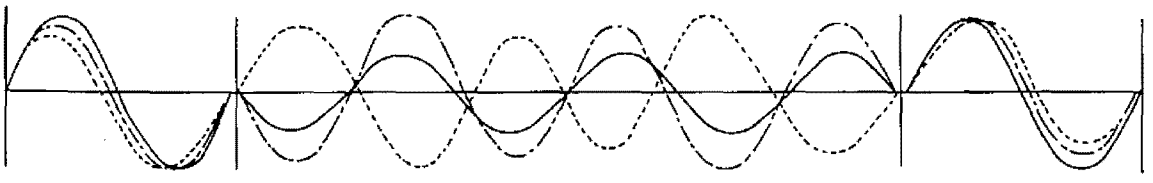

4th Mode

Fig 2.13 Anti-Symmetric Mode of Free Vibrations

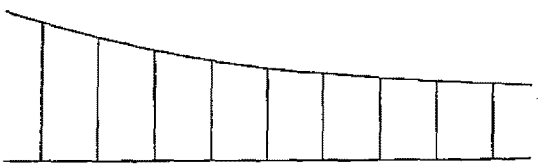

Vertical Hanger System

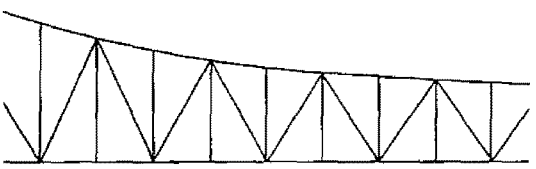

Three Members Hanger System

Fig. 2.14 Types of Hanger Systems

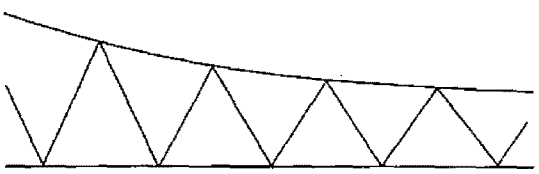

Warren Type Hanger System

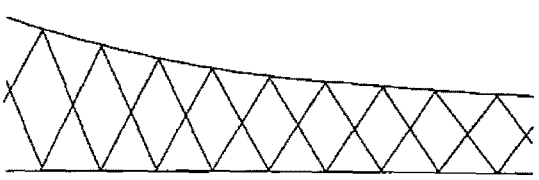

Double Warren Type Hanger System

Fig. 2.15 Types of Hanger Systems

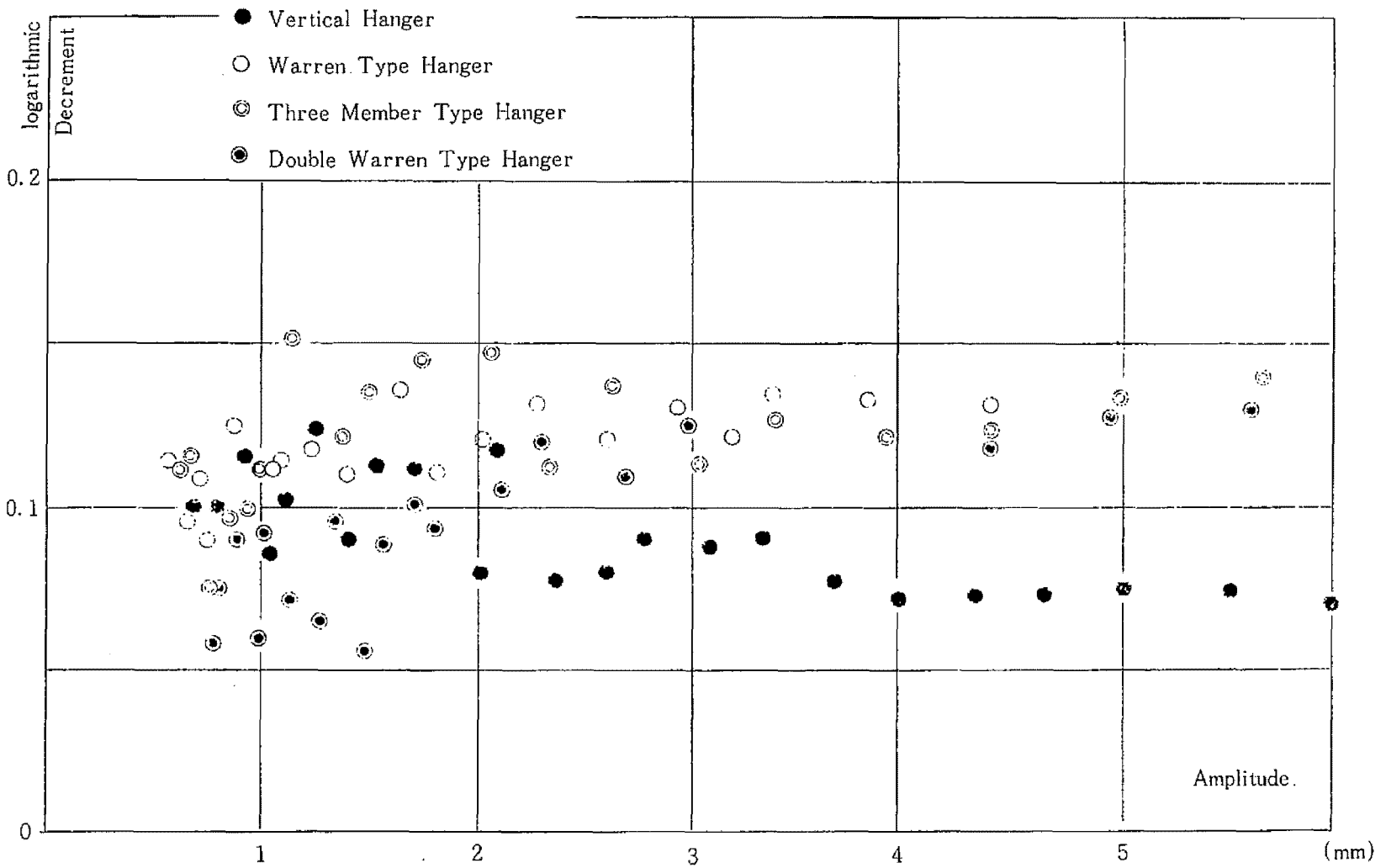

Fig. 2.16 Logarithmic Decrement—Amplitude Relations (1st Symmetric Mode)

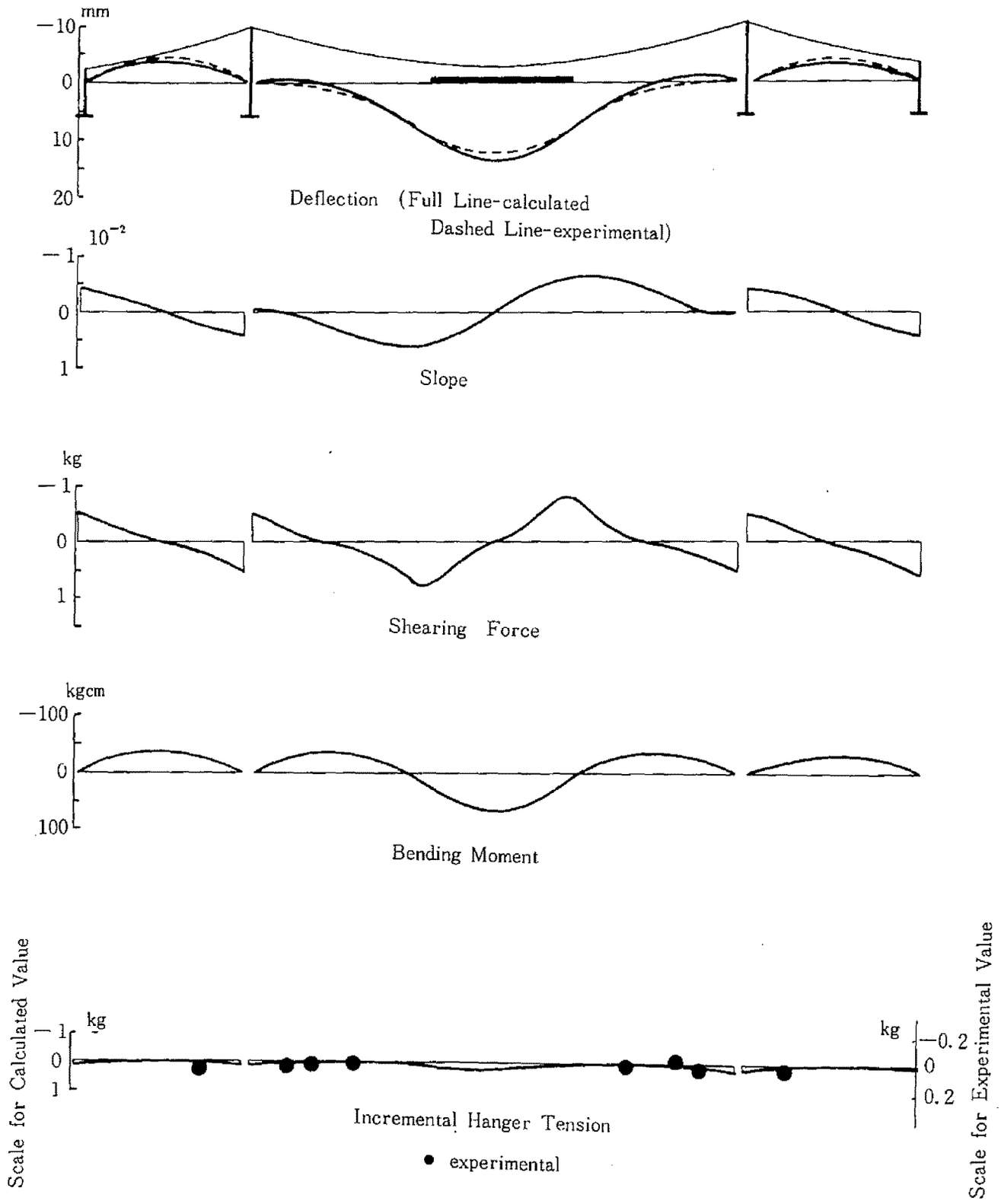

Fig. 2.17 Vertical Hanger System (Symmetric Partial Load on Main Span)

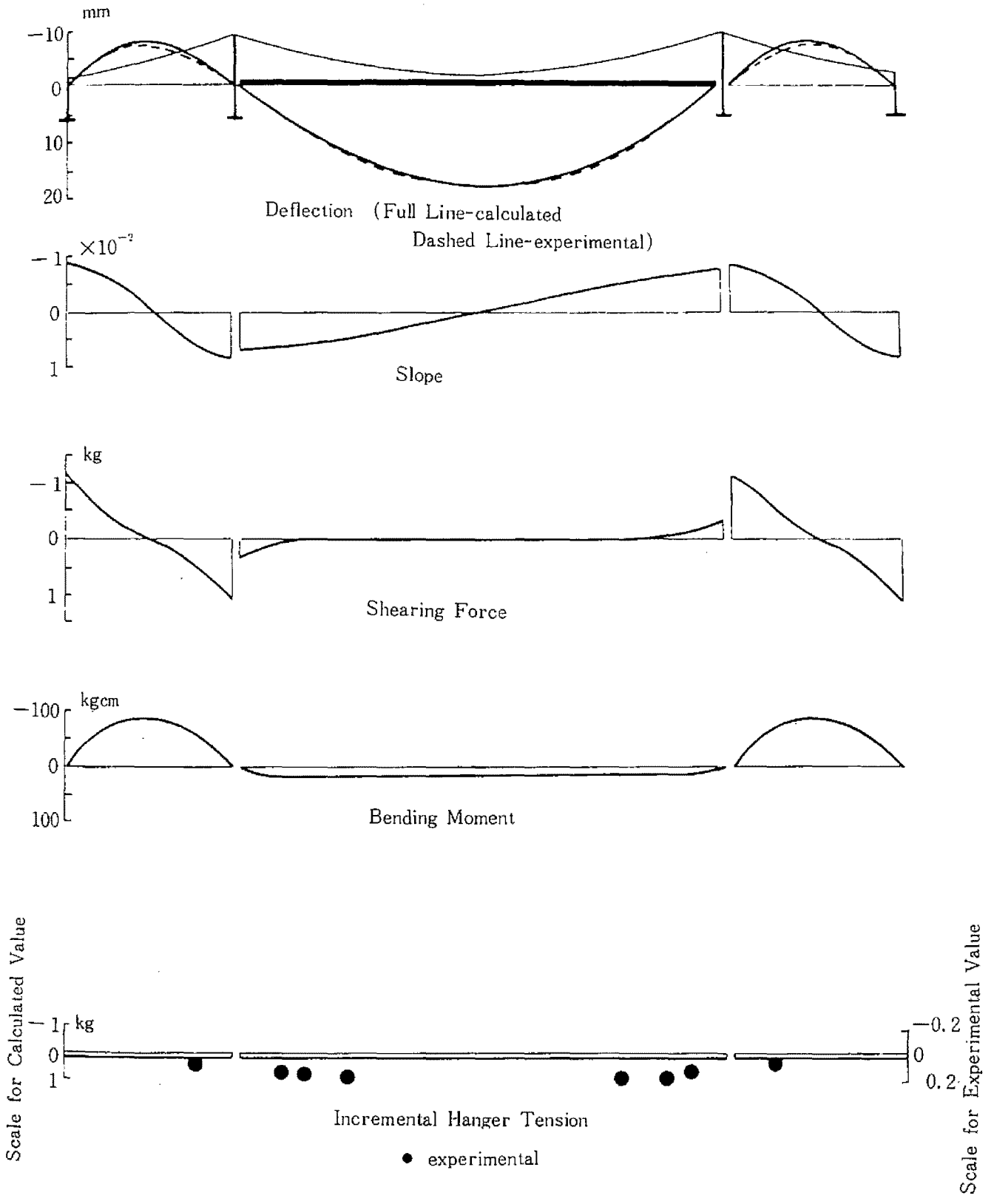

Fig. 2.18 Vertical Hanger System (Fully Loaded on Main Span)

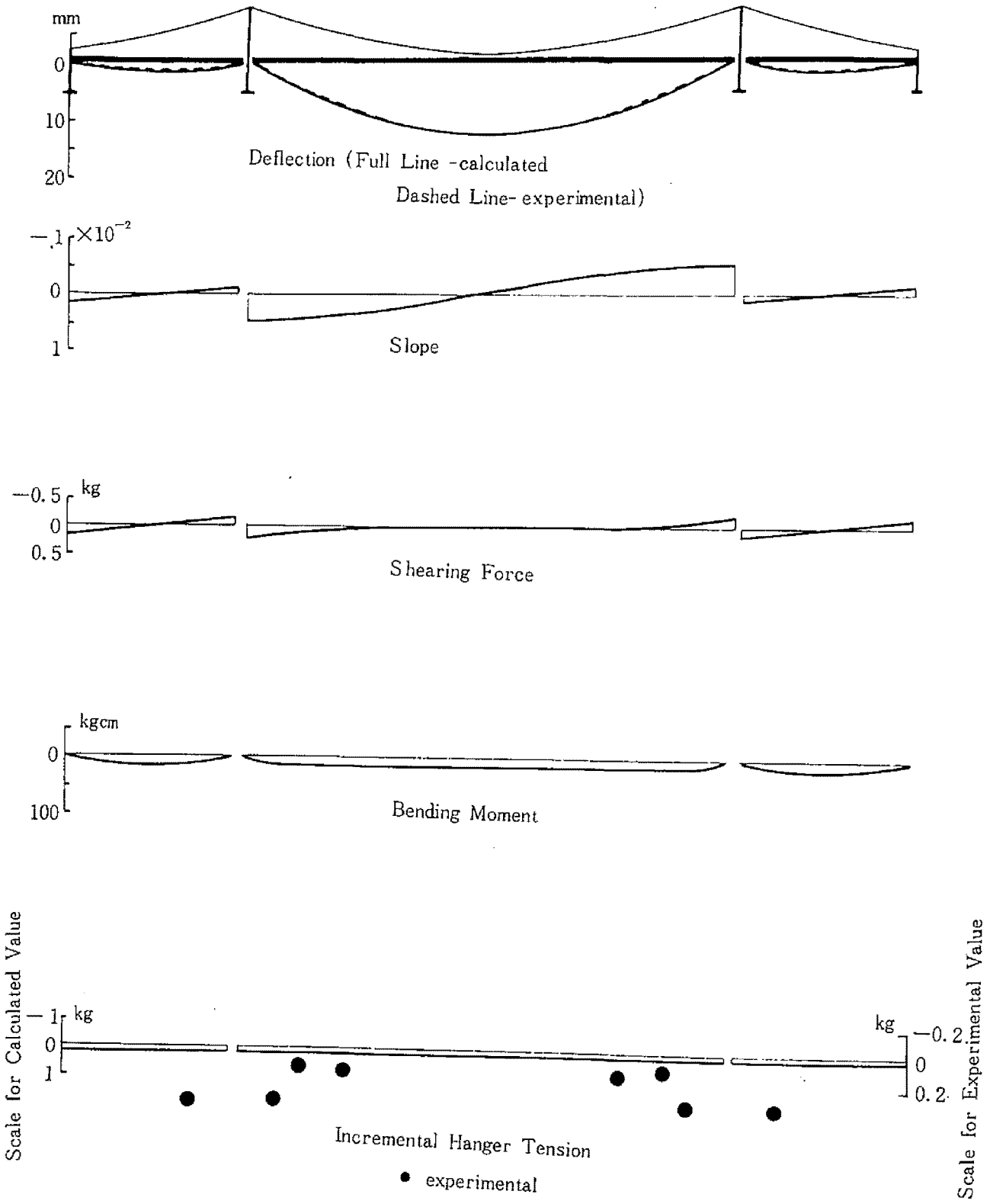

Fig. 2.19 Vertical Hanger System (Fully Loaded)

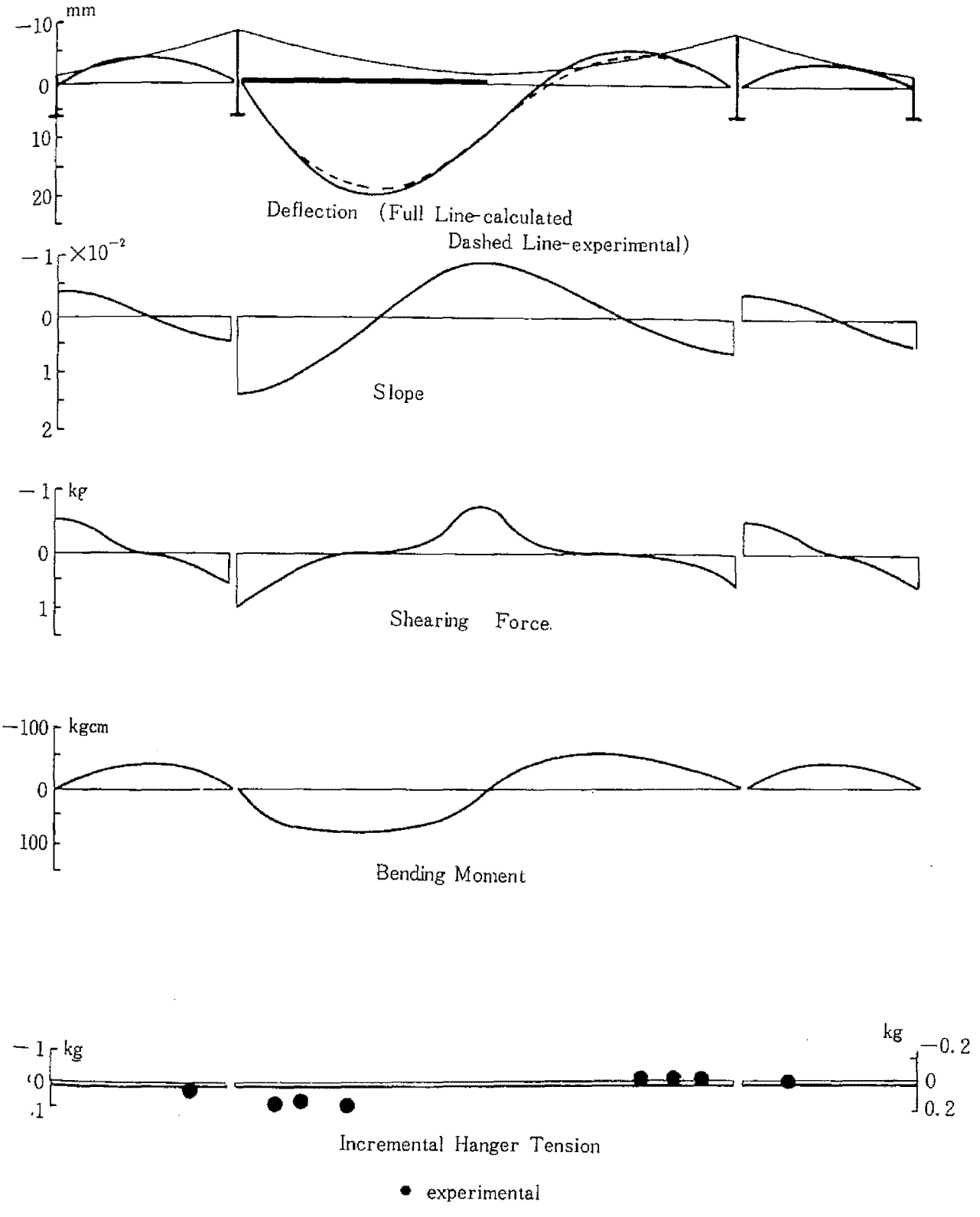

Fig. 2.20 Vertical Hanger System(Asymmetric Load on Main span)

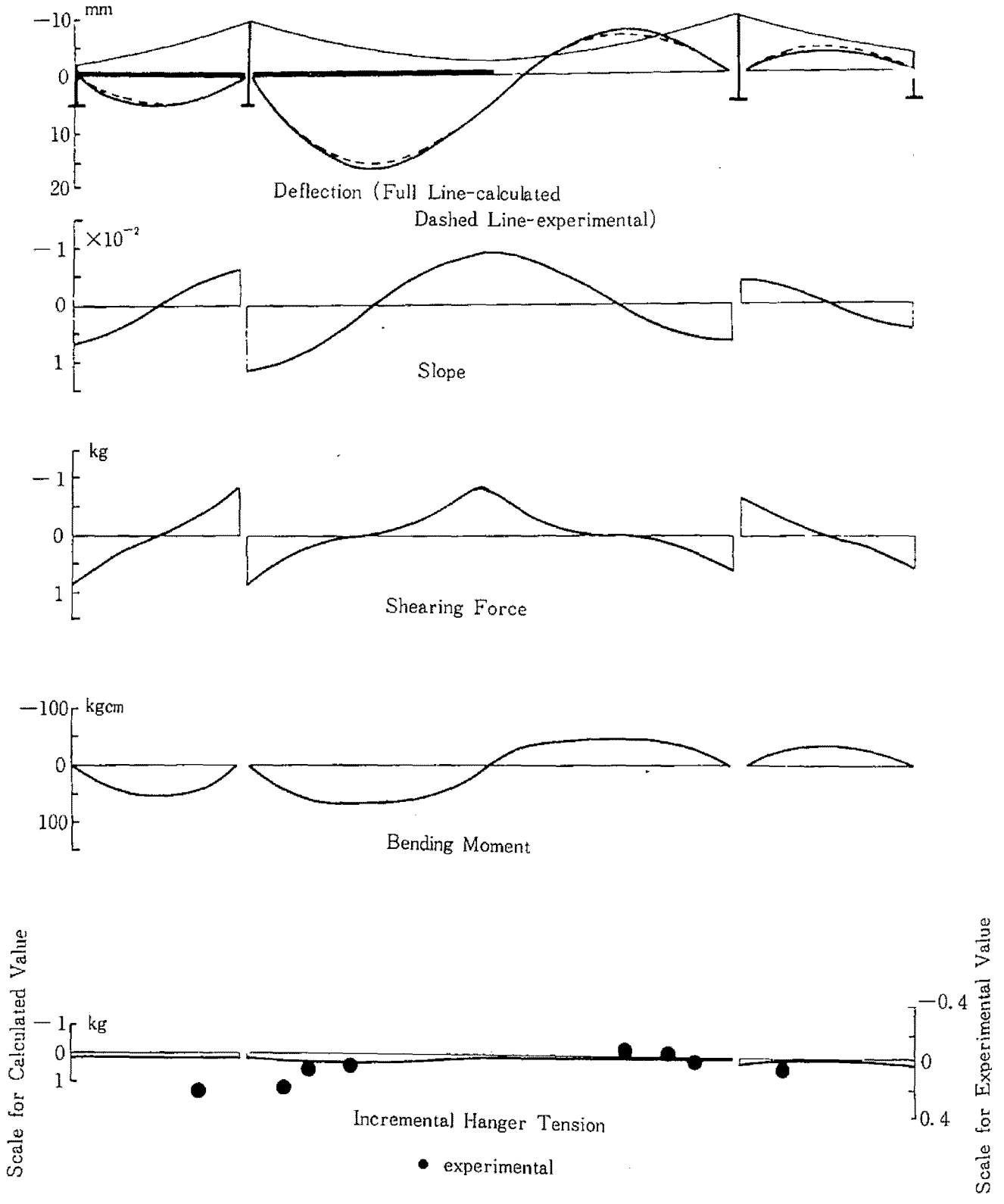

Fig. 2.21 Vertical Hanger System (Asymmetric Load on Main & Side Spans)

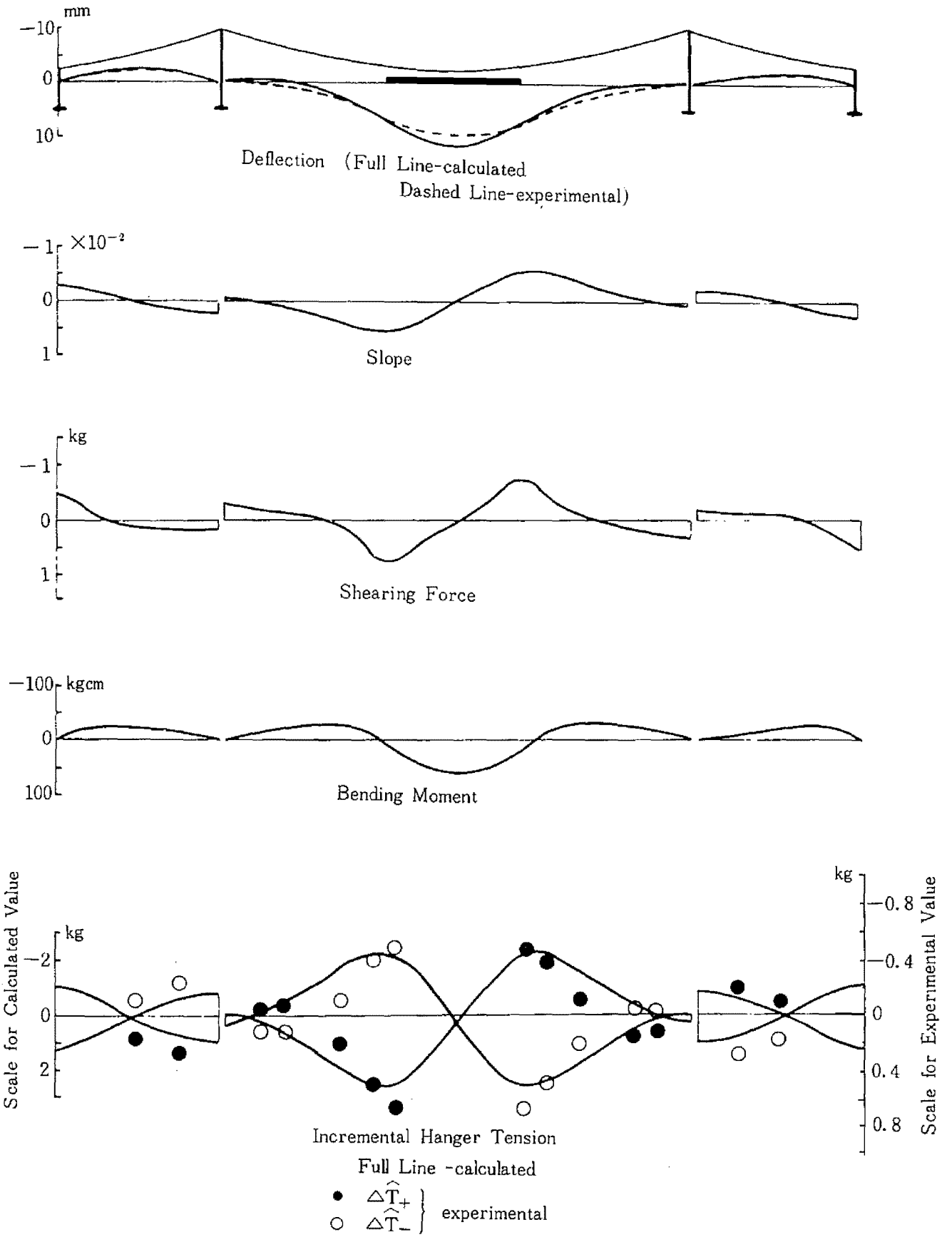

Fig. 2.22 Inclined Hanger System (Sysmetric Partial Load) $\Lambda m=\Lambda s=5.2763 kg/cm$

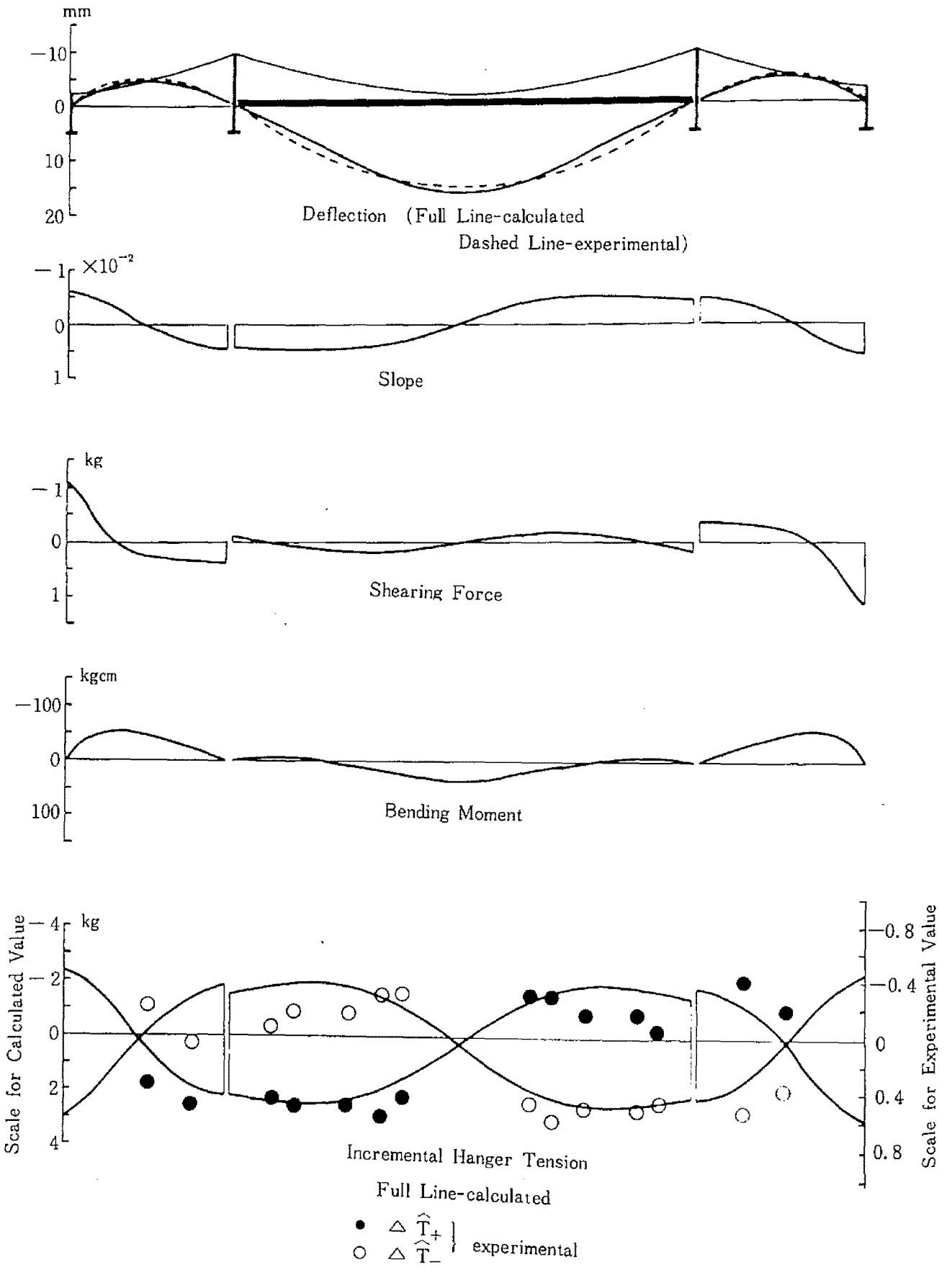

Fig. 2.23 Inclined Hanger System (Fully Loaded on Main Span)

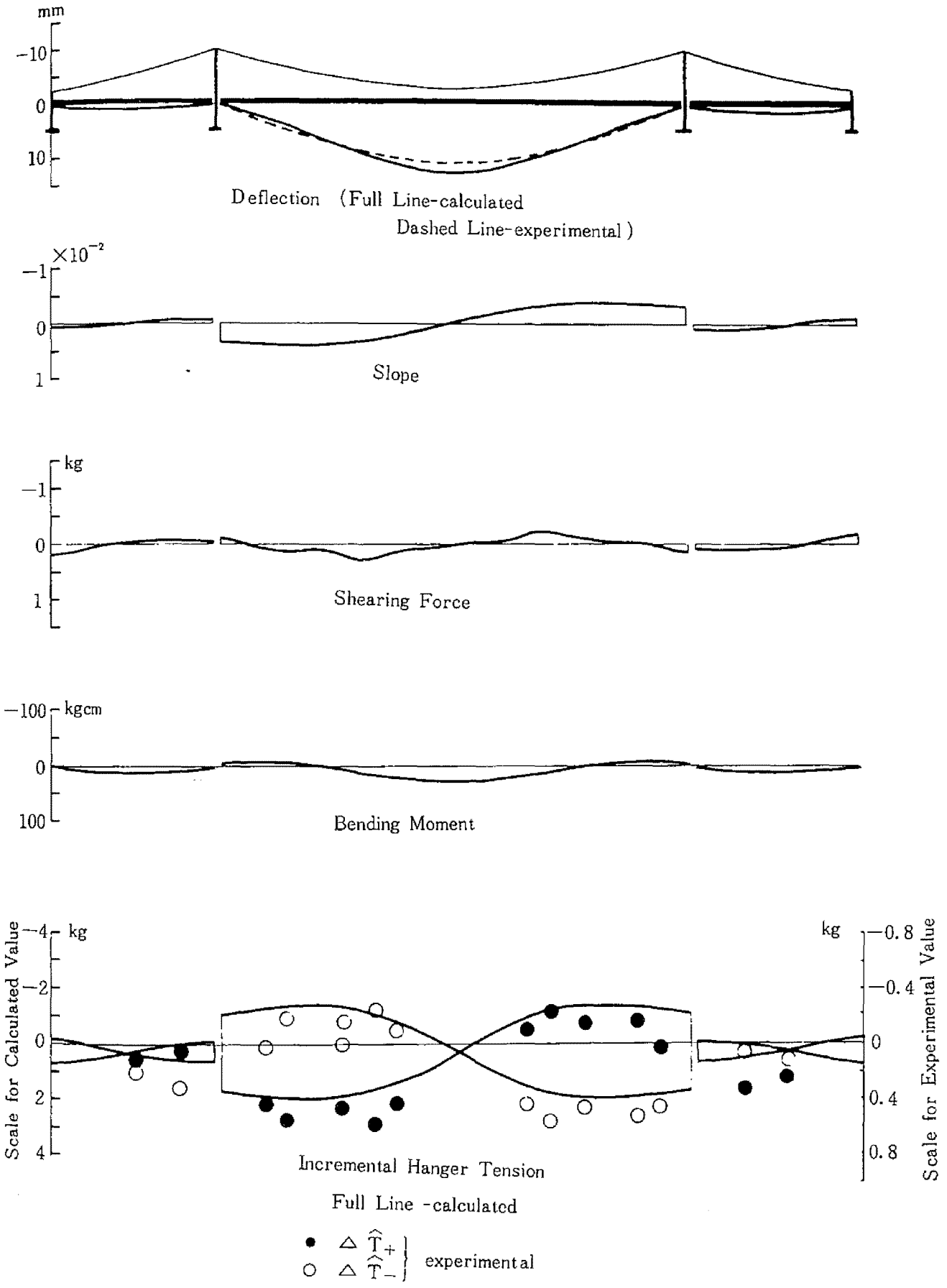

Fig. 2.24 Inclined Hanger System (Fully Loaded)

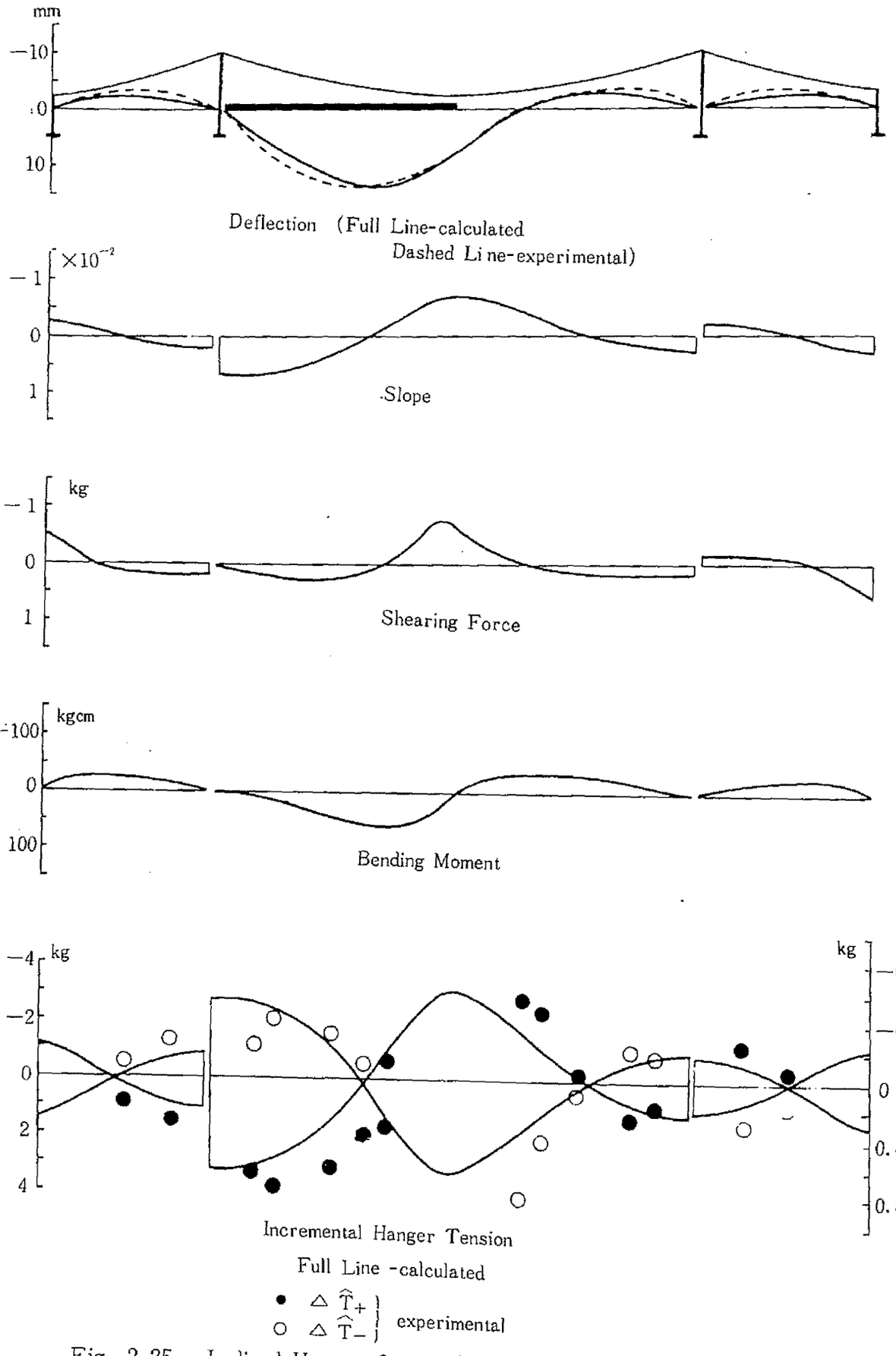

Fig. 2.25 Inclined Hanger System (Asymmetric Load on Main Span)

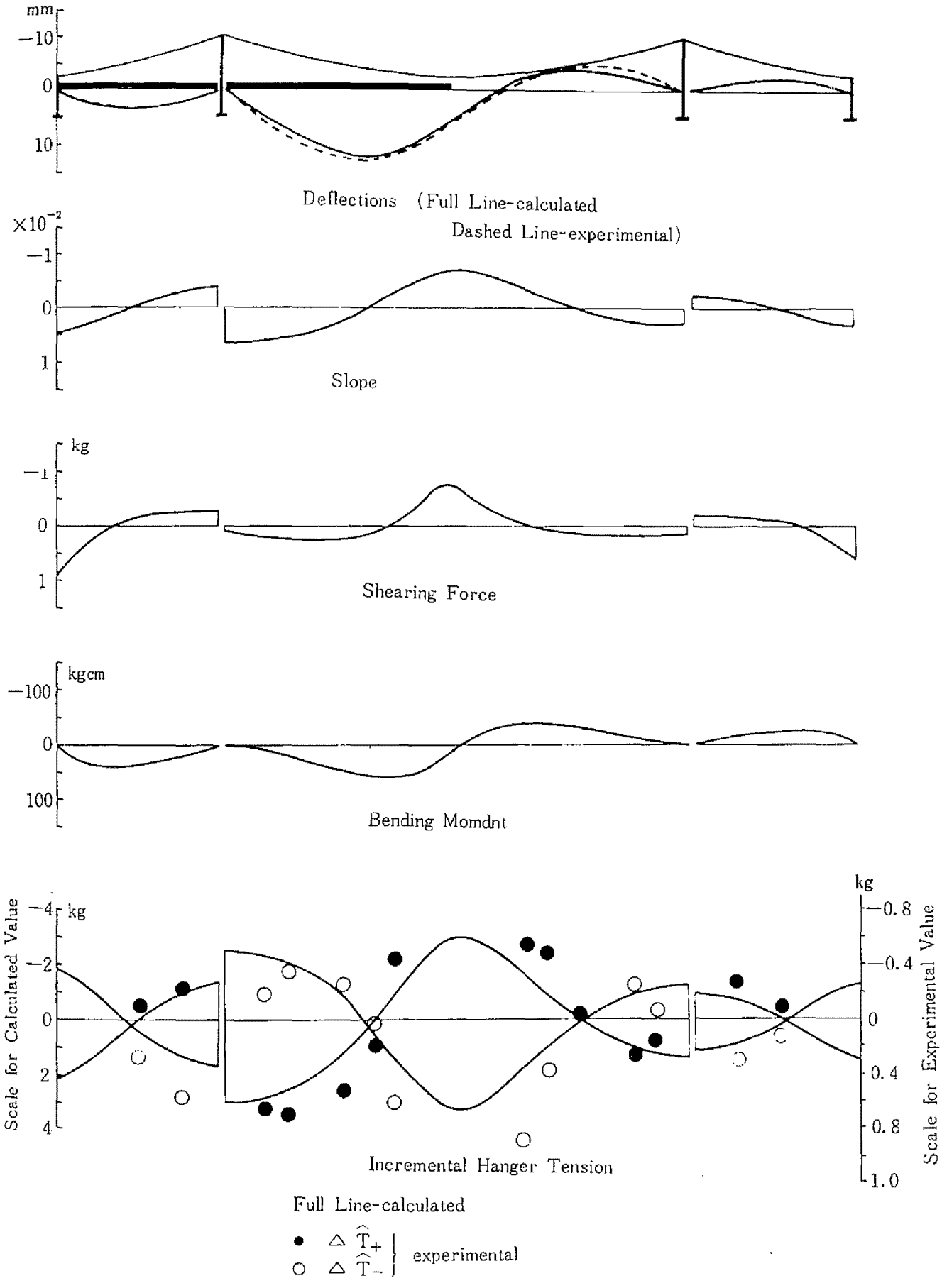

Fig. 2.26 Inclined Hanger System (Asymmetric Load on Main and Side Spans)

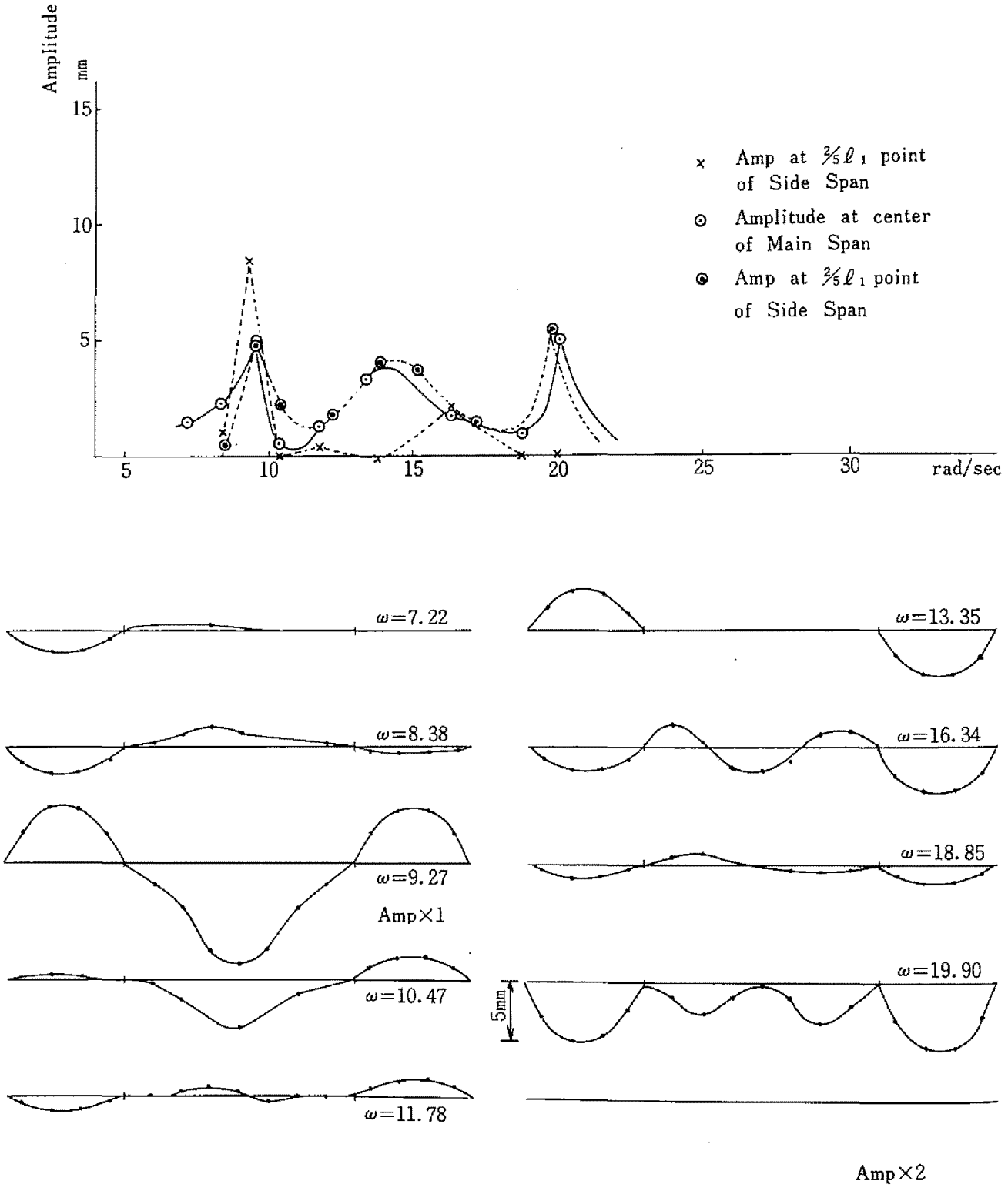

Fig. 2.27 Forced Vibration Test for Vertical Hanger System (Forced at the Center of Side Span)

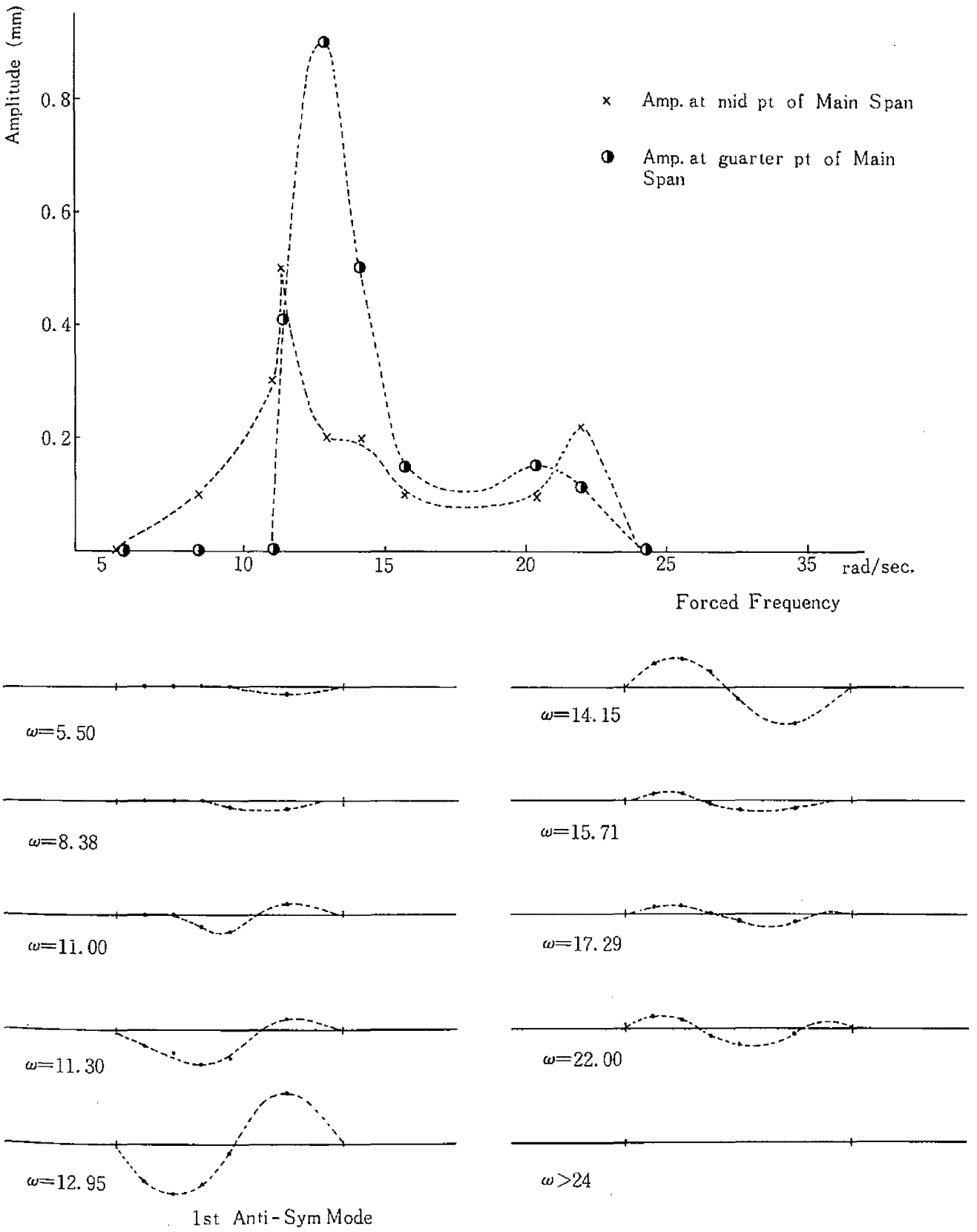

Fig. 2.28 Forced Vibration Test for Vertical Hanger System
(Forced at a quarter point of Side Span)

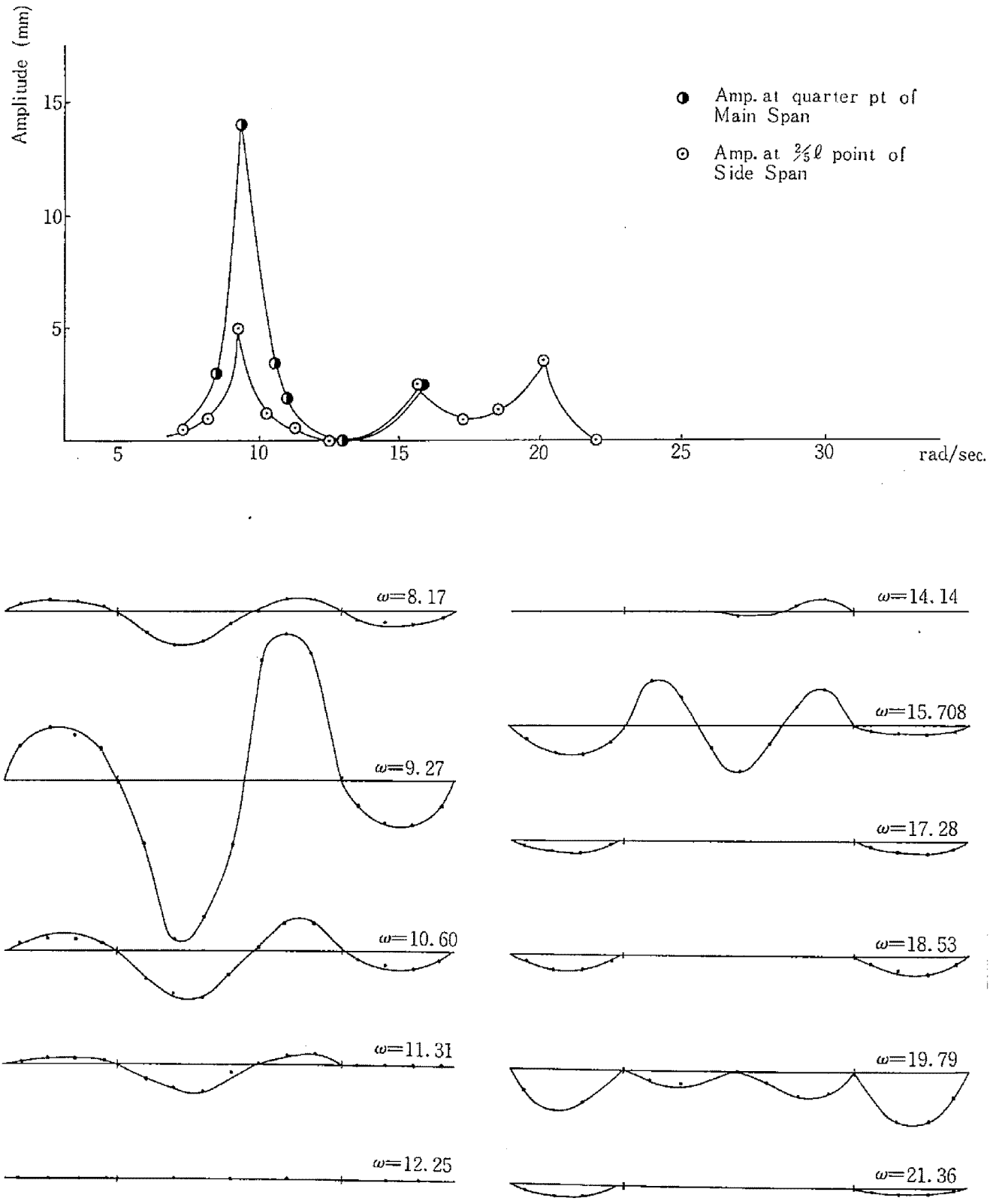

Fig. 2.29 Forced Vibration Test for Vertical Hanger System
(Forced at a quater point of Main Span)

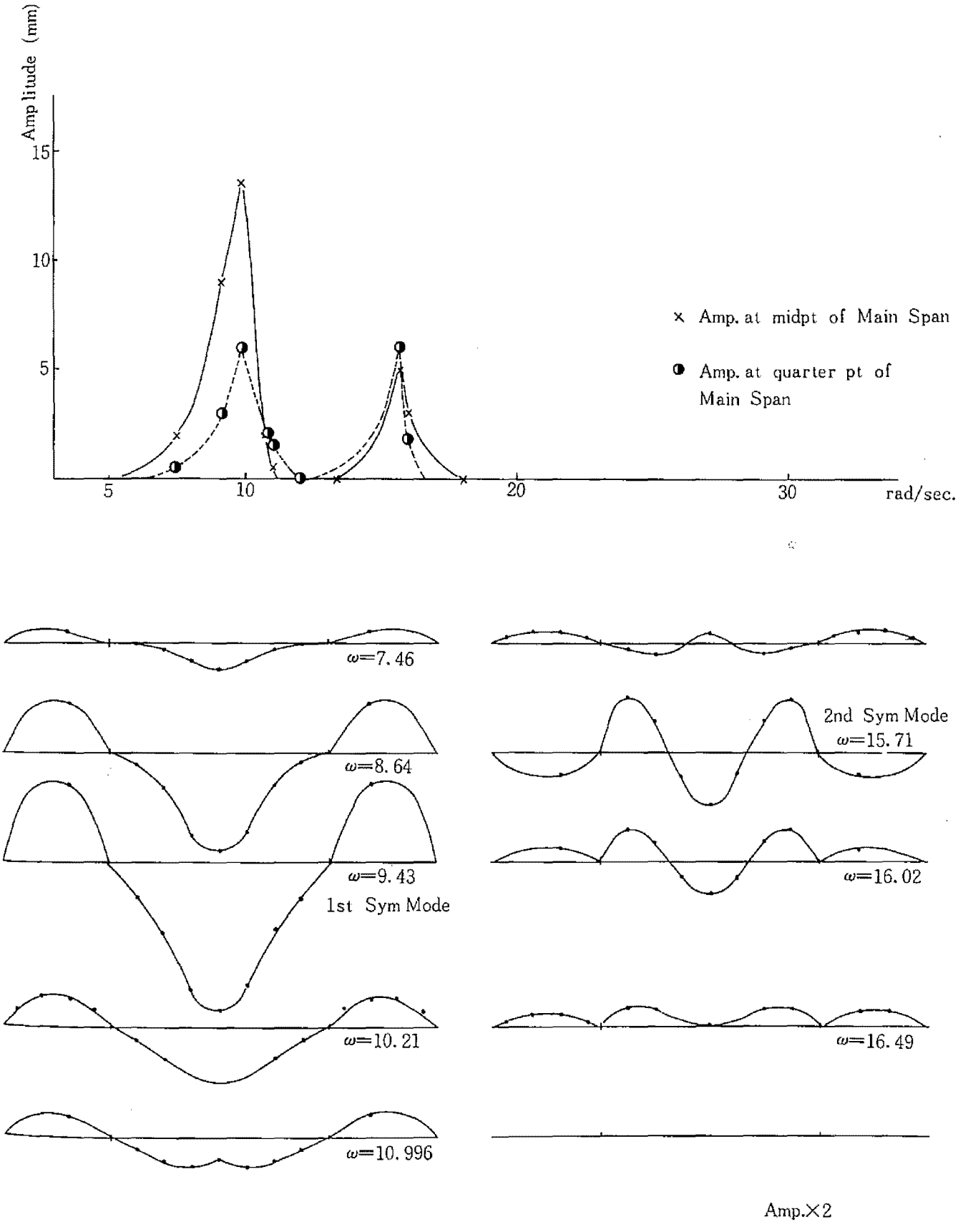

Fig. 2.30 Forced Vibration Test for Vertical Hanger System
(Forced at the center of Main Span)

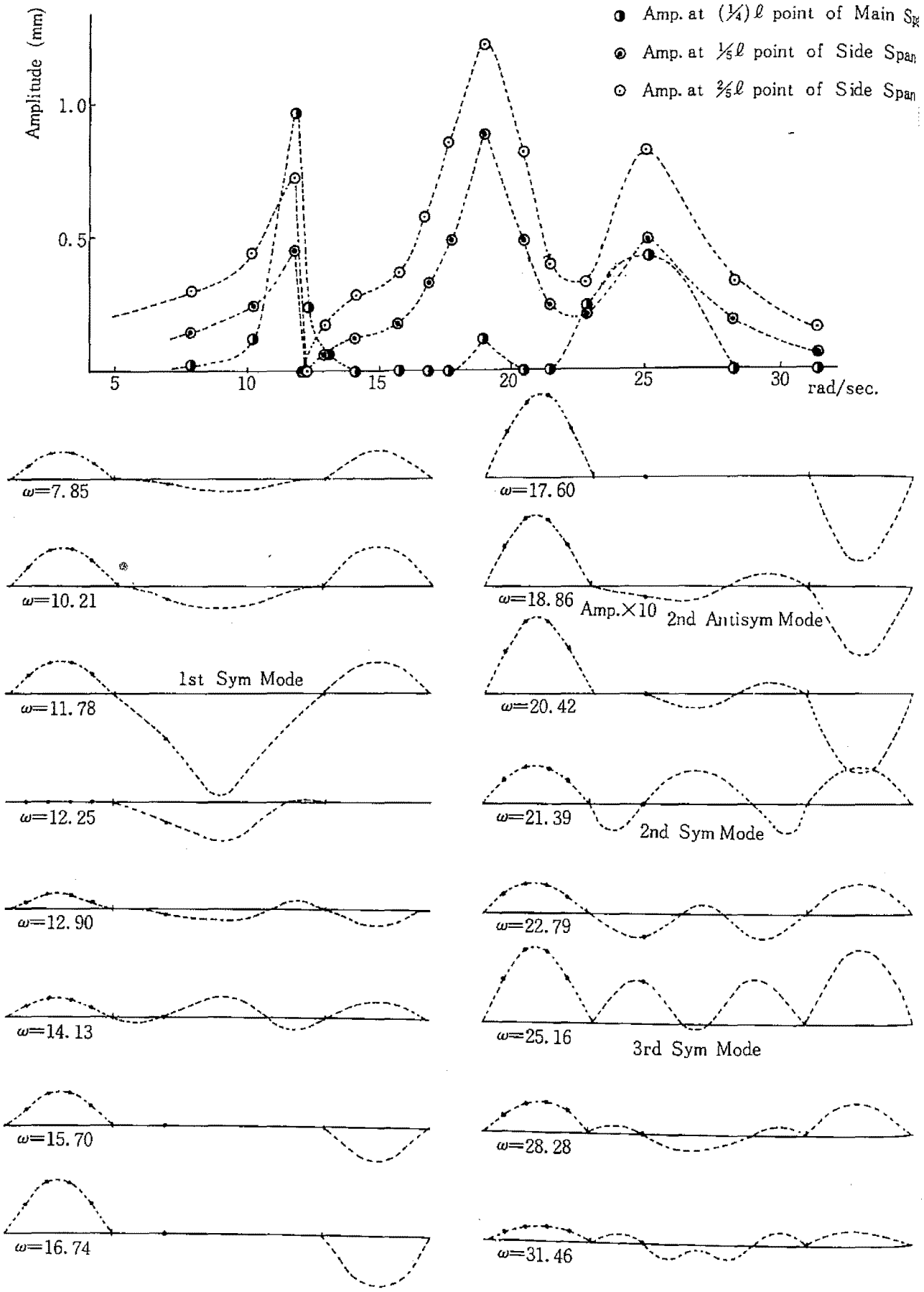

Fig. 2.31 Forced Vibration Test for Double Warren Type Hanger System (Forced at center of Side Span)

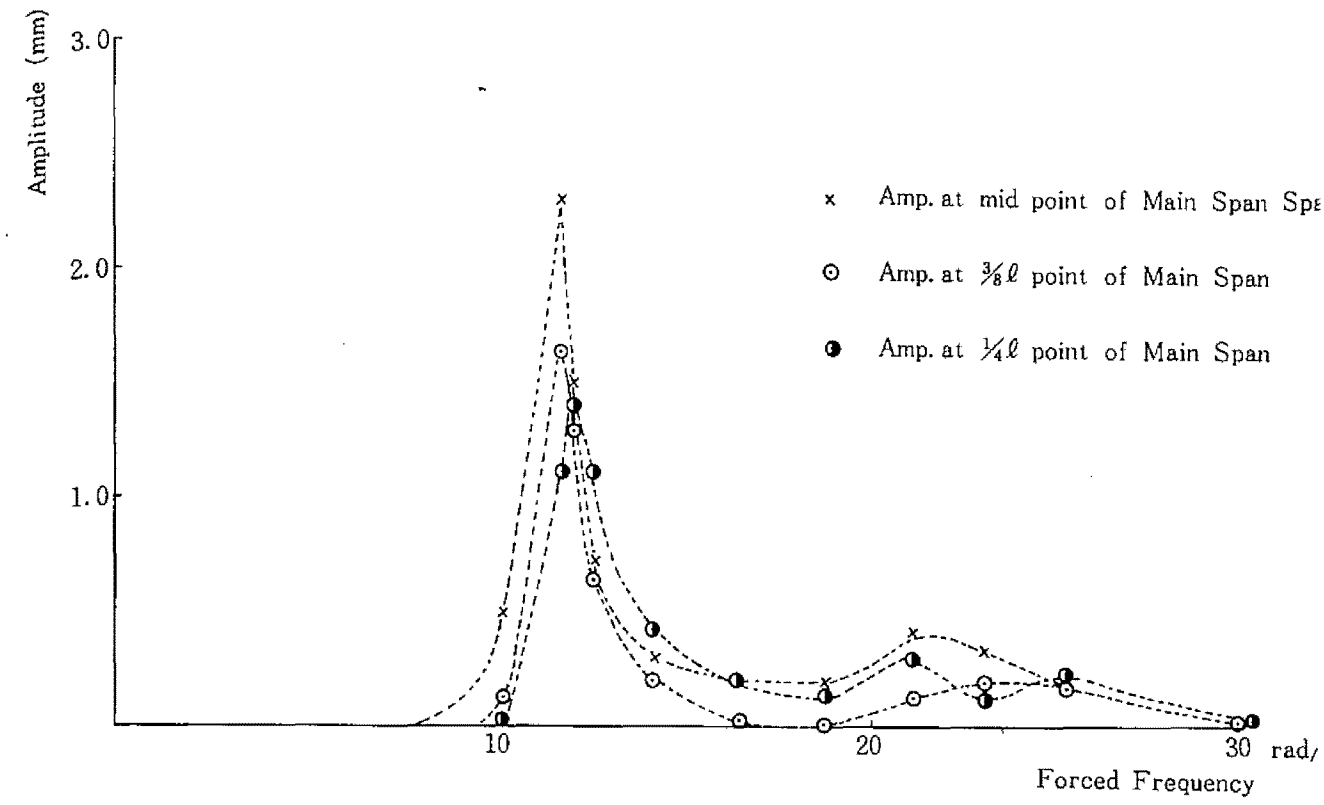

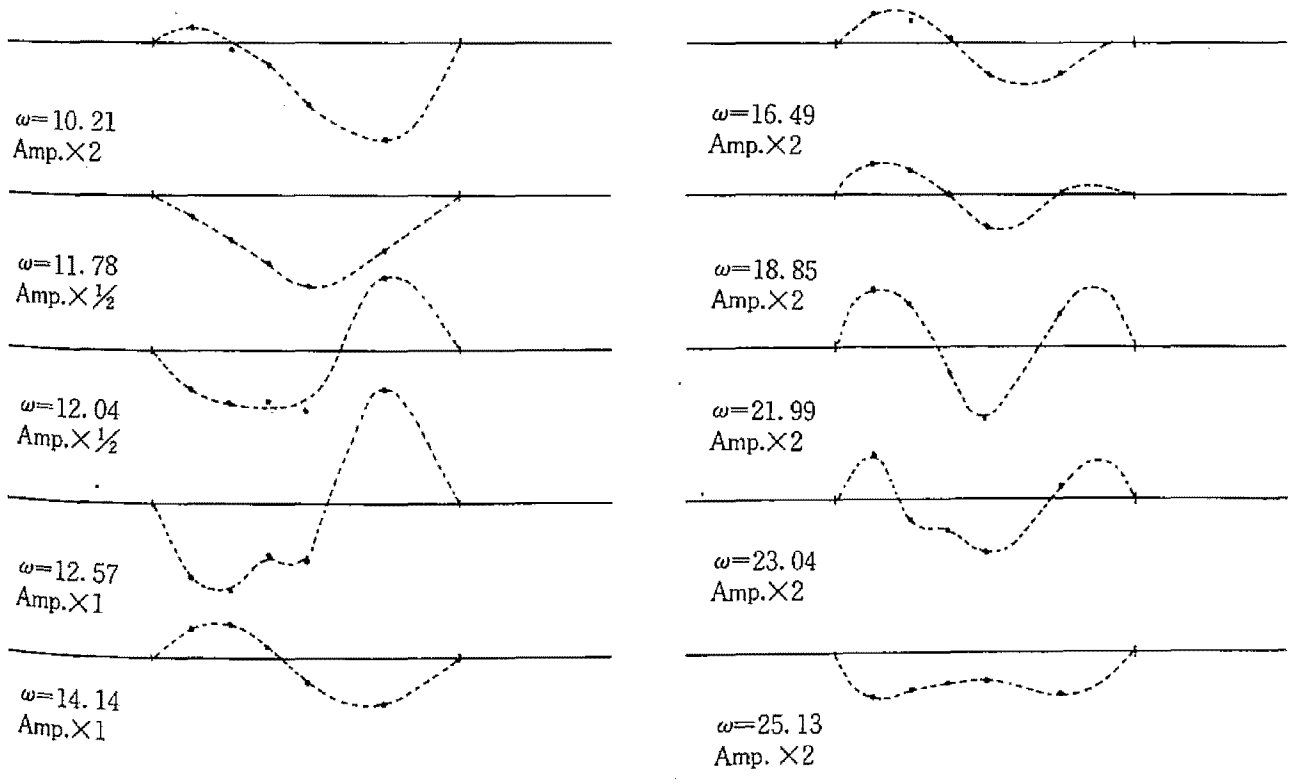

Fig. 2.32 Forced Vibration Test for Double Warren Type Hanger System
(Forced at a quarter point of Main Span)

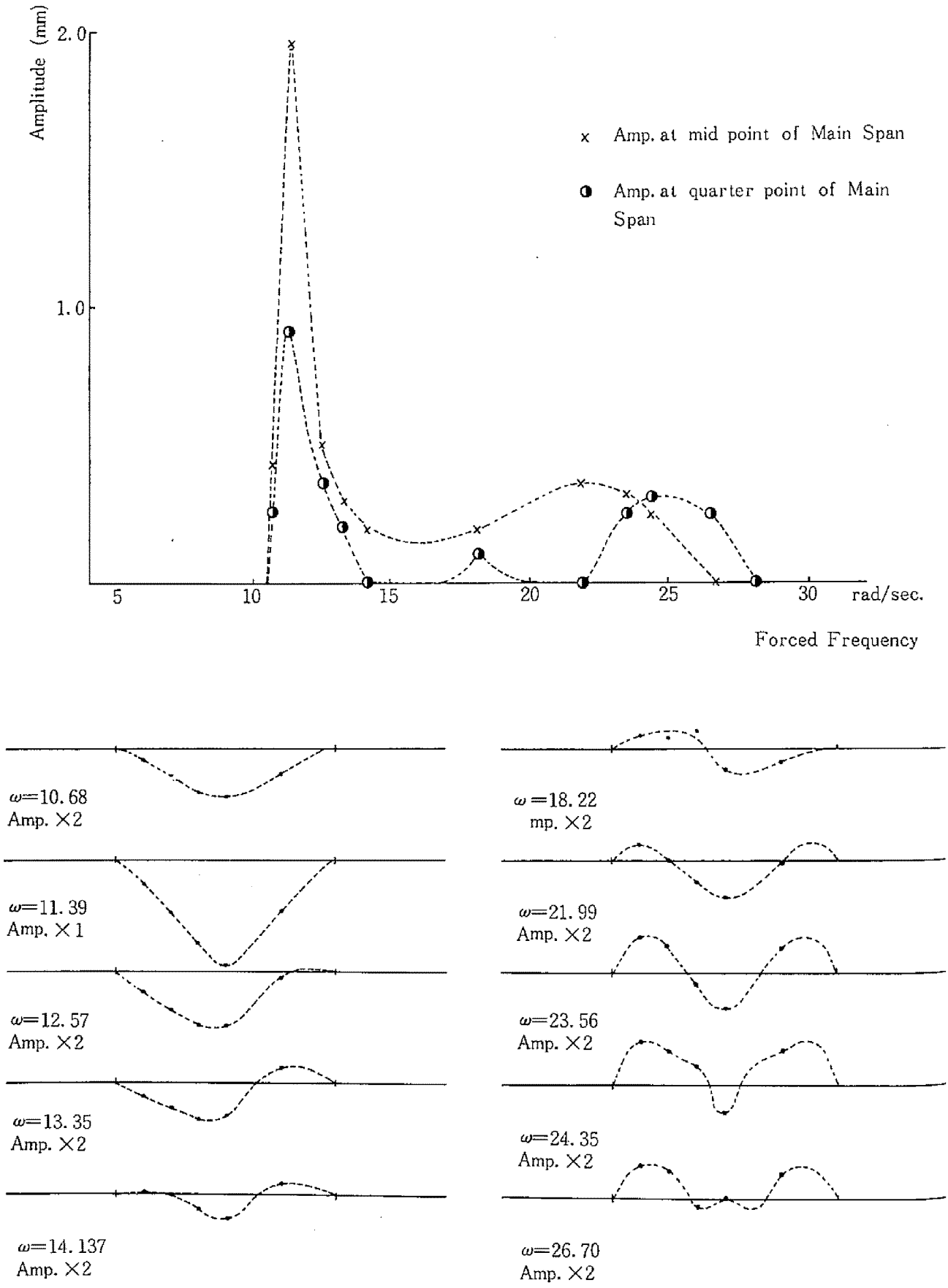

Fig. 2.33 Forced Vibration Test for Double Warren Type Hanger System (Forced at midpoint of Main Span)

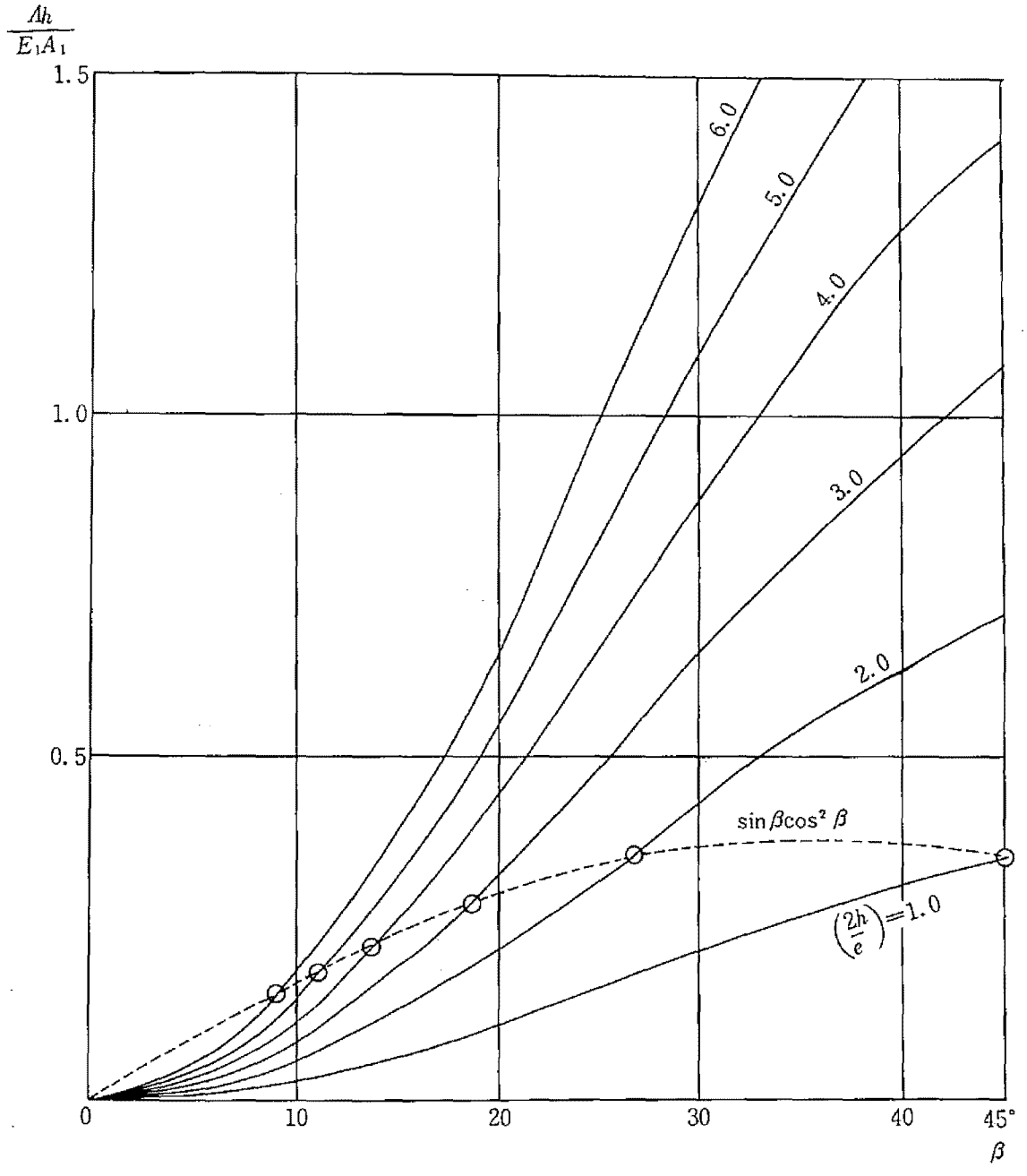

Fig. 2. 34 $\Delta h = E_1 A_1 \left(\frac{2h}{e}\right) \sin^2 \beta \cos \beta$—Curve

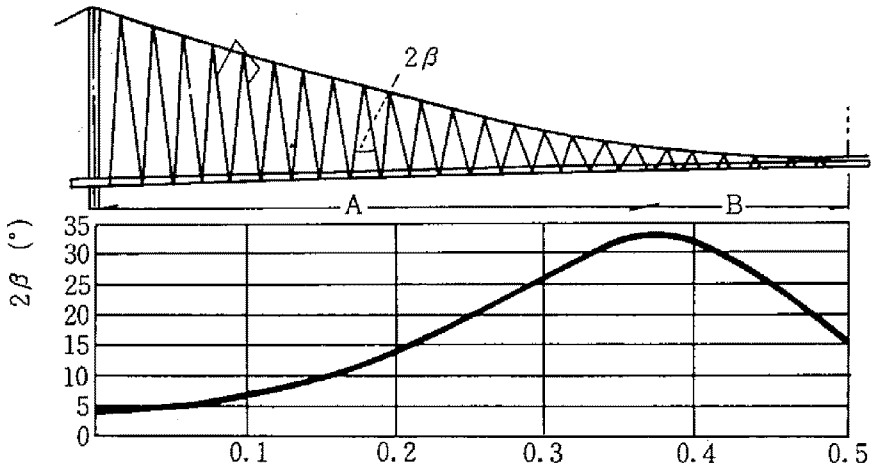

Fig. 2. 35 Distance from tower expressed as a fraction of the span

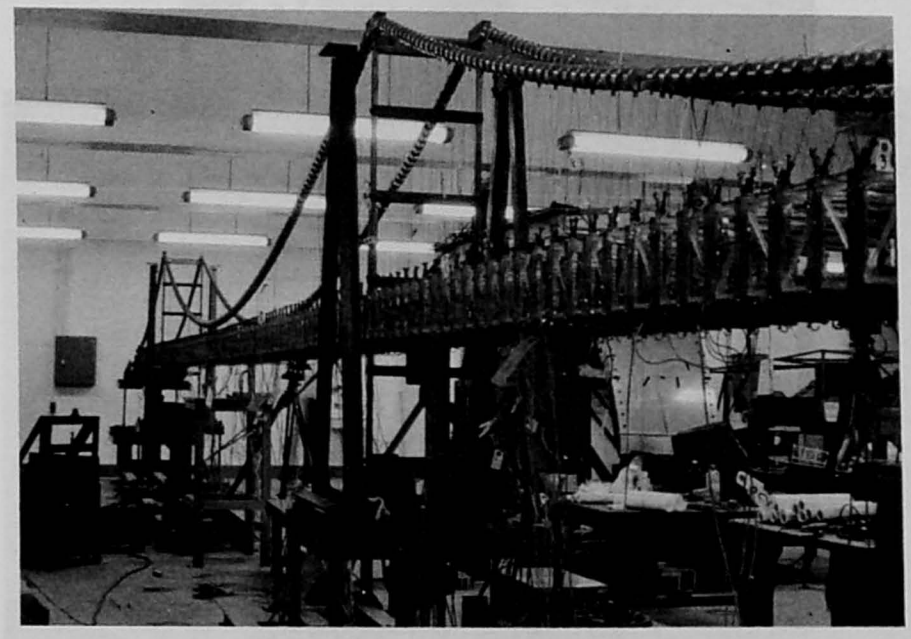

Photo 2.1 General Views of Model

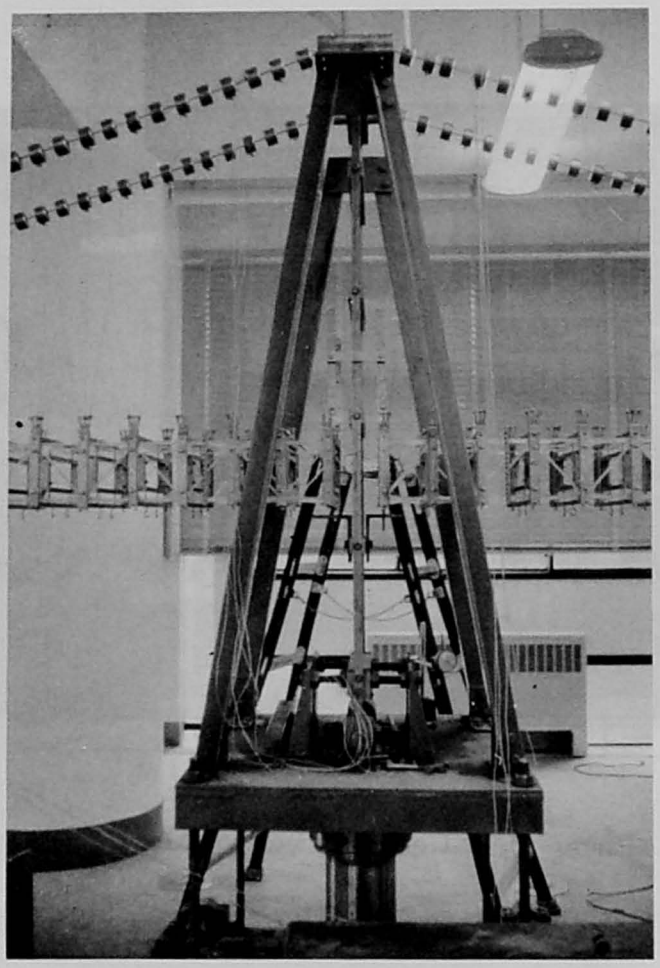

Photo 2.2 Tower and Supporting Angles

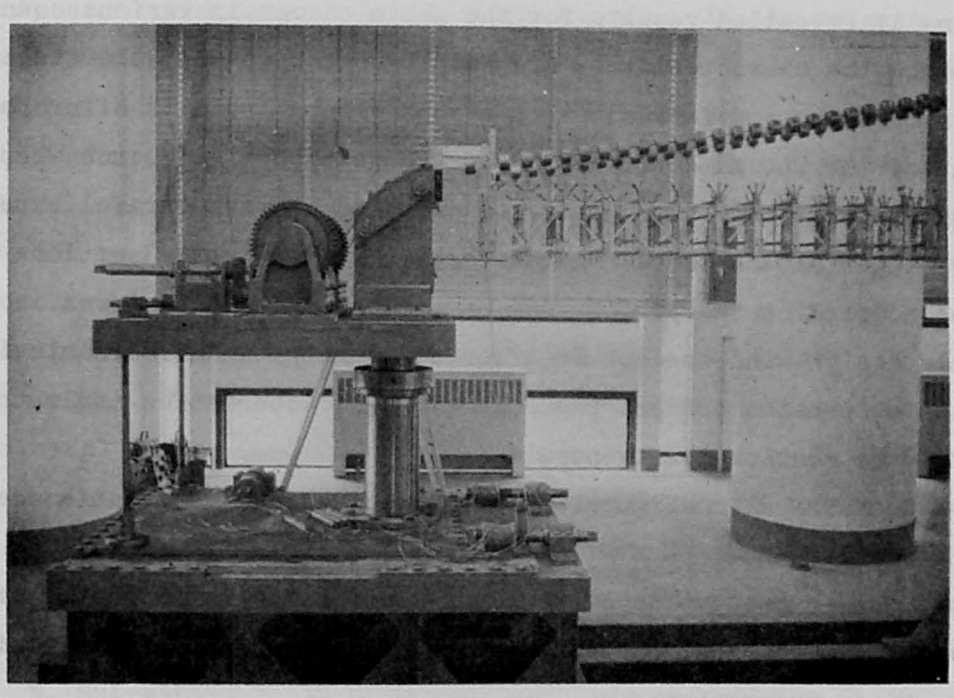

Photo 2.3 Details for Anchorage and Cable Bent Shoes

CHAPTER 3 AEROELASTIC BEHAVIOURS OF LONG-SPANNED STRUCTURES

3.1 INTRODUCTION

The wind-induced dynamic behaviours of a long-spanned suspension bridge have presented for long time one of the most controversial problems on an account of its complexity in interrelation of aerodynamic forces acting on rather complicate compound of number of structural members. The formally revealled results for the above themes in various countries to disclose the characteristics are mainly concerned with the stability of the structures and fortunately numerous eminent results after the accident of the Tacoma Narrows Bridge have been obtained since whenever the long-spanned suspension bridge be planned the most careful experimental investigations on the aerodynamic stability of bridge sections are required to predict the performance of the concerned structures in the available design wind speed. In order to clarify the aerodynamic instability of suspension bridges the following characteristics and methodology should be mentioned in general:

1) Geometrical configuration of structures and aerostatic characteristic
2) Dynamic properties of structures and aerodynamic characteristics
3) Fluidmechanical characteristics of air-stream and its statistical properties
4) Influences of neighbouring structures and boundaries; buffetting and scattering
5) Methodology of wind resistant design of structures
6) Experimentation for aerodynamic performance of prototype by use of model and its representation.

These problems are considered mutually related with each other and still there remains a number of facts unexplained satisfactorily.
As Prof. F. B. Farquharson quoted, however, the systematically inconclusive achievement of above researches should not be interpreted as repre-

senting any lack of confidence in the data accumulated but rather as arising from the fact that but a fraction of the field has been covered by the endeavor.

The first problem of aerostatic characteristics of structures provides one of the fundamental approaches to evaluate qualitatively and quantitatively the fluid forces on the structures induced by the air-stream. The second problem of dynamic properties and aerodynamic characteristics forms a basis to predict the flutter instabilities such as the classical flutter, the stall flutter, etc., in the relation with the experimentation for measurement of the non-steady aerodynamic forces and with the similarity requirement between the protorype and the model. This fraction of investigation is previously researched by aeronautical engineers and the importance of the results tends to increase rapidly with tendency of elevating the heights and widening the span-length of structures. As the main recent contributions one may mention the analysis on the Severn and Forth Bridges by R. A. Frazer, C. Scruton[2], D. E. Walshe[3], the investigation on the classical flutter by A. Selberg[4], the aerodynamic analysis of H-section by D. Dicker[5] and the non-linear problem of aeroelastic oscillator of square prism by G. V. Parkinson and J. D. Smith[6]. The theoretical consideration on the flutter stability of suspension bridge taking into an account of the horizontal spanwise variation of wind velocity is given by I. Konishi, N. Shiraishi, H. Utsunomiya[7] and independently by T. Narutomi, M. Kawashima[8]. The third problem is closely concerned with the meteorological studies, which is firstly systematically investigated by A. G. Davenport[9] introducing the statistical concept into the wind-induced behaviours of structures. The stochastic and statistical properties of atmospheric turbulence and turbulent flows are studied by such investigators as H. Shiotani[10], H. Ishizaki[11], M. Hino[12], Y. Mitsuta[13], etc., in our country and by H. E. Cramer[14], H. W. Liepman[15], Y. C. Fung[16], etc., in other nations. From the structural engineering point of views G. Vincent[17), 18] introduces the concepts of " wind efficiency " and " the time to build instability " as the result of observations and

investigations of wind-induced oscillations of the Golden Gate Bridge and it is directly applied for the wind resistant design of the New Quebec Bridge by L. R. Cayes[19]. The influences of neighbouring structures and boundaries are considered as one of causes of turbulence in air stream to produce the buffetting and scattering of structural motions as investigated by C. Scruton[20]. The wind resistant design methods of the long-spanned suspension bridge are presented by D. B. Steinman[21], F. Bleich[22], and A. G. Davenport[23] as well as A. Hirai[24], who considers the ultimate stage of collapse by the aerodynamic instability to relate the torsional buckling of bridge sections, and S. Komatsu[25].

The sixth problem of experimentation and similarity calls at present mostly for more eleborate modifications of customary methods. Recently, however, the measurement technique of non-steady aerodynamic forces developed by S. Kawashima[26] is successively applied by N. Ukeguchi, H. Sakata, and H. Nishitani[27] for various types of bridge sections and the alternate method by R. H. Scanlan and Ali Sabzevari[28] is presented by use of the so called free vibration method.

In this field of investigations the contributions by J. P. den Hartog[29] and Y. Rocard[30] should be noted to disclose some of basic aerodynamic properties of instability of structures on wind stream. However of great difficulty remains the problem to anticipate the probable performance of long spanned suspension bridge in wind stream at the initiation, diverging, and final stages of vibrations of structures.

3.2 STATIC AEROELASTIC FORCES ON BRIDGE STRUCTURES

The static aeroelastic forces act on the structures in air stream as shown in Fig's 3.2.1. & 3.2.2. and these are expressed according to the specifications for wind resistant design of the Proposed Honshu-Shikoku Bridge in Japan as

$$\left.\begin{aligned} L\ (Lift) &= \frac{1}{2} C_L \rho V^2 B \quad (kg/m) \\ D\ (drag) &= \frac{1}{2} C_D \rho V^2 A \quad (kg/m) \\ M\ (pitching\ moment) &= \frac{1}{2} C_M \rho V^2 B^2 \quad (kg-m/m) \end{aligned}\right\} \qquad (3\cdot2\cdot1)$$

where ρ is the air density, V is the wind velocity, A is the projected area per unit length to normal plane to two dimensional wind stream, B is the width of structure and C_L, C_D, C_M are non-dimensional aeroelastic coefficients for lift, drag & pitching moment. Additionally three dimensional aeroelastic forces are defined as the side force, the rolling and the yawing moments, but an ordinary type of long-spanned suspension bridges is considered to receive dominantly the above two-dimensional aeroelastic forces which mainly depend on the following factors; (1) Structural Factors, size, geometrical shape and configurations of members, (2) Fluidmechanical Factors, friction between structures and fluid, (3) Environmental Factors. In evaluation of above aeroelastic forces an attention should be particularly placed on the influences of the Reynolds numbers and the aspect ratio which are briefly reviewed as follows:

Influence of the Reynolds Number: The close relationship between the geometrical shape and configuration of structural members and the skin friction of the fluid on the surfaces of structural elements are known and investigated by number of researchers. Some of the results indicate the relations between the drag coefficients and the Reynolds numbers. Generally speaking, the skin friction of the fluid with the structural surfaces can vary with the wind velocity,

which attribute the change of aerodynamic coefficients to the movement of separation points of flow. For the ordinary scale for suspension bridges the Reynolds number takes

3×10^5 to 5×10^6 for main cables

2×10^6 to 4×10^7 for towers

6×10^6 to 6×10^7 for stiffening girders

and these are so bluff and squared shaped except for the cables and hangers that the separation points are considered insensitive with the wind velocity to result in little dependence of aerodynamic performance of structures on the Reynolds number.

Influence of the Aspect Ratio : As mentioned below the horizontal wind-induced force, the drag, takes an important role in consideration on the static deflectional characteristics and the static instability. According to T. von Karman the drag is characterized as

drag ---- { pressure drag ---- { induced drag / wake drag } / frictional drag }

Experimentally the relations between the lift and the drag coefficients as shown in Fig. 3.2.3 depend significantly on the aspect ratio, viz., the structural configuration. However a corrective evaluation for this relation is possible if one applies the lifting line theory by L. Prandtl so that the drag coefficient C_D is proportional to the squared lift coefficient C_L^2 and inversely proportional to the aspect ratio. Fig. 3.2.4 is the result of correction for Fig. 3.2.3 by the lifting line theory. From a practical point of views C. Scruton suggests the corrective coefficient for the drag coefficients for various aspect ratios which are also adopted in the specifications for wind resistant design for the Proposed Honshu-Shikoku Bridges in Japan.

As discussed in the preceding paragraph the static aeroelastic forces possibly cause to increase the aeroelastic instability. Some

of the fundamental consideration on aeroelastic instability taking into an account the static wind induced forces are described in the followings.

A) Selfexcited oscillations due to stationary aeroelastic forces

The instability phenomenon exemplified by oscillations of transmission lines is investigated by J. P. den Hartog[29], that is, the galloping phenomenon and the den Hartog criteria for stability is established as follows.

Let us define the resultant lift and drag forces as

$$L = \frac{1}{2}\rho V_{rel}^2 A \cdot C_L \quad , \quad D = \frac{1}{2}\rho V_{rel}^2 A \cdot C_D$$

then the lift force for the relative angle of attack $\dot{y}/V$ due tc the deflection y is

$$L_{\dot{y}} = -\left\{ \left(\frac{\partial C_L}{\partial \alpha} + C_D \right) \frac{1}{2}\rho V_{rel}^2 A \left(\frac{\dot{y}}{V} \right) \right\}$$

by which the equation of motion of a single degree of freedom with the system of mass m and spring constant k is expressed by

$$m\ddot{y} + \left(\frac{\partial C_L}{\partial \alpha} + C_D \right) \frac{1}{2}\rho V_{rel}^2 A \frac{\dot{y}}{V} + k y = 0 \qquad (3.2.2)$$

Thus the stability is determined by the conditions that

$$\begin{aligned} &\frac{\partial C_L}{\partial \alpha} + C_D > 0 && \text{stable} \\ &\frac{\partial C_L}{\partial \alpha} + C_D < 0 && \text{unstable} \end{aligned} \qquad (3.2.3)$$

In general, the drag coefficient C_D being positive the instability occurs necessarily when $\partial C_L / \partial \alpha < 0$ so that the theory by the above criteria is termed as the negative slope theory. The experimental values for aeroelastic forces acting on bridge sections are shown in

3.4 from which the negative inclination of the lift coefficient is frequently obtained for an H-type cross sectional shape of stiffening girder of suspension bridge. A usual type of cross section for suspension bridge is so arranged as to increase an aerodynamic stability, so there is scarcely possible to find the region of the negative slope for the lift coefficient-angle of attack relation. This indicates the fact that an aerodynamic instability of the galloping type is seldom expected, and it is also confirmed experimentally and theoretically by the investigation by N. Ukeguchi, H. Sakata, et al[31].

In their investigations the aerodynamic forces are assumed to act not only such directional forces as lift and drag but the pitching moment on the bridge sections to couple the deflectional and the torsional motions as written as

$$\ddot{y} + \omega_\eta^2 y = \frac{1}{2}\rho V^2 \frac{(2b)}{M}\left\{-\left(\frac{\partial C_L}{\partial \alpha} + C_D\right)\left(\varphi - \frac{\dot{y}}{V}\right)\right\}$$

$$\ddot{\varphi} + \omega_\alpha^2 \varphi = \frac{1}{2}\rho V^2 \frac{(2b)^2}{I}\left(\frac{\partial C_M}{\partial \alpha}\right)\left(\varphi - \frac{\dot{y}}{V}\right) \qquad (3.2.4)$$

where

M	:	mass per unit length (kg sec^2/m^2)
I	:	moment of inertia per unit length (kg sec^2)
ω_η , ω_α	:	circular frequencies for deflectional and torsional free vibrations (rad/ sec)
2b	:	width (m)
C_L	:	aeroelastic lift coefficient
C_D	:	aeroelastic drag coefficient
C_M	:	aeroelastic pitching moment coefficient
y	:	deflection of neutral axis (m)
φ	:	angle of rotation (rad)

Let μ, ν, τ, z, be defined as

$$\mu = \frac{M}{\frac{1}{2}\rho b^2}, \quad \nu = \frac{I}{\frac{1}{2}\rho b^4}, \quad \tau = \left(\frac{\omega_\eta}{\omega_\alpha}\right)^2, \quad z = \left(\frac{b\omega_\alpha}{V}\right)^2$$

then the Routh descriminant gives the criteria for stability as follows

$$-\left(\frac{\partial C_L}{\partial \alpha} + C_D\right) > 0 \qquad \text{(a)}$$

$$\nu z - 4\frac{\partial C_M}{\partial \alpha} > 0 \qquad \text{(b)}$$

$$\frac{\partial C_M}{\partial \alpha}(\tau - 1) > 0 \qquad \text{(c)}$$

for which the expressions (a), (b) give the galloping instability and the divergence condition to form aperiodic divergent solution, respectively. The third expression is only valid for $\partial C_M / \partial \alpha < 0$ since we have in general $\tau < 1$. Applying the above theory for the truss-type stiffening girder of suspension bridge only the divergence condition is physically valid and it results in comparatively higher critical wind velocity than the critical velocity for the flutter phenomenon, and one obtains similar tendency for the plate girder type of stiffening system. Apparently this estimation for stability does not accord with the experimental results for aerodynamic instability of suspension bridge so that it is possibly concluded that an application of the negative slope theory will be inappropriate and analysis of the aerodynamic instability of an ordinary truss-stiffened and an improved closed shaped stiffening girders of suspension bridges.

B) Lateral Torsional Buckling Instability Criteria

From the different point of views from the abovementioned an instability criteria is investigated by A. Hirai taking into an account the static aerodynamic forces on the suspension bridge proportional to the displacements[24]. The fundamental equations for this problem are written as

$$EI\eta'''' - 2H\eta'' + (\bar{M}\varphi)'' - L = 0$$

$$EC_W\varphi'''' - KG\varphi'' - \frac{H}{2}b^2\varphi'' + \bar{M}\eta'' - M_t = 0$$

where L and M_t denote the lift and the pitching moment per unit length, while $\bar{M}$ denote the resultant bending moment due to the horizontal drag force. Evaluating the above aerodynamic forces as

$$\bar{M} = \frac{C_D \rho V^2 b \ell^2}{2\sqrt{128}} \quad , \quad L = \frac{1}{2} \rho V^2 b \frac{\partial C_L}{\partial \alpha} \varphi \quad , \quad M_t = \frac{1}{2} \rho V^2 b \frac{\partial C_M}{\partial \alpha} \varphi$$

the critical stability is obtained from the above fundamental equations, where ρ is the air density, b the width, ℓ the spanlength, V the velocity, C_D the drag coefficient, $\partial C_L/\partial\alpha$ the inclination of lift coefficient and $\partial C_M/\partial\alpha$ the inclination of pitching moment coefficient.

C) Vortex Induced Oscillations

For the analysis of aeroelastic responses of structures the turbulence in the fluid takes an important role as the facts that various aeroelastic and aerodynamic effects largely depend on the magnitude and the stability of vortices. In the range of comparatively low Reynolds number the alternating stable Benard Karman trail of vortices is generated, while for the high Reynold number range one also observes a dominant periodic change of velocity in the neighbourhood of obstacles in the fluid. It is therefore considered that the vortex may excite the structures in the steady flow of low Reynolds number and in the turbulent flow of the high Reynolds number. The periodicity of the Karman vortex is observed firstly by Strouhal that the frequency N of the oscillations of the transmission lines is proportional to the wind velocity V and independent of the elastic modulus to reduce an expression as

$$S = Nd/V$$

in which d is the width of resistance area, as shown in Fig. 3.2.5, and S is termed as the Strouhal number. Experimentally Fage and Johansen obtained S = 0.15 for a plate, while Roshko found the Universal Strouhal

number S* = 0.16 by correcting the velocity and the width of structures according to the types of free stream lines, which is eventually independent from the types and shapes of structures.

The drag forces when a vortex is produced in the wake are theoretically evaluated by von Karman and the relation between the drag coefficients and the Strouhal number is analyzed experimentally by Ippen et al to yield to

$$S = \frac{0.22}{C_D}$$

This is known as the fundamental relation of the Strouhal number and the drag coefficients and for various shapes as illustrated in Fig. 3.2.6. For the suspension bridge structures the vertical oscillations are more easily produced than the horizontal lateral movement and the alternate vortex trail generates in the lateral direction to the flow the resultant periodic forces as follows

$$L = \beta \left(\frac{1}{2} \rho V^2\right) C_D \, d \, \sin \, 2\pi N t$$

in which β is the coefficient proposed by Y. Rocard[30]. The value of β takes 0.05 for a circular cross section and 0.25 to 0.30 for an ordinary type bridge structures. When the Strouhal number be 0.16 then we have

$$2\pi N = 2\pi \times 0.16 V / d \doteq V / d$$

$$\therefore \; L = \beta \left(\frac{1}{2} \rho V^2\right) C_D \, d \, \sin \, V t / d$$

Applying the above considerations for a three spans suspension bridge ($\ell_1 + \ell + \ell_1$), the natural frequencies ω_n are determined by the characteristic equations, viz.,

$$\tan \mu_n + 2 \tan \alpha \, \mu_n = (1 + 2\alpha) \, \mu_n \qquad \alpha = \ell_1 / \ell < \frac{1}{2}$$

so that

$$\omega_n^2 = \frac{16\,\mu_n^4\,EI}{m\ell^4} + \frac{g}{2f}\,\mu_n^2$$

according to Y. Rocard. When the wind acts normal to and uniform to the bridge, the lift force is vertically produced and the vortices appear as immense rolls parallel to the deck, discharged in phase along the bridge. On the contrary the anti-symmetric modes are supposed to occur, then obviously the resultant effect will cancell out to annihilate the assumed modes of vibrations. For the case $\mu_n^2 >> \mu_n^4$, the frequency is proportional to the degree of modes, n and to the wind velocity. Since the symmetrical vibrations with 2n + 1 half sine waves along the bridge receive from the vortices a resultant excitation on one half sine wave, the overall excitation of all the other half sine wave cancelling out, the amplitude of the force exciting the mode n will be proportional to 1/n. Thus according to the aerodynamic expression $\beta\frac{1}{2}\rho V^2 C_D$ the excitation of the mode n leads to the exciting force $\frac{1}{n} \times \beta C_D \frac{1}{2}\rho V^2$ which is proportional to n. For very high harmonics the natural frequencies ω tend to vary with n^2 so that the wind speed V is proportional to n^2 and consequently the exciting forces increase with n^3 for the vibrating nth modes. Applying the preceding remark for the Tacoma Narrows Bridge the lift force of 2 lbs/ft (= 3 kg/m) is required for the 9th mode under the wind celocity V = 60 ft/sec (= 19 m/sec). Y. Rocard also investigates the possibility for the bridge to vibrate stationary by the vortex excitation in the range of resonance which tendency is also experimentally observed. In the investigation by Roçard the vortex excitation is shown in a single region of the amplitude-wind velocity relations, while two or more possible stable limit cycles exist in the latter experimental results. An explanation is made for the high ranges of limit cycles as the non-linear charecteristics of excited oscillations and the other as a kind of such instability as galloping by Ohtsuki and Washizu[32].

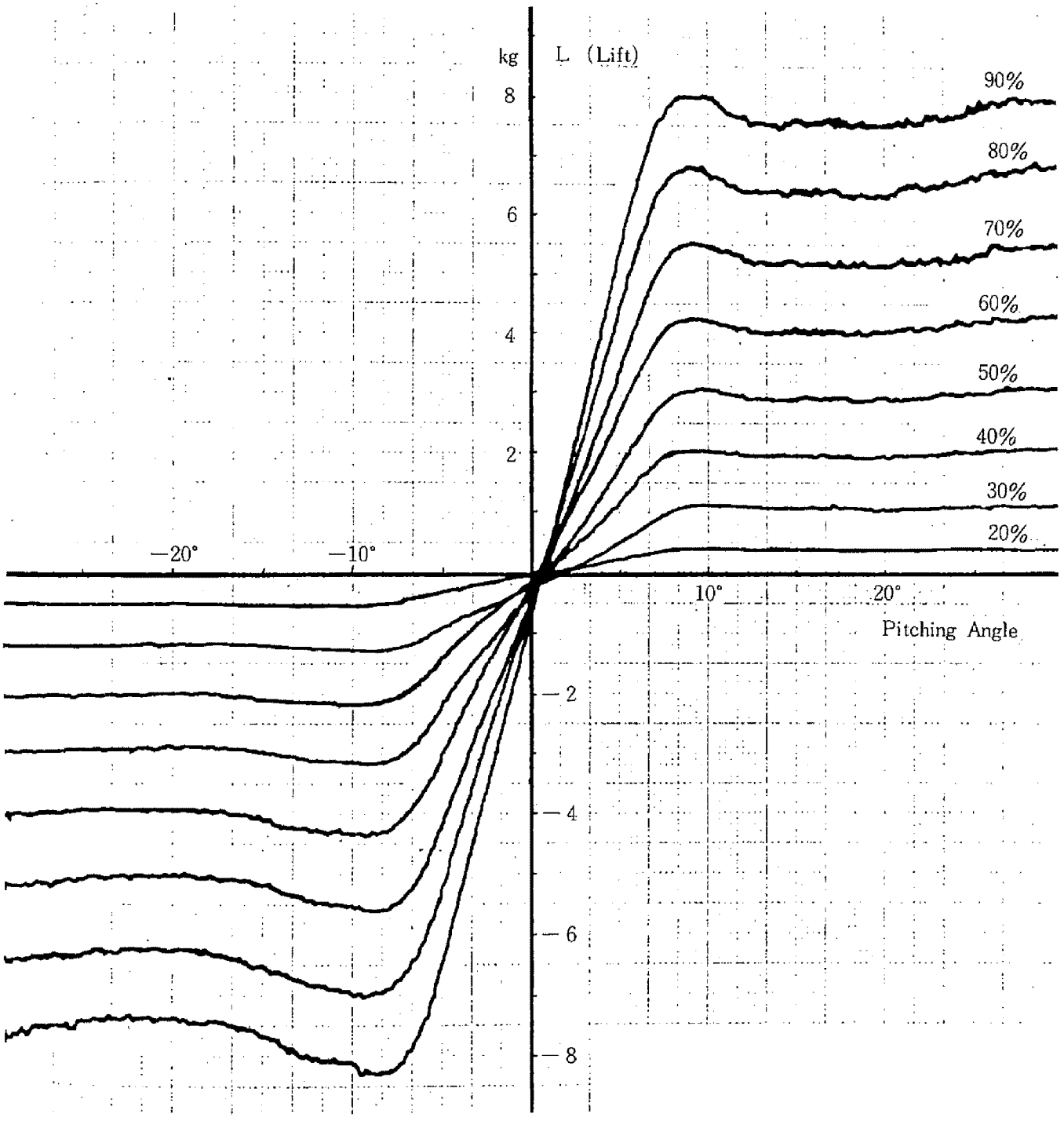

Fig. 3.2.1 Lift-Pitching Angle Relation of Plate for various wind speeds

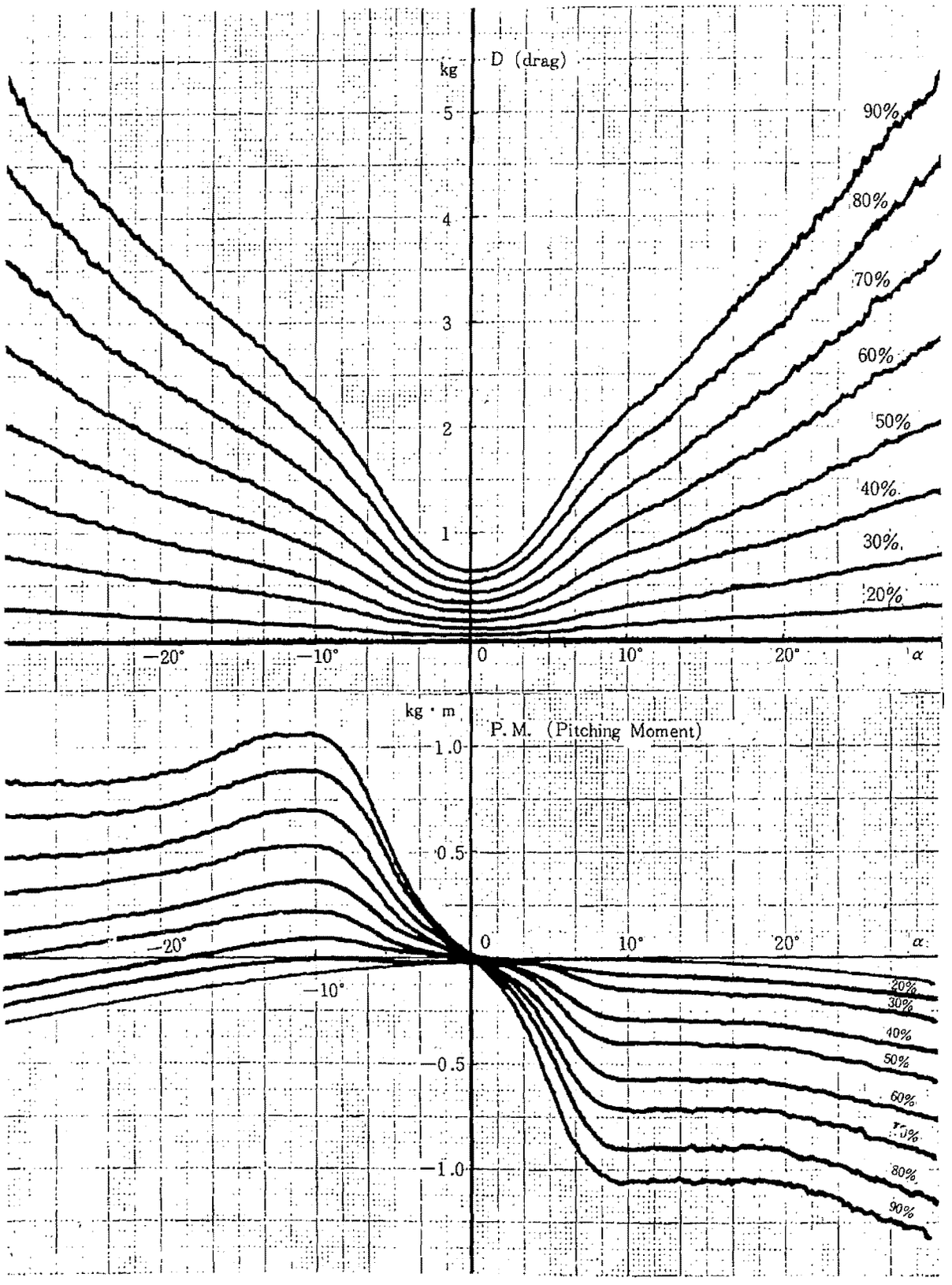

Fig. 3.2.2 Drag and Pitching Moment for Plate

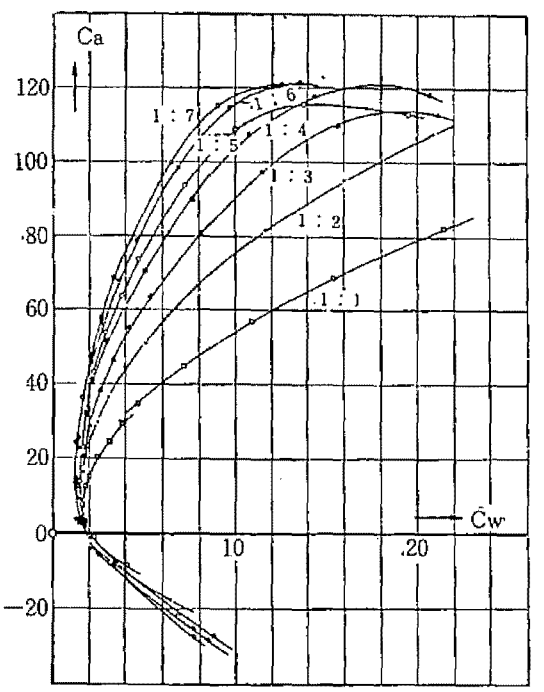

Fig. 3.2.3 Experimental values of lift coefficient Ca to drag coefficient Cw for wings of different aspect ratio (von Karman)

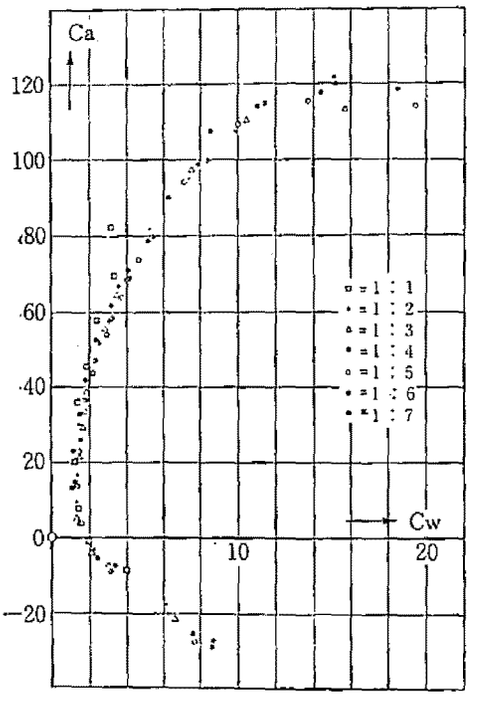

Fig. 3.2.4 Corrected relation of lift coofficient and drag coefficient by the lifting line theory (von Karman)

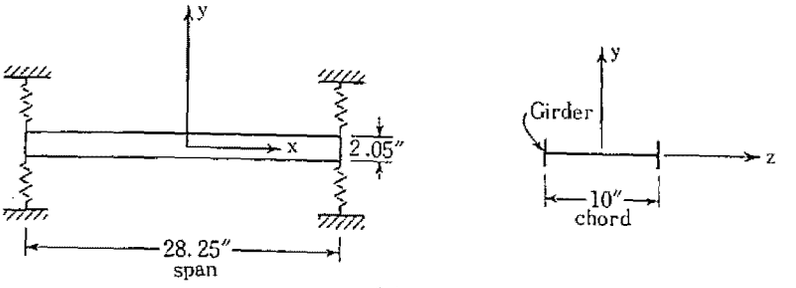

(a)

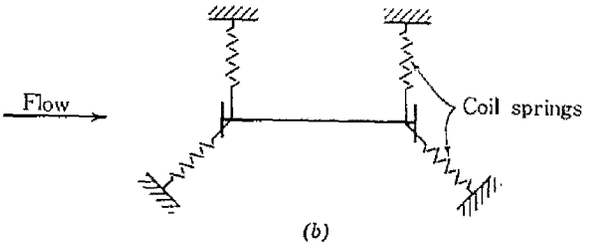

(b)

Experimental arrangments in Dunn's tests.

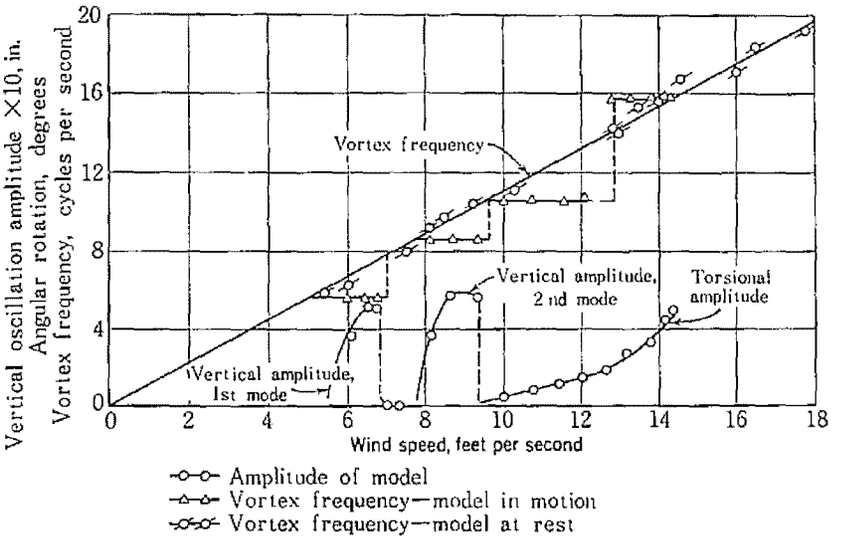

Vortex frequency vs. wind speed .

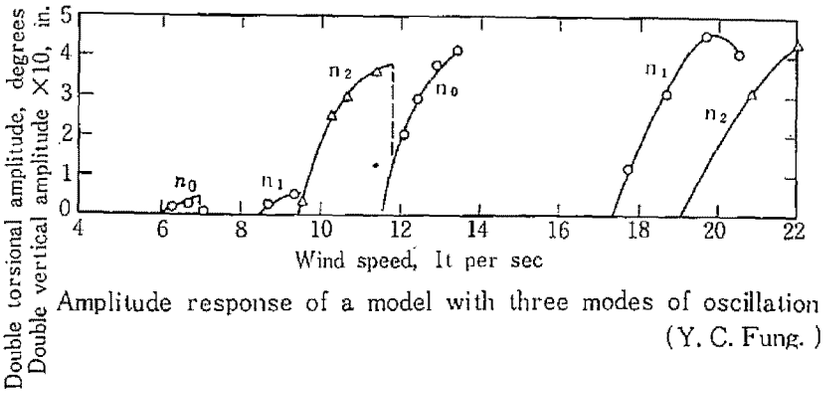

Amplitude response of a model with three modes of oscillation (Y. C. Fung.)

Fig. 3.2.5

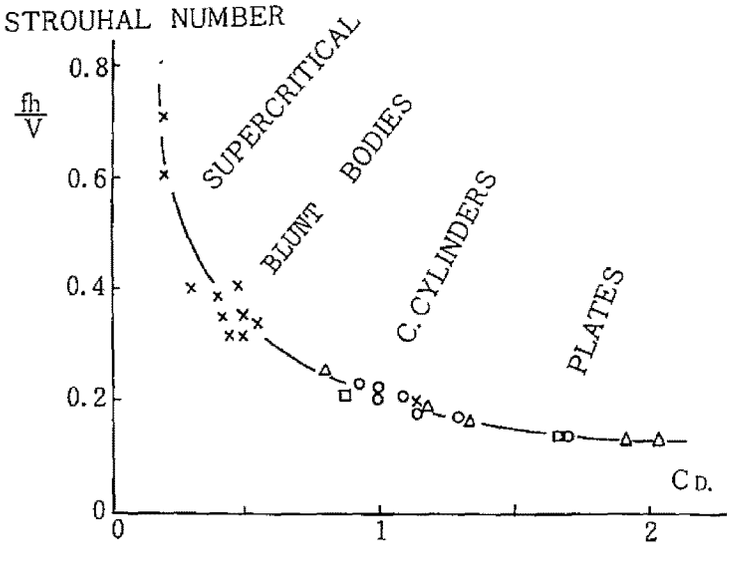

Fig. 3. 2. 6 Strouhal number and drag coefficient of various shapes in essentially two-dimensional flow, at Reynolds numbers $>10^3$. (Washizu & Ohtsuki)

3.3 DYNAMIC AEROELASTIC FORCES ON BRIDGE STRUCTURES

Aerodynamic investigations on the long-spanned suspension bridges are required inevitably for almost any kinds of projects to guranttee the most important factors of safety. For reconstruction of the Tacoma Narrows Bridge T. von Karman, F. B. Farquharson , G. Vincent et al worked to characterize the detrimental factors to cause the failure of the Tacoma Narrows Bridge and to disclose the fact that the torsional stiffness of the failed structure remains remarkably small and the stiffening girder of the so called plate girder type forms unbeneficial cross-sectional shape aerodynamically.

From the dynamic point of views the most important feature is considered as instability phenomenon of wind induced self excitation and F. Bleich[22] and Y. Rocard[30] applied the aerodynamic forces for a plate derived by T. Theodorsen for this instability problem of the classical flutter, namely the coupling of torsional and flexural vibrational modes by the wind stream. This theoretical investigation accords sufficiently with the experimental results as for the Tacoma Bridge but on the contrary explains unsatisfactorily for the Golden Gate Bridge. Phenomenologically the classical flutter is the instability due to the coupling of flexural and torsional vibrational modes, for which case the air stream is assumed to flow along the structural surface without accumlating any kinematical energy on oscillating structure. The typical feature of the classical flutter is exemplified by the fact that beyond the critical wind velocity at which the steady state remains the amplitude increase remarkably to yield to failure of the structure.

However it is already mentioned by Panovko & Gubanova et al that the stall flutter due to the separation of flow due to structural member may take an important role in characterization of unstable oscillation of a bluff structure in air stream. In such case the separated flow from structural surface may reattach with certain phase difference which results in supplying the energy to structure to form finally negative damping. It is also said that the torsional mode of vibrations becomes dominant in the stall flutter state. As for the classical flutter there

is a number of theoretical and experimental investigations to confirm this instability phenomenon, while the stall flutter is considered too complicate to investigate theoretically at the present stage. The stall flutter is caused by the flow separation around the structure in wind stream to produce the phase lag between the aerodynamic forces and the induced deformations to form the positive workdone on the oscillators from the stream. The phase lag for the classical flutter is termed as the Wagner effect which can be expressed mathematically, while for the stall flutter the phase difference varies in more involved manner so that there appear not too many references except for the instability problems for propellas, the screw blades, etc.

It should therefore be noted that the aerodynamic investigations for structures in civil engineering are comparatively involved because of the fact that the structure is not fully susceptible to streamlining and produces the turbulent flow of air even in uniform wind to cause whorls and vortices, for which case the phase lag of the aerodynamic forces and induced deformations takes inherently an important role in the resultant responses of structures.

According to Y. C. Fung[34] the stall flutter is defined as "a periodic self-excited oscillation of the structure with mass and elastic effects in the airstream which is possibly separated partially or wholy in its vibrations". Although this definition characterizes a general feature of the stall flutter, as Scanlan & Rosenbaum pointed out, the flow separation does not always produce regular periodic forces, but in some instances this separation occurs in an unstable way so that fluctuating conditions ranging from near-potential flow conditions to very turbulent conditions (buffeting) obtains. The latter type of instability is in general termed as the buffeting flutter but it is less clearly distinguished from the former. A. G. Rainy illustrates the difference as follows:

Since the buffeting is the structural response for turbulent external forces, namely the forced vibration, the force-response relation is valid only for the positive damping. For the negative damping the equilibrium

problem of the force-response relation is transformed to the stability problem, viz., the stall flutter. Thus the stall flutter and the buffeting differ from each other depending on the sign of the damping terms. General speaking for the stall flutter one observes the following characteristics:

1) The flutter velocity drops severely in comparison with the case of the classical flutter.
2) The flutter frequency rises slowly toward the natural torsional oscillation frequency of the structure in still air.
3) The torsional motion predonimates. Whereas in classical flutter the torsional strain and bending strain are of the same order of magnitude, in stall flutter the amplitude of the bending oscillation becomes negligibly small in comparison with that of the torsion, although the axis of rotation is in general not the elastic axis.
4) Usually the flutter speed reaches a minimum and rises again as the structure becomes completely stalled.
5) There is a large phase shift at the transition from classical flutter to stall flutter. The phase difference between the bending and torsion drops by about 45°, sometimes vanishing completely.
6) Variation of the structural properties of the airfoils has very different effects on the stall flutter as compared with the classical flutter. The ratio of the uncoupled bending and torsion frequencies in still air has little effect on stall flutter, for which the critical speed is often higher when the ratio is equal to 1 than at other values.

The stall flutter was for the first time observed by W. S. Farren and H. L. Stueder and investigated by R. L. Halfman et al to notice that the pitching moment - pitching angle curve near the stall angle forms the 8-shaped hysteresis to supply the positive energy from the air stream to oscillating structure in course of time.

In general the pitching moment and the angle is expressed as

$$\frac{M}{2\rho V^2 b S \alpha_0} = C_0 + \sum_j a_j \cos j\omega t + \sum_j b_j \sin j\omega t \qquad (a)$$

$$\alpha = \bar{\alpha} + \alpha_0 \sin \omega t \qquad (b)$$

where ρ ; air density
V ; wind velocity
b ; half chord length
s ; span length
α_0; amplitude
$\bar{\alpha}$; average angle of attack
ω ; circular frequency

Thus the workdone by pitching moment per one cycles is given as

$$W = \oint M d\alpha = 2\pi \rho V^2 b^2 \alpha_0^2 b_1 \qquad (c)$$

If $b_1 < 0$, then $W < 0$ gives positive torsional damping (stable) but if $b_1 > 0$, then $W > 0$ gives negative torsional damping (unstable).

Therefore the lowest coefficient b_1 of the third terms in eq. (a) contribute to the positive workdone depending on its sign, namely the characteristics of the phase lag. There appears two types of approaches for investigation on the stall flutter. The one pursues the relationship with the classical flutter and the other is to use the oscillating aerodynamic forces in separated flow, obtained experimentally. The former type of investigations is done by Victory and Mendelson. Victory introduces the torsional damping term which is obtained from the oscillation tests of large amplitude instead of that of classical flutter and showed a good accordance with the experimental result by Stueder. Mendelson obtained the relationship of the critical velocity and the

pitching angle for the stall flutter assuming the appropriate phase difference on aerodynamic restoring force and damping forces. The latter type of investigations is done by Haley, Schnittger, Sisto, Vaccaro, et al, but there remains a number of difficulties for applying these investigations on the actual design of long-spanned suspension bridges.

So far the self-excited oscillations of structures in wind stream are considered in the form of the classical flutter and the stall flutter. For the aerodynamic characteristics of the long-spanned suspension bridges it is obviously noticed that both types of instabilities should be considered depending on the geometrical shapes and configurations of stiffening girders. Recently an attention is paid on the direct measurement of aerodynamic forces in oscillating structure by use of the so called free vibration method and the forced vibration method.

The fundamental equations for a linear system of two degrees of freedom in air stream are written[28] as

$$\ddot{\eta} + 2\zeta_\eta \omega_\eta \dot{\eta} + \omega_\eta^2 \eta = H_1 \dot{\eta} + H_2 \dot{\varphi} + H_3 \varphi \qquad (3\cdot3\cdot1)$$

$$\ddot{\varphi} + 2\zeta_\alpha \omega_\alpha \dot{\varphi} + \omega_\alpha^2 \varphi = A_1 \dot{\eta} + A_2 \dot{\varphi} + A_3 \varphi \qquad (3\cdot3\cdot2)$$

where
- η ; deflection
- φ ; torsional angle
- ζ_η, ζ_α ; damping ratio in vertical, torsional oscillations in still air
- ω_η, ω_α ; natural frequencies in uncoupled vertical, torsional oscillations
- H_i, A_i $(i=1.2.3)$; aerodynamic coefficients

The above introduced aerodynamic coefficients yield for a plate to

$$H_1^* = \frac{m}{\rho\omega b^2} H_1 = -2A_1^* = -\frac{2\pi}{k}|C(k)| \qquad A_1^* = \frac{I_\rho}{\rho b^3 \omega} A_1 = \frac{\pi}{k}|C(k)|$$

$$H_2^* = \frac{m}{\rho\omega b^3} H_2 = -\left(\frac{\pi}{k} + A_1^*\right) \qquad A_2^* = \frac{I_\rho}{\rho b^4 \omega} A_2 = \frac{1}{2}\left(A_1^* - \frac{\pi}{k}\right) \qquad (3\cdot3\cdot3)$$

$$H_3^* = \frac{m}{\rho\omega^2 b^3} H_3 = -\frac{2}{k} A_1^* \qquad A_3^* = \frac{I_p}{\rho b^4 \omega^2} A_3 = \frac{A_1^*}{k}$$

Based on eq's (3.3.1) and (3.3.2) Scanlan and Sabzevari measured the aerodynamic coefficients for an ordinary type of bridge models to note that the coefficient A_2 in above expression takes the most important role. For a plate this coefficient remains negative, while for a truss type of cross section it remains positive.

Alternatively Ukeguchi and Sakata[27] applied the forced vibration method for measurement of aerodynamic forces for oscillating structure for which the lift and the pitching moment for steady motion are written as

$$L = \frac{\pi\rho b^3 \omega^2}{m} \left\{ C_{\ell h} \frac{\eta_0}{b} + C_{\ell \alpha} \alpha_0 \right\} \tag{3·3·4}$$

$$M = \frac{\pi\rho b^4 \omega^2}{I} \left\{ C_{mh} \frac{\eta_0}{b} + C_{m\alpha} \alpha_0 \right\} \tag{3·3·5}$$

for which

$$\begin{aligned} C_{\ell h} &= (C_{\ell h})_R + i (C_{\ell h})_I \\ C_{\ell \alpha} &= (C_{\ell \alpha})_R + i (C_{\ell \alpha})_I \\ C_{mh} &= (C_{mh})_R + i (C_{mh})_I \\ C_{m\alpha} &= (C_{m\alpha})_R + i (C_{m\alpha})_I \end{aligned} \tag{3·3·6}$$

As far as the linear aeroelastic characteristics of bridge structures are concerned, the aerodynamic instability problem should be considered as the most important factor for the safety of the structures and its typical patterns are given as the classical flutter and the stall flutter depending as the geometrical shapes of cross sections and the aerodynamic characteristics of structures. These features are at the present stage best known and confirmed experimentally for which one may apply the forced vibration method or the free vibration method. In this paper the application of the free vibration method for evaluation of

aerodynamic coefficients is discussed and the fundamental consideration on various types of stiffening girders of suspension bridges is given in the following paragraphs.

3.4 AEROELASTIC CHARACTERISTICS AND STATIC WIND TUNNEL TESTS

As previously reviewed in 3.2 the static aeroelastic forces on the structures in the air stream are considered to cause the various types of instability phenomena and also they take an important role in the structural design for the static forces. The main difficulties on the aeroelastic analysis of the bridge structures are due to the complexity of structural configuration of bridges and the bluffness of the members. Though there are closed forms of theoretical solutions for induced aeroelastic forces for several simple cross sections such as plates, cylinders and airfoils, the bridge cross sections, on the contrary, are aeroelastically so complicate that the turbulences due to various fluid-mechanical discontinuities and singularities can not be solved analytically yet. Whatever the bridge sections be, ordinary trussed girder type or modern streamlined box type, additional stiffening members such as handrails, road-lamp-poles, etc., cause inevitably to the disturbance of the stream lines to result in the particular types of aeroelastic forces. Therefore, at present, an experimental analysis is considered as the most reliable method of evaluation of the aeroelastic forces acting on the bridge structures.

In this investigation the non-dimensional aeroelastic coefficients for lift, drag and piticing moment (C_L, C_D, C_M) are determined by using the section models as illustrated in Tables 3.4.1 and 3.4.2. In order to disclose the fundamental aeroelastic properties of bridge section, the models simply consist of deck with two girders and two end plates; two types of girders are employed namely trussed and plate girder with or without lower flanges and three slots are placed in the deck as shown in the tables. The static aeroelastic experiment is performed by use of the following equipments.

The Eiffel type Wind Tunnel (Mitsubishi Heavy Industry Co., Ltd) is used by which wind velocity can vary continuously up to 25 m/sec at the maximum which is considered two dimensionally uniform throughout the effective cross section of 1.5 x 2.5 m^2. (Photo 3.1)

Lift, Drag and Pitching Moment are measured and recorded independ-

ently on the X-Y recorders by the Shimadzu Six Components Pyramidal Balance (Shimadzu Seisakusho Co., Ltd) (Photo 3.2)

Wind velocity is measured by the Betz type Manometer and the NPL type Pitot tube (Rikasieki Kogyo Co., Ltd)

The experimental results are illustrated in Fig. 3.4.1 to Fig. 3.4.13 for the aeroelastic coefficients C_L, C_D, C_M versus the pitching angle, from which the following characteristics are mentioned:

(i) Effects of the girder types

a) The lift coefficient C_L curve; The truss-stiffened models show eventually the similar tendency of variation of induced lift force as the case of the plates. The lift force increases almost linearly with the pitching angle up to 15°, beyond which the variation tends to vanish to be almost parallel to the abscissa. For the plate girder type a region of the negative inclination appears clearly and the higher the height of girder, the wider region of pitching angle in which the negative slope of the lift curve appears is obtained.

b) The drag coefficient C_D curve; The drag curves obtained vary in general concavely for both truss and plate girder types, while the magnitudes are significantly different; namely the drag forces induced for the plate girder types are more than twice as large as those for the truss types.

c) The pitching moment foefficient C_M curve; The variation of the pitching moment ciefficient seems to be considered apparently similar with the variation of the lift coefficient for both the truss models and the plate girder models.

(ii) Effects due to Slots of Deck

From the fluidmechanical point of views the existence of slots of deck never fails to disturb the stream lines to induce the complicate variation of aeroelastic forces with respect to the change of pitching angle. Obviously the lift forces are reduced for trussed type girder

with slit deck so that the inclination of lift coefficient curve $(\partial C_L/\partial\alpha)_{\alpha=0}$ is largely reduced. For the plate girder $(\partial C_L/\partial\alpha)_{\alpha=0}$, which is negative in this case, also is reduced though the region of the negative slope becomes wider.

(iii) Effect of Flanges

For the plate girder type the flanges take an important role in the design of structures. However the existence of flanges aeroelastically tends to increase the negative inclination of lift and pitching moment curves as well as the drag forces for the solid deck, while, on the contrary, it decreases the negative inclination of the lift coefficient curve for the slit deck.

(iv) Influence of the ratio of the width to height (b/d)

As for the trussed girders type models the exposed areas for the wind pressure being comparatively small, the effect due to various height of girders is relatively small; while as for the plate girders type models the higher the height of girders the more inclined the negative slope of the lift curve. When the ratio of the width to height remains larger than about 3.0, there appears very little tendency of the negative slope in the lift curve so that the induced aeroelastic forces are considered to be determined by the characteristics of the decks.

In order to analyze the aeroelastic charecteristics of the plate girder type model a different series of experimental study is performed in which the 18 kinds of models are used, as shown in Table 3.4.2. The results of the lift coefficients are given in Table 3.4.3 by which the most significant factor, the inclination of lift coefficient curve, indicates the tendency that, the higher the height, the more unstable characteristics increase. Typical relations of the aeroelastic coefficients versus the pitching angle are also illustrated in Figs. 3.4.11, 3.4.12 and 3.4.13. From these it is considered that as long as the

pitching angle changes within $\pm 5^{\circ}$ the slot configuration as given as the I-type is responsible for the smaller magnitudes of aeroelastic forces. Though the numbers and kinds of models are so limited, the above results apparently confirm the previous results done by various investigators and it is therfore concluded that the trussed models behave so similarly as the plate while the plate girders models show quite different types of the induced forces depending on the position of deck, the height to width ratio, the slot configurations, the types of flanges, etc.

Table 3.4.1

Width / height	x	Type of Model	Cross Section	Type of Model	Cross Section
3.0	0.50	A−T T A−P P	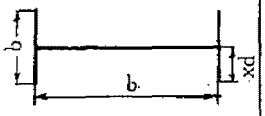	A−T T−S A−P P−S	
3.0	0.75	A′−T T A′−P P	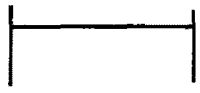	A′−T T−S A′−P P−S	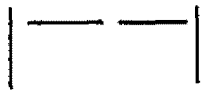
3.0	1.00	A″−T T A″−P P		A″−T T−S A″−P P−S	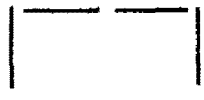
3.0	0.50	A−T T−F A−P P−F		A−T T−F S A−P P−F S	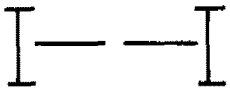
3.0	0.75	A′−T T−F A′−P P−F	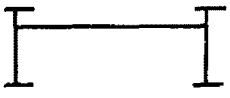	A′−T T−F S A′−P P−F S	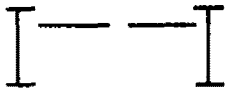
3.0	1.00	A″−T T−F A″−P P−F		A″−T T−F S A″−P P−F S	
2.0	0.50	B−T T B−P P		B−T T−S B−P P−S	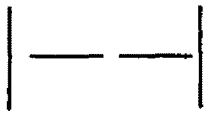
2.0	0.50	B−P P−F	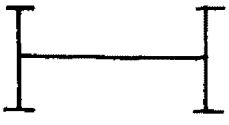	B−P P−F S	
1.5	0.50	C−T T C−P P	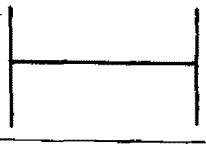	C−T T−S C−P P−S	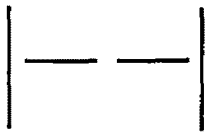
1.5	0.50	C−P P−F		C−P P−F S	

Table 3.4.2

Type	height mm	height / width	Cross-section
D P 40	40	0.133	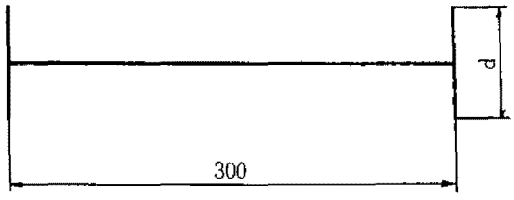
D P 60	60	0.200	
D P 80	80	0.267	
E P 40	40	0.133	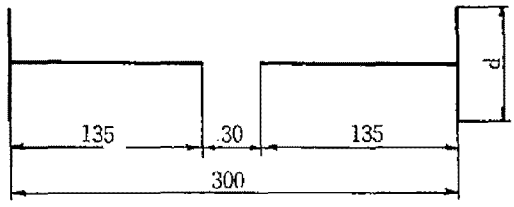
E P 60	60	0.200	
E P 80	80	0.267	
F P 40	40	0.133	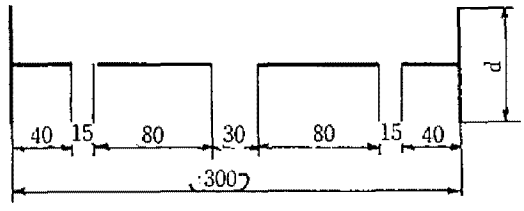
F P 60	60	0.200	
F P 80	80	0.267	
G P 40	40	0.133	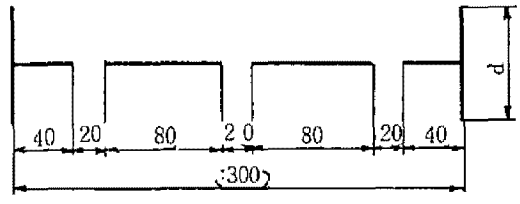
G P 60	60	0.200	
G P 80	80	0.267	
H P 40	40	0.133	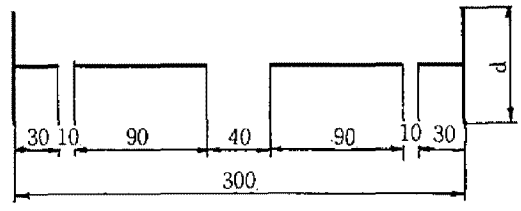
H P 60	60	0.200	
H P 80	80	0.267	
I P 40	40	0.133	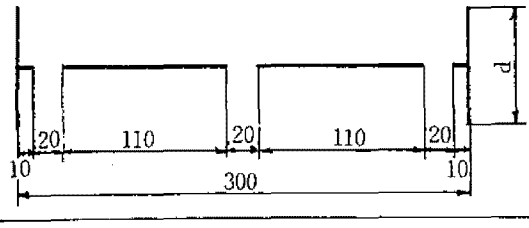
I P 60	60	0.200	
I P 80	80	0.267	

Table 3. 4. 3

Type	$(C_L)_{\alpha=5°}$	$(C_L)_{\alpha=-5°}$	$\triangle C_L$	$(\partial C_L/\partial\alpha)_{\alpha=0}$
DP 40	1.05	−0.44	1.49	8.54
60	0.64	−0.21	0.85	4.87
80	0.29	−0.03	0.32	1.83
EP 40	0.66	−0.41	1.07	6.10
60	0.25	−0.05	0.30	1.74
80	0.23	0.00	0.23	1.32
FP 40	0.59	−0.07	0.66	3.78
60	0.31	0.03	0.28	1.60
80	0.18	0.06	0.12	0.69
GP 40	0.56	0.04	0.55	3.13
60	0.25	0.10	0.15	0.86
80	0.16	0.10	0.06	0.34
HP 40	0.59	−0.09	0.68	3.90
60	0.28	0.08	0.20	1.15
80	0.09	0.06	0.03	0.17
IP 40	0.47	−0.07	0.54	3.09
60	0.12	0.04	0.08	0.46
80	0.11	0.17	−0.06	−0.34

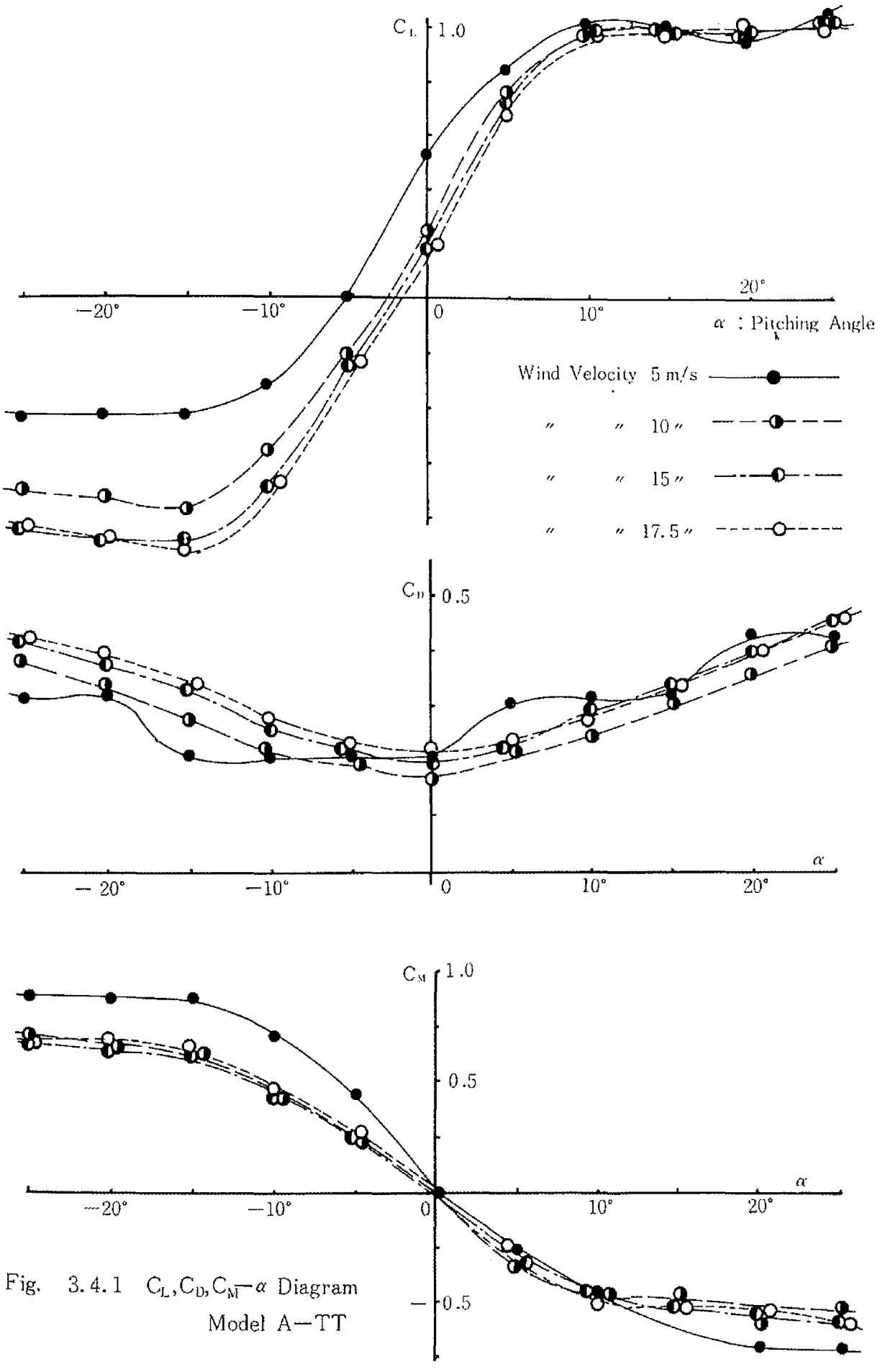

Fig. 3.4.1 $C_L, C_D, C_M - \alpha$ Diagram
Model A—TT

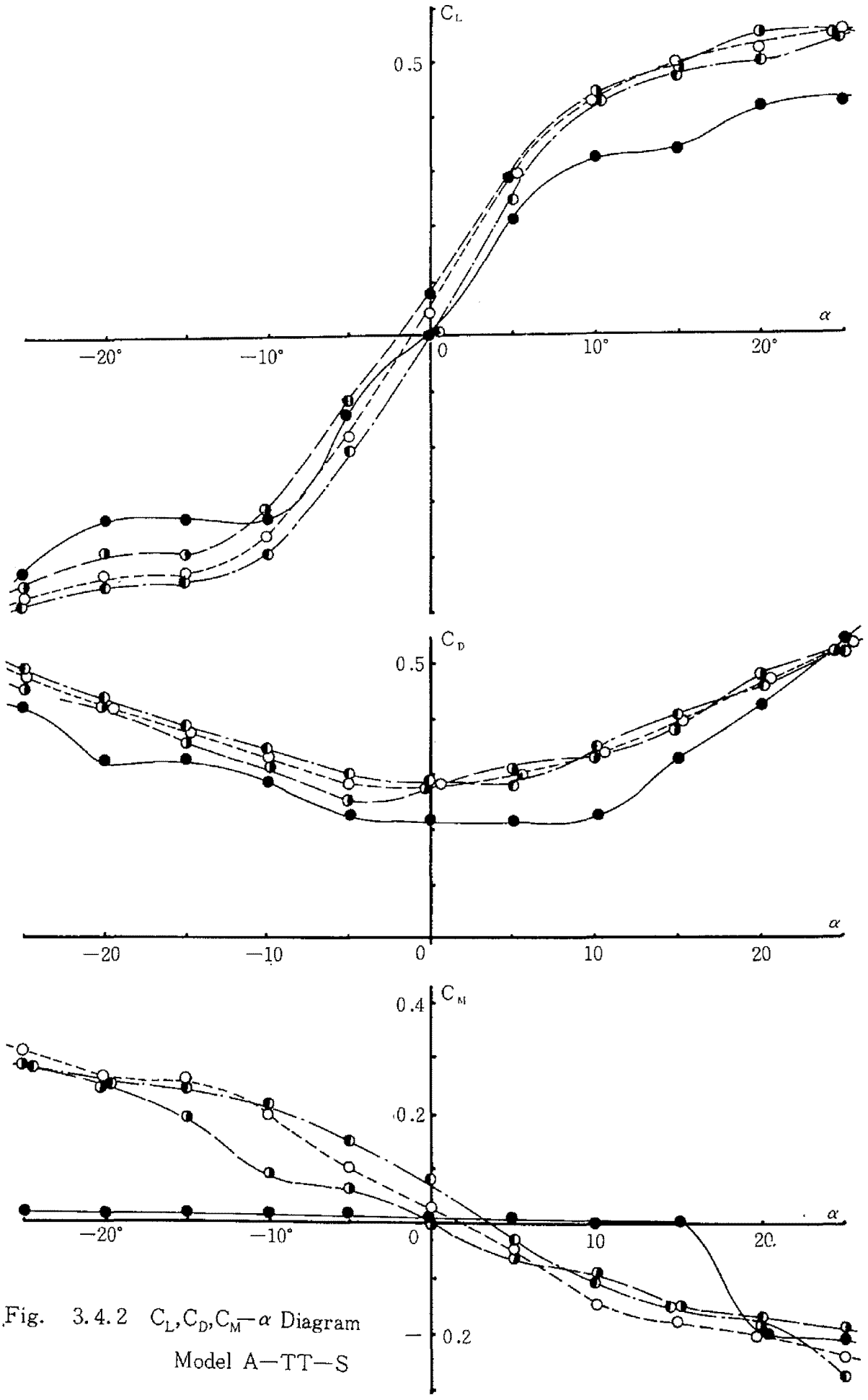

Fig. 3.4.2 $C_L, C_D, C_M - \alpha$ Diagram
Model A—TT—S

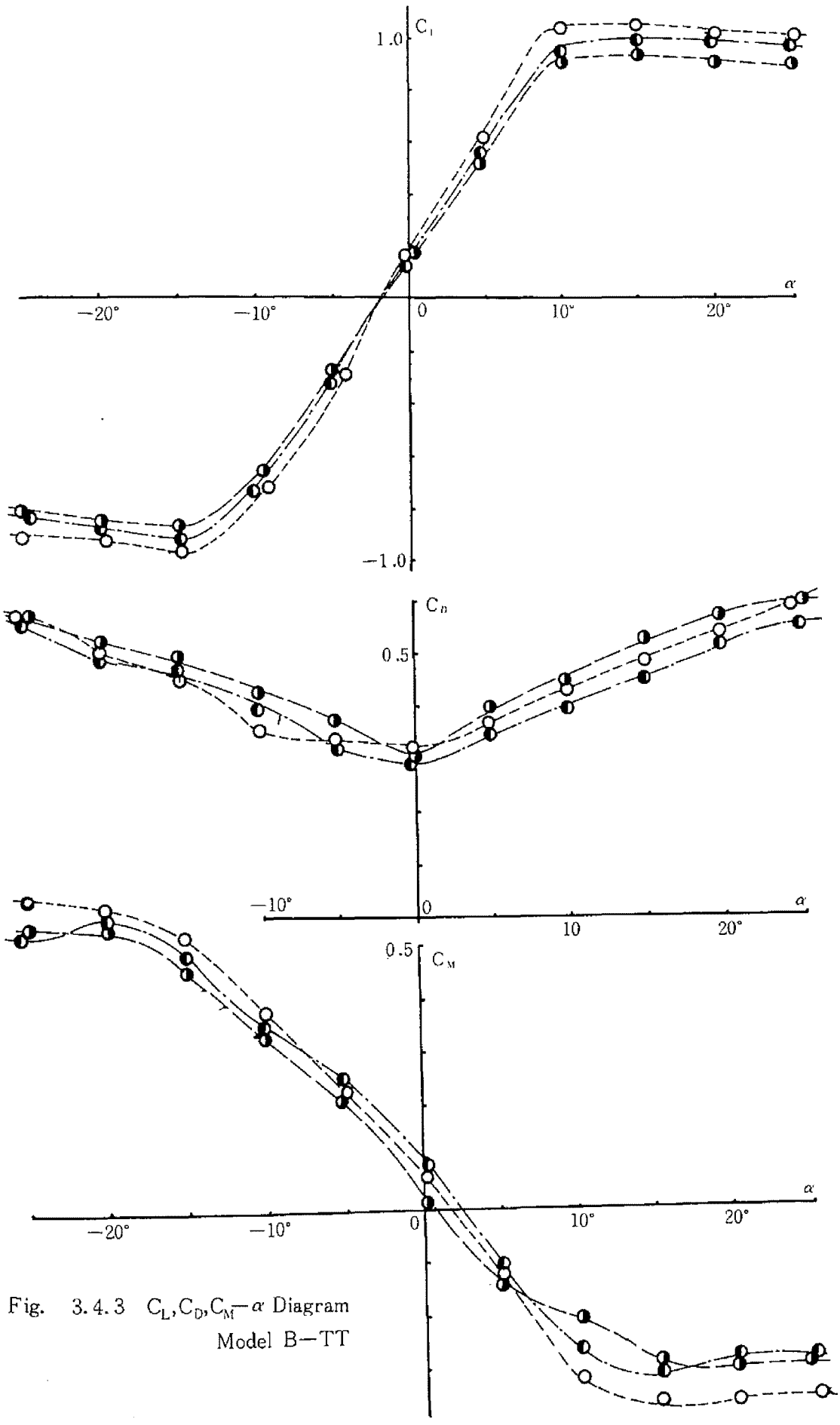

Fig. 3.4.3 $C_L, C_D, C_M - \alpha$ Diagram
Model B—TT

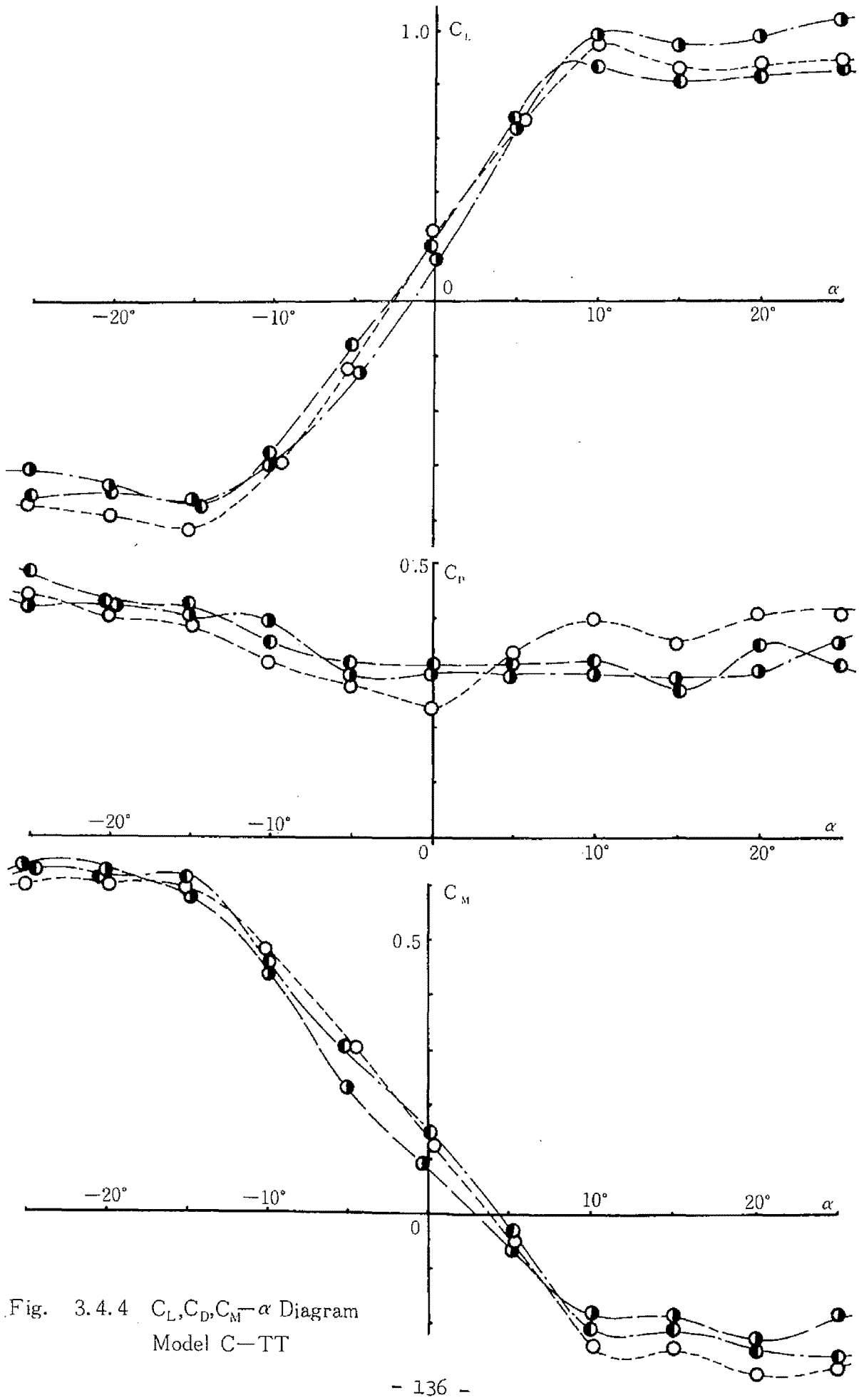

Fig. 3.4.4 $C_L, C_D, C_M - \alpha$ Diagram
Model C—TT

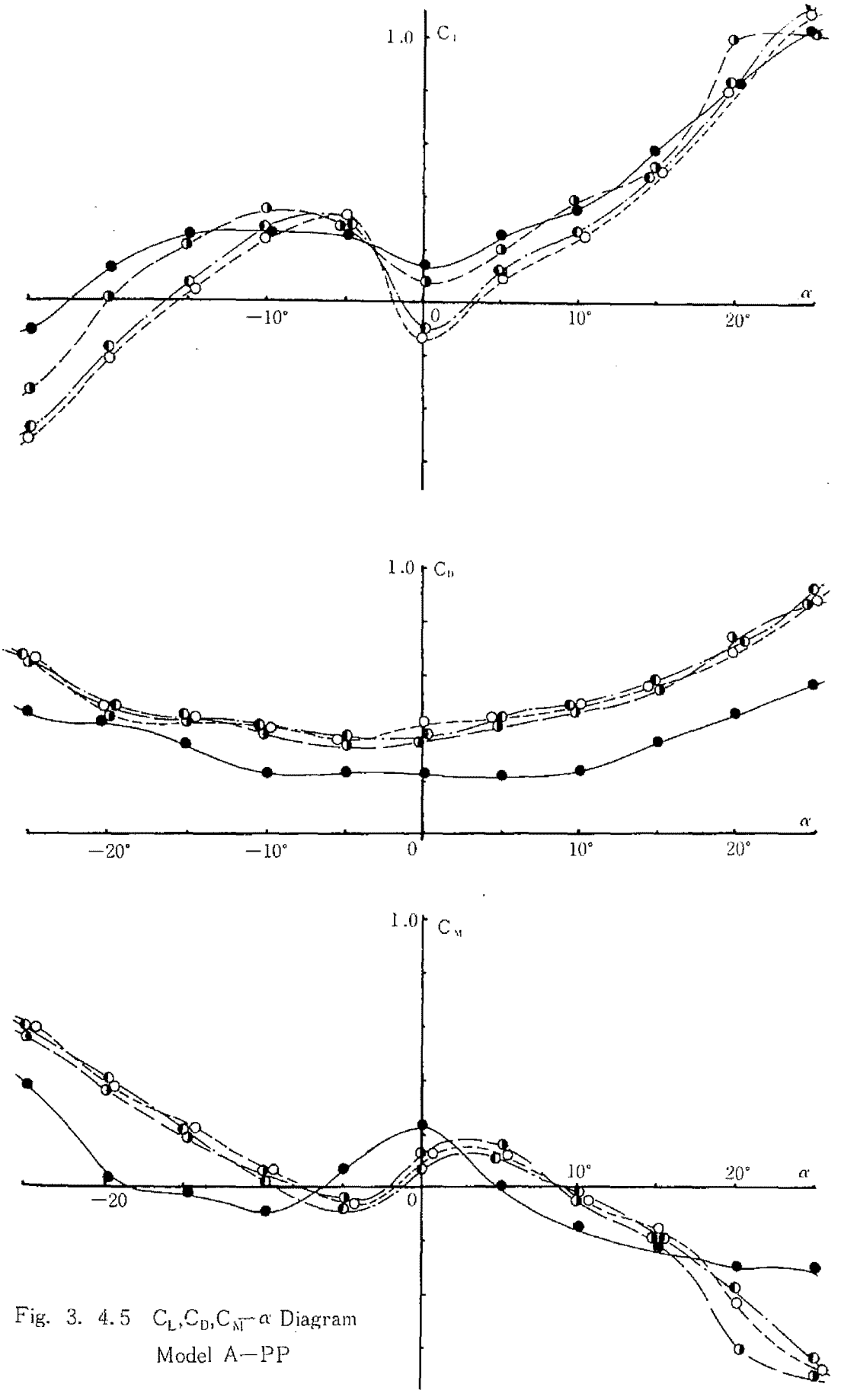

Fig. 3. 4.5 C_L, C_D, C_M—α Diagram
Model A—PP

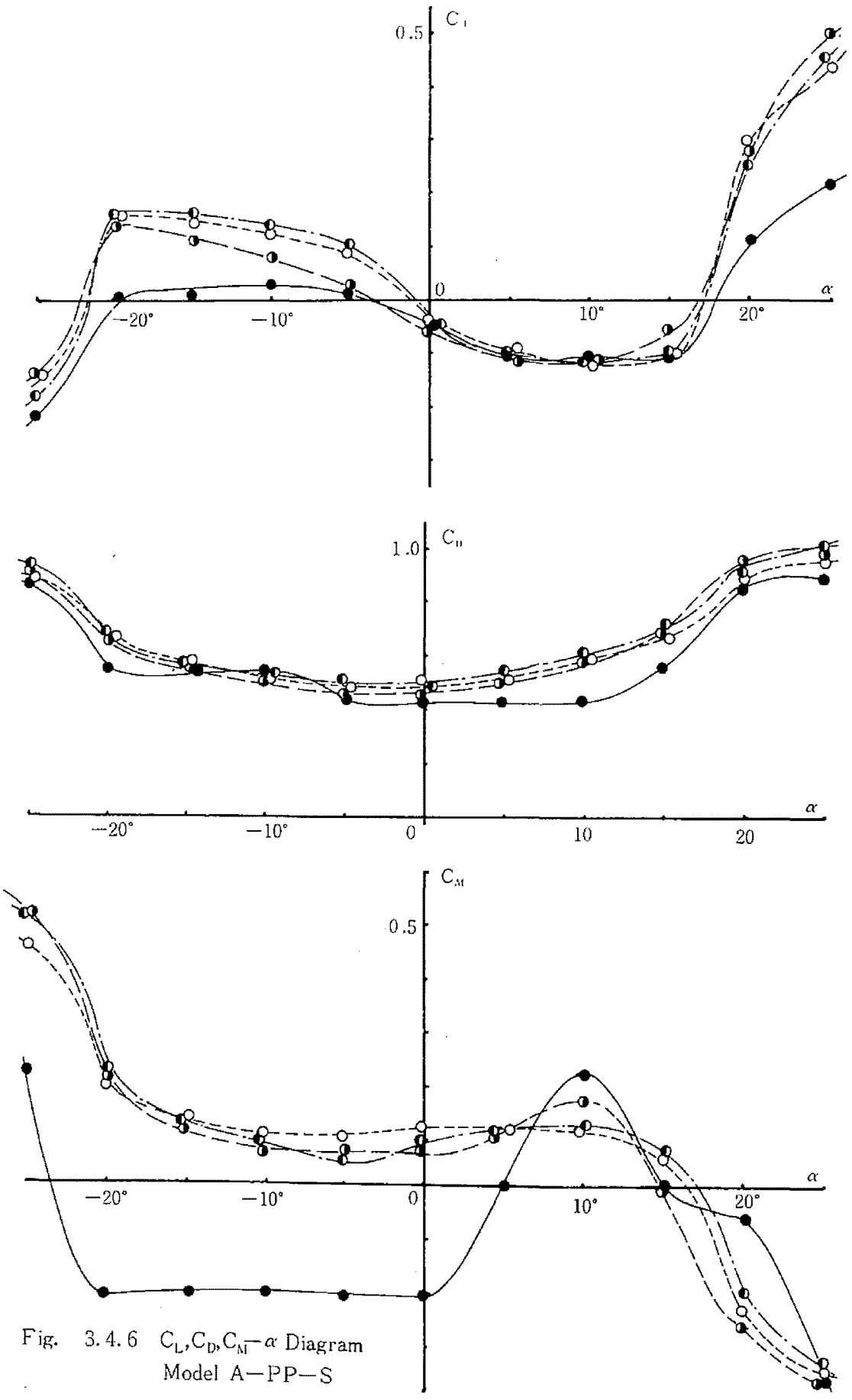

Fig. 3.4.6 $C_L, C_D, C_M - \alpha$ Diagram
Model A—PP—S

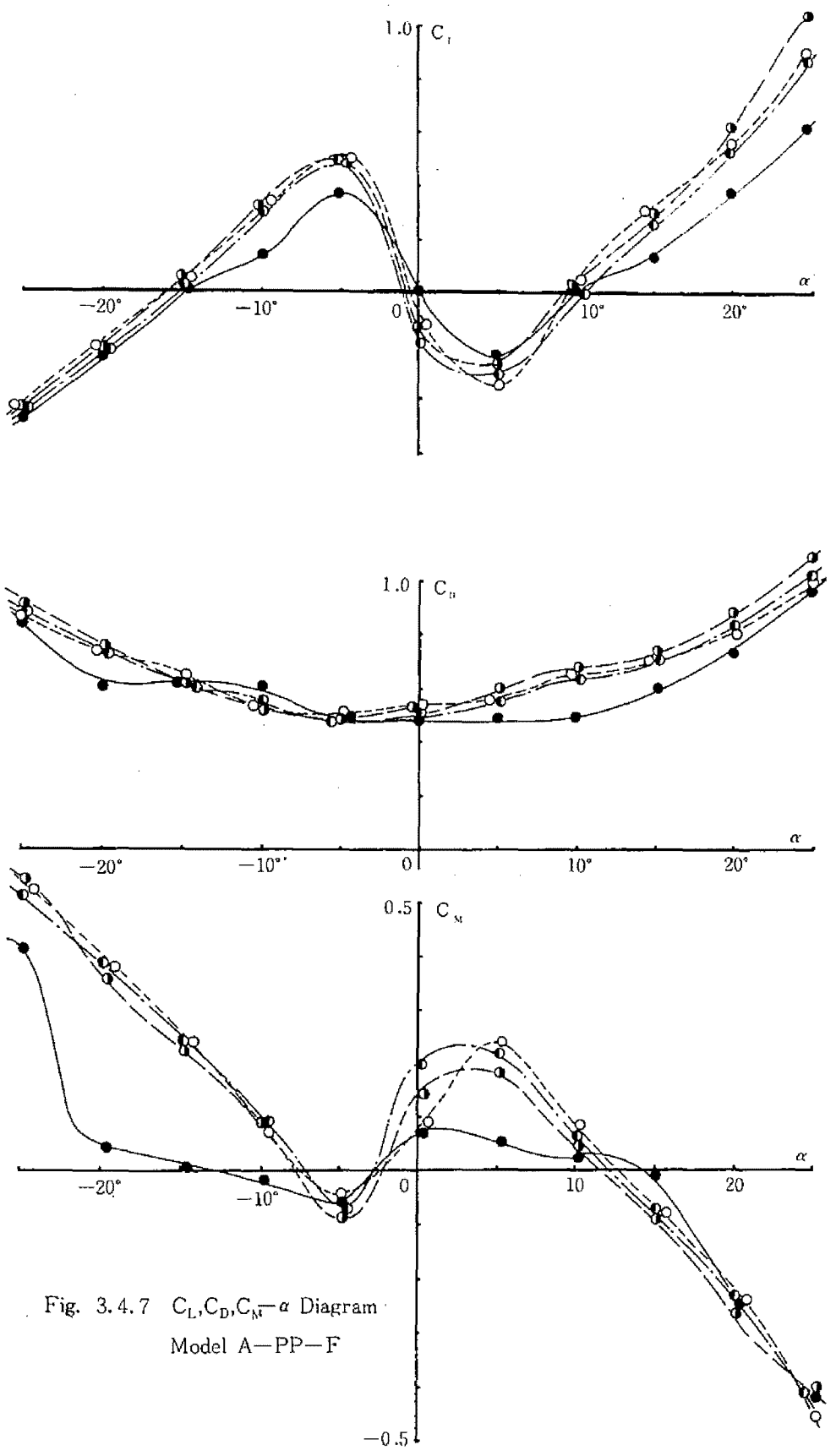

Fig. 3.4.7 $C_L, C_D, C_M - \alpha$ Diagram
Model A—PP—F

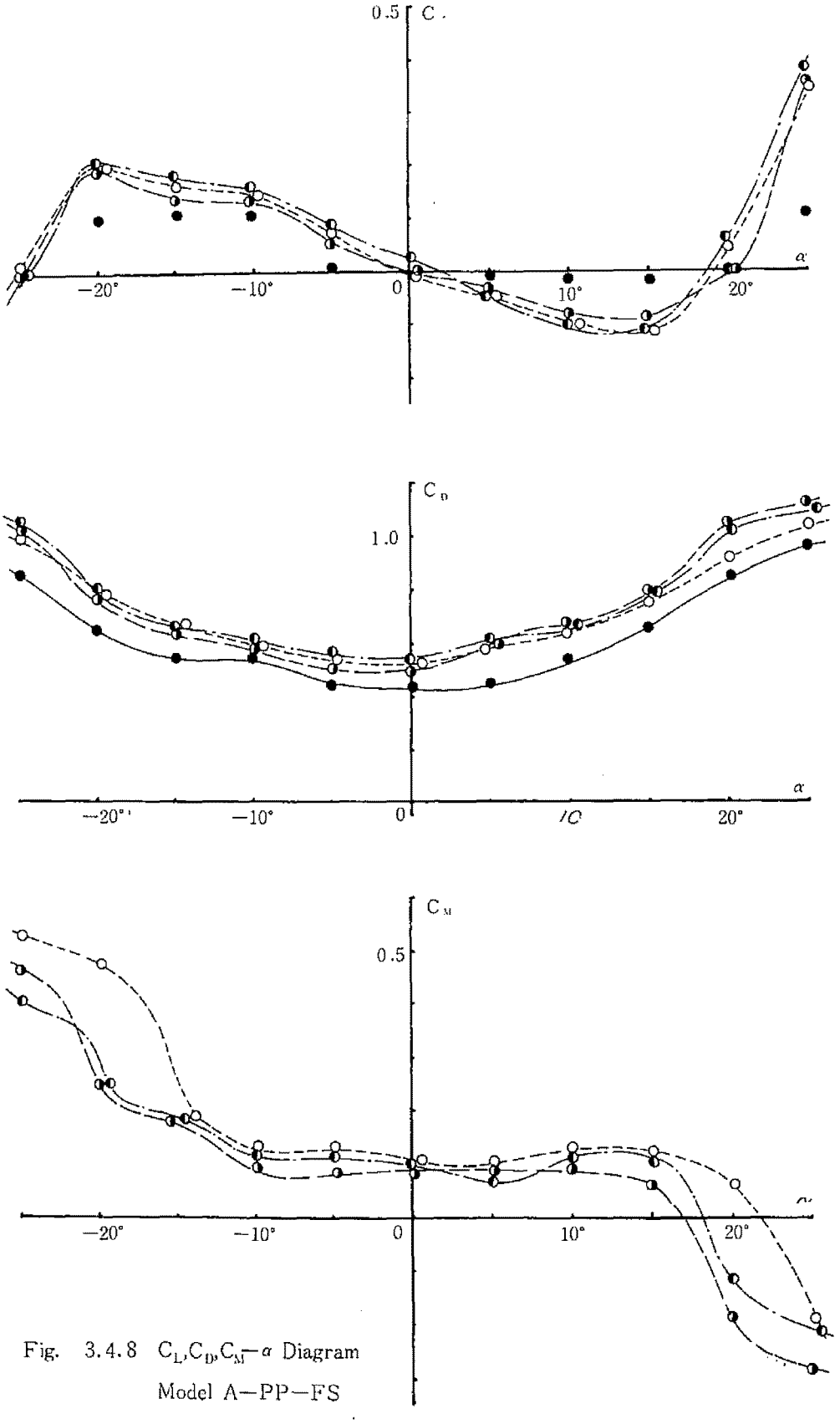

Fig. 3.4.8 $C_L, C_D, C_M - \alpha$ Diagram
Model A—PP—FS

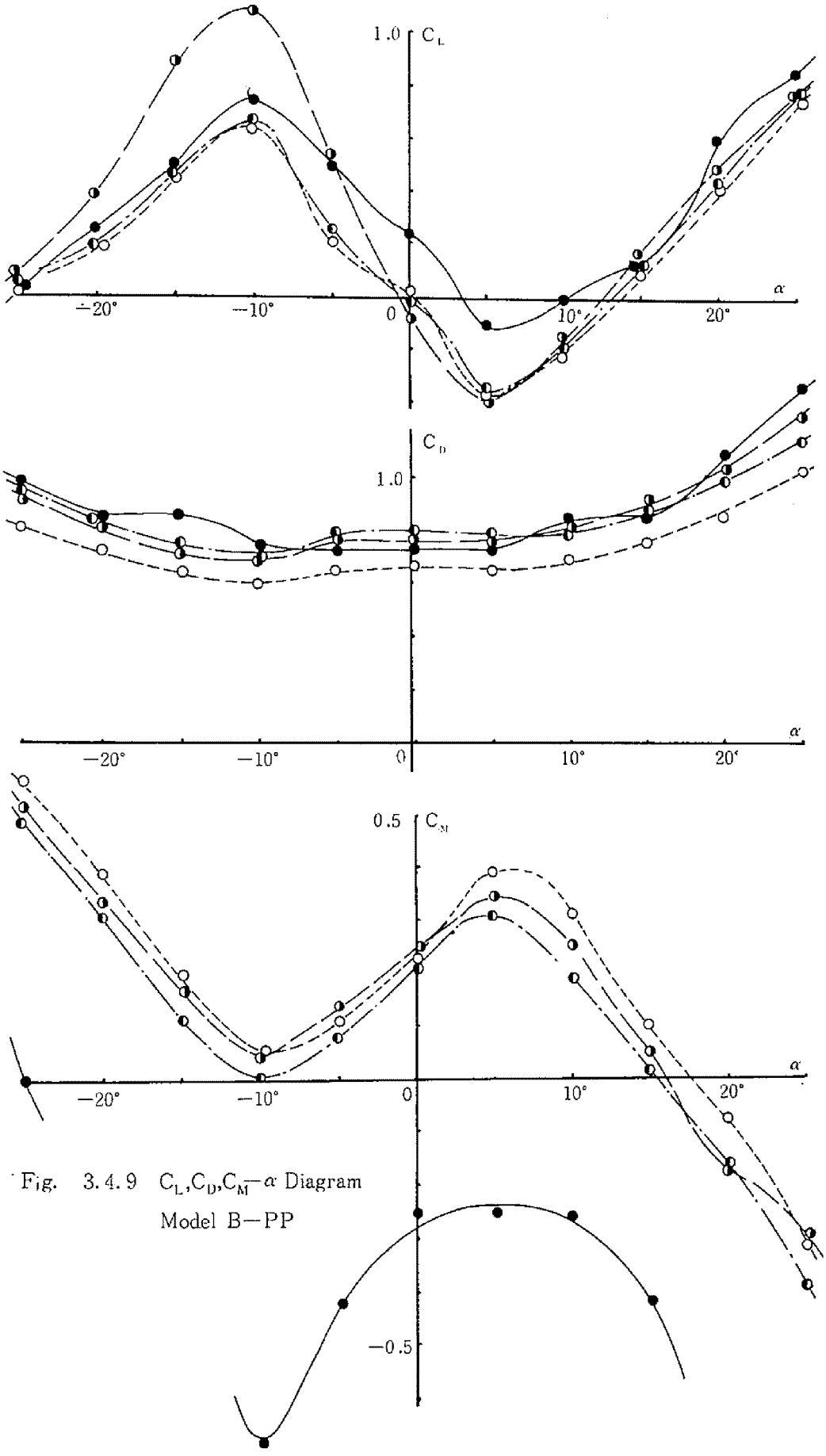

Fig. 3.4.9 C_L,C_D,C_M—α Diagram
Model B—PP

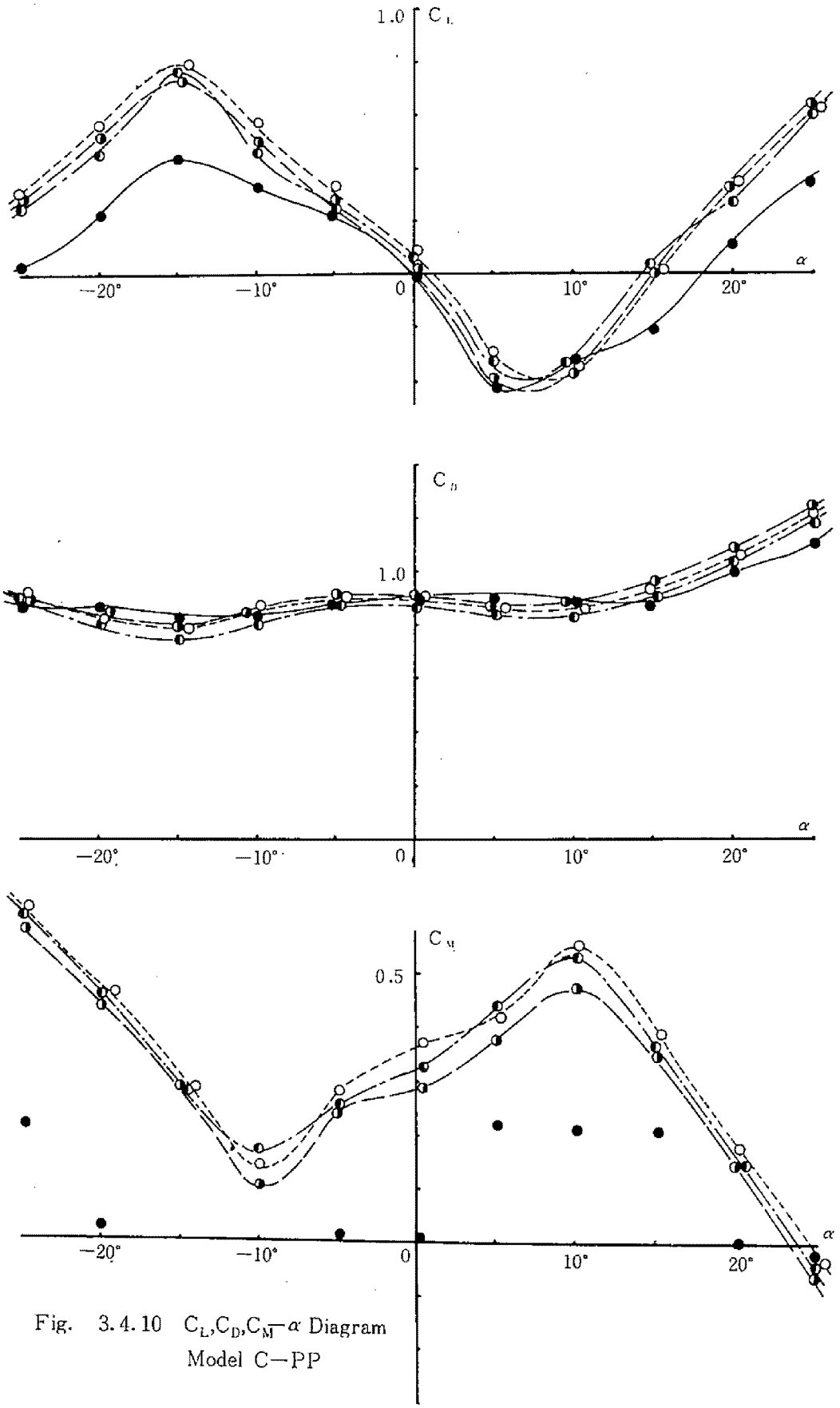

Fig. 3.4.10 $C_L, C_D, C_M - \alpha$ Diagram
Model C—PP

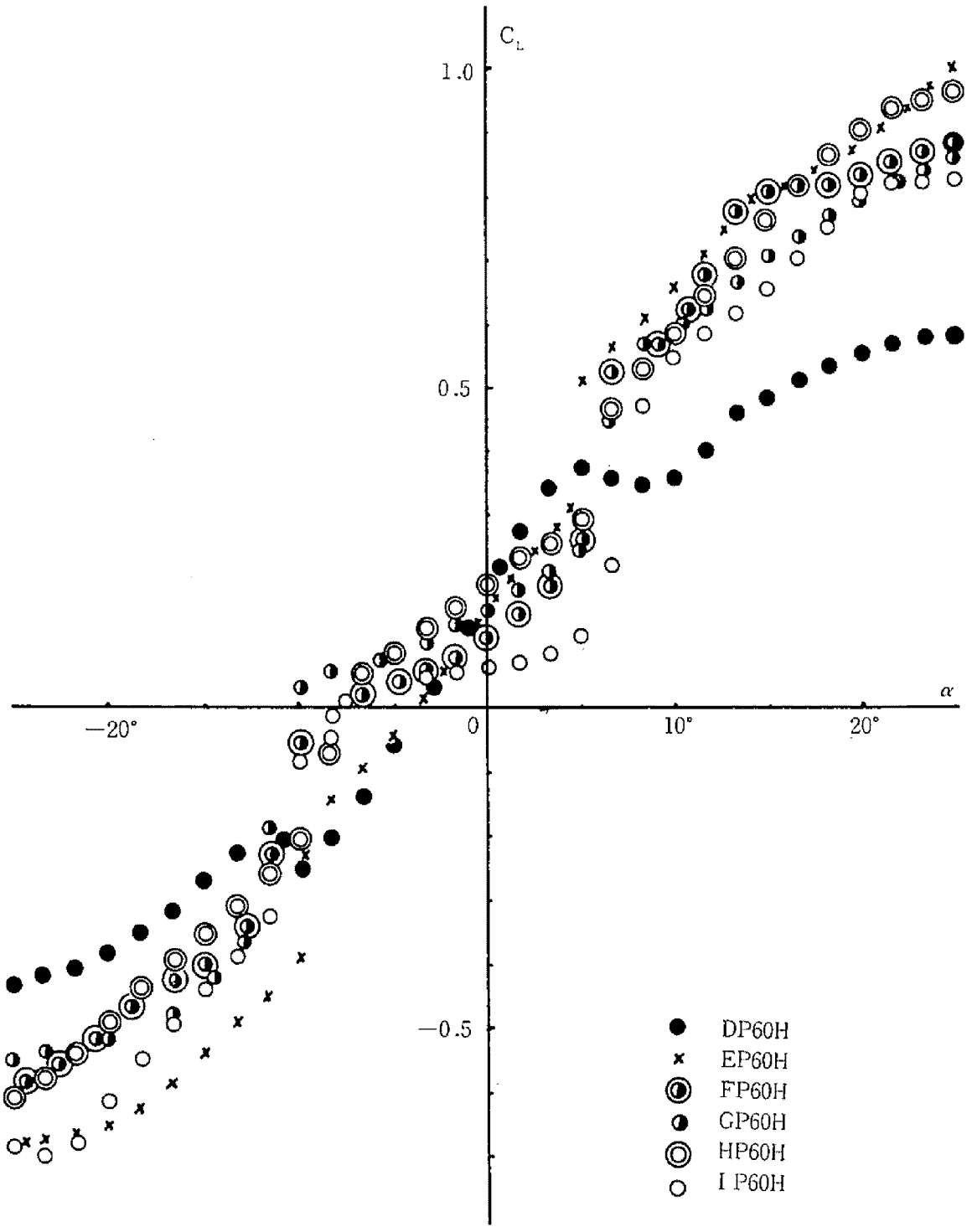

Fig. 3.4.11

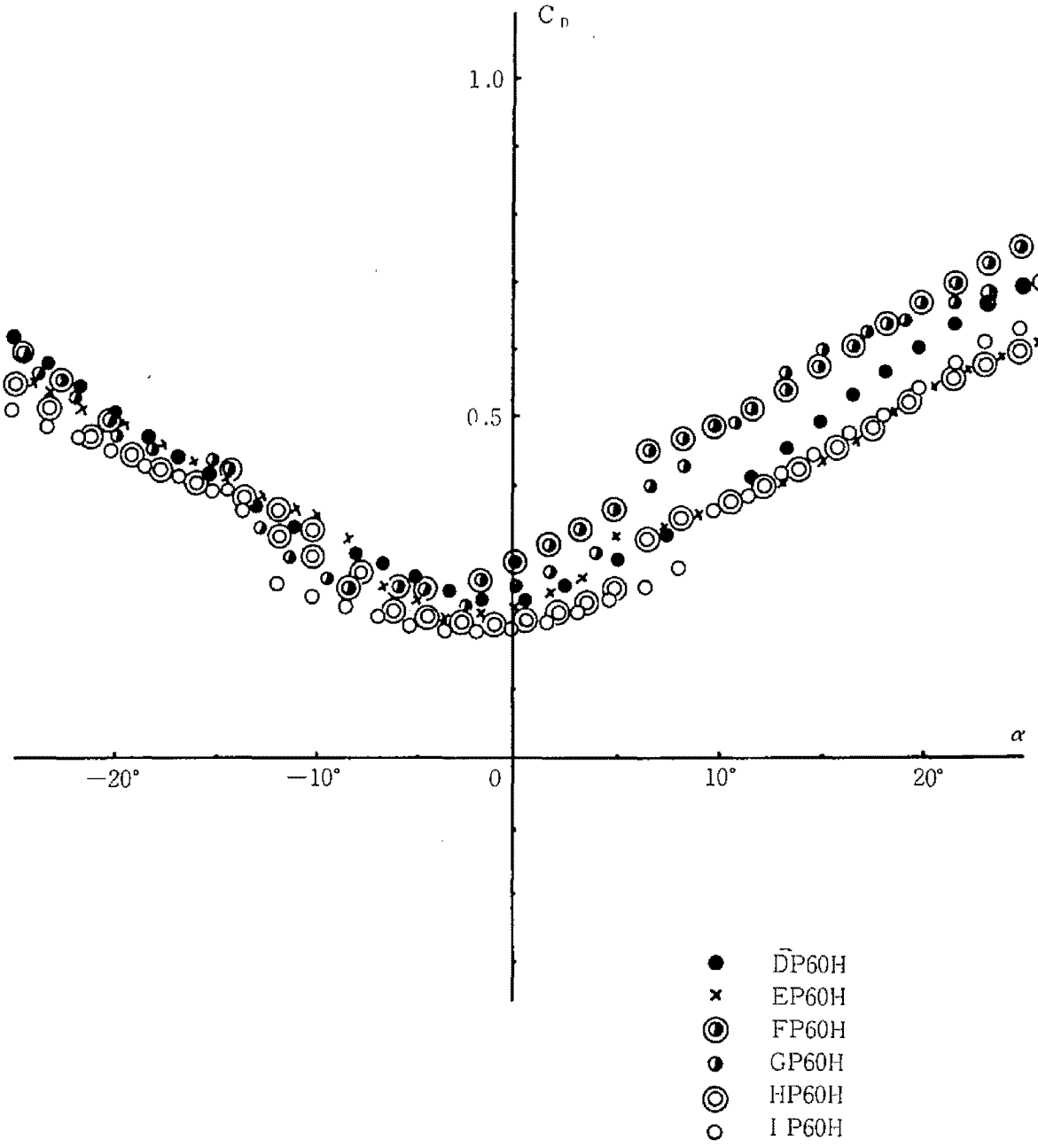
C_D
1.0
0.5
α
−20°
−10°
0
10°
20°
DP60H
EP60H
FP60H
GP60H
HP60H
I P60H

Fig. 3.4.12

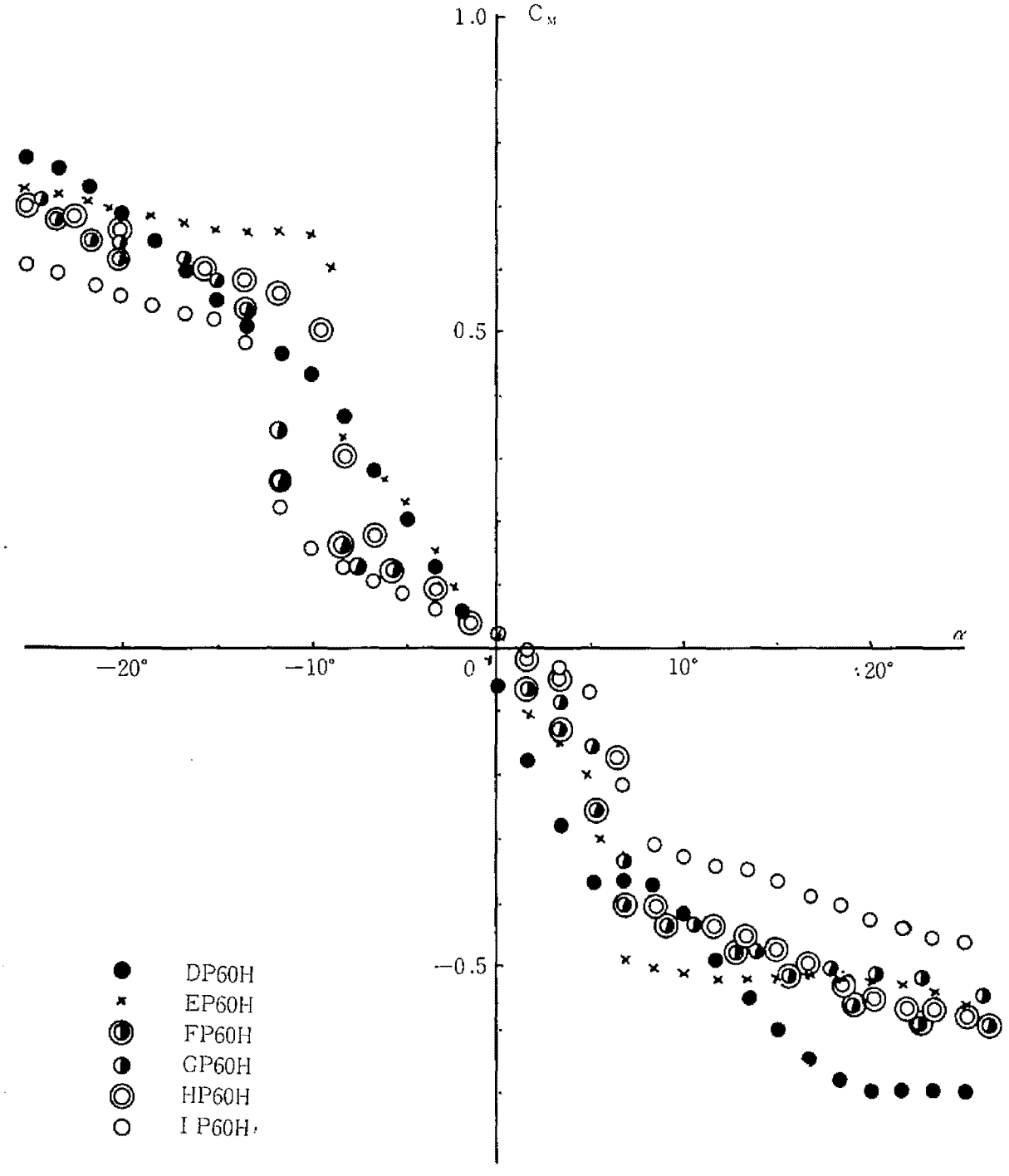
1.0
C_M
0.5
α
−20°
−10°
0
10°
20°
−0.5
DP60H
EP60H
FP60H
GP60H
HP60H
I P60H

Fig. 3.4.13

3.5 AERODYNAMIC CHARACTERISTICS AND DYNAMIC WIND TUNNEL TESTS

1) Introduction :

In continuation with the aeroelastic experimental tests a series of the dynamic tests by the same models as used in the static tests is performed by use of the Eiffel type Wind Tunnel in the Department of Civil Engineering, Kyoto University, and as the same as before the wind velocity is measured by the Betz Manometer and the NPL type-Pitot tube.
In the first series of experiment the models in Table 3.4.1 are used in order to disclose the kinds of effective factors to charecterise the flutter phenomenon in the typical forms of cross sections for bridge, namely the truss-stiffened and the plate girder type of models.
The dependence of the critical wind velocity on the frequency ratio (the ratio of the frequencies of the torsional to the deflectional modes), the ratio of the width to the height of the cross sections, and the configuration of slots on the deck are examined qualitatively.
In the second series of experiments the ten kinds of models are so chosen to clarify the aerodynamic characteristics associated with the types of girder systems, as shown in Fig. 3.5.6. In this test the steady torsional amplitudes of the flutter state are obtained for certain reduced velocity. In the third series of the experiment an attention is placed on the inherent capacity of damping effects in the model mountings. Similarily as the second series of experiment the flutter amplitude are obtained and plotted with the reduced velocity.

2) Similarity Requirement

In order to analyze the aerodynamic behaviour of the bridge structures, such as a suspension bridge, by use of the model tests both geometrical and vibrational similarities are required so that the flow pattern with vibrating structures might be assumed to be similar with the prototype. Through the dimension analysis C. Scruton defined the similarity parameters as follows

a) $I_\theta / \rho B^4$, $I_z / \rho B^2$

b) $S_\theta / \rho V^2 B^2$, $S_z / \rho V^2$

c) $\delta_{\theta S}$, δ_{zS}

where I_θ : the polar moment of inertia per unit spanwise length, calculated with respect to axis of rotation for torsional oscillations

I_z : the mass per unit spanwise length for vertical oscillations

S_θ , S_z : elastic stiffness corresponding to I_θ , I_z, respectively

ρ : air density

B : width of bridge

V : wind speed

$\delta_{\theta S}$, $\delta_{\theta z}$: logarithmic decrements for torsional and vertical oscillations respectively due to structural damping

As known already there is a controversial problem of applicability of the so called section model instead of the full size model in the wind tunnel test. If the experimental apparatus and stations be sufficiently large enough, the full size model test is obviously recommended placing an attention on the damping and the aerodynamic similarity requirements as well as the geometrical similarity. However it is also noted that the main aerodynamic feature of suspension bridge is in general determind by the geometrical and the kinematical characteristics of stiffening girder system and a number of previous investigations have confirmed this presumption as far as the two dimensional flow is concerned.

In this investigation stress being placed on the aerodynamic behaviours of the idealized from of bridge sections, no similarity rule is particularly considered except the fact that the frequency ratio of the torsional to the deffectional modes remains in the range from 1.0 to 2.5 approximately.

3) Description of models and their mountings

As mentioned before, in this series of experiments, about 30 kinds

models are used as shown in Tables 3.5.1, 3.5.2 and 3.5.3 (Photo 3.3 ~ 3.5). All models are attached to the end plates which are supported at the center of cross section in such a way that the mounting apparatus permits both vertical and pitching motions as shown in Fig. 3.5.1.
The natural frequencies for deflectional and torsional models can be adjusted by use of eight coiled springs of appropriate spring constants and the proper distances (Sb) of spring positions.
The deflection is measured by a channel form of copper gauges (G_1) with the electric wire strain gauge and the torsional deformation is recorded as the difference of the two gauges (G_2) as shown in Fig. 3.5.1.

4) Experimental results

In order to analyze the aerodynamic instability of bridge section the preliminary inrestigation, namely the first series of experiment, was performed, by which the flutter frequency and the flutter wind velocity were obtained as shown in Tables 3.5.1. ~ 3. As illustrated in Table 3.4.1 the A-type model such as A-TT and A-PP-F in Table 3.5.1 is such a model as the ratio of the height to the width of the deck is 3.0 and it should be noted that the static wind tunnel tests show the negative inclination of the lift coefficient-pitching angle curve for the plate girder type model of this kind. However the height of girders being smaller than approximately 1/3 of the width of deck there appears very little tendency of the negative inclination in both the lift coefficient and the pitching moment coefficient curves. Dynamically the negative inclination in the lift coefficient curve seems us to take less important role in the flutter phenomena since, as far as this investigation is concerned, the torsional mode in the flutter state is so dominant to compare with the deflectional modes. From the results the plate girder type model with or without slots on the deck vibrates with flutter frequency which almost accords with the frequency of free torsional vibrations, while the flutter frequency of the truss-stiffened girder type models remains between the frequencies of free deflectional

and free torsional vibrations. In this experiment the flutter velocity is obtained by measuring the damping of free vibrations in wind stream induced by initial small disturbances. Several examples are illustrated in Figs. 3.5.5 and the flutter velocity is defined as the wind velocity for intersecting point of the abscissa and the damping curve.
The relation between the flutter wind velocity and the frequency ratio is shown in Figs. 3.5.2, 3.5.3 and 3.5.4. Though a number of results is limited it can be said that the flutter velocity tends to increase with the frequency ratio.
As long as the truss-stiffened girder type models are concerned the slot deck is responsible for increasement of the flutter velocity but for the plate girder type models the configurations and the dimensions of slots on the desk, the height of girders and the type of flanges, effect on the flutter velocity dependent on the frequency ratios. Through the preliminary tests it is considered that the flutter wind velocity and the flutter frequency are some indications of the aerodynamic instability phenomena of the bridges.
In the second and the third series of experiments therefore it is aimed to disclose the mechanisms of initiation and annihilation of instability so that for some typical types of models as illustrated in Fig. 3.5.6 the initial steady and final stages of flutter phenomena are searched by varying wind velocity continuously.

In the second series of flutter experiments the torsional and deflectional amplitudes in the steady state are obtained for the nondimensional reduced velocity. The flutter states in this tests apparently are classified into two types depending on the plate type response and the plate girder type response. The former type responses, as shown in Fig. 3.5.7 ~ 3.5.11, is characterized as follows; at the critical reduced velocity the amplitudes start to increase suddenly so that as decreasing the velocity there exists the steady amplitude. Again decreasing the wind velocity, the steady amplitude may decrease or increase depending on the type of models and the frequency ratio. This indicate clearly that the wind velocity at which the flutter starts and the wind velocity

at which flutter vanishes are different and, so far, the former is approximately 20 ~ 30% larger than the latter. For the plate girder type response as shown in Fig. 3.5.12 ~ 15 the starting flutter velocity also differs from the ending flutter velocity as same as the former case. However the steady amplitudes vary gradually with the wind velocity. It is also noted that for this type the torsional mode is so dominant that the vertical deflection can be disregarded. For a particular type of model (EP type) the relation of the steady flutter amplitude and the reduced wind velocity shows that as increasing the wind velocity the amplitude increases until about 2.0 of the reduced velocity beyond which the amplitude gradually decreases as Fig. 3.5.15.

The third series of experimental study is performed for the same models as used in the second series of experiment in order to comfirm the flutter amplitude and the reduced velocity relations obtained previously, as Fig. 3.5.16 ~ 24. In this study the same results are obtained for the plate and truss types models except the fact that there exist small steady amplitude below the starting flutter velocity. For the plate girder type models the torsional amplitude increases remarkably above the ending flutter velocity but the relation can not coincide with each other for increasing and decreasing wind velocity.

Through this experimental study it is concluded that the flutter amplitude-reduced wind velocity relation can characterize the flutter phenomena for bridge structures and this relation seems to be sufficiently sensitive for the types of stiffening girders, slots configurations, deck positions, etc. However since it is so sensitive, aerodynamic characteristic is considered to be quite involved so that it is hard to illustrate the detailed flutter properties by these relations. In order to determine specific factors of aerodynamic instability for bridge section it is desired to measure directly the aerodynamic forces acting on the bridge sections which will be considered the next paragraph 3.6.

Table 3. 5. 1

Model	Natural Freq.		$\frac{\omega_{\alpha_0}}{\omega_{h_0}}$	Flutter Frequency ω_F	Flutter Velocity V_F m/s
	Defl. ω_{h_0} rad/s	Torsional ω_{α_0} rad/s			
A–PP	8.69	11.08	1.28	10.05	3.65
	8.66	12.36	1.43	11.90	—
	8.66	13.80	1.59	13.30	5.32
	8.66	15.39	1.78	15.15	7.80
A–TT	9.10	11.42	1.26	10.03	6.89
	9.10	12.51	1.38	11.61	9.04
	9.15	14.60	1.60	13.25	9.75
	9.13	16.44	1.80	14.89	11.62
A–PP–F	8.58	11.08	1.29	10.59	3.65
	8.54	12.56	1.47	12.10	4.08
	8.56	13.83	1.62	13.41	4.28
	8.58	15.70	1.83	14.96	5.16
A–PP–S	8.91	11.36	1.28	8.83	8.01
	8.88	13.22	1.49	8.60	8.56
	8.87	14.31	1.61	8.62	8.80
	8.86	15.06	1.70	8.70	8.94
A–TT–S	9.45	11.74	1.26	10.79	10.17
	9.30	13.22	1.42	12.19	12.53
	9.30	14.78	1.59	14.14	15.55
	9.30	15.94	1.71	15.16	15.97
A–PP–FS	8.08	11.50	1.31	11.48	7.85
	8.78	12.53	1.43	12.50	8.90
	8.78	14.34	1.63	14.34	9.96
	8.78	14.95	1.70	15.00	10.80

Table 3. 5. 2

Model	Natural Frequency		$\frac{\omega_{\alpha_0}}{\omega_{h_0}}$	Flutter Frequency	Flutter Velocity
	ω_{h_0}	ω_{α_0}		ω_F	V_F
DP40	9.27	13.20	1.43	12.96	3.31
	9.28	14.71	1.59	14.52	3.45
	9.23	17.17	1.85	16.72	4.03
DP60	9.18	13.36	1.46	13.36	3.69
	9.02	14.93	1.65	14.15	3.91
	9.02	16.47	1.82	16.47	4.52
DP80	9.06	11.78	1.30	11.60	3.48
	9.16	14.31	1.58	13.80	3.94
	9.04	16.69	1.84	16.40	4.91
DT40	9.43	13.65	1.45	12.92	5.06
	9.41	14.91	1.58	14.70	5.69
	9.42	17.26	1.83	16.11	8.56
DT70	9.43	13.53	1.43	12.81	6.91
	9.58	14.61	1.55	13.85	8.26
	9.44	17.59	1.86	15.67	12.09
EP40	9.35	13.36	1.42	12.75	3.48
	9.35	14.91	1.58	14.91	3.70
	9.42	16.72	1.77	17.25	4.92
EP60	9.03	12.71	1.40	12.56	2.26
	9.08	14.52	1.60	14.52	2.92
	9.16	16.80	1.85	16.50	3.20
EP70	9.27	14.50	1.56	14.40	2.95
	9.27	16.80	1.81	16.50	3.47
	—	—	—	—	—
EP80	9.11	12.90	1.42	12.70	3.06
	9.11	14.30	1.57	13.95	3.20
	9.10	16.70	1.84	15.95	3.92

Table 3. 5. 3.

Model	Natural Frequency		$\frac{\omega_{\alpha_0}}{\omega_{h_0}}$	Flutter Frequency ω_F	Flutter Velocity V_F
	ω_{h_0}	ω_{α_0}			
FP40	9.44	13.57	1.44	13.35	2.73
	9.44	14.61	1.58	14.52	2.92
	9.44	17.25	1.83	16.90	3.92
FP60	9.42	13.51	1.43	12.88	2.74
	9.35	14.53	1.56	14.22	2.92
	9.35	16.89	1.80	16.49	2.92
FP80	—	—	—	—	—
GP40	9.44	13.66	1.42	13.52	2.93
	9.33	14.92	1.58	14.92	3.58
	9.44	16.97	1.80	17.26	3.70
GP60	—	—	—	—	—
GP80	—	—	—	—	—
HP40	9.44	13.36	1.42	13.36	2.93
	9.44	14.93	1.58	14.93	3.21
	9.44	17.70	1.88	17.25	3.22
HP60	—	—	—	—	—
HP80	9.26	12.90	1.39	12.90	2.61
	9.30	14.60	1.57	14.60	3.20
	9.40	17.30	1.86	16.60	3.46
IP40	9.44	13.35	1.41	13.35	2.46
	9.44	14.93	1.58	14.93	2.63
	9.44	17.70	1.88	17.25	3.22
IP60	9.31	13.27	1.41	12.95	2.63
	9.42	14.71	1.56	14.47	3.22
	9.43	16.62	1.76	16.50	4.24
IP80	9.16	12.97	1.41	12.56	3.22
	9.23	14.61	1.59	14.33	—
	9.21	16.50	1.79	—	—

Table 3. 5. 4

Model \ Dimension		Deflectional Vibration			Torsional Vibration			Freq. Ratio.
		m Kg·sec²/m²	δ_{h_0}	ω_{h_0} rad/sec	I Kg·m·sec²/m	δ_{α_0}	ω_{α_0} rad/sec	$\omega_{\alpha_0}/\omega_{h_0}$
	Plate	.7587	.0290	8.93	.02798	.0896	8.80	0.99
					.02867	.0650	10.54	1.18
					.02957	.0481	12.22	1.37
					.03069	.0300	13.87	1.55
D-type	DT70H	.8173	.0189	8.70	.02941	.0901	10.26	1.18
					.03011	.0823	11.60	1.33
					.03101	.0446	11.83	1.36
	DP40H	.8217	.0118	8.63	.02951	.0963	8.32	0.96
					.03020	.0745	9.94	1.15
					.03111	.0578	11.77	1.36
					.03222	.0423	13.43	1.56
	DP70H	.8543	.0135	8.64	.03033	.0585	8.41	0.97
					.03193	.0317	11.75	1.36
	DP70H F30	.8945	.0177	8.30	.03105	.0343	8.48	1.02
					.03265	.0256	11.61	1.42
E-type	ET70H	.8326	.0228	8.64	.02960	.1144	8.25	0.95
					.03029	.0805	10.33	1.20
					.03119	.0518	11.88	1.38
					.03231	.0369	13.63	1.58
	EP40H	.8369	.0228	8.63	.02969	.0947	8.54	0.99
					.03038	.0551	10.27	1.19
					.03129	.0405	12.05	1.40
					.03240	.0296	13.53	1.57
	EP70H	.8695	.0231	8.46	.03051	.0948	8.43	1.00
					.03120	.0692	9.94	1.17
					.03211	.0428	11.83	1.40
					.03322	.0213	13.45	1.59
	EP70H F30	.9097	.0139	8.29	.03123	.1000	8.44	1.02
					.03193	.0750	9.89	1.19
					.03283	.0550	11.54	1.39
F-type	FT70H	.8282	.0185	8.64	.02949	.1177	8.64	1.00
					.03018	.0568	10.47	1.21
					.03109	.0385	11.94	1.38
					.03220	.0306	13.59	1.57
	FP40H	.8326	.0241	8.64	.02959	.0911	8.64	1.00
					.03028	.0644	10.21	1.18
					.03118	.0382	11.78	1.36
					.03230	.0279	13.59	1.57
	FP70H	.8651	.0222	8.47	.03040	.0764	8.49	1.00
					.03110	.0533	10.19	1.20
					.03200	.0431	11.84	1.40
	FP70H F30	.9053	.0213	8.24	.03113	.0933	8.37	1.02
					.03182	.0792	10.05	1.22
					.03272	.0627	11.67	1.42

Table 3. 5. 5

Model \ Dimension		Deflectional Vibration			Torsional Vibration			Freq. Ratio.
		m Kg·sec²/m²	δ_{h_0}	ω_{h_0} rad/sec	I Kg·sec²	δ_{α_0}	ω_{α_0} rad/sec	$\omega_{\alpha_0}/\omega_{h_0}$
Plate		.4473	.0376	11.69	.01631	.0217	17.80	1.52
			.0391	11.62	.01941	.0284	19.64	1.69
			.0342	11.62	.02401	.0218	21.54	1.85
			.0391	11.52	.03017	.0237	23.25	2.02
			.0425	11.52	.03540	.0176	24.08	2.09
Truss type model	DT70H	.5426	.0367	10.60	.01794	.0214	17.06	1.61
			.0380	10.60	.02104	.0176	18.85	1.78
			.0376	10.55	.02564	.0278	20.74	1.97
			.0421	10.52	.03180	.0193	22.44	2.13
			.0406	10.37	.03703	.0157	23.34	2.25
	DT70π	.5440	.0368	10.54	.01718	.0198	16.80	1.59
			.0412	10.47	.02026	.0210	18.59	1.78
			.0331	10.61	.02488	.0216	19.39	1.83
			.0524	10.54	.03105	.0112	23.62	2.24
			.0347	10.40	.03628	.0383	23.27	2.24
	ET70H	.5802	.0283	10.60	.01806	.0190	16.96	1.60
			.0313	10.60	.02117	.0243	18.85	1.78
			.0299	10.54	.02557	.0141	20.65	1.96
			.0363	10.52	.03193	.0113	23.04	2.19
	ET70π	.5802	.0344	10.66	.01822	.0296	16.85	1.59
			.0399	10.56	.02133	.0200	18.71	1.77
			.0405	10.60	.02593	.0292	20.75	1.86
			.0342	10.60	.03209	.0100	22.53	2.13
			.0321	10.60	.03732	.0171	23.15	2.17
Plategirder type model	DP70H F30	.6161	.0254	9.89	.01829	.0290	16.03	1.62
			.0225	9.89	.02140	.0319	17.76	1.80
			.0185	9.84	.02600	.0174	19.93	2.03
			.0188	9.89	.03216	.0165	21.64	2.19
			.0189	9.84	.03739	.0120	22.37	2.27
	DP70π F30	.5954	.0241	10.05	.02003	.0422	16.16	1.61
			.0230	10.05	.02414	.0296	18.07	1.80
			.0281	10.05	.02773	.0271	19.90	1.98
			.0233	10.05	.03389	.0249	21.67	2.16
			.0235	9.94	.03913	.0361	23.02	2.32
	DP70H F30	.6339	.0382	9.41	.01742	.0187	15.84	1.68
			.0373	9.87	.02050	.0173	17.73	1.80
			.0380	9.87	.02512	.0319	19.68	2.00
			.0390	9.84	.03129	.0119	21.58	2.19
			.0348	9.72	.03652	.0177	22.50	2.32
	EP70π F30	.5966	.0363	10.05	.02007	.0307	16.10	1.60
			.0330	10.21	.02318	.0245	18.07	1.77
			.0352	10.17	.02778	.0192	19.97	1.96
			.0354	9.95	.03394	.0226	21.60	2.17
			.0360	9.82	.03917	.0157	22.68	2.31
Severn		.4553	.0432	11.47	.01463	.0331	17.07	1.49
			.0413	11.55	.01771	.0274	18.93	1.64
			.0522	11.47	.02233	.0176	20.87	1.82

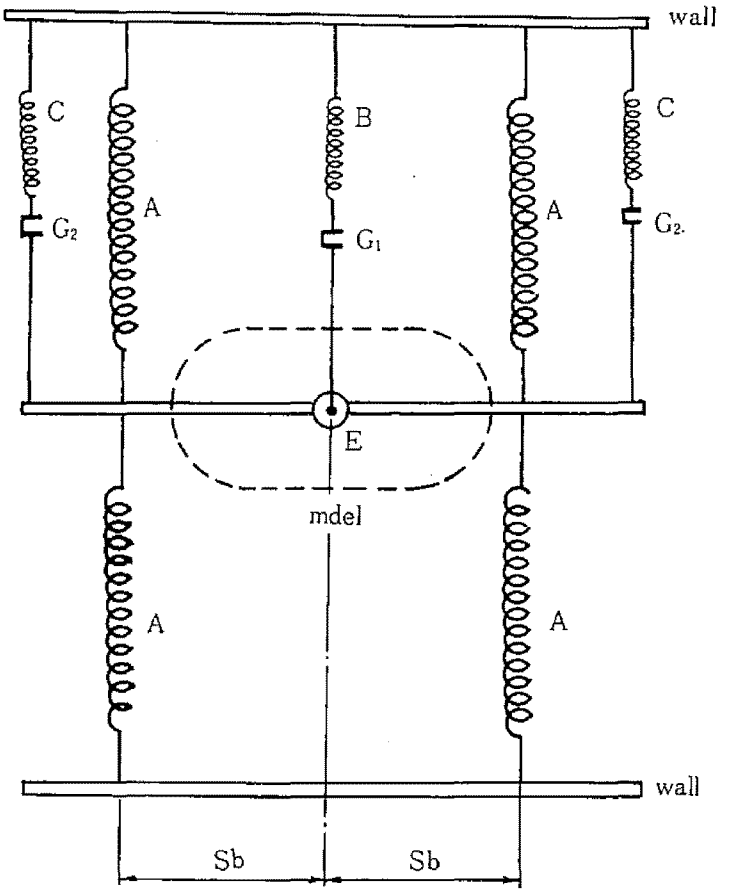

A, B, C : Springs

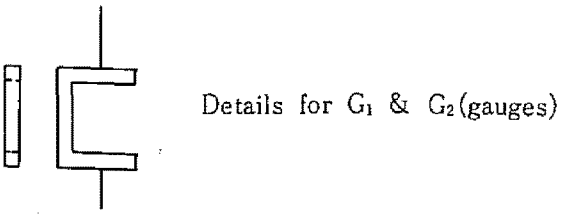

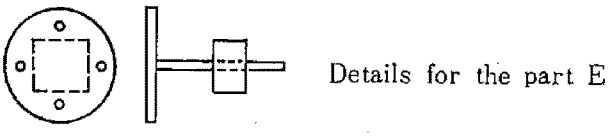

Fig. 3.5.1 Mounting Arrangement

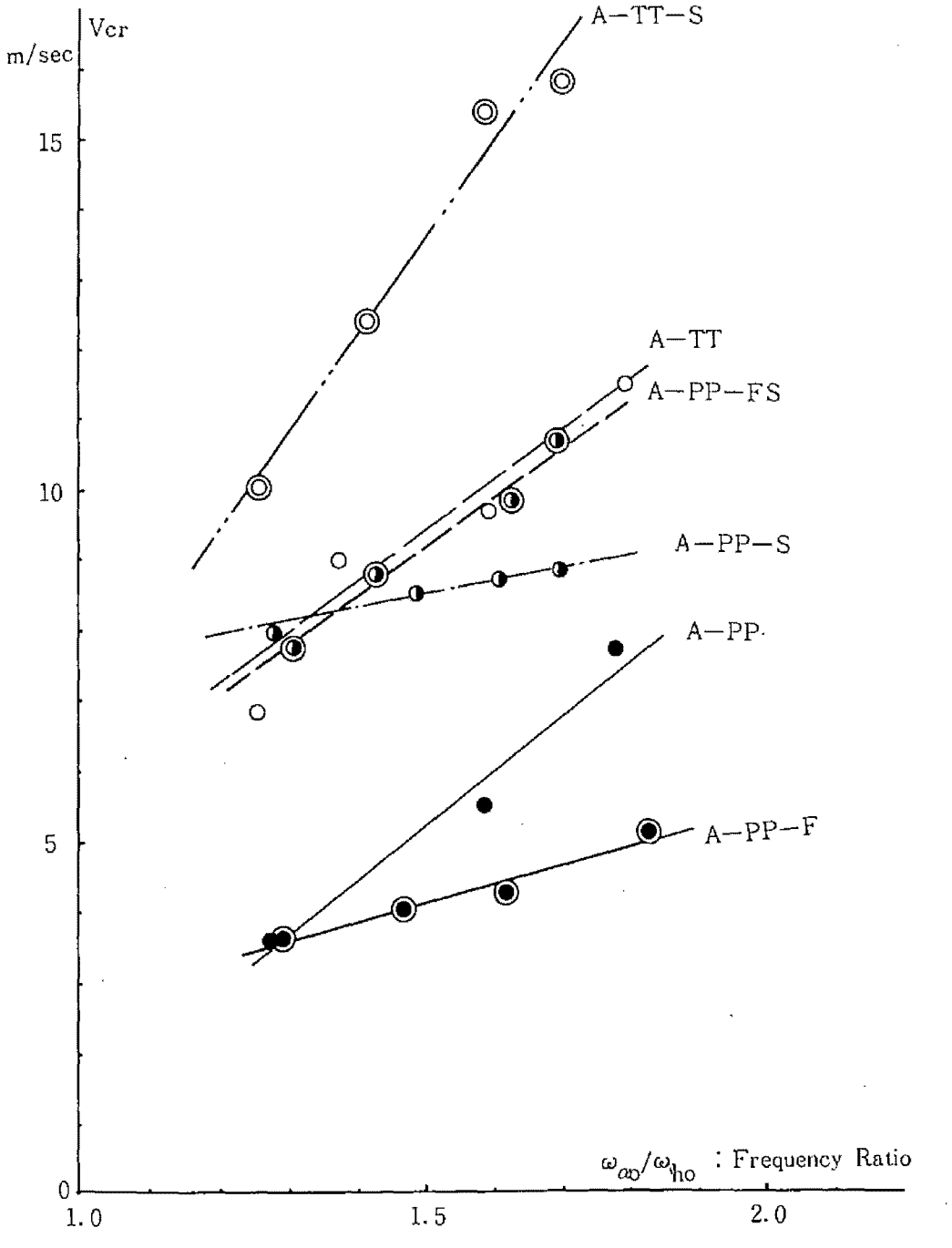

Fig. 3.5.2 Critical Wind Velocity-Frequency Ratio Relation

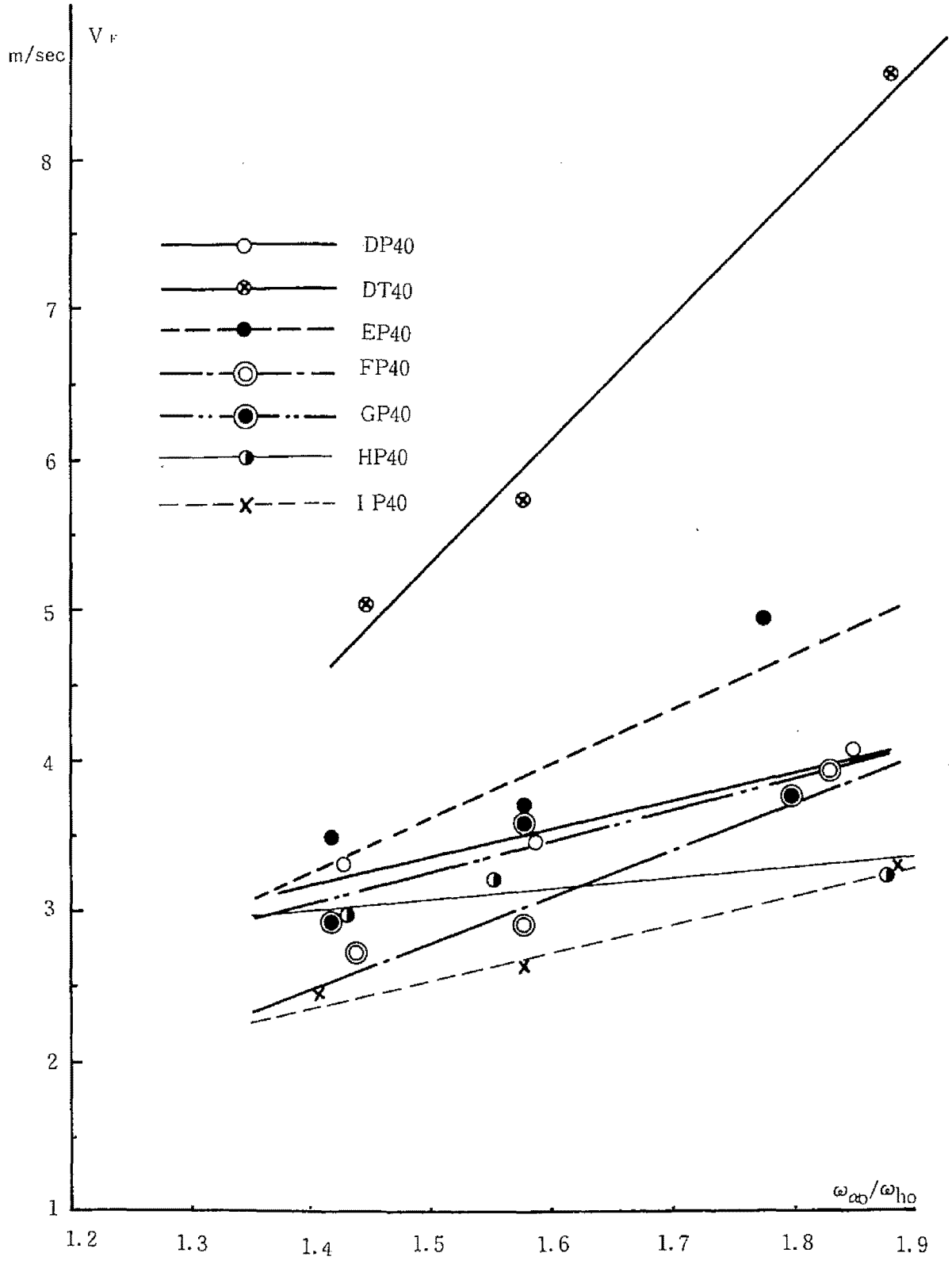

Fig. 3.5.3 Critical Wind Velocity -Frequency Ratio Relation

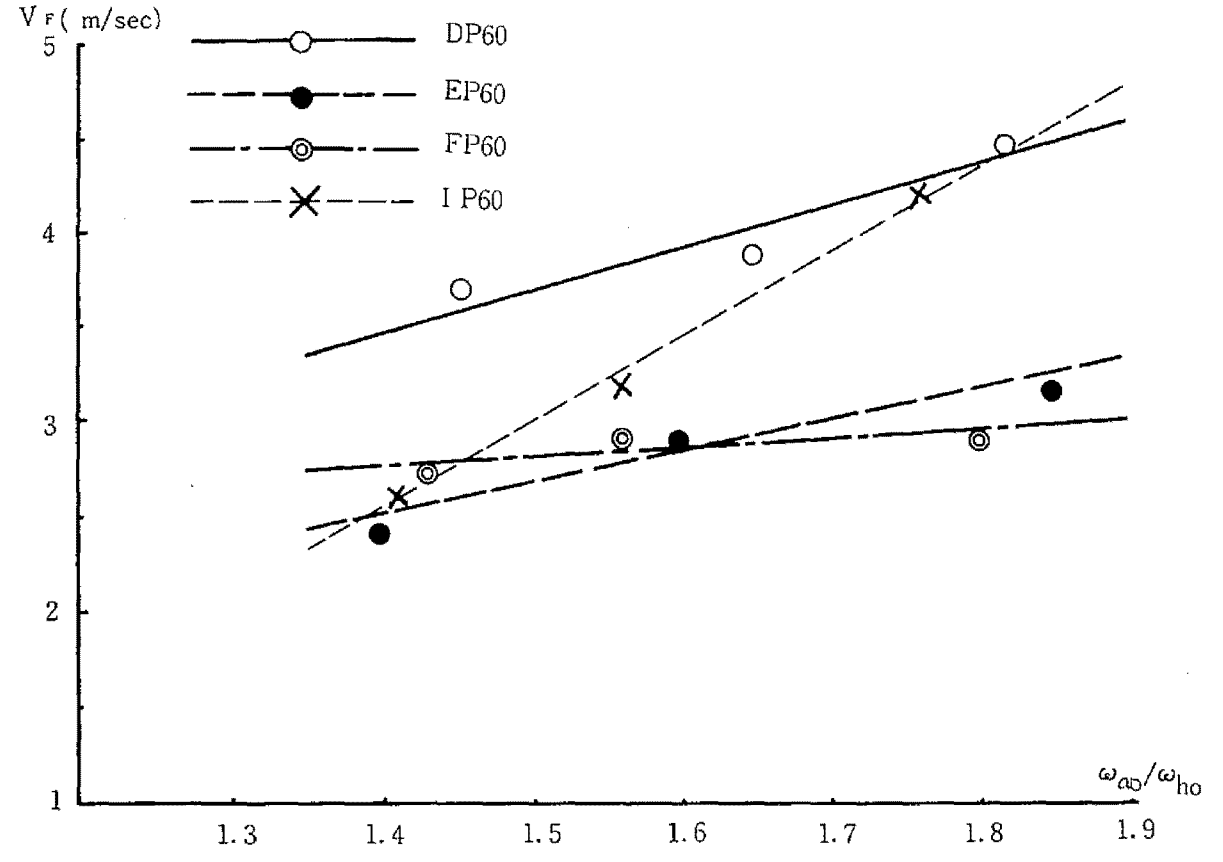

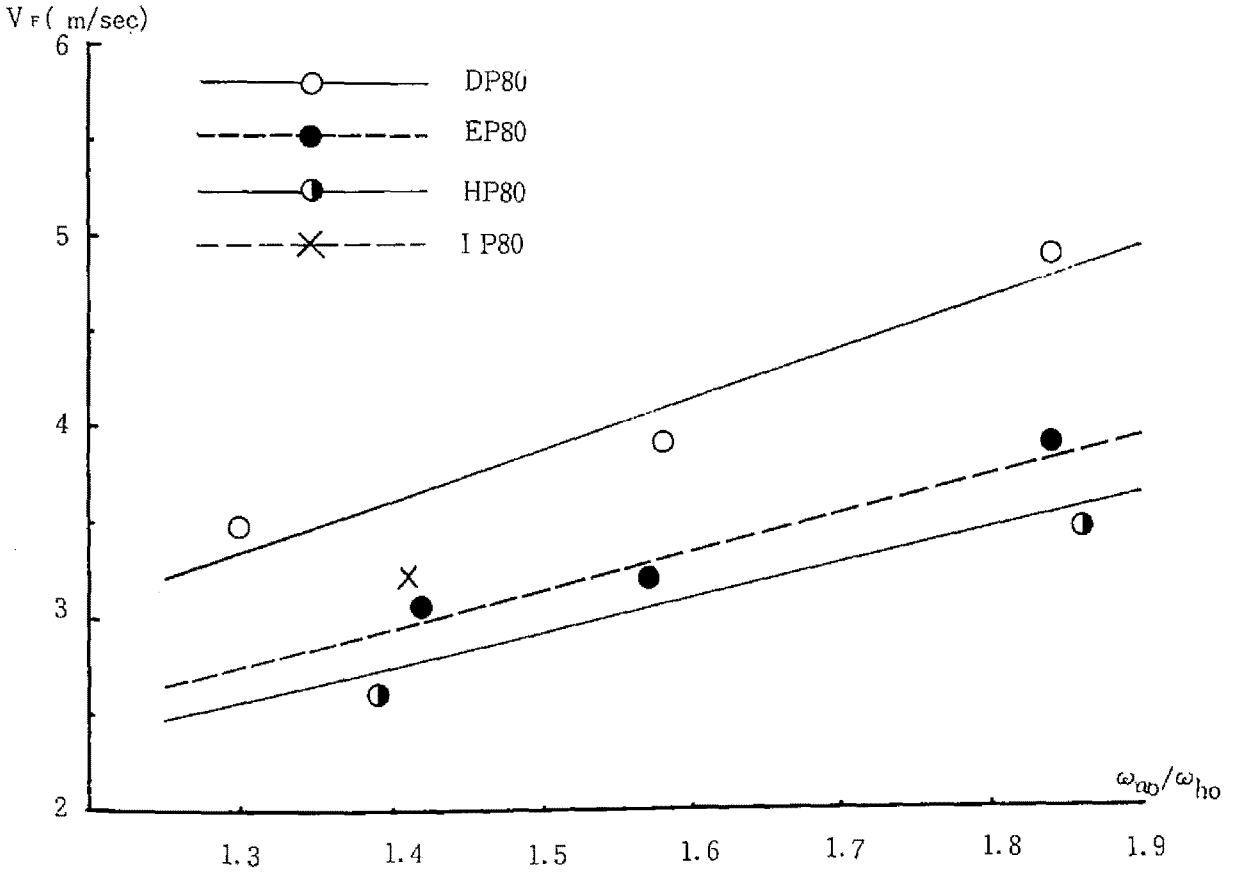

Fig. 3.5.4 Critical Wind Velocity-Frequency Ratio Relation

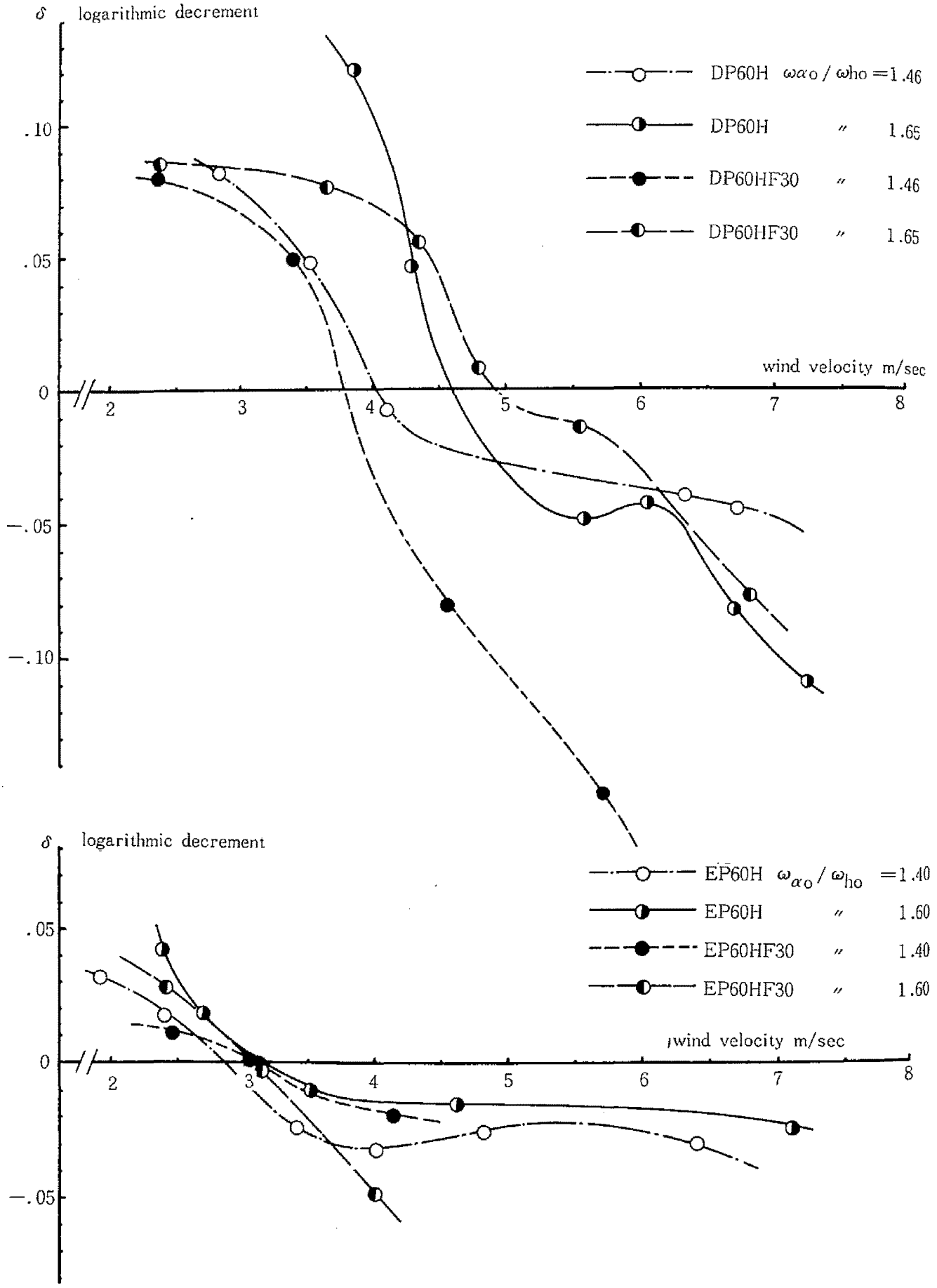

Fig. 3.5.5 Logarithmic Decrement-Wind Velocity Relation (Plate Girder type Model)

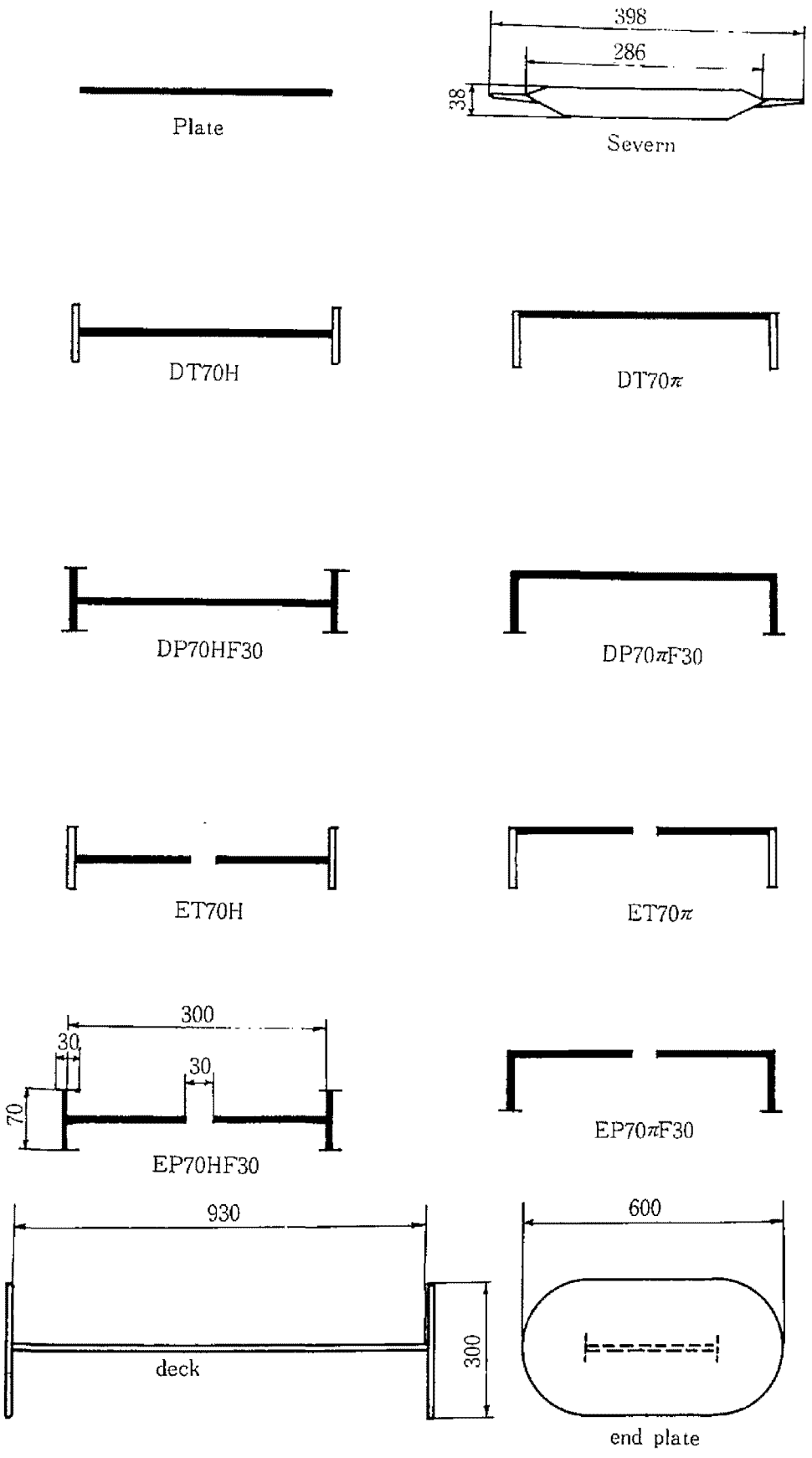

Fig. 3.5.6 Dimensions & Configurations of Models

Fig. 3.5.7

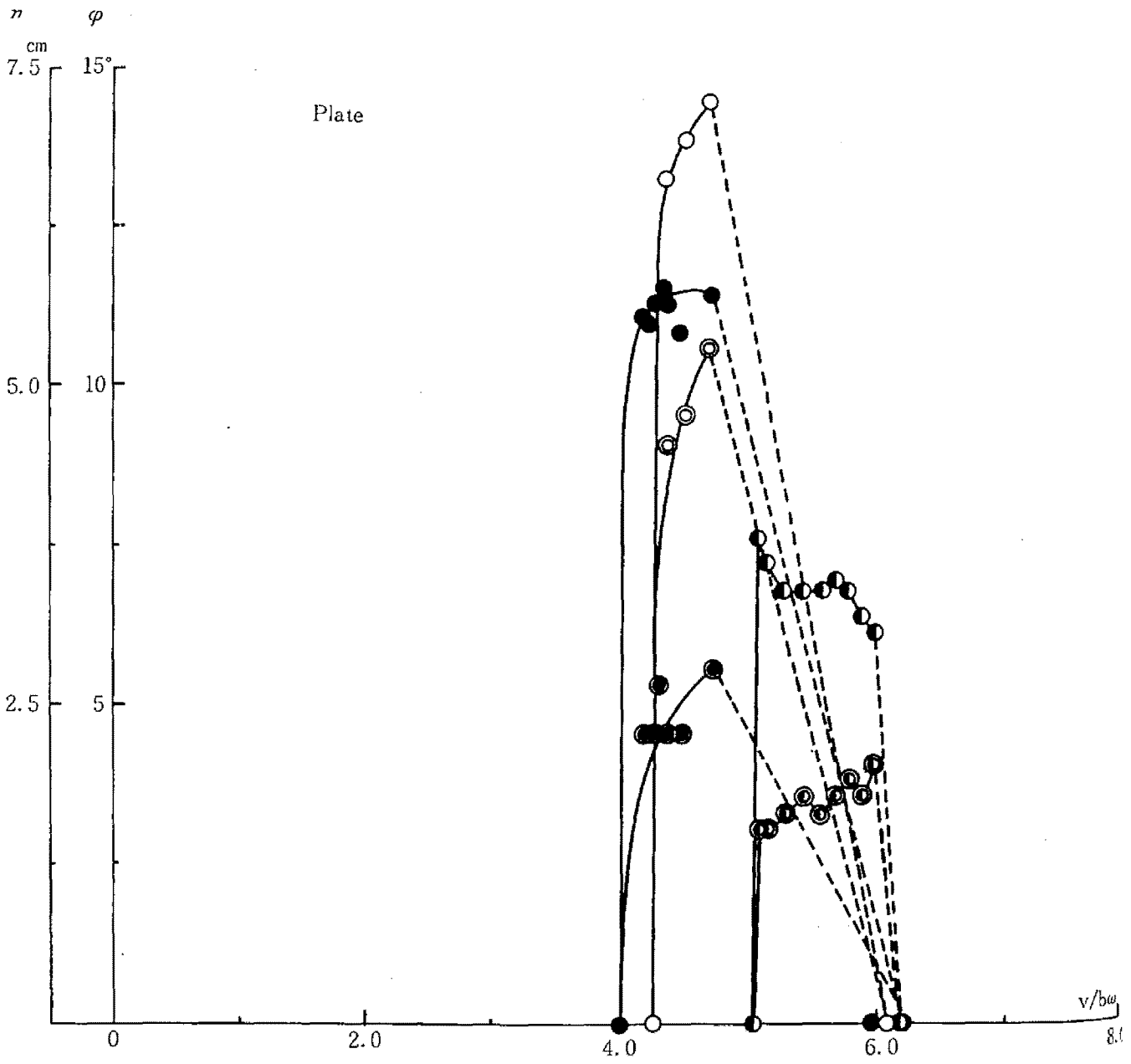

Vcr^S	Vcr^E	ω_η	$\omega\alpha$	ζ_η	ζ_α	$\omega_\alpha/\omega_\eta$	Test No.	Notation
11.76	8.26	10.014	13.273	.00466	.00255	1.325	11—13	φ○ η◎
13.89	8.96	10.210	15.708	.00385	.00245	1.538	11—11	● ●
15.73	12.83	10.210	18.326	.00446	.00214	1.795	11—12	◐ ◐

Fig. 3.5.8

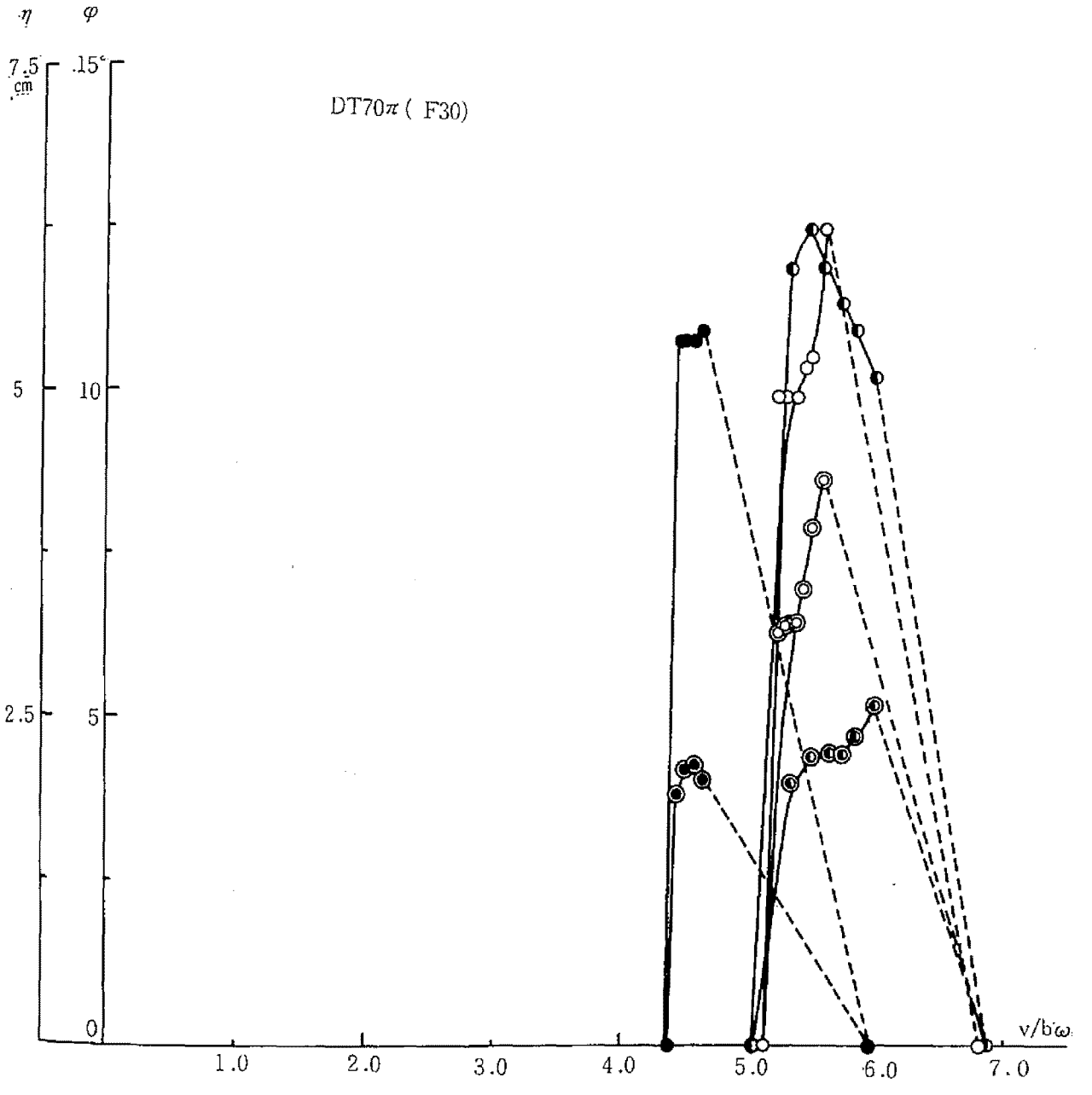

Vcr^S	Vcr^E	ω_η	ω_φ	ζ_η	ζ_φ	$\omega_\varphi/\omega_\eta$	Test No.	Notation
11.63	8.76	9.032	12.30	.00355	.00290	1.362	11—30	φ ○ η ◎
13.17	9.66	9.032	14.73	.00432	.00259	1.630	11—31	● ◉
16.08	11.90	9.163	17.20	.00395	.00284	1.877	11—32	◐ ◉

Fig. 3.5.9

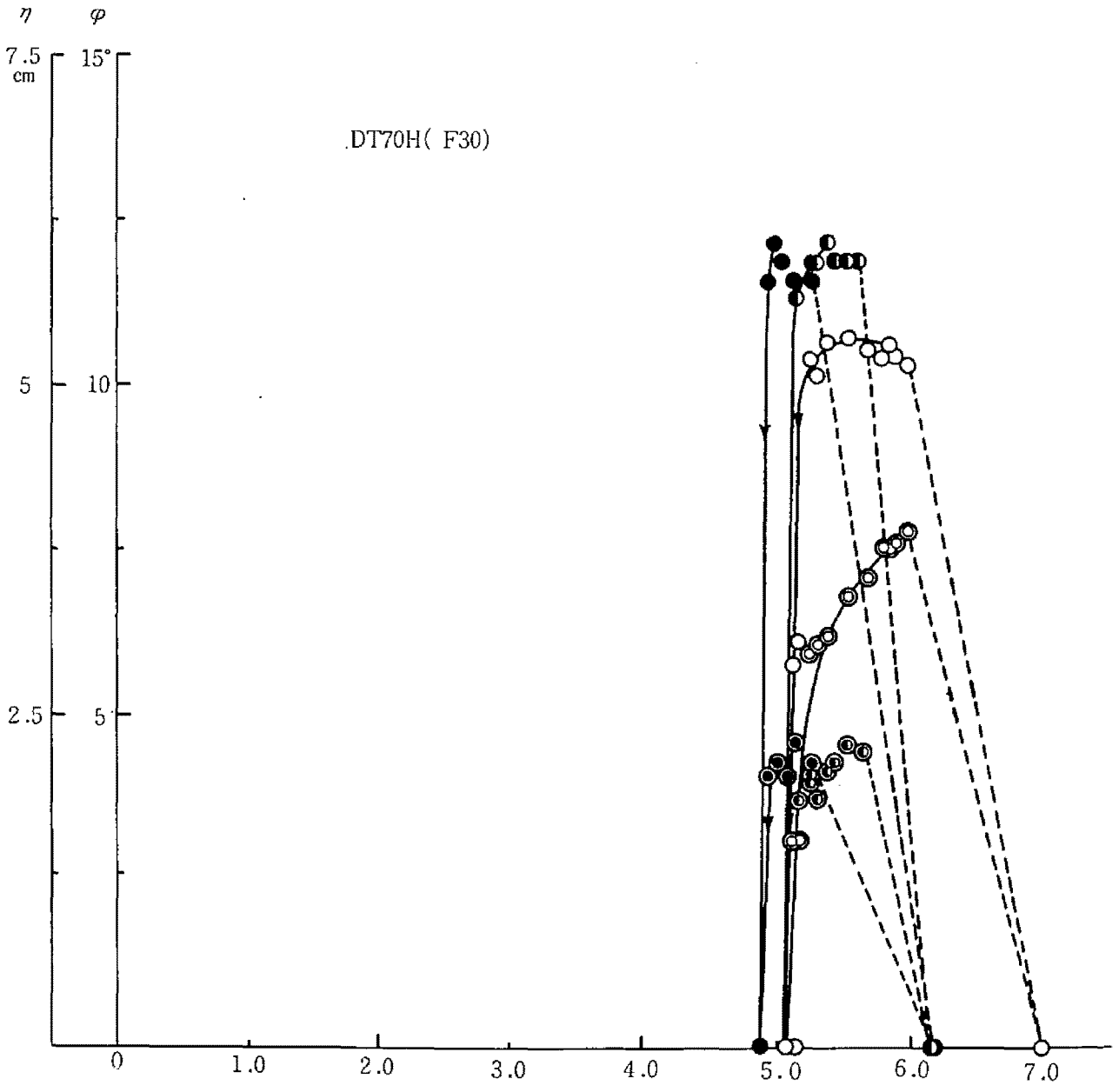

Vcr^S	Vcr^E	ω_η	ω_φ	ζ_η	ζ_φ	$\omega_\varphi/\omega_\eta$	Test No.	Notation	v/b
12.34	8.95	9.032	12.25	.00355	.00251	1.357	11—33	φ ○ η ◎	
12.94	10.26	9.032	14.66	.00355	.00290	1.623	11—34	● ◉	
15.23	12.60	9.032	17.20	.00373	.00184	1.904	11—35	◐ ◉	

Fig. 3.5.10

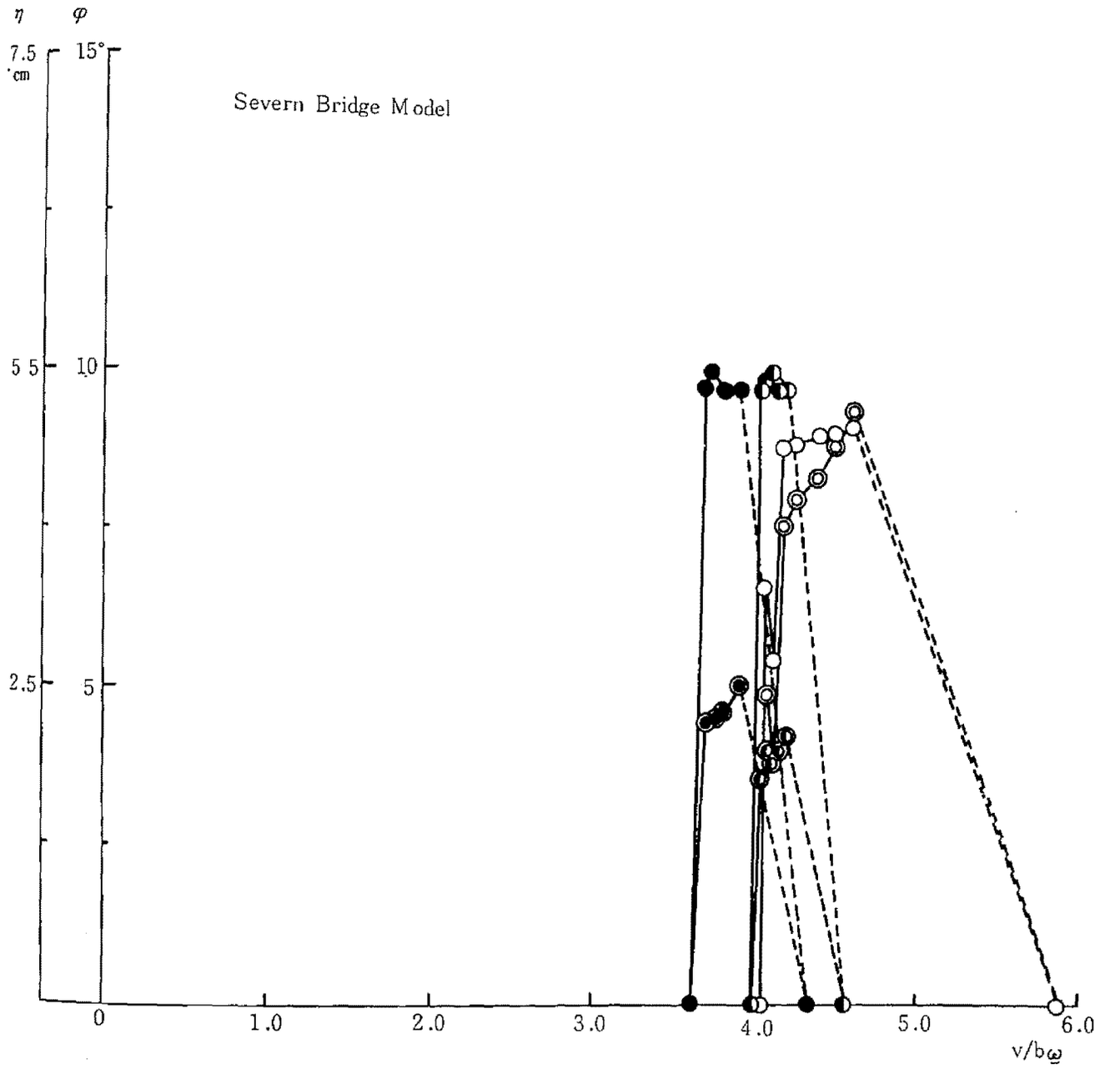

Vcr^S	Vcr^E	ω_η	ω_α	ζ_η	ζ	ω_α / ω	Test No.	Notation
14.40	9.91	10.01	13.09	.00545	.00284	1.307	11—26	φ ○ η ◎
12.70	10.42	10.13	15.65	.00735	.00274	1.545	11—27	● ◉
14.68	12.92	10.21	18.06	.00735	.00274	1.769	11—28	◐ ◑

Fig. 3.5.11

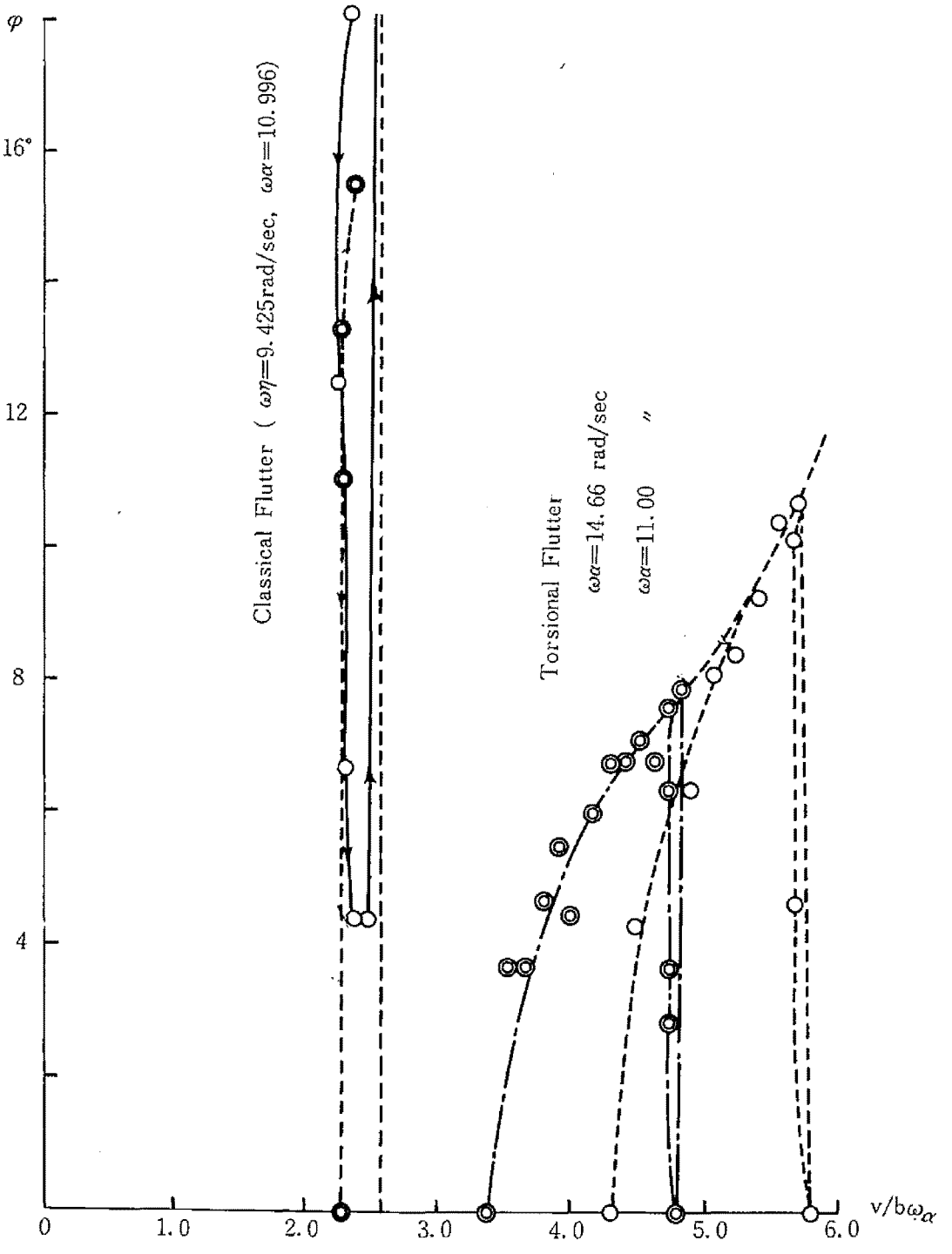

Severn Bridge Type Model

○ ωα=11.00rad/sec

◎ ωα=14.66rad/sec

Fig. 3.5.12

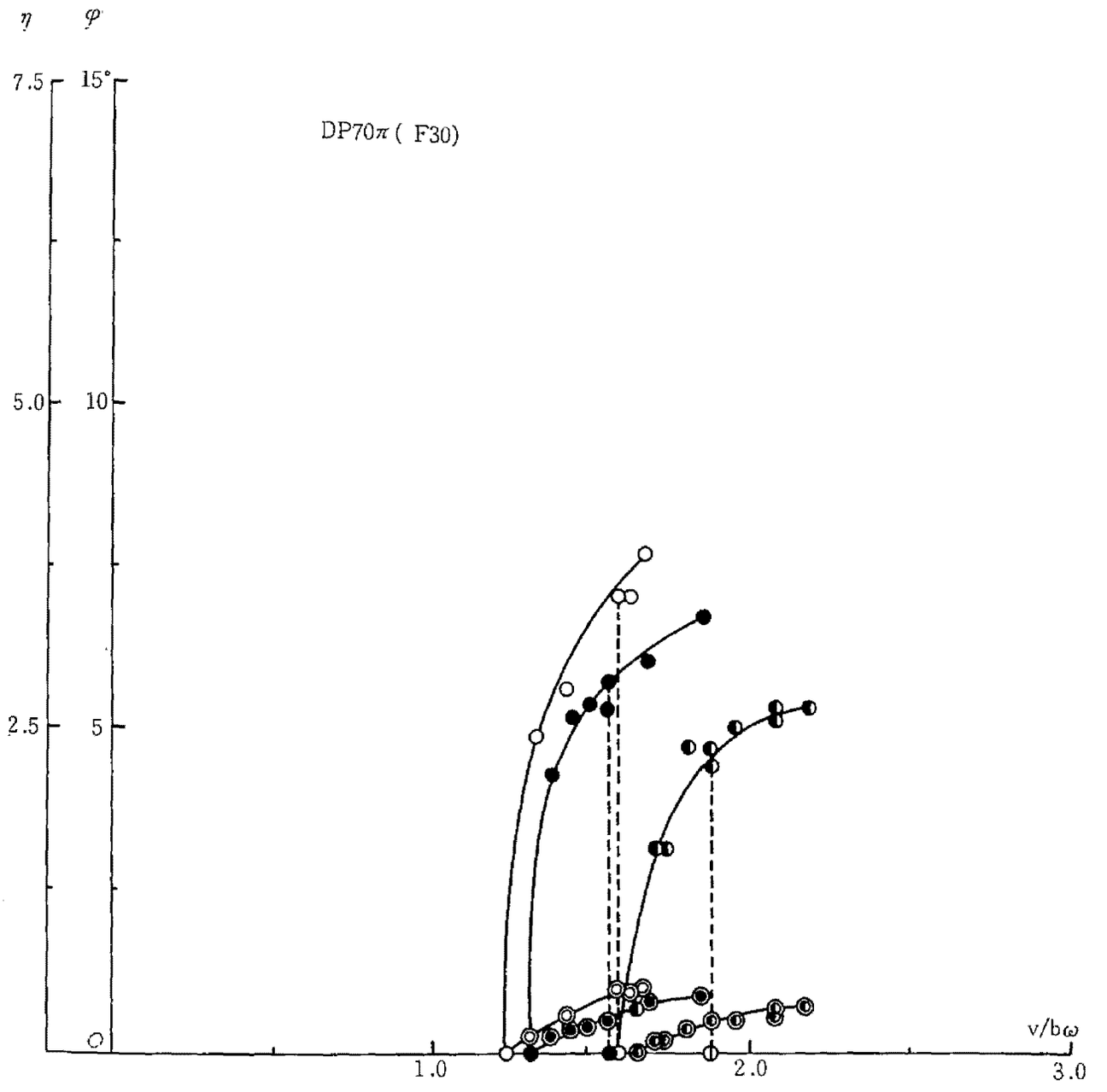

Model, DP70πF30.

Vcr^S	Vcr^E	ω_η	ω_φ	ζ_η	ζ_φ	$\omega_\eta/\omega_\varphi$	Test No.	Notation φ	Notation η
2.83	2.20	8.639	11.938	.00324	.00253	1.382	11—14	○	◎
3.35	2.83	8.796	14.451	.00355	.00302	1.643	11—15	●	◉
4.71	3.97	8.836	16.755	.00299	.00505	1.896	11—16	◐	◉

Fig. 3.5.13

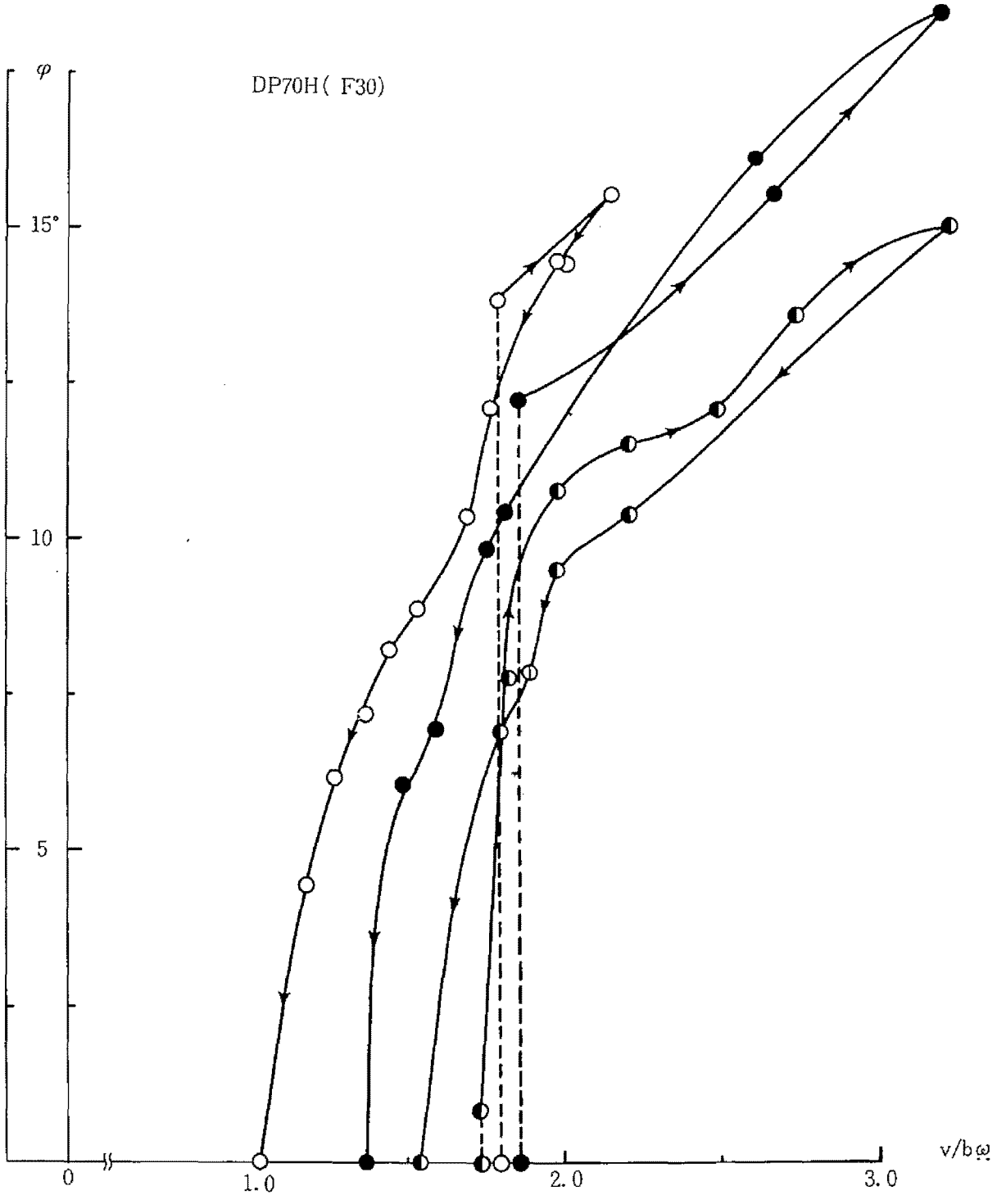

Vcr^S	Vcr^E	ω_1	ω_2	ζ_1	ζ_2	ω_2/ω_1	Test No.	Notation
3.22	1.80	8.727	11.912	.00322	.00290	1.365	11—25	○
3.96	2.90	8.691	14.216	.00418	.00290	1.636	11—24	●
4.59	3.84	8.727	16.650	.00384	.00298	1.908	11—23	◐

Fig. 3.5.14

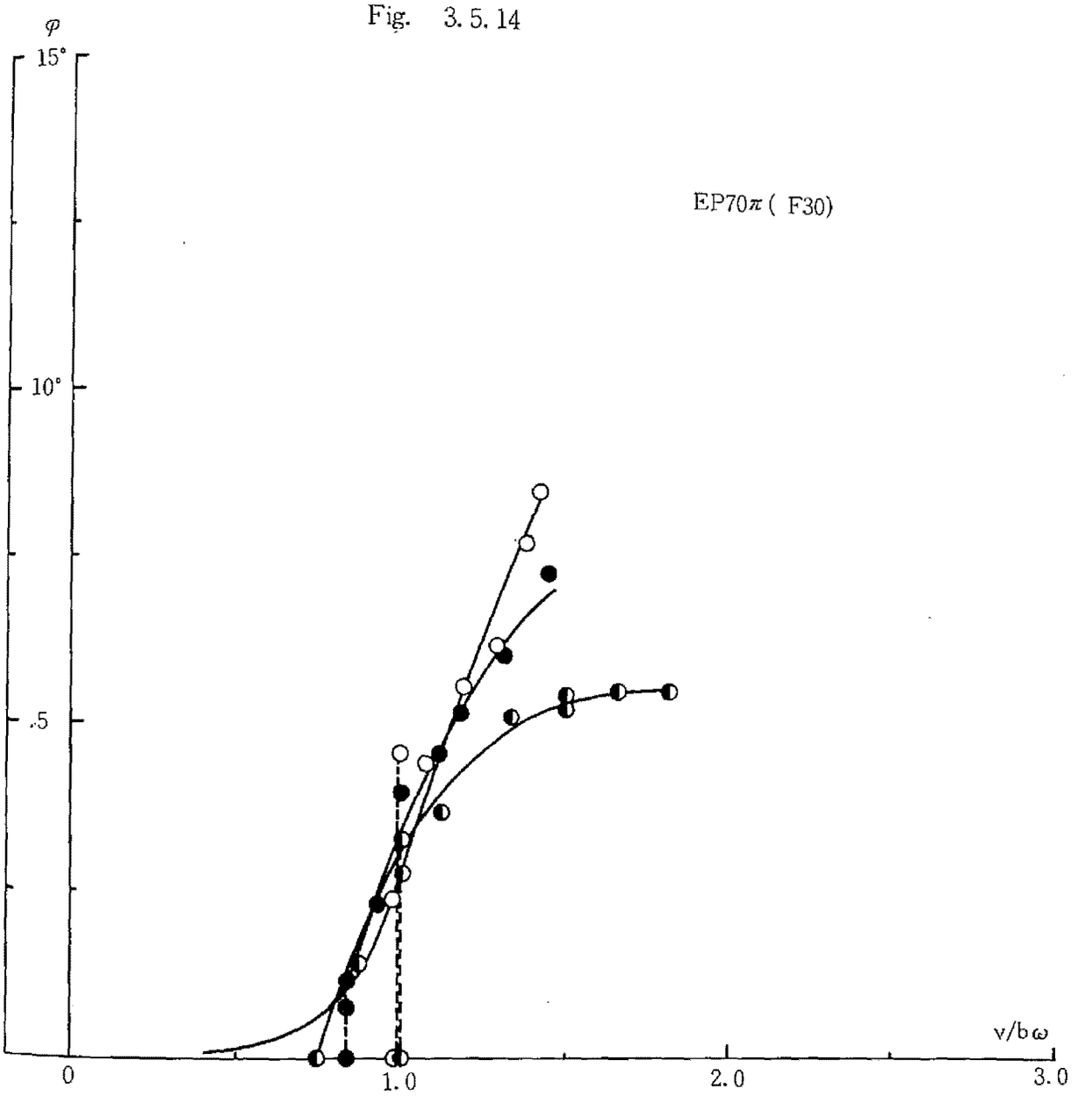

V_{cr}^{S}	V_{cr}^{E}	ω_η	ω_α	ζ_η	ζ_α	$\omega_\alpha/\omega_\eta$	Test No.	Notation
1.80	0	8.650	11.94	.00536	.00290	1.380	11−19	○ ◎
1.80	0	8.836	14.36	.00645	.00367	1.625	11−18	● ◉
2.54	1.88	8.844	16.89	.00561	.00410	1.909	11−17	◐ ◑

Fig. 3.5.15

EP70H(F30)

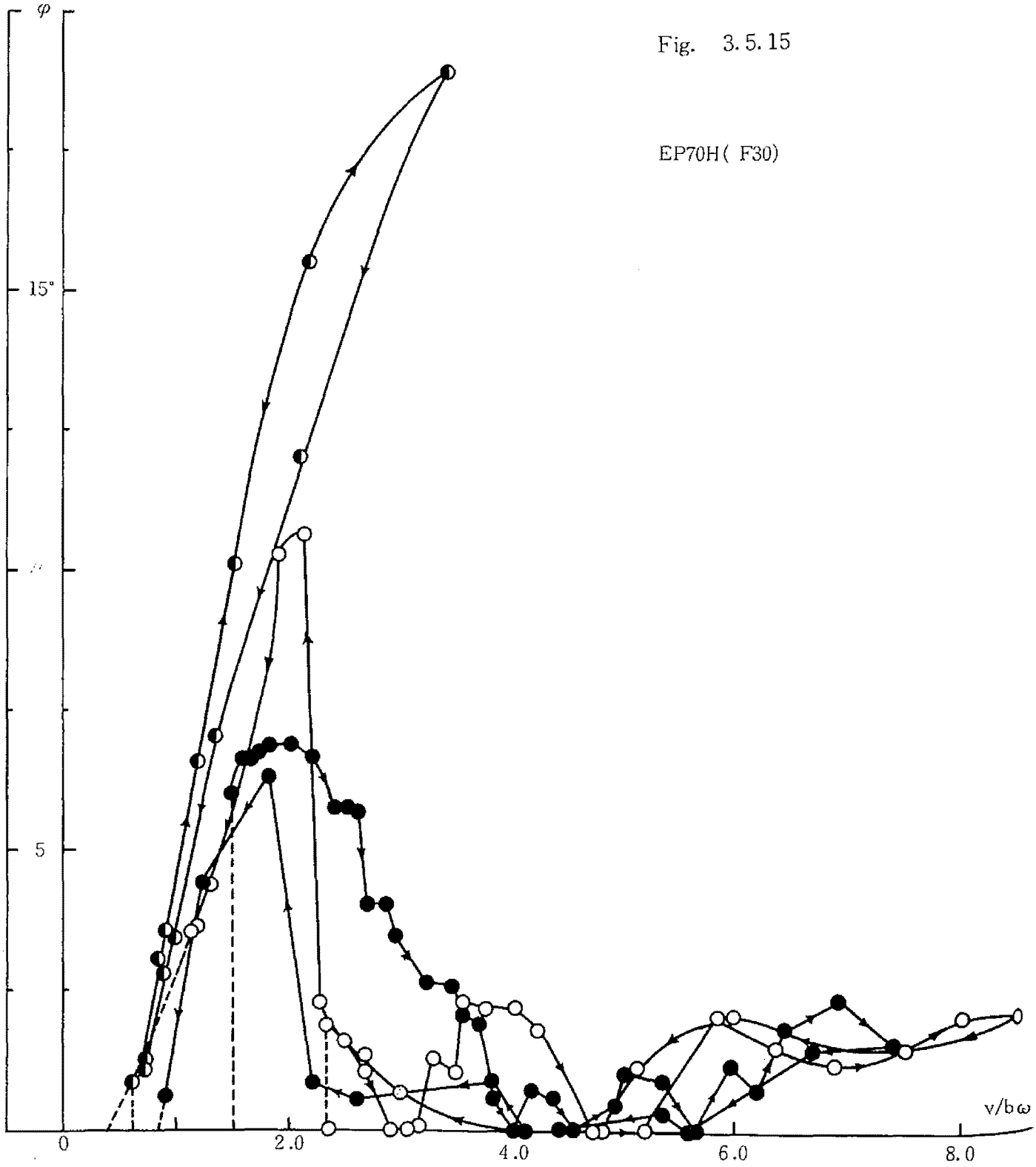

Vcr^S	Vcr^E	ω_η	ω_ξ	ζ_η	ζ_ξ	ω_ξ/ω_η	Test No.	Notation
4.16	2.02	8.718	11.868	.00513	.00344	1.361	11—20	○
3.22	1.97	8.770	14.361	.00458	.00397	1.638	11—21	●
1.56	—	8.796	16.755	.00626	.00290	1.905	11—22	◐

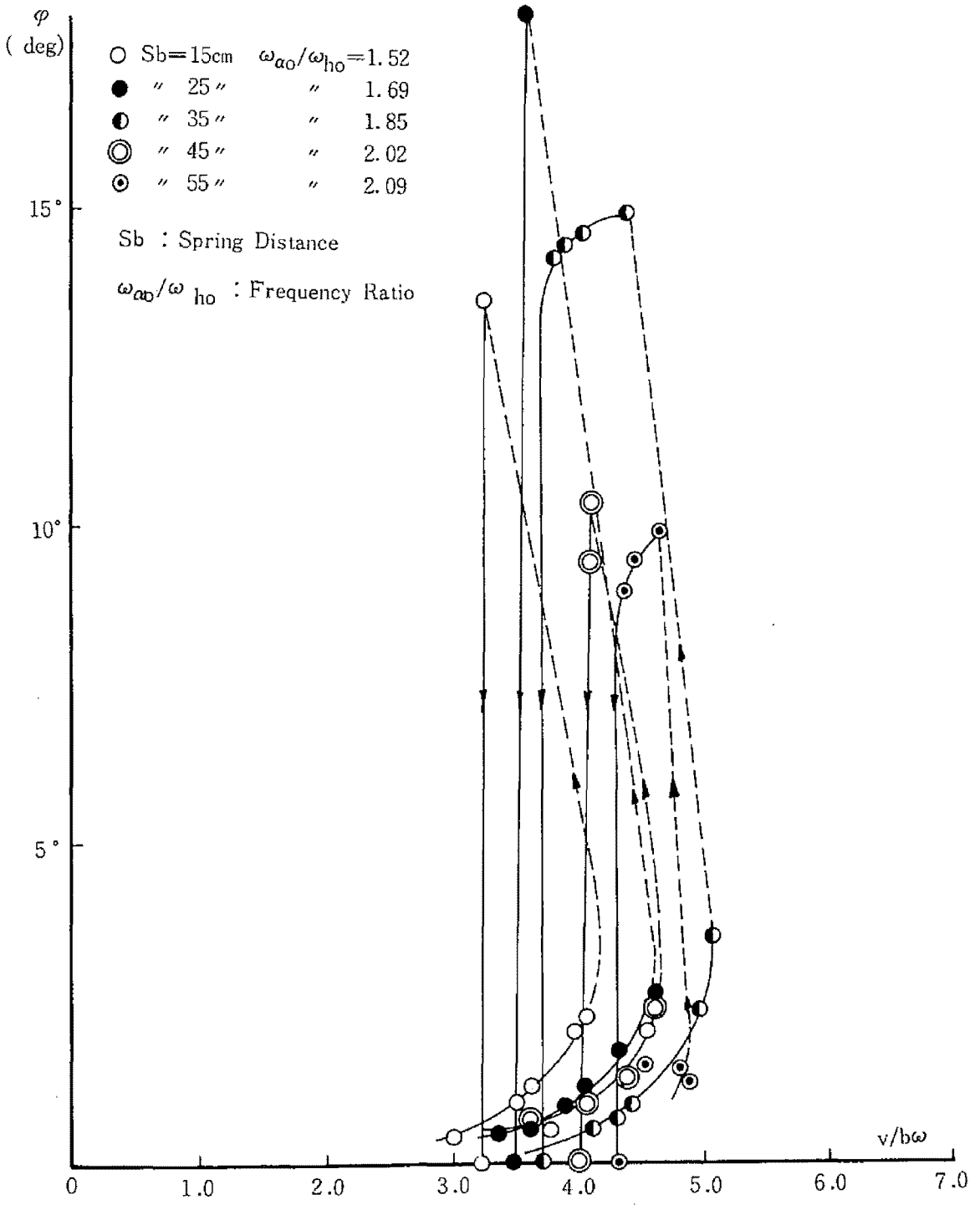

Fig. 3.5.16 Flutter Amplitude-Reduced Velocity Relation, Model : Plate

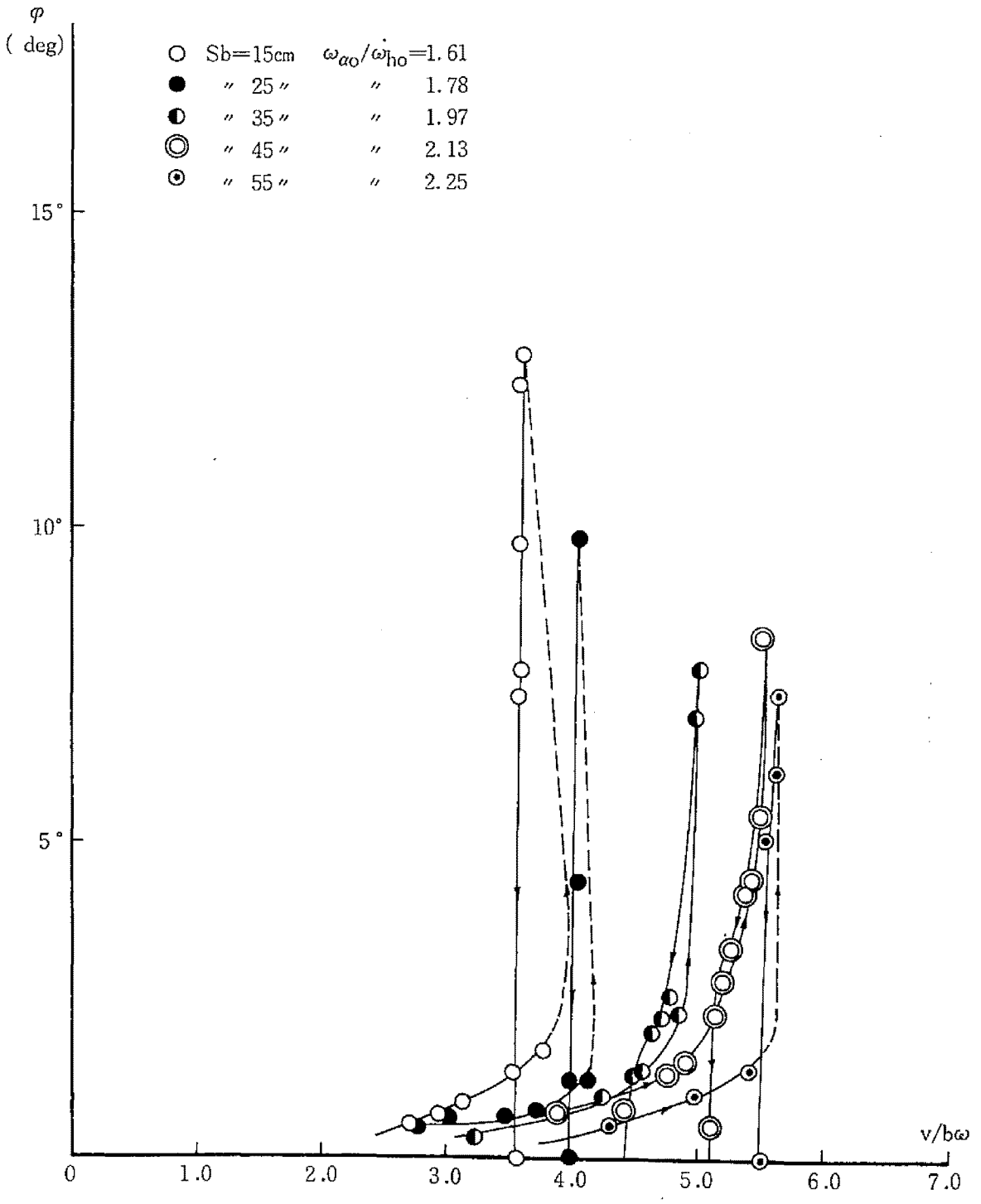

Fig. 3.5.17 Flutter Amplitude-Reduced Velocity Relation, Model : DT70H

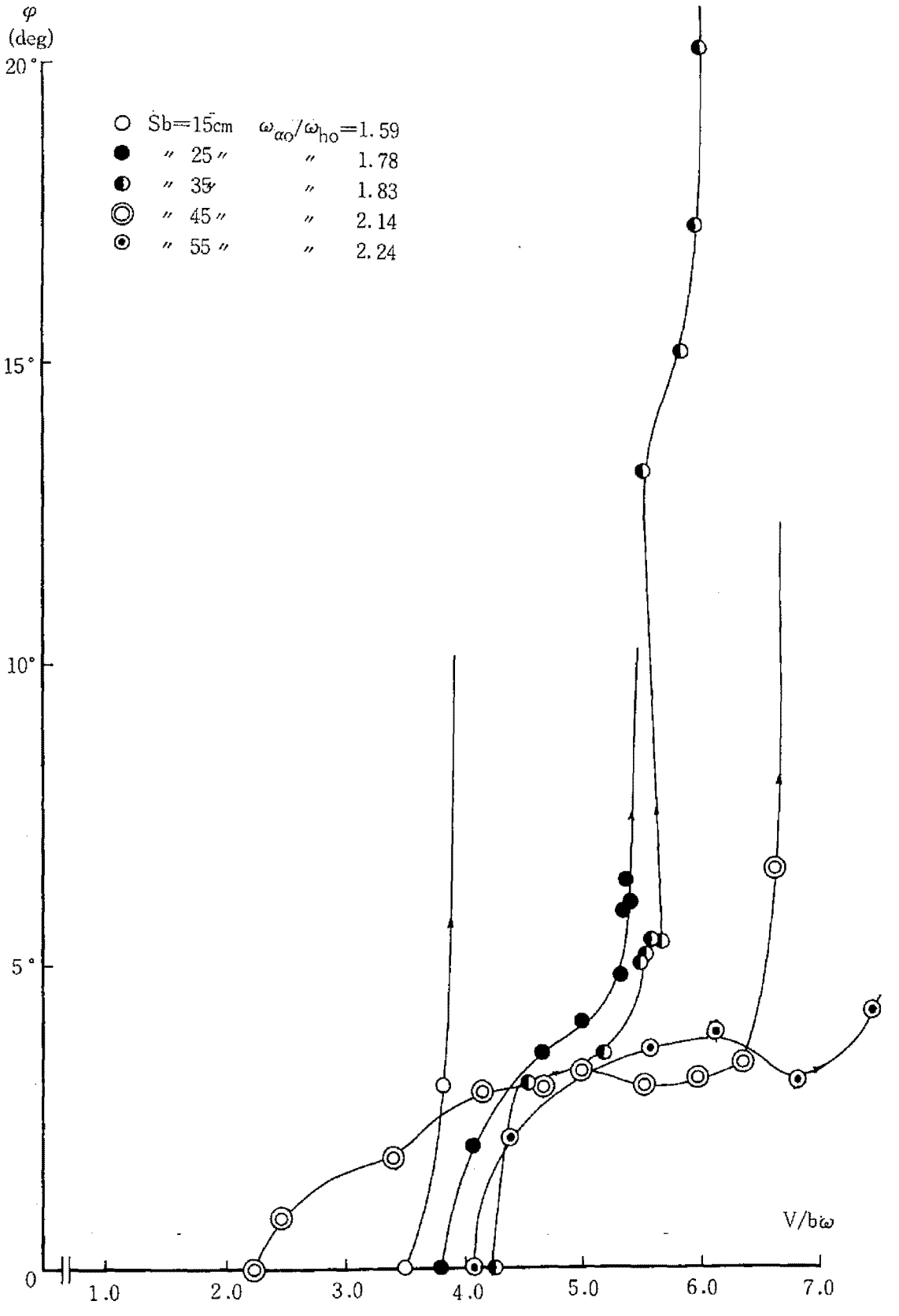

Fig. 3.5.18 Flutter Amplitude-Reduced Velocity Relation, Model : DT70π

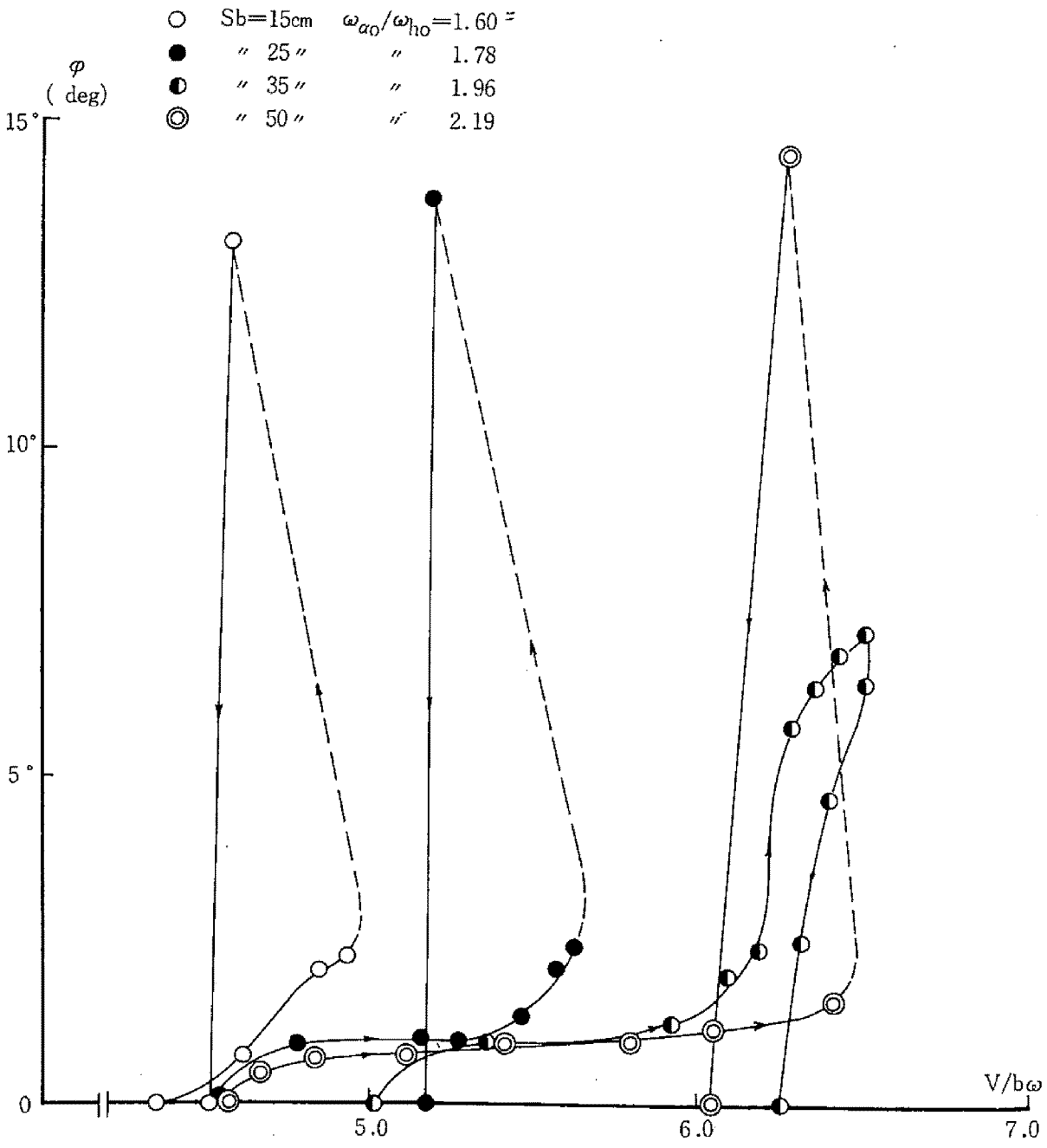

Fig. 3.5.19 Flutter Amplitude-Reduced Velocity Relation, Model : ET70H

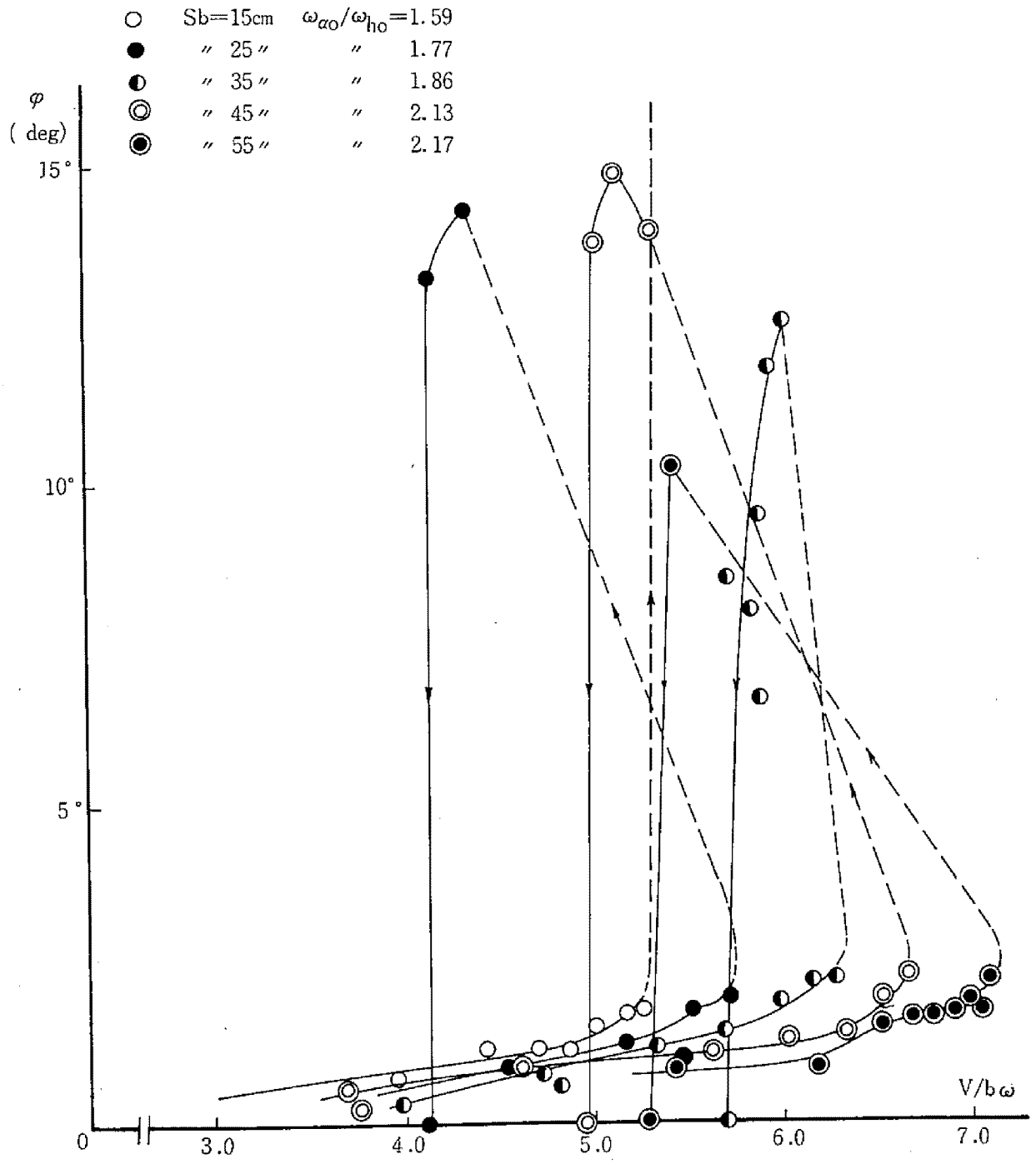

Fig. 3.5.20 Flutter Amplitude-Reduced Velocity Relation, Model : ET70π

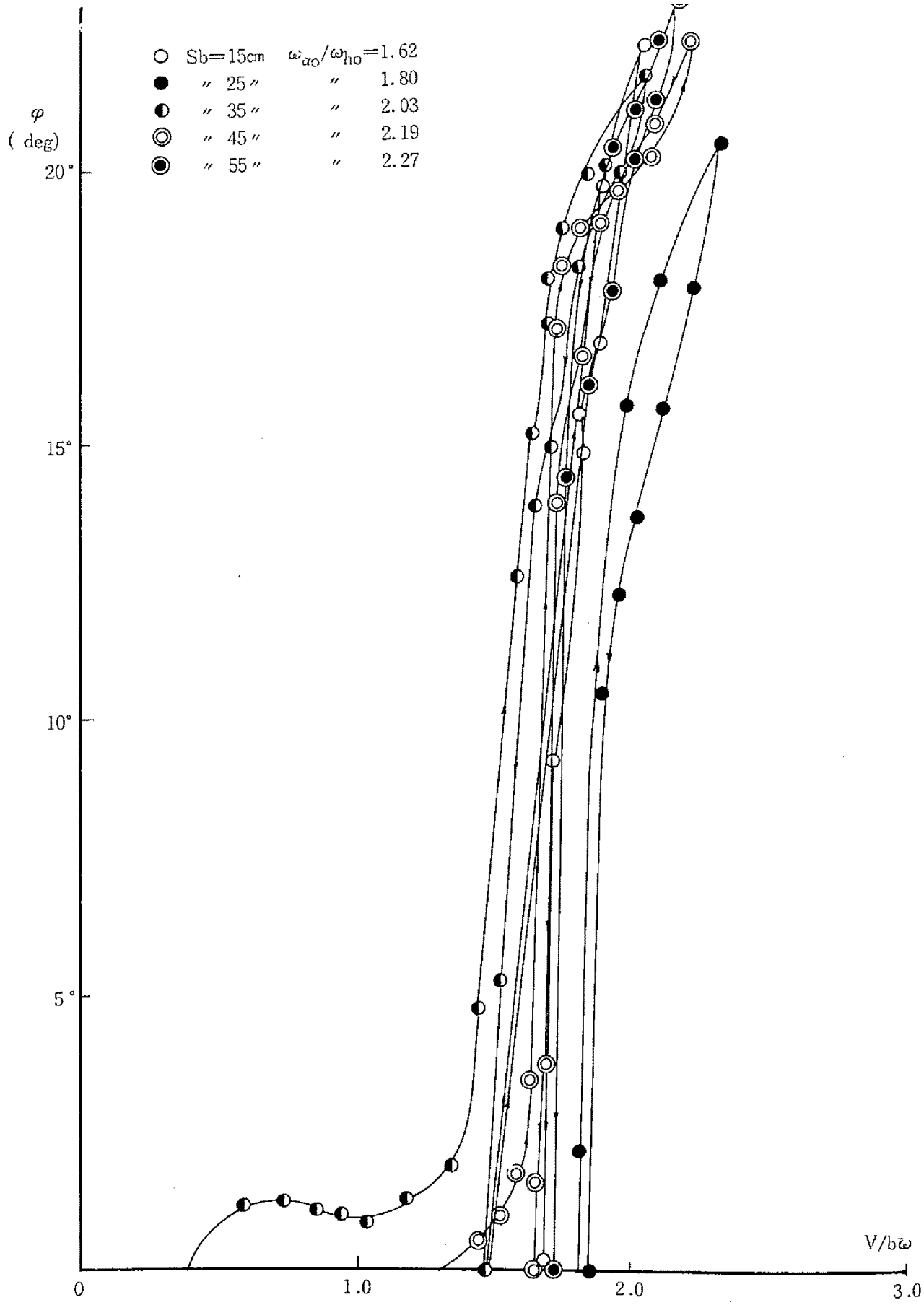

Fig. 3.5.21 Flutter Amplitude-Reduced Velocity Relation , Model : DP70HF30

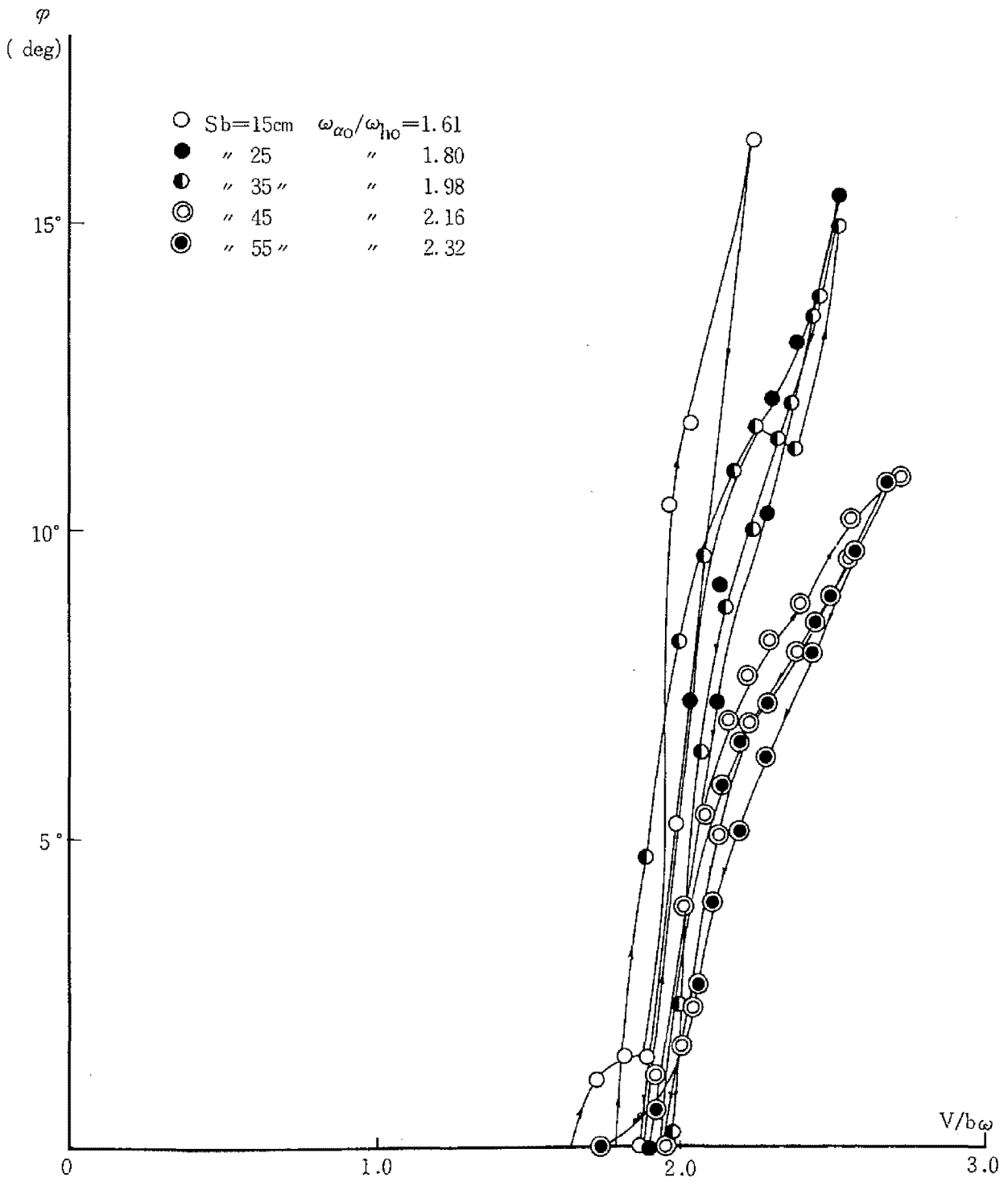

Fig. 3.5.22 Flutter Amplitude-Reduced Velocity Relation, Model : DP70πF30

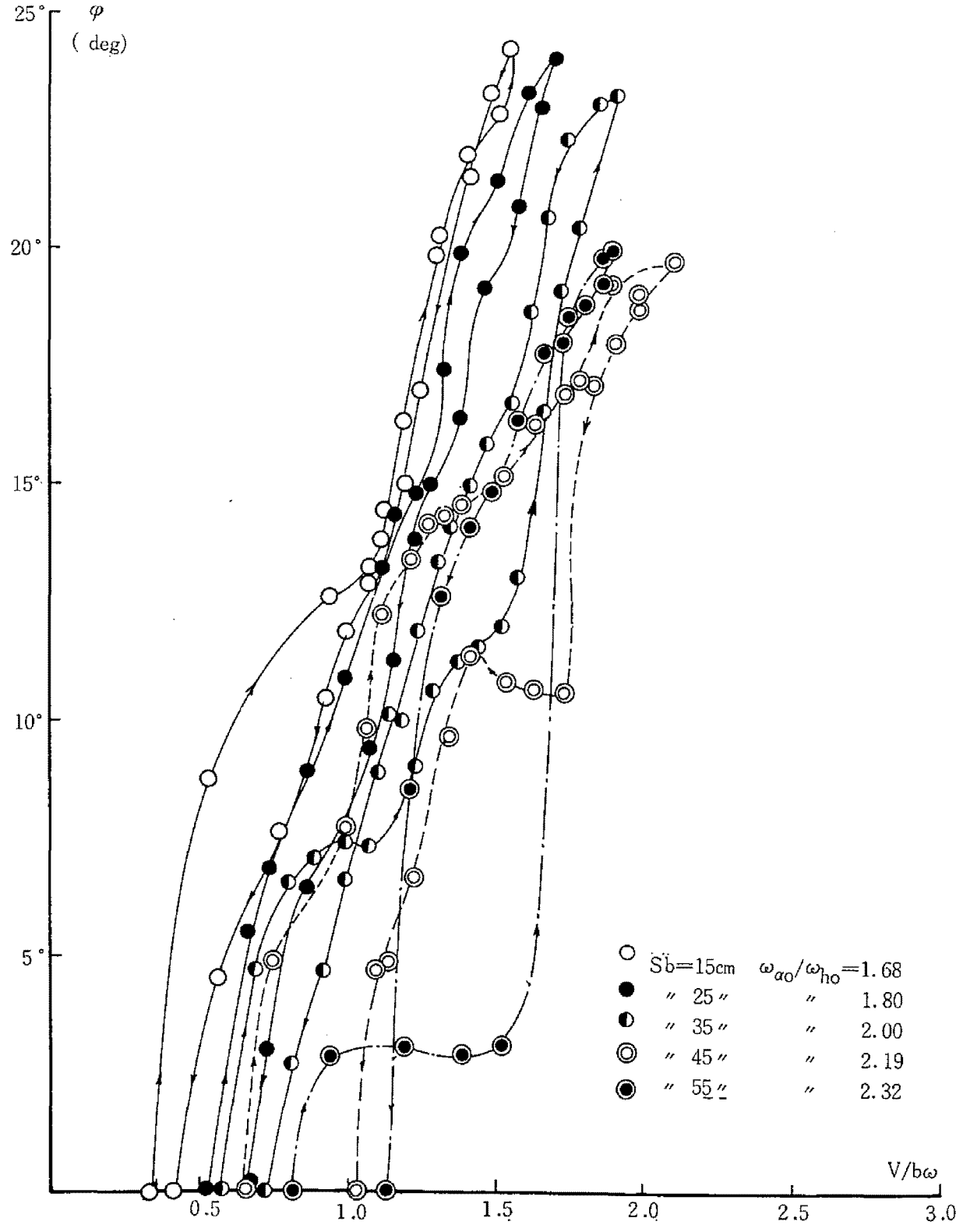

Fig. 3.5.23 Flutter Amplitude-Reduced Velocity Relation, Model : EP70HF30

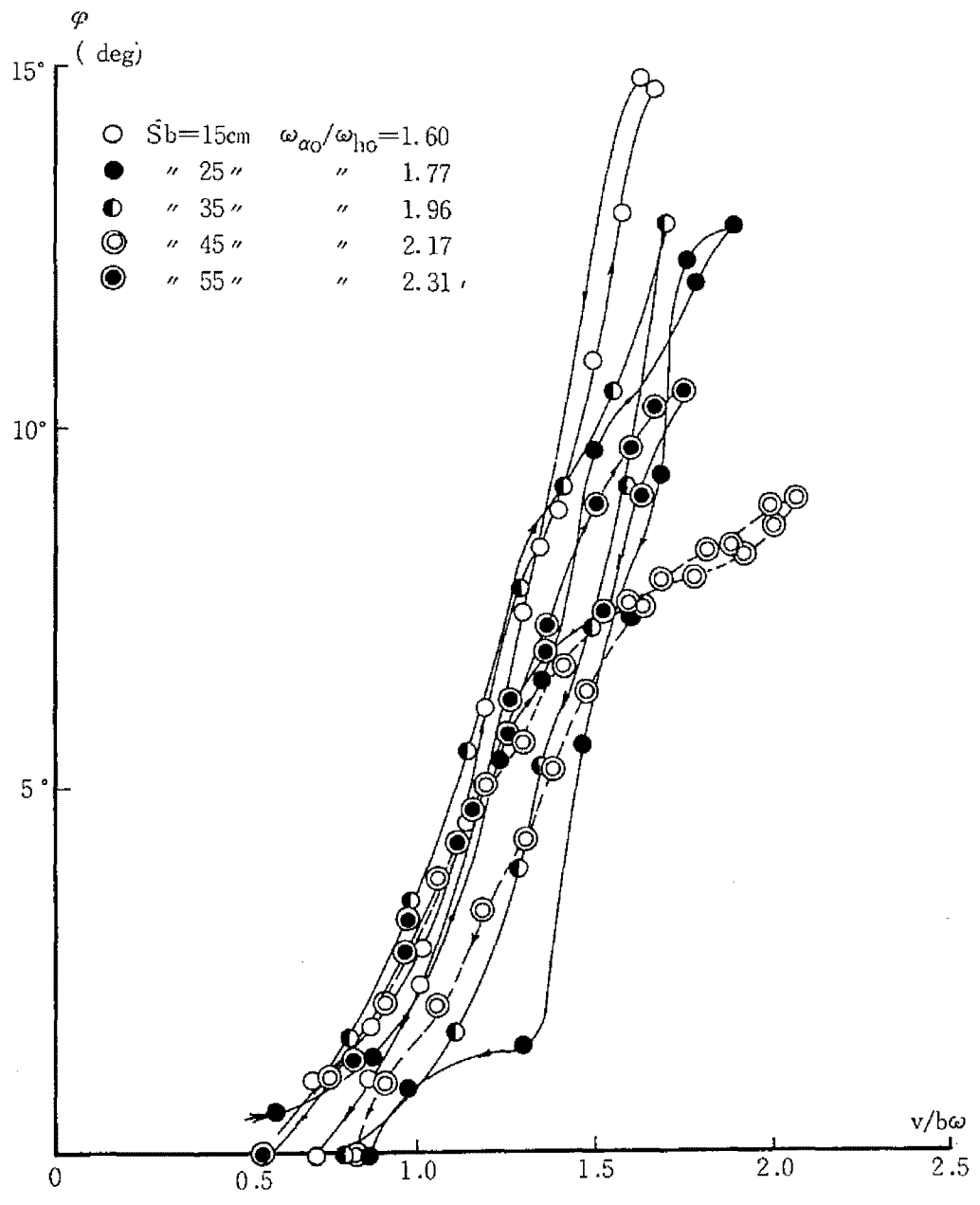

Fig. 3.5.24 Flutter Amplitude-Reduced Velocity Relation, Model : EP70πF30

3.6 MEASUREMENT OF AERODYNAMIC FORCES ACTING ON MODEL IN WIND TUNNEL

As shown in previous paragraphs 3.4 and 3.5 the aerodynamic charecteristics of bridge sections are disclosed by the static and dynamic wind tunnel tests. By the so-called static test in our problem the steady aeroelastic coefficients, C_L(lift coefficient), C_D(drag coefficient), and C_M(pitching moment coefficient), are obtained, while by the dynamic tests the critical wind velocity for instability is determined.

However the critical wind velocity and the flutter frequencies for the flutter phenomena, for instance, indicate insufficiently the aerodynamic characteristics of the so complicate system of bridge sections.

It is well known that for determination of aerodynamic forces acting on airfoils there are two representative methods, namely the free vibration method and the forced vibration method. The forced vibtation method is used by R. L Halfman to compare the Theodorsen theory with the actually acting aerodynamic forces on the aerofoil, NACA0012 sections of two degrees of freedoms. The results show a good accordance with each other. The principle of measurement method by Halfman is again used by Ukeguchi, Sakata and Nishitani with an improved idea to subtract the inertial forces from the total dynamic forces to find the differential forces, aerodynamic forces, using as additional dummy model. In other words this method is to obtain the aerodynamic forces as the difference between the dynamic forces received by a model in air stream and the dynamic forces received by the other model in still air, both of which move simultaneously together. It should be mentioned that the forced vibration method due to Halfman et al is only valid for the small amplitudes in the linear region of responses. As illustrated previously the free vibration method is recently applied by Scanlan and Sabzevari reviwing the flutter phenomenon of suspension bridge to assure the fact that the plate girder type bridge section is clearly characterized by the dominant aerodynamic coefficient A_2 which is defined in the set of equations, (3.3.1) and (3.3.2) in 3.3.

The relations of aerodynamic coefficients defined by the forced vibration method and the free vibration method are tabled in Table 3.6.1.

According to the investigation by Ukeguchi, Sakata and Nishitani the plate girder type model and the truss-stiffened plate type model with some angle of attack show the positive phase angle $\beta[C_{m\alpha}]$ as shown in Fig. 3.6.1, while the absolute values of coeficients are considered less remarkably varying with the types of models and they tend to increase as the reduced velocity increases. It is easily seen that the plate with no angle of attack is associated with the negative value of phase angle $\beta[C_{m\alpha}]$, so that the positiveness of this phase angle is considered to relate to some extent with discontinuous separation of flow from the body of models.

The aerodynamic coefficients defined by the free vibration method are illustrated as in Fig. 3.6.6 for the plate by the Theodorsen's theory. By use of the models in our investigations the characteristic aerodynamic coefficients A_2 and A_3 are obtained experimentally as shown in Fig.'s 3.6.7 ~ 3.6.12. In Fig.3.6.13 one of the remaining coefficient H_1 is shown as the non-dimensional quantity vs the reduced velocity. The similar relations of A_2*, A_3* with the reduced velocity are figured qualitatively in Fig.'s 3.6.14 and 3.6.15 using the experimental results. The characteristic phase angle $\beta[C_{m\alpha}]$, defined in the forced vibration method, is easily determined as shown in Table 3.6.1; based on the aerodynamic coefficients A_2* and A_3* some of the test results are plotted in Fig.'s 3.6.16 and 3.6.17 which reveal, generally speaking, that the plate or the truss-stiffened plate type is associated with the negative value of the phase angle β and, however, the plate girder type model is associated with positive as already remarked in the investigations by Ukeguchi et al.

In our investigations the free vibration method is used to determine the aerodynamic forces acting on the bridge sections according to the method proposed by Scanlan and Sabzevari. The results indicate that measurement of frequencies and damping coefficients is easily done with sufficient accuracy, while the measurement of phase angle between the deflection and the torsional deformations is comparatively difficult and it effects directly on the coupling aerodynamic coefficients A_1*, H_2*

and H_3*. In order to eliminate this difficulty a combined method for determination of aerodynamic coefficients is considered to use the both types of methods, namely the free vibration method and the forced vibration method to determine the uncoupled aerodynamic coefficients, H_1*, A_2*, and A_3* and secondly to use the forced vibration method to determine the coupled aerodynamic coefficients, A_1*, H_2* and H_3*.
The principle to use the forced vibration method is as follows;
If the steady vertical force is applied for models, the equations of motion are written as

$$\ddot{\eta} + 2\zeta_\eta \omega_\eta \dot{\eta} + \omega_\eta^2 \eta - H_1 \dot{\eta} - H_2 \dot{\varphi} - H_3 \varphi = L / m$$

$$\ddot{\varphi} + 2\zeta_\alpha \omega_\alpha \dot{\varphi} + \omega_\alpha^2 \varphi - A_1 \dot{\eta} - A_2 \dot{\varphi} - A_3 \varphi = 0$$

Since $L = L_0 \sin(\omega t + \Psi)$, we have $\eta = \eta_0 \sin \omega t$, $\varphi = \varphi_0 \sin(\omega t - \theta)$
Substitution of above deflectional modes into the second equation yields to

$$A_1 = \frac{1}{\omega} \left(\frac{\varphi_0}{\eta_0}\right) \left[(\omega^2 - \omega_\alpha^2 - A_3) \sin\theta + (2\zeta_\alpha \omega_\alpha - A_2)\, \omega \cos\theta \right]$$

where the right side is known as given values ; ω_α, ζ_α are initially given natural frequencies and damping codfficient, A_2, A_3 are determined by the free vibration method, and ω, η_0, φ_0, θ are the forced frequency, the amplitudes, and the phase angle of deflectional modes.
The steady forced vibration is remarkably stable so that it is easily done to find the phase angle between the torsional deformation and the deflectional deformation from the Lissajous' diagram.

If the steady pitching moment is applied for models, the equations of motion are written as

$$\ddot{\eta} + 2\zeta_\eta \omega_\eta \dot{\eta} + \omega_\eta^2 \eta - H_1 \dot{\eta} - H_2 \dot{\varphi} - H_3 \varphi = 0$$

$$\ddot{\varphi} + 2\zeta_\alpha \omega_\alpha \dot{\varphi} + \omega_\alpha^2 \varphi - A_1 \dot{\eta} - A_2 \dot{\varphi} - A_3 \varphi = M_t / I_p$$

By similar fashion as before the coupling aerodynamic coefficients H_2, H_3 can be determined from the responses defined by the first equation of the above set of equations as follows

$$H_2 = \frac{1}{\omega}\left(\frac{\eta_0}{\varphi_0}\right)\left[\,(\omega_\eta^2 - \omega^2)\sin\theta + (2\zeta_\eta\,\omega_\eta - H_1)\,\omega\cos\theta\right]$$

$$H_3 = -\frac{\eta_0}{\varphi_0}\left[\,(\omega^2 - \omega_\eta^2)\cos\theta + (2\zeta_\eta\,\omega_\eta - H_1)\,\omega\sin\theta\right]$$

According to the preliminaty experimental investigation by this method the aerodynamic coefficients obtained for a plate coincide satisfactorily with the theoretical values, so the method is applied for a truss-stiffened bridge section model, RT-1 as shown in Photo 3.5. The results are indicated in Fig.'s 3.6.18 and 3.6.19. In Fig. 3.6.18 the aerodynamic coefficients determined from uncoupled free vibrations, namely H_1^*, A_2^*, A_3^* are shown in comparison with those defined by the Theodorsen's theory. As far as this results are concerned, A_2^* is considered to accord with the theoretical values, while A_3^* is remarkably smaller and H_1^* is comparatively smaller than the Theodoren's theory. For the aerodynamic coefficients A_1^*, H_2^*, H_3^* to result in the coupling effects the following facts should be particularly noticed that A_1^* is negligibly small and H_2^* shows a peak value at approximately $V/b\omega = 8.0$ and H_3^* decreases monotonically in the large value of the reduced velocity. It is interesting to note that the peak value H_2^* occurs at the reduced velocity 8.0 approximately which is equal to the critical reduced velocity as shown in Fig. 3.6.20.

It is rather difficult to conclude the general aerodynamic behaviours of large spanned bridge structures, because the aerodynamic effects on the bridges can differ from one another depending on the types of structures and the dynamic characteristics. However the experimental method as mentioned above seems us to have an advantages for the sake of simpleness and rapidness to characterise the flutter phenomenon of the bridge sections.

Table 3. 6. 1

Coefficients	General Structure	Plate (Theory)
C_{lh}	$\frac{1}{\pi} \mid H_1^* \mid$	$\frac{2}{k} \mid C(k) \mid$
β	$\frac{3}{2}\pi$	$\frac{3}{2}\pi$
$C_{l\alpha}$	$\frac{1}{\pi} (H_2^*)^2 + (H_3^*)^2$	$\frac{1}{k} \{1+\mid C(k) \mid\}^2 + \{\frac{2 \mid C(k) \mid}{k}\}^2$
β	$\pi + \tan^{-1} \frac{H_2^*}{H_3^*}$	$\pi + \tan^{-1} \frac{k\{1+\mid C(k) \mid\}}{2 \mid C(k) \mid}$
C_{mh}	$\frac{1}{\pi} A_1^*$	$\frac{1}{k} \mid C(k) \mid$
β	$\frac{\pi}{2}$	$\frac{\pi}{2}$
$C_{m\alpha}$	$\frac{1}{\pi} (A_2^*)^2 + (A_3^*)^2$	$\frac{1}{k} \{\frac{1-\mid C(k) \mid}{2}\}^2 + \{\frac{\mid C(k) \mid}{k}\}^2$
β	$\tan^{-1} \frac{A_2^*}{A_3^*}$	$-\tan^{-1} \frac{k\{1-\mid C(k) \mid\}}{2 \mid C(k) \mid}$

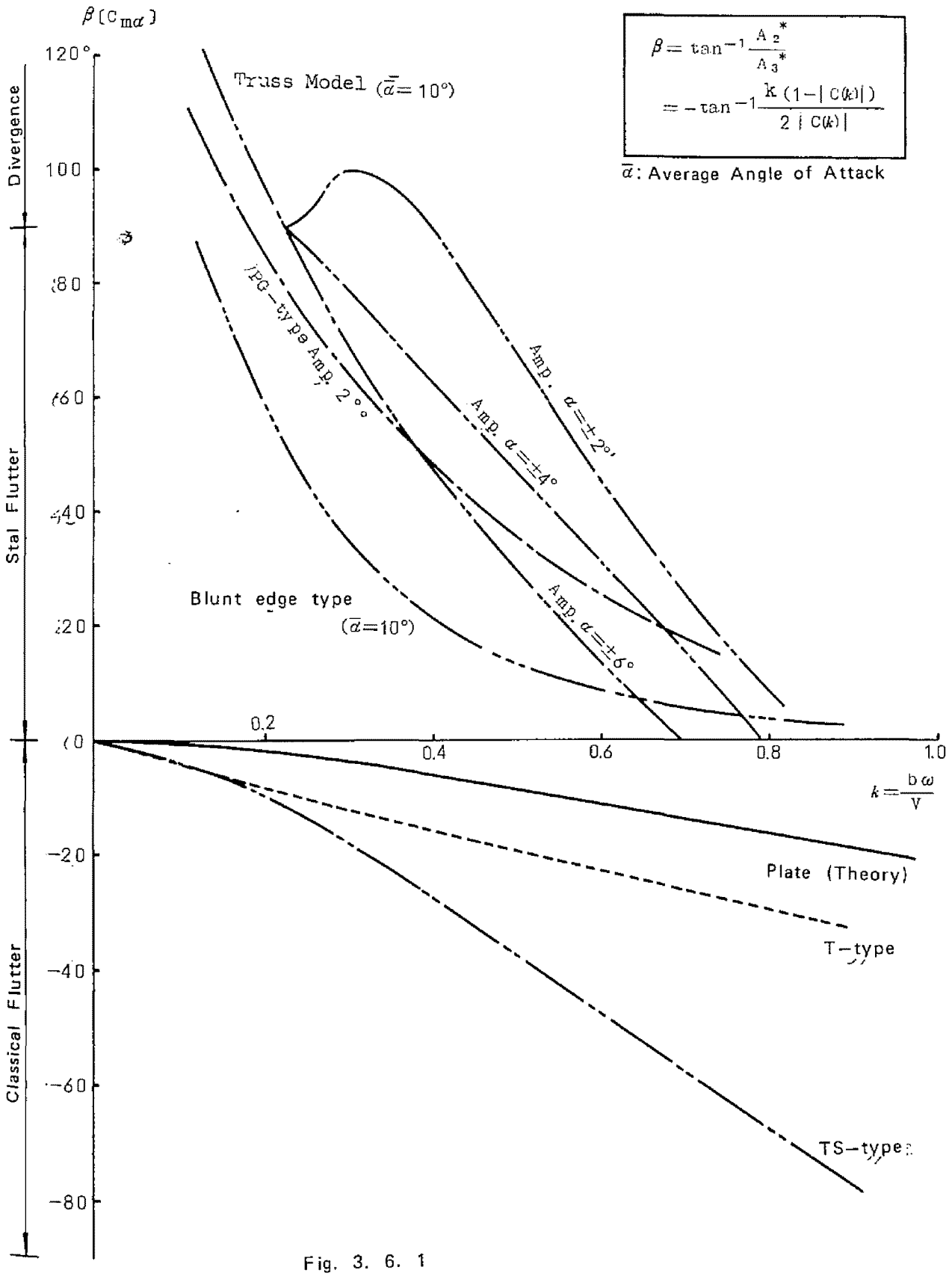
$\beta(C_{m\alpha})$
$\beta = \tan^{-1}\frac{A_2^*}{A_3^*} = -\tan^{-1}\frac{k(1-|C(k)|)}{2|C(k)|}$
$\bar{\alpha}$: Average Angle of Attack
Truss Model ($\bar{\alpha}$= 10°)
Amp. $\alpha = \pm 2°$
Amp. $\alpha = \pm 4°$
Amp. $\alpha = \pm 6°$
IPG-type Amp. 2°
Blunt edge type
($\bar{\alpha}$=10°)
Plate (Theory)
T-type
TS-type
Divergence
Stal Flutter
Classical Flutter
120°
100
80
60
40
20
0
-20
-40
-60
-80
0.2
0.4
0.6
0.8
1.0
$k = \frac{b\omega}{V}$

Fig. 3. 6. 1

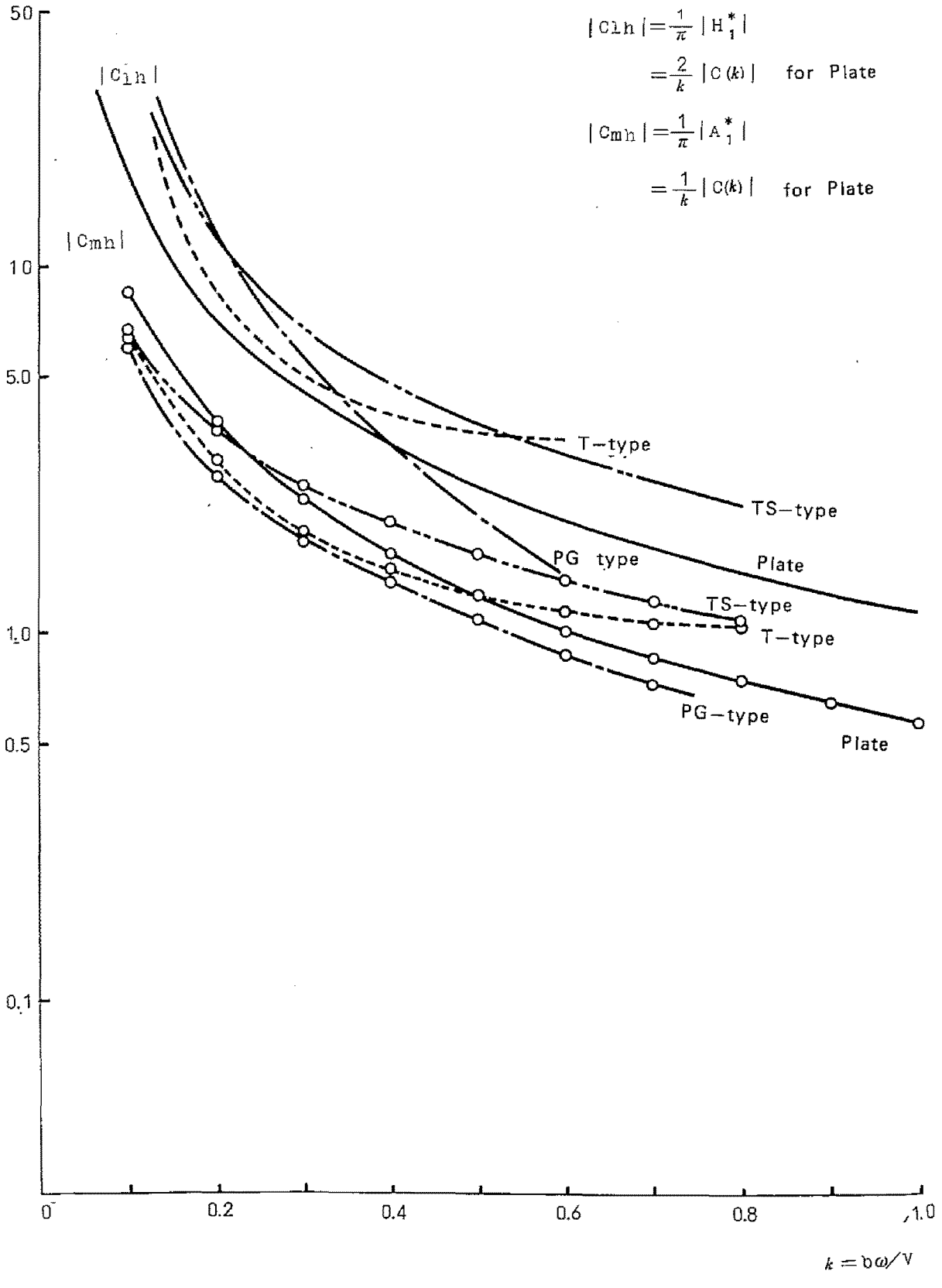
$|C_{lh}| = \frac{1}{\pi}|H_1^*|$
$= \frac{2}{k}|C(k)|$ for Plate
$|C_{mh}| = \frac{1}{\pi}|A_1^*|$
$= \frac{1}{k}|C(k)|$ for Plate
$|C_{lh}|$
$|C_{mh}|$
50
10
5.0
1.0
0.5
0.1
0
0.2
0.4
0.6
0.8
1.0
T-type
TS-type
Plate
PG type
TS-type
T-type
PG-type
Plate
$k = b\omega/V$

Fig. 3. 6. 2

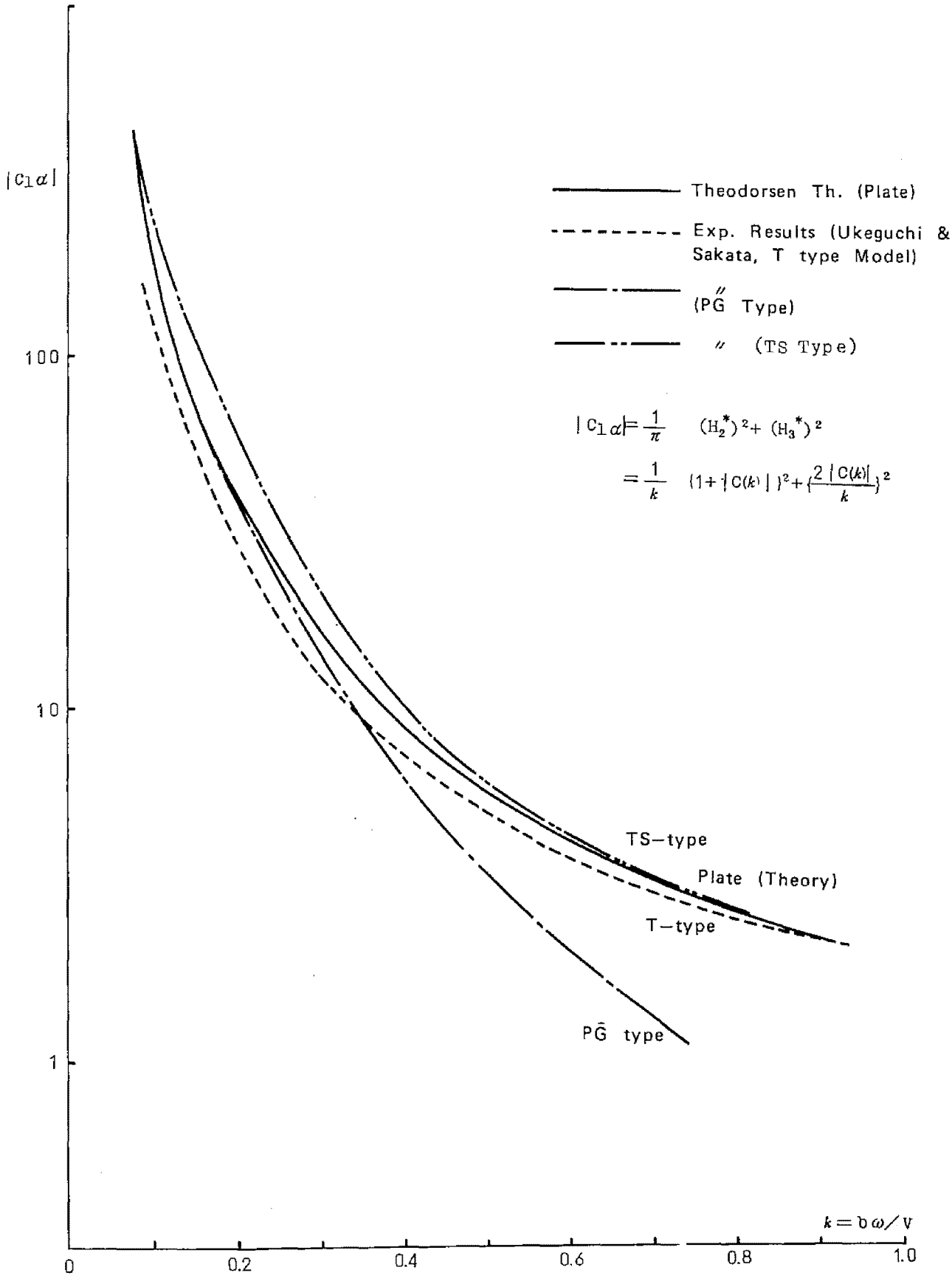
$|C_{l\alpha}|$
100
10
1
0
0.2
0.4
0.6
0.8
1.0
$k = b\omega / V$
Theodorsen Th. (Plate)
Exp. Results (Ukeguchi & Sakata, T type Model)
〃 (PG̃ Type)
〃 (TS Type)
$|C_{l\alpha}| = \frac{1}{\pi} (H_2^*)^2 + (H_3^*)^2$
$= \frac{1}{k} (1 + |C(k)|)^2 + (\frac{2|C(k)|}{k})^2$
TS−type
Plate (Theory)
T−type
PG̃ type

Fig. 3. 6. 3

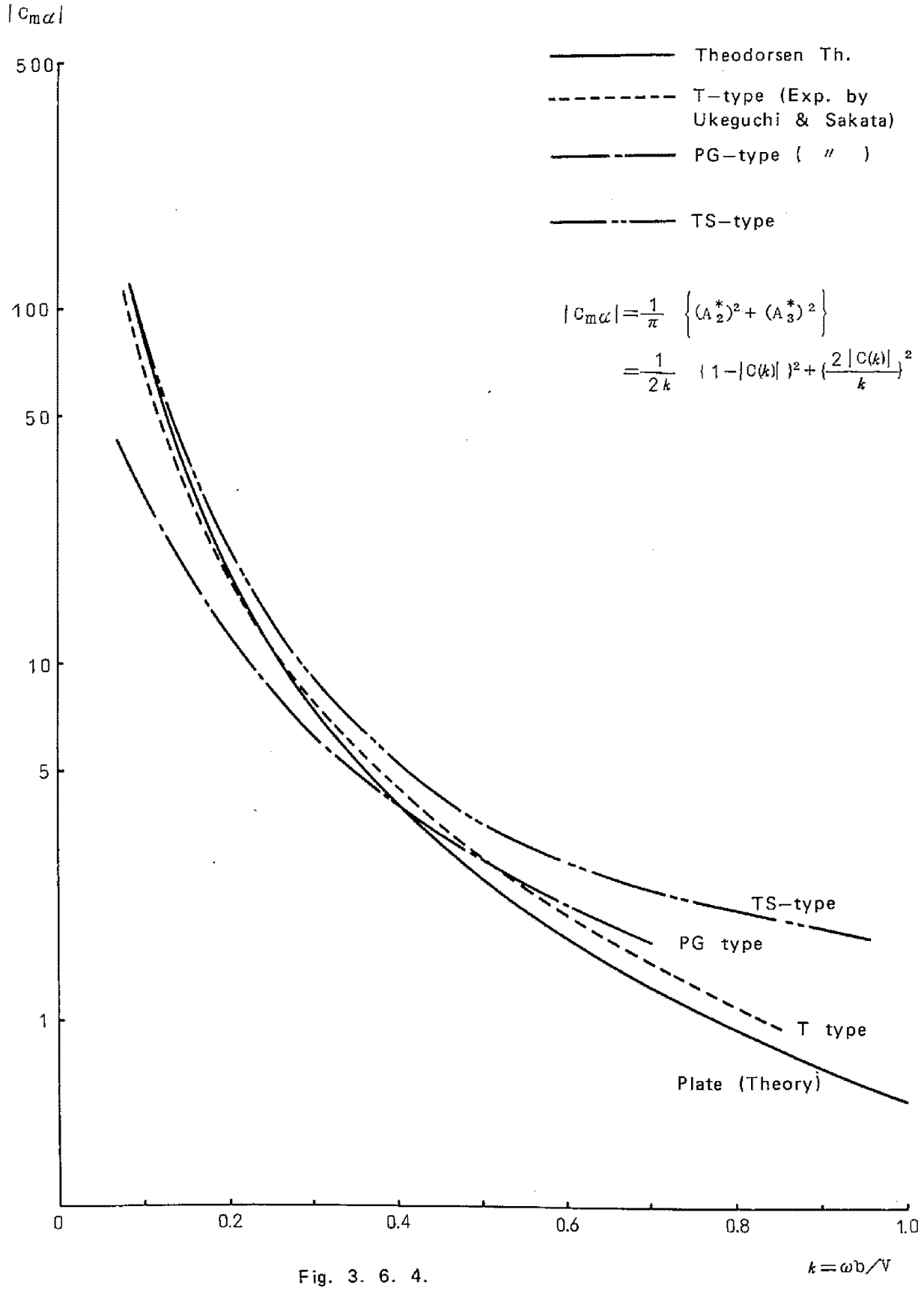
$|C_{m\alpha}|$
500
100
50
10
5
1
0
0.2
0.4
0.6
0.8
1.0
$k=\omega b/V$
Theodorsen Th.
T−type (Exp. by Ukeguchi & Sakata)
PG−type (〃)
TS−type
$|C_{m\alpha}|=\frac{1}{\pi}\left\{(A_2^*)^2+(A_3^*)^2\right\}$
$=\frac{1}{2k}\left\{1-|C(k)|\right)^2+\left\{\frac{2|C(k)|}{k}\right\}^2$
TS−type
PG type
T type
Plate (Theory)

Fig. 3. 6. 4.

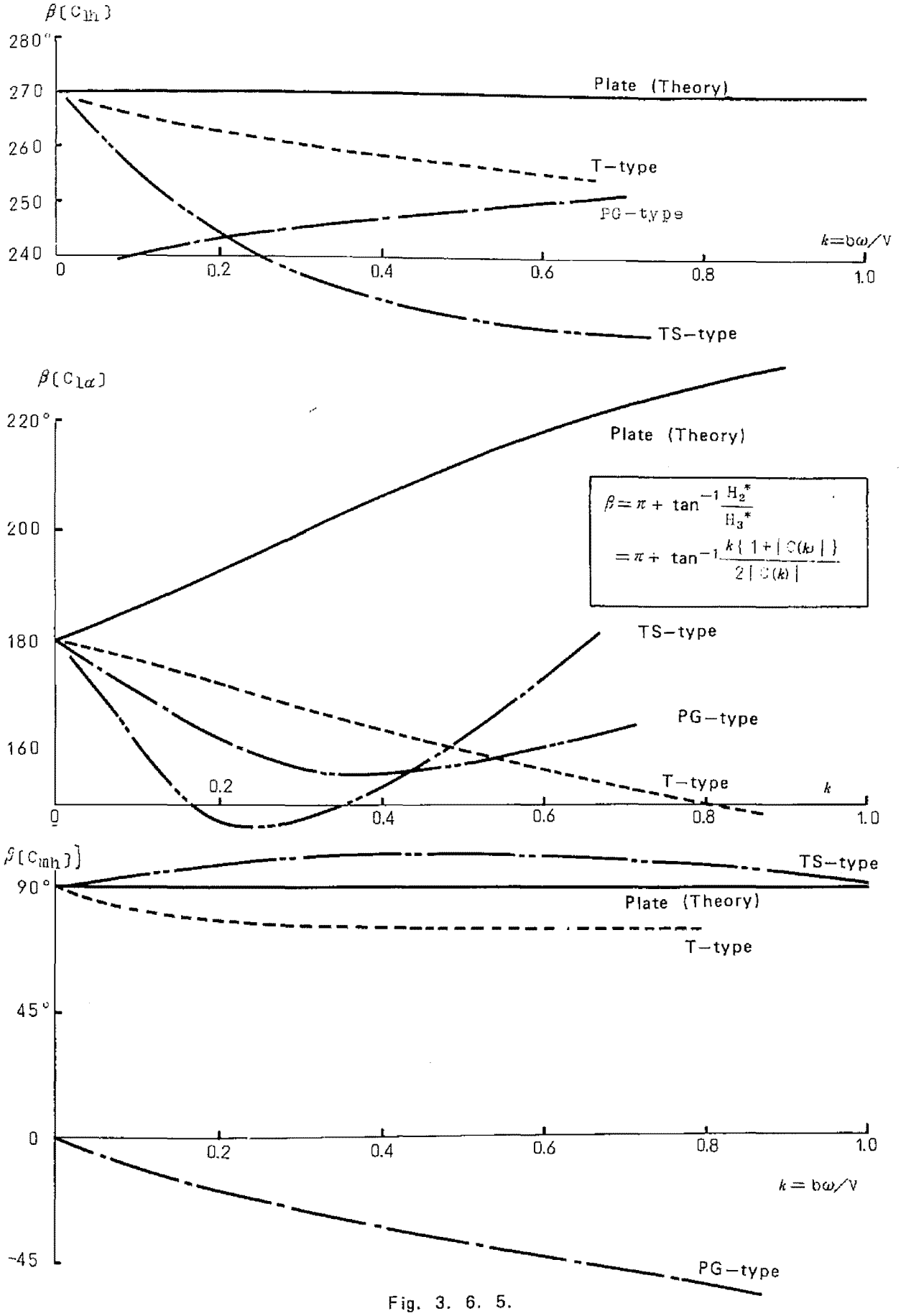
β[C_lh]
280°
270
260
250
240
Plate (Theory)
T-type
PG-type
TS-type
k=bω/V
0
0.2
0.4
0.6
0.8
1.0
β[C_lα]
220°
200
180
160
Plate (Theory)
β = π + tan⁻¹ H₂*/H₃*
= π + tan⁻¹ k{1+|C(k)|}/2|C(k)|
TS-type
PG-type
T-type
k
β[C_mh]
90°
45°
0
-45
TS-type
Plate (Theory)
T-type
PG-type
k = bω/V

Fig. 3. 6. 5.

Fig. 3.6.6 Aerodynamic Coefficients by Theodorsen's Theory

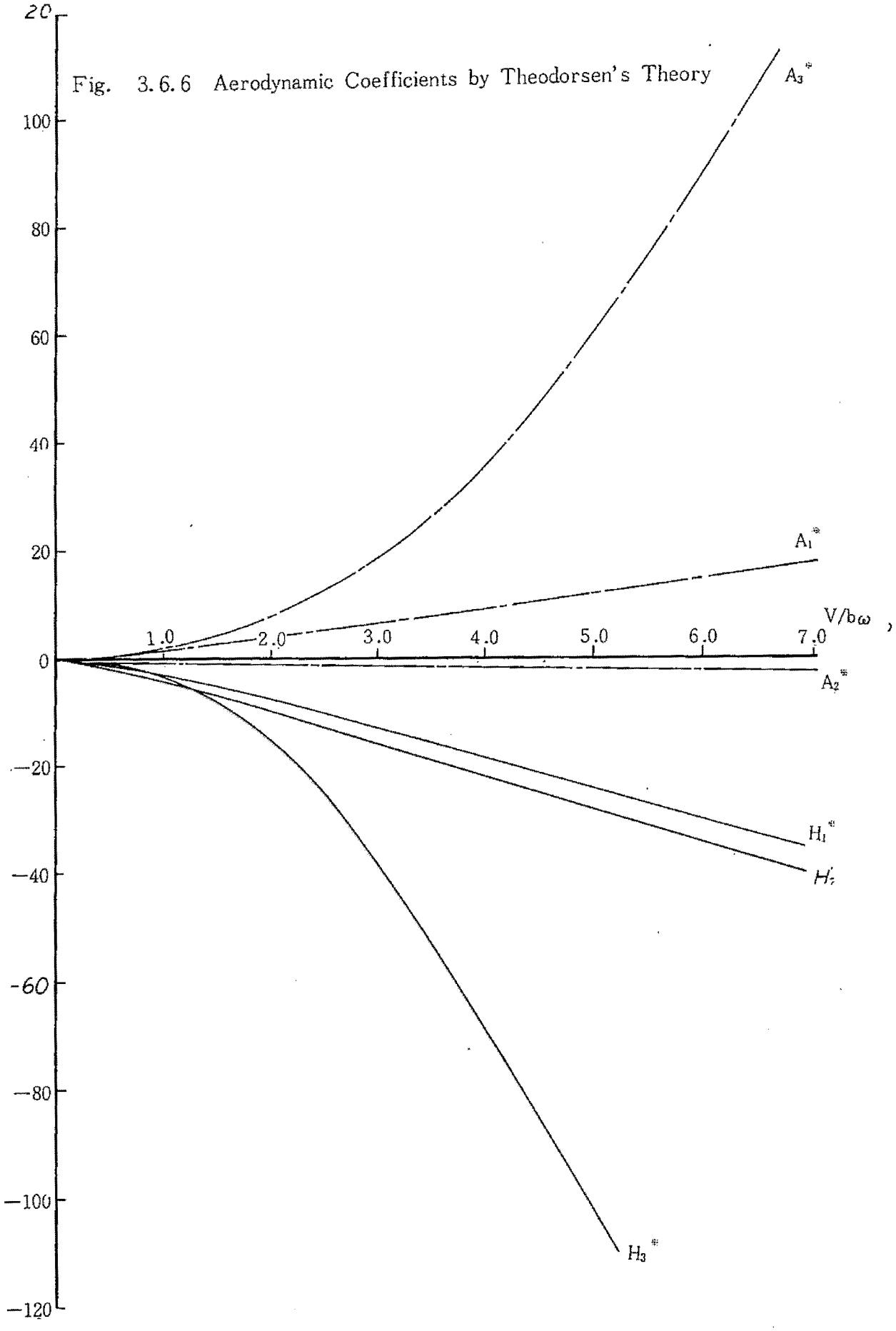

Aerodynamic Coefficients for Model DP70H (F30)

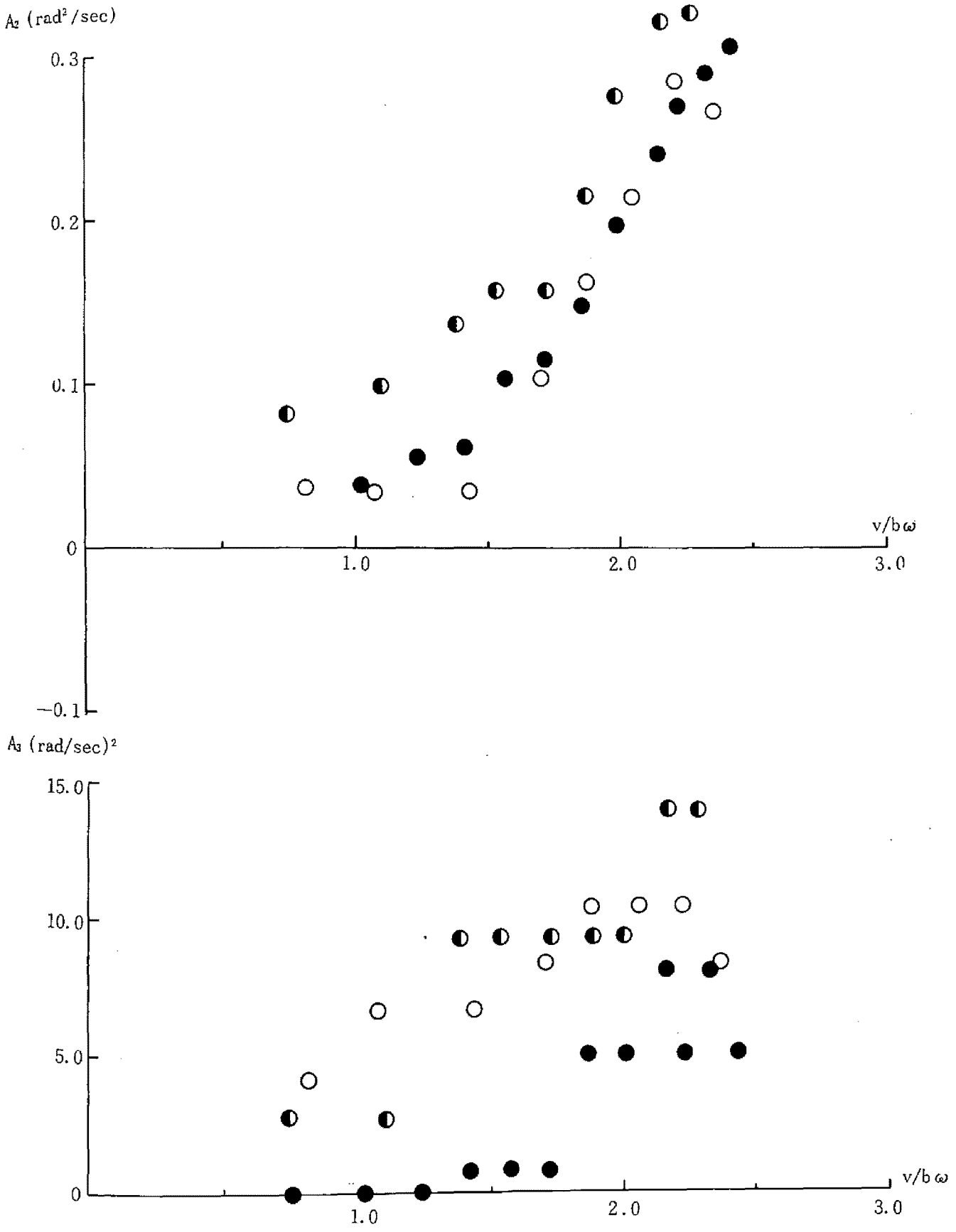

Fig. 3.6.7

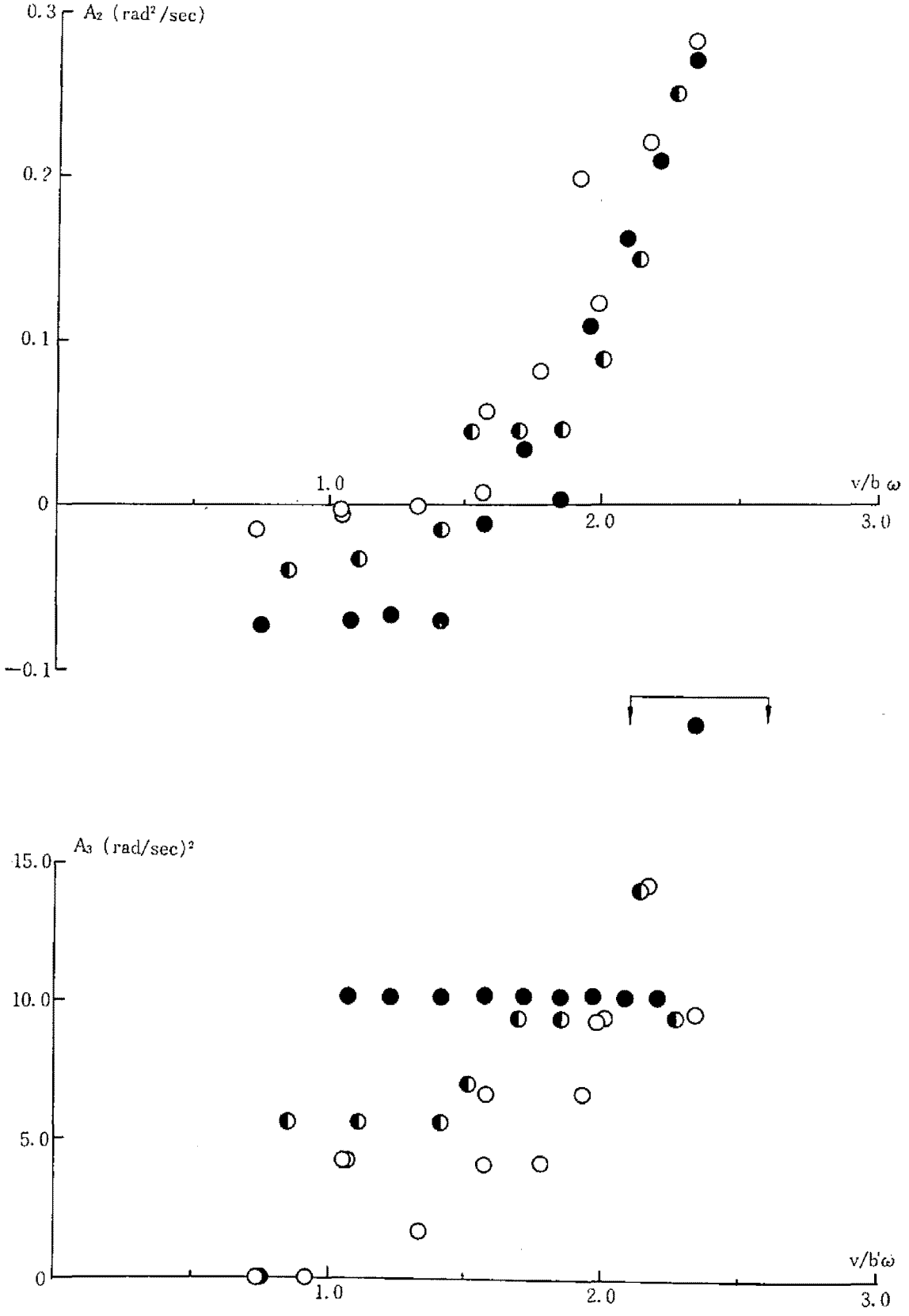
0.3
A₂ (rad²/sec)
0.2
0.1
0
−0.1
1.0
2.0
3.0
v/b ω
15.0
A₃ (rad/sec)²
10.0
5.0
0
1.0
2.0
3.0
v/b'ω

Fig. 3.6.8

Aerodynamic Coefficient for Model ET70π

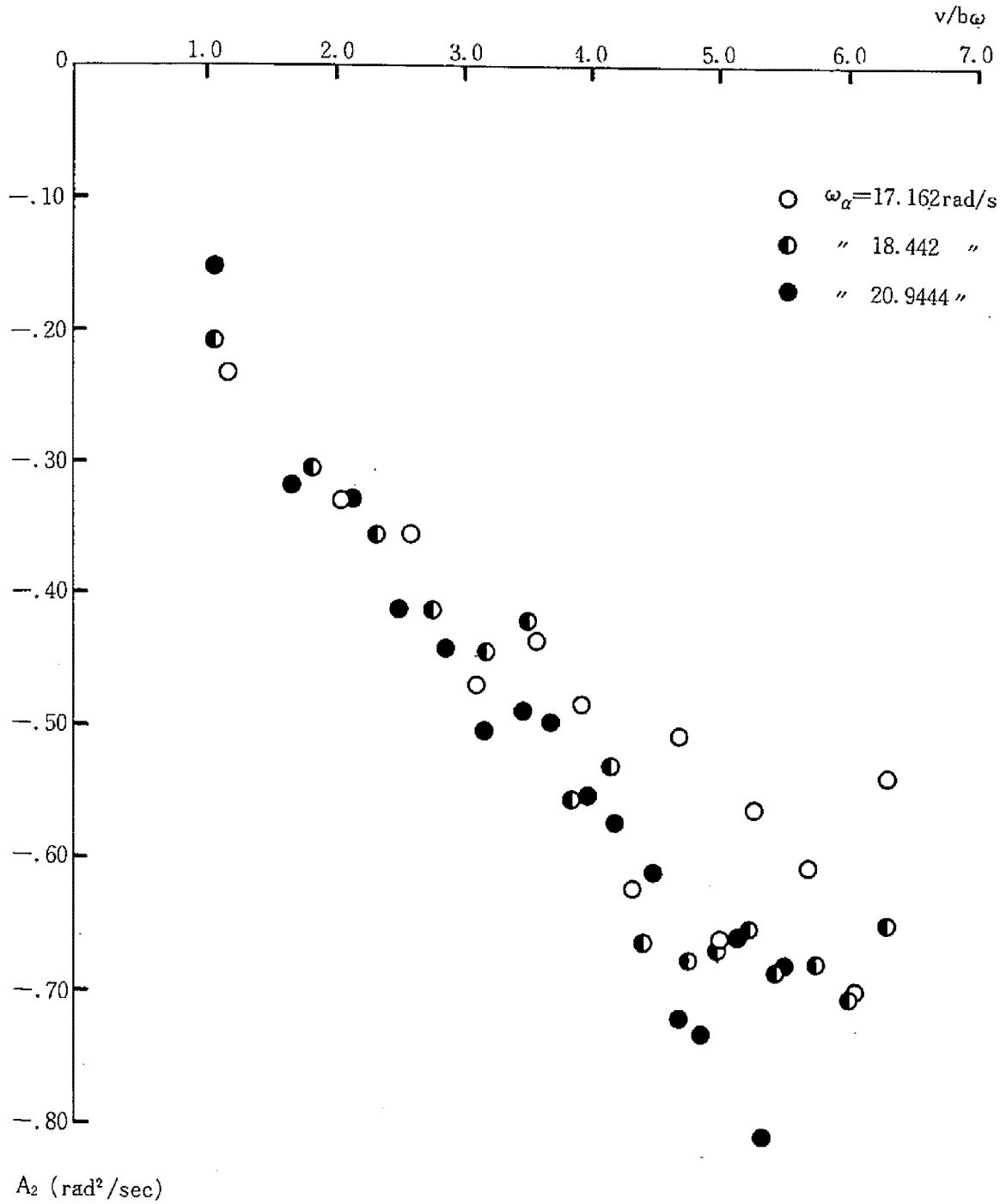

Fig. 3.6.9

Aerodynamic Coefficient for Model ET70π

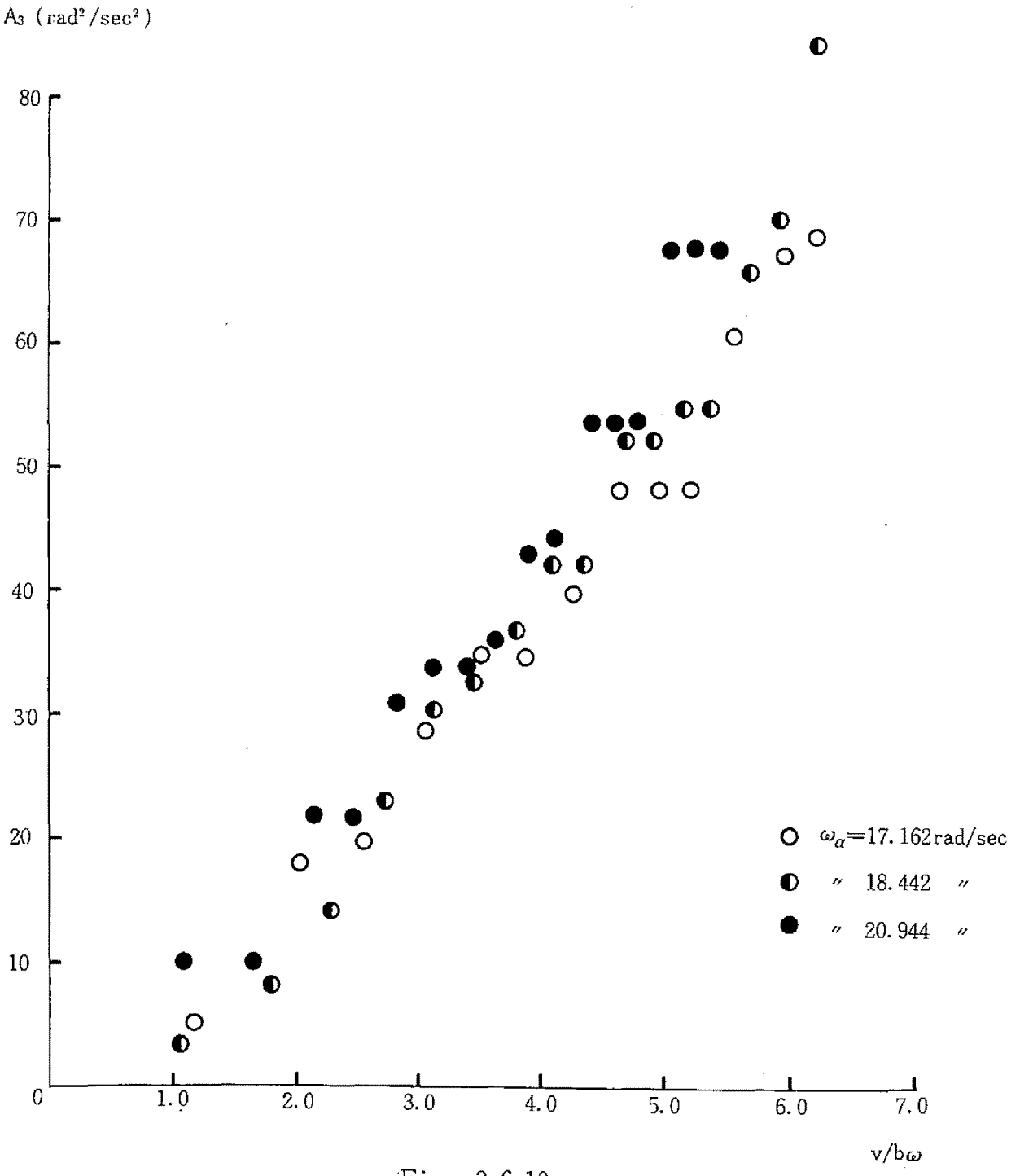

Fig. 3.6.10

Aerobynamic Coefficient for Model ET70H

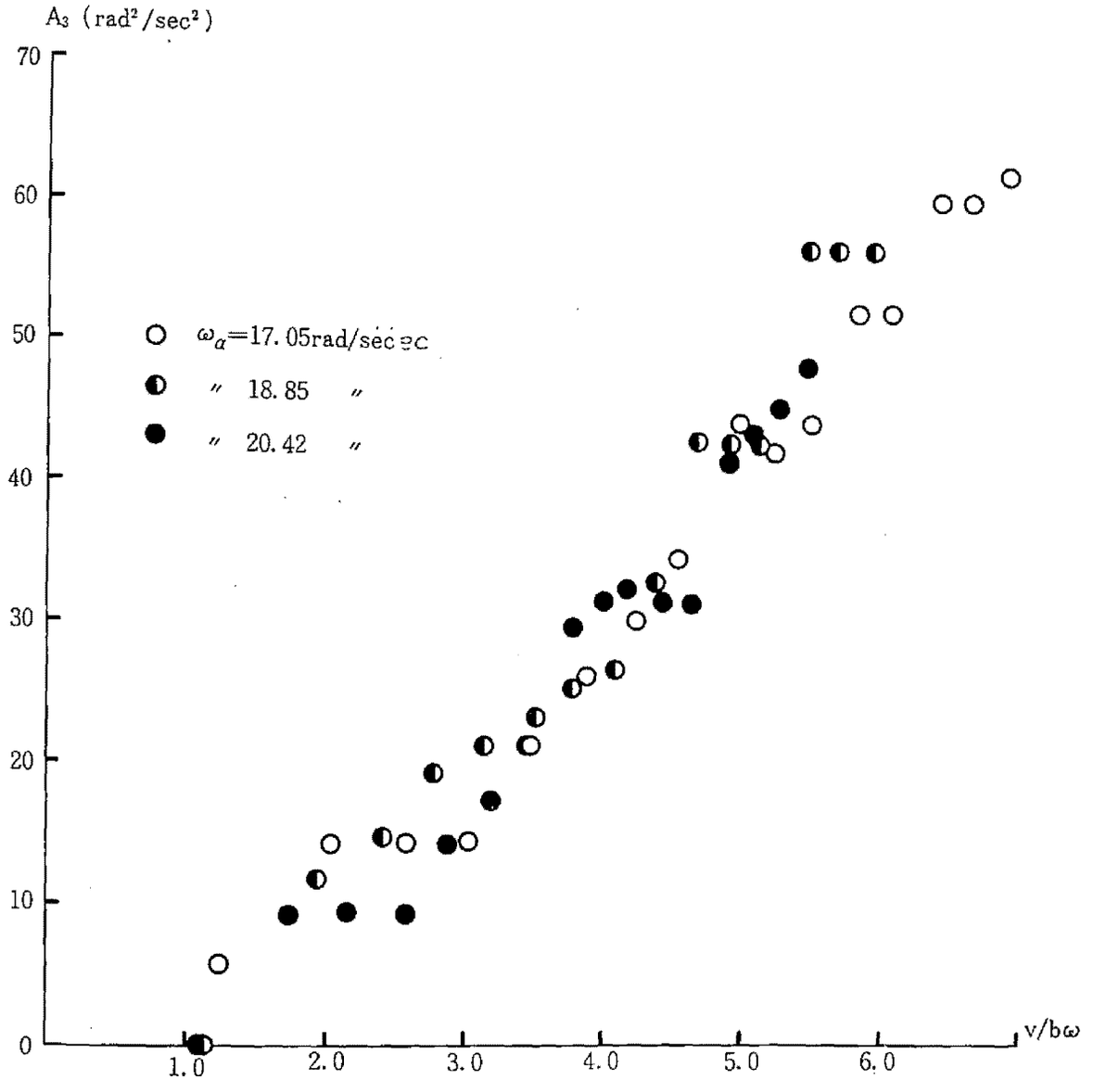

Fig. 3.6.11

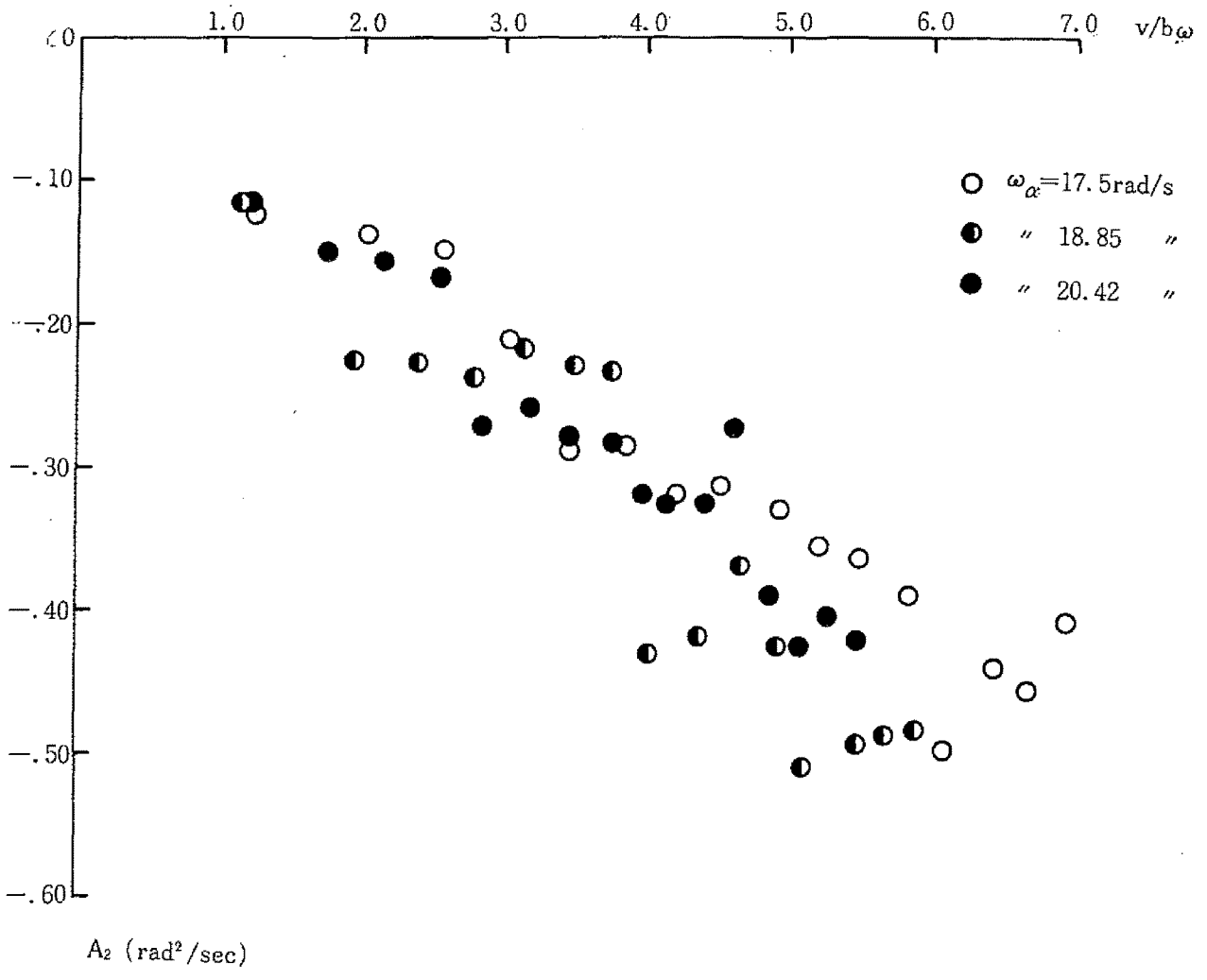

Fig 3.6.12 Aerodynamic Coefficient for Model ET70H

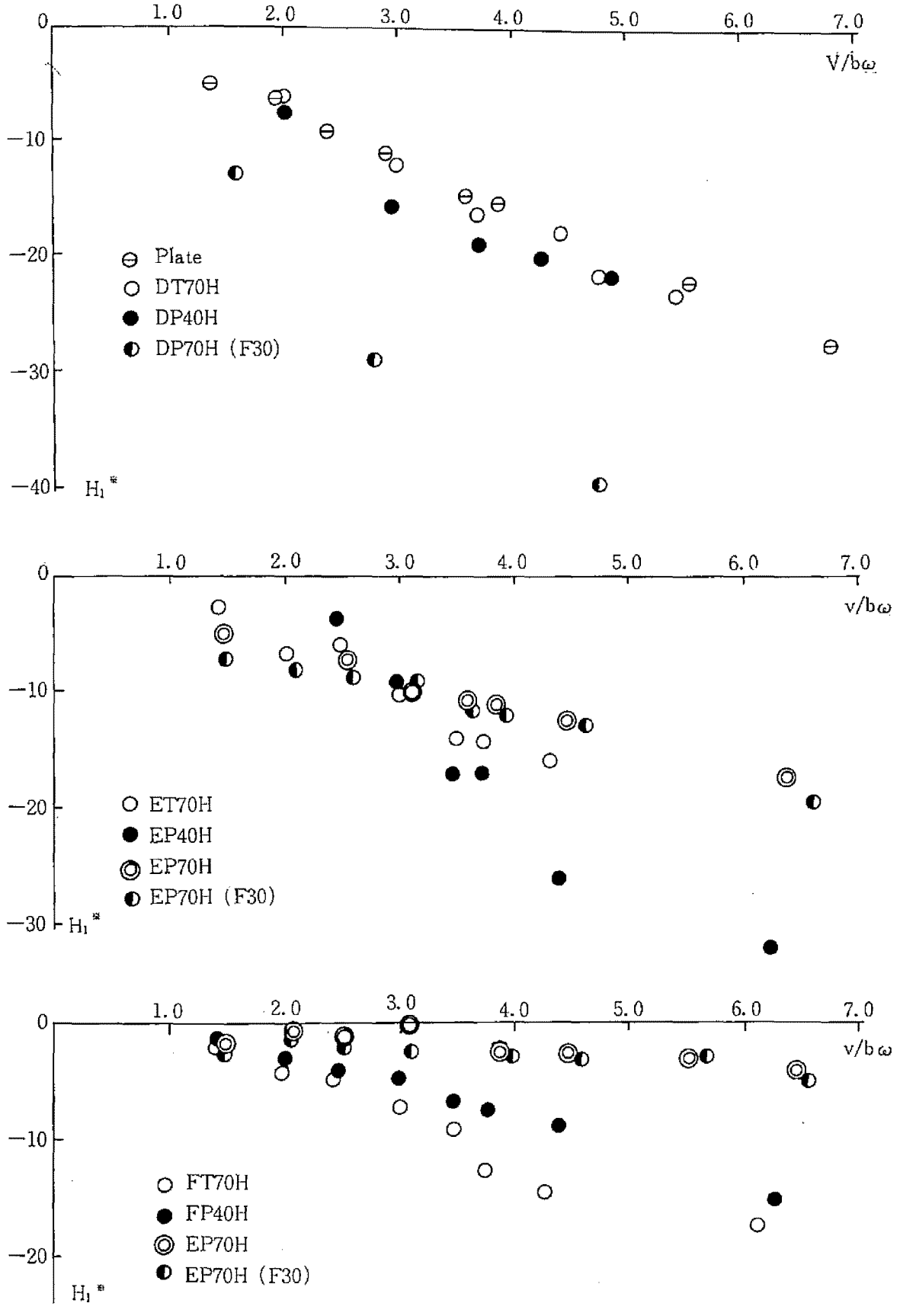

Fig. 3.6.13 Aerodynamic Coefficient H_1^*—Reduced Velocity Relation

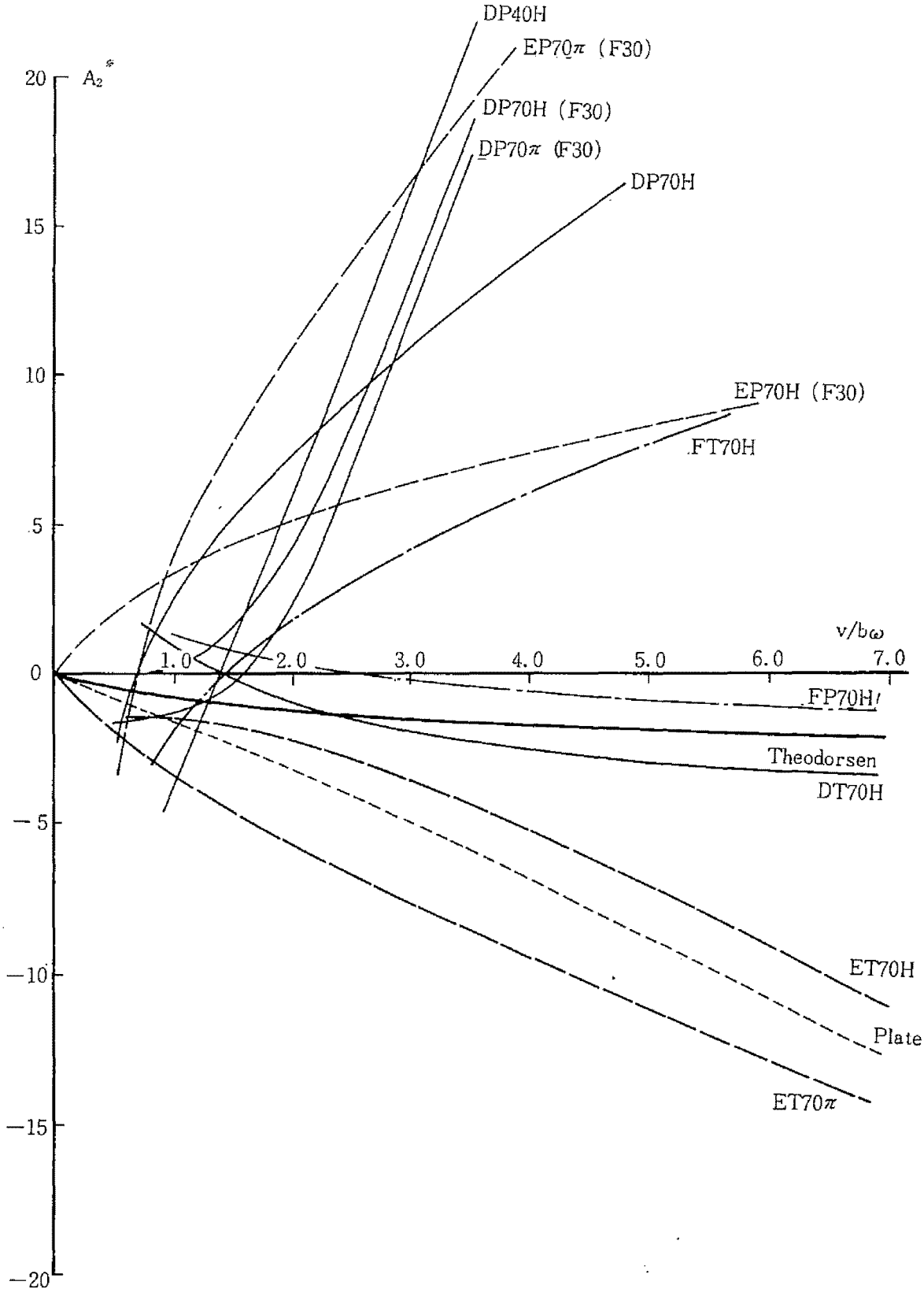

Fig. 3.6.14 Aerodynamic Coefficient A_2^*—Reduced Velocity Relation

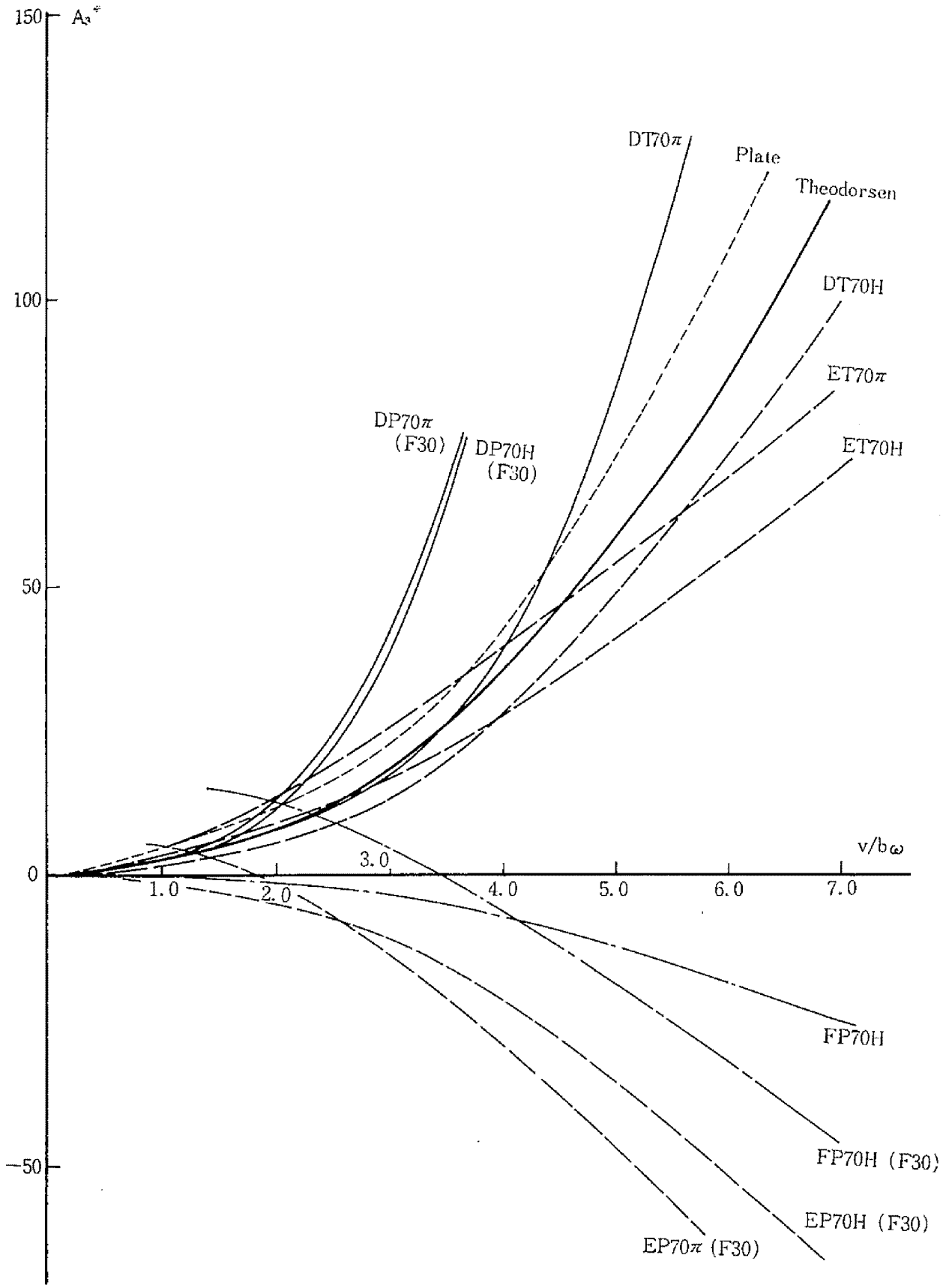

Fig. 3.6.15 Aerodynamic Coefficient A_3^*—Reduced Velocity Relation

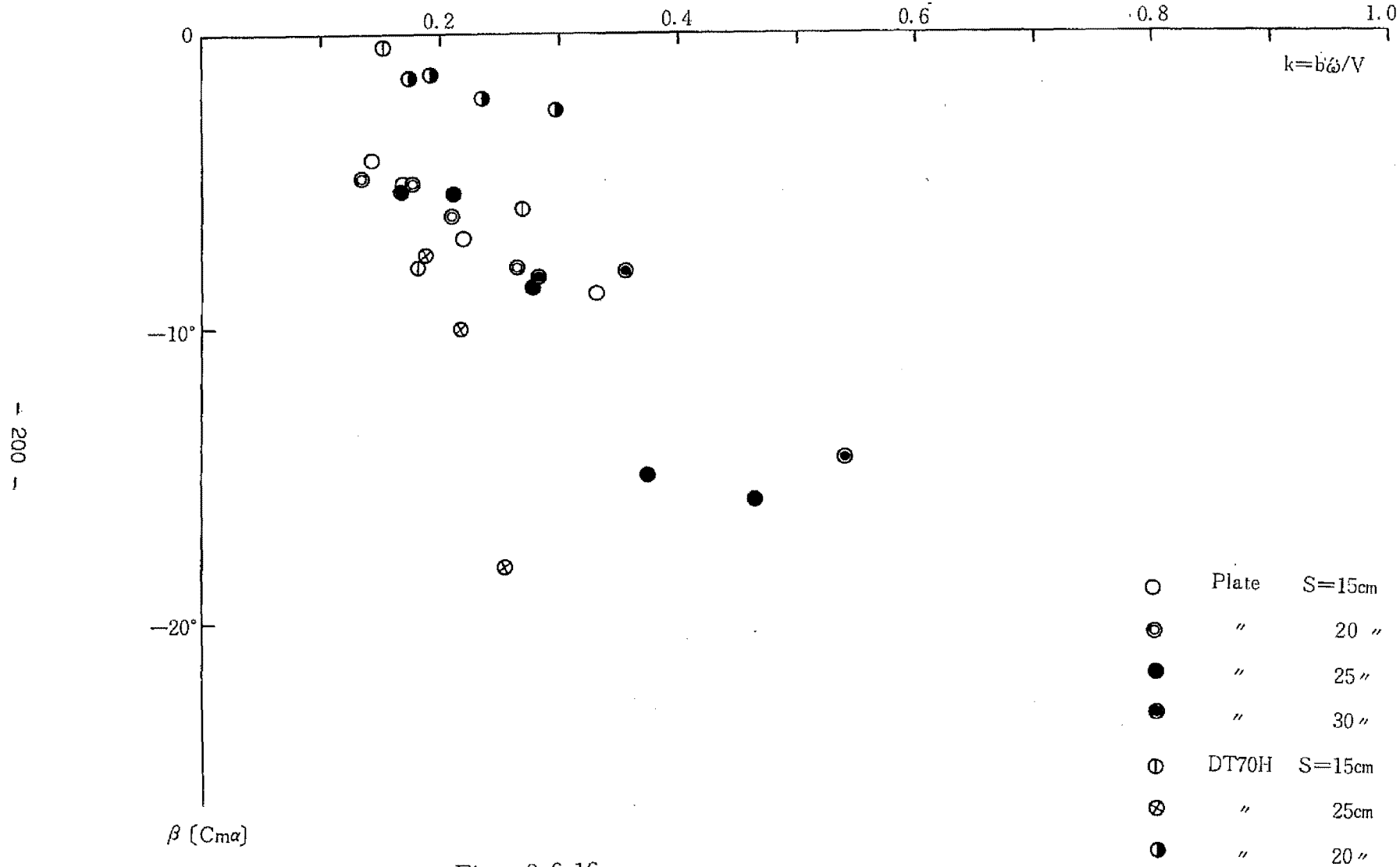
0
0.2
0.4
0.6
0.8
1.0
k=bω/V
−10°
−20°
β (Cmα)
200
Plate S=15cm
〃 20 〃
〃 25 〃
〃 30 〃
DT70H S=15cm
〃 25cm
〃 20 〃

Fig. 3.6.16

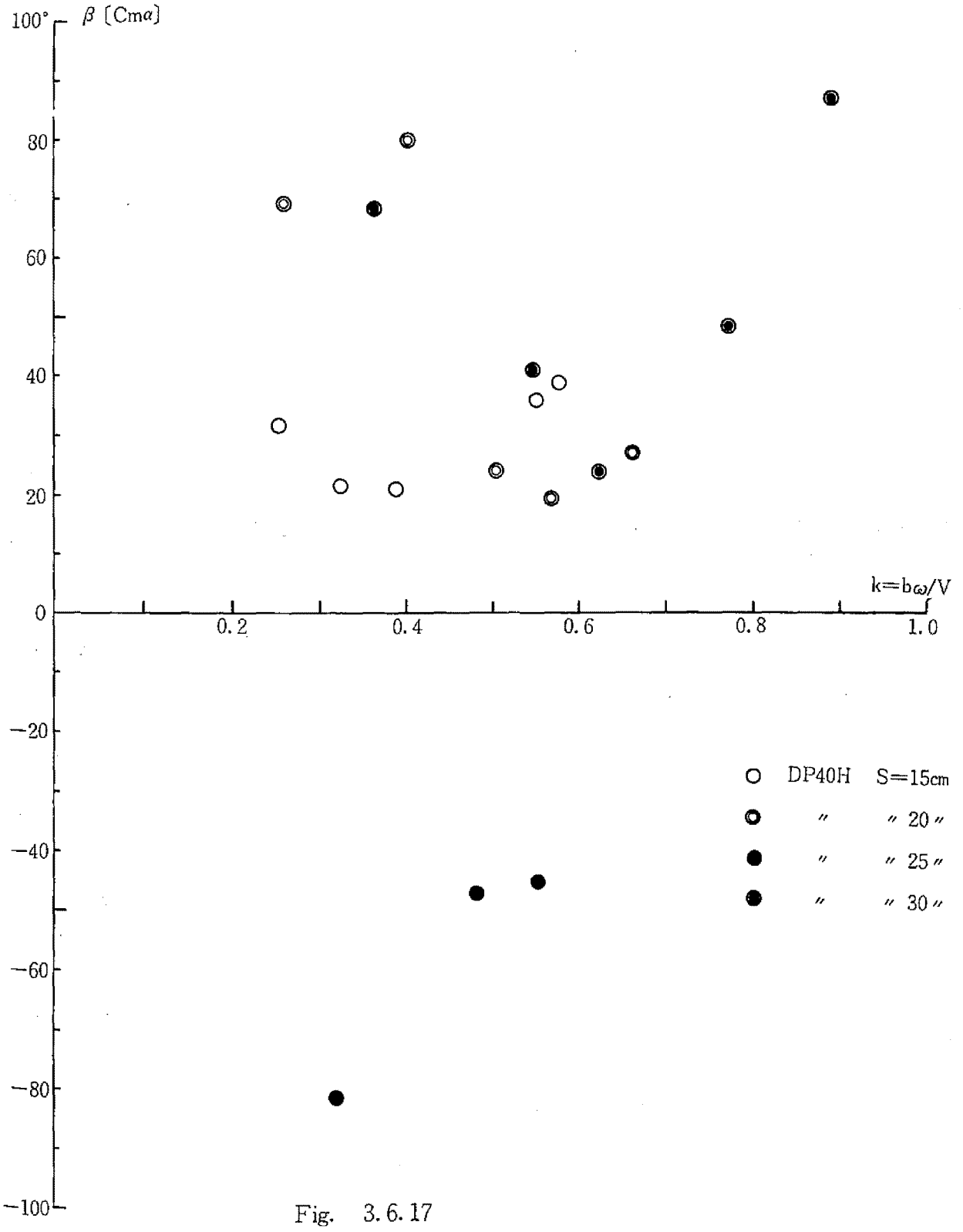
100°
β [Cmα]
80
60
40
20
0
−20
−40
−60
−80
−100
0.2
0.4
0.6
0.8
1.0
k=bω/V
DP40H S=15cm
〃 〃 20〃
〃 〃 25〃
〃 〃 30〃

Fig. 3.6.17

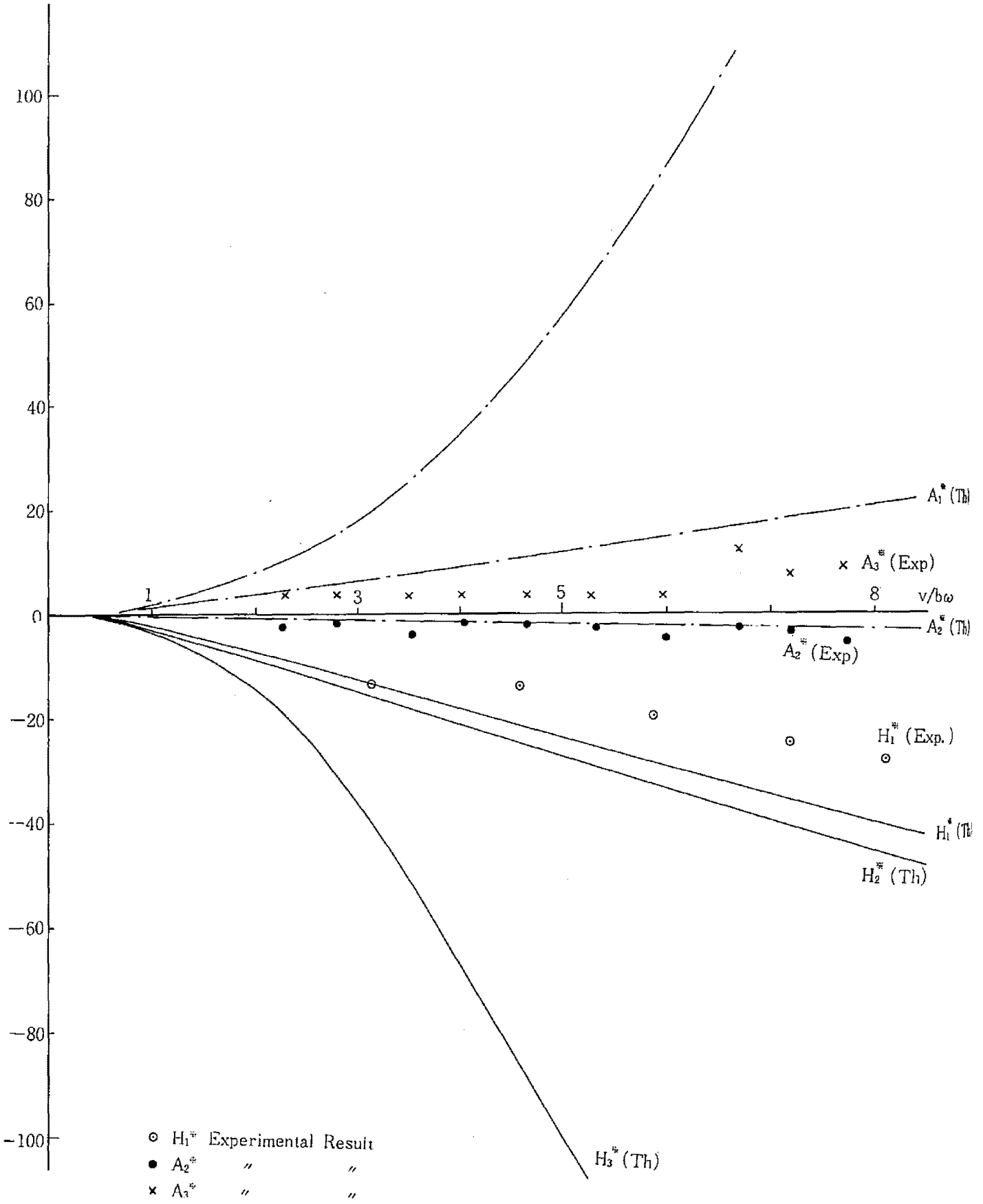

Model RT—1 with Track

Fig. 3.6.18

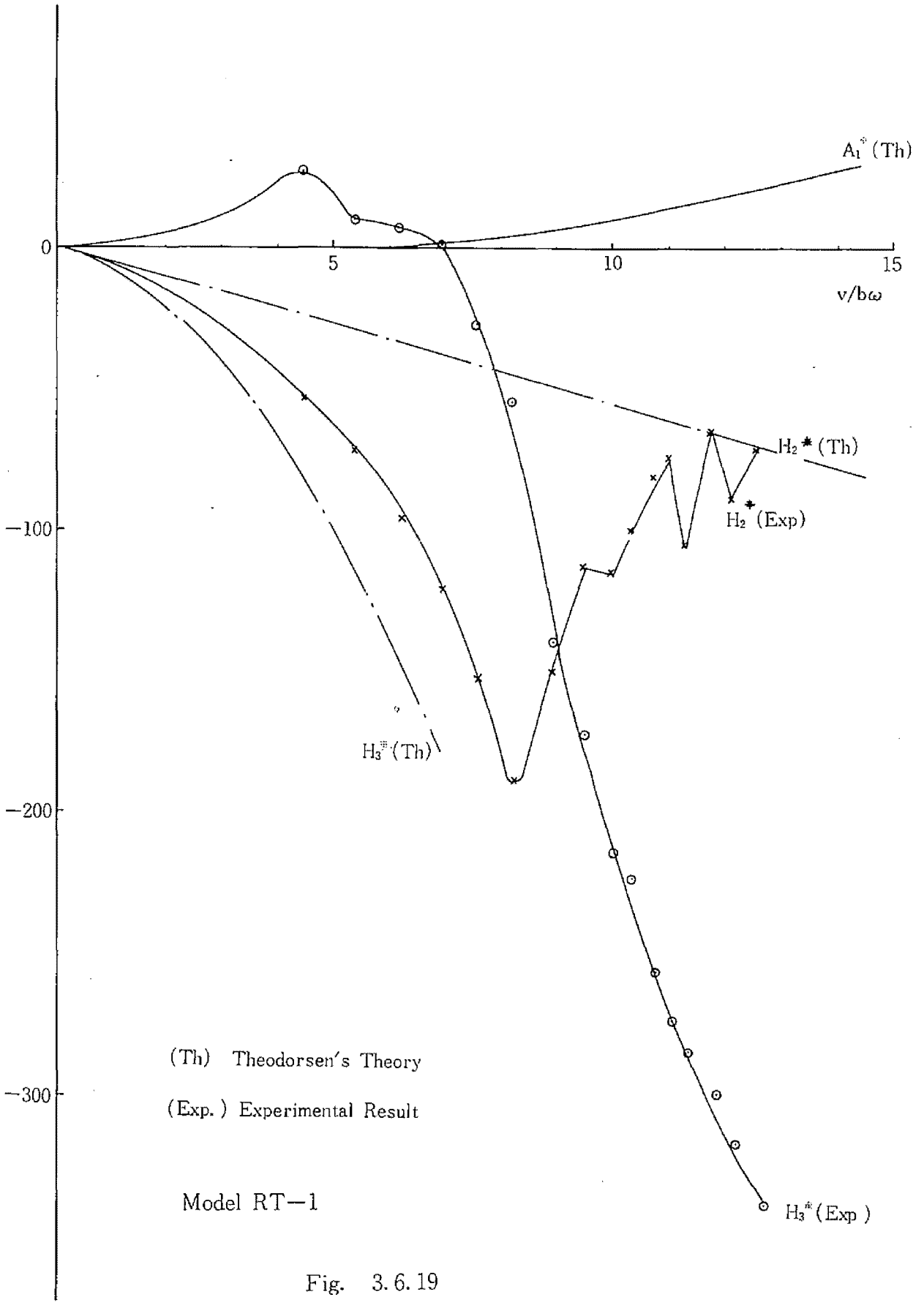
A_1^* (Th)
0
5
10
15
v/bω
H_2^* (Th)
H_2^* (Exp)
−100
H_3^* (Th)
−200
(Th) Theodorsen's Theory
(Exp.) Experimental Result
−300
Model RT−1
H_3^* (Exp)

Fig. 3.6.19

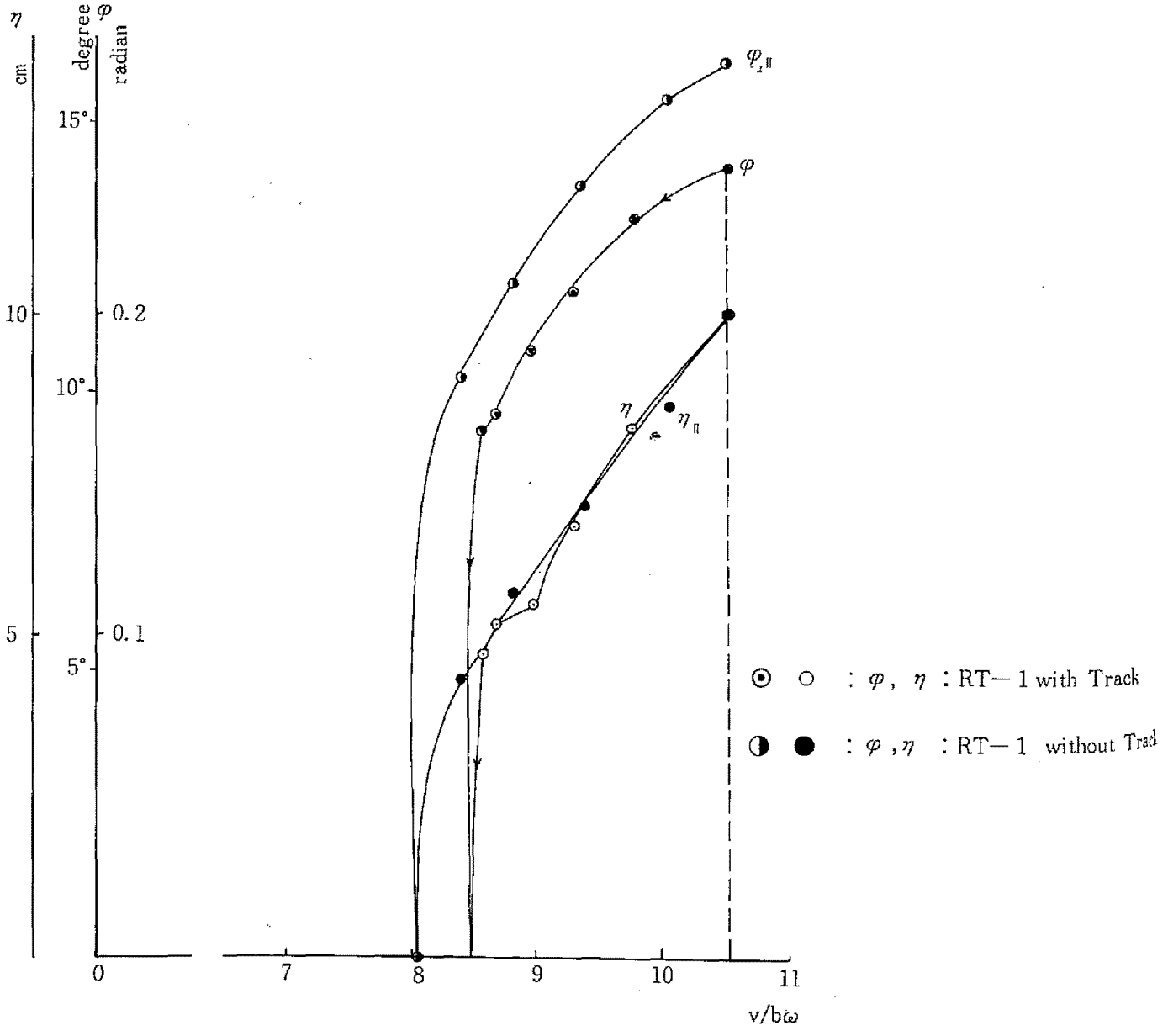
η
cm
φ
degree
radian
15°
10°
5°
0.2
0.1
10
5
0
7
8
9
10
11
v/bω
φ⊥∥
φ
η
η∥
⊙ ○ : φ , η : RT— 1 with Track
◑ ● : φ , η : RT— 1 without Trad

Fig. 3. 6. 20

3.7 DISCUSSIONS AND CONCLUDING REMARKS

From the investigations above mentioned the aerodynamic and aeroelastic responses of long-spanned bridge structures should be examined experimentally by use of the wind tunnel test, because the theoretical considerations for arbitrary shapes and combinations of structural members are so complicate aerodynamically that it is considered quite difficult to anticipate quantitatively the wind induced behaviours of bridge structures. However it seems very important to engineers to know at least qualitatively the aerodynamic effects of various structural factors for aerodynamic instability. An indicated in 3.4, 3.5, 3.6 the most important factors particularly for the flutter phenomena are considered as the frequency ratio of deflectional to torsional vibrations, the damping factors, mass effects, the angle of attack, the aerodynamic coefficients, etc. In this paragraph several fundamental aerodynamic characteristics are considered theoretically as well as experimentally in comparison with various investigators' results. As matter of fact, the bridge section of long-spanned suspension bridge forms in general a box type cross section with two main trussed stiffening walls and two horizontal trussed or deck systems, and the frequency ratio of torsional to deflectional modes varies from 2.0 to 3.0. From the structural point of view, the damping coefficients are comparatively small compared with other types of bridge structures. Experimental results so far indicate the fact that the most important aerodynamic characteristic is the flutter phenomenon of coupled or uncoupled modes depending on the structural and vibrational characteristics of the bridge. Therefore an attention is placed on the flutter type instability and main considerations and discussions are given on this instability from the following points of views: (1) the linear characteristics of aerodynamic coefficients to determine the critical wind velocity by use of the analog simulations, (2) the experimental method for determination of critical wind velocity and associate factors, (3) some influent factors for critical wind velocity and (4) some recommendations for aerodynamic stability problems of long-spanned bridge.

(1) Application of analog simulation method

The basic characteristics of the linear aerodynamic responses of bridges are described by the following set of defferential equations as mentioned already;

$$\ddot{\eta} + 2\zeta_\eta \omega_\eta \dot{\eta} + \omega_\eta^2 \eta = H_1 \dot{\eta} + H_2 \dot{\varphi} + H_3 \varphi$$
$$\ddot{\varphi} + 2\zeta_\alpha \omega_\alpha \dot{\varphi} + \omega_\alpha^2 \varphi = A_1 \dot{\eta} + A_2 \dot{\varphi} + A_3 \varphi \qquad (3\cdot7\cdot1)$$

where η, φ indicate the deflectional and torsional responses and H_i, A_i ($i = 1 \sim 3$) the aerodynamic coefficients, which can be rewritten of the non-dimensional form as follows

$$H_1^* = \frac{m}{\rho\omega b^2} H_1 = -2A_1^* = -\frac{2\pi}{k} \mid C(k) \mid$$
$$H_2^* = \frac{m}{\rho\omega b^3} H_2 = -\left(\frac{\pi}{k} + A_1^*\right)$$
$$H_3^* = \frac{m}{\rho\omega^2 b^3} H_3 = -\frac{2}{k} A_1^*$$
$$A_1^* = \frac{I_p}{\rho b^3 \omega} A_1 = \frac{\pi}{k} \mid C(k) \mid \qquad (3\cdot7\cdot2)$$
$$A_2^* = \frac{I_p}{\rho b^4 \omega} A_2 = \frac{1}{2}\left(A_1^* - \frac{\pi}{k}\right)$$
$$A_3^* = \frac{I_p}{\rho b^4 \omega^2} A_3 = \frac{A_1^*}{k}$$

The right handed expressions are valid for the case of thin plate for which the Theodorsen's function C(K) takes an important role for determination of its aerodynamic behaviours. For the quasi-steady state the coefficients H_i, A_i in eq's (3.7.1) are written as

$$H_1 = -\frac{\rho b V}{m}\left(\frac{\partial C_L}{\partial \alpha}\right), \quad H_2 = -\frac{\rho b^2 V}{2m}\left(\frac{\partial C_L}{\partial \alpha}\right), \quad H_3 = -\frac{\rho b V^2}{m}\left(\frac{\partial C_L}{\partial \alpha}\right)$$
$$A_1 = \frac{\rho b^2 V}{2I_p}\frac{\partial C_L}{\partial \alpha}, \quad A_2 = -\frac{\rho b^3 V}{2I_p}\left(\pi - \frac{1}{2}\frac{\partial C_L}{\partial \alpha}\right), \quad A_3 = \frac{\rho b^2 V^2}{\partial \alpha}\left(\frac{\partial C_L}{\partial \alpha}\right) \qquad (3\cdot7\cdot3)$$

It should be mentioned that eq's (3.7.3) give the fact that all aerodynamic coefficients but H_3 and A_3 are proportional to the wind velocity, while H_3 and A_3 are proportional to the squared magnitude of the wind velocity. Since the smaller the aerodynamic coefficients the more stable the bridge, the stability increases when the inclination of lift coefficient decreases in general. For A_2 the decreasement of $\partial C_L/\partial\alpha$ results in increasement of the magnitude so that the torsional damping term may increase to tend to be stable.

In order to determine the critical wind velocity of the classical flutter phenomenon there are various numerical methods proposed by a number of investigators. One of the most simplified empirical formula is presented by A. Selberg as follows

$$V_F = 0.88\,\omega_\alpha\, b\,\sqrt{\frac{\sqrt{\nu}}{\mu}\left(1-\frac{\omega_\eta^2}{\omega_\alpha^2}\right)} \tag{3.7.4}$$

Notations are below mentioned.

In this investigation an analog simulation is performed for eq's (3.7.1), by use of which result an approximate formula for the critical wind velocity is derived.

From eq's (3.7.1) we have

$$\begin{aligned} &\ddot{\eta} + (2\zeta_\eta\omega_\eta - H_1)\dot{\eta} + \omega_\eta^2\,\eta - H_2\dot{\varphi} - H_3\varphi = 0 \\ &\ddot{\varphi} + (2\zeta_\alpha\omega_\alpha - A_2)\dot{\varphi} + (\omega_\alpha^2 - A_3)\varphi - A_1\dot{\eta} = 0 \end{aligned} \tag{3.7.5}$$

which are also reduced to

$$\begin{aligned} &\dddot{\varphi} + (2\zeta_\alpha\omega_\alpha + 2\zeta_\eta\omega_\eta - H_1 - A_2)\ddot{\varphi} + \{(\omega_\alpha^2 - A_3) + \omega_\eta^2 + (2\zeta_\eta\omega_\eta - H_1)(2\zeta_\alpha\omega_\alpha - A_2) \\ &- A_1H_2\}\ddot{\varphi} + \{(2\zeta_\eta\omega_\eta - H_1)(\omega_\alpha^2 - A_3) + (2\zeta_\alpha\omega_\alpha - A_2)\omega_\eta^2 - A_1H_3\}\dot{\varphi} \\ &+ \omega_\eta^2(\omega_\alpha^2 - A_3)\varphi = 0 \end{aligned} \tag{3.7.6}$$

Eq. (3.7.6) is the fundamental differential equation for the present problem and the stable solution requires to satisfy the following Routh condition as written as

$$B_3 \equiv 2\zeta_\alpha \omega_\alpha + 2\zeta_\eta \omega_\eta + |H_1| + |A_2| > 0 \qquad \text{(a)}$$

$$B_2 \equiv \omega_\alpha^2 - A_3 + \omega_\eta^2 + (2\zeta_\eta \omega_\eta + |H_1|)(2\zeta_\alpha \omega_\alpha + |A_2|) + A_1 |H_2| > 0 \qquad \text{(b)}$$

$$B_1 \equiv (\omega_\alpha^2 - A_3)(2\zeta_\eta \omega_\eta + |H_1|) + \omega_\eta^2 (2\zeta_\alpha \omega_\alpha + |A_1|) + A_1 |H_3| > 0 \qquad \text{(c)}$$

$$B_0 \equiv \omega_\eta^2 (\omega_\alpha^2 - A_3) > 0 \qquad \text{(d)}$$

$$R \equiv B_3 B_2 B_1 - B_3^2 B_0 - B_1^2 > 0 \qquad \text{(e)}$$

As long as $\omega_\alpha^2 - A_3 > 0$, eq's (a) ~ (b) hold as required. This condition is already mentioned by Y. Rocard in his investigation.

In Rocard's investigation the aerodynamic coefficients defined as eq's (3.7.2) are uniquely determined by a single coefficient A_1* as shown in eq's (3.7.2) since a plate is only considered. Therefore the Routh condition, eq (e) is to determine the condition for A_1*, from which the formula for critical wind velocity can be derived.

In order to know the effects of each aerodynamic coefficients on the instability the analog simulation is used by use of the analog computor ALS-1000 (Photo 3.6), for which case the analog block diagram is written as Fig. 3.7.1 based on eq's (3.7.5).

As shown in Fig's 3.7.2 ~ 3.7.7 obtained by use of the analog computer for a plate, the uncoupled and the coupled modes of oscillations tend to converge and also the coupled modes, considering the aerodynamic coefficients, A_1, H_2, H_3, A_1 and H_2, H_2 and H_3, converges for given initial deformations. However for the case when A_1 and H_3 are taken into an account, the divergent oscillations are obtained in our calculations, and there appears no divergent oscillations without simultaneous existence of A_1 and H_3. Therefore it is considered that the critical Routh condition eq. (e) can be written as follows;

$$\frac{B_2 B_3}{2}\left\{1+\sqrt{1-\frac{4B_0}{B_2^2}}\right\}-D>A_1|H_3| \tag{3.7.7}$$

where

$$D=(\omega_\alpha^2-A_3)(2\zeta_\eta\omega_\eta+|H_1|)+\omega_\eta^2(2\zeta_\alpha\omega_\alpha+|A_2|)$$

By eq's (3.7.2) we have

$$A_1|H_3|=\frac{\rho^2 b^6\omega^3}{mI_p}\frac{2}{k}\quad A_1^{*2}=\frac{2\pi^2\rho^2 b^3}{mI_p}|C(k)|^2V^3$$

and by eq's (3.7.3) we have alternatively

$$A_1|H_3|=\frac{\rho^2 b^3V^3}{2mI_p}\left(\frac{\partial C_L}{\partial\alpha}\right)^2$$

Thus the critical wind velocity V_{cr} can be obtained as

$$V_{cr}=\sqrt[3]{\frac{mI_p}{2\pi^2\rho^2 b^3|C(k)|^2}\left\{\frac{B_2B_3}{2}\left(1+\sqrt{1-\frac{4B_0}{B_2^2}}\right)-D\right\}} \tag{3.7.8}$$

or

$$V_{cr}=\sqrt[3]{\frac{2mI_p}{\rho^2 b^3\left(\frac{\partial C_L}{\partial\alpha}\right)^2}\left\{\frac{B_2B_3}{2}\left(1+\sqrt{1-\frac{4B_0}{B_2^2}}-D\right)\right\}} \tag{3.7.9}$$

Since we have approximately the following expression

$$\frac{B_2B_3}{2}\left(1+\sqrt{1-\frac{4B_0}{B_2^2}}\right)-D\doteqdot(\omega_\alpha^2-\omega_\eta^2)(2\zeta_\alpha\omega_\alpha+|A_2|)$$

eq (3.7.8) and eq (3.7.9) yield to

$$V_{cr} = \sqrt[3]{\frac{m I_p (2\zeta_\alpha \omega_\alpha + |A_2|)}{2\pi^2 \rho^2 b^3 |C(k)|^2} (\omega_\alpha^2 - \omega_\eta^2)}$$

and

$$V_{cr} = \sqrt[3]{\frac{2 m I_p (2\zeta_\alpha \omega_\alpha + |A_2|)}{\rho^2 b^3 \left(\frac{\partial C_L}{\partial \alpha}\right)^2} (\omega_\alpha^2 - \omega_\eta^2)}$$

Introducing the same notations as A. Selberg used

$$\mu = \frac{2\pi\rho b^2}{m} \quad , \qquad \nu = \frac{2r^2}{b^2} \quad , \qquad I_p = m r^2$$

we have

$$\left.\begin{aligned} V_{cr} &= K \omega_\alpha b \sqrt[3]{\frac{\nu}{\mu^2}\left(1 - \frac{\omega_\eta^2}{\omega_\alpha^2}\right)} \\ &= \frac{K}{\sqrt[3]{2\pi^2}} \omega_\alpha b \sqrt[3]{\left(\frac{m}{\rho b^2}\right)\left(\frac{I}{\rho b^4}\right)\left(1 - \frac{\omega_\eta^2}{\omega_\alpha^2}\right)} \end{aligned}\right\} \qquad (3.7.10)$$

where

$$K = \sqrt[3]{\frac{1}{|C(k)|}\left(2\zeta_\alpha + \frac{|A_2|}{\omega_\alpha}\right)} \quad or \quad K = \sqrt[3]{\frac{4\pi^2}{\left(\frac{\partial C_L}{\partial \alpha}\right)^2}\left(2\zeta_\alpha + \frac{|A_2|}{\omega_\alpha}\right)} \qquad (3.7.11)$$

Eq (3.7.10) is of similar expression for the critical wind velocity for the classical flutter as eq.(3.7.4) except for the fact that the coefficient K also depend on the critical velocity. For eq. (3.7.11) it is obtained by eq's. (3.7.2) that

$$\frac{|A_2|}{\omega_\alpha} = \frac{\rho b^4}{2 I_p}\left(\frac{\omega}{\omega_\alpha}\right)\frac{\pi}{k}\left\{1 - |C(k)|\right\} = \frac{\mu}{2\nu}\left(\frac{\omega_\alpha}{\omega}\right)\frac{|1 - C(k)|}{k}$$

so that the above term may be considered the dynamic correction factor for damping coefficient. Apparently it depends on the flutter frequency ω, the kinematic factors μ and ν, the reduced frequency k and the lift reduction factor C(k). A far as the similarity rule holds for the inertia, the frequency, the wind parameter and the damping parameter, eq.(3.7.11) is therefore determined experimentally.

So far our considerations are restricted to the classical flutter which can be apparently characterized by the fact that $A_2 < 0$, but for the case $A_2 > 0$ the coupling of torsional and deflectional modes takes less important role and the critical wind velocity can be obtained by

$$A_2 = 2\zeta_\alpha \omega_\alpha$$

or

$$A_2^* = 2\pi\zeta_\alpha \frac{\nu}{\mu} \qquad (3\cdot7\cdot12)$$

which indicates that the critical wind velocity increases as the torsional stiffness, the torsional damping factor, torsional frequency and the mass of structures increase.

(2) Experimental method for determination of critical wind velocity and associate factors.

In order to determine the aerodynamic stability of the bridge the most probable method is at present considered to examine the proposed bridges section experimentally by use of the wind tunnel. However one should mention the fact that there exist apparently two different types of factors to be considered, namely the insensitive and the sensitive factors. The former factors are for example the frequency ratio, the size of the model, etc., and the latter are the angle of attack, the damping ratio, the slot area of the deck, et al. In generally the kinematic parameters contribute rather insensitively on the critical wind velocity, while the aerodynamic parameters contribute sensitively on it.

In this paragraph a few fundamental considerations for determination of the critical wind velocity of the bridge section concerned are given as follows: firstly the experimental method is described and secondly the significantly sensitive factors are illustrated based on the experimental analysis.

As the results of a number of previous investigators on the aerodynamic problems of bridge sections the experimental examination is considered unavoidable for which the similarity requirements and the experimental accuracy is inevitably satisfied as required. Usually the two degrees of freedom model-mounting is adapted so as to the deflectional and the torsional oscillations possible. Since the vibrations are characterized by inertia, damping, and restoring forces, the similarity is required on the following parameters:

1) mass parameter : $m/\rho b^2$, $I/\rho b^4$
2) damping parameter : ζ_η , ζ_α
3) frequency parameter : $\omega_\alpha/\omega_\eta$

in which the mass parameter indicates the similarity on the magnitudes the aerodynamic forces, the damping parameter the similarity on the dissipative to nondissipative forces and the frequency parameter the similarity on the aerodynamic flow configuration around the model. As for the mass parameter requirement an attention should be placed on the fact that the set-up model usually has an additional mass effects of so attached parts as springs and supporting bars. The most reliable method of determining the inertia forces is considered to calculate in the following manners; namely the natural frequencies ω_1 and ω_2 on at least two different spring systems where spring constants are assumed k_1 and k_2. Then the mass M is determined by

$$M = \frac{k_1 - k_2}{\omega_1^2 - \omega_2^2}$$

In the exactly same fashion the inertia forces for torsional motion are determined by

$$I = \frac{S_b^2 (k_1 - k_2)}{\omega_{\alpha_1}^2 - \omega_{\alpha_2}^2}$$

where S_b indicates the half spring distance and ω_{α_1}, ω_{α_2} the natural torsional frequencies on the corresponding spring system.

For the damping parameter there appears no definite method of estimation on the damping capacity on the actual bridge, so that it is usually recommended to have as small damping ratio as possible in experimental analysis.

It is rather easy to satisfy the frequency similarity requirement experimentally. By the above manner, the similarity laws can be satisfied prior to the experimental examination as far as the linear response is concerned, but obviously an adjustment is required particularly for the inertia parameters and the frequency parameters.

For determination of an aerodynamic stability two approaches are considered, which are alternatively related with each other. The first method is a direct experimental work by which the flutter phenomena are obtained by varying the wind velocity, while the second is an indirect experimental work in which the unsteady aerodynamic forces are measured. The former method provides directly the aerodynamic characteristics of the structure concerned taking into an account the geometrical and vibrational features simultaneously, while the latter method provides particularly the individual aerodynamic coefficients which has an advantages that the obtained coefficients are considered independent from the inertia and frequency similarity requirements and only dependent on the velocity parameter. Accuracy of measurement and experimental informations can be affirmed by combining the above two methods, namely the direct measurement of critical velocity and the indirect measurement method. At present the measurement methods of unsteasy aerodynamic forces are considered the so called forced vibration method and the free vibration method, either of which are appropriate for use to analyse the aerody-

namic characteristics of bridge sections. There remains the controversial problem for the size of models and the structural idealization, namely the full-scaled model or the section model. It is naturally desired to use the fully scaled model instead of the latter. However the inherent damping capacity and the accuracy of wind velocity variations should be examined properly when the fully scaled model is used. As far as the aerodynamic instability is concerned, the section model is considered to provide sufficient informations experimentally.

(3) Influent factors for the critical wind velocity of the flutter phenomenun of bridge sections.

A number of various kinematical and aerodynamic factors may influence the stability and the responses of bridge sections in wind stream. As pointed out already there exist complicate interaction between associate factors, but it should be noticed that for a flat plate eq's(3.7.2) indicate the fact that the non-dimensional form of aerodynamic coefficients is given by one parameter, for example, the lift reduction factor C(K). So far, an approximate estimation for the critical wind velocity by such ones as A. Selberg presented gives, to be brief, the influential factors and their form of contributions which comprise fundamentally the frequency ratio, the ratio of width to the radius of gyration, the mass, the damping ratio, the aerodynamic coefficients et al, as a whole. It is hard at present to enumerate qualitatively as well as quantitatively which factors are predominate to others. However, at this point, the angle of attack and the slit deck are particularly considered since these factors are not taken into an account theoretically.

The angle of attack is considered as one of the significant factors to determine the critical wind velocity of the comparatively flat cross sections. One of the typical experimental results for a flat plate is shown in Fig. 3.7.8, which indicates that the small change of angle of attack reduces the critical velocity remarkably but it tends to increase the flutter frequency by comparatively small magnitude up to the angle of attack approximately equal to 10° as long as this experiment is con-

cerned. According to the quasi-steady state analysis the effect of angle of attack is only taken into an account the form of the varying relative angle of attack, so that by replacing the wind velocity V by Vrel = V sec α (α= angle of attack) one obtains roughly the results that the reduced velocity decreases by cosα. This explains unlikely the previously illustrated experimental result. To envidage the aerodynamic characteristics due to the angle of attack the amplitude-damping-reduced velocity relations are illustrated in Fig's 3.7.9 ~ 3.7.11 for various angles of attack for a flat plate. With no angle of attack it can be said that the torsional and deflectional amplitudes apparently do not depend on the wind velocity, while increasing the angle of attack there appears one to one correspondence between the steady state amplitudes and the wind velocity. As long as the linear form of fundamental differential equations is concerned, the steady state amplitudes should be independent on the wind velocity; thus the effect of angle of attack is considered as the result of the non-linear responses of the structures in wind stream. It is interesting to note that the change of angle of attack is clearly determined theoretically for the aeroelastic problem, while for aerodynamic problem it should be characterized by the non-linear problem, which is not solved theoretically at present. In spite of the fact that the angle of attack effects significantly on the critical wind velocity, there is an independent problem, namely, the reasonable determination of angle of attack from the moteorological observations at the sites. C. Scruton induced from the observations at the site of the Severn Bridge that the effective angle of attack decreases with the wind velocity at such open area as the water level.

On this problem H. Ishizaki[37], H. Arai[38] et al reported some observational results of the vertical component of natural wind velocity at various sites. Thus the present investigations on the aerodynamic characteristics of bridge sections call for more detailed analysis both on the nonlinear problems of aerodynamic forces and on the natural wind velocity at the sites.

Another aerodynamic factor influent on the critical wind velocity

which is considered here is the effect of slot on the deck part of the stiffening girder system. Most modern type of trussed girder system of suspension bridge employs the slit deck and particular girders supporting decks. As shown in Fig's 3.7.12 and 3.7.14 the model test indicates that the equi-damping curves in the amplitude-wind velocity relations behave in a complicate fashion, so that one may not easily factor out the effect of slot on the critical wind velocity. In order to analyse the aerodynamic characteristics of slit deck a few fundamental considerations are given on the classical flutter phenomena of an idealized slit flat plate. As the preliminary experiments three types of truss-stiffened models as shown in Tables 3.7.1 and 3.7.2 are used for the aeroelastic tests and six types of truss-and girder-stiffened models are used for the flutter tests (Table 3.7.3)

As shown in Fig's 3.7.15 the C_L and C_M curves may vary less sensitively to compare the model with slit deck with the one with solid deck, while the C_D- curve for the slit deck tend to increase in comparison with the C_D- curve for the case of solid deck because the wind stream can deform to result in increase of the drag force. The flutter tests, on the contrary, indicate, as shown in Table 3.7.2 and Fig. 3.7.16, that the critical wind velocity increases by the slit deck quite sensitively. In order to investigate the effect of slot an approximate estimation method is considered on the critical wind velocity of flat plate by use of the unsteady air forces given by the Theodorsen's Function. Formulation is based on the assumptions that the aerodynamic forces associate with the vibrating plate with a slot comprise with those acting on individual solid parts and the reduction factors of aerodynamic forces remain unchanged with those for the case of plate without slot. Though insufficient to express the flow pattern around a plate with slot since the vorticities in wake and the effect of upstream part on the down stream part are ignored, such assumptions may be allowed because main contributions of flows on the aerodynamic forces are due to those expressed by the bound vortices. For sake of brevity the aerodynamic forces on a plate with slit as shown in Fig. 3.7.17 is considered, the lift L and

the pitching moment M of which are given as

$$L = \pi\rho c^2 \left(\frac{c-s}{\sqrt{2c}}\right) \ddot{\eta} + 2\pi\rho U c\ C(k) \left(\frac{c-s}{c}\right) \dot{\eta}$$
$$+ \left\{ \pi\rho c^2 U + \pi\rho U c^2 C(k) \right\} \left(\frac{c-s}{\sqrt{2c}}\right)^2 \dot{\varphi}$$
$$+ 2\pi\rho U^2 c C(k) \left(\frac{c-s}{c}\right) \varphi$$

$$M = 2\pi\rho U C(k)\, b^2\, \dot{\eta}$$
$$+ \left[\pi\rho b^2 (-bU) + 2\pi\rho U C(k) \left\{ \frac{b^3}{2} - 2b\ (s+b)^2 \right\} \right] \dot{\varphi}$$
$$+ 2\pi\rho c U C(k)\, \varphi$$
$$+ \pi\rho b^2 \left(-\frac{b^2}{4} - 2\ (s+b)^2 \right) \ddot{\varphi}$$

Taking into an account only the terms proportional to the velocity and the displacement the above expressions yield to

$$L = 2\pi\rho c U C(k)\, S_1(\phi)\, \dot{\eta} + \pi\rho U \left\{ 1 + C(k) \right\} S_2(\phi)\, \dot{\varphi}$$
$$+ 2\pi\rho c U^2 C(k)\, S_1(\phi)\, \varphi$$

$$M = \pi\rho c^2 U C(k)\, S_2(\phi)\, \dot{\eta} + \pi\rho c^2 U \frac{c}{2} \dot{\varphi} \left[(1 - C(k))\, 2\, S_3(\phi) + S_4(\phi) \right]$$
$$+ \pi\rho c^2 U^2 C(k)\, S_2(\phi)\, \varphi$$

in which ρ = air density, U = mean wind velocity, η = deflectional displacement, φ = torsional displacement, C(k) = Theodorsen function, k = reduced frequency $b\omega/U$, $S_i(\phi)[i = 1\sim4]$ = modifying functions, ϕ = opening ratio (s/c).

The modifying functions $S_i(\phi)$ in above expressions are limited to

four types as described in Fig. 3.7.18. It is interesting to note that S_1, S_2, S_3 are decreasing functions with the opening ratio ϕ while S_4 increases up to $\phi = 1/3$ then decreases to vanish at $\phi = 1.0$. Another point with respect to the modifying functions is featured at the fact that the above expressions may not be reduced to those for the solid plate when $\phi = 0$ but in the lift force the second term yields to 1/2 and in the pitching moment the first and the third terms yield to 1/2 and the terms with C(k) yield to 1/4 and 3/4 in the second term, in comparison with a solid plate. This means that the Kutta conditions assumed in this approximation hold when s=0 so that one should pay an attention on existence of physical discontinuity.

By use of above approximate expressions for unsteady lift forces and pitching moments the critical wind velocity can be obtained theoretically as usaul manner.

The dashed curves are those approximated by A. Selberg's empirical formula in the way as Tanaka and Ito[35] indicated. The numerical results show that the dependence of critical wind velocity on the opening ratio is sensitively influenced by the frequency ratio. The smaller the frequency ratio, the more steeply the critical wind velocity increases. For affirmation of the above approximate considerations an experiment is performed by use of the model of flat plate (b = 15 cm) with slot (s = 1.5 cm) at the central part of chord, which is shown in Fig. 3.7.19. As long as this result is concerned the method considered provides a satisfactory accordance of theoretical and experimental results at the smaller frequency ratios such as $\omega_\alpha/\omega_\eta = 1.1 - 1.5$ when ϕ is also small. For the large ratio of ϕ it is without saying required that an effect of wakes due to upstream parts on the down stream parts is taken into consideration.

(4) Some recommendations for aerodynamic stability problems of long-spanned bridge.

In this chapter a fundamental consideration is given on the aerodynamic stability problems associate with a long-spanned suspension

bridge. Since the fall of the Tacoma Narrows Bridge there are a number of eminent investigations by various researchers on this point theoretically and experimentally. The aerodynamic characteristics of bridge sections, up to this date, are qualitatively clarified mainly by Farquharsen, T. von Karman et al. As the theoretical evaluation of critical wind velocity accords generally insufficiently with experimentl results, it is considered evitable to perform the wind tunnel test to know the aerodynamic forces by the methods previously discussed. However to design the bridge aerodynamically stable there are a number of factors to be possibly capable of taking into an account; namely the natural frequencies of torsional and deflectional modes, the inertia effects, the effects of radius of gyration to chord length. It is expected that the larger the mass and the smaller the inclination of lift curve (assumed positive slope) the more stable the bridge. For example the slot on the deck may reduce the lift force per unit length of chord at least aeroelastically. However a particular stress should be placed on the following points; the non-linear characteristics on aerodynamic forces are essential in order to describe the aerodynamic stability since the steady responses of structures (amplitudes) depend on the wind velocity, which can not be obtained in the linear form of fundamental equations. To compare the model test with the field performance of proto-type structures, one ought to find great difficulty in reasonable judgement which case is safe. G. Vincent considered, generally speaking, that a model can response so sensitively in wind tunnel because the effective absorption of energy from flow is steady to shorten the time to build up an instability, while for the proto-type the efficiency may decrease due to turbulence of wind and phase lags of aerodynamic forces for so called truss type girder system.

As the previous considerations we can recommend the following terms in order to assure the aerodynamic stability of bridge sections:

1) Wind tunnel test is necessary to find the type of instability and to obtain the aerodynamic forces.

2) For classical flutter the frequency ratio should be taken as large as possible, namely the torsional rigidity should be increased, and inertia effect should be utilized effectively.

3) For stall flutter and galloping type of instability particular attention should be placed on the damping effect as well as the non-linear responses.

4) To improve the aerodynamic stability the configuration and the position of slots on deck should be so considered as appropriate structurally and aerodynamically.

5) The mean angle of attack effects sensitively on aerodynamic stability in spite of the fact that there remains an uncertainty in the idealization to be taken into an account in design.

Apparently there exists a large number of factors which should be mentioned when one considers the aerodynamic stability problems of bridge structures. Recent work by T. Miyata and I. Okauchi[36] intend specifically to analyse the initiation of aerodynamic instability by use of the quasi-steady non-linear characteristics, as G. Parkinson showed. It is considered that one needs to devote to the investigations on the non-linear characteristics particularly in order to clarify the aerodynamic instability more specifically and thoroughly.

Table 3. 7. 1

b/d	x	Notations	Cross Sections
3.0	0.5	A-TT	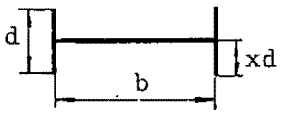
3.0	0.5	A-TT-S	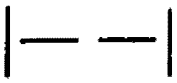
2.0	0.5	B-TT	
1.5	0.5	C-TT	

b = 30Cm

length of model = 94Cm

Slit distances are 20, 25, 20mm

(opening ratio $\phi = 0.217$)

Table 3. 7. 2

Models	A-PP			A-TT				A-PP-F				A-PP-S				A-TT-S		
defl. freq. $\omega\eta$	8.69	8.66	8.66	9.10	9.10	9.15	9.13	8.58	8.54	8.56	8.58	8.91	8.88	8.87	8.86	9.30	9.30	9.30
tor. freq. $\omega\alpha$	11.1	13.8	15.4	11.4	12.5	14.6	16.4	11.1	12.6	13.8	15.7	11.4	13.2	14.3	15.1	13.2	14.8	15.9
frequency ratio $\omega\alpha/\omega\eta$	1.28	1.59	1.78	1.26	1.38	1.60	1.8	1.29	1.47	1.62	1.83	1.28	1.49	1.61	1.70	1.42	1.59	1.71
flutter freq.	10.1	13.3	15.2	10.0	11.6	13.3	14.9	10.6	12.1	13.4	15.0	8.83	8.60	8.62	8.70	12.2	14.1	15.2
flutter velocity	3.65	5.32	7.80	6.89	9.04	9.75	11.6	3.65	4.08	4.28	5.16	8.01	8.56	8.80	8.94	12.5	15.6	16.0

Table 3. 7. 3 Flutter Characteristics for Plate–Like Structures.

Model	m kgsec^2/m^2	I kgsec^2	ω_η rad/sec	ω_α rad/sec	$\omega_\alpha/\omega_\eta$	μ	ν	$V_{cr}/b\omega_\alpha$ (exp.)	K
	.4473	.01631	11.69	17.80	1.52	.03951	3.241	3.603	.341
	.4473	.01941	11.62	19.64	1.69	.03951	3.857	4.269	.365
PLATE	.4473	.02401	11.62	21.54	1.85	.03951	4.771	4.687	.361
	.4473	.03017	11.52	23.25	2.02	.03951	5.995	4.426	.310
	.4473	.03540	11.52	24.08	2.09	.03951	7.035	4.681	.309
	.5426	.01794	10.60	17.06	1.61	.03257	2.939	3.486	.291
	.5426	.02104	10.60	18.85	1.78	.03257	3.447	3.938	.301
DT70H	.5426	.02564	10.55	20.74	1.97	.03257	4.200	4.638	.323
	.5426	.03180	10.52	22.44	2.13	.03257	5.209	5.213	.333
	.5426	.03703	10.37	23.34	2.25	.03257	6.066	5.323	.320
	.5802	.01806	10.60	16.96	1.60	.03046	2.767	4.669	.382
	.5802	.02117	10.60	18.85	1.78	.03046	3.243	5.326	.398
ET70H	.5802	.02557	10.54	20.65	1.96	.03046	3.917	6.075	.415
	.5802	.03193	10.52	23.04	2.19	.03046	4.892	6.122	.380
	.5440	.01718	10.54	16.80	1.59	.03248	2.807	4.224	.360
	.5440	.02026	10.47	18.59	1.78	.03248	3.310	4.879	.379
DT70H	.5440	.02488	10.61	19.39	1.83	.03248	4.065	5.290	.379
	.5440	.03105	10.54	23.62	2.24	.03248	5.073	5.606	.358
	.5440	.03628	10.40	23.27	2.24	.03248	5.928	5.690	.345
	.5802	.01822	10.66	16.85	1.59	.03046	2.971	4.901	.393
	.5802	.02133	10.56	18.71	1.77	.03046	3.268	5.267	.393
ET70H	.5802	.02593	10.60	20.75	1.86	.03046	3.973	5.613	.387
	.5802	.03209	10.60	22.53	2.13	.03046	4.916	5.936	.369
	.5802	.03732	10.60	23.15	2.17	.03046	5.718	6.208	.366
	.4553	.01463	11.47	17.07	1.49	.03881	2.856	3.802	.373
Severn	.4553	.01771	11.55	18.93	1.64	.03881	3.458	4.116	.364
	.4553	.02233	11.47	20.87	1.82	.03881	4.360	4.471	.354

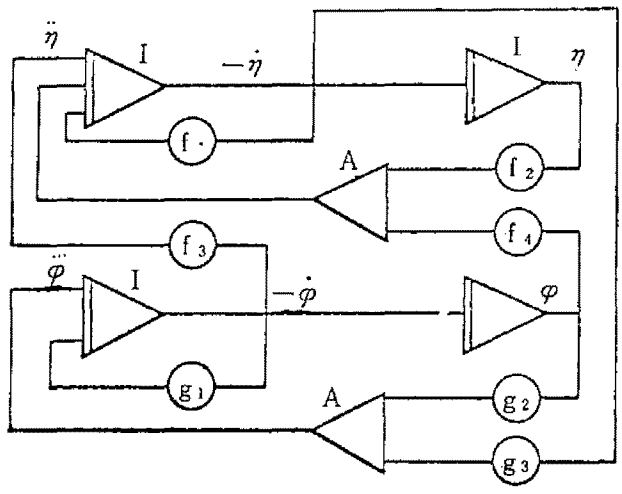

Fig. 3.7.1 Analog Block Diagram for Flutter Simulation

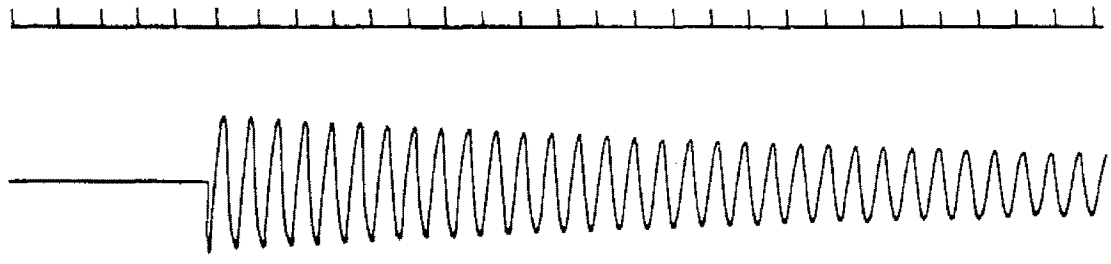

η (50volt)

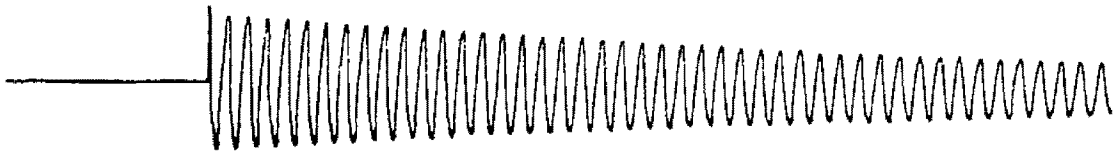

φ (50volt)

Fig. 3.7.2 Simulated Free Vibrations Deflectional and Torsional Modes

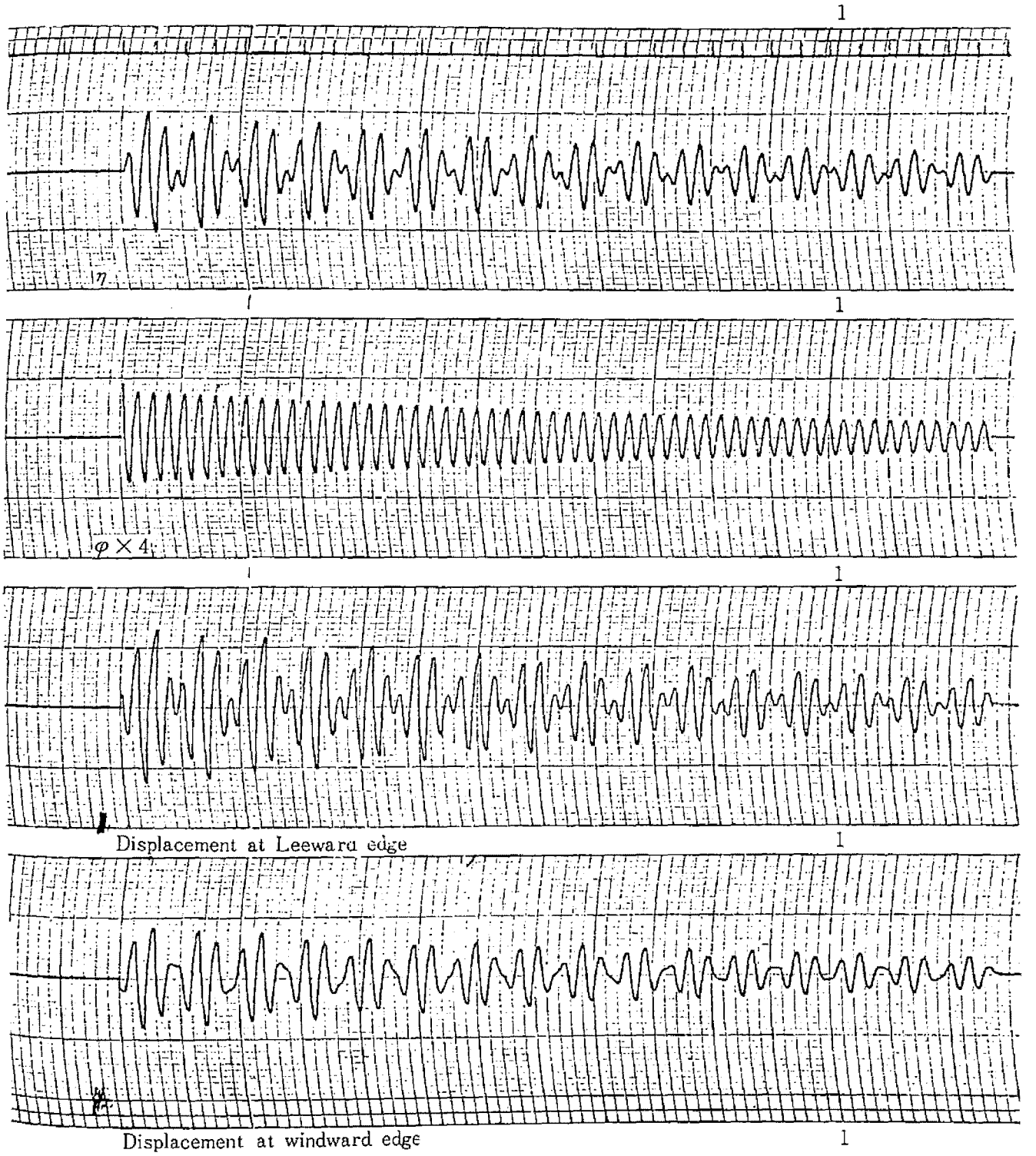

Fig. 3.7.3 Convergent Oscillations in one term coupling H_3

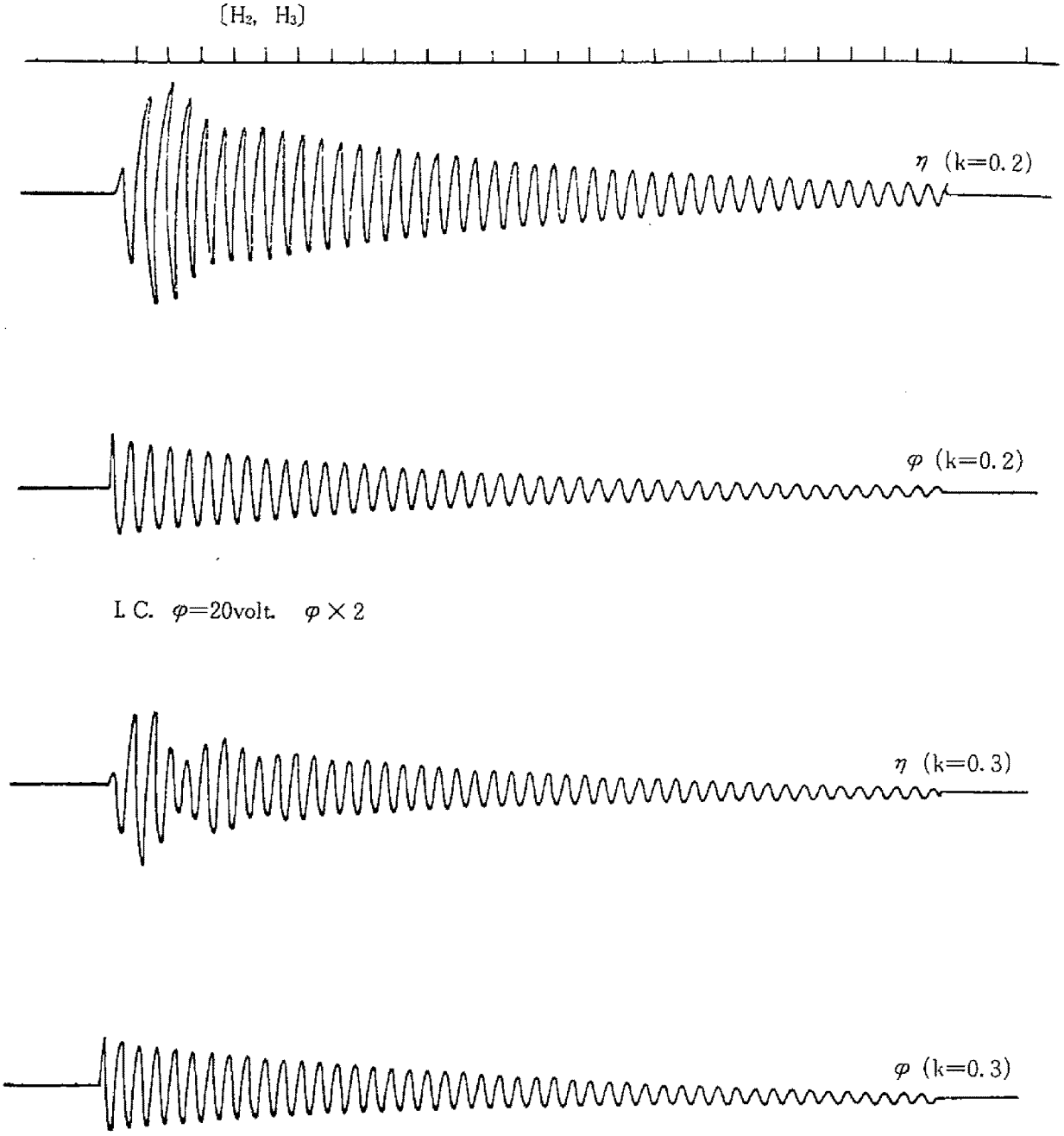

Fig. 3.7.4 Convergent Oscillations in two terms coupling of H_2 and H_3

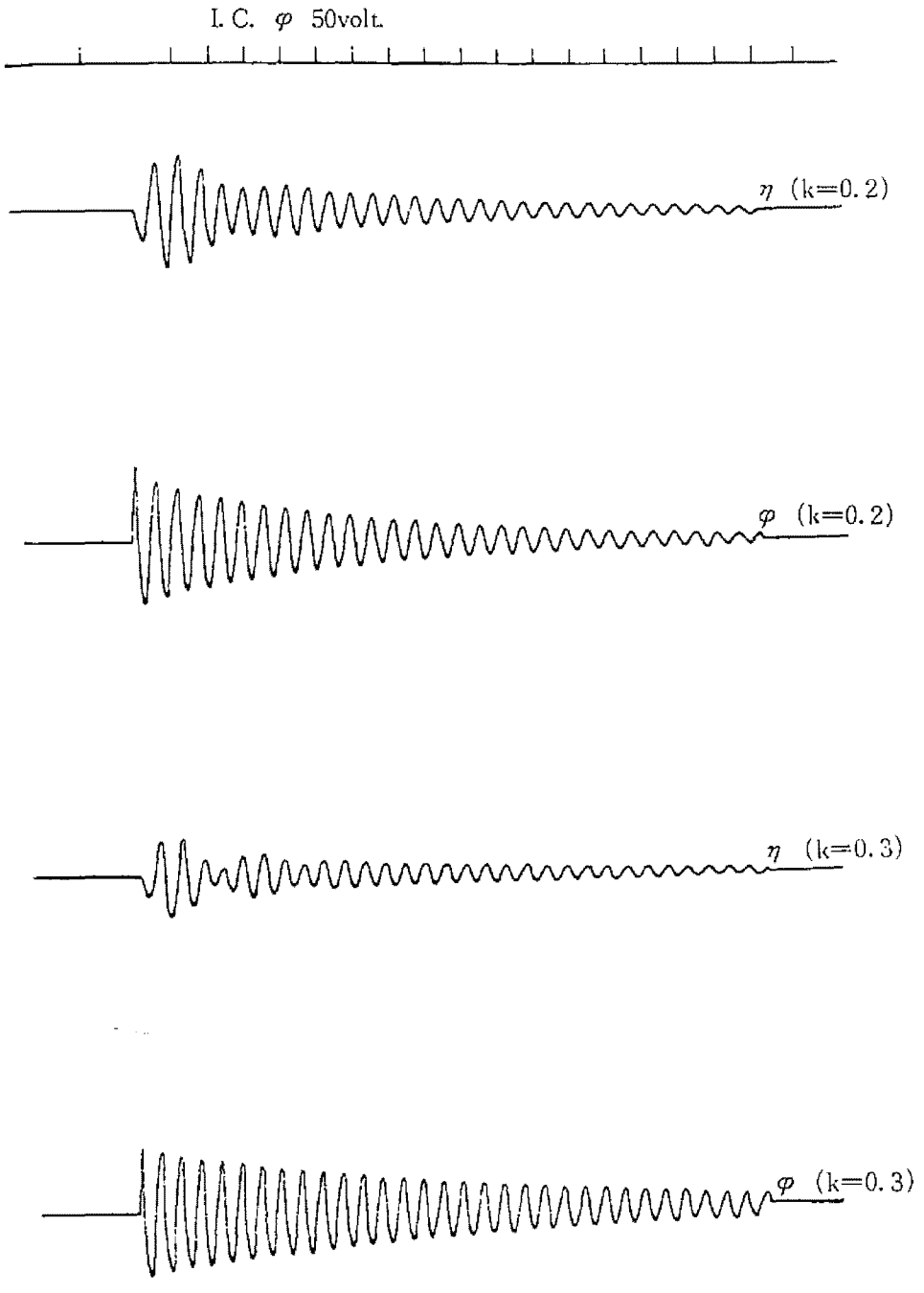

Fig. 3.7.5 Convergent Oscillations in two terms coupling of A_1 and H_2

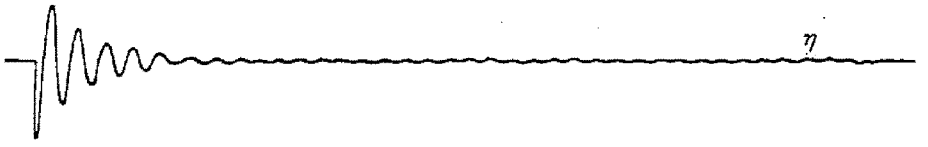

I. C. η=50volt.
k=0.3

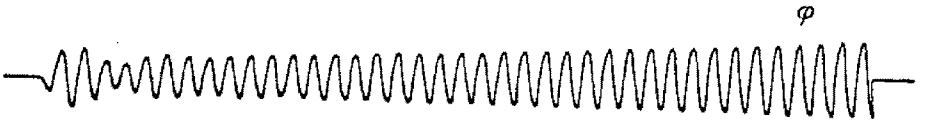

$\varphi \times 10$

Fig. 3.7.6 Divergent Oscillations due to Coupling Aerodynamic Coefficients A_1 and H_3 (k=reduced frequency)

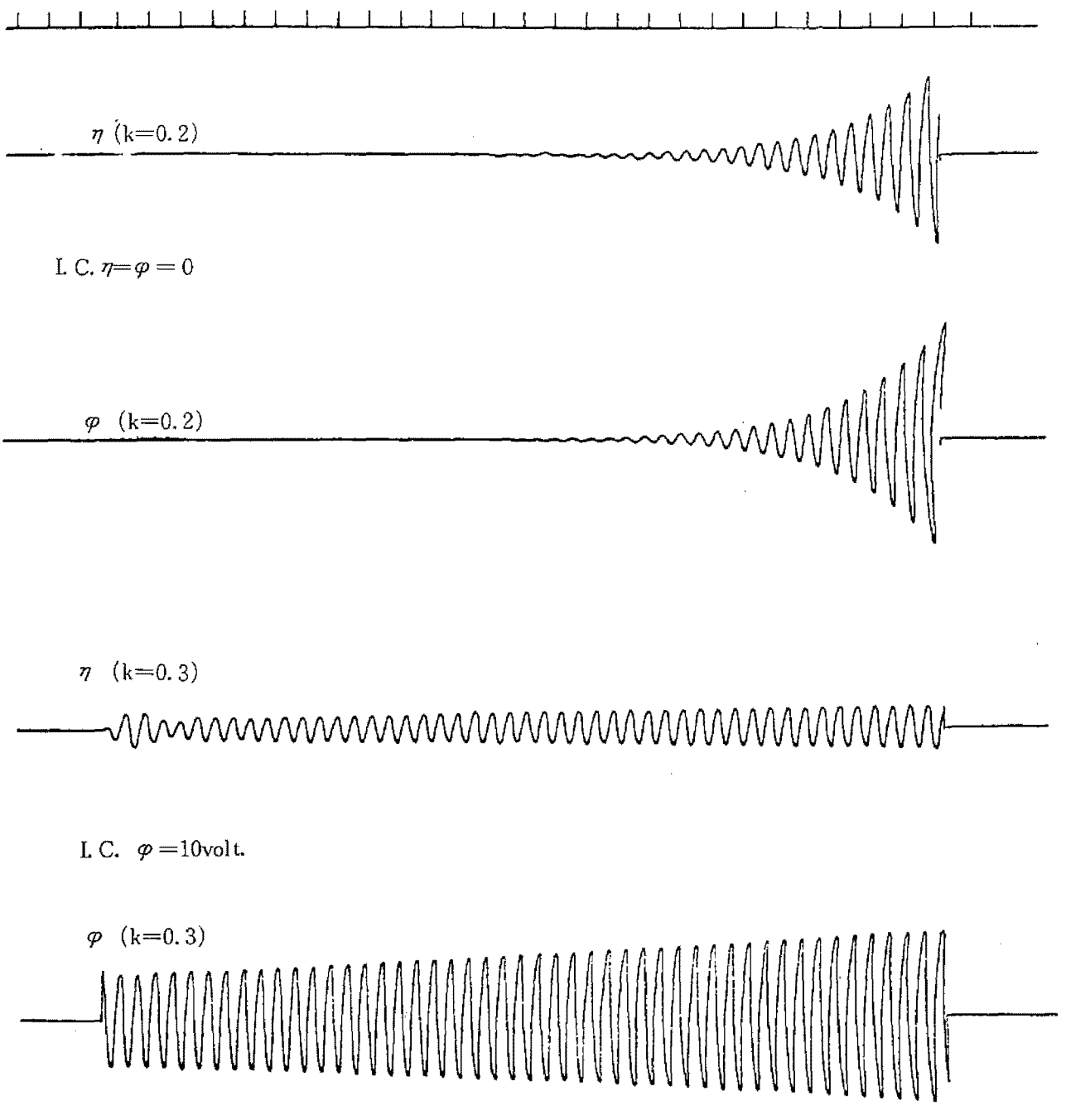

Fig. 3.7.7 Simulated Divergent Oscillations in Air Stream

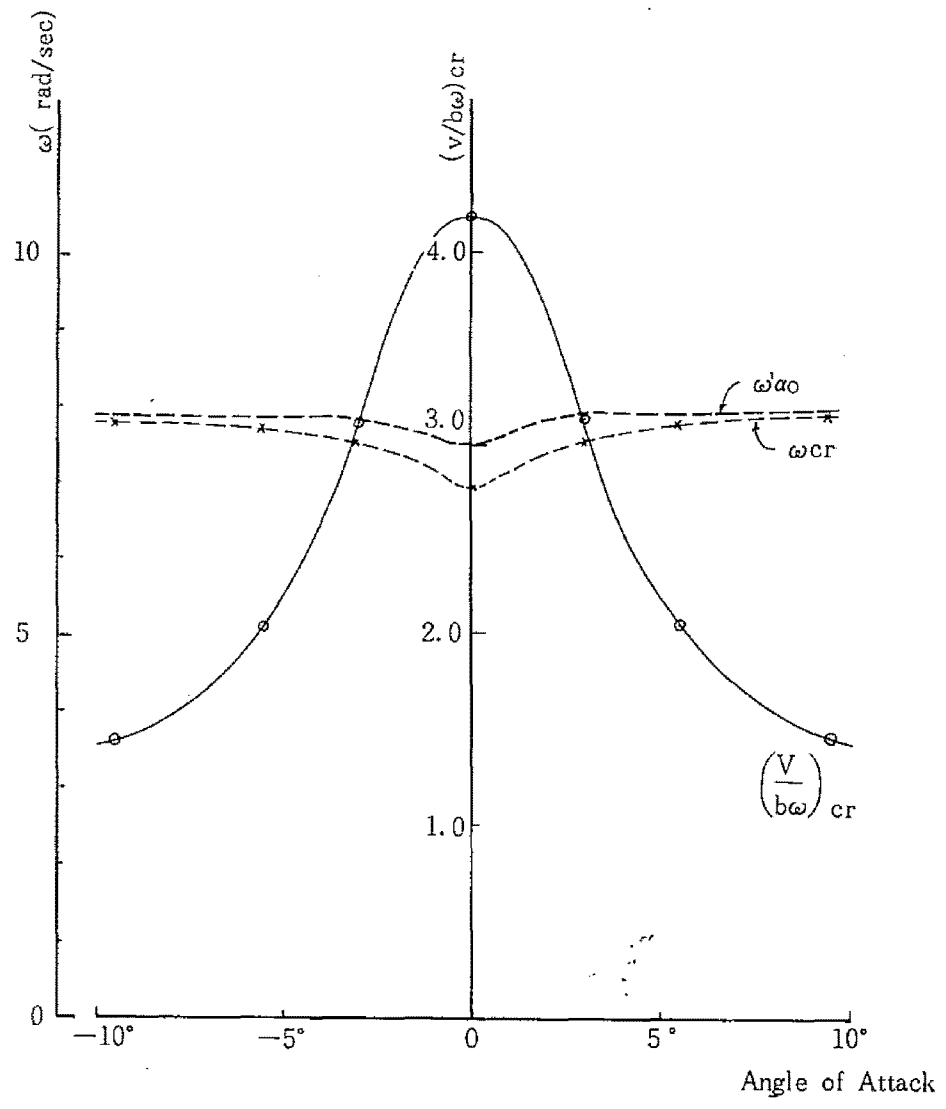

Fig. 3.7.8 Critical Reduced Velocity, Flutter Frequency—Mean Angle of Attack Relation (Plate)

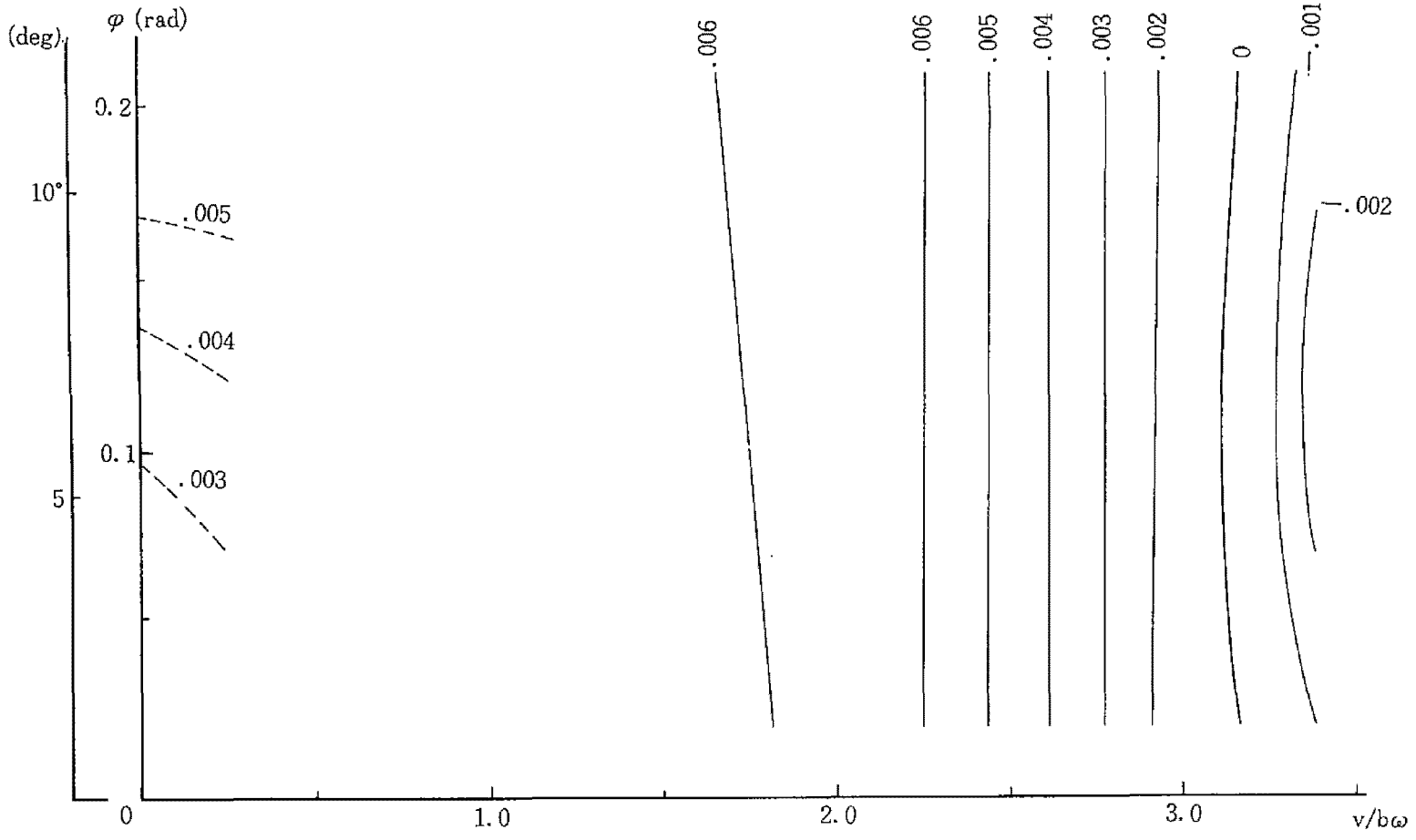

Fig. 3.7.9 Amplitude—Velocity—Damping Relation (Plate, $\alpha=3.1°$ $\omega_\alpha/\omega_\eta=1.385$)

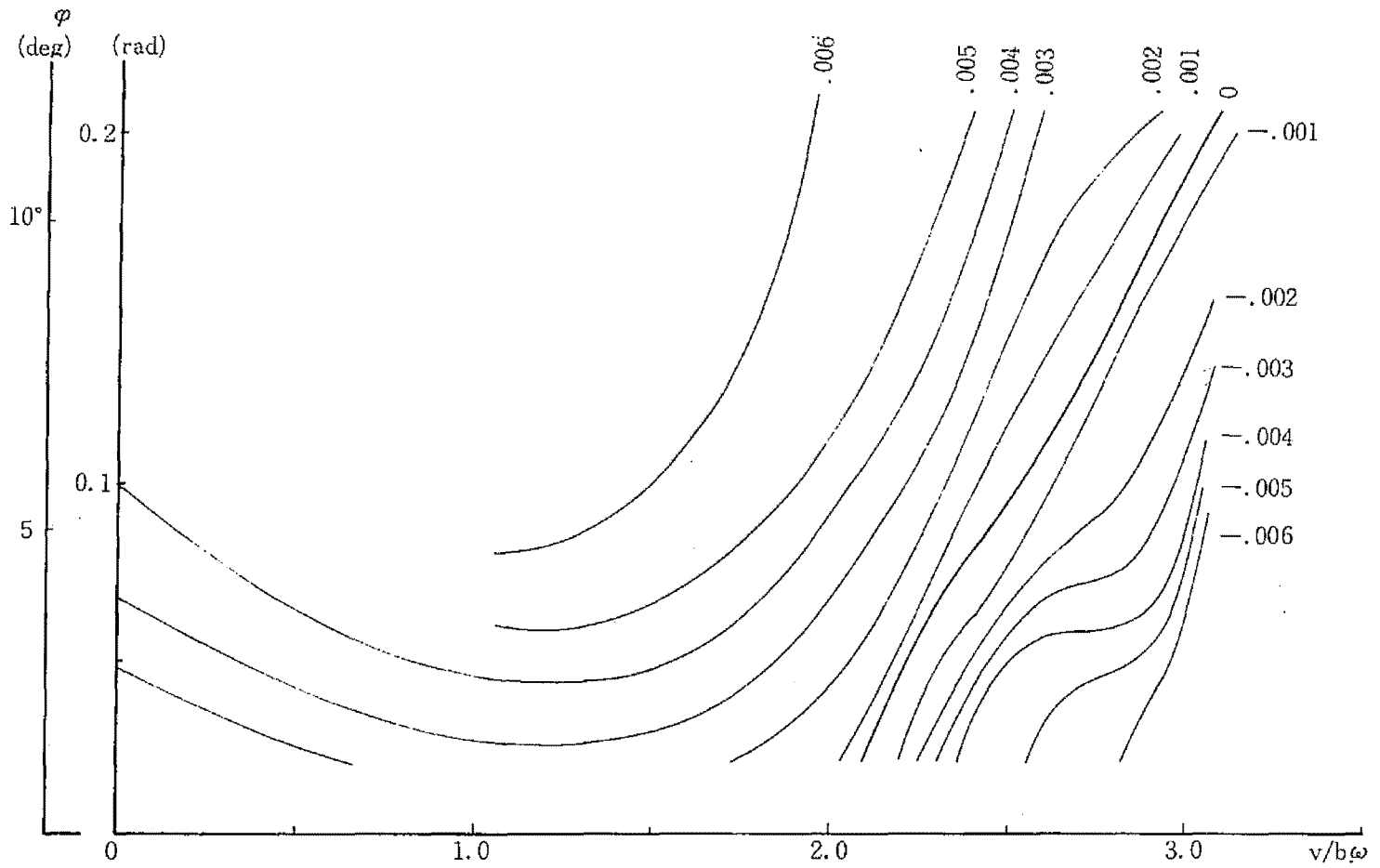

Fig. 3.7.10 Amplitude—Velocity—Damping Relation ¯ (plate, α=5.5 , $\omega_\alpha/\omega_\eta$=1.381)

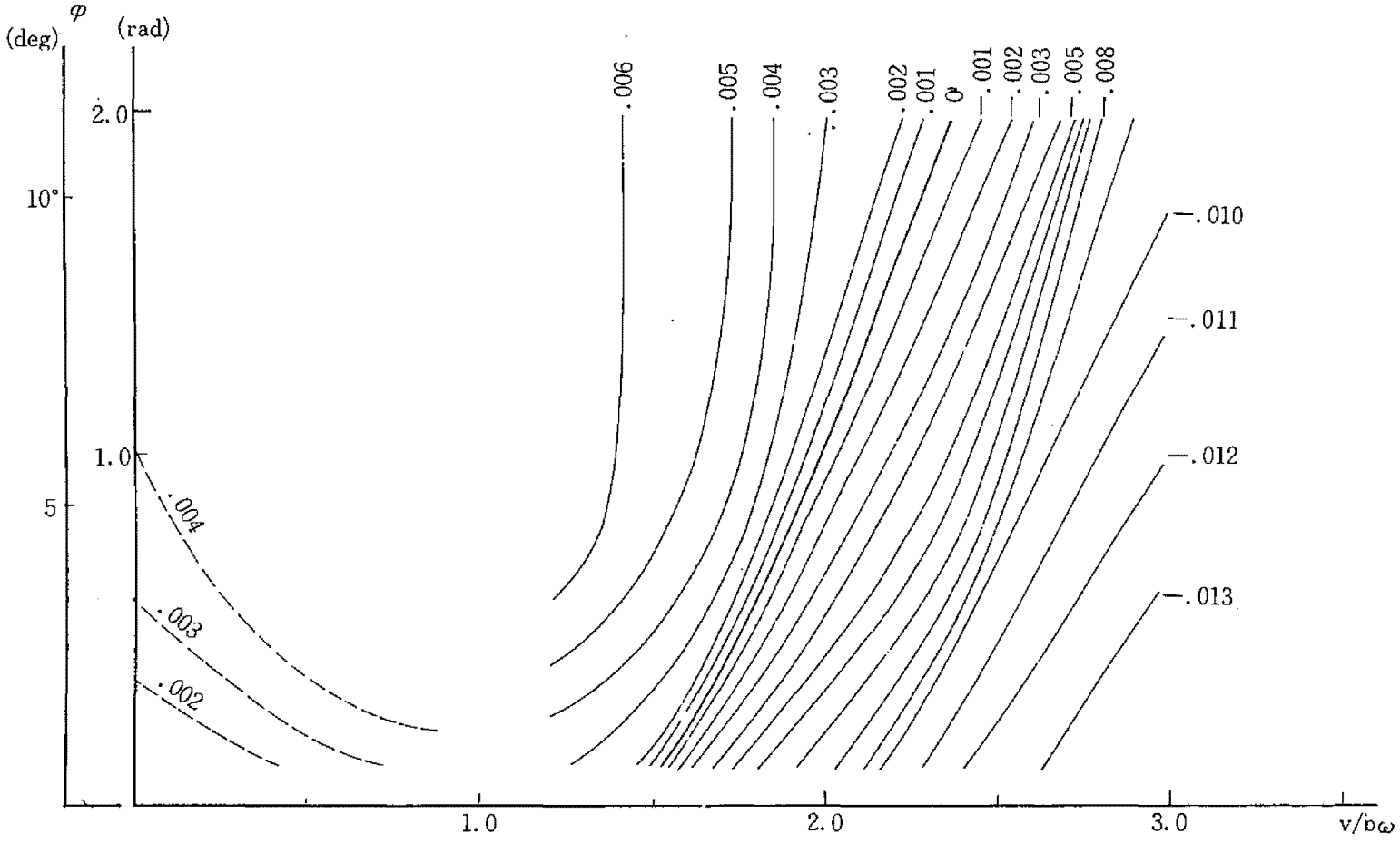

Fig. 3.7.11 Amplitude—Velocity—Damping Relation (Plate, α=9.7°, $\omega_\alpha/\omega_\eta$=1.394)

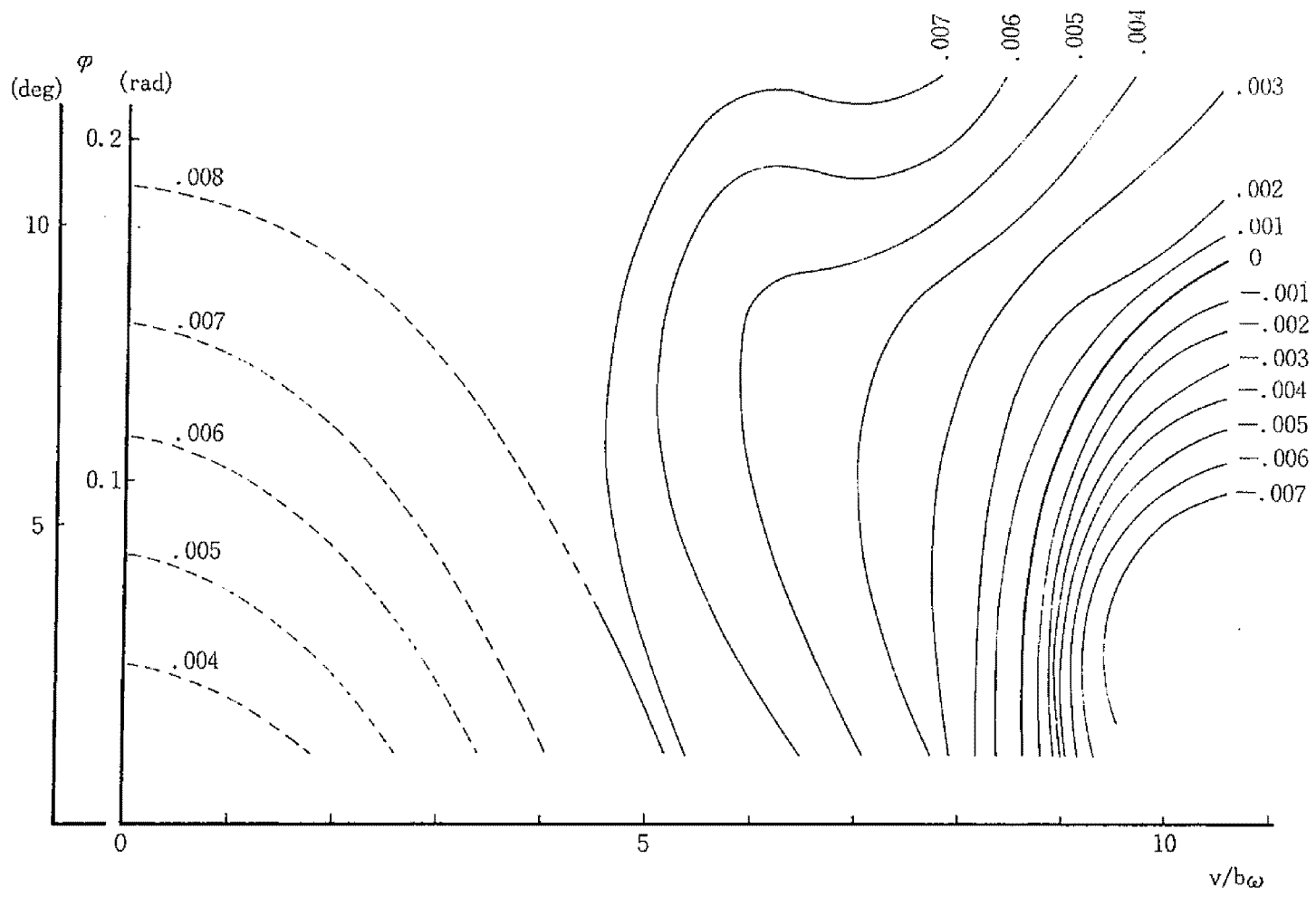

Fig. 3.7.12 Amplitude—Velocity—Damping Relation Model RT—1 $\alpha=0$ $\omega_\alpha/\omega_\eta=1.372$

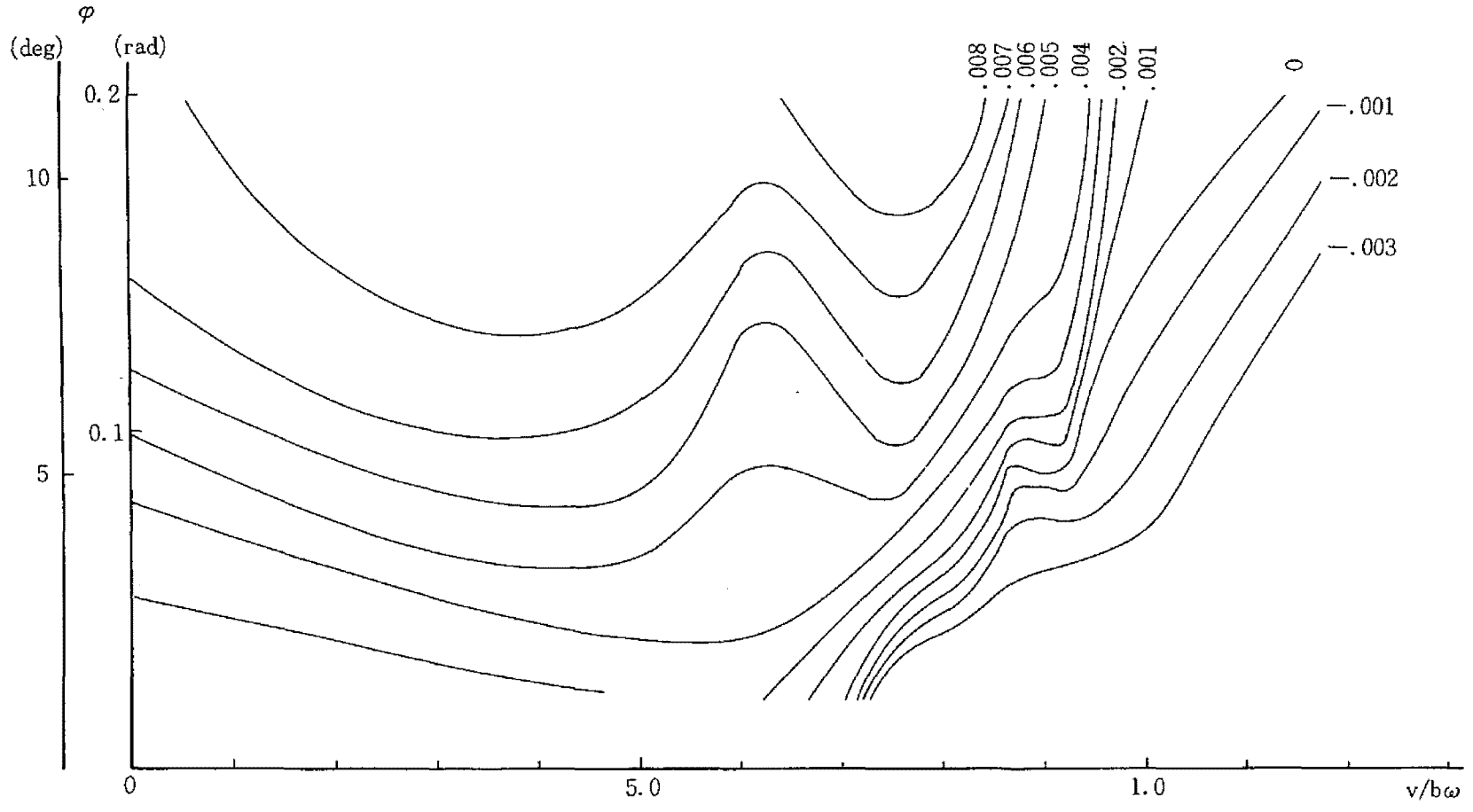

Fig. 3.7.13 Amplitude—Velocity—Damping Relation (Model RT—1, $\alpha=-3.3°$ $\omega_\alpha/\omega_\eta=1.367$)

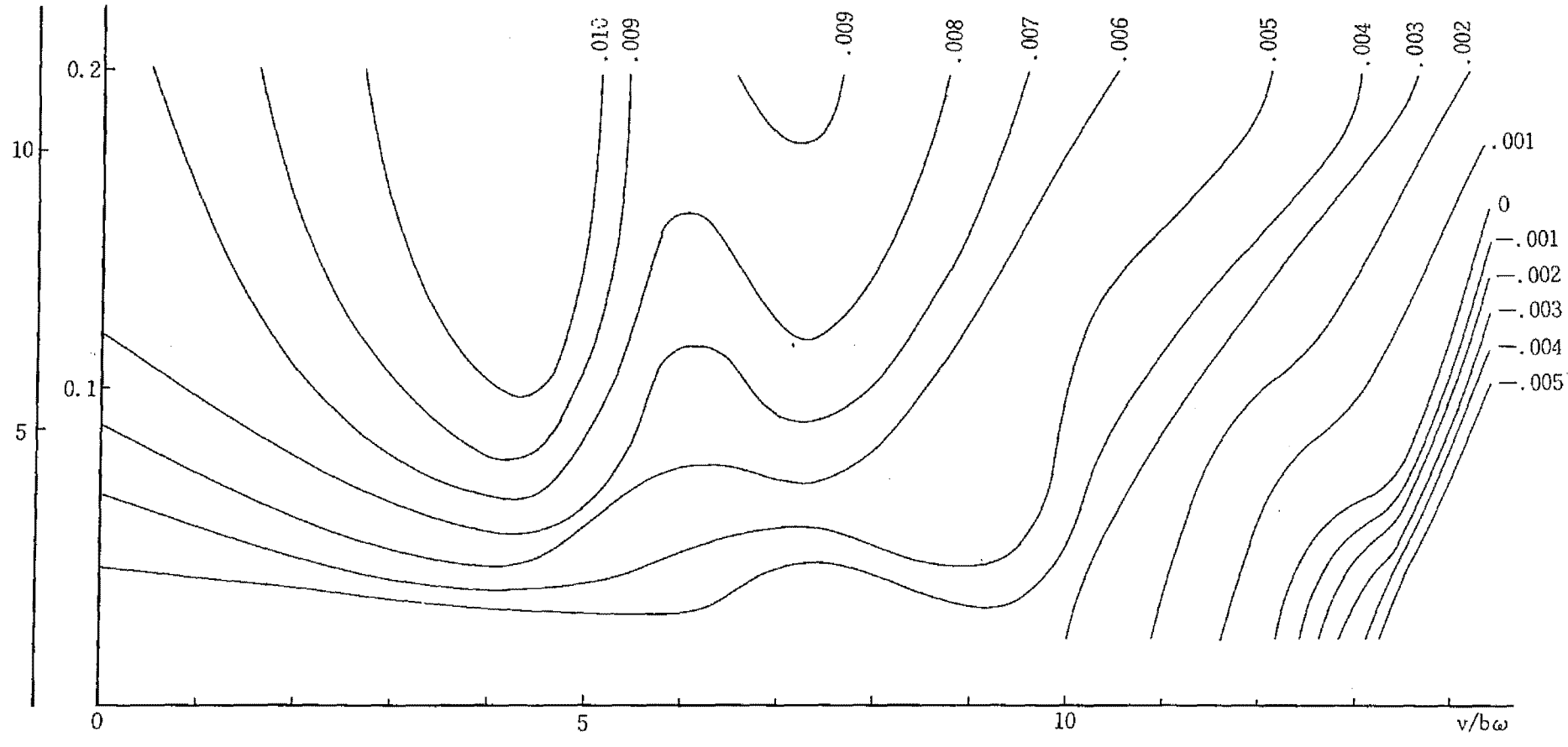

Fig. 3.7.14 Amplitude—Velocity—Damping Relation (Model RT—1, $\alpha=-7.0$, $\omega_\alpha/\omega_\eta=1.378$)

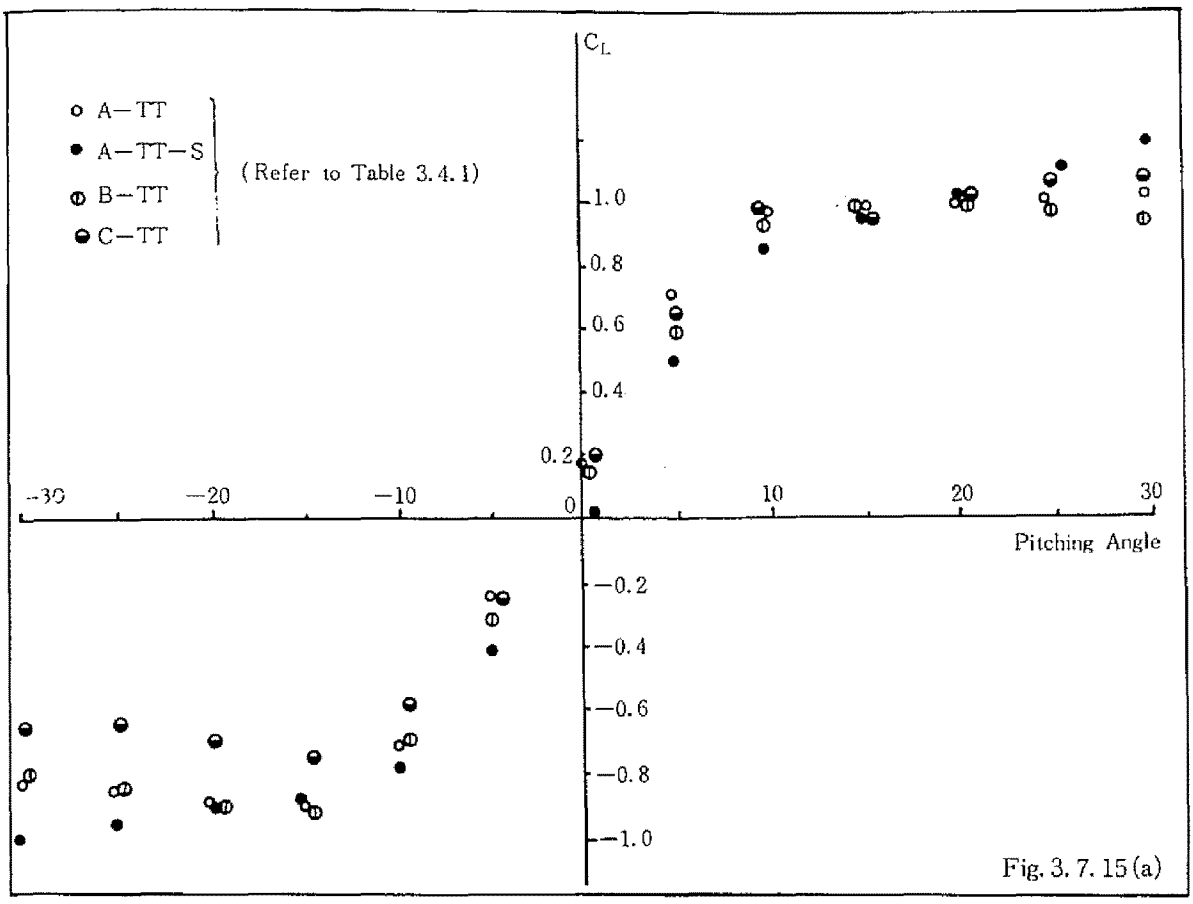

Fig. 3.7.15(a)

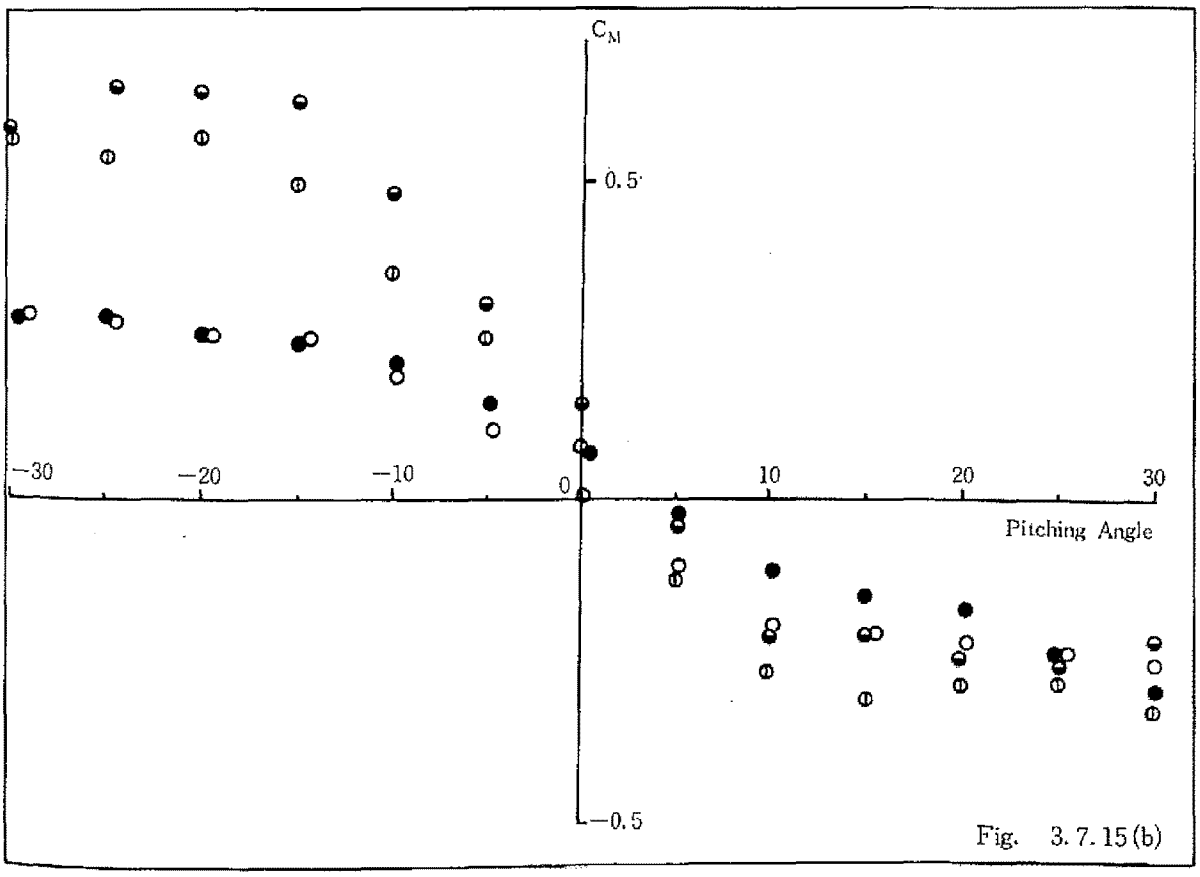

Fig. 3.7.15(b)

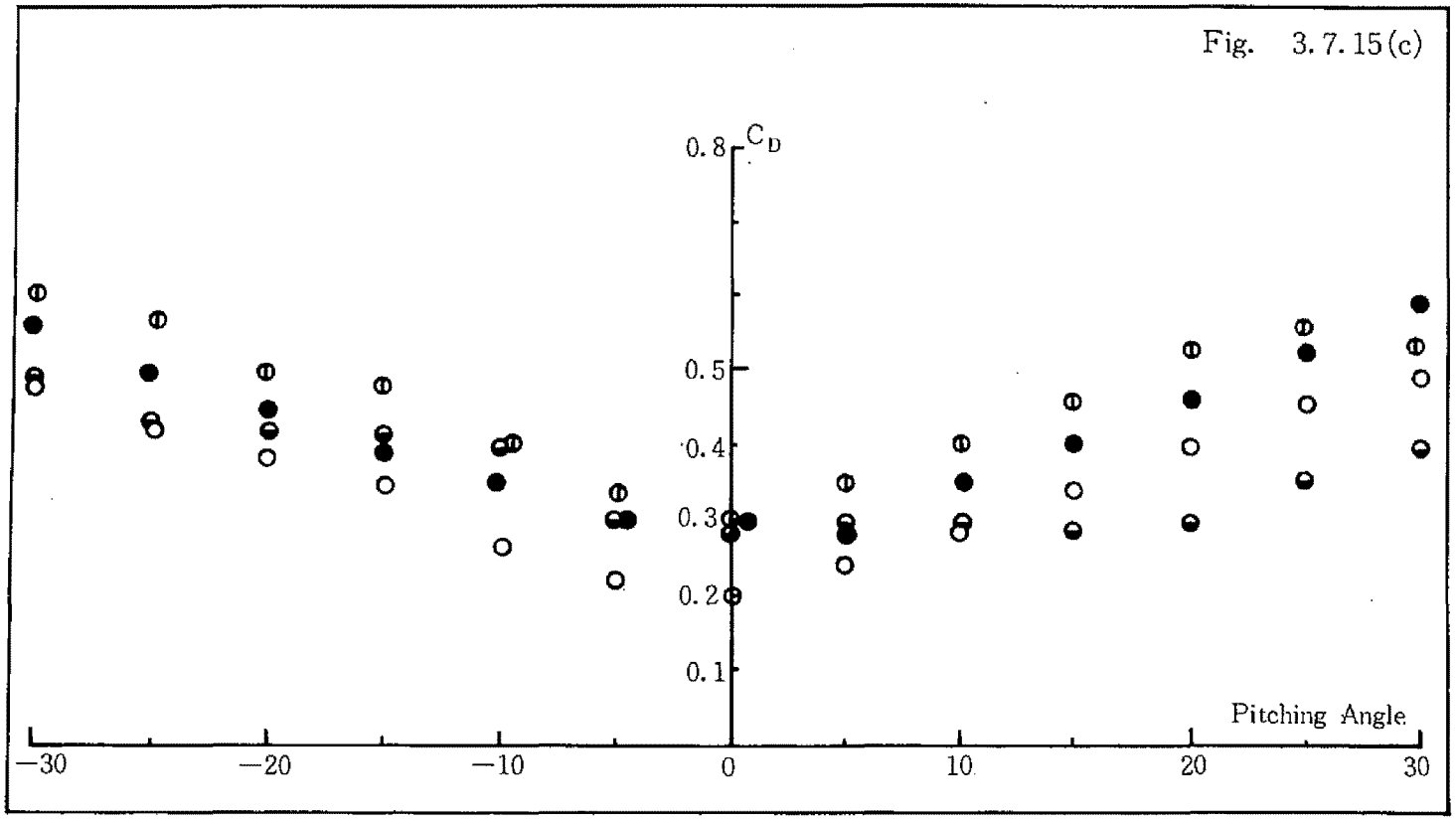

F g. 3.7.15 Lift, Drag, Pitching Moment Coefficients (wind Velocity=15m/sec)

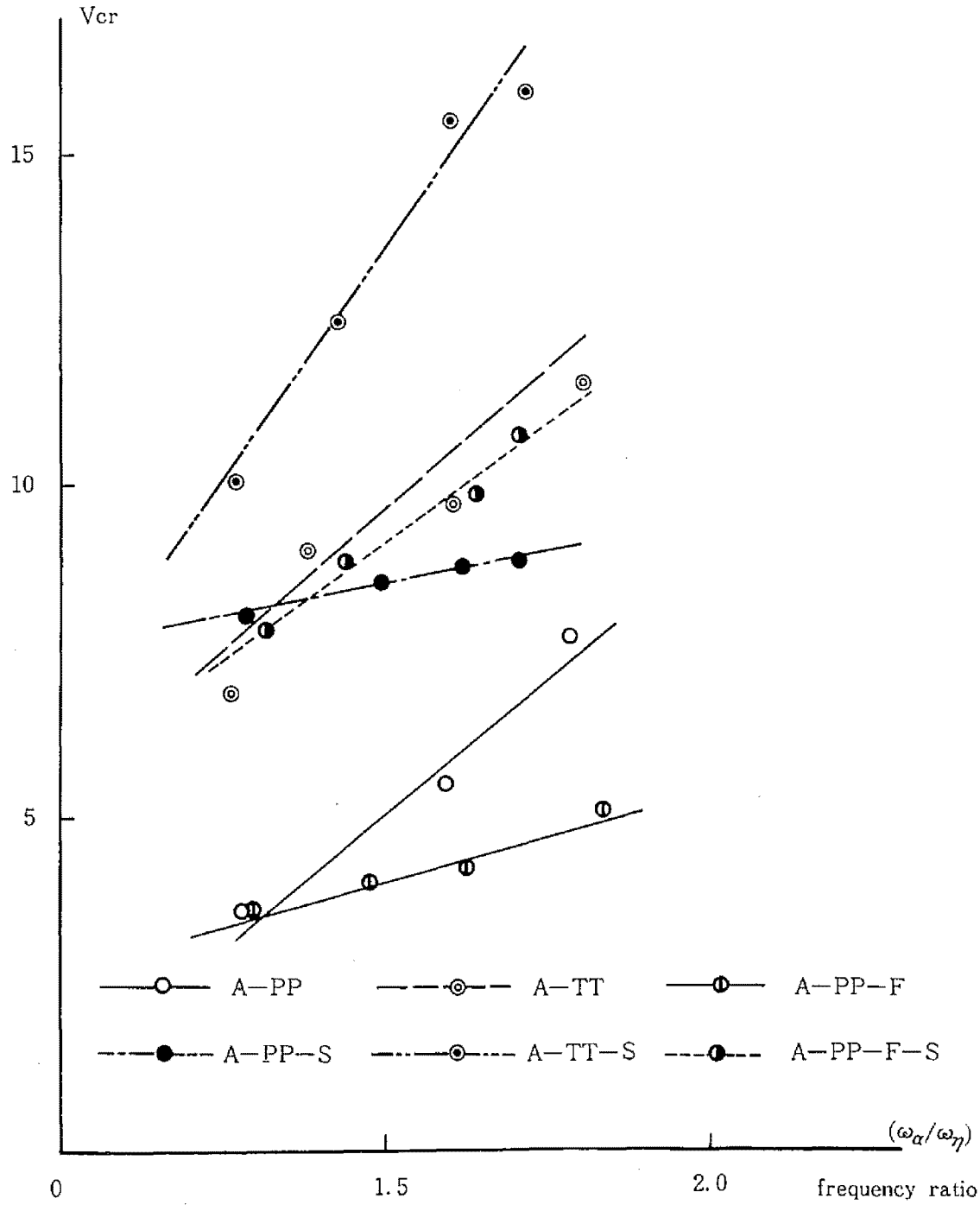

Fig. 3.7.16 Critical Velocity–Frequency Ratio Relation

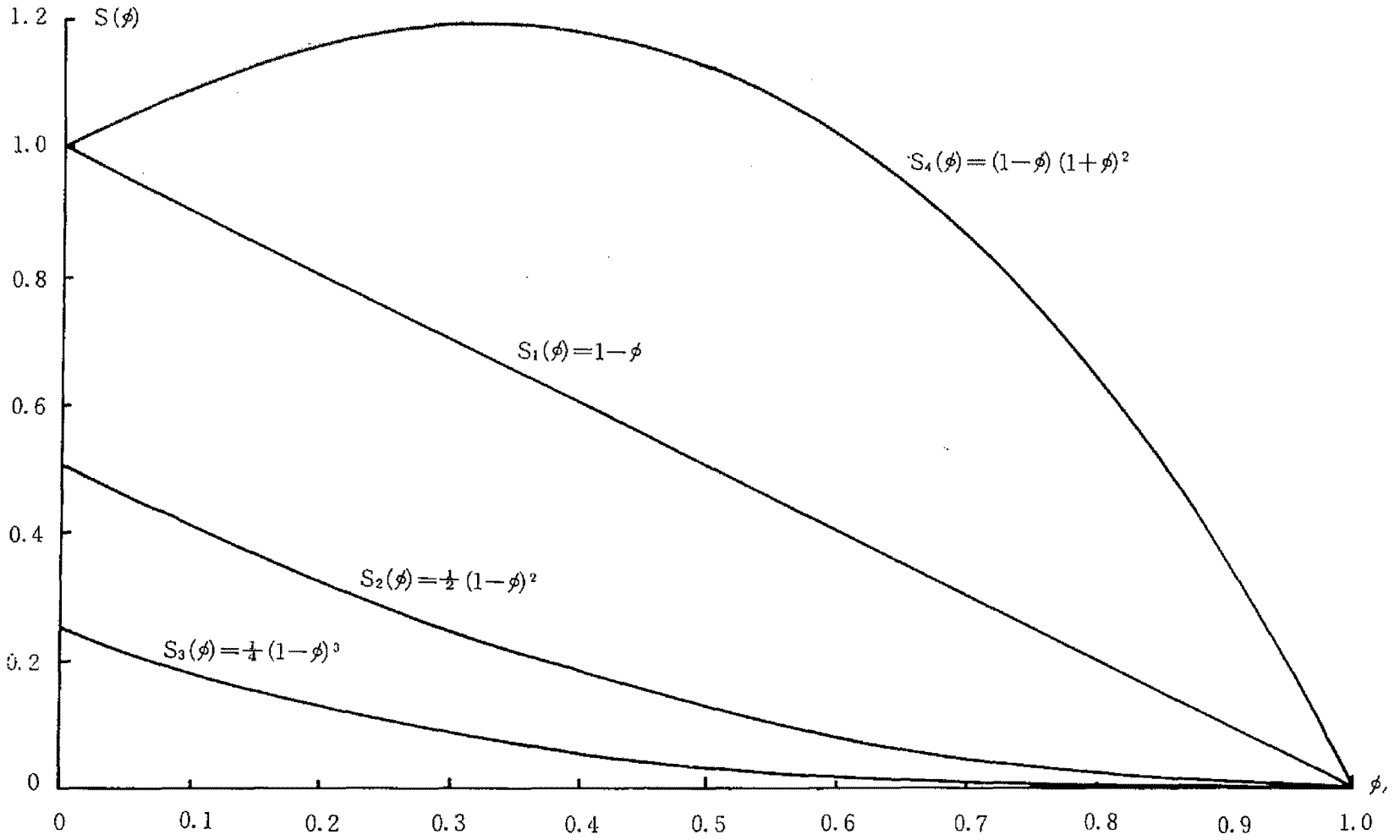

Fig. 3.7.17 Corrective Function for Slit Deck for Plate

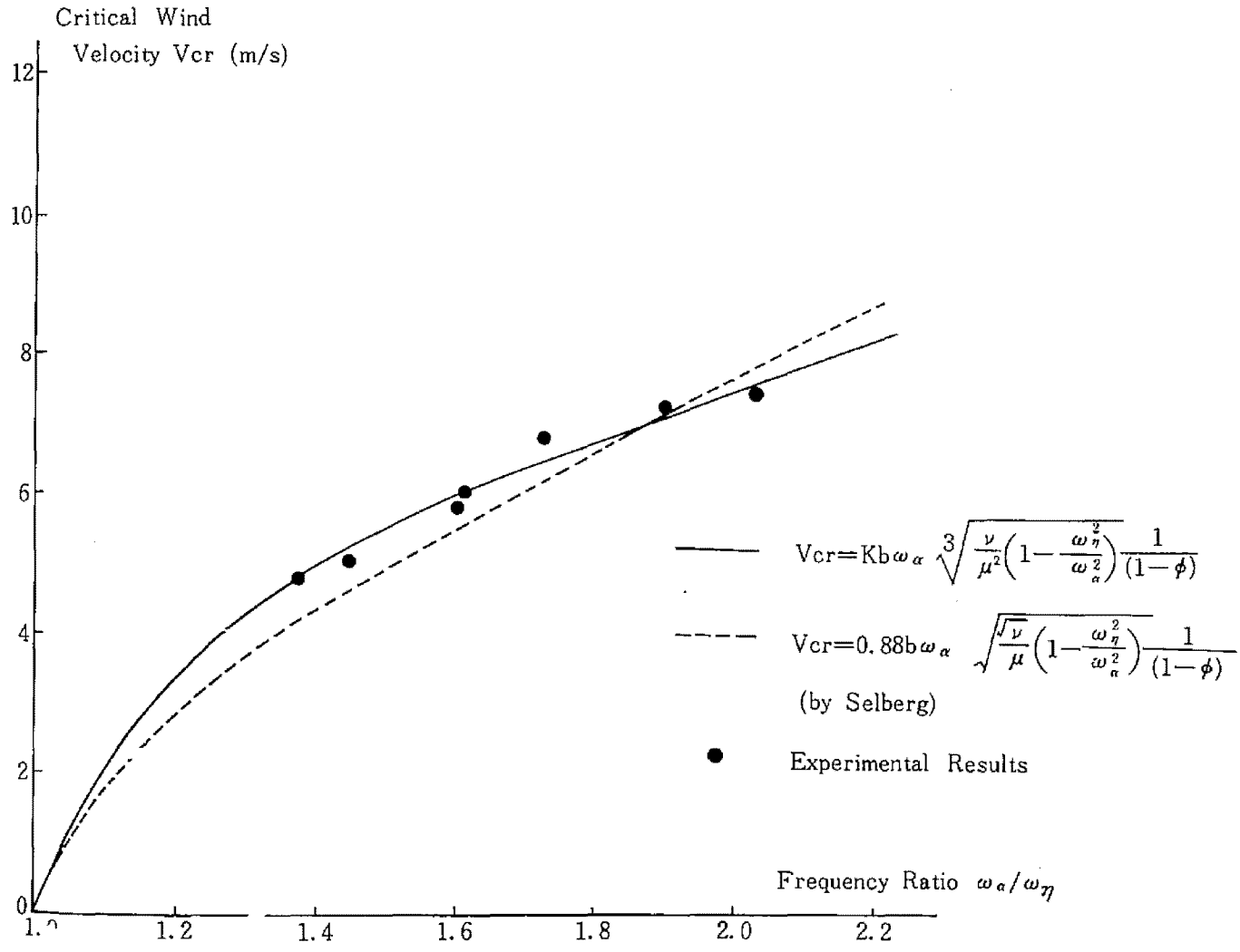

Fig. 3.7.18 Critical Wind Velocity-Frequency Ratio Relation
(Plate with slot at mid-chord, $\phi=0.1$)

APPENDIX : MEASUREMENT OF UNSTEADY AERODYNAMIC COEFFICIENTS OF PLATE AND PLATE-LIKE STRUCTURE BY MEANS OF THE FREE VIBRATION METHOD

In the paragraph 3.6 the measurement method of unsteady aerodynamic forces is presented to use both the free vibration method and the forced vibration method. The accuracy of obtained values in this method is largely dependent on the preciseness of the amplitudes and the phase angle between flexural and torsional displacements. Through the experiments in wind tunnel this difficulty is found to be eliminated by using the low pass filter and by recording the Lissajous diagram on the dual beam synchroscope. Some typical cases are exemplified in Photo*.
Using such data the unsteasy aerodynamic coefficients for a plate (940 × 200 × 2) and plate-like model (DT70H) are obtained as shown in Fig's A.1 and A.2, which yield to the similar results as those obtained previously. All aerodynamic coefficients for plate and simple plate-like model are so far satisfactorily coincident with the Theodorsen's theory except those propertional to the rate of torsional deformations, namely A_2^* and H_2^* To compare the case for plate with the case for DT70H the coefficient A_2^* is considered to be on different curves, while H_2^* to be on same curve. It is irteresting to note that both coefficients are much more smaller than the Theodorsen's theory.

*Photos A.1, A.2, A.3; pp 394 - 395

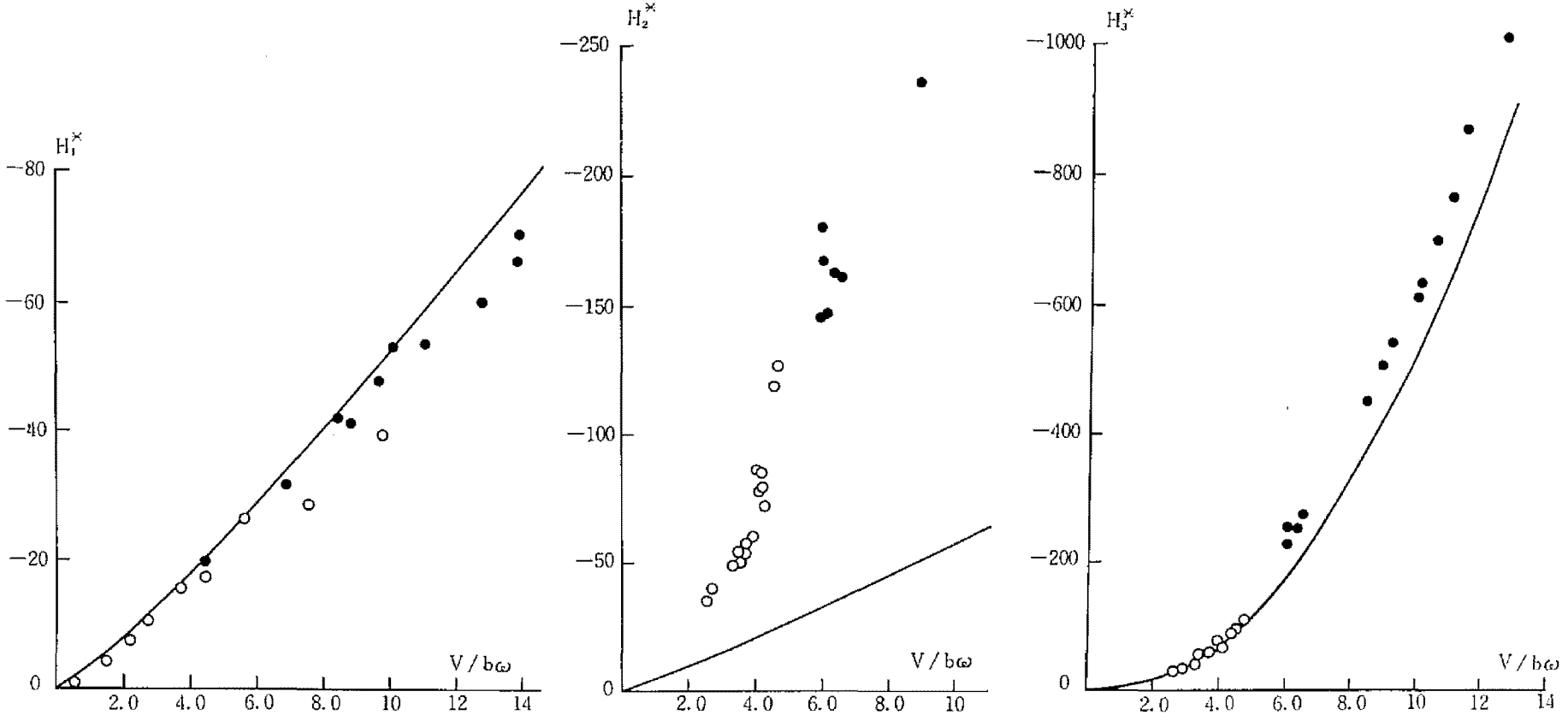

●plate. ○DT70H. —Theodorsen's theoretical curve.

Fig. A. 1 Experimental results of aerodynamic coefficients of plate and plate-like model (DT70H)

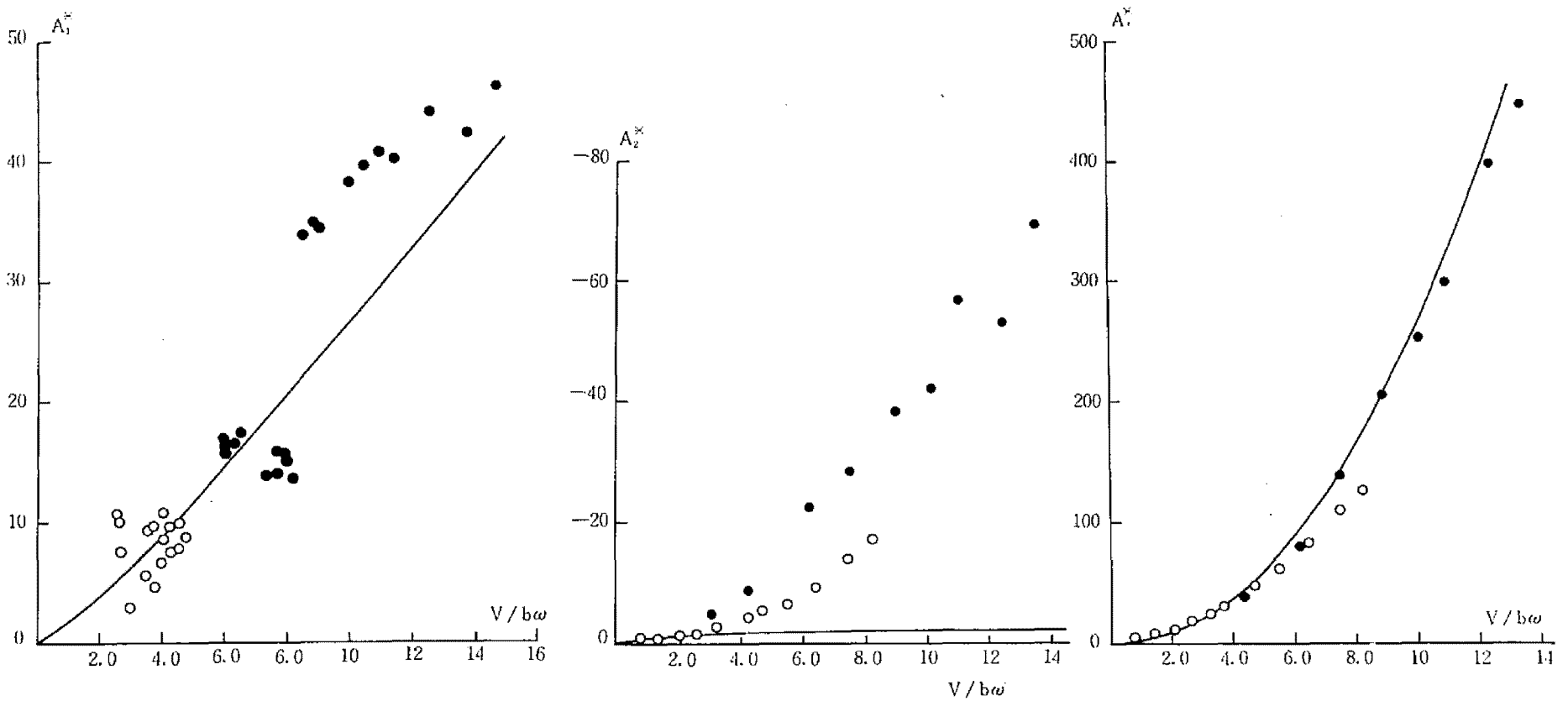

● plate. ○ DT70H. —Theodorsen's theoretical curve.

Fig. A. 2 Experimental results of aerodynamic coefficients of plate and plate-like model (DT70H)

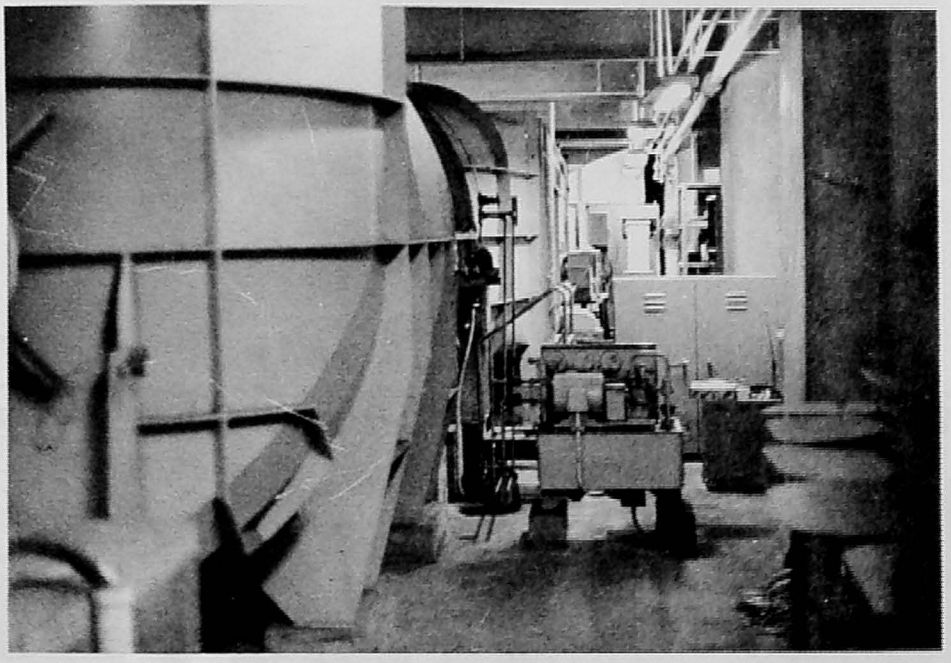

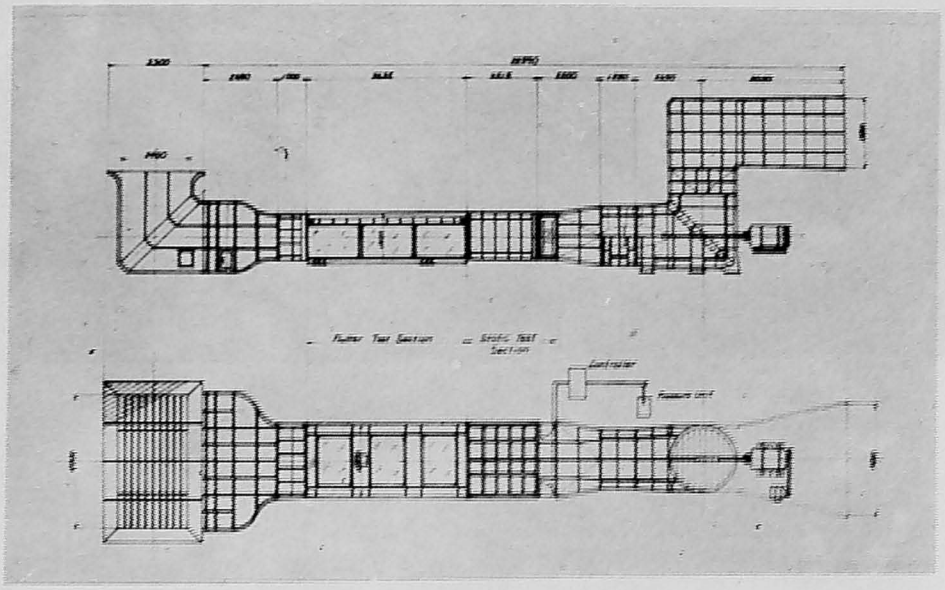

Photo 3.1 Eiffel Type Wind Tunnel

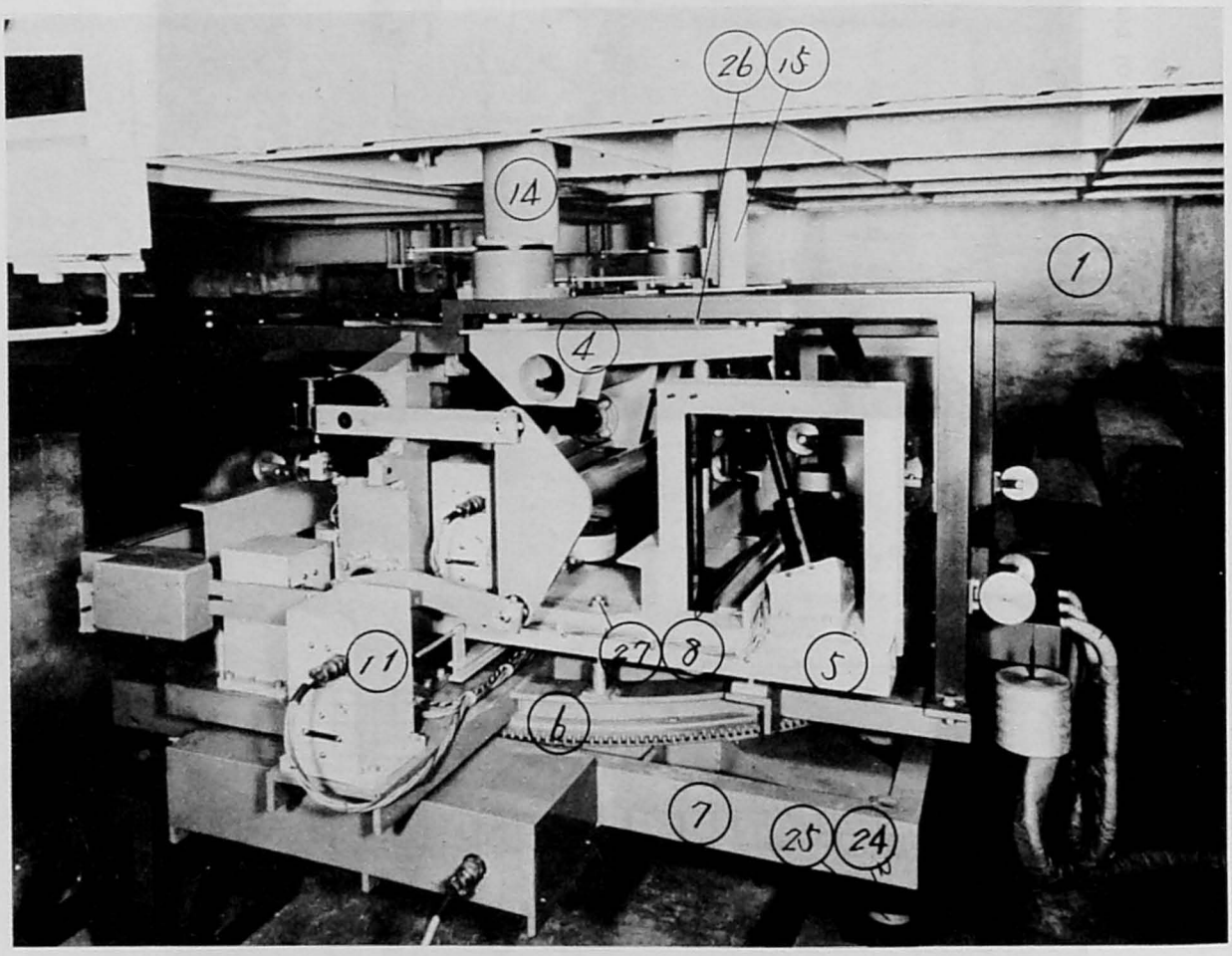

Photo 3.2 Six Components Balance

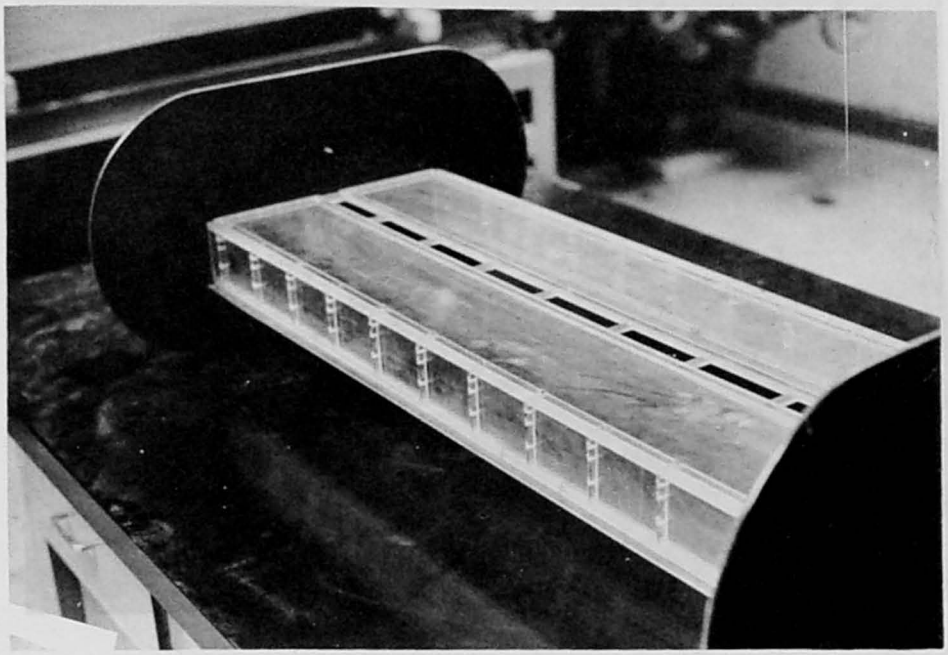

Photo 3.3 Model(EP70π(F30))

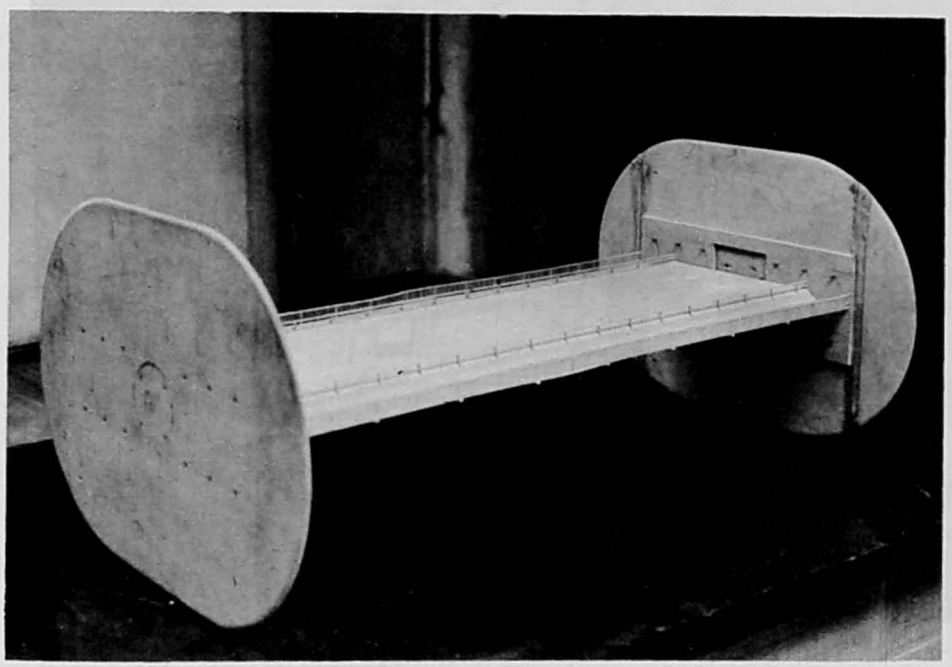

Photo 3.4 Model(Severn Type)

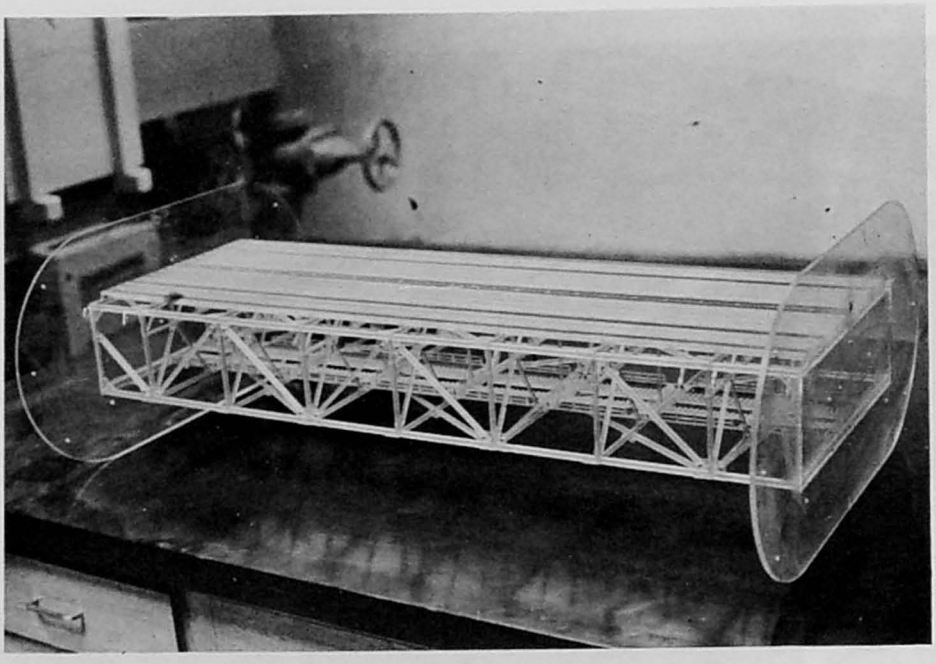

Photo 3.5 Model (RT－1)

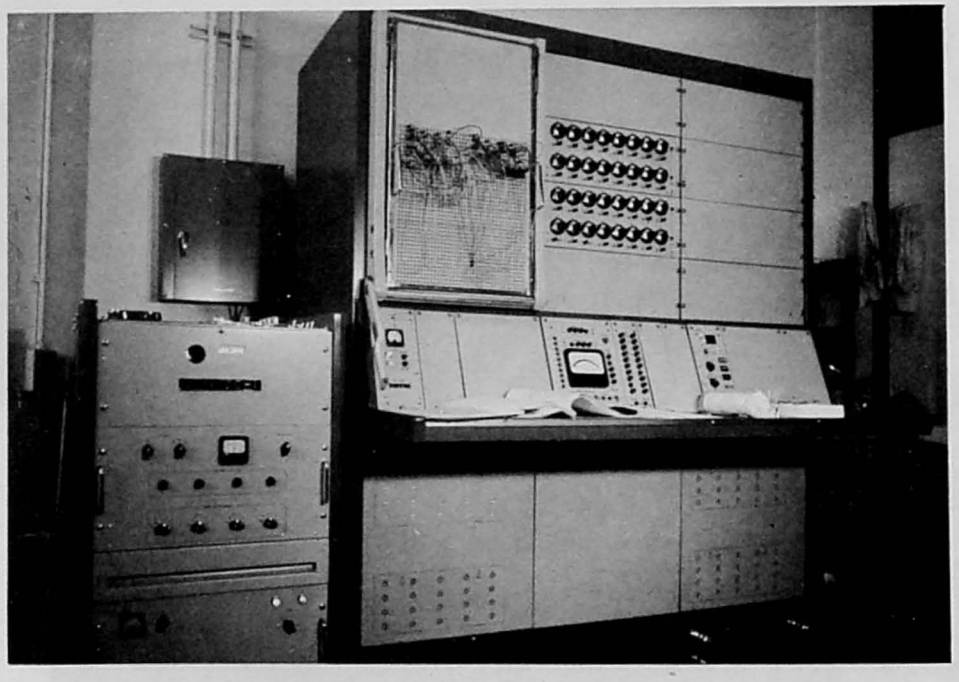

Photo 3.6 Analog Computer (HITACHI ALS1000)

References

3.1) F.B.Farquharson, Aerodynamic stability of suspension bridges, Bull. U. of Washington, No. 116, Part I, 1950.

3.2) R.A.Frazer & C.Scuton, A summarised account of the Severn Bridge aerodynamic investigation, NPL/Aero/222 Feb., 1952.

3.3) D.E.Walshe, A resume of the aerodynamic investigations for the Forth Road and Severn Bridges, Proc. Inst. Civil Eng., Vol. 37, May, 1967, pp. 87/108.

3.4) A.Selberg, Aerodynamic effects on suspension bridges, Proc. Int'l Conf. on Wind Effects, Paper 11, 1963.

3.5) D.Dicker, Aerodynamic stability of H sections, Jnl. of Eng'g Mechanics Division, Proc. ASCE, EM2, April 1966, pp 1/23.

3.6) G.V.Parkinson & S.D.Smith, The square prism as an aeroelastic non-linear oscillator, Quart. Jnl. Mech. and Applied Math., Vol. XVII,Pt. 2, 1964,
On the aeroelastic instability of bluff cylinders, Jnl. Applied Mech., Trans. ASME, June, 1961, pp. 252/258.

3.7) I.Konishi, N.Shiraishi & H.Utsunomiya, A theoretical investigation on aerodynamic stability of long-spanned suspension bridges, Trans. JSCE, No. 128, April, 1966.

3.8) T.Naritomi & M.Kawashima, Flutter calculation of suspension bridges under uniform wind velocity distribution and non-uniform distribution, Mitsubishi Heavy Industries Tech. Review, Vol. 3, No. 6, 1966, pp. 104/110.

3.9) A.G.Davenport, A statistical approach to the treatment of wind loading on tall masts and suspension bridges, PhD Thesis, Univ. of Bristal, March, 1967.

3.10) M.Shiotani, Turbulence in the lowest layers of the atmosphere, Sci. Rep. Tohoku Univ. Ser. 5, Geophysics, No. 2, pp. 167/201.

3.11) M.Ishizaki, Variation of wind pressure against structures in the event of typhoon, Annals, D. P. E. I., Kyoto Univ. No. 30, 1959, pp. 1/15.

3.12) H.Hino, Relationships between the instantaneous peak values and the evaluation time-A theory of the gust factor, Trans. JSCE, No. 117, May, 1965, pp. 23/33.

3.13) Y. Mitsuta, On the power spectrum of turbulence in storm wind, Annals, D. P. E. I., Kyoto Univ., 1963, pp. 1o4/112.

3.14) H.E.Cramer, Measurement of turbulence structure near the ground with the frequency range from 0.5 to 0.01 cps, Advances in Geophysics, 1959, pp. 75/96, Academic Press.

3.15) H.W.Liepman, On the application of statistical concepts to the buffeting problem, J.Aero. Sci. Vol. 19, 1952, pp.793/800.

3.16) Y.C.Fung, Statistical aspects of dynamic loads, Journ. Aero. Sci. Vol. 20, No. 5, 1953, pp. 317/330.

3.17) G.S.Vincent, Golden Gate Bridge vibration studies, Trans. ASCE, Vol. 127, Part II, 1962, pp. 667/702.

3.18) Ditto, Correlation of predicted and observed suspension bridge behaviour, Trans. ASCE, Vol. 127, Part II, 1962, pp. 646/662.

3.19) L.R.Cayes, Aerodynamic stability of proposed New Quebec Suspension Bridge, Bureau of Public Roads, Office of Research and Development, Oct., 1966.

3.20) C. Scruton, Aerodynamic buffeting of bridges, The Engineer, 1955, pp. 654/667.

3.21) D.B.Steinman, Aerodynamic theory of bridge oscillations, Trans. ASCE, Vol. 115, 1950.

3.22) F.Bleich, Dynamic instability of truss-stiffened suspension bridge under wind action, Trans. ASCE, Vol. 114,. 1949.

3.23) ibid(9)

3.24) A.Hirai, On the aerodynamic stability of suspension bridge, Trans. JSCE, 1947.

3.25) S.Komatsu, Design methods and safety of long-span suspension bridge against wind, Trans. JSCE, No. 142, June, 1967, pp. 10/19.

3.26) S.Kawashima, H.Kimura & T.Shibato, Measurement of aerodynamic forces on oscillating airfoil, Proc. 13th Japan Nat'l Congr, for App. Mechanics, 1963.

3.27) N.Ukeguchi, H.Sakata, H.Nishitani et al, Study on aeroelastic instability of suspension bridges subject to horizontal wind, Mitsubishi Heavy Industries Tech. Review Vol. 3, No. 6, 1966.

3.28) R.H.Scanlan & Ali Sabzevari, Suspension bridge flutter revisited, ASCE, Str. Eng'g Conf. /Seattle, Washington. May, 1967.

3.29) J.P. den Hartog, Mechanical Vibrations, 1956, MacGraw Hill.

3.30) Y.Rocard, Dynamic Instability, 1957, Ungar.

3.31) N.Ukeguchi, H.Sakata, S.Takai, K.Hirota: "Study on the characteristics of Statical Aerodynamic Forces Acting on Bridges" : Mitsubishi Heavy Industries Tech. Rev., Vol. 3, No. 6, 1966, pp. 78 - 87.

3.32) T.Ohtsuki & K.Washizu: "Wind Tunnel Tests on Square Building Model" : Tech. Rep. to the subcomittee of Wind Resistant Design, JSCE, No. 168, 1967, (unpublished)

3.33) Y.G.Panovko.& I.I.Gubanova: "Stability and Oscillations of Elastic Systems", Consultants Bureau, New York, 1965. pp. 228 - 231.

3.34) Y.C.Fung: "The Theory of Aeroelasticity," J.Wiley, 1955. pp. 320 - 330.

3.35) H.Tanaka & M.Ito: "The Characteristics of Aerodynamic Forces in Self-Excited Oscillations of Bluff Structures" Trans. JSCE, No. 168, 1969, pp. 15 - 24.

3.36) T.Miyata & I.Okauchi: "A Study of the Self-Excited Oscillations of Suspension Bridges by Wind" Trans. JSCE, No. 173, 1970, pp. 19 - 34.

3.37) H.Ishizaki & Y. Mitsuta: Observations and investigations on design wind loads for the proposed Akashi Strait Bridge, Chosa-geppo (Monthly Report of Kobe City), No. 64, Dec., 1969 pp. 5 - 11.

3.38) H.Arai et al; Vertical distribution of wind velocity above sea waters, Report of Japan Railway Technical Research Institute, No. 67 - 41, March, 1967

CHAPTER 4 AERODYNAMIC RESPONSES OF STRUCTURES IN TRANSVERSELY & CHORDWISELY FLUCTUATING GUSTS

4.1 INTRODUCTION

The aerodynamic investigations on the long-spanned suspension bridge are so far mainly concerned with the aerodynamic instability due to the flutter phenomenon in the uniform air stream. However there is an aspect of the problem other than the stationariness of air flow, which should be considered; that is, the fact that timely and spatially varying nature of natural wind velocity possibly causes the fluctuations of responses of such flexible structures as suspension bridges. The actual structure is so required to be designed as sufficiently resistant to various types of wind loadings and feasibly stable for various aerodynamic destabilizing factors. As already mentioned, the latter problem is closely related with the flutter and the galloping types of instability problems, while for the former problem the randomness of wind velocity takes an important role to produce timely and spatially fluctuating respones. One of the significant contributions has been achieved by A. G. Davenport[1] since 1960. His statistical approach extends over most of flexible structures such as tall masts, tall buildings and long-spanned suspension bridges. After A. G. Davenport's investigations there are numbers of papers presented by applying his method directly and some by modifying it from various points of views.[2),3),4),5)] Fundamental scheme for analysis due to A. G. Davenport is to disclose the aerodynamic mechanisms that fluctuations of wind velocity are responsible for the fluctuations of induced aerodynamic forces for the structures to receive timely and spatially varying responses. In order tc investigate this theme, therfore, the following problems are considered to be clarified:

(1) meteorological characteristics of natural winds
(2) fluidmechanical properties of fluctuating wind velocity
(3) unsteady aerodynamic forces due to fluctuating wind velocity
(4) statistical effectiveness of aerodynamic forces on structures
(5) frequency response characteristics of structures

(6) probabilistic estimation of variation of aerodynamic responses
(7) stabilizing and destabilizing effects due to fluctuations of wind velocity

In this investigation stress is placed on the above problems (3), (5), and (7) particularly, considering two-dimensional air flows.

The unsteady aerodynamic forces of lift and pitching moments acting on a plate due to transversely fluctuating wind velocity are investigated by Th. von Karman and W. R. Sears[6] who succeed in defining the so-called Sears function by which the periodically fluctuating wind velocity is easily taken into an account for estimation of the corresponding aerodynamic forces[7]. R. Isaacs[8] investigates the lift force of airfoil due to the chordwisely fluctuating wind velocity when the angle of attack exists and the theory for this effect is more precisely estabilished by J. H. Horlock[9]. Based on the Horlock's investigations the aerodynamic forces due to chordwisely fluctuating wind velocity for a vibrating plate are derived theoretically in this investigation. The stabilizing and destabilizing mechanisms for a plate under action of fluctuating wind velocity is discussed here.

In statistical analysis of random phenomena in mechanical system it is important to find the frequency response function for the given system. In connection with suspension bridge the coupling of deflectional and torsional modes of vibrations is inevitable under the action of wind. A general coupled form of frequency response function for the plate-like structures in air stream is illustrated here.

Wind tunnel tests are performed by using the same models as shown in the previous chapter in artificially generated flows by setting the wooden grids in the tunnel.

4.2 STATISTICAL CONEEPTS IN ANALYSIS ON AERODYNAMIC PROBLEMS OF SUSPENSION BRIDGES DUE TO A.G.DAVENPORT[10) ~ 16)]

In this paragraph the fundamental concept and the method of analysis by A. G. Davenport are briefly introduced, related with the present concerns.

4.2.1 Aerodynamic Forces due to Fluctuating Flow

1) General Problem for resistance in unsteady flow.

In general the resistance in fluctuating flow can be expressed as

$$P(t)=\frac{1}{2}\rho C_D(n) V(t)|V(t)| + C_m(n)\rho\frac{A_0}{D}\frac{dV(t)}{dt} \qquad (4\cdot2\cdot1)$$

where

P(t) = force per unit area for the object at time t

V(t) = velocity of the fluid at time t

ρ = fluid density

D = diameter of object

A_o = a reference area for the additional mass

$C_D(n)$ = coefficient of drag (assumed to be a function of the fluctuation frequency n)

$C_m(n)$ = coefficient of additional mass (including the equivalent mass of the fluid and object itself -also assumed to be a function of n)

In uniform flow, the average velocity in the region is obviously equal to the velocity at any point in the region. In turbulent flow, however, the average velocity differs from the velocity at a point owing to the variations in phase and randomness of the fluctuations within the region.

If we assume a correlation function for the fluctuating wind velocity of the type

$$R_{XX'} = e^{-\frac{|x-x'|}{L(n)}} \qquad (4\cdot2\cdot2)$$

where L(n) is the scale of the fluctuations at frequency n, then the correlation over the whole area is of the form

$$C = \int_0^b \int_0^b \int_0^D \int_0^D e^{-\frac{|x-x'|}{L_x(n)}} \quad e^{-\frac{|z-z'|}{L_z(n)}} \quad dx\,dx'\,dz\,dz' \qquad (4\cdot2\cdot3)$$

Eq.(4.2.3) can be written as

$$C(\xi) = \frac{2}{(7\xi)^2}\left(7\xi - 1 + e^{-7\xi}\right) \qquad (4\cdot2\cdot4)$$

where $\xi = nD/\overline{V}$ (reduced frequency), Fig. 4.1 and Fig. 4.2, if one takes the scale of fluctuations L(n) as

$$L_x(n) \doteq L_z(n) = \frac{1}{7}\frac{\overline{V}}{n} \qquad and \qquad b = D$$

The characteristics can be described as follows:

1. For reduced frequencies less than 0.1 the velocity fluctuations within the region of the flow likely to affect the pressures on the structure are fairly uniform: thus the resistance in turbulent flow at these reduced frequencies probably approaches that in uniform fluctuating flow.
2. For reduced frequencies greater than 1, fluctuations in the turbulent flow have negligible effect in inducing pressures on structures.
3. For $0.1 < \xi < 1$ there is a transition region in which the resistance diverges from the uniform flow in 1 and decreases until it is negligible as in 2.

2) Drag

For the present analysis eq.(4.2.1) can be written as

$$P = \frac{1}{2}\rho\overline{V}^2 C_D(0) + \rho C_D(\xi)\overline{V}\,D V_e \sin 2\pi n t$$

$$= \overline{P} + 2\overline{P}\frac{C_D(\xi)}{C_D(0)}\frac{V_e}{\overline{V}}\sin 2\pi n t$$

where $\overline{P}$ = the mean pressure = $(1/2)\rho C_D(0)\overline{V}^2 D$

The spectrum of the $S_p(n)$ is written as

$$S_p(n) = 4\overline{P}^2 |\chi_A(n)|^2 \frac{S_V(n)}{\overline{V}^2}$$

$$|\chi_A(n)|^2 = C(\xi)\,[C_D(\xi)/C_D(0)]^2$$

where $C(\xi)$ = velocity correlation over the postuated region of influence, eq.(4.2.4)

$S_V(n)$ = spectrum of horizontal velocity at a point

Since, at the reduced frequencies for which $C_D(\xi)/C_D(0)$ becomes significantly greater than unity, $C(\xi)$ diminishes rapidly to very small values, it seems adequate to assume that

$$|\chi_A(\xi)| \cong C(\xi)$$

3) Lift Forces

It is characteristic of most bridge decks that they will experience a vertical force when the wind is inclined to the plane of the deck. The forces that develop are large even at small angles of inclination. If the deck and the mean wind are horizontal, this angle of inclination, or angle of attack of the deck to the wind, α is the angle between the horizontal and the instantaneous wind velocity. Approximataly,

$$\alpha = \frac{w}{\overline{V}}$$

where w = the vertical component of velocity.

For most bridge decks it is possible, over a limited range, to represent the change in lift force with angle of attack by a straight line. Suppose that the slope of this line, i.e., the rate of change of lift force with α, is denoted by $dZ/d\alpha$, then the vertical force P is given by

$$P = \frac{dZ}{d\alpha} \frac{w_e}{\bar{V}}$$

where w_e is an effective vertical velocity. The best assumption we can make regarding w_e is that it is the average vertical velocity over some hypothetical region of influence. The expression for the spectrum of vertical lift force can be written as

$$S_p(n) = \left(\frac{dZ}{d\alpha}\right)^2 \frac{S_w(n)}{\bar{V}^2} \left| \chi_A(n) \right|^2$$

where $S_w(n)$ is the vertical velocity spectrum and

$$\left| \chi_A(n) \right|^2 = C(\xi)$$

4.2.2 Aerodynamic Responses to Fluctuating Flow

For the mechanical system considered the fundamental vibrational characteristics are determined by usual method of calculations. Let n_r and $\mu_r(x)$ be the natural frequencies and the corresponding mode of the r-th degree, then the joint mode acceptances are given as

$$|J_r(n)|^2 = \frac{1}{N_r^2} \int_0^\ell \int_0^\ell R_{XX'}(n)\, \mu_r(x)\, \mu_r(x')\, dx\, dx'$$

where $R_{XX'}(n)$ is the cross correlation ceofficient of the form

$$R_{XX'}(n) = e^{-\frac{7|x-x'|n}{\bar{V}}}$$

and dynamic magnification factors $|\chi_r(n)|^2$ are calculated as

$$|\chi_r(n)|^2 = \frac{1}{\left\{1-\left(\frac{n}{n_r}\right)^2\right\}^2 + \left(\frac{\delta_r}{\pi}\right)^2 \left(\frac{n}{n_r}\right)^2}$$

where δ_r is the total logarithmic damping decrements consisting of aerodynamic and mechanical damping. So the normalized variance of the dynamically magnified mode components of the pressure,

$$\frac{\sigma_r^2(P)}{\bar{P}^2} = \int_0^\infty |\chi_r(n)|^2\, |J_r(n)|^2 \frac{S_p(n)}{\bar{P}^2}\, dn$$

The second moment of the pressure spectra is written as

$$\frac{\{\sigma_r'(P)\}^2}{\bar{P}^2} = \int_0^\infty n^2\, |\chi_r(n)|^2\, |J_r(n)|^2 \frac{S_p(n)}{\bar{P}^2}\, dn$$

which is required in calculating "the responce factors", ν_T.

For the beam-like strectures, the root mean square shear and bending

moment at the station x, $\sigma_Q(x)$ and $\sigma_M(x)$ can be written as

$$\sigma_Q^2(x) = \sum_{r=1}^{\infty} \sigma_r^2(P)\ q_r^2(x)$$

$$\sigma_M^2(x) = \sum_{r=1}^{\infty} \sigma_r^2(P)\ m_r^2(x)$$

where $q_r(x)$ and $m_r(x)$ are the shear force and bending moment at station x due to unit r-th mode load distribution. Similarly, the second moments of the shear and bending moment spectra are given by

$$\left\{ \sigma_Q'(x) \right\}^2 = \sum_{r=1}^{\infty} \left\{ \sigma_r'(P) \right\}^2 q_r^2(x)$$

$$\left\{ \sigma_M'(x) \right\}^2 = \sum_{r=1}^{\infty} \left\{ \sigma_r'(P) \right\}^2 m_r^2(x)$$

When the distribution of statistical quantity is given as the Gaussian type, the distribution of its maximum value, which is the main concern, is easily determined by the theory of extreme values. Applying this theory the gust factor defined as

$$g\ (\nu T)\ \sigma(y) / \overline{y}$$

where

$$g\ (\nu T) = \sqrt{2 \log \nu T} + \frac{1}{\sqrt{2 \log \nu T}}$$

is derived by A. G. Davenport, which is considered as the most significant quantity in the analysis of structural responses in fluctuating flows.

4.3 AERODYNAMIC FORCES INDUCED BY CHORDWISELY AND TRANSVERSELY FLUCTUATING WIND VELOCITY

4.3.1 Aerodynamic Forces induced by Transverse Periodic Gust Velocity

According to Th. von Karman and W. R. Sears the lift force L and the pitching moment M are expressed as

$$\left.\begin{aligned} L &= 2\pi\rho b U\, v_0\, e^{i\nu t}\, S\,(k') \\ M &= \pi\rho b^2 U\, v_0\, e^{i\nu t}\, S\,(k') \end{aligned}\right\} \qquad (4\cdot3\cdot1)$$

when a plate is subjected to transverse periodic gust velocity of the form

$$v\,(x,\,t) = v_0\, e^{i\nu\,(t-\frac{x}{U})} \qquad (4\cdot3\cdot2)$$

where U : mean velocity

ν : fluctuating circular frequency

t : time

x : coordinate parameter

ρ : air density

b : half chord length

$k' = \nu b/U$: reduced frequency

and

$$S\,(k') = \frac{J_0\,(k')\,K_1\,(ik') + iJ_1\,(k')\,K_0\,(ik')}{K_1\,(ik') + K_0\,(ik')} = \frac{1}{ik'\,(K_0\,(ik') + K_1\,(ik'))} \qquad (4\cdot3\cdot3)$$

in which J_n and K_n signify the Bessel and the modified Bessel functions of n-th degree.

Experimental justification for Karman-Sears results is investigated by A. M. Kuethe and W. R. Sears[17] and it is shown that the theoretical estimation satisfactorily accords with the experimental results.

However, N. H. Kemp[18] shows the modified form of the Sears function as

$$K\ (k'\ ,\ \lambda)$$

by introducing the fluctuating velocity profile such as

$$v\ (x\ ,\ t) = v_0\ e^{i\nu t}\ e^{-i\frac{\mu x}{U}} \qquad (\nu \neq \mu)$$

The lift force for this case is given as

$$L = 2\pi\rho b U v_0\ e^{i\nu t}\ K\ (k'\ ,\ \lambda) \qquad (4\cdot3\cdot4)$$

where $\lambda = \mu b / U$

and $$K\ (k',\ \lambda) = \left\{ J_0(\lambda) - i J_1(\lambda) \right\} C\ (k') + i\frac{k'}{\lambda}\ J_1(\lambda) \qquad (4\cdot3\cdot5)$$

$$C\ (k') = \frac{K_1\ (i k')}{K_0\ (i k') + K_1\ (i k')}$$

in which the C(k') function is the well known Theodorsen function.
So it is easily shown that

$$K\ (k'\ ,\ k') = S\ (k')$$

and

$$K\ (k'\ ,\ 0) = C\ (k') + \frac{i k'}{2}$$

which is considered as a form of extended Sears function.

4.3.2 Aerodynamic Forces induced by Chordwise Periodic Gust Velocity

The aerodynamic forces due to horizontal periodic gust when an airfoil receives angle of attack α are considered by R. Isaacs and studied in more general way by J. H. Horlock[9] on the basis of the Karman-Sears theory[6], explained briefly in 4.3.1. Let the fluctuation of horizontal gust u be given by

$$u = u_0 \left(\sin \nu t \cos k' x - \cos \nu t \sin k' x \right) = u_0 \sin \left(\nu t - k' x \right) \tag{4·3·6}$$

where $k' = \dfrac{\nu b}{U}$

Then the lift force subjected to the horizontal gust as eq.(4.3.6) is obtained by J. H. Horlock of the form

$$L_u = 2\pi\rho b U u_0 \alpha e^{i\nu t} T_0 (k') \tag{4·3·7}$$

in which

$$T_0 (k') = J_0 (k') \left\{ 1 + ReC(k') \right\} + J_1 (k') ImC(k') + i \left[J_1 (k') \left\{ 2 - ReC (k') \right\} + J_0 (k') ImC(k') \right] \tag{4·3·8}$$

and α is the constant angle of attack.

Suppose that the wind velocity fluctuates transversely and chordwisely with the phase angle β, one can write

$$u = w_0 e^{i \left(\nu t - \frac{x}{U} \right)} \cos \beta$$

$$v = w_0 e^{i \left(\nu t - \frac{x}{U} \right)} \sin \beta \tag{4·3·9}$$

so that the resultant lift is expressed as

$$L_w = 2\pi\rho b U w_0 e^{i\nu t} \alpha \{ \cos\beta T_0 (k') + \sin \beta S(k') \} \tag{4·3·10}$$

When a plate receives the fluctuating velocity transversely and chordwisely as in eq.(4.3.9), the general form of the lift forces can be given by eq.(4.3.10).

It should be noted that the pitching moment acting on a plate in this case is given by multiplying a quarter length of chord for the lift when the effect of apparent mass is neglected.

4.3.3 Generalization of the Horlock Theory

In the previous paragraph the Sears and the Horlock theories are briefly described which provide the fundamental concepts for analysis of aerodynamic responses of bridge sections under action of fluctuating wind velocity. According to J. H. Horlock there exists no aerodynamic force induced by horizontally fluctuating winds when a structure receives no angle of attack, excluding the effect of drag force. In order to investigate the effects of fluctuating wind velocity on the bridge section at certain oscillatory state it is considered necessary to find the aerodynamic forces for the case that the angle of attack varies with a certain frequency. Using the Karman-Sears theory generalization of the Horlock theory is illustrated as follows:

If a plate oscillates in certain specified manner and subjects to a periodically fluctuating wind, the effect of vertical gust may not be changed by the specified vibrations, while the effect of horizontal gust is altered since the relative angle changes from time to time.

Let the chord length be 2 and $\gamma_s(x)$, $\gamma_o(x,t)$ and $\gamma_1(x,t)$ be the bound, the quasi-steady and the induced vorticities by the veroticity in the wake $\gamma(\xi, t)$, respectively, for which x extends over the plate and ξ extends over from 1 to ∞.
Thus the lift force for a plate[6] is expressed as

$$L=\rho\int_{-1}^{1} u\gamma_s(x)\,dx+\rho U\int_{-1}^{1}\gamma_0(x,t)\,dx-\rho\frac{\partial}{\partial t}\int_{-1}^{1}\gamma_0(x,t)\,x\,dx+\rho U\int_{-1}^{\infty}\frac{\gamma(\xi)}{\sqrt{\xi^2-1}}\,d\xi \quad (4\cdot3\cdot11)$$

where U is the mean velocity and u is the fluctuating horizontal gust.

Let the relative angle of attack be α, then the transverse velocity component of a plate due to the horizontal gust u can be given as

$$\int_{-1}^{1}\frac{\gamma_0(x,t)}{2\pi(x'-x)}\,dx' = -\alpha u \quad (4\cdot3\cdot12)$$

which is the fundamental equation to determine the quasi-steady vorticity in terms of the relative angle of attack and the fluctuating wind

velocity. Once the quasi-steady vorticity is known, then eq.(4.3.11) can be expressed only by the mean and fluctuating velocities and the relative angle of attack since the bound vorticity is determined by the customary airfoil theory and the effect of vorticity in the wake is also expressed in terms of the quasi-steady vorticity.

In order to solve eq.(4.3.12) let us assume that

$$\left.\begin{aligned} \gamma_0 &= 2U\left\{A_0 \cot\frac{\theta}{2} + \sum_{n=1}^{\infty} A_n \sin n\theta\right\} \\ \alpha &= \varphi + \frac{1}{U}(\dot{\eta} + \dot{\varphi} x) \\ u &= u_0 \sin(\nu t - k' x) \\ x &= -\cos\theta \end{aligned}\right\} \qquad (4\cdot3\cdot13)$$

and substituting eq's (4.3.13)[19] into eq.(4.3.12), then it is written that

$$U(-A_0 + \sum_{n=1}^{\infty} A_n \cos n\theta)$$

$$= -u_0\left(\varphi + \frac{\dot{\eta}}{U} - \frac{\dot{\varphi}}{U}\cos\theta\right)\left\{\sin\nu t \cos(k'\cos\theta) + \cos\nu t \sin(k'\cos\theta)\right\}$$

Therefore indetermined coefficients A_n(n = 0,.....) in eq. (4.3.13) are now given as

$$U\int_0^{\pi} A_0\, d\theta = u_0\left(\varphi + \frac{\dot{\eta}}{U}\right)\left\{\sin\nu t\int_0^{\pi}\cos(k'\cos\theta)\, d\theta + \cos\nu t\int_0^{\pi}\sin(k'\cos\theta)\, d\theta\right\}$$

$$-\frac{u_0}{U}\dot{\varphi}\left\{\sin\nu t\int_0^{\pi}\cos\theta\cos(k'\cos\theta)\, d\theta + \cos\nu t\int_0^{\pi}\cos\theta\sin(k'\cos\theta)\, d\theta\right\} \qquad (4\cdot3\cdot14)$$

and

$$U\int_0^{\pi} A_n \cos^2 n\theta \, d\theta = -u_0\left(\varphi+\frac{\dot{\eta}}{U}\right)\left\{\sin \nu t \int_0^{\pi}\cos n\theta \cos\left(k'\cos\theta\right) d\theta\right.$$

$$\left. + \cos \nu t \int_0^{\pi}\cos n\theta \sin\left(k'\cos\theta\right) d\theta \right\}$$

$$+\frac{u_0}{U}\dot{\varphi}\left\{\sin \nu t \int_0^{\pi}\cos\theta \cos n\theta \cos\left(k'\cos\theta\right) d\theta\right.$$

$$\left. + \cos \nu t \int_0^{\pi}\cos\theta \cos n\theta \sin\left(k'\cos\theta\right) d\theta\right\} \qquad (4\cdot3\cdot15)$$

By use of the formulas

$$\int_0^{\pi}\cos n\theta \cos\left(k'\cos\theta\right) d\theta = \pi\cos\frac{n\pi}{2} J_n\left(k'\right)$$

$$\int_0^{\pi}\cos n\theta \sin\left(k'\cos\theta\right) d\theta = \pi\sin\frac{n\pi}{2} J_n\left(k'\right)$$

eq's (4.3.14) and eq. (4.3.15) can be rewritten as

$$A_0 = \frac{u_0}{U}\left(\varphi+\frac{\eta}{U}\right) J_0\left(k'\right)\sin \nu t - \frac{u_0}{U^2}\dot{\varphi} J_1\left(k'\right)\cos \nu t$$

$$A_n = -\frac{2u_0}{U}\left(\varphi+\frac{\dot{\eta}}{U}\right)\left\{\sin \nu t \cos\frac{n\pi}{2} J_n\left(k'\right) + \cos \nu t \sin\frac{n\pi}{2} J_n\left(k'\right)\right\}$$

$$-\frac{u_0}{U^2}\dot{\varphi}\left[\sin \nu t\left\{\cos\frac{(n+1)\pi}{2} J_{n+1}\left(k'\right) + \cos\frac{(n-1)\pi}{2} J_{n-1}\left(k'\right)\right\}\right.$$

$$\left. + \cos \nu t\left\{\sin\frac{(n+1)\pi}{2} J_{n+1}\left(k'\right) + \sin\frac{(n-1)\pi}{2} J_{n-1}\left(k'\right)\right\}\right]$$

$$(4\cdot3\cdot16)$$

so one finds that

$$T_0 = 2u_0\left(\varphi+\frac{\dot{\eta}}{U}\right)\left[\sin \nu t\, J_0\left(k'\right)\cot\frac{\theta}{2}\right.$$

$$\left. - \sum_1^{\infty}\left\{2\sin \nu t \cos\frac{n\pi}{2} J_n\left(k'\right) + 2\cos \nu t \sin\frac{n\pi}{2} J_n\left(k'\right)\right\}\sin n\theta\right]$$

$$- \frac{2u_0}{U}\dot{\varphi}\ \{\cos \nu t\, J_1\,(k')\cot\frac{\theta}{2}$$

$$- \sum_1^{\infty}\{\,2\sin \nu t\,\Big(\cos\frac{(n+1)\pi}{2}J_{n+1}\,(k') + \cos\frac{(n-1)\pi}{2}J_{n-1}\,(k')$$

$$+ 2\cos \nu t\,\Big(\sin\frac{(n+1)\pi}{2}J_{n+1}\,(k') + \sin\frac{(n-1)\pi}{2}J_{n-1}\,(k')\Big)\,\}\sin n\theta\,] \qquad (4\cdot3\cdot17)$$

In determination of the lift force in eq. (4.3.11) let us write each term as follows;

$$\begin{aligned} I_1 &= \rho\int_{-1}^{1} u\,\gamma_s(x)\,dx \\ I_2 &= \rho U\int_{-1}^{1}\gamma_0\,(x\,,\,t)\,dx \\ I_3 &= -\rho\,\frac{\partial}{\partial t}\int_{-1}^{1}\gamma_0\,(x\,,\,t)\,dx \\ I_4 &= \rho U\int_1^{\infty}\frac{\gamma(\xi)}{\sqrt{\xi^2-1}}\,d\xi \end{aligned} \qquad (4\cdot3\cdot18)$$

then we have, according to the Karman-Sears' theory,

$$I_4 = -\,I_2\frac{K_0\,(ik')}{K_0\,(ik')+K_1\,(ik')}$$

so that

$$L = I_1 + I_2 C\,(k') + I_3 \qquad (4\cdot3\cdot19)$$

where C(k') is the Theodorsen's function.

(1) The intergral I_1

Since the bound vorticity[19] is given as

$$\gamma_s(x) = \gamma_s(\theta) = 2U\varphi\frac{1+\cos\theta}{\sin\theta}$$

by the Glauert's formula, we have

$$I_1 = 2\rho U u_0 \varphi \int_0^{\pi} \{ \sin \nu t \cos (k' \cos\theta) + \cos \nu t \sin (k' \cos\theta) \} (1 + \cos\theta) \, d\theta$$

$$= 2\pi\rho U u_0 \varphi \{ \sin \nu t \, J_0(k') + \cos \nu t \, J_1(k') \} \qquad (4 \cdot 3 \cdot 20)$$

(2) The integral I_2

The integral I_2 is written by J. H. Horlock as

$$I_2 = 2\pi\rho U^2 \left(A_0 + \frac{A_1}{2} \right)$$

so by use of eq's (4.3.16) for n = 0 and 1 we have

$$I_2 = 2\pi\rho U u_0 \left(\varphi + \frac{\dot{\eta}}{U} \right) \{ J_0(k') \sin \nu t - J_1(k') \cos \nu t \}$$

$$- 2\pi\rho u_0 \dot{\varphi} \left\{ -\frac{1}{2} \left(J_0(k') - J_2(k') \right) \sin \nu t + J_1(k') \cos \nu t \right\} \qquad (4 \cdot 3 \cdot 21)$$

(3) The integral I_3

Similarily we have

$$I_3 = 2\rho U \frac{\partial}{\partial t} \left\{ \frac{\pi}{2} \left(A_0 + \frac{A_2}{2} \right) \right\}$$

$$= 2\pi\rho U u_0 \left[\left\{ \left(\varphi + \frac{\dot{\eta}}{U} \right) J_1(k') - \frac{\ddot{\varphi}}{U^2} \frac{J_2(k')}{k'} \right\} \cos \nu t \right.$$

$$\left. + \left\{ \frac{\dot{\varphi}}{U} J_2(k') - \left(\frac{\dot{\varphi}}{U} - \frac{\ddot{\eta}}{U^2} \right) \frac{J_1(k')}{k'} \right\} \sin \nu t \right] \qquad (4 \cdot 3 \cdot 22)$$

Therefore the substitution of eq's (4.3.20), (4.3.21) and (4.3.22) into eq. (4.3.19) yields to

$$L = 2\pi\rho U u_0 \varphi \left\{ \sin \nu t \, J_0(k') + \cos \nu t \, J_1(k') \right\}$$

$$+ 2\pi\rho U u_0 \left(\varphi + \frac{\dot{\eta}}{U} \right) \left\{ \sin \nu t \, J_0(k') - \cos \nu t \, J_1(k') \right\} C(k')$$

$$+ 2\pi\rho u_0 \dot{\varphi} \left\{ \sin \nu t \, \frac{J_0(k') - J_2(k')}{2} + \cos \nu t \, J_1(k') \right\} C(k')$$

$$+ 2\pi\rho U u_0 \left[\left\{ \left(\varphi + \frac{\dot{\eta}}{U} \right) J_1(k') - \frac{\ddot{\varphi}}{U^2} \frac{J_2(k')}{k'} \right\} \cos \nu t \right.$$

$$\left. + \left\{ \frac{\dot{\varphi}}{U} J_2(k') - \left(\frac{\dot{\varphi}}{U} - \frac{\ddot{\eta}}{U^2} \right) \frac{J_1(k')}{k'} \right\} \sin \nu t \right]$$

$$= 2\pi\rho U u_0 \left[\varphi \left\{ \sin \nu t \, J_0(k') \left(1 + C(k') \right) + \cos \nu t \, J_1(k') \left(2 - C(k') \right) \right\} \right.$$

$$+ \frac{\dot{\eta}}{U} \left\{ \sin \nu t \, J_0(k') \, C(k') + \cos \nu t \, J_1(k') \left(1 - C(k') \right) \right\}$$

$$+ \frac{\dot{\varphi}}{U} \left\{ \sin \nu t \, \frac{J_0(k') - J_2(k')}{2} \left(1 - C(k') \right) + \cos \nu t \, J_1(k') \, C(k') \right\}$$

$$- \frac{\ddot{\varphi}}{U^2} \left\{ \frac{J_2(k')}{k'} \right\} \cos \nu t$$

$$\left. + \frac{\ddot{\eta}}{U^2} \left\{ \frac{J_1(k')}{k'} \right\} \sin \nu t \right] \qquad (4 \cdot 3 \cdot 23)$$

Alternatively, when the horizontal gust velocity is given in complex form

$$u = u_0 \, e^{i\nu\left(t - \frac{x}{U}\right)} \qquad (4 \cdot 3 \cdot 24)$$

which imaginary part is equal to eq. (4.3.6), then eq. (4.3.23) can be written as

$$L = 2\pi\rho U u_0 \, e^{i\nu t} \left[T_0(k') \varphi + T_1(k') \frac{\dot{\eta}}{U} + T_2(k') \frac{\dot{\varphi}}{U} + T_3(k') \frac{\ddot{\varphi}}{U^2} + T_4(k') \frac{\ddot{\eta}}{U^2} \right]$$

$$(4 \cdot 3 \cdot 25)$$

where

$$T_0(k')=J_0(k')\{1+C(k')\}+iJ_1(k')\{2-C(k')\}$$

$$T_1(k')=J_0(k')C(k')+iJ_1(k')\{1-C(k')\}=S(k')$$

$$T_2(k')=\frac{1}{2}\{J_0(k')-J_2(k')\}\{1-C(k')\}+iJ_1(k')C(k') \qquad (4\cdot3\cdot26)$$

$$T_3(k')=-i\frac{J_2(k')}{k'}=-i\frac{J_1(k')+J_3(k')}{4}$$

$$T_4(k')=\frac{J_1(k')}{k'}=\frac{1}{2}\{J_0(k')+J_2(k')\}$$

Note that the function $T_0(k')$ defined in eq. (4.3.26) is exactly same function of eq. (4.3.8) and furthermore in eq. (4.3.25) half length of chord being taken as the unit length, we have for the chord equal to 2b the following lift expression,

$$L=2\pi\rho bU u_0 e^{i\nu t}\left[T_0(k')\varphi+T_1(k')\frac{\tilde{\eta}}{U}+T_2(k')\frac{b\dot{\varphi}}{U}+T_3(k')\frac{b^2\ddot{\varphi}}{U^2}+T_4(k')\frac{b\ddot{\eta}}{U^2}\right] \qquad (4\cdot3\cdot27)$$

The vector diagrams for the functions defined in eq. (4.3.26) are shown in Fig's 4.3 ~ 4.8

As for the functions to characterize the aerodynamic magnification factors, it should be noted that the functions of $T_0(k')$, $T_2(k')$ and $T_3(k')$ signify the frequency dependence of lift with respect to torsional deformation and those of $T_1(k')$ and $T_4(k')$ that with respect to flexural deformation, where $T_1(k')$ is identical with the Sears' function of eq. (4.3.3).

4.3.4 Aerodynamic forces induced by a few patterns of transverse periodic gust velocity

Case 1 Rectangular Transverse Gust

Given a rectangular transverse gust velocity as shown in Fig. 4.9, the gust pattern is expressed by Fourier Cosine series as

$$f(x)=\sum_{m=1}^{\infty}\frac{4}{\pi(2m-1)}(-1)^{m+1}\cos\frac{(2m-1)\pi}{2b}x$$

Thus a complex form of periodic transverse gust velocity of rectangular shape can be written as

$$v(x,t)=\sum_{m=1}^{\infty}v_0\frac{4(-1)^{m+1}}{\pi(2m-1)}e^{i\left(\nu t-\frac{(2m-1)\pi}{2b}x\right)} \qquad (4\cdot3\cdot28)$$

where v_0 : amplitude of the gust velocity

ν : circular frequency of fluctuating gust

t : time

x : coordinate distance

b : quarter wave length

By use of eq. (4.3.4) one obtains the lift force and the pitching moment for a plate of chord length 2b in the mean velocity U as follows,

$$\left.\begin{aligned}L&=2\pi\rho bUv_0e^{i\nu t}\sum_{m=1}^{\infty}\frac{4(-1)^{m+1}}{\pi(2m-1)}K_L(k',\lambda_m)\\M&=2\pi\rho b^2Uv_0e^{i\nu t}\sum_{m=1}^{\infty}\frac{4(-1)^{m+1}}{\pi(2m-1)}K_M(k',\lambda_m)\end{aligned}\right\} \qquad (4\cdot3\cdot29)$$

where

$$\lambda_m=\frac{(2m-1)\pi}{2},\quad k'=\frac{\nu b}{U}$$

and

$$\left.\begin{aligned}K_L(k',\lambda_m)&=\{J_0(\lambda_m)-iJ_1(\lambda_m)\}C(k')+i\frac{k'}{\lambda_m}J_1(\lambda_m)\\K_M(k',\lambda_m)&=\{J_0(\lambda_m)-iJ_1(\lambda_m)\}C(k')\end{aligned}\right\} \qquad (4\cdot3\cdot30)$$

Note that the apparent mass does not contribute to the pitching moment for this case. When the wave length of rectangular transverse gust is infinite λm tends to vanish so that we have, from eq. (4.3.30),

$$K_L\ (k',\ o) = C(k') + \frac{ik'}{2}\ , \qquad K_M = C(k')$$

and

$$\sum_{m=1}^{\infty} \frac{4}{\pi} \frac{(-1)^{m+1}}{(2m-1)} = 1$$

so that lift force and the pitching moment are reduced to

$$L = 2\pi\rho bU v_0\, e^{i\nu t} \left\{ C(k') + \frac{ik'}{2} \right\}$$

$$M = \pi\rho b^2 U v_0\, e^{i\nu t}\ C(k')$$

In other words, the infinite wave length actually corresponds to the aerodynamic forces due to translatory oscillation of structures and the above expressions yield exactly to Karman-Sears results.[6),7)]

Case 2 Triangular Transverse Gust

For triangular transverse gust the corresponding expression for eq. (4.3.28) is now given as

$$v(x,\ t) = \sum_{m=1,3,5}^{\infty} -\frac{4v_0}{m^2\pi^2} \sin\frac{m\pi x}{2b} \sin\nu t \sin\frac{m\pi}{2}$$

An alternative form is written for the above expression as

$$v(x,\ t) = \sum_{m=1,2,3}^{\infty} \frac{4v_0}{(2m-1)^2\pi^2}(-1)^{m+1} e^{i\left(\nu t - \frac{2m-1}{2b}x\right)}$$

An attention should be placed on evaluation of aerodynamic forces for such transverse gust as this case. By the Karman-Sears theory[6] the pitching moment is induced by the wake if one ignores the apparent mass effect, while the lift consists of those due to both the wake effect and the quasi-steady effect. Therefore the lift force and the pitching moment are now written as

$$\left.\begin{aligned} L &= 2\pi\rho b U v_0 \, e^{i\nu t} \sum_{m=1}^{\infty} \frac{4(-1)^{m+1}}{(2m-1)^2\pi^2} K_L(k', \lambda_m) \\ M &= \pi\rho b^2 U v_0 \, e^{i\nu t} \sum_{m=1}^{\infty} \frac{4(-1)^{m+1}}{(2m-1)^2\pi^2} K_M(k', \lambda_m) \end{aligned}\right\} \qquad (4\cdot3\cdot32)$$

and

$$\lambda_m = \frac{(2m-1)}{2}\pi$$

$$K_L(k', \lambda_m) = \{ J_0(\lambda_m) - iJ_1(\lambda_m) \} C(k') + i\frac{k'}{\lambda_m} J_1(\lambda_m)$$

$$K_M(k', \lambda_m) = 1 - K_L(k', \lambda_m)$$

4.4 AERODYNAMIC RESPONSES OF STRUCTURES OF TWO-DEGREES OF FREEDOM IN TWO DIMENSIONAL FLOWS

4.4.1 Frequency Response Functions for Structures of Two Degrees of Freedom in Two Dimensional Air Flows

In order to analyse the aerodynamic responses of suspension bridge there appears a number of factors to be taken into an account, which, generally speaking, form complicate mutual interactions. Particular attention is placed on the aerodynamic responses of structures in two dimentional air flow which displace only deflectionally and torsionally in this paragraph. Restricting ourselves to the above case the fundamental equations of motions are written, according to Scanlan and Sabzevari's notations, as follows,

$$\left.\begin{aligned} &\ddot{\eta} + 2\zeta_\eta \omega_\eta \dot{\eta} + \omega_\eta^2 \eta = H_1 \dot{\eta} + H_2 \dot{\varphi} + H_3 \varphi + \frac{L}{m} \\ &\ddot{\varphi} + 2\zeta_\alpha \omega_\alpha \dot{\varphi} + \omega_\alpha^2 \varphi = A_1 \dot{\eta} + A_2 \dot{\varphi} + A_3 \varphi + \frac{M}{I} \end{aligned}\right\} \qquad (4\cdot4\cdot1)$$

where L and M are the periodic lift force and periodic pitching moment.

By usual method for determination of frequency response function the Fourier transform is applied for the system given by eq. (4.4.1)

$$\left.\begin{aligned} &\ddot{\eta} + 2\zeta_\eta \omega_\eta \dot{\eta} + \omega_\eta^2 \eta = H_1 \dot{\eta} + H_2 \dot{\varphi} + H_3 \varphi + \begin{pmatrix} \delta \\ o \end{pmatrix} \\ &\ddot{\varphi} + 2\zeta_\alpha \omega_\alpha \dot{\varphi} + \omega_\alpha^2 \varphi = A_1 \dot{\eta} + A_2 \dot{\varphi} + A_3 \varphi + \begin{pmatrix} o \\ \delta \end{pmatrix} \end{aligned}\right\} \qquad (4\cdot4\cdot1')$$

where δ signifies the Dirac's Delta Function.

Thus the frequency response function for eq. (4.4.1') can be written as

$$H(\omega) = \begin{vmatrix} H_\eta(\omega) & H_\alpha(\omega) \\ \theta_\eta(\omega) & \theta_\alpha(\omega) \end{vmatrix} \qquad (4\cdot4\cdot2)$$

where

$$H_\eta(\omega) = \frac{\omega_\alpha^2 - \omega^2 - A_3 + i\ (2\zeta_\alpha \omega_\alpha - A_2)\ \omega}{D_R + i D_I}$$

$$H_\alpha(\omega) = \frac{H_3 + i\omega H_2}{D_R + i D_I}$$

$$\theta_\eta(\omega) = \frac{i\omega A_1}{D_R + i D_I}$$

$$\theta_\alpha(\omega) = \frac{\omega_\eta^2 - \omega^2 + i(2\zeta_\eta \omega_\eta - H_1)\ \omega}{D_R + i D_I}$$

and

$$D_R = (\omega_\eta^2 - \omega^2)(\omega_\alpha^2 - \omega^2 - A_3) - \omega^2 (2\zeta_\eta \omega_\eta - H_1)(2\zeta_\alpha \omega_\alpha - A_2) + \omega^2 A_1 H_2$$

$$D_I = (\omega_\eta^2 - \omega^2)(2\zeta_\alpha \omega_\alpha - A_2)\ \omega + (\omega_\alpha^2 - \omega^2 - A_3)(2\zeta_\eta \omega_\eta - H_1)\ \omega + \omega A_1 H_3$$

in which the aerodynamic coefficients H_i, A_i $(i = 1,2,3)$ are assumed real functions of reduced frequency $b\omega/U$.

For example the aerodynamic coefficients for a plate are given as

$$H_1 = -\frac{\pi \rho b U}{m} |C(k)| \qquad A_1 = \frac{\pi \rho b^2 U}{2I} |C(k)|$$

$$H_2 = -\frac{\pi \rho b^2 U}{m} \{1 + |C(k)|\} \qquad A_2 = -\frac{\pi \rho b^3 U}{2I} \{1 - |C(k)|\} \qquad (4\cdot4\cdot1'')$$

$$H_3 = -\frac{2\pi \rho b U^2}{m} |C(k)| \qquad A_3 = \frac{\pi \rho b^2 U^2}{I} |C(k)|$$

$$k = \frac{b\omega}{U}$$

It will be convenient to characterise the frequency response function $/H(\omega)$, given by eq. (4.4.2), in terms of the gain factor and the phase factor as follows:

$$/H(\omega) = \begin{vmatrix} |H_\eta(\omega)|\ e^{i\theta_{\eta\eta}} & |H_\alpha(\omega)|\ e^{i\theta_{\eta\alpha}} \\ |\theta_\eta(\omega)|\ e^{i\theta_{\alpha\eta}} & |\theta_\alpha(\omega)|\ e^{i\theta_{\alpha\alpha}} \end{vmatrix} \qquad (4\cdot4\cdot3)$$

so that

$$\left.\begin{aligned}\text{Gain Factor} &= \begin{vmatrix} |H_\eta(\omega)| & |H_\alpha(\omega)| \\ |\theta_\eta(\omega)| & |\theta_\alpha(\omega)| \end{vmatrix} \\ \text{Phase Factor} &= \begin{vmatrix} \theta_{\eta\eta} & \theta_{\eta\alpha} \\ \theta_{\alpha\eta} & \theta_{\alpha\alpha} \end{vmatrix}\end{aligned}\right\} \qquad (4\cdot4\cdot4)$$

for which

$$|H_\eta(\omega)| = \left[\left\{(\omega_\alpha^2-\omega^2-A_3)D_R+(2\zeta_\alpha\omega_\alpha-A_2)\omega D_I\right\}^2+\left\{\omega(2\zeta_\alpha\omega_\alpha-A_2)D_R-(\omega_\alpha^2-\omega^2-A_3)D_I\right\}^2/(D_R^2+D_I^2)^2\right]^{\frac{1}{2}}$$

$$|H_\alpha(\omega)| = \left\{(H_3D_R+\omega H_2D_I)^2+(H_3D_I-\omega H_2D_R)^2/(D_R^2+D_I^2)^2\right\}^{\frac{1}{2}}$$

$$|\theta_\eta(\omega)| = \omega A_1 \,/\, (D_R^2+D_I^2)^{\frac{1}{2}}$$

$$|\theta_\alpha(\omega)| = \left[\left\{(\omega_\eta^2-\omega^2)D_R+(2\zeta_\eta\omega_\eta-H_1)\omega D_I\right\}^2+\left\{\omega(2\zeta_\eta\omega_\eta-H_1)D_R-(\omega_\eta^2-\omega^2)D_I\right\}^2/(D_R^2+D_I^2)^2\right]^{\frac{1}{2}}$$

$$\tan\theta_{\eta\eta} = \frac{(2\zeta_\alpha\omega_\alpha-A_2)\omega D_R-(\omega_\alpha^2-\omega^2-A_3)D_I}{(\omega_\alpha^2-\omega^2-A_3)D_R+(2\zeta_\alpha\omega_\alpha-A_2)\omega D_I}$$

$$\tan\theta_{\eta\alpha} = \frac{H_3D_I-\omega H_2D_R}{H_3D_R+\omega H_2D_I} \qquad \tan\theta_{\alpha\eta} = -\frac{D_R}{D_I}$$

$$\tan\theta_{\alpha\alpha} = \frac{\omega(2\zeta_\eta\omega_\eta-H_1)D_R-(\omega_\eta^2-\omega^2)D_I}{(\omega_\eta^2-\omega^2)D_R+(2\zeta_\eta\omega_\eta-H_1)\omega D_I} \qquad (4\cdot4\cdot5)$$

Using the frequency functions the aerodynamic responses are obtained as in the following sections.

4.4.2 Aerodynamic responses due to periodic Transverse gust

Case 1 Sinusoidal Transverse Gust

When a structure subjects to the sinusoidal transverse gust the aerodynamic forces are given by eq.(4.3.1) and the fundamental equations yield to

$$\ddot{\eta}+2\zeta_\eta\omega_\eta\dot{\eta}+\omega_\eta^2\eta=H_1\dot{\eta}+H_2\phi+H_3\varphi-\frac{2\pi\rho b}{m}\,U v_0\,e^{i\nu t}\,S(k')$$

$$\ddot{\varphi}+2\zeta_\alpha\omega_\alpha\dot{\varphi}+\omega_\alpha^2\varphi=A_1\dot{\eta}+A_2\dot{\varphi}+A_3\varphi+\frac{\pi\rho b^2}{I}\,U v_0\,e^{i\nu t}\,S(k')$$

where k' = νb/U and U is the mean velocity, while m and I indicate the mass and the inertia moment of unit length. Let $Ye^{i\nu t}$ and $\Psi e^{i\nu t}$ be the responses for the above equations, one obtains that

$$\left\{\omega_\eta^2-\nu^2+i\nu\,(2\zeta_\eta\omega_\eta-H_1)\right\}Y-(H_3+i\nu H_2)\,\Psi=-\frac{2\pi\rho b}{m}\,U v_0\,S(k')$$

$$-A_1\nu Y+\left\{\omega_\alpha^2-\nu^2-A_3+i\nu\,(2\zeta_\alpha\omega_\alpha-A_2)\right\}\Psi=\frac{\pi\rho b^2}{I}\,U v_0\,S(k')$$

$$\begin{Bmatrix}Y\\ \Psi\end{Bmatrix}=\begin{bmatrix}\omega_\eta^2-\nu^2+i\nu\,(2\zeta_\eta\omega_\eta-H_1) & -(H_3+i\nu H_2)\\ -A_1\nu & \omega_\alpha^2-\nu^2-A_3+i\nu\,(2\zeta_\alpha\omega_\alpha-A_2)\end{bmatrix}^{-1}\begin{Bmatrix}-\frac{2\pi\rho b}{m}\,U v_0\,S(k')\\ \frac{\pi\rho b^2}{I}\,U v_0\,S(k')\end{Bmatrix}$$

namely

$$\left.\begin{aligned}Y&=-\frac{2\pi\rho b}{m}U v_0\,S(k')\,H_\eta(\nu)+\frac{\pi\rho b^2}{I}U v_0\,S(k')\,H_\alpha(\nu)\\ \Psi&=-\frac{2\pi\rho b}{m}U v_0\,S(k')\,\Theta_\eta(\nu)+\frac{\pi\rho b^2}{I}U v_0\,S(k')\,\Theta_\alpha(\nu)\end{aligned}\right\}\qquad(4\cdot4\cdot6)$$

and

$$
\left.
\begin{aligned}
Y^2 = \{ &\left(\frac{2\pi\rho b}{m}\right)^2 |H_\eta(\nu)|^2 - 2\left(\frac{2\pi\rho b}{m}\right)\left(\frac{\pi\rho b^2}{I}\right)|H_\eta(\nu)|\cdot|H_\alpha(\nu)|\cos(\theta_{\eta\eta}-\theta_{\eta\alpha}) \\
&+\left(\frac{\pi\rho b^2}{I}\right)^2 |H_\alpha(\nu)|^2 \} U^2 v_0^2 S^2(k') \\
\Psi^2 = \{ &\left(\frac{2\pi\rho b}{m}\right)^2 |\Theta_\eta(\nu)|^2 - 2\left(\frac{2\pi\rho b}{m}\right)\left(\frac{\pi\rho b^2}{I}\right)|\Theta_\eta(\nu)|\cdot|\Theta_\alpha(\nu)|\cos(\theta_{\alpha\eta}-\theta_{\alpha\alpha}) \\
&+\left(\frac{\pi\rho b^2}{I}\right)^2 |\Theta_\alpha(\nu)|^2 \} U^2 v_0^2 S^2(k')
\end{aligned}
\right\} \quad (4\cdot4\cdot7)
$$

in which $S^2(k')$ is the squared absolute value of the Sear's function, eq. (4.3.3). It should be noted that responses due to transverse gust velocity are characterized for the system considered here by the following functions.

$$
\widetilde{Y}^2(\nu) = \left(\frac{2\pi\rho b}{m}\right)^2 |H_\eta(\nu)|^2 - 2\left(\frac{2\pi\rho b}{m}\right)\left(\frac{\pi\rho b^2}{I}\right)|H_\eta(\nu)|\cdot|H_\alpha(\nu)|\cos(\theta_{\eta\eta}-\theta_{\eta\alpha}) + \left(\frac{\pi\rho b^2}{I}\right)^2 |H_\alpha(\nu)|^2
$$

$$
\widetilde{\Psi}^2(\nu) = \left(\frac{2\pi\rho b}{m}\right)^2 |\Theta_\eta(\nu)|^2 - 2\left(\frac{2\pi\rho b}{m}\right)\left(\frac{\pi\rho b^2}{I}\right)|\Theta_\eta(\nu)|\cdot|\Theta_\alpha(\nu)|\cos(\theta_{\alpha\eta}-\theta_{\alpha\alpha}) + \left(\frac{\pi\rho b^2}{I}\right)^2 |\Theta_\alpha(\nu)|^2
$$

Case 2 Rectangular Transverse Gust

In this case the lift force and the pitching moment are given by eq. (4.3.29) as follows

$$
L = 2\pi\rho b U v_0 e^{i\nu t} \sum_{m=1}^{\infty} \frac{4(-1)^{m+1}}{\pi(2m-1)} K_L(k', \lambda_m)
$$

$$
M = \pi\rho b^2 U v_0 e^{i\nu t} \sum_{m=1}^{\infty} \frac{4(-1)^{m+1}}{\pi(2m-1)} K_M(k', \lambda_m)
$$

where

$$
K_L(k', \lambda_m) = \{ J_0(\lambda_m) - i J_1(\lambda_m) \} C(k') + i\frac{k'}{\lambda_m} J_1(\lambda_m)
$$

$$
K_M(k', \lambda_m) = \{ J_0(\lambda_m) - i J_1(\lambda_m) \} C(k')
$$

and $\lambda_m = \dfrac{(2m-1)}{2}\pi \quad , \quad k' = \nu b / U$

Therefore the responses can be expressed by aid of eq. (4.4.8) as

$$Y^2 = \widetilde{Y}^2(\nu)\left[\left\{\sum_{m=1}^{\infty}\frac{4(-1)^{m+1}}{\pi(2m-1)}K_{LR}(k',\lambda_m)\right\}^2+\left\{\sum_{m=1}^{\infty}\frac{4(-1)^{m+1}}{\pi(2m-1)}K_{LI}(k',\lambda_m)\right\}^2\right]U^2 v_0^2$$

$$\widetilde{\Psi}^2 = \widetilde{\Psi}^2(\nu)\left[\left\{\sum_{m=1}^{\infty}\frac{4(-1)^{m+1}}{\pi(2m-1)}K_{MR}(k',\lambda_m)\right\}^2+\left\{\sum_{m=1}^{\infty}\frac{4(-1)^{m+1}}{\pi(2m-1)}K_{MI}(k',\lambda_m)\right\}^2\right]U^2 v_0^2 \qquad (4\cdot4\cdot9)$$

in which

$$K_{LR} = Re\,K_L \quad , \quad K_{LI} = Im\,K_L$$

$$K_{MR} = Re\,K_M \quad , \quad K_{MI} = Im\,K_M \qquad (4\cdot4\cdot10)$$

Case 3 Triangular Transverse Gust

In the exactly same manner as Case 2 we have responses of structures subjected to the triangular transverse gust, expressed by eq. (4.3.31), as follows,

$$Y^2 = \widetilde{Y}^2(\nu)\left[\left\{\sum_{m=1}^{\infty}\frac{4(-1)^{m+1}}{\pi^2(2m-1)^2}K_{LR}(k',\lambda_m)\right\}^2+\left\{\sum_{m=1}^{\infty}\frac{4(-1)^{m+1}}{\pi^2(2m-1)^2}K_{LI}(k',\lambda_m)\right\}^2\right]U^2 v_0^2$$

$$\Psi^2 = \widetilde{\Psi}^2(\nu)\left[\left\{\sum_{m=1}^{\infty}\frac{4(-1)^{m+1}}{\pi^2(2m-1)^2}K_{MR}(k',\lambda_m)\right\}^2+\left\{\sum_{m=1}^{\infty}\frac{4(-1)^{m+1}}{\pi^2(2m-1)^2}K_{MI}(k',\lambda_m)\right\}^2\right]U^2 v_0^2$$

for which (4·4·11)

$$K_{LR}(k',\lambda_m) = J_1(\lambda_m)F(k') - J_0(\lambda_m)G(k') - \frac{k'}{\lambda_m}J_1(\lambda_m)$$

$$K_{LI}(k',\lambda_m) = J_0(\lambda_m)F(k') + J_1(\lambda_m)G(k')$$

$$K_{MR}(k',\lambda_m) = 1 - K_{LR}$$

$$K_{MI}(k',\lambda_m) = -K_{LI}$$

$$C(k') = F(k') + iG(k')$$

4.4.3 Aerodynamic responses due to periodic chordwise gust

For periodic chordwise gust no aerodynamic force is induced unless the relative angle of attack is taken into an account (refer to 4.3.2). In this paragraph a few typical cases are illustrated according to a variaty of the angle of attack, considering only sinusoidal horizontal gust.

Case 1 Constant angle of attack,

Suppose that a structure receives the constant angle of attack α the induced lift force and pitching moment are given by J. H. Horlock as expressed by eq. (4.3.7),

$$L = 2\pi\rho b U v_0 \alpha e^{i\nu t} T_0(k')$$

$$M = \pi\rho b^2 U v_0 \alpha e^{i\nu t} T_0(k') \qquad (4\cdot4\cdot12)$$

Substituting them into eq. (4.4.1) the responses are easily found as

$$Y^2 = \widetilde{Y}^2 T_0^2(k') U^2 u_0^2 \alpha^2$$

$$\Psi^2 = \widetilde{\Psi}^2 T_0^2(k') U^2 u_0^2 \alpha^2 \qquad (4\cdot4\cdot13)$$

in which

$$T_0^2(k') = \left[J_0(k')\left\{2 - Re\frac{K_0(ik')}{K_0(ik')+K_1(ik')}\right\} - J_1(k') I_m\left(\frac{K_0}{K_0+K_1}\right)\right]^2$$

$$+ \left[J_1(k')\left\{1 + Re\frac{K_0}{K_0+K_1}\right\} - J_0(k') I_m\frac{K_0}{K_0+K_1}\right]^2$$

Case 2 When structure oscillates periodically with the frequency ω_0 deflectionally or torsionally

When structures oscillates periodically in such way as

$$\eta = \eta_0 e^{i\omega_0 t}$$

and also subjects to the horizontal periodic gust

$$u = u_0 e^{i\nu\left(t-\frac{x}{U}\right)}$$

the induced lift force and pitching moment are given by eq. (4.3.27) as

$$L = 2\pi\rho U u_0 \left[i T_1(k') \frac{b\omega_0}{U} - T_4(k') \left(\frac{b\omega_0}{U}\right)^2 \right] \eta_0 e^{i(\omega_0+\nu)t}$$

$$M = \pi\rho b U u_0 \left[i T_1(k') \left(\frac{b\omega_0}{U}\right) - T_4(k') \left(\frac{b\omega_0}{U}\right)^2 \right] \eta_0 e^{i(\omega_0+\nu)t}$$

Let $T_\eta(k', k_0)$ be

$$T_\eta(k', k_0) = T_\eta^R + i T_\eta^R = i T_1(k') k_0 - T_4(k') k_0^2 \qquad (4\cdot4\cdot14)$$

where

$$k_0 = \frac{b\omega_0}{U}, \qquad k' = \frac{\nu b}{U}$$

$$T_1(k') = J_0(k') C(k') + i J_1(k') \left\{1 - C(k')\right\}$$

$$T_4(k') = \frac{1}{2}\left\{J_0(k') + J_2(k')\right\}$$

then responses corresponding to eq's (4.4.1) can be obtained as

$$\left.\begin{aligned} Y^2 &= \widetilde{Y}^2(\omega_0+\nu)\, U^2 u_0 \left| T_\eta(k', k_0) \right|^2 \left(\frac{\eta_0}{b}\right)^2 \\ \Psi^2 &= \widetilde{\Psi}^2(\omega_0+\nu)\, U^2 u_0 \left| T_\eta(k', k_0) \right|^2 \left(\frac{\eta_0}{b}\right)^2 \end{aligned}\right\} \qquad (4\cdot4\cdot15)$$

It should be mentioned that the effect of phase differences between the horizontal gust and the oscillatory displacement is ignored here.

Alternatively the responses due to horizontal gust when structure vibrates torsionally in such way as

$$\varphi = \varphi_0 e^{i\omega_0 t}$$

are obtained as following. By eq. (4.3.27) the aerodynamic forces are

$$L = 2\pi\rho b U u_0 e^{i(\omega_0+\nu)t} \left[T_0(k') + i k_0 T_2(k') - k_0^2 T_3(k') \right] \varphi_0$$

$$\overset{def}{=} 2\pi\rho b U u_0 e^{i(\omega_0+\nu)t} T_\varphi(k', k_0)\varphi_0$$

$$M = \pi\rho b^2 U u_0 e^{i(\omega_0+\nu)t} T_\varphi(k', k_0)\varphi_0$$

so we have

$$\left.\begin{aligned} Y^2 &= \widetilde{Y^2}(\omega_0+\nu) U^2 u_0^2 \left| T_\varphi(k', k_0) \right|^2 \varphi_0^2 \\ \Psi^2 &= \widetilde{\Psi^2}(\omega_0+\nu) U^2 u_0^2 \left| T_\varphi(k', k_0) \right|^2 \varphi_0^2 \end{aligned}\right\} \qquad (4\cdot4\cdot16)$$

where

$$T_\varphi(k', k_0) = T_0(k') + i k_0 T_2(k') - k_0^2 T_3(k')$$

$$T_0(k') = J_0(k')\left\{1 + C(k')\right\} + i J_1(k')\left\{2 - C(k')\right\} \qquad (4\cdot4\cdot17)$$

$$T_2(k') = \frac{1}{2}\left\{J_0(k') - J_2(k')\right\}\left\{1 - C(k')\right\} - i J_1(k') C(k')$$

$$T_3(k') = -\frac{i}{4}\left\{J_1(k') + J_3(k')\right\}$$

It is interesting to note that there is a significant difference about the response characteristics between the horizontal and the vertical gusts; that is, the frequency response functions depend on the sum of the specified frequency ω_0 and the gust frequency ν for the former case, while the frequency response functions merely vary with the gust frequency ν for the latter case. The fact seems an important character to consider the effect of fluctuating wind velocity on the aerodynamic

stability which will be considered in 4.5.

Case 3 When structure subjects to flexure-torsion flutter

The flexure-torsion flutter of a structure in air stream is considered as one of the most important aerodynamic problems particularly for long spanned suspension bridges. Suppose that one is restricted to two dimensional analysis, then the deflectional and torsional deformations can be written as

$$\eta = \eta_0 e^{i\omega_0 t} \qquad \varphi = \varphi_0 e^{i(\omega_0 t - \phi_0)} \tag{4.4.18}$$

where η_0, ϕ_0 are the deflectional and the torsional amplitudes and ω_0, ψ_0 are the flutter frequency and phase difference, respectively.

Substituting eq. (4.4.18) into eq. (4.3.7) the lift force is expressed as

$$L = 2\pi\rho b U u_0 \left[T_\varphi(k', k_0)\, \varphi_0 e^{-i\phi_0} + T_\eta(k', k_0) \frac{\eta_0}{b} \right] e^{i(\omega_0 + \nu)t} \tag{4.4.19}$$

when the horizontal gust is given by

$$u = u_0 e^{i\nu\left(t - \frac{x}{U}\right)}$$

Thus the responses due to fluctuating horizontal gust are obtained similarily as

$$\left.\begin{aligned} Y^2 = \widetilde{Y}^2(\omega_0+\nu) U^2 u_0^2 \Big[& |T_\varphi(k', k_0)|^2 \varphi_0^2 + 2|T_\varphi(k', k_0)|\,|T_\eta(k', k_0)| \cos\psi_0 \cdot \varphi_0 \cdot \left(\frac{\eta_0}{b}\right) \\ & + |T_\eta(k', k_0)|^2 \left(\frac{\eta_0}{b}\right)^2 \Big] \\ \Psi^2 = \widetilde{\Psi}^2(\omega_0+\nu) U^2 u_0^2 \Big[& |T_\varphi(k', k_0)|^2 \varphi_0^2 + 2|T_\varphi(k', k_0)|\,|T_\eta(k', k_0)| \cos\psi_0 \cdot \varphi_0 \cdot \left(\frac{\eta_0}{b}\right) \\ & + |T_\eta(k', k_0)|^2 \left(\frac{\eta_0}{b}\right)^2 \Big] \end{aligned}\right\} \tag{4.4.20}$$

As considered in the previous chapter, the phase difference ψ_o between the deflectional and torsional deformations in the flutter state of plate or plate-like structures tends to vanish when the frequency ratio of torsional and deflectional frequencies becomes large. So in eq. (4.4.20) $\cos \psi_o$ can be replaced by unity for most types of actual suspension bridges.

4.4.4 Aerodynamic responses due to periodic transverse and chordwise gusts

When horizontal and vertical components of fluctuating gusts are given as

$$u = w\cos\beta \qquad v = w\sin\beta \tag{4·4·21}$$

where β indicates the phase angle between u and v, then one obtains

$$L = -2\pi\rho b U w_0 e^{i\nu t}\left[\left\{T_\eta(k', k_0)\frac{\eta_0}{b} + T_\varphi(k', k_0)\varphi_0 e^{-i\phi_0}\right\} e^{i\omega_0 t}\cos\beta + S(k')\sin\beta\right] \tag{4·4·22}$$

for which $w = w_0 e^{i\nu t}$ and η_0, ϕ_0 are the responsive amplitudes in deflectional and torsional modes of specified vibrations and ψ_0, ω_0 ($k_0 = \omega_0 b/U$) correspond to the phase angle and the frequency specified. The expression for the pitching moment can be obtained by multiplying quarter length of chord for the lift, eq. (4.4.22). From eq. (4.4.6) and eq. (4.4.15) the responses subjected to the fluctuating gust given by eq. (4.4.21) are also written as

$$\left.\begin{aligned}
\eta &= \left\{-\frac{2\pi\rho b}{m}H_\eta(\nu) + \frac{\pi\rho b^2}{I}H_\alpha(\nu)\right\}\left(S(k')\sin\beta\right) U w_0 e^{i\nu t} \\
&+ \left\{-\frac{2\pi\rho b}{m}H_\eta(\omega_0+\nu) + \frac{\pi\rho b^2}{I}H_\alpha(\omega_0+\nu)\right\}\left(T_\eta\frac{\eta_0}{b} + T_\varphi\varphi_0 e^{-i\phi_0}\right) U w_0 e^{i(\omega_0+\nu)t} \\
\text{and} \\
\varphi &= \left\{-\frac{2\pi\rho b}{m}\Theta_\eta(\nu) + \frac{\pi\rho b^2}{I}\Theta_\alpha(\nu)\right\}\left(S(k')\sin\beta\right) U w_0 e^{i\nu t} \\
&+ \left\{-\frac{2\pi\rho b}{m}\Theta_\eta(\omega_0+\nu) + \frac{\pi\rho b^2}{I}\Theta_\alpha(\omega_0+\nu)\right\}\left(T_\eta\frac{\eta_0}{b} + T_\varphi\varphi_0 e^{-i\phi_0}\right) U w_0 e^{i(\omega_0+\nu)t}
\end{aligned}\right\} \tag{4·4·23}$$

For the case that a structure receives only constant angle of attack eq. (4.4.23) are greatly simplified as

$$\left.\begin{aligned}\eta &= \left\{-\frac{2\pi\rho b}{m} H_\eta(\nu) + \frac{\pi\rho b^2}{I} H_\alpha(\nu)\right\} \left\{S(k')\sin\beta + \varphi_0 T_0(k')\cos\beta\right\} U w_0 e^{i\nu t} \\ \varphi &= \left\{-\frac{2\pi\rho b}{m} \theta_\eta(\nu) + \frac{\pi\rho b^2}{I} \theta_\alpha(\nu)\right\} \left\{S(k')\sin\beta + \varphi_0 T_0(k')\cos\beta\right\} U w_0 e^{i\nu t}\end{aligned}\right\} \quad (4\cdot4\cdot24)$$

where S(k') and $T_0(k')$ are the functions defined by W. Sears and J. H. Horlock, respectively. Eq. (4.4.24) implies the fact that both of the frequency response functions and the aerodynamic magnification factors are uniquely determined by the frequency ν, while eq. (4.4.23) implies that the aerodynamic magnification factors are determined by the frequency ν but the frequency response functions are associated with the sum of the frequencies of ω_o and ν. It is considered that the horizontal gusts effect on the structure at the fluttering state, for example, in rather complicate way and the overall responses depend on their combination so that there is no definite amplitude of vibration and it will be a time varying and distorted form.

4.5 STABILIZING AND DESTABILIZING EFFECTS OF FLUCTUATING GUSTS

4.5.1 General Remarks

In the previous chapter the aerodynamic stability of suspension bridges are considered from a fundamental point of views, and it is known that various types of aerodynamic instability should be analyzed in order to have sufficient safety of reliability depending on the structural configurations and vibrational characteristics of the structure. Generally the aerodynamic stability is classified into two types, that is, the galloping and the flutter phenomena, the latter of which is furthermore classified into the so-called stall flutter and the flexure-torsion flutter. The galloping appears for aeroelastically unstable sections such as H-sections and near right rectangular cross sections, which is due to the non-linear characteristics of lift-coefficient curves. For the stall flutter, there appears no well-established theoretical base but it can be due to non-linear hystresis of aerodynamic forces and responses. In this investigations we restrict ourselves to the problems of linear aerodynamic responses and particular consideration is placed on the destabilizing and stabilizing effects on the structures which aerosynamic stability is concerned with flexure-torsion flutter phenomenon. However it should be naturally mentioned that the non-linear aerodynamic problems are of primary importance to be analyzed in near future.

4.5.2 Destabilizing effect due to fluctuating gust

For sake of theoretical brevity a plate possible to vibrate deflectionally and torsionally is considered in two dimensional air flow. If a plate oscillates periodically under the action of periodic forces, the fundamental equations are written as eq. (4.4.1), viz.,

$$\ddot{\eta} + 2\zeta_\eta \omega_\eta \dot{\eta} + \omega_\eta^2 \eta = H_1 \dot{\eta} + H_2 \dot{\varphi} + H_3 \varphi + \frac{L}{m}$$

$$\ddot{\varphi} + 2\zeta_\alpha \omega_\eta \dot{\varphi} + \omega_\alpha^2 \varphi = A_1 \dot{\eta} + A_2 \dot{\varphi} + A_3 \varphi + \frac{M}{I}$$

where the aerodynamic coefficients are given as eq's (4.4.1")

Suppose that L and M is periodic with frequencey ν, then the aerodynamic coefficients are functions of the mean velocity U and the reduced frequency $k' = \nu b / U$, Therefore the stability of the system at the given reduced frequency is our main concerns, which is easily examined by the Routh-Hurwitz's criteria as follows (refer to 3.8 (1));

$$B_3 = 2\zeta_\alpha \omega_\alpha + 2\zeta_\eta \omega_\eta - H_1 - A_2 > 0$$

$$B_2 = \omega_\alpha^2 - A_3 + \omega_\eta^2 + (2\zeta_\eta \omega_\eta - H_1)(2\zeta_\alpha \omega_\alpha - A_2) - A_1 H_2 > 0$$

$$B_1 = (\omega_\alpha^2 - A_3)(2\zeta_\eta \omega_\eta - H_1) + \omega_\eta^2 (2\zeta_\alpha \omega_\alpha - A_2) - A_1 H_3 > 0$$

$$B_0 = \omega_\eta^2 \ (\omega_\alpha^2 - A_3) > 0$$

$$R = B_3 B_2 B_1 - B_3^2 B_0 - B_1^2 > 0$$

It should be mentioned that the instability criteria stated here differ from that of the classical flutter theory. Without forcing aerodynamic force the fundamental equations are of the form of eq's (4.4.1), so if

$$\eta = \bar{\eta}_0 \ e^{\lambda t} \ , \quad \varphi = \bar{\varphi}_0 \ e^{\lambda t}$$

are assumed then non trivial solutions are obtained when

$$\begin{vmatrix} \lambda^2 + (2\zeta_\eta \omega_\eta - H_1)\lambda + \omega_\eta^2 & -(\lambda H_2 + H_3) \\ -A_1 \lambda & \lambda^2 + (2\zeta_\alpha \omega_\alpha - A_2)\lambda + (\omega_\alpha^2 - A_3) \end{vmatrix} = 0$$

The aerodynamic coefficients of eq's (4.4.1") are rewritten of the form of

$$H_1 = -\frac{\pi \rho b^2}{m} \frac{|C(k)|}{k} \omega \qquad A_1 = \frac{\pi \rho b^3}{I} \frac{|C(k)|}{k} \omega$$

$$H_2 = -\frac{\pi \rho b^3}{m} \frac{1+|C(k)|}{k} \omega \qquad A_2 = -\frac{\pi \rho b^4}{2I} \omega \frac{1-|C(k)|}{k}$$

$$H_3 = -\frac{2\pi \rho b^3}{m} \frac{|C(k)|}{k^2} \omega^2 \qquad A_3 = \frac{\pi \rho b^4}{I} \frac{|C(k)|}{k} \omega^2$$

One method to determine the flutter frequency and the critical reduced frequency is to fix ω at first to calculate the aerodynamic coefficients, which are numerically obtained for specified value of k. Thus, changing the value of k, the solutions are required to be sought until these satisfy the Routh condition and $\lambda = i\omega$ in the above determinant. This is one of the typical method to analyze the torsion-bending flutter state. Once the reduced frequency $k' = \nu b/U$ is uniquely determined, then substitution of k' into eq's (4.4.1") yields to aerodynamic coefficients of function of mean velocity U. Thus the Routh criteria provides the critical wind velocity beyond which the systems becomes unstable. Since the Theodorsen function indicates physically the reduction of aerodynamic forces due to the reduced frequency by taking into an account the effect of vorticity in the wake, the excitation below the flutter frequency recults in the lift reduction and consequently the critical mean velocity decreases which is, therfore, considered as the destabilizing effect due to fluctuating gust. The lowest critical velocity, or the lower bound, is now obtained by setting k' = o (which corresponds to initiation of flutter) by the following conditions.

$$B_3 = 2\zeta_\alpha\omega_\alpha + 2\zeta_\eta\omega_\eta + \frac{2\pi\rho b}{m} V \geqq 0$$

$$B_2 = \omega_\alpha^2 + \omega_\eta^2 + 4\zeta_\alpha\omega_\alpha\zeta_\eta\omega_\eta + \frac{2\pi\rho b}{m}(2\zeta_\alpha\omega_\alpha)V + \frac{\pi\rho b^2}{I}\left(\frac{2\pi\rho b^2}{m} - 1\right)V^2 \geqq 0$$

$$B_1 = \omega_\alpha^2(2\zeta_\eta\omega_\eta) + \omega_\eta^2(2\zeta_\alpha\omega_\alpha) + \frac{2\pi\rho b}{m}\omega_\alpha^2 V - \frac{\pi\rho b^2}{I}(2\zeta_\eta\omega_\eta)V^2 \geqq 0$$

$$B_0 = \omega_\eta^2\left(\omega_\alpha^2 - \frac{\pi\rho b^2}{I}V^2\right) \geqq 0$$

$$R = B_3 B_2 B_1 - B_3^2 B_0 - B_1^2 \geqq 0 \qquad (4\cdot5\cdot25)$$

It is easily known that B_3, B_2, B_1, B_0 take secondary role and the critical condition is R = 0 for usual case.

From considerations in 4.4 the possibility that the forcing excitation is below the flutter frequency occurs only by the transverse gust, so that the destabilizing effect is considered due to the vertical component of the fluctuating wind velocity. Approximate method of determine the flutter velocity in 3.8 gives the destabilized critical wind velocity of lower bound roughly as

$$(U_{\nu=0})_{cr} = U_{cr} \sqrt[3]{\frac{|C(k)|}{|C(o)|}}$$

$$= 0.826\ U_{cr} \qquad (4\cdot5\cdot26)$$

if the critical reduced frequency is taken as 0.2, which means about 20% decrease of critical wind velocity.

4.5.3 Stabilizing Effect due to Fluctuating Gust

As considered in 4.5.2 the aerodynamic stability of a structure can be defined in exactly same way for the case that the excitation frequency is higher than the flutter frequency in uniform air stream by the Routh criteria. Since the lift reduction tends to increase when the frequency becomes larger the aerodynamic frequency characteristics become smaller effect up to $|C(k)|_{k=\infty}=1/2$.

If a plate is considered, the ultimate values for aerodynamic coeffi-cients are

$$H_1 = -\frac{\pi\rho b}{m} V \qquad A_1 = \frac{\pi\rho b^2}{2I} V$$

$$H_2 = -\frac{3}{2}\frac{\pi\rho b^2}{m} V \qquad A_2 = -\frac{\pi\rho b^3}{4I} V$$

$$H_3 = -\frac{\pi\rho b}{m} V^2 \qquad A_3 = \frac{\pi\rho b^2}{2I} V^2$$

for which the critical conditions are given as

$$B_3 = 2\zeta_\alpha\omega_\alpha + 2\zeta_\eta\omega_\eta + \left(\frac{\pi\rho b}{m} + \frac{\pi\rho b^3}{4I}\right) V \geqq 0$$

$$B_2 = \omega_\eta^2 + \omega_\alpha^2 + 4\zeta_\eta\zeta_\alpha\omega_\eta\omega_\alpha + \left\{(2\zeta_\eta\omega_\eta)\left(\frac{\pi\rho b^3}{4I}\right) + (2\zeta_\alpha\omega_\alpha)\left(\frac{\pi\rho b}{m}\right)\right\} V + \frac{\pi\rho b^2}{I}\left(\frac{\pi\rho b^2}{m} - \frac{1}{2}\right) V^2 \geqq 0$$

$$B_1 = (2\zeta_\eta\omega_\eta)\omega_\alpha^2 + (2\zeta_\alpha\omega_\alpha)\omega_\eta^2 + \frac{\pi\rho b}{m}\omega_\alpha^2 V - \frac{\pi\rho b^2}{2I}(2\zeta_\eta\omega_\eta) V^2 \geqq 0$$

$$B_0 = \omega_\eta^2\left(\omega_\alpha^2 - \frac{\pi\rho b^2}{2I} V^2\right) \geqq 0$$

$$R = B_3 B_2 B_1 - B_3^2 B_0 - B_1^2 \geqq 0 \qquad (4\cdot5\cdot27)$$

An approximate method as used in the previous paragraph gives the result that, if the critical reduced frequency is taken as 0.2, the upper bound ($k = \infty$) for critical wind velocity $U_{\nu=\infty,cr}$ is approximately

$$U_{\nu=\infty} = U_{cr} \sqrt[3]{\frac{|C(k)|}{|C(\infty)|}}$$

$$= 1.32\, U_{cr} \qquad (4\cdot5\cdot28)$$

When k is small enough to be zero , then we have , approximately ,

$$U_{\nu=\infty} = U_{cr} \sqrt[3]{4} = 1.6\, U_{cr}$$

Let us consider now the stabilizing effect on torsion-bending flutter due to fluctuating wind velocity. When transversely or chordwisely flutctuating gusts act on a plate, the fundamental equations are associated with the excitated frequency. For horizontal gust the aerodynamic responses have always the higher frequenties than the flutter frequency ω_o and also there is a possibility that the transverse gust has the higher frequencies than the flutter frequency, so that it is considered to act on the safety side, namely the stabilizing effect on the torsion-bending flutter.

4.6 STATISTICAL CONSIDERATIONS OF AERODYNAMIC RESPONSES OF PLATE-LIKE STRUCTURES DUE TO TWO DIMENSIONALLY FLUCTUATING GUSTS.

4.6.1 Introduction to random vibration analysis

In generally a timely random physical quantity x(t) defined in duration T can be expressed in the form of the Fourier series as

$$x(t) = a_0 + \sum_{n=1}^{\infty} (a_n \cos n\omega_0 t + b_n \sin n\omega_0 t) \qquad (4\cdot6\cdot1)$$

where $\omega_0 = 2\pi/T$. Thus the mean squared value for x(t) is given by

$$\overline{x^2(t)} = \frac{1}{T}\int_{-T/2}^{T/2} x^2(t)\,dt = a_0^2 + \frac{1}{2}\sum_{n=1}^{\infty}(a_n^2 + b_n^2) \qquad (4\cdot6\cdot2)$$

Instead of eq. (4.6.1) one has alternatively

$$x(t) = \sum_{n=-\infty}^{\infty} C_n e^{in\omega_0 t} \qquad (4\cdot6\cdot3)$$

for which

$$\overline{x^2(t)} = \sum_{n=-\infty}^{\infty} |C_n|^2 \qquad (4\cdot6\cdot4)$$

Let the quantity be responsive for continuous spectrum and let $F(\omega)$ be the Fourier Transform of x(t), then we have

$$x(t) = \frac{1}{2\pi}\int_{-\infty}^{\infty} F(\omega)\, e^{i\omega t}\, d\omega \;, \qquad F(\omega) = \int_{-\infty}^{\infty} x(t)\, e^{-i\omega t}\, dt \qquad (4\cdot6\cdot5)$$

and

$$\int_{-\infty}^{\infty} x^2(t)\,dt = 2\int_{-\infty}^{\infty} |F(\omega)|^2\, d\omega$$

by the Parseval theorem.

As well known the power spectral density function $S(\omega)$ and the auto-correlation function $R(\tau)$ are defined as

$$\overline{x^2(t)} \overset{def}{=} 2\int_0^\infty S(\omega)\, d\omega \qquad (4\cdot6\cdot6)$$

and

$$R(\tau) = \overline{x(t)\,x(t+\tau)} \;/\; \overline{x^2(t)} \qquad (4\cdot6\cdot7)$$

for which the super bar is to take the average with respect to time. By the Winer-Khinchine's relation the power spectral density function and the autocorrelation function are mutually related as follows;

$$S(\omega) = 2\int_0^\infty R(\tau)\cos\omega\tau\, d\tau$$

$$R(\tau) = \frac{1}{\pi}\int_0^\infty S(\omega)\cos\omega\tau\, d\omega \qquad (4\cdot6\cdot8)$$

4.6.2 Spectral Analysis of Aerodynamic Responses due to Fluctuating Gusts

For the system given by eq's (4.4.1) the frequency response function is shown as eq's (4.4.3). Suppose that S_y and S_x are the power spectral density function (PSD) as

$$S_y = \begin{bmatrix} S_{\eta\eta} & S_{\eta\varphi} \\ S_{\varphi\eta} & S_{\varphi\varphi} \end{bmatrix} \qquad S_x = \begin{bmatrix} S_{LL} & S_{LM} \\ S_{ML} & S_{MM} \end{bmatrix} \tag{4·6·9}$$

then we have[20]

$$S_y = |H(\omega)| \cdot S_x \cdot |H^*(\omega)| \tag{4·6·10}$$

where $|H^*(\omega)$ is the conjugate transpose of $|H(\omega)$ and S_{LL}, S_{MM} are the power spectral density functions of lift and pitching moment and $S_{\eta\eta}$ and $S_{\phi\phi}$ are the power spectral density functions of deflectional and torsional deformations respectively. Eq (4.6.10) yields, thus, to

$$\begin{aligned} S_{\eta\eta} &= |H_\eta|^2 S_{LL} + 2|H_\eta|\cdot|H_\alpha| \cos(\theta_{\eta\eta}-\theta_{\eta\alpha}) S_{LM} + |H_\alpha|^2 S_{MM} \\ S_{\varphi\varphi} &= |\theta_\eta|^2 S_{LL} + 2|\theta_\eta|\cdot|\theta_\alpha| \cos(\theta_{\alpha\alpha}-\theta_{\alpha\eta}) S_{ML} + |\theta_\alpha|^2 S_{MM} \end{aligned} \tag{4·6·11}$$

When the transverse and horizontal gusts v and u act on a plate like structure which receives a constant angle of attack, power and cross spectral density functions for lift and pitching moment are written as following;

$$\left.\begin{aligned} S_{LL} &= \left(\frac{2\pi\rho bU}{m}\right)^2 \left\{ S^2\left(\frac{\omega b}{U}\right) S_{vv} + 2S\left(\frac{\omega b}{U}\right) T_0\left(\frac{\omega b}{U}\right) S_{uv} + T_0^2\left(\frac{\omega b}{U}\right) S_{uu} \right\} \\ S_{MM} &= \left(\frac{\pi\rho b^2 U}{I}\right)^2 \left\{ S^2\left(\frac{\omega b}{U}\right) S_{vv} + 2S\left(\frac{\omega b}{U}\right) T_0\left(\frac{\omega b}{U}\right) S_{uv} + T_0^2\left(\frac{\omega b}{U}\right) S_{uu} \right\} \\ S_{LM} &= S_{ML} = -\left(\frac{2\pi\rho bU}{m}\right)\left(\frac{\pi\rho b^2 U}{I}\right) \left\{ S^2\left(\frac{\omega b}{U}\right) S_{vv} + 2S\left(\frac{\omega b}{U}\right) T_0\left(\frac{\omega b}{U}\right) S_{uv} + T_0^2\left(\frac{\omega b}{U}\right) S_{uu} \right\} \end{aligned}\right\} \tag{4·6·12}$$

where

$$\left.\begin{aligned}\overline{u^2(t)} &= 2\int_0^\infty S_{uu}(\omega)\,d\omega \\ \overline{u(t)\,v(t)} &= 2\int_0^\infty S_{uv}(\omega)\,d\omega \\ \overline{v^2(t)} &= 2\int_0^\infty S_{vv}(\omega)\,d\omega\end{aligned}\right\} \qquad (4\cdot6\cdot13)$$

and S(ωb/U) and T(ωb/U) are the Sears and Horlock functions.

If the fluctuating winds are obtained and the spectral analysis is done, then by eq.(4.6.11), (4.6.12) and (4.6.13) the variances of responses are found as

$$\left.\begin{aligned}\sigma_{\eta\eta}^2 &= 2\int_0^\infty S_{\eta\eta}(\omega)\,d\omega \\ \sigma_{\varphi\varphi}^2 &= 2\int_0^\infty S_{\varphi\varphi}(\omega)\,d\omega\end{aligned}\right\} \qquad (4\cdot6\cdot14)$$

Applying A. G. Davenport's considerations for eq's (4.6.14) the response factor ν is obtained as

$$\left.\begin{aligned}\nu_\eta &= 2\pi\sqrt{\frac{\int_0^\infty \omega^2 S_{\eta\eta}(\omega)\,d\omega}{\int_0^\infty S_{\eta\eta}(\omega)\,d\omega}} \\ \nu_\varphi &= 2\pi\sqrt{\frac{\int_0^\infty \omega^2 S_{\varphi\varphi}(\omega)\,d\omega}{\int_0^\infty S_{\varphi\varphi}(\omega)\,d\omega}}\end{aligned}\right\} \qquad (4\cdot6\cdot15)$$

so that the gust factors[10] for duration T are rewritten as

$$\left.\begin{aligned}g_\eta(\nu T) &= \sqrt{2\log\nu_\eta T} + \frac{1}{\sqrt{2\log\nu_\eta T}} \\ g_\varphi(\nu T) &= \sqrt{2\log\nu_\varphi T} + \frac{1}{\sqrt{2\log\nu_\varphi T}}\end{aligned}\right\} \qquad (4\cdot6\cdot16)$$

When one considers only the transverse gust the expressions for power spectral density functions are so simplified in eq's (4.6.11) and (4.6.12) to

$$S_{\eta\eta} = \widetilde{Y}(\omega)\, U^2\, S\left(\frac{b\omega}{U}\right) S_{vv}$$

$$S_{\varphi\varphi} = \widetilde{\Psi}(\omega)\, U^2\, S\left(\frac{b\omega}{U}\right) S_{vv}$$

with no effect of cross-spectrum of transverse and chordwise gust by use of eq's (4.4.8).

When a structure is subjected to certain periodic oscillatory state, the T (ωb/U) in eq (4.6.12) should be replaced by the function defined in eq's (4.3.25) and (4.3.26) and the similar expressions are easily obtained. Consequently for spectral analysis of fluctuating gusts it is required to have the power spectral and cross-spectral functions for gusts, the aerodynamic admittance such as Sears function and the frequency response functions of the structure considered. It should be noticed that there is no average responses in our considerations and the aerodynamic responses, therefore, are eventually due to the fluctuating gusts to be evaluated in the form of $g_\eta\ (\nu Y)\ \sigma_{\eta\eta}$ and $g_\phi\ (\nu T)\ \sigma_{\phi\phi}$.

4.6.3 Spectral Characteristics of Gusts

As considered in 4.6.2 the aerodynamic responses are directly responsive for the spectral characteristics of gusts. There are a number of investigations about statistical and probabilistic characteristics of atmospheric turbulence. As for the horizontal gustivess A. G. Davenport proposes an expression for the spectral density[1] as

$$\frac{S_{uu}(n)}{U^2} = 2K_r \frac{x_D^2}{(1+x_D^2)^{4/3}} \qquad (4\cdot6\cdot17)$$

where $x_D = 1{,}200 \frac{n}{U}$ (1/m)

K_r = the drag coefficient for the surface (referred to the mean velocity at standard reference height, 10m)

Eq. (4.6.17) is comparatively satisfactory expression in comparison with observations of horizontal components of natural winds.

The spectrum expression for vertical gustiness is proposed by Panofsky and McCorwick[1] as

$$\frac{n\,S_W(n)}{U^2} = 3K_r \frac{f_r^2}{(1+4f_r)^2} \qquad (4\cdot6\cdot18)$$

where $f_r = nz/\overline{U}$ and $\overline{U}$ is the mean velocity at the height Z. The fundamental difference between eq. (4.6.17) and (4.6.18) is the fact that the former depends merely on the frequency and the mean velocity at reference height, while the later depends on the height Z and the corresponding mean velocity and the frequency. Only the effect of vertical gustiness being considered, the statistical analysis can be performed by use of eq. (4.6.17). When a constant angle of attack or a certain excitation on the structure exists, one is required to know the horizontal and vertical gustinesses as well as their co-spectrum as indicated in

the eq's (4.6.12)

Recently M. Shiotani[21] reports the observation results of stormy winds at Tokushima in the Shikoku Island, Japan. It indicates that the results satisfactorily coincide with the previous investigations as eq's (4.6.17) and (4.6.18) and the cross-correlation between horizontal and vertical gusts remains about -0.2 to -0.37 which coherence is, roughly, considered independent from the frequency.

An approximate method for spectral analysis is to assume that the autocorrelation function $R(\tau)$ is of the form

$$R(\tau) = e^{-\frac{\tau}{\tau_0}} \tag{4.6.19}$$

then the scale of turbulence L_x can be obtained by the Taylor's hypothesis[22] as follows

$$L_x = U \int_0^\infty R(\tau)\, d\tau = U\, \tau_0 \tag{4.6.20}$$

The associate powers spectral density is now written as

$$S(n) = \frac{2\sigma^2}{L_x U} \frac{1}{(\frac{1}{L_x})^2 + (\frac{2\pi n}{U})^2} \tag{4.6.21}$$

where U is the mean velocity and σ^2 is the variance. The peak value for S(n) occurs in eq. (4.6.21) at

$$(\frac{n}{U})_{max} = \frac{1}{2\pi L_x} \tag{4.6.22}$$

The observed results give L_x = 100 ∿ 200m so that the average duration of wind action can be 2.5 ∿ 5 sec for the mean velocity 40m/sec at the site of structures.

Similarly an alternative method is to assume

then $$R(\tau) = e^{-a|\tau|} \cos 2\pi n_0 \tau$$

$$\frac{S(n)}{\sigma^2} = 2a \left\{ \frac{1}{a^2 + 4\pi^2 (n+n_0)^2} + \frac{1}{a^2 + 4\pi^2 (n-n_0)^2} \right\} \qquad (4 \cdot 6 \cdot 23)$$

which form can be useful in practical application.

4.7 WIND TUNNEL TEST

In order to clarify the effect of fluctuating gusts on the structure used as stiffening girder system of suspension bridge, wind tunnel test is performed using same models as used in Chapter 3, for which turbulent flow is generated by the grids placed at 6.50m windward from the model (mountings of models and grids are shown in Photo 4.1, 4.2).

* Experimental apparatus and Models Configurations

Vibrational characteristics of models are shown in Table 4.2. Deformations are measured by use of Dynamic Strain Meters (DS6/MTX Shinkou Electric Co. Ltd) and recorded in the magnetic recorder (TEAC Co. Ltd 351F-type). Mean Wind Velocity is obtained by Betz-type manometer and NPL-type Pilot tube (Rika Seiki Co. Ltd) and horizontal gust velocity is measured by the constant temperature anemometer (Nihon Kagaku Kogyo Co. Ltd IAM-60/28, IV type).

* Grids

Grids are so set as shown in Photo4.3, 4.4, 4.5 and their demensions and configurations are given in Table 4.3.

* Experimental Results

Deformation and fluctuating velocity data are digitalized by the A-D converter and the 2500 values are used in calculations which are sampled at the sampling frequency 400 cps. Using the Blackman and Tukey's Method[23] the autocorrelation functions are obtained as shown in Fig's 4.11, 4.12, 4.13 and the intensity of turbulence and the scale of average vorticity are calculated as in Table 4.3.

By these results it is considered that the larger the grid size the larger the intensity of turbulence and the intensity tends to decrease when the mean velocity increases. From the autocorrelation functions obtained for horizontal gust the peak values of the power spectrum are considered somewhere between 2 and 4 cps and are considered to increase

as the mean velocity increases.

The spectrums of responses of models are shown in Fig's 4.14 ∿ 4.22 which indicate that vertical vibrations are dominate at the wind velocity below the critical wind velocity for the plate and truss girder models and similar characteristics seem to be expected for both types of models as the wind velocity increases; namely the spectral density tends to decrease as the grid size decreases. On the contrary the spectral density of responses of the plate girder model tends to increase as the grid size decreases.

In this experimental work special attention is placed on the effect of fluctuating gusts on the critical velocity. Experimental results are shown in Table 4.3, which indicate that the critical wind velocity tends to increase in the turbulent flow for plate and truss-girder models, while it seems to decrease for the plate-girder model. This means that the fluctuating gusts work as the stabilizing effect for the plate and truss-girder models as long as this experiment is concerned. Similar flutter test is performed in uniform and turbulent flow using the models as shown in Fig. 4.23 for which the amplitudes-reduced velocity relations are given in Fig's 4.24, 4.25. Again the same tendency of stabilizing and destabilizing effect due to fluctuating winds is obtained using the grid size of 300x250.

It is unfortunate that we have only the horizontal gust components in this experimental work because of the lack of experimental apparatus. The measurement of vertical and horizontal components of gust is essential in the analysis of aerodynamic responses of structures in turbulent flows. In spite of the lack of data, however, it can be said that experimental results indicate affirmatively the theoretical characteristics given in the previous paragraphs. The stabilizing effect on the critical wind velocity due to fluctuating gusts in wind tunnel test is also reported by G. Vincent (A. G. Davenport[24]) for the model tests of the Golden Gate Bridge. However, caution must be placed on the destabilizing characteristics as mentioned in 4.5.2 which is also considered closely related with initiation mechanisms of flutter phenomena. It is required thus

to have more thoroughful analysis in theoretical and experimental works of the effects due to fluctuating gusts on the aerodynamic reliability of suspension bridge.

4.8 DISCUSSIONS AND CONCLUDING REMARKS

Generally speaking, the oscillations of structures excited by wind are ascribed to a number of aerodynamic mechanisms. In this chapter particular considerations are placed on the plate-like structures which can respond to unsteady nature of natural winds. Their oscillatory displacements can become unlikely large because of their randomness. A. G. Davenport investigates the statistical responses of flexible structures such as suspension bridges and tall masts in turbulent winds to conclude that the responses are possibly characterized by

1) fluid characteristics - power spectral density function of fluctuating gusts and the mean velocity
2) dynamic characteristics - mechanical and aerodynamic magnification factors
3) statistical considerations on extreme values - gust factors or response factor and duration

As illustrated in 4.2 A. G. Davenport contributes to large extent for clarification on fluid characteristics and statistical evaluation of responses by applying the extreme value theory; on the other hand a modification or the improvement for dynamic characteristics seems to be reasonable by this investigations. Frequency response functions used by Davenport is the one by taking into an account the aerodynamic coefficients for damping term, which may be justified if one considers uncoupled lateral and transverse vibrations of structures. For most types of suspension bridge the vibrations of stiffening girders are uncoupled approximately laterally transverely and torsionally in free vibrations but they are essentially coupled transversely and torsionally in air flows. Thus the aerodynamic mechanism which produces the lift is inevitably responsible for simultaneous action of pitching moment, and the corresponding frequency response functions are therefore required to be obtained from a coupled form of fundamental equations. As for aerodynamic magnification factor Davenport introduces statistically the average or expected value of spatial correlation over the cross section,

$C(\xi)$ where ξ is the reduced frequency which should be modified by the aerodynamic magnification factors introduced by W. R. Sears, and J. H. Horlock, depending on the configurations and the components of gusts when the plate-like structures are analyzed.

Although there is no comparable experimental result obtained, the above mentioned theoretical considerations seem to be feasible in order to describe the aerodynamic responses due to the fluctuating gusty winds. An important feature is now the stabilizing and destabilizing effects on the aerodynamic stability problem for the plate-like structures. As shown in previous paragraphs the horizontal component of gust may act as stabilizing effect while the vertical component as destabilizing effect, which indicates to some extent the explanation for the obtained results of G. Vincent and of ours. In other words the turbulent flows in the wind tunnel should be examined to have comparative amount of tansverse gustiness; otherwise the stabilized responses are noted and the destabilizing effect is not taken into an account. When a structure subjects to external excitations, the characteristics are no longer same as before and in the analysis for this case not only the power spectrum of transverse gustiness but also that of chordwise gustiness as well as the co-spectrum should be specified as eq's (4.6.12), and the aerodynamic magnification factors consist of the Sears function and the extended Horlock functions as defined in eq. (4.3.27). Then the way of analysis is considered eventually same as before so that statistical evaluations may be performed in similar manner.

As for experimental verifications it calls for the more reasonable methods of work and complete accumulations of data on fluctuating gustiness for which we have obtained so far unsatisfactorily.

The more detailed investigations are needed to assure the satisfactory reliability of such large scale structures as suspension bridge, particularly to take into an account the three-dimensional effects and to establish the similarity law of natural winds.

References

4.1) A. G. Davenport; A statistical approach to the treatment of wind loading on tall masts and suspension bridges, PhD Dissertation, Univ. of Bristol, March, 1061

4.2) B. J. Vickery; Load fluctuations of bluff shapes in turbulent flow, Engineering Science Research Report BLWT-4-67, Univ. of Western Ontario, Canada, 1967.

4.3) J. Vellozzi & E. Cohen; Gust response factors, Jn'l of the Structural Division, Proc. ASCE, ST6, 1968, pp. 1295-1313.

4.4) A. N. L. Chiu; Response of structures to time-varying wind loads, Jn'l of the structural division, Proc. ASCE, ST2, 1970, pp 381-391

4.5) M. Novak & A. G. Davenport; Aeroelastic instability of prisms in turbulent flow, Jn'l of Engineering Mechanics, Proc. ASCE, EM1. 1970, pp 17-39

4.6) Th. von Karman & W. R. Sears; Airfoil theory for non-uniform motion, J. Aeron. Sci., Vol. 5, No.10, 1938, pp 379-390

4.7) W. R. Sears; Some aspects of non-stationary airfoil theory and its practical application, J. Aeron. Sci., Vol. 8, No. 3, 1941, pp 104-108

4.8) R. Isaacs; Airfoil theory for flows of variable velocity, J. Aeron. Sci., Vol. 12, 1945, pp 113-117

4.9) J. H. Horlock; Fluctuating lift forces on airfoil moving through transverse and chordwise gust, Jnl of Basic Eng'g, Trans. ASME, 1968, pp 494-500

4.10) A. G. Davenport; The application of statistical concepts to the wind loading of structures, Inst. Civ. Eng., Proc. Vol. 19, 1961, pp 449-472

4.11) A. G. Davenport; The buffeting of a suspension bridge by storm winds, Jnl of Str. Div., ASCE, Vol. 88, ST3, 1962, pp 233-267

4.12) A. G. Davenport; The causes of wind induced vibration, RILEM Sym. of the vibrations of structures, Theme 3 Supplementary Reports, 1963, pp 445-474

4.13) A. G. Davenport; Buffeting of structures by gusts, Proc. of the 1963 Int'l Sym. on the effects of winds on structures, London, 1965

4.14) A. G. Davenport; The action of wind on suspension bridges, Proc. Int'l Conf. Suspension Bridges, Lisbon, 1966, pp 79-100

4.15) A. G. Davenport; Gust loading factors, Jnl of Str. Div., ASCE, ST3, 1967. pp 11-34

4.16) A. G. Davenport and N. Isyumov; The application of the boundary layer wind tunnel to the prediction of wind loading, Int'l Research Seminar, Wind Effects on Buildings and Structures, Ottwa, 1967, pp 201-230

4.17) A. M. Kuethe & W. R. Sears; The growth of circulation of an airfoil flying through a gust, J. Aeron,Sci. Vol 6, 1939 1939, pp 376-378

4.18) N. H. Kemp; On the lift and circulation of airfoils in some unsteady flow problems, J. Aeron. Sci., Vol. 19, 1952 pp 713-714.

4.19) Y. C. Fung; The theory of Aeroelasticity, J. Wiley, 1955, pp 187-193.

4.20) J. S. Bendat & A. G. Piersol; Measurement and Analysis of Random Data, J. Wiley, 1967. p. 110

4.21) M. Shiotani; Structures of gusts in high winds, Interim report Part 4 to the Japan Railway Construction Cooporation, March, 1970.

4.22) G. K. Batchelor; The Theory of Homogeneous Turbulence, Cambridge Univ. Press, 1956. p. 35

4.23) R. B. Blackman & J. W. Tukey; The Measurement of power spsctra, Dover 1958.

4.24) A. G. Davenport, Ref. (4.14) p. 87

k'	$T_1(k') = S(k')$	$T_2(k')$	$T_3(k')$	$T_4(k')$
0	1.000,0	0	0	.500,0
0.1	.821,3 − .163,5 i	.083,7 + .123,2 i	− .012,5 i	.499,4
0.2	.701,6 − .159,6 i	.134,2 + .156,4 i	− .024,9 i	.497,5
0.3	.623,5 − .125,6 i	.161,9 + .173,0 i	− .037,2 i	.494,4
0.4	.567,9 − .085,0 i	.176,4 + .185,6 i	− .049,3 i	.490,1
0.5	.524,6 − .044,0 i	.182,5 + .197,3 i	− .061,2 i	.484,5
0.6	.488,4 − .004,0 i	.182,9 + .209,0 i	− .072,8 i	.477,8
0.8	.426,0 + .065,9 i	.171,8 + .232,2 i	− .094,8 i	.461,0
1.0	.3686 + .125,9 i	.149,8 + .253,4 i	− .114,9 i	.440,0
1.2	.312,0 + .175,3 i	.120,3 + .271,7 i	− .132,8 i	.415,2
1.5	.225,6 + .229,6 i	.067,0 + .290,0 i	− .154,7 i	.372,0
2.0	.081,6 + .268,0 i	− .031,4 + .285,6 i	− .176,4 i	.288,4
3.0	− .145,2 + .177,8 i	− .184,2 + .159,7 i	− .162,0 i	.113,0
4.0	− .198,0 − .020,7 i	− .188,9 − .038,3 i	− .091,0 i	− .016,5
6.0	.081,3 − .141,0 i	+ .098,0 − .134,4 i	+ .040,5 i	− .046,1
10.0	− .124,0 + .002,5 i	− .125,0 + .020,0 i	− .025,5 i	.004,3
∞	0	0	0	0

Table 4・1 Aerodynamic Magnification Factors

Table 4・2 Vibrational Characteristics

	Plate	*Trussed Girder (DT70H)*	*Plate-Girder (DP70H)*
mass per unit length m ($g\,sec^2\,cm^{-2}$)	0.265	0.361	0.384
inertia moment per unit length, I ($kg\,sec^2$)	0.0085	0.0113	0.0118
deflectional natural frequency (rad/sec)	9.50 (1.51 *cps*)	8.64 (1.375 *cps*)	8.81 (1.402 *cps*)
torsional natural frequency (rad/sec)	12.54 (2.00 *cps*)	12.18 (1.939 *cps*)	12.78 (2.034 *cps*)
logarithmic decrement in defl. vibration	.024	.025	.038
logarithmic decrement in tor. vibration	.032	.020	.031

Table 4・3

Grid Type	*Grid Size (ctc)*	*Open Area*	*OPening Ratio*
A	400 × 350	340 × 320	77.7 %
B	200 × 350	140 × 320	64.0
C	200 × 100	140 × 70	49.0

Intensity of Turbulence

Grid Type \ *Mean Wind Velocity*	*m/sec* 2.00	4.19	7.41	9.40
A	.053	.047	.046	.043
B	.052	.044	.040	.041
C	.033	.030	.027	.028

Scale of Average Vorticity (m)

Grid Type \ *Mean Wind Velocity*	*m/sec* 2.00	4.19	7.41	9.40
A	.058	.122		.103
B	.118	.190	.173	.108
C	.084	.061	.039	.071

Critical Wind Velocity (m/sec)

Grid Type \ *Model Type*	*Plate*	*Truss Type*	*H-Section*
A	10.67	9.52	3.92
B	10.29	9.48	3.92
C	10.21	9.48	5.01
None	> 8.92	9.01	6.43

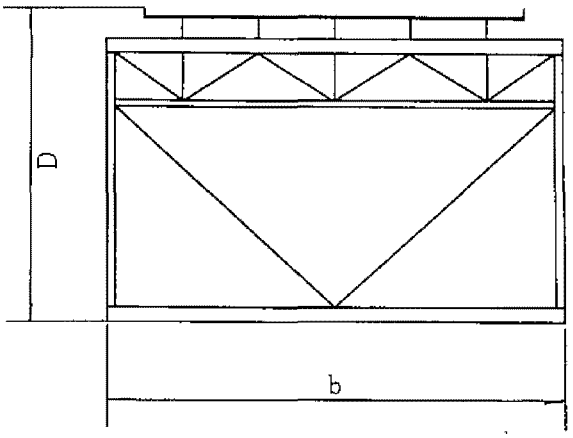

Fig. 4.1 Region of flow affecting pressure

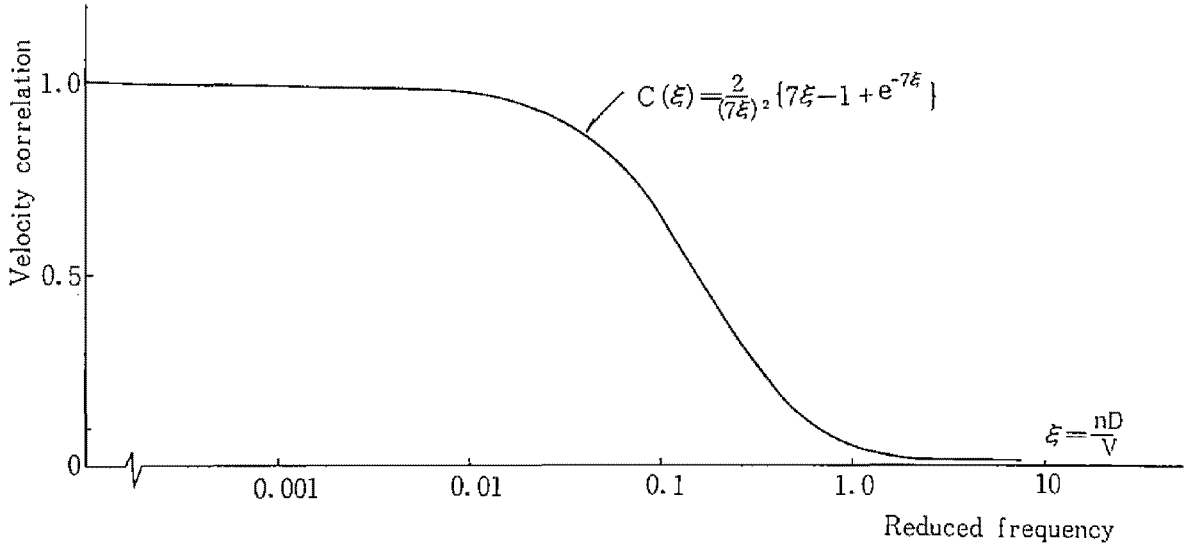

Fig. 4.2 Velocity correlation- Reduced Frequency Relation

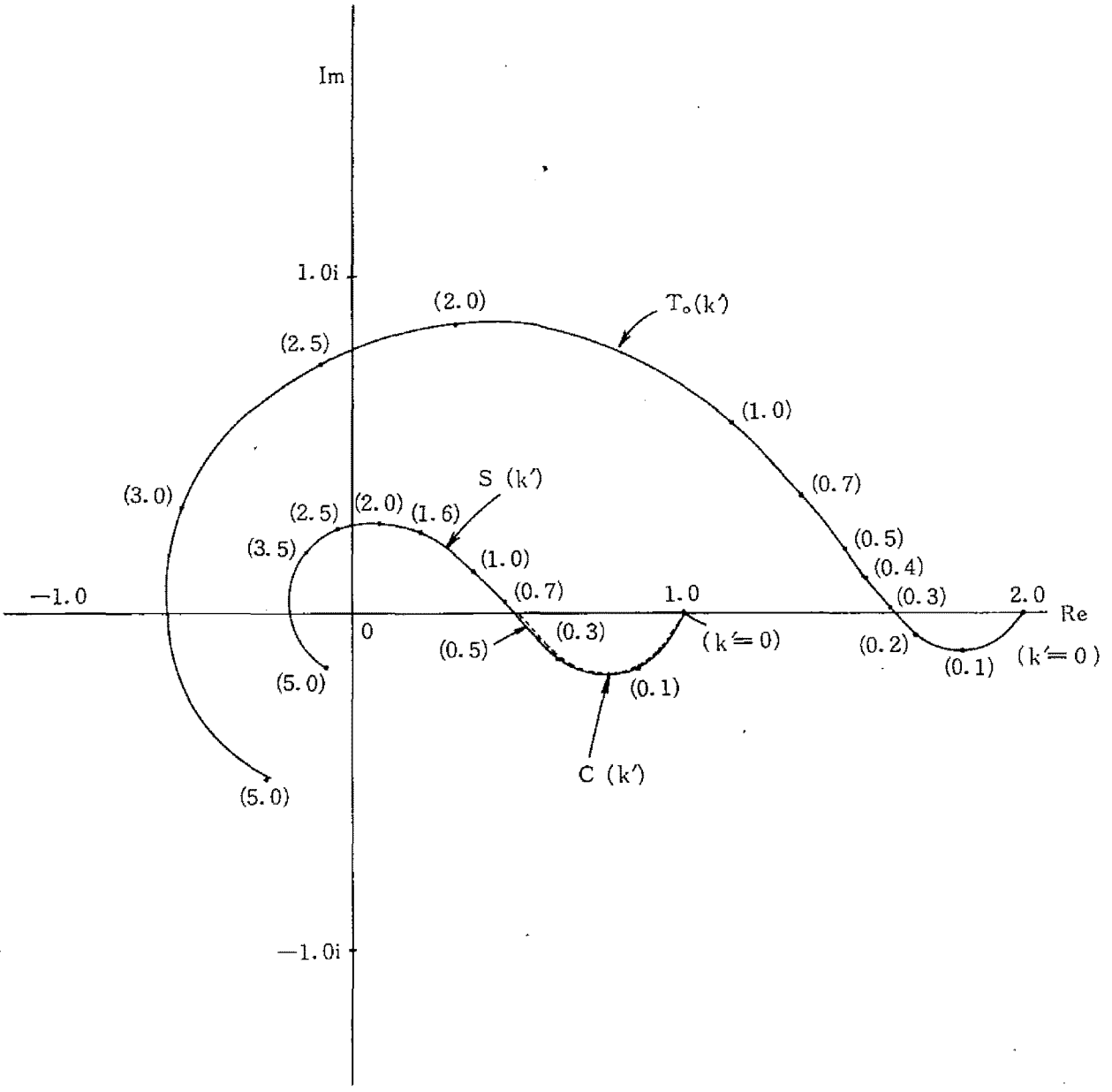

Fig. 4.3 Vector Diagrams of C (k').S(k') and T_o (k')

C (k') : Theodorsen Function

S (k') : Sears Function

T_o (k') : Horlock Function

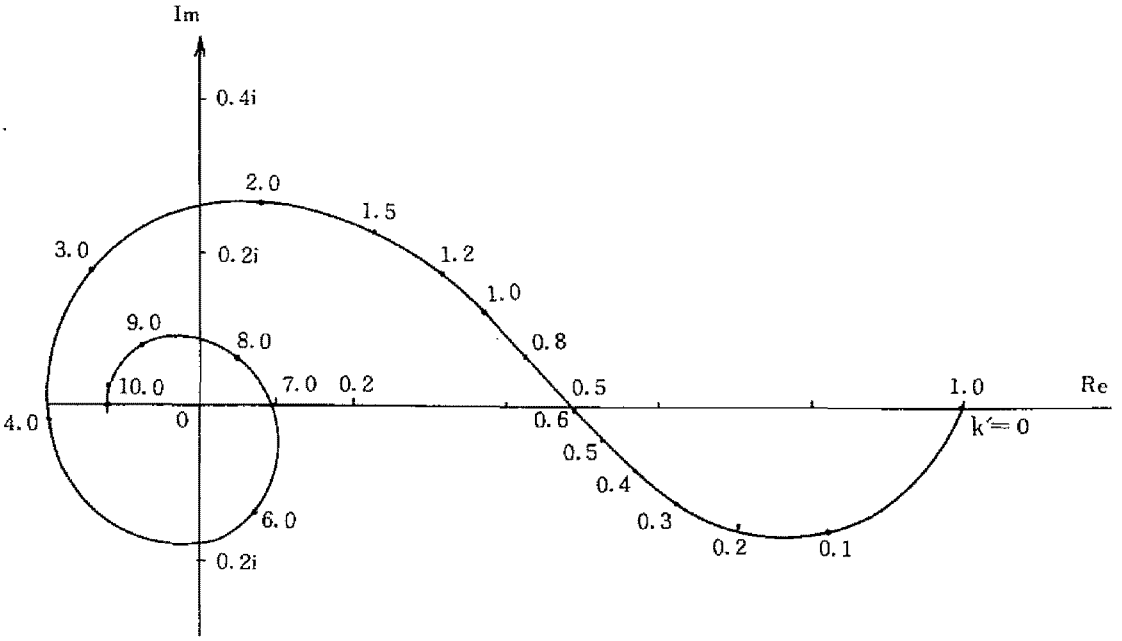

Fig. 4.4 Vector Diagram of T_1 (k')

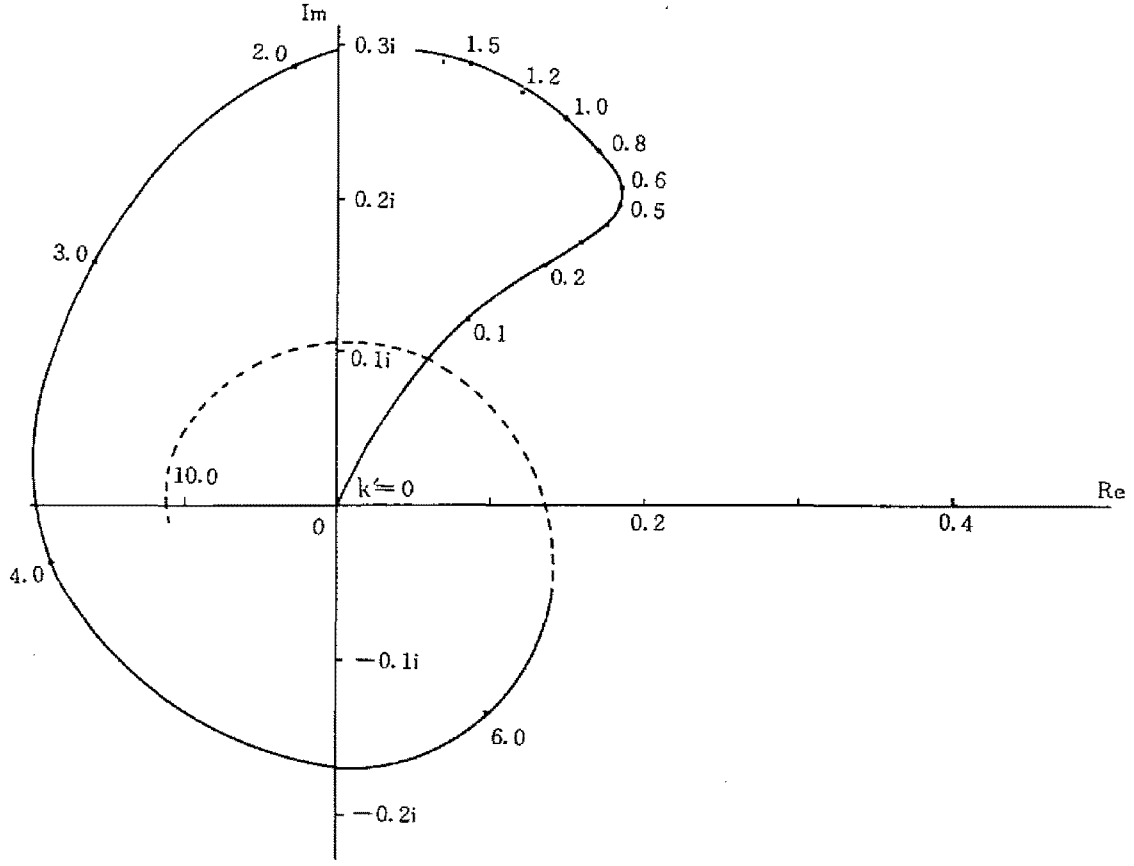

Fig. 4.5 Vector Diagram of T_2 (k')

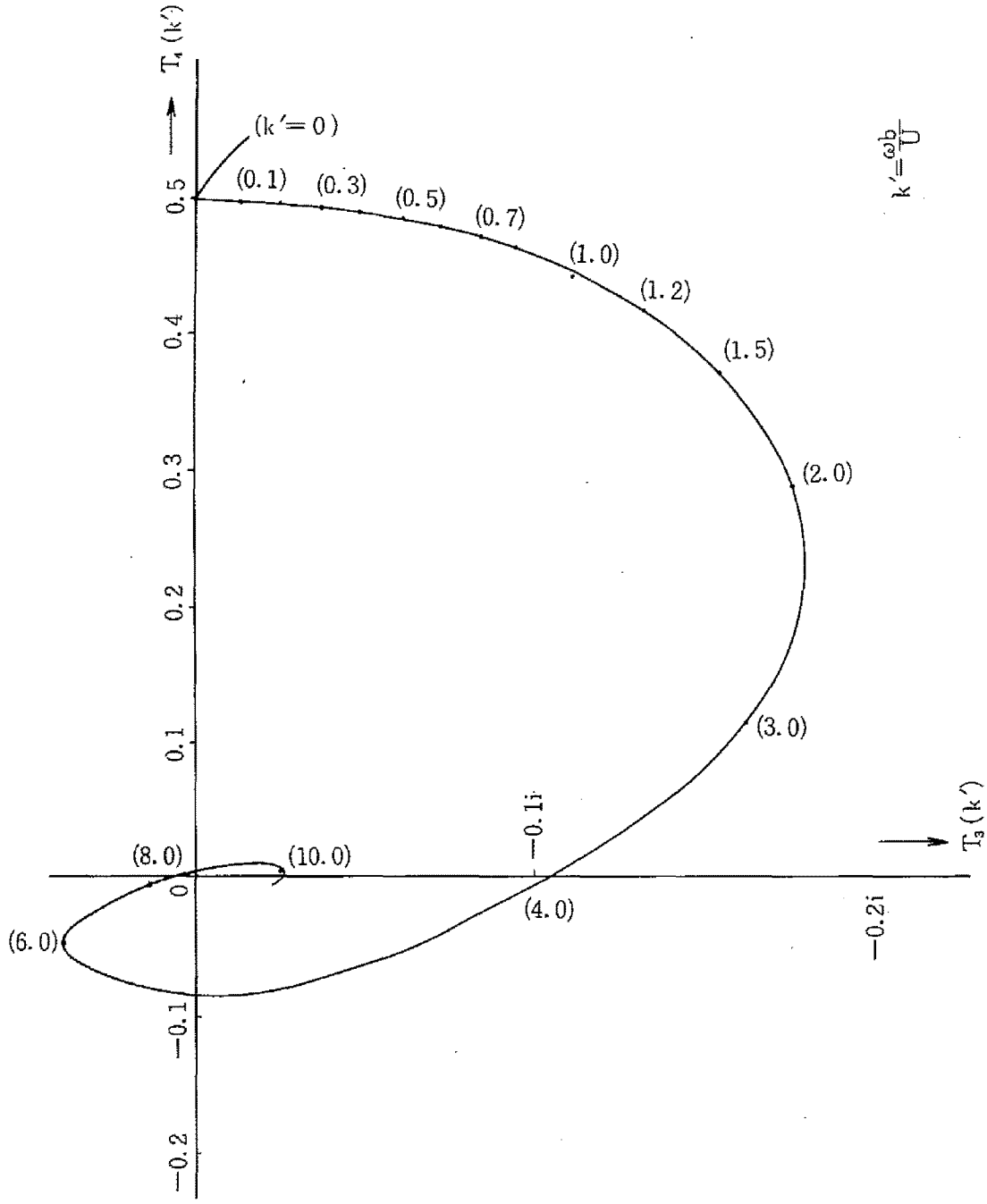

Fig. 4.6 Aerodynamic Magnification Factor. $T_3(k').T_4(k')$

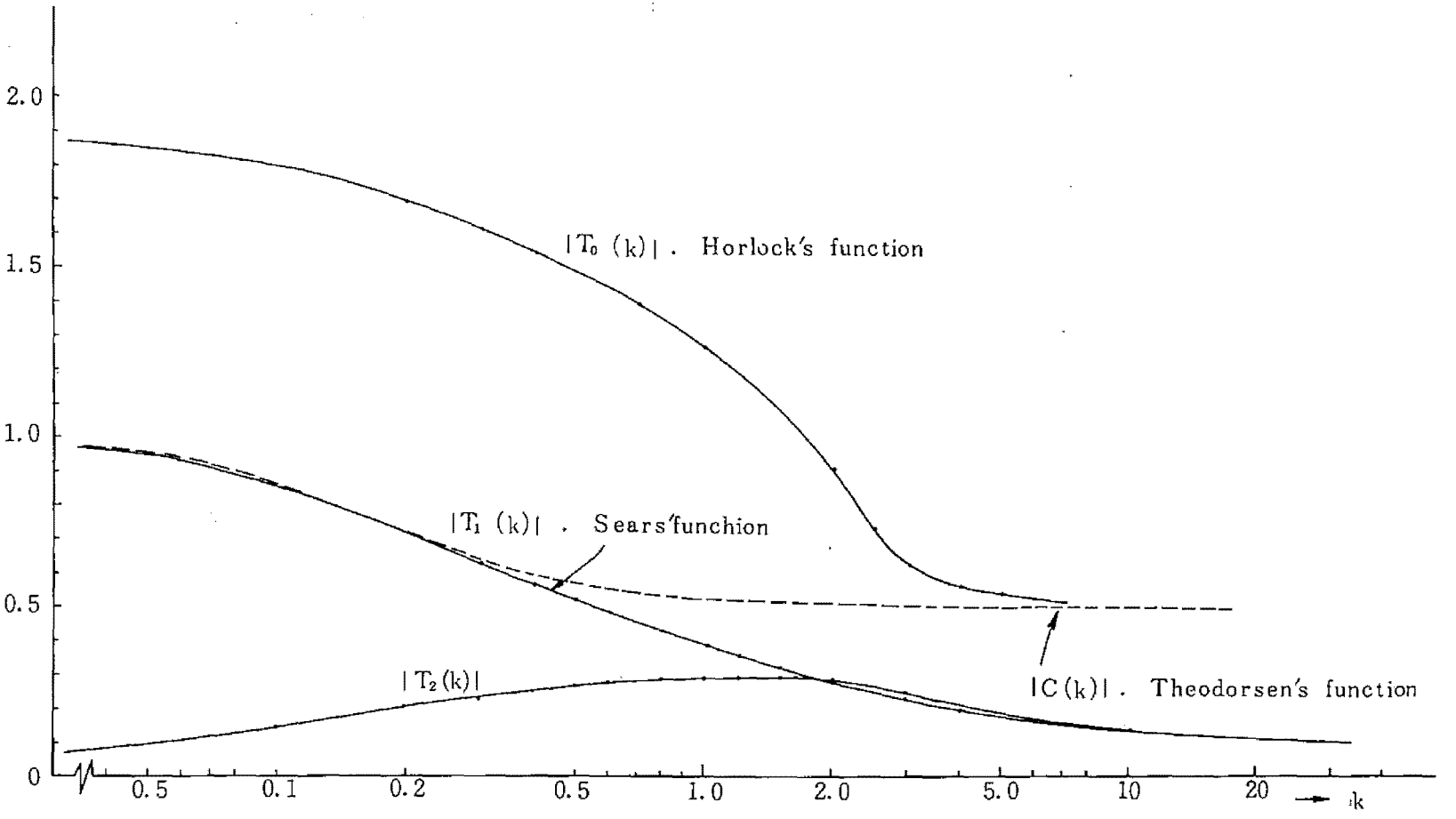

Fig. 4.7 Absolute Values of Aerodynamic Magnification Factors

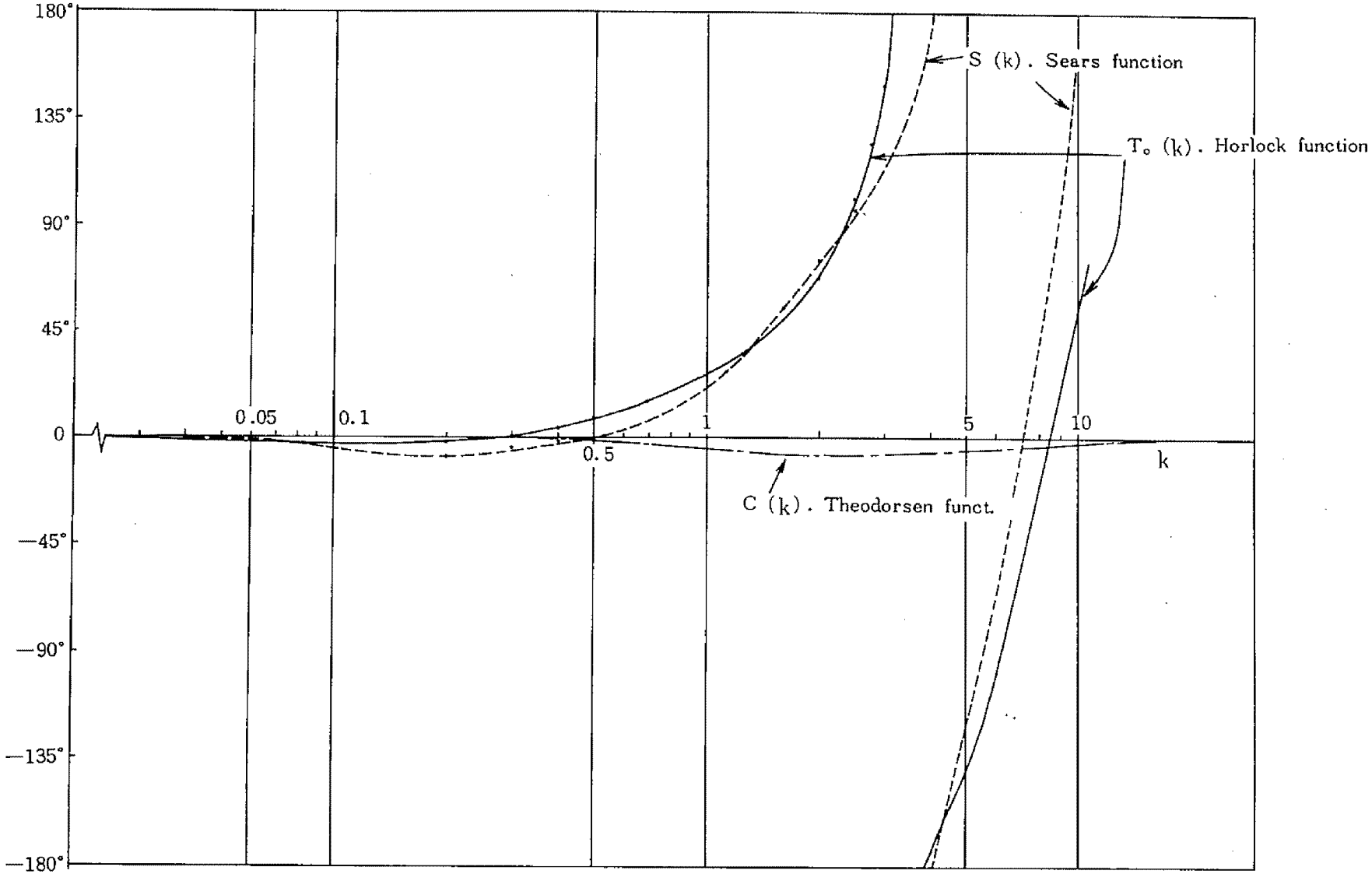

Fig. 4.8 Phase Charcteristics of Aerodynamic Magnification Factors

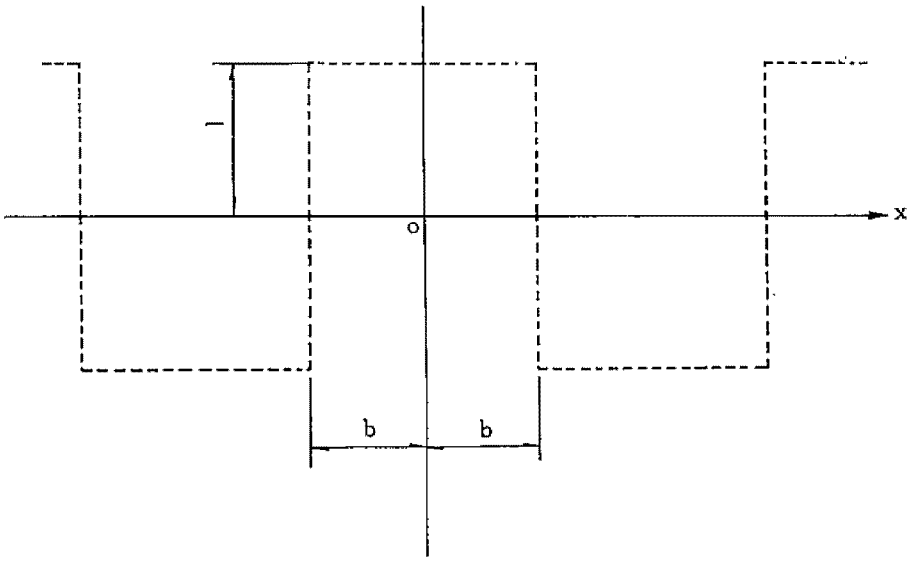

Fig. 4.9 Rectangular Transverse Gust Pattern

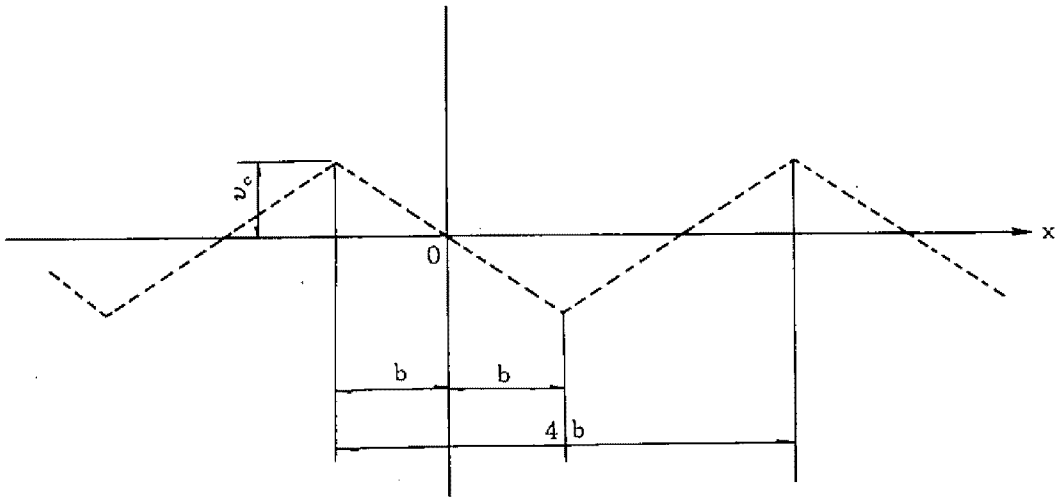

Fig. 4.10. Triangular Transverse Gust Pattern

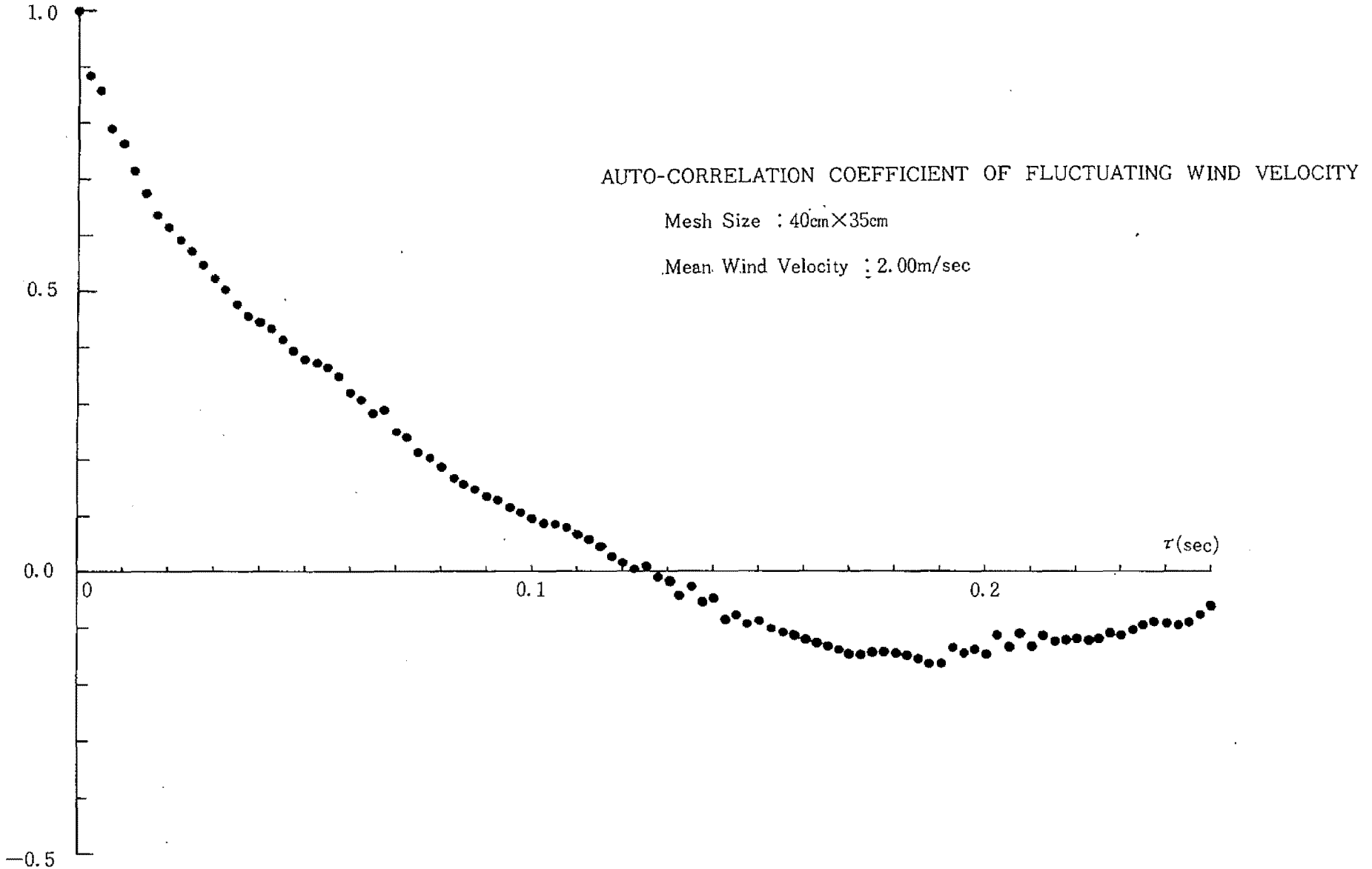
AUTO-CORRELATION COEFFICIENT OF FLUCTUATING WIND VELOCITY
Mesh Size : 40cm×35cm
Mean Wind Velocity : 2.00m/sec
1.0
0.5
0.0
−0.5
0
0.1
0.2
τ(sec)

Fig. 4.11(a)

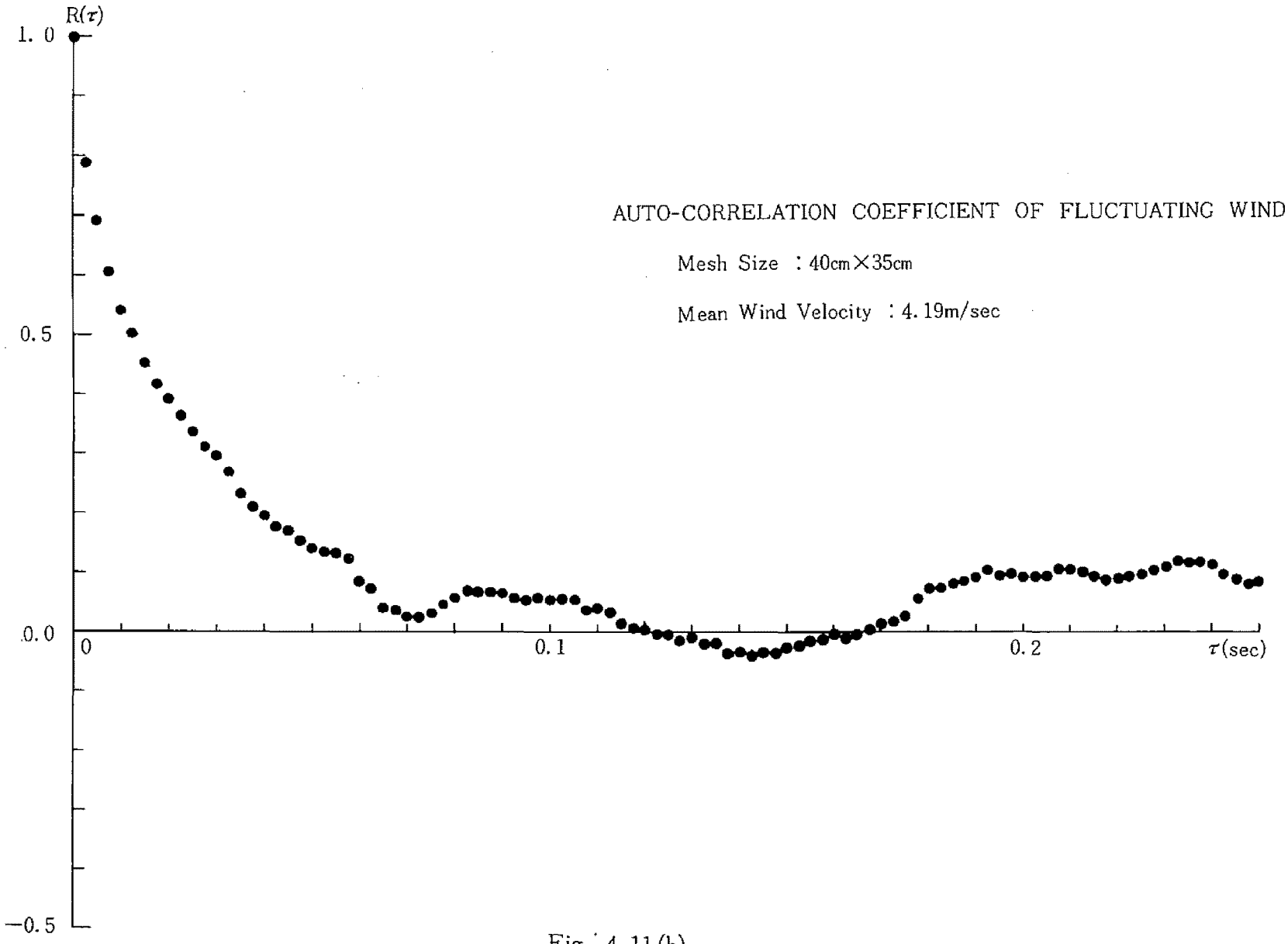
R(τ)
1.0
0.5
0.0
−0.5
0
0.1
0.2
τ(sec)
AUTO-CORRELATION COEFFICIENT OF FLUCTUATING WIND VELOCITY
Mesh Size : 40cm×35cm
Mean Wind Velocity : 4.19m/sec

Fig. 4.11 (b)

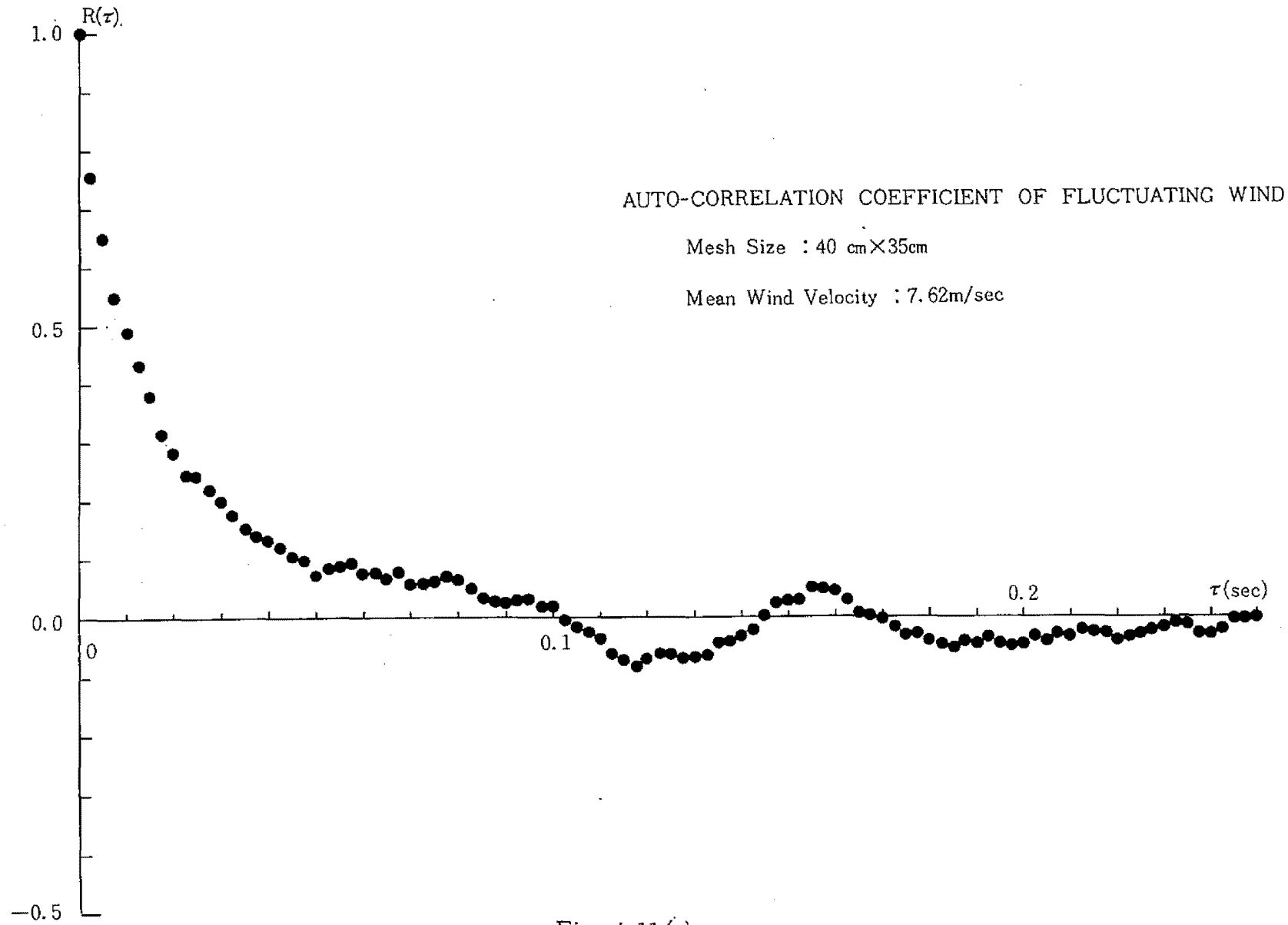

AUTO-CORRELATION COEFFICIENT OF FLUCTUATING WIND VELOCITY

Mesh Size : 40 cm×35cm

Mean Wind Velocity : 7.62m/sec

Fig. 4.11(c)

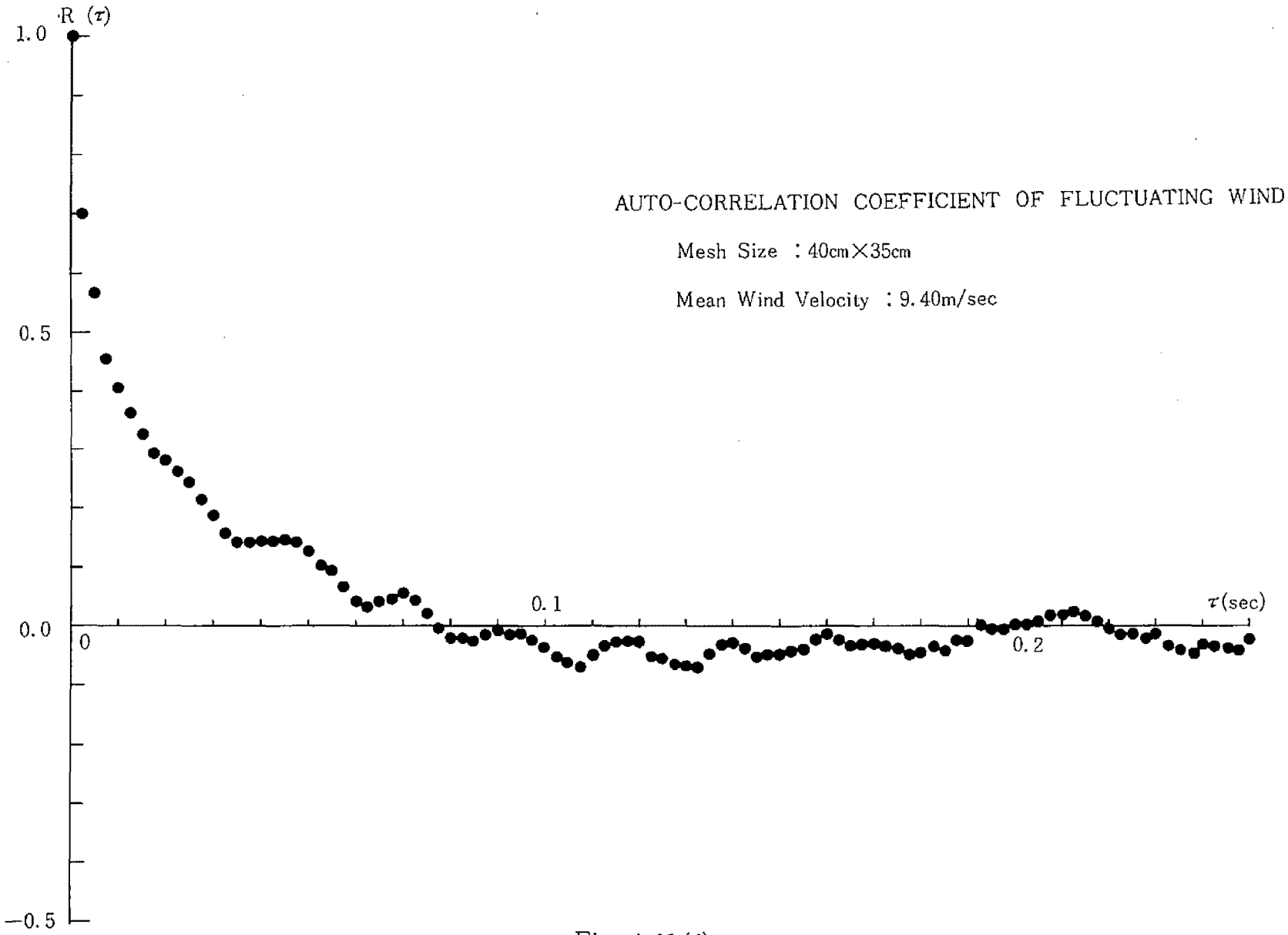

AUTO-CORRELATION COEFFICIENT OF FLUCTUATING WIND VELOCITY

Mesh Size : 40cm×35cm

Mean Wind Velocity : 9.40m/sec

Fig. 4.11 (d)

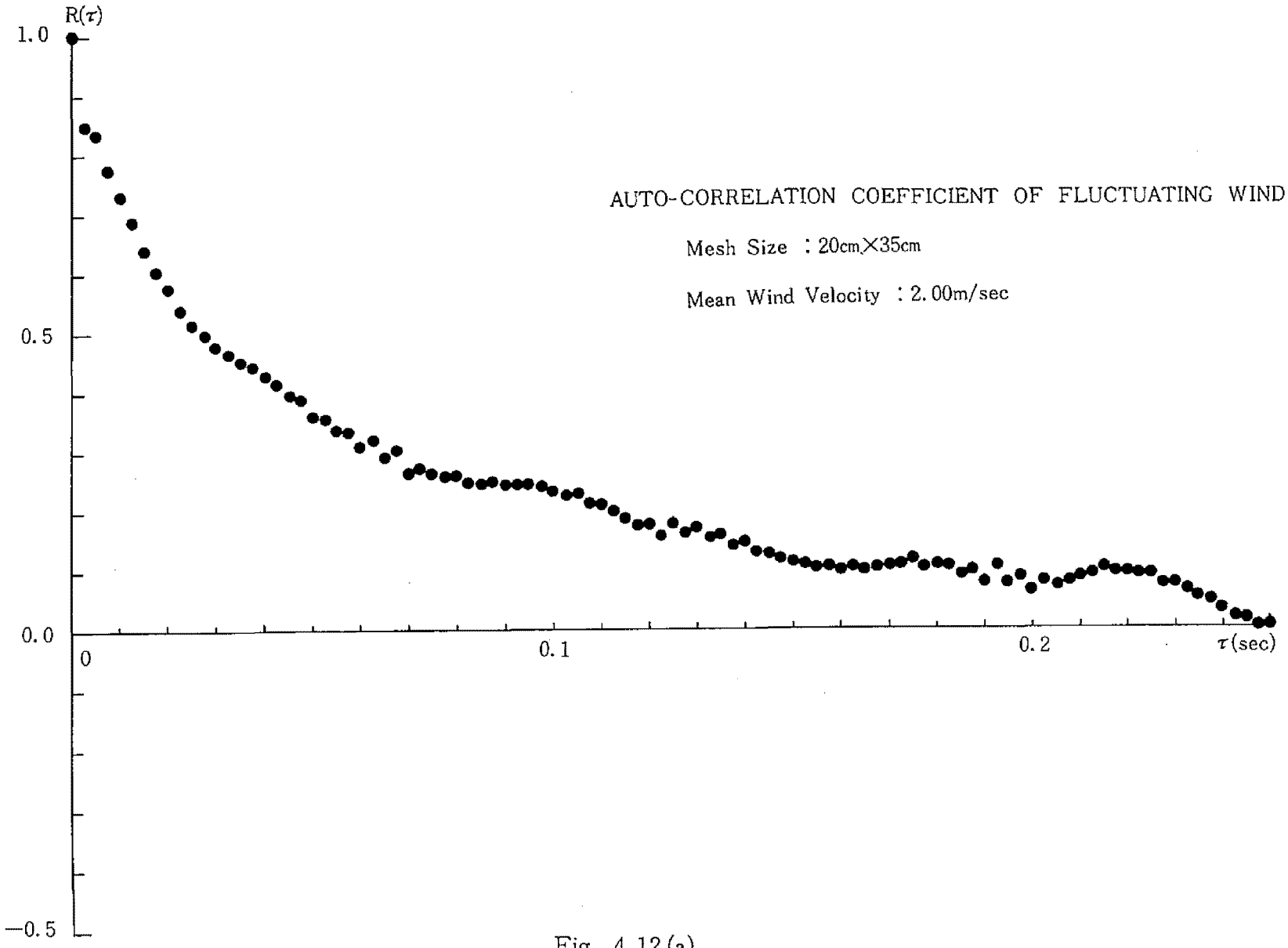
R(τ)
1.0
0.5
0.0
−0.5
0
0.1
0.2
τ(sec)
AUTO-CORRELATION COEFFICIENT OF FLUCTUATING WIND VELOCITY
Mesh Size : 20cm×35cm
Mean Wind Velocity : 2.00m/sec

Fig. 4.12 (a)

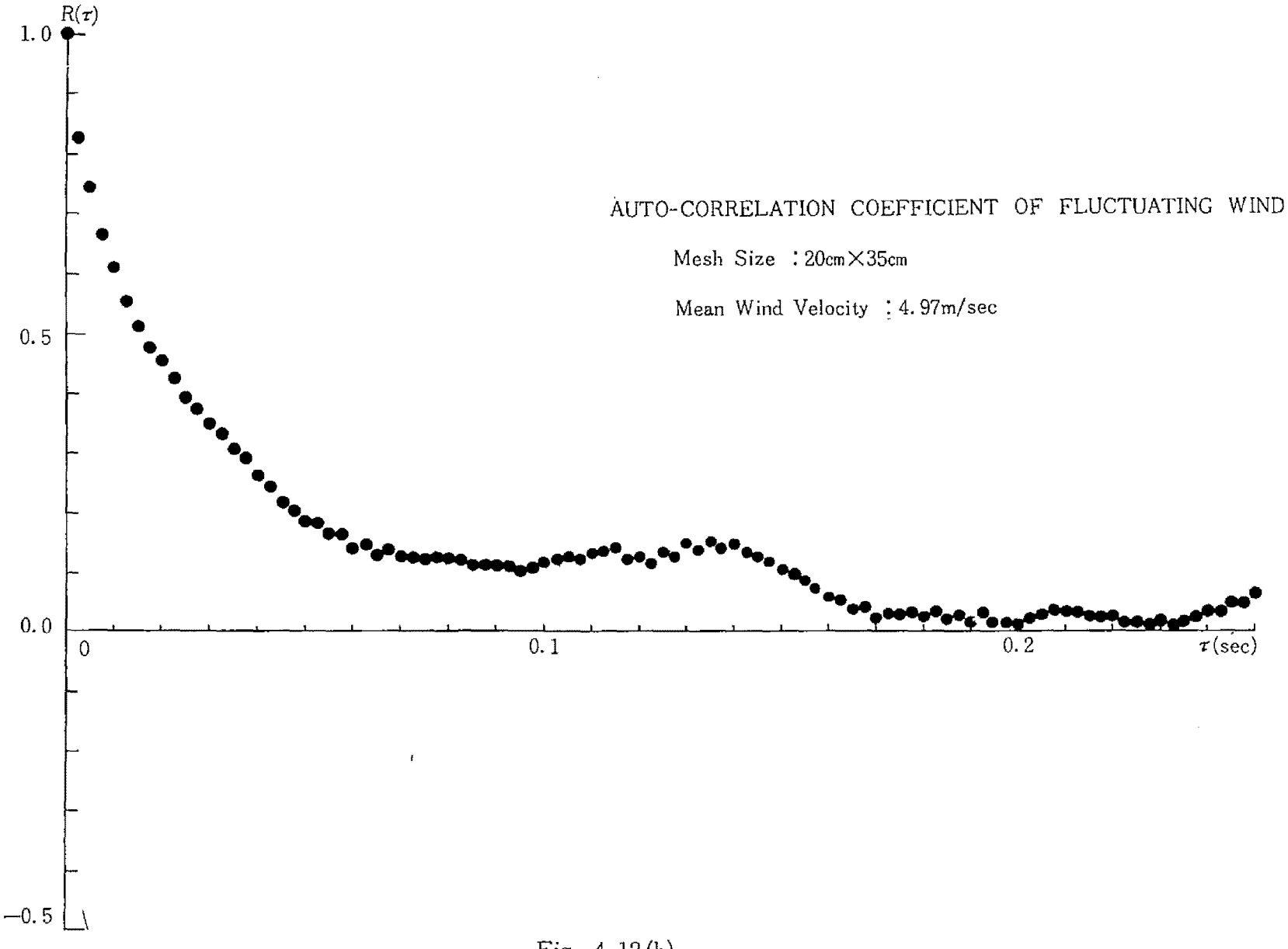
R(τ)
1.0
0.5
0.0
−0.5
0
0.1
0.2
τ(sec)
AUTO-CORRELATION COEFFICIENT OF FLUCTUATING WIND VELOCITY
Mesh Size : 20cm×35cm
Mean Wind Velocity : 4.97m/sec

Fig. 4.12(b)

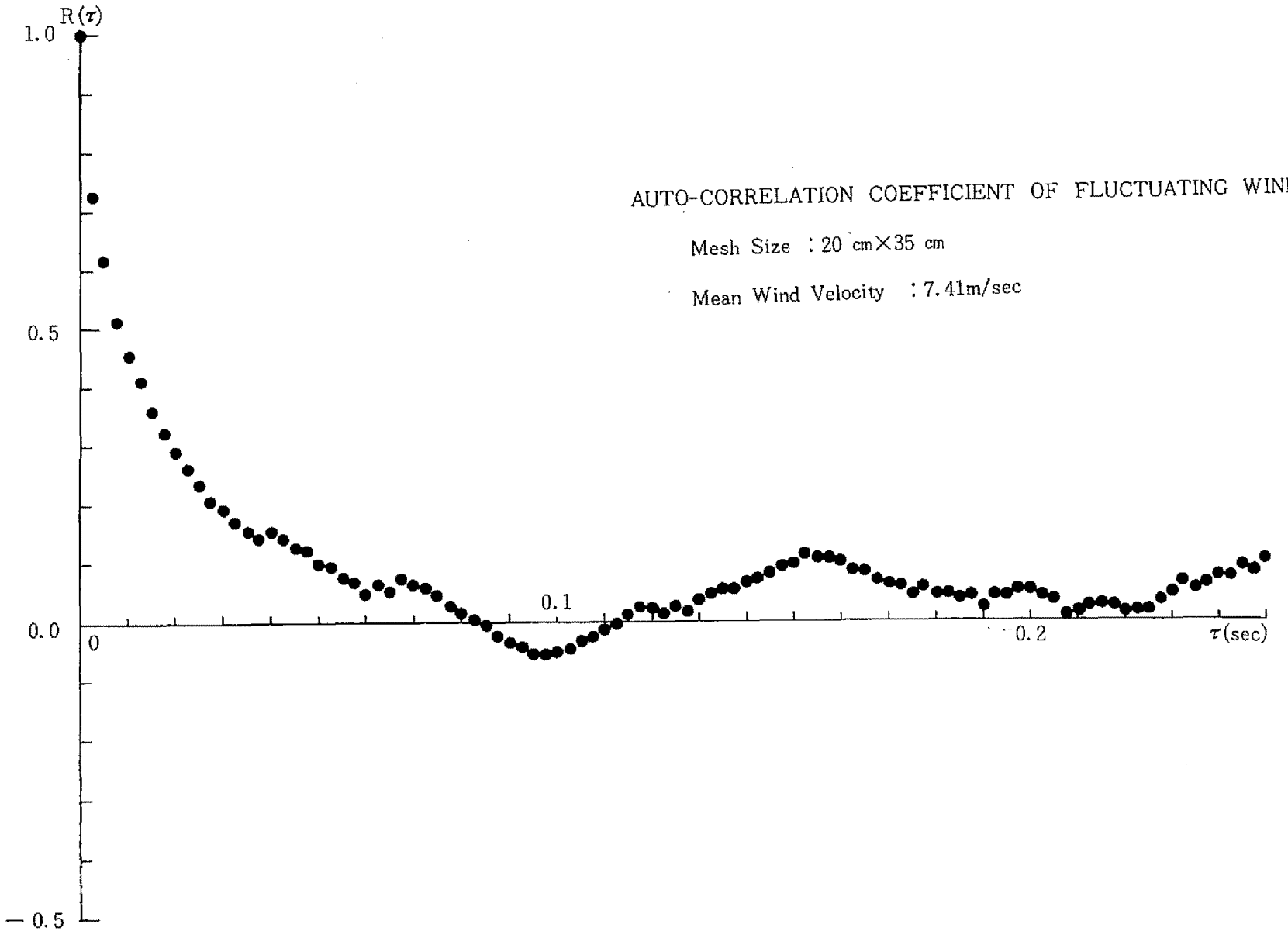
R(τ)
1.0
0.5
0.0
−0.5
0
0.1
0.2
τ(sec)
AUTO-CORRELATION COEFFICIENT OF FLUCTUATING WIND VELOCITY
Mesh Size : 20 cm×35 cm
Mean Wind Velocity : 7.41m/sec

Fig. 4.12(c)

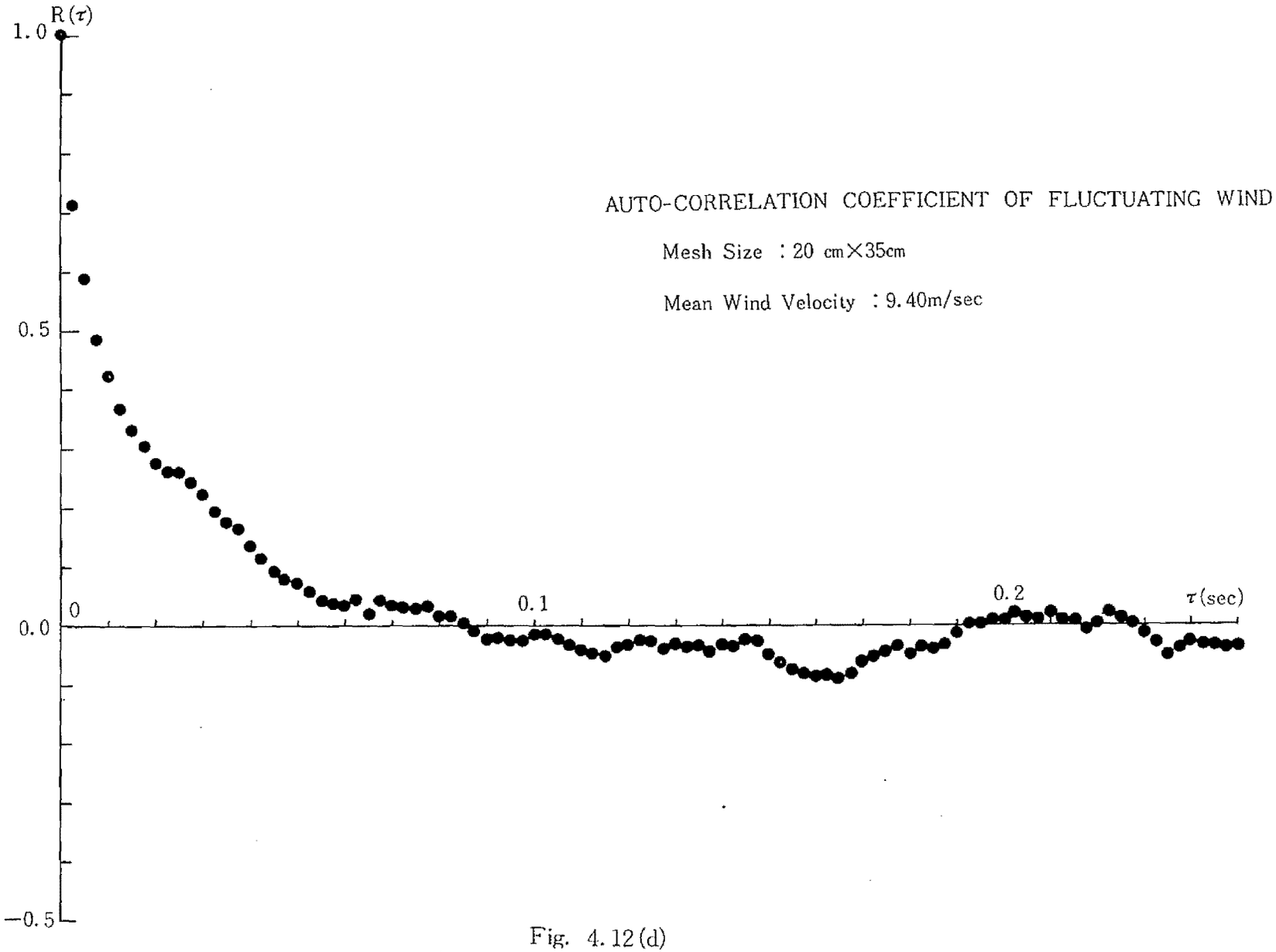
AUTO-CORRELATION COEFFICIENT OF FLUCTUATING WIND VELOCITY
Mesh Size : 20 cm×35cm
Mean Wind Velocity : 9.40m/sec
R(τ)
1.0
0.5
0.0
−0.5
0
0.1
0.2
τ(sec)

Fig. 4.12(d)

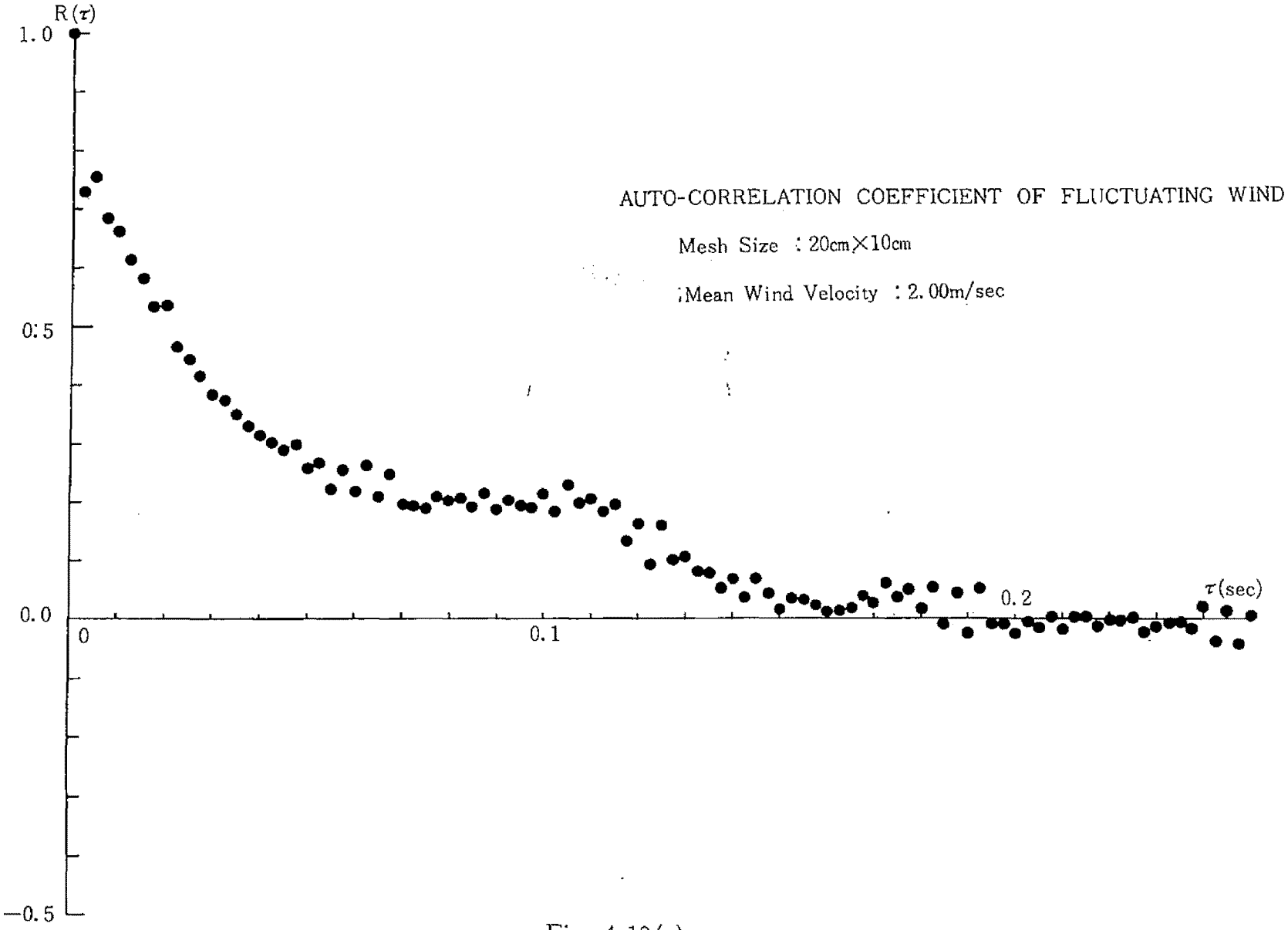
R(τ)
1.0
0.5
0.0
−0.5
0
0.1
0.2
τ(sec)
AUTO-CORRELATION COEFFICIENT OF FLUCTUATING WIND VELOCITY
Mesh Size : 20cm×10cm
Mean Wind Velocity : 2.00m/sec

Fig. 4.13(a)

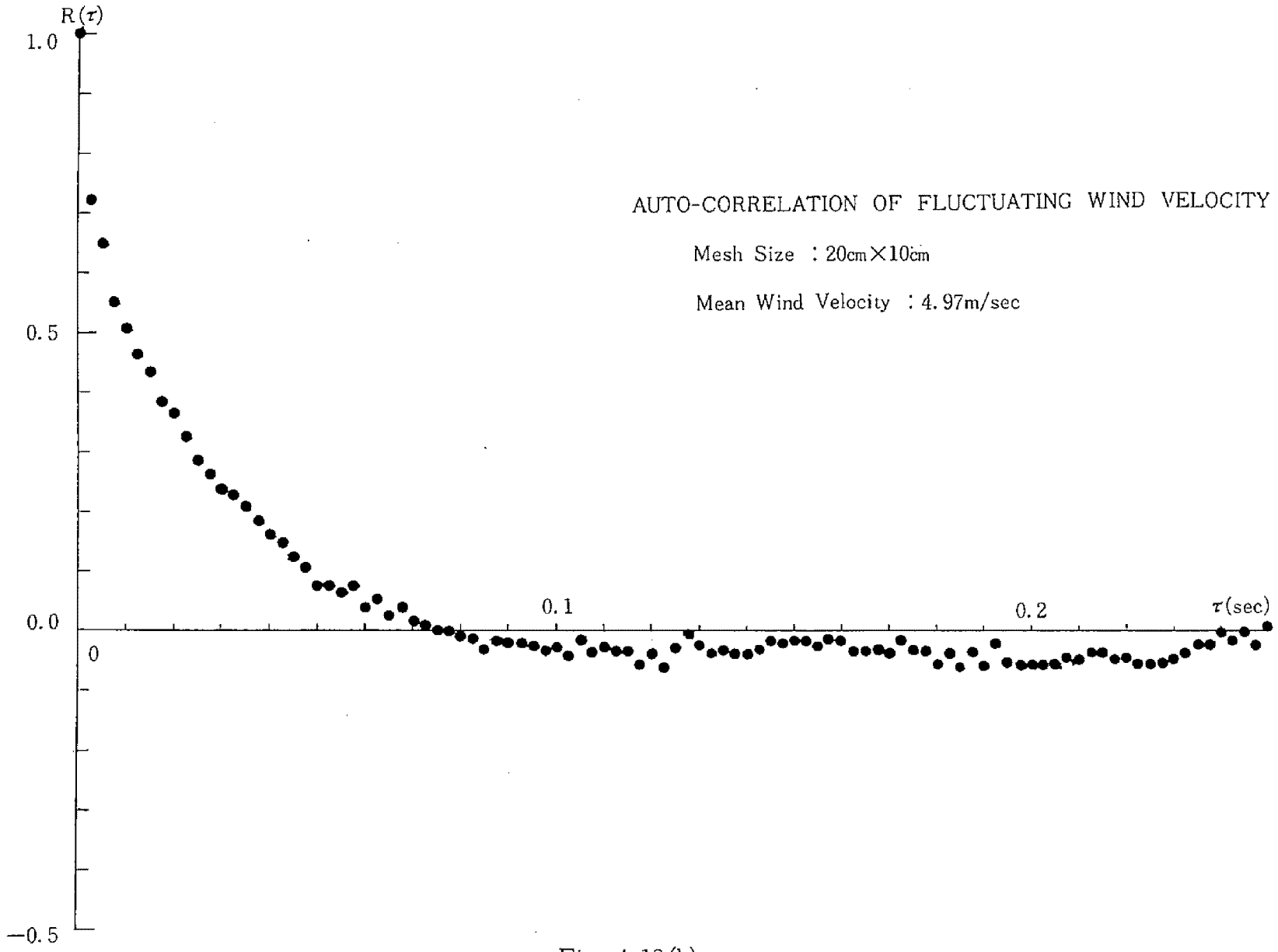
R(τ)
1.0
0.5
0.0
−0.5
0
0.1
0.2
τ(sec)
AUTO-CORRELATION OF FLUCTUATING WIND VELOCITY
Mesh Size : 20cm×10cm
Mean Wind Velocity : 4.97m/sec

Fig. 4.13(b)

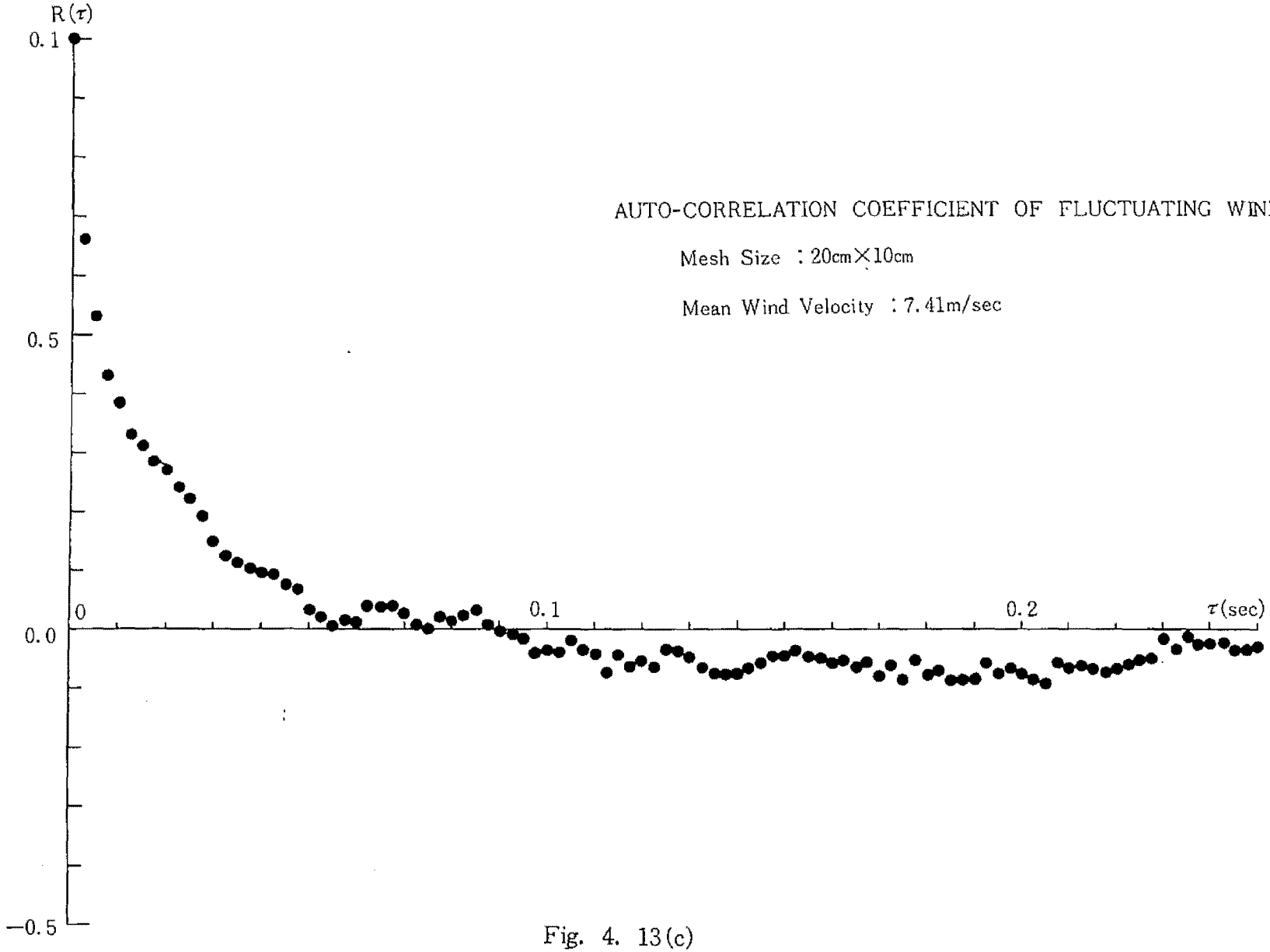
R(τ)
0.1
0.5
0.0
−0.5
0
0.1
0.2
τ(sec)
AUTO-CORRELATION COEFFICIENT OF FLUCTUATING WIND VELOCITY
Mesh Size : 20cm×10cm
Mean Wind Velocity : 7.41m/sec

Fig. 4. 13(c)

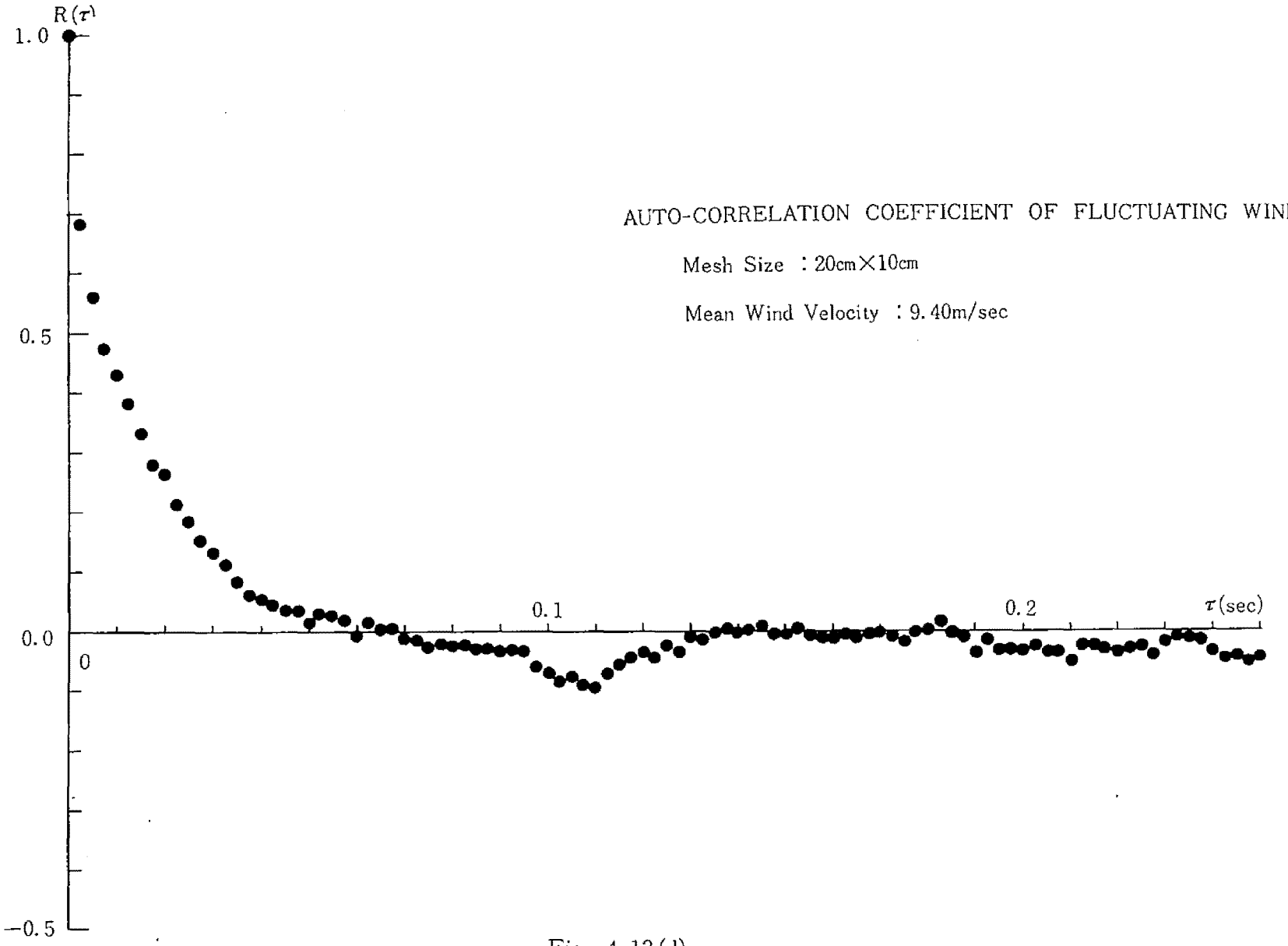

AUTO-CORRELATION COEFFICIENT OF FLUCTUATING WIND VELOCITY

Mesh Size : 20cm×10cm

Mean Wind Velocity : 9.40m/sec

Fig. 4.13(d)

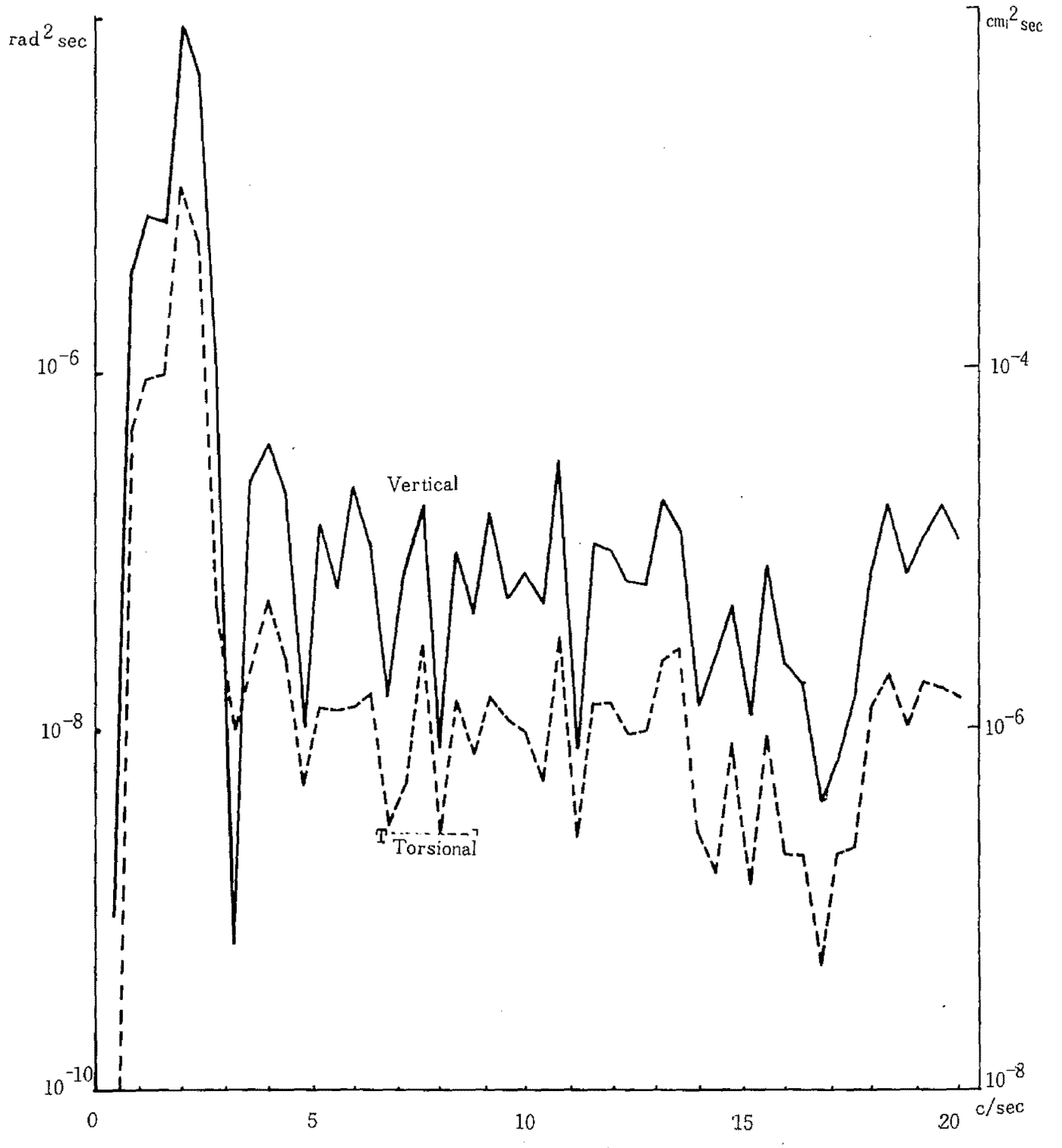

Fig. 4.14(a) Power Spectrum of Model-Response
Model ; Plate
Mesh Size ; 40cm×35cm
Mean Wind Velocity ; 2.00m/sec

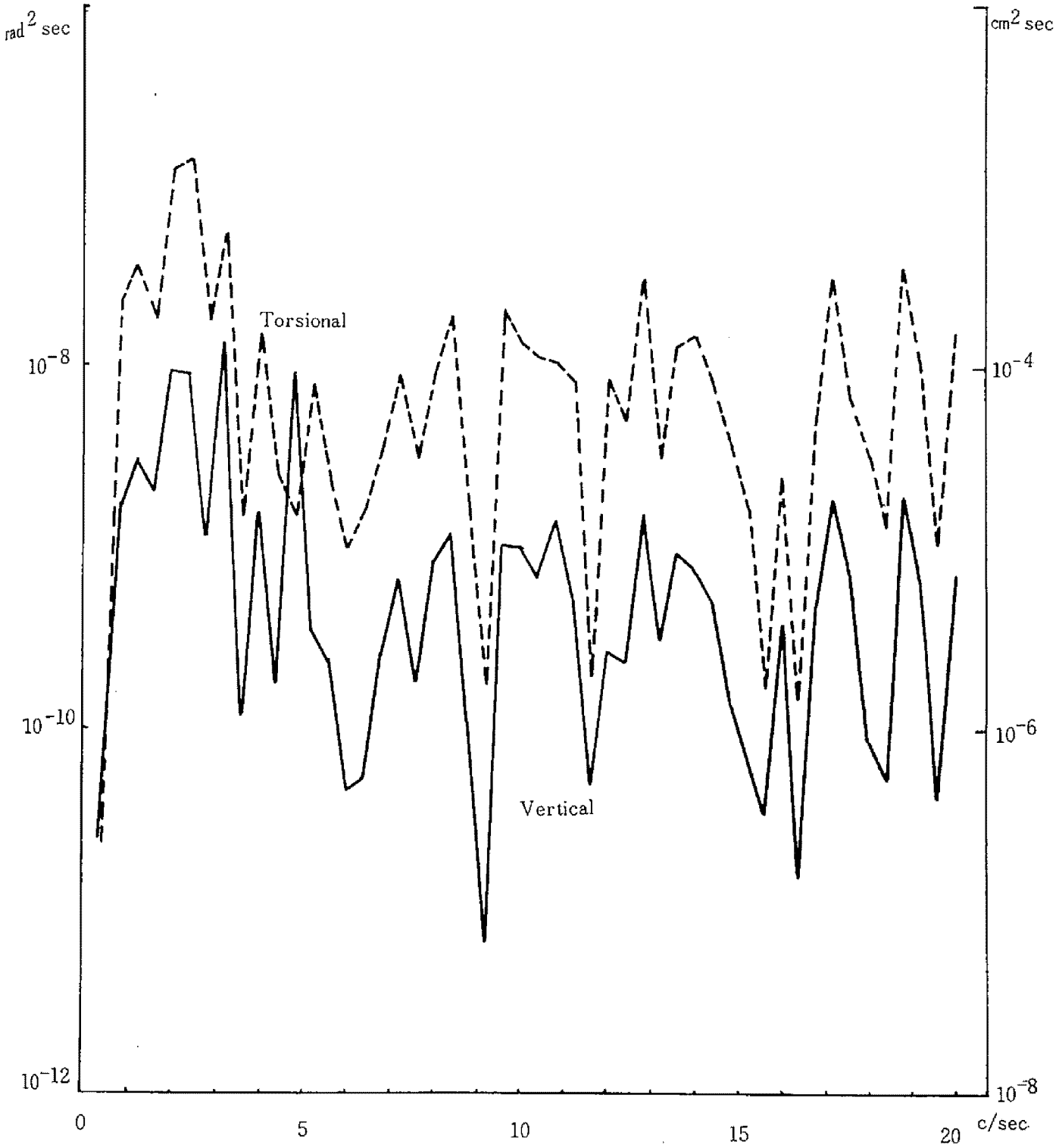

Fig. 4.14(b) Power Spectrum of Model-Response
Model ; Plate
Mesh Size ; 40cm×35cm
Mean Wind Velocity ; 4.19m/sec

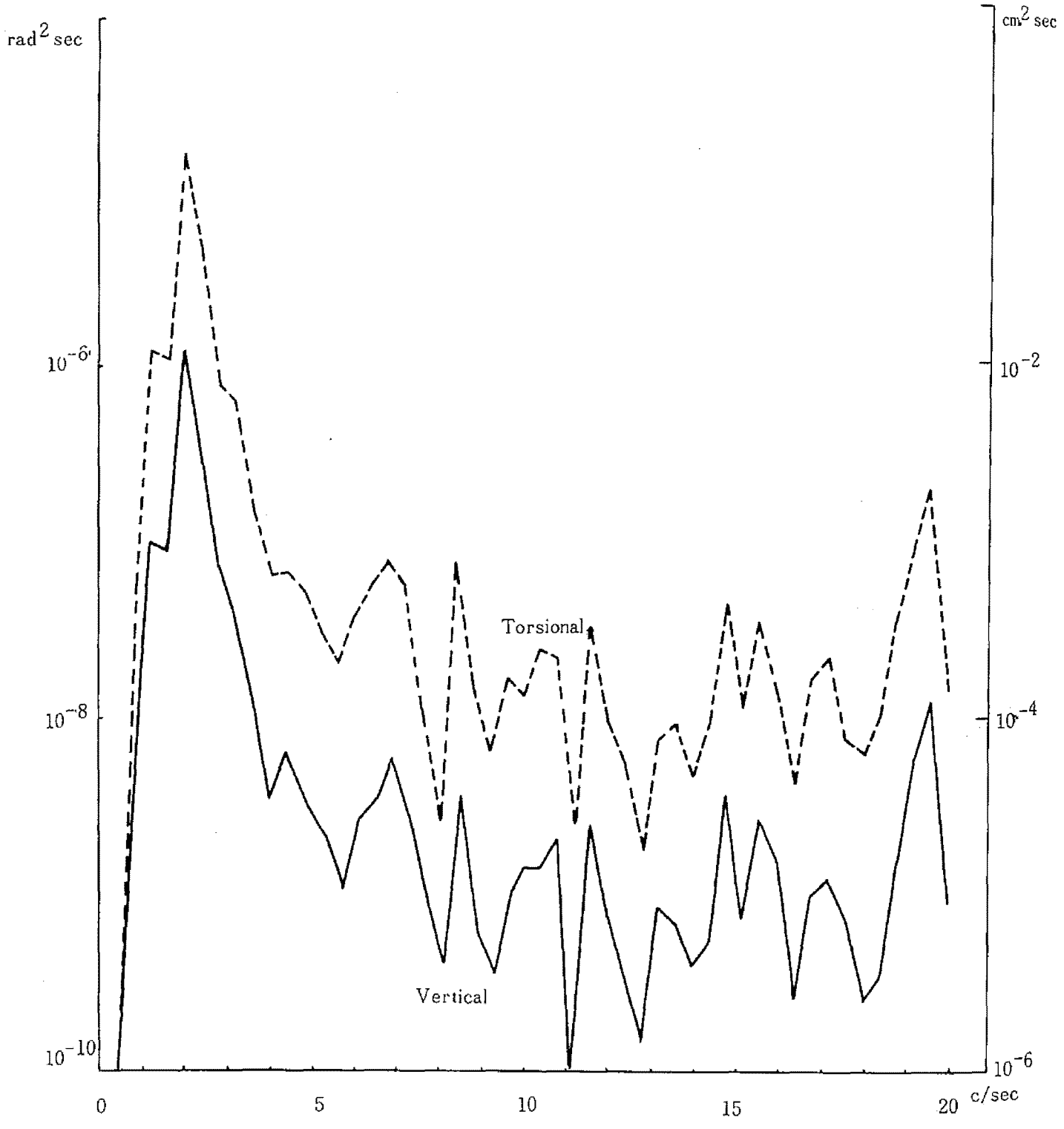

Fig. 4.14(c) Power Spectrum of Model-Response
Model ; Plate
Mesh Size ; 40cm×35cm
Mean Wind Velocity ; 7.26 m/sec

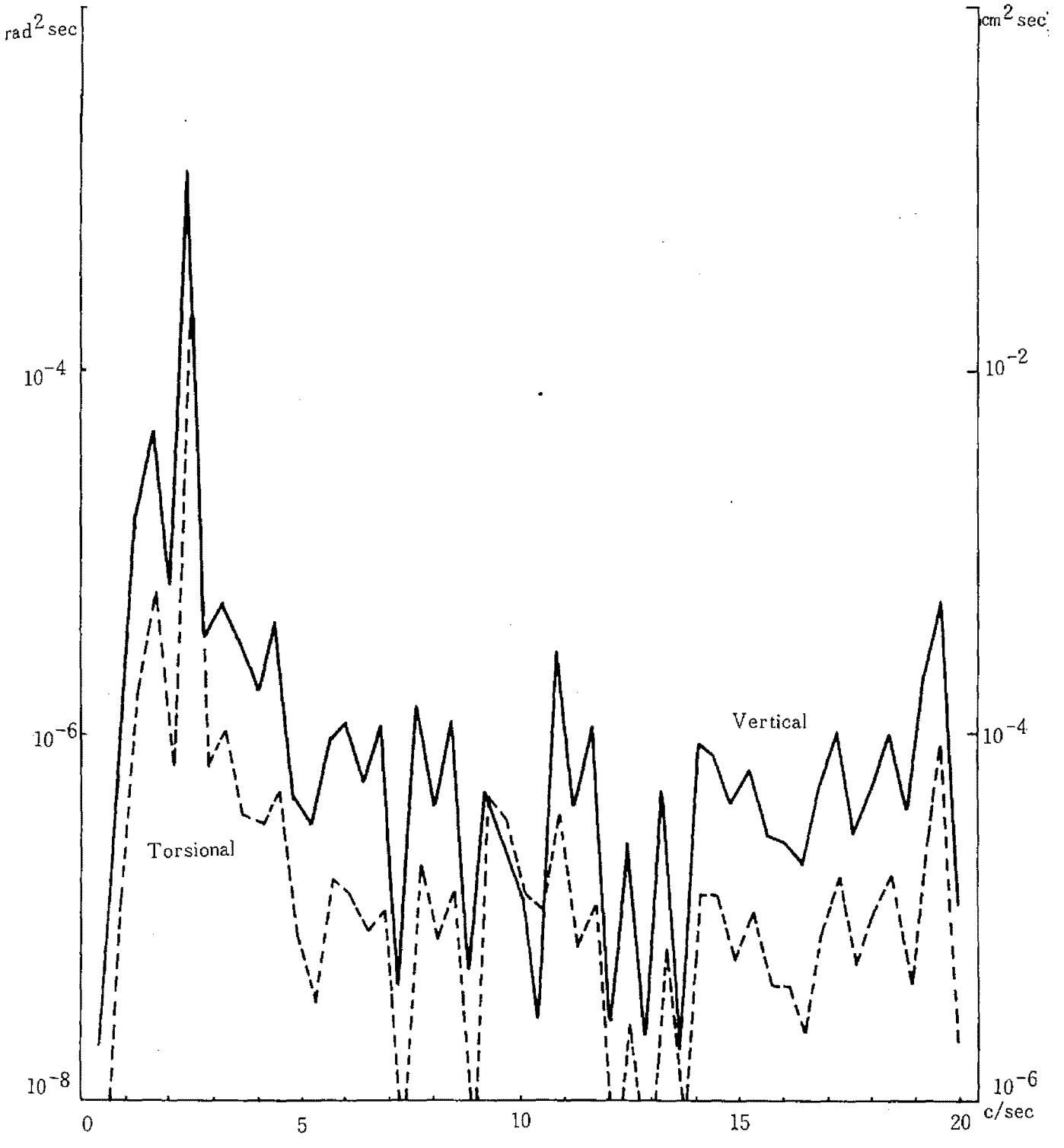

Fig. 4.14(d) Power Spectrum of Model-Response
Model ; Plate
Mesh Size ; 40cm×35cm
Mean Wind Velocity ; 9.40m/sec

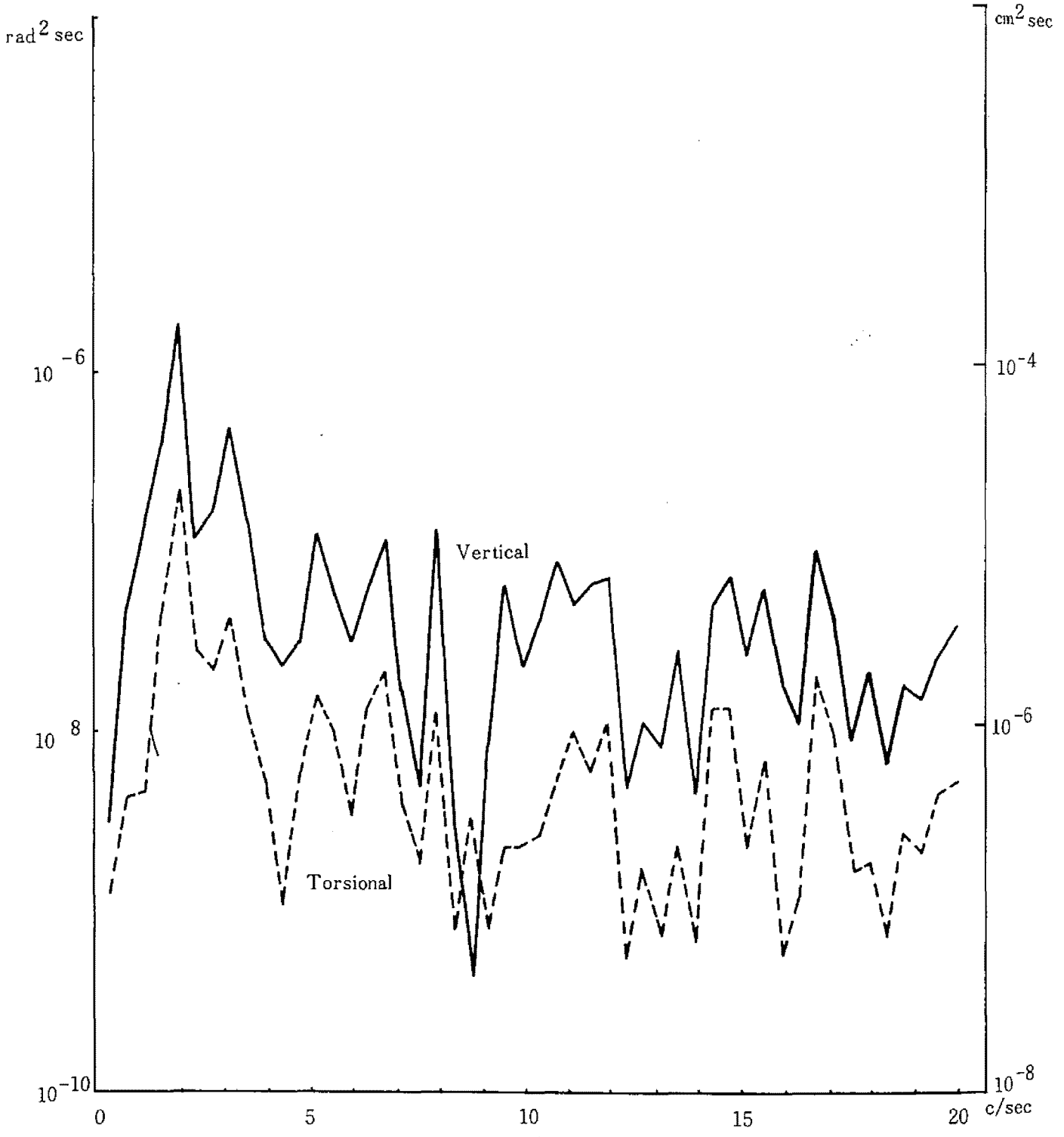

Fig. 4.15(a) Power Spectrum of Model-Response
Model ; Plate
Mesh Size ; 20cm×35cm
Mean Wind Velocity ; 2.00 m/sec

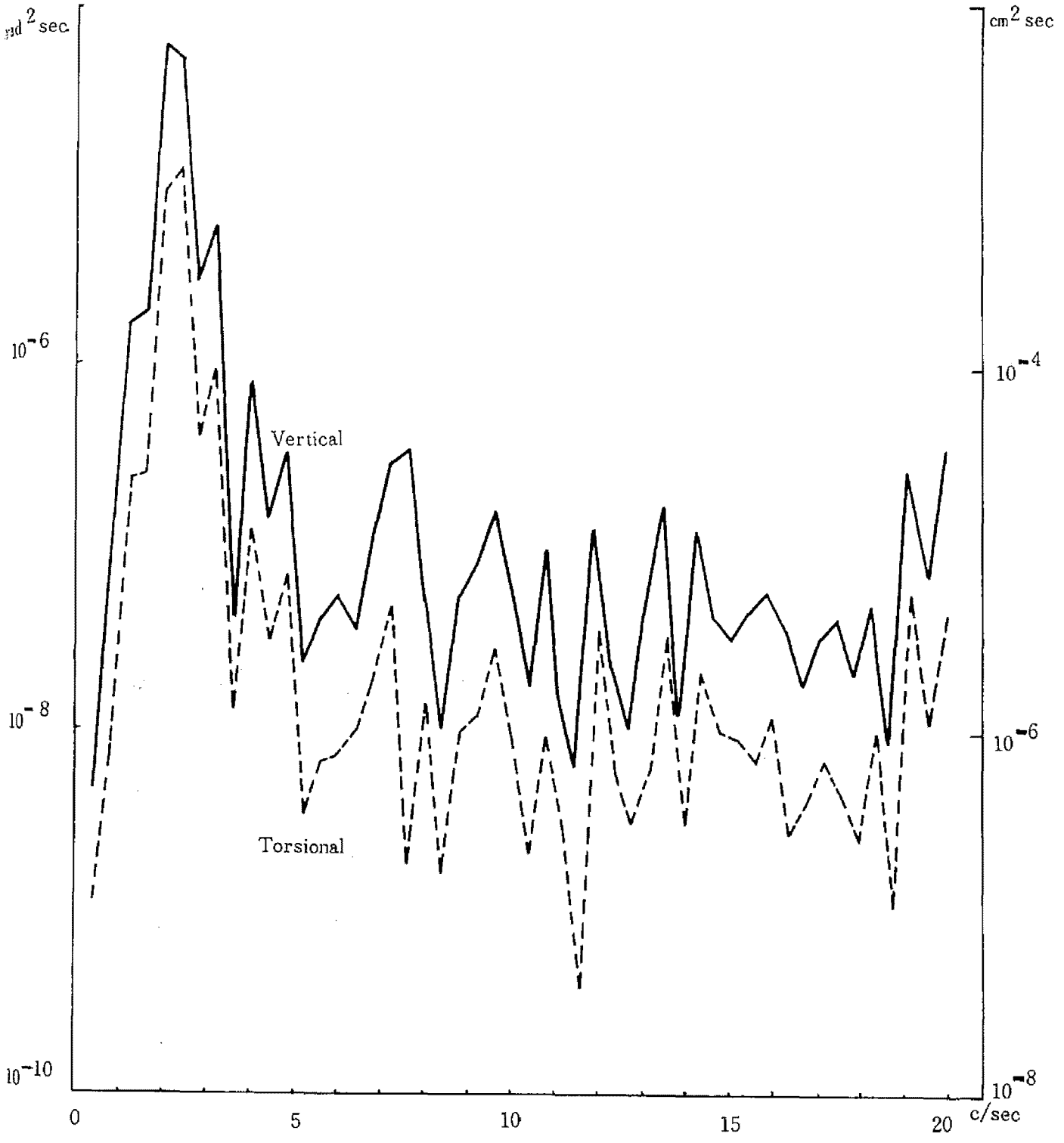

Fig. 4.15(b) Power Spectrum of Model-Response
Model ; Plate
Mesh Size ; 20cm×35cm
Mean_Wind Velocity ; 4.19 m/sec

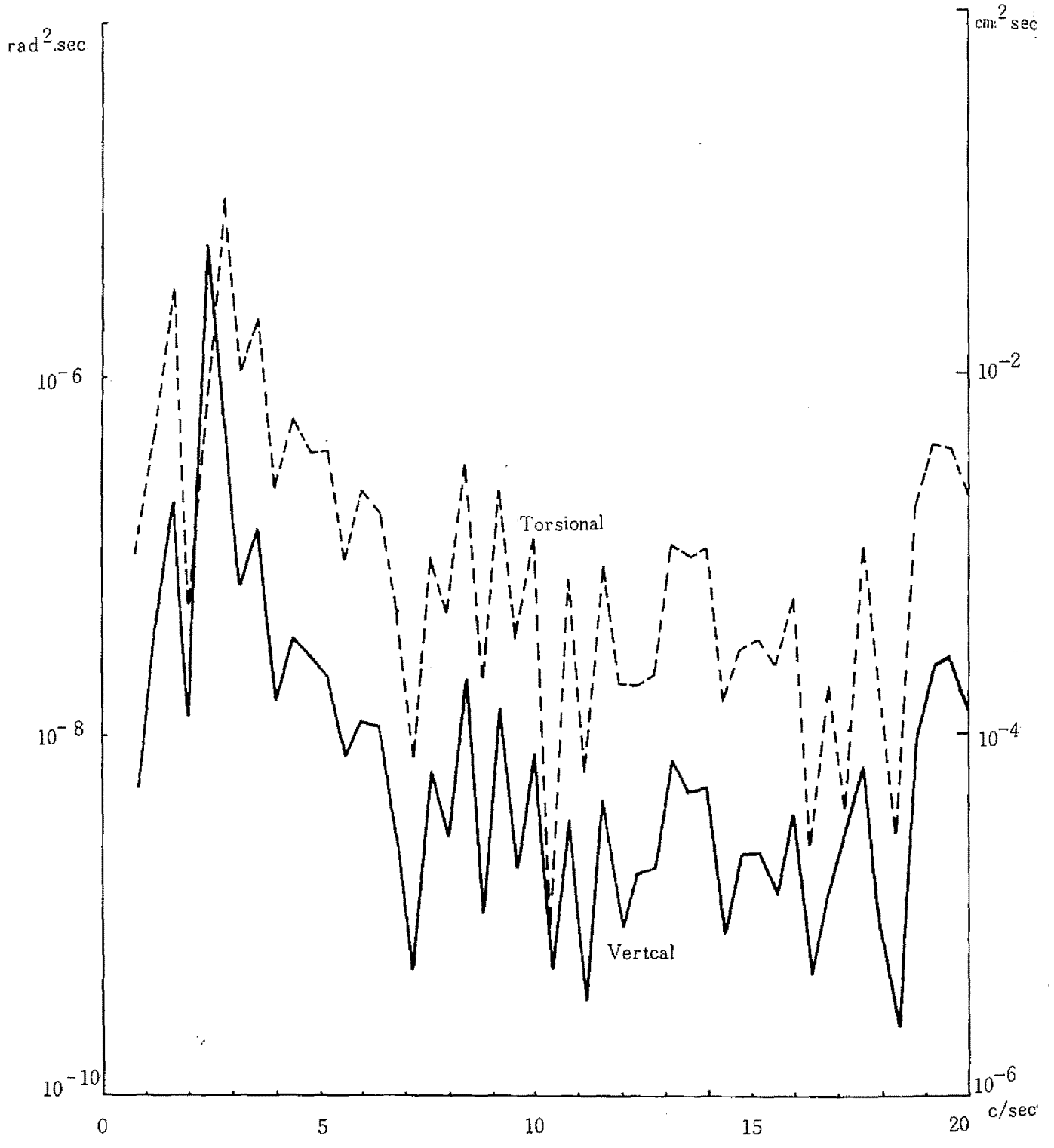

Fig. 4.15(c) Power Spectrum of Model-Response
Model ; Plate
Mesh Size ; 20mm×35cm
Mean wind Velocity ; 7.26m/sec

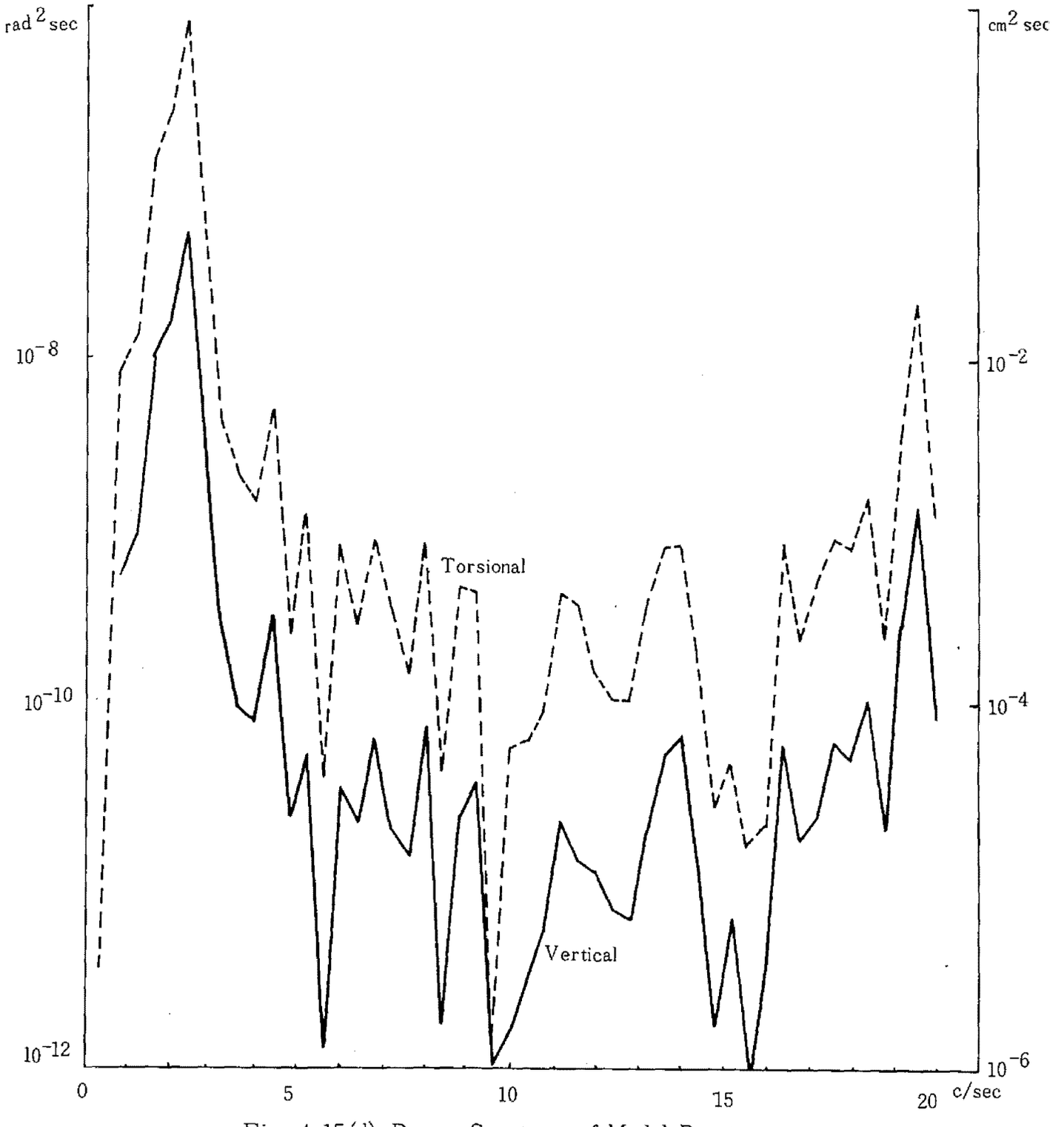

Fig. 4.15(d) Power Spectrum of Model Response
Model ; Plate
Mesh Size ; 20cm×35cm
Mean Wind Velocity ; 9.40 m/sec

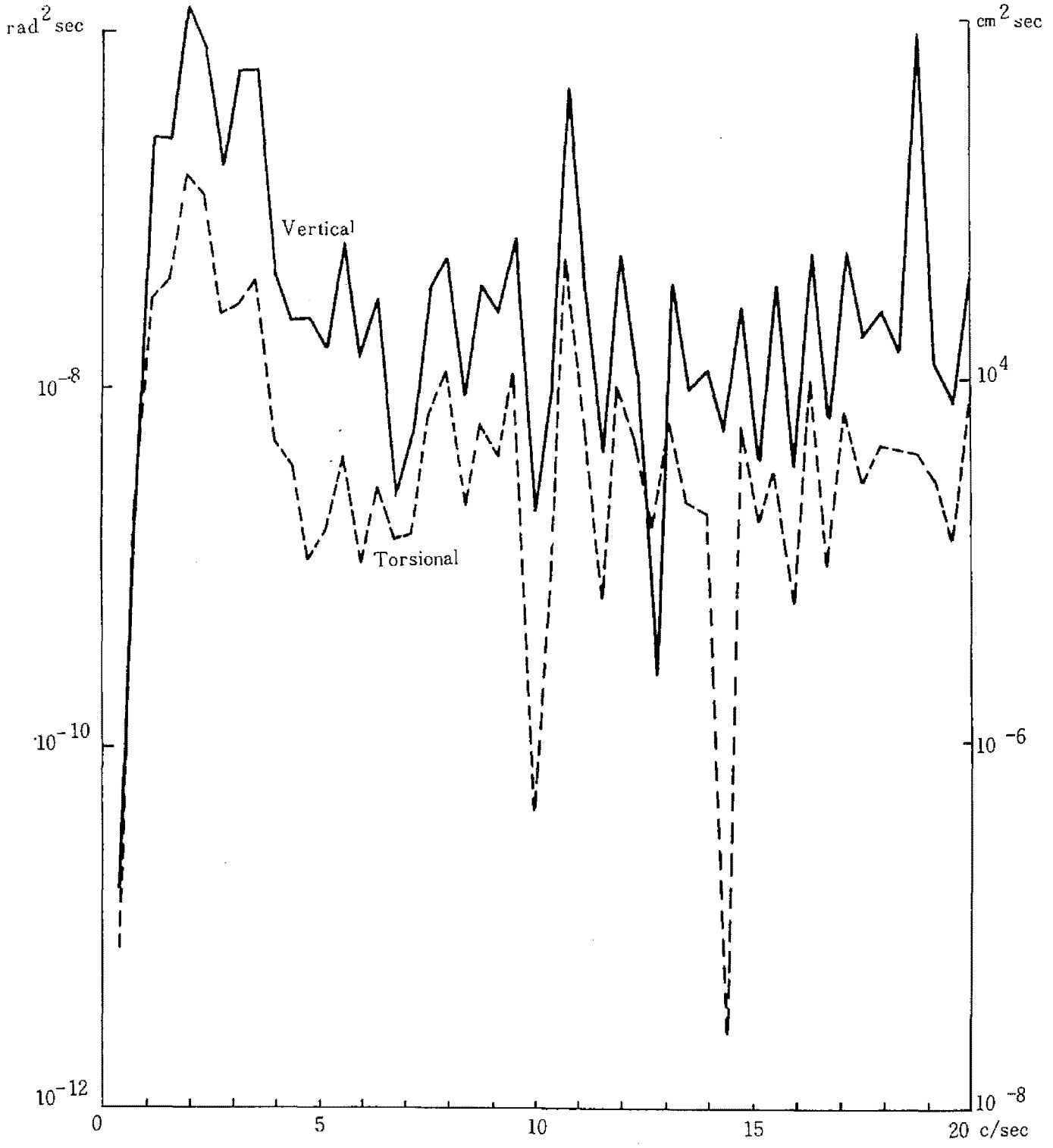

Fig. 4.16(a) Power Spectrum of Model Response
Model ; Plate
Mesh Size ; 20cm×10cm
Mean Wind Velocity ; 2.00m/sec

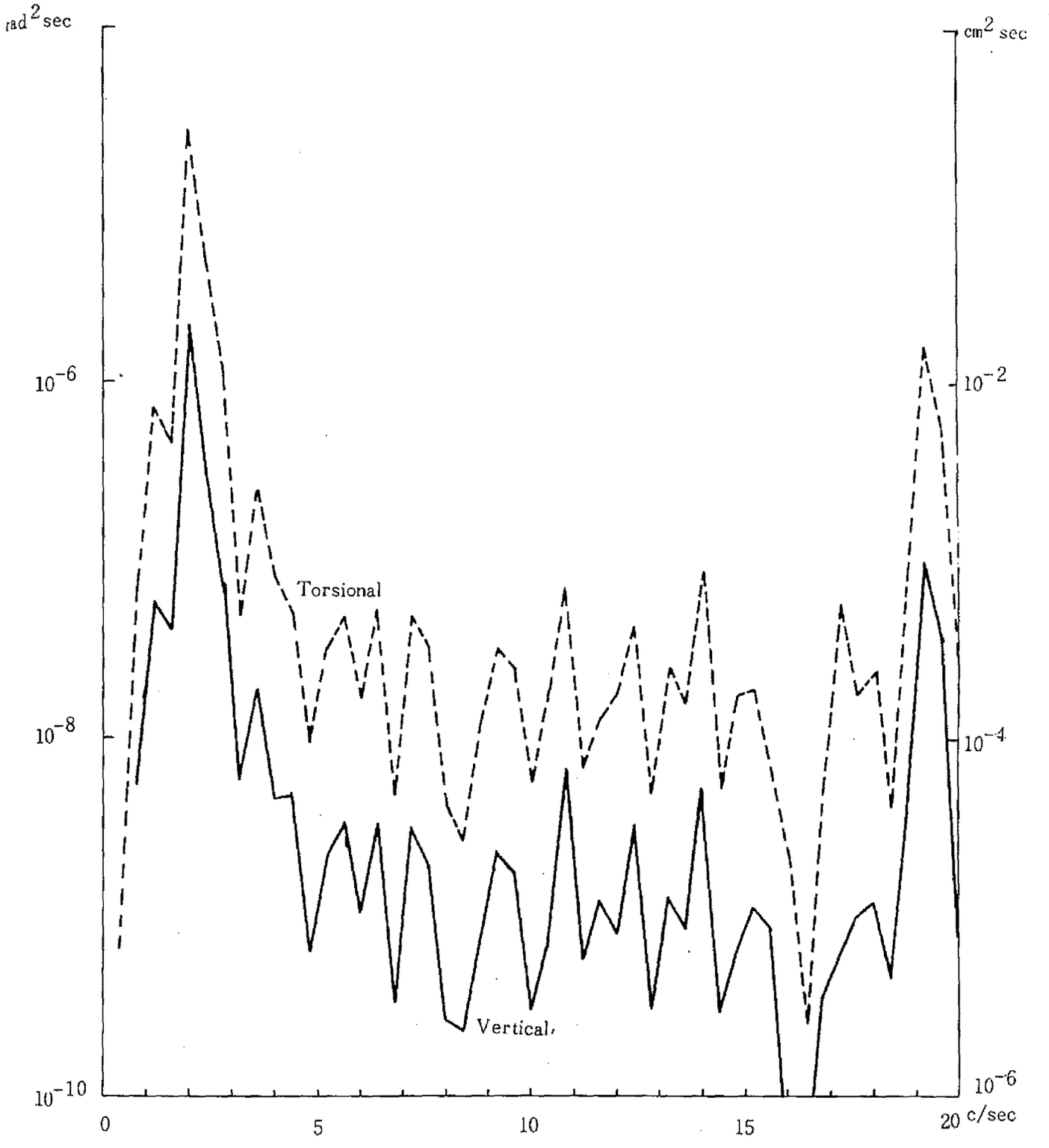

Fig. 4.16(b) Power Spectrum of Model-Responses
Model ; Plate
Mesh Size ; 20cm×10cm
Mean Wind Velocity ; 7.62m/sec

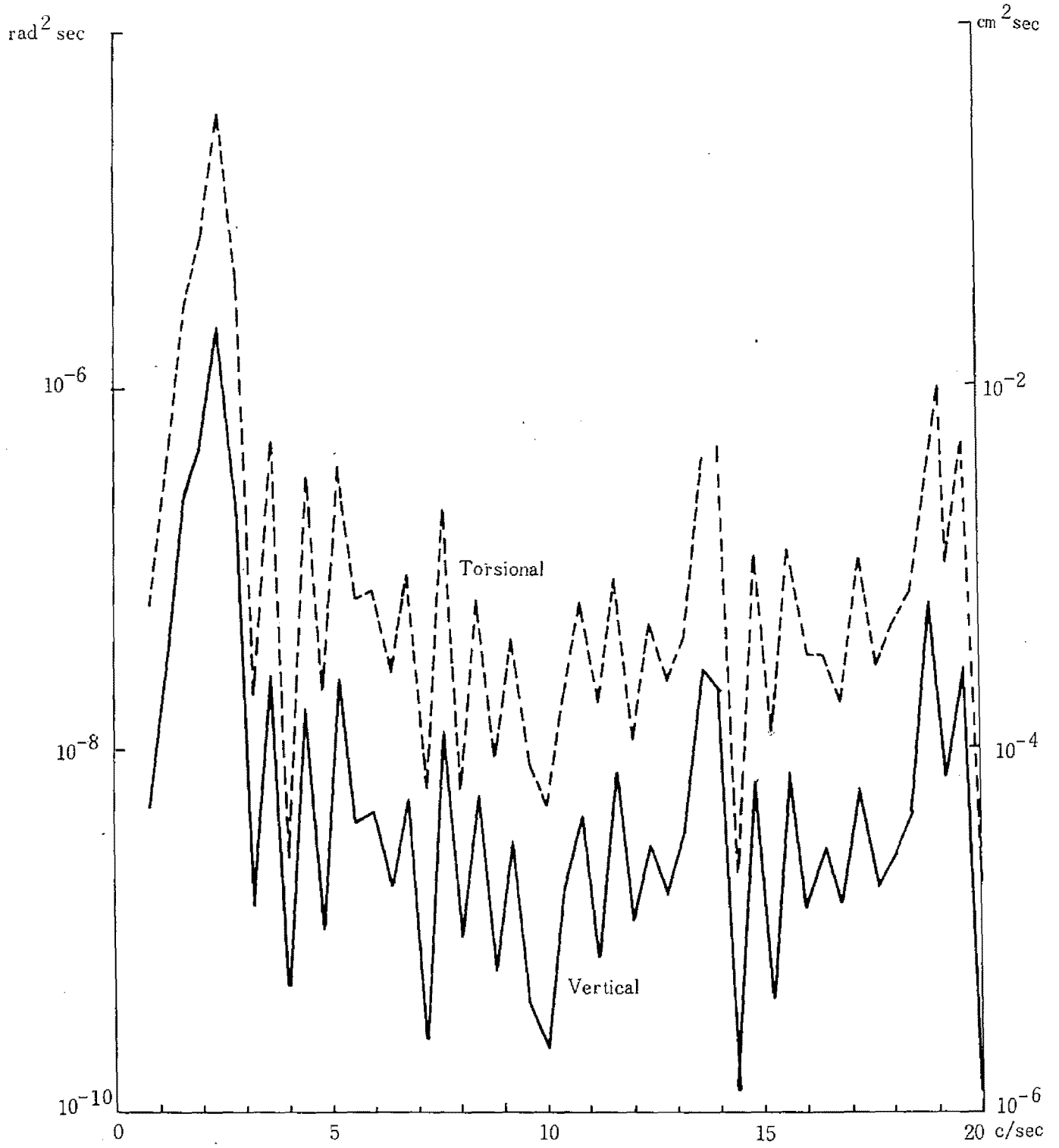

Fig. 4.16(c) Power Spectrum of Model Response
Model ; Plate
Mesh Size ; 10cm×20cm
Mean Wind Velocity ; 9.40 m/sec

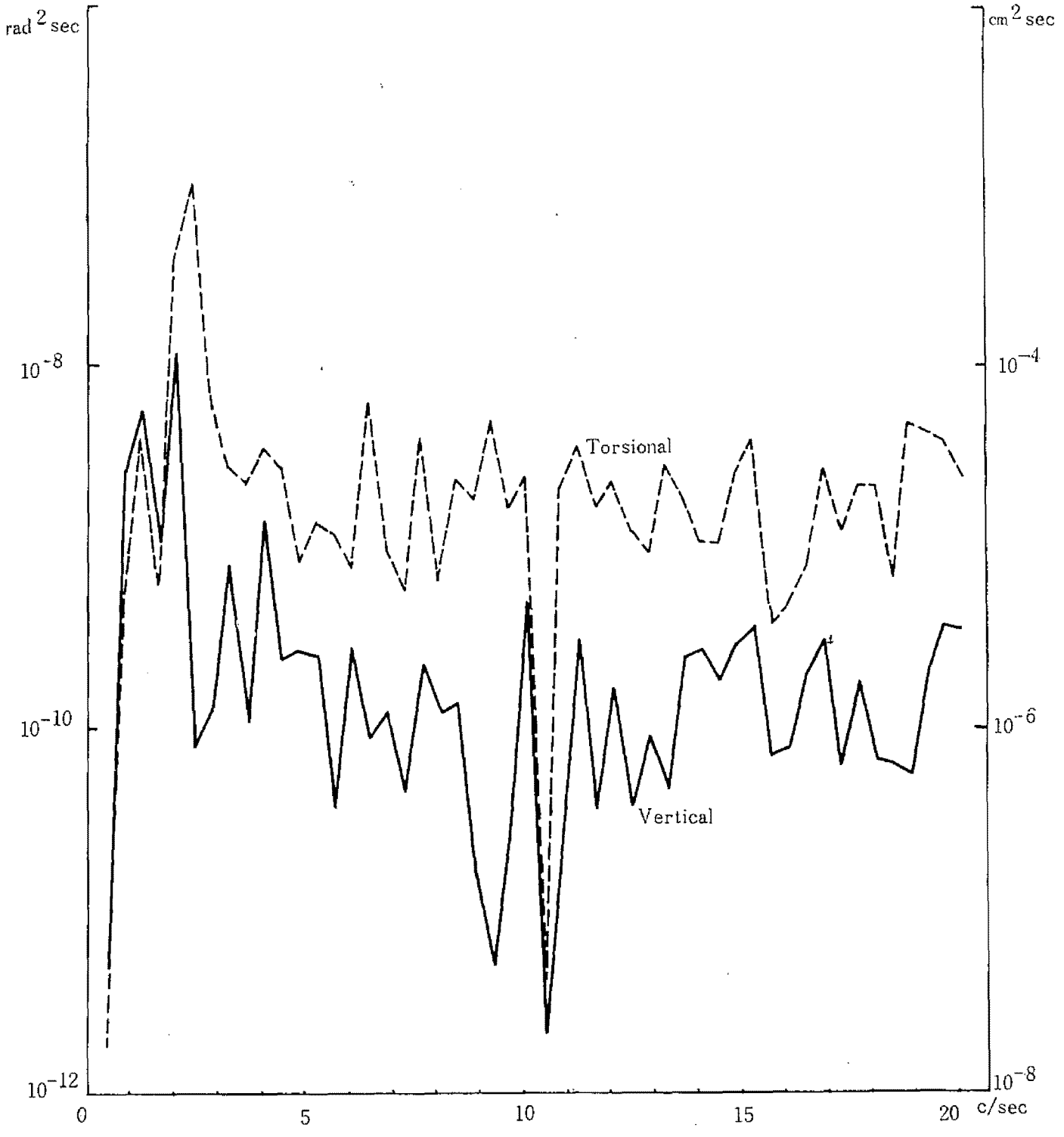

Fig. 4.17(a) Power Spectrum of Model Response
Model ; Truss
Mesh Size ; 40cm×35cm
Mean Wind Velocity ; 2.01 m/sec

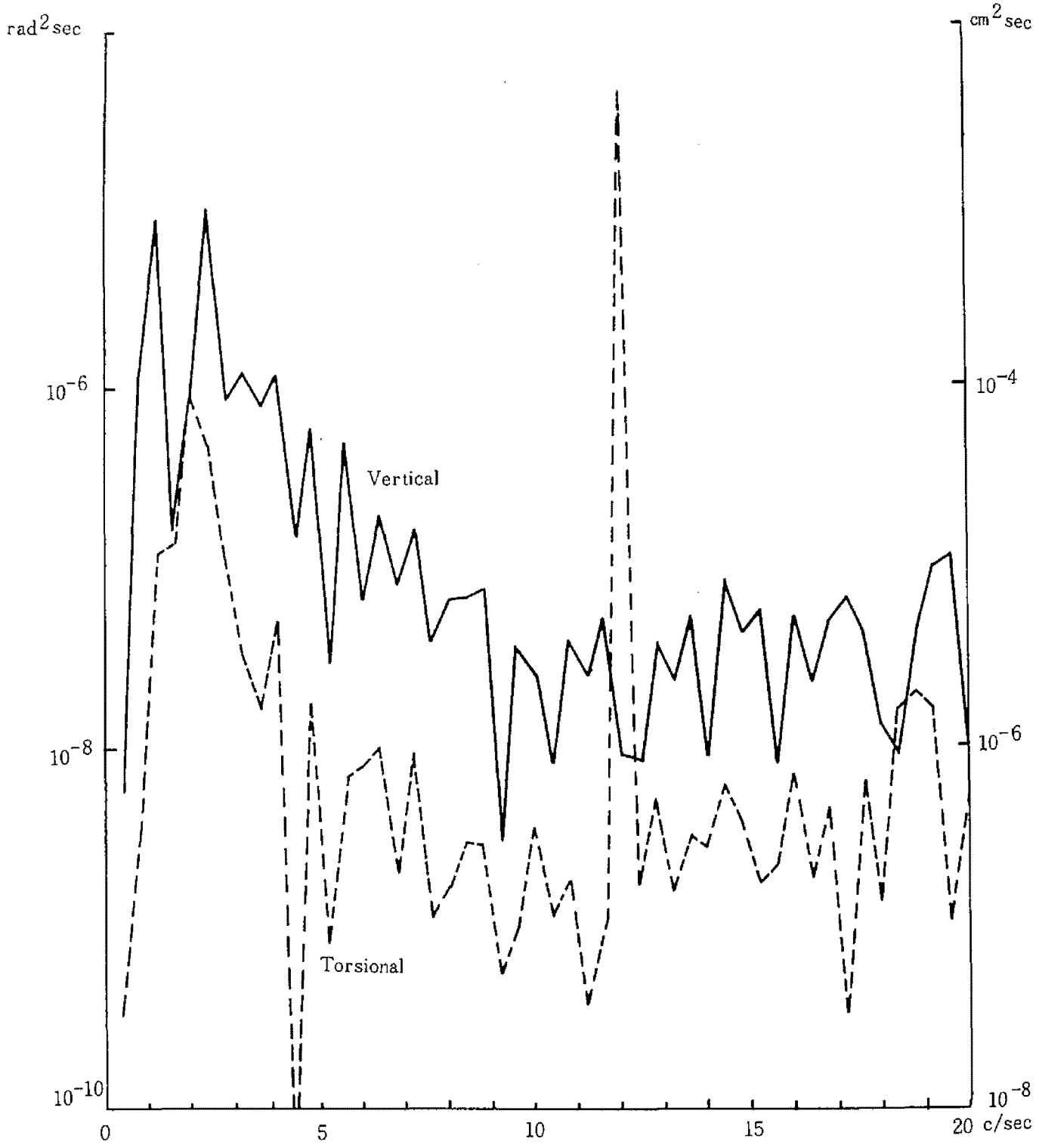

Fig. 4.17(b) Power Spectrum of Model-Response
Model ; Truss
Mesh Size ; 40 cm×35cm
Mean Wind Velocity ; 5.09m/sec

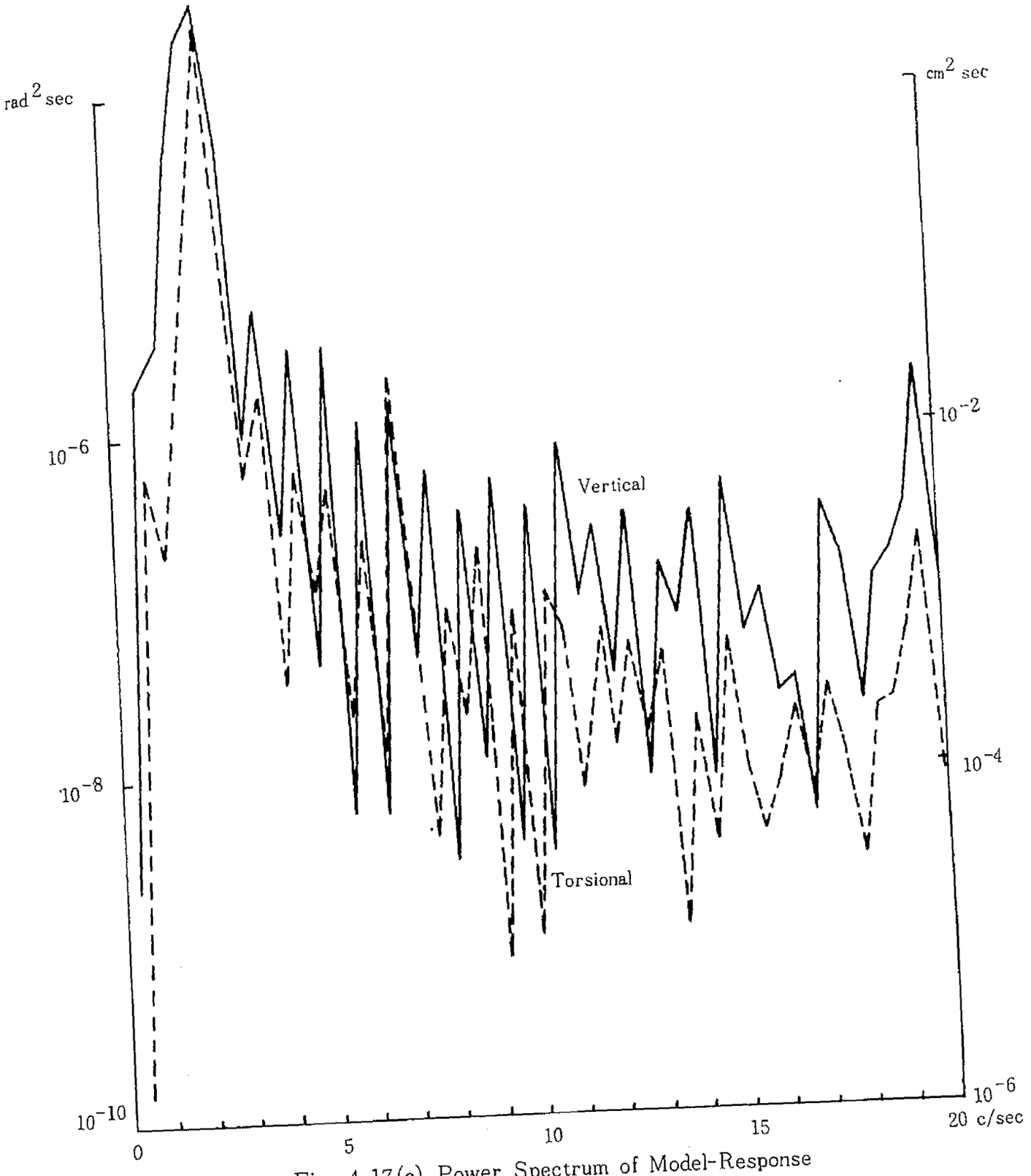

Fig. 4.17(c) Power Spectrum of Model-Response
Model ; Truss
Mesh Size ; 40cm×35cm
Mean Wind Velocity ; 7.02m/sec

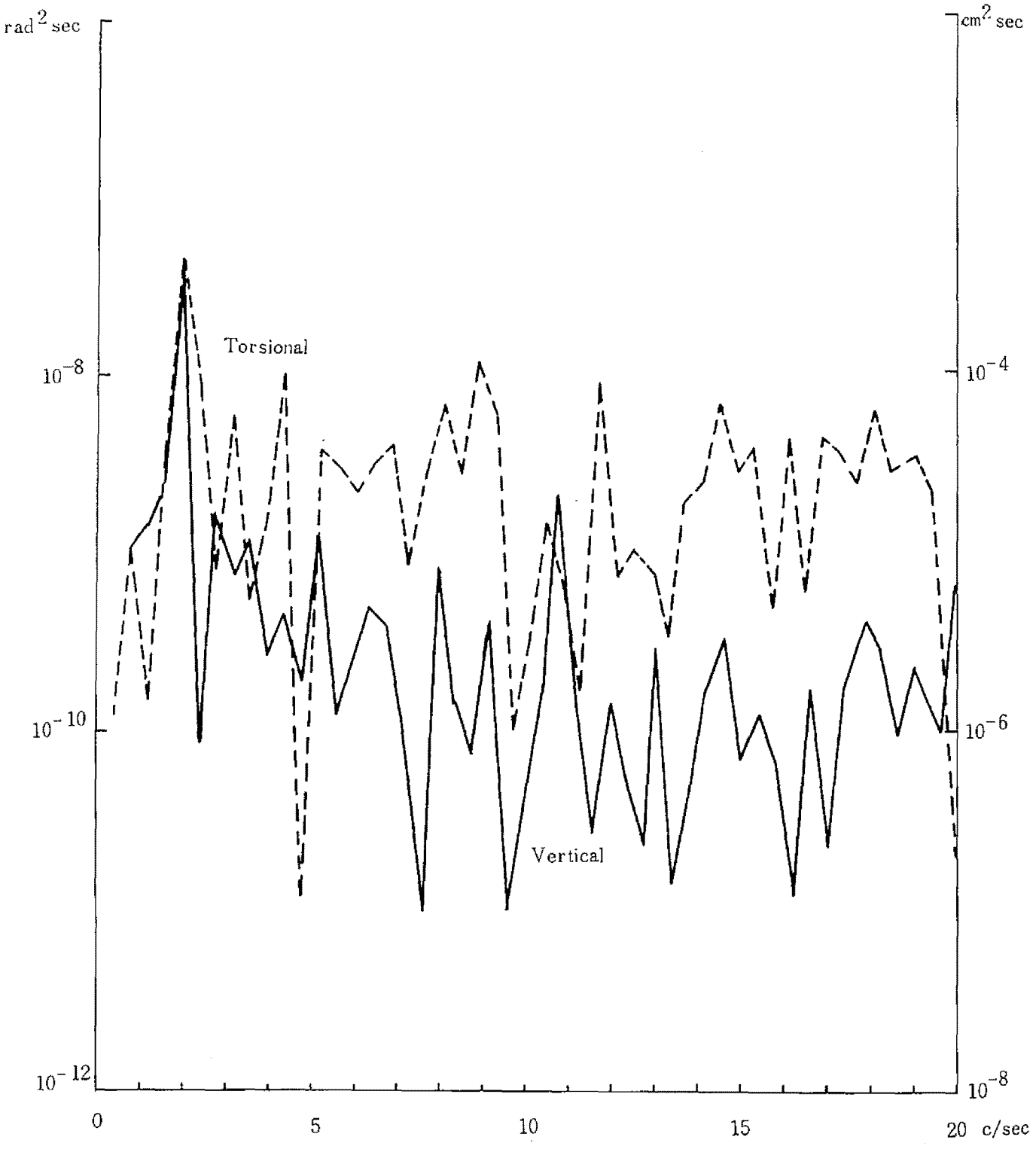

Fig. 4.18(a) Power Spectrum of Model-Response
Model ; Truss
Mesh Size ; 20cm×35cm
Mean Wind Velocity ; 2.01m/sec

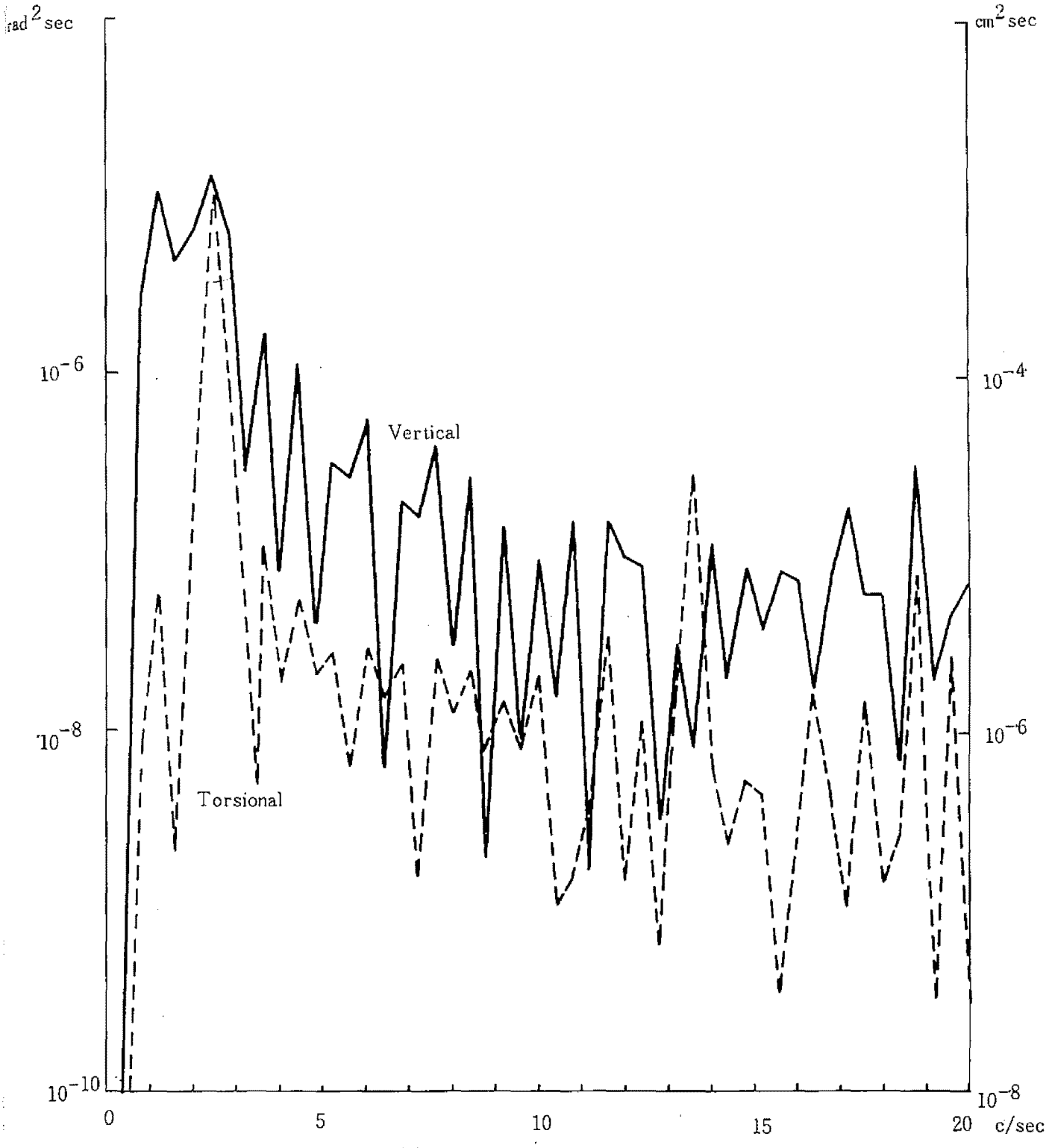

Fig. 4.18(b) Model ; Truss
Mesh Size ; 20cm×35cm
Mean Wind Velocity ; 5.09m/sec

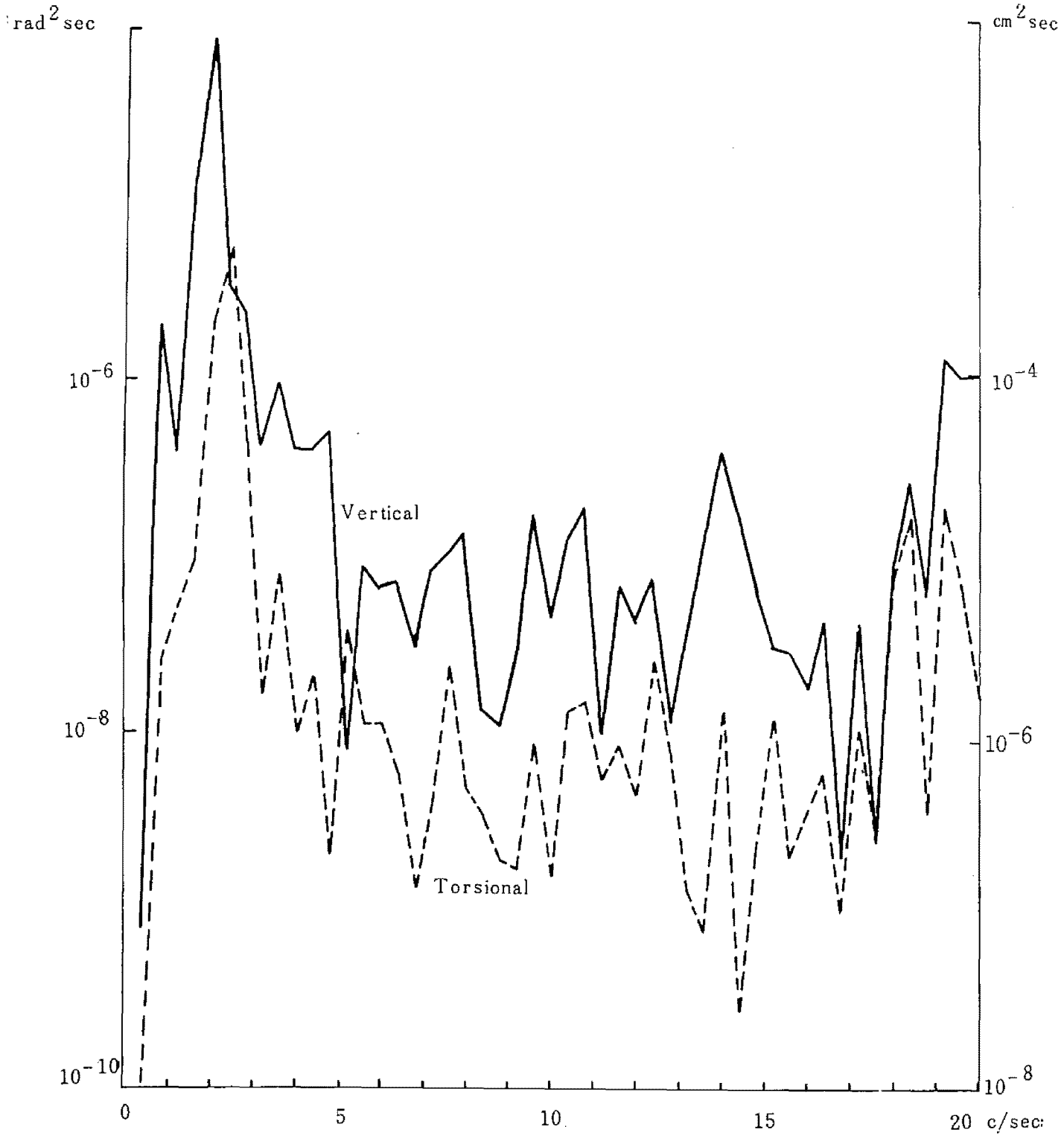

Fig. 4.18(c) Power Spectrum of Model-Response
Model ; Truss
Mesh Size ; 20cm×35cm
Mean Wind Velocity ; 7.02m/sec

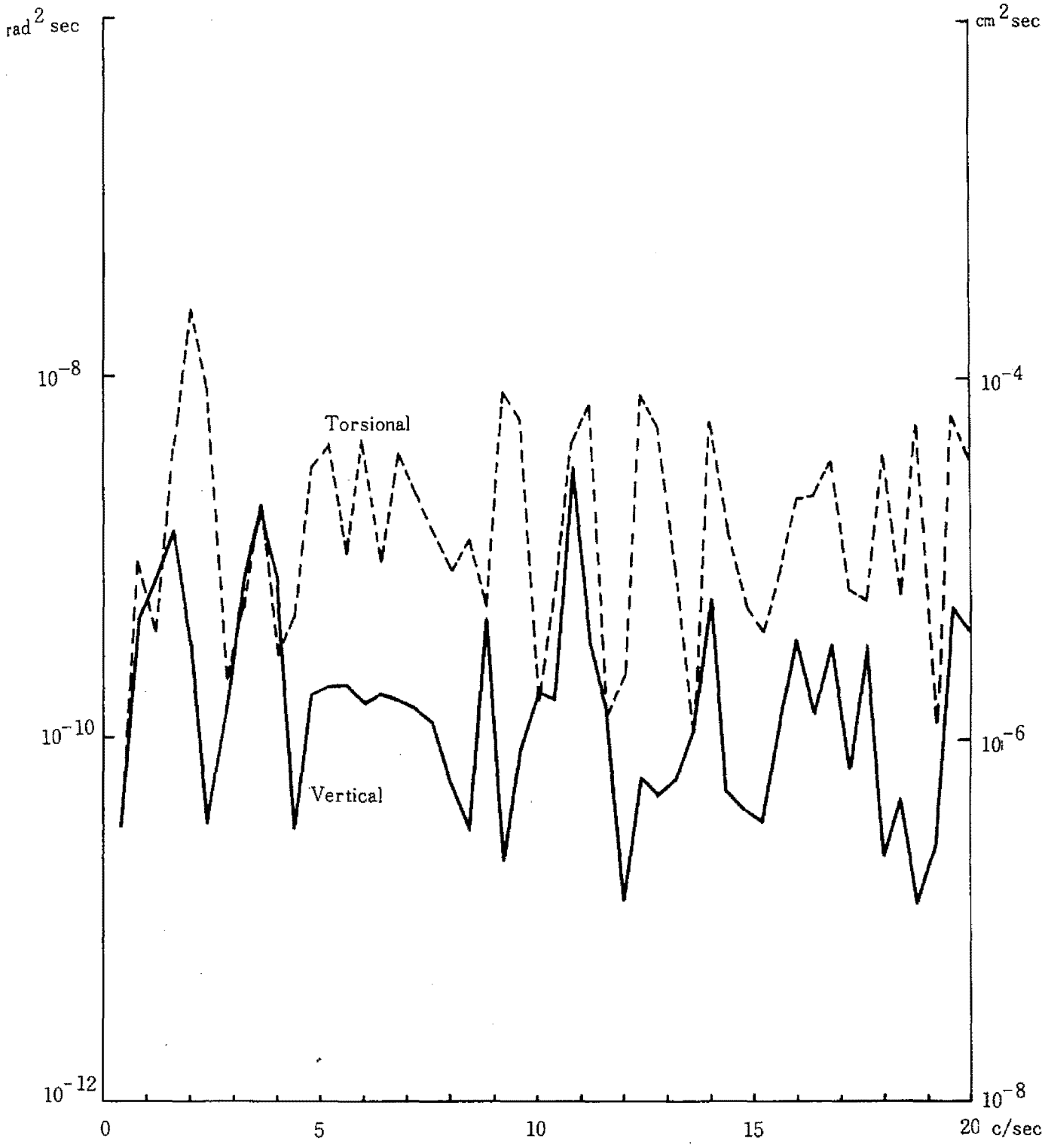

Fig. 4.19(a) Power Spectrum of Model-Response
Mesh Size ; 20cm×10cm
Mean Wind Velocity ; 2.01m/sec
Model Truss

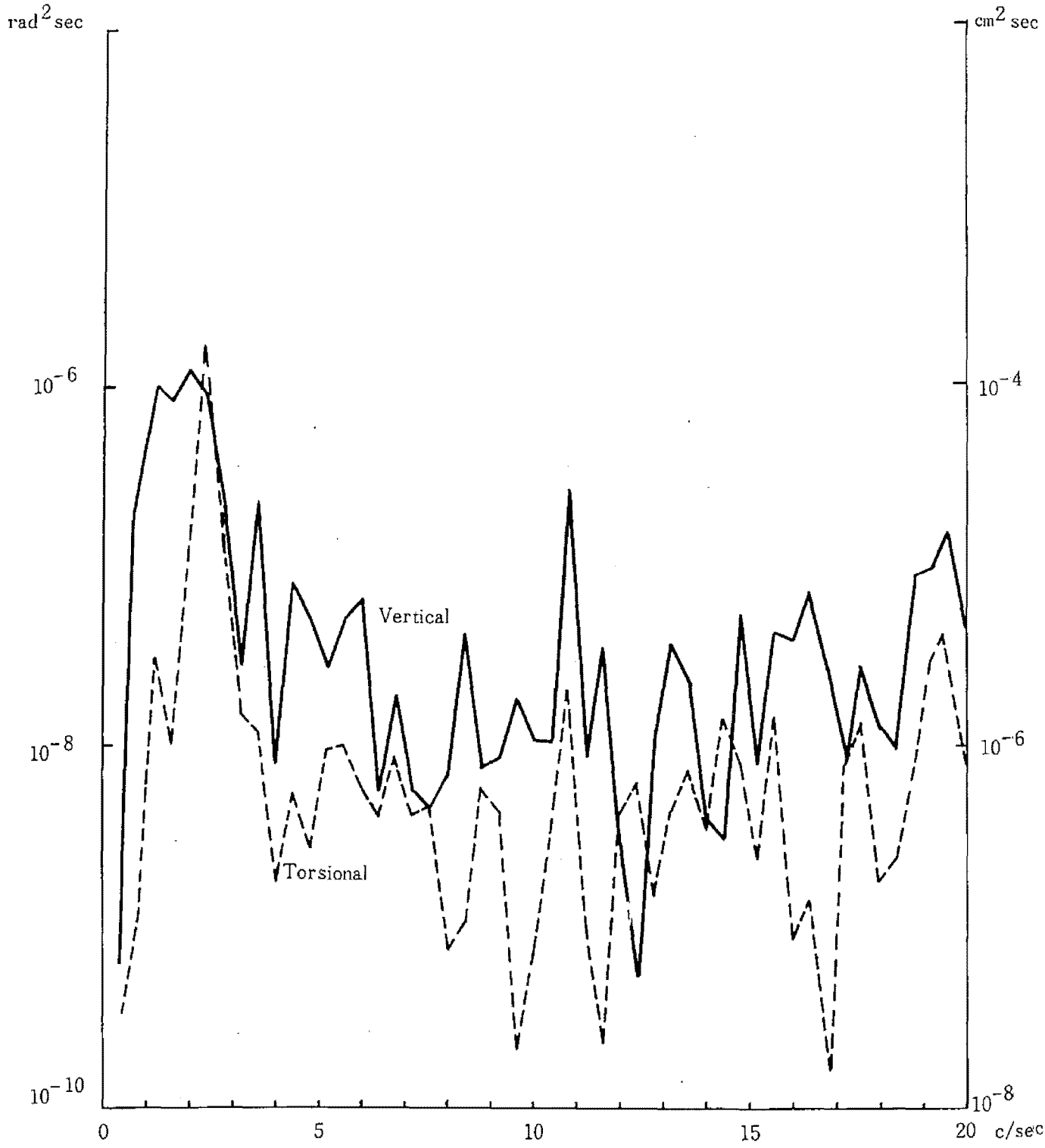

Fig. 4.19(b) Power Spectrum of Model-Response
Mesh Size ; 20cm×10cm
Model ; Truss
Mean Wind Velocity ; 5.09m/sec

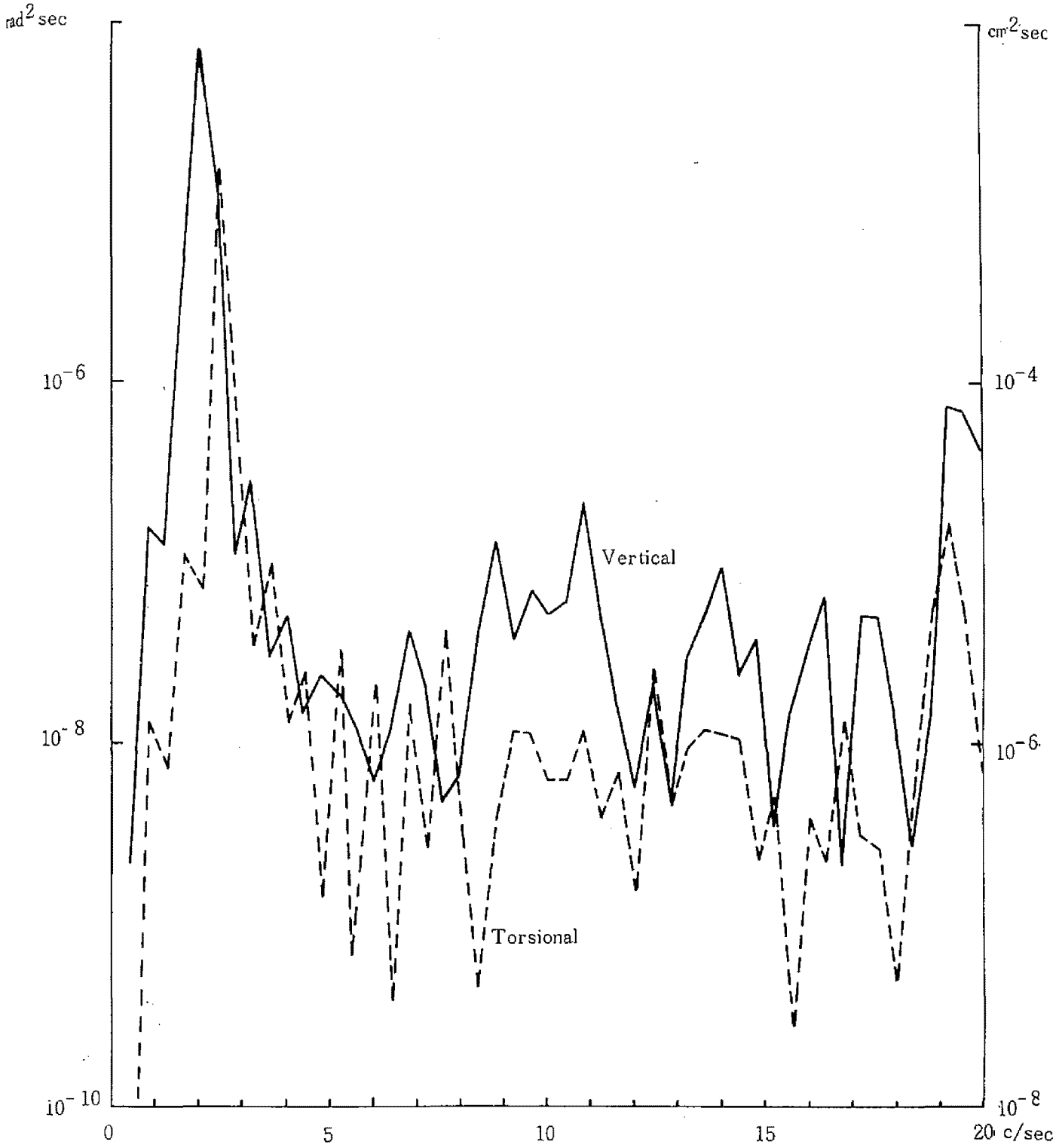

Fig. 4.19(c) Model; Truss
Mesh Size ; 20cm×10cm
Mean Wind Velocity ; 7.20 m/sec

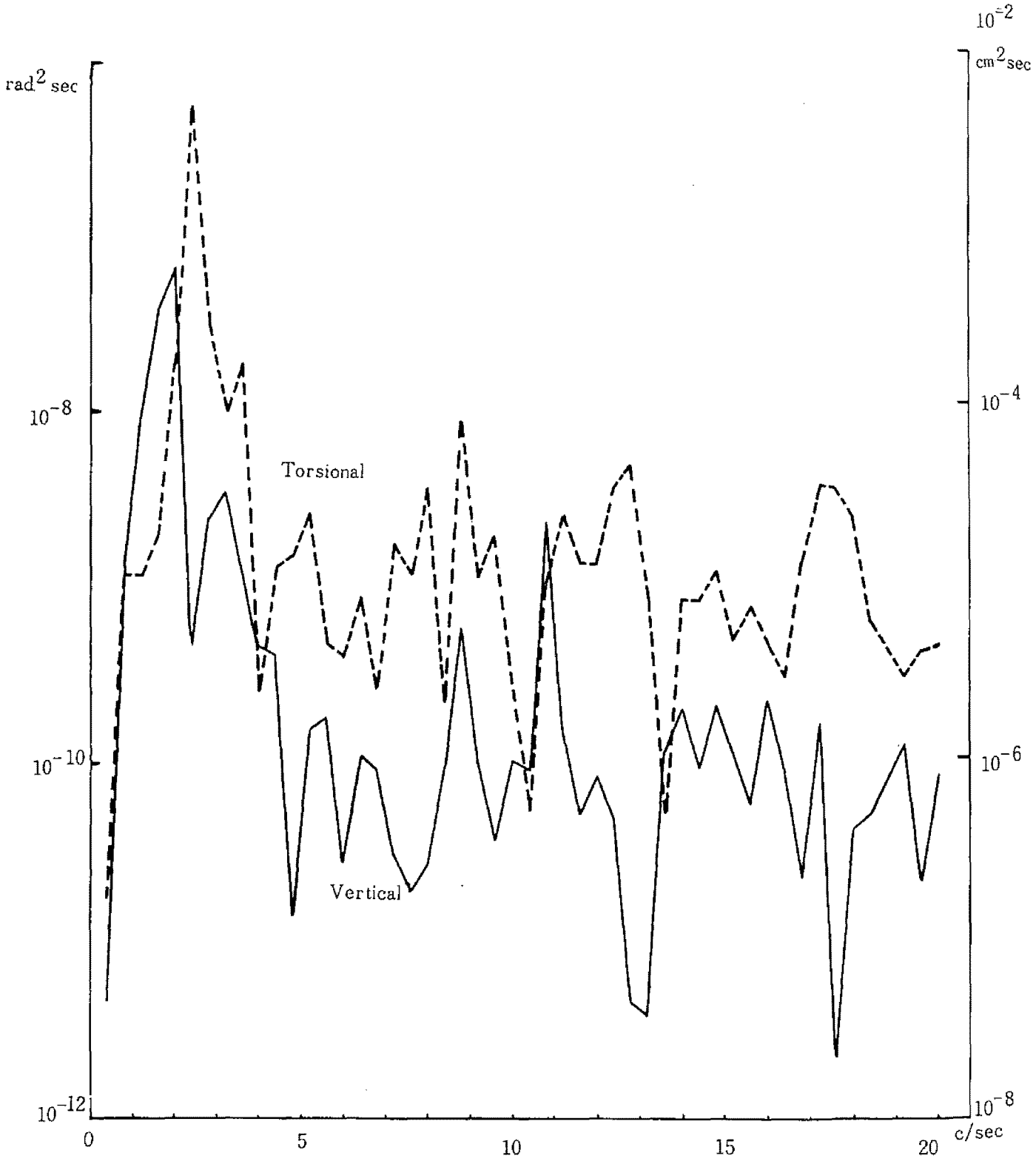

Fig. 4.20(a) Power Spectrum of Model-Response
Model ; H-Section
Mesh Size ; 40cm×35cm
Mean Wind Velocity ; 2.01m/sec

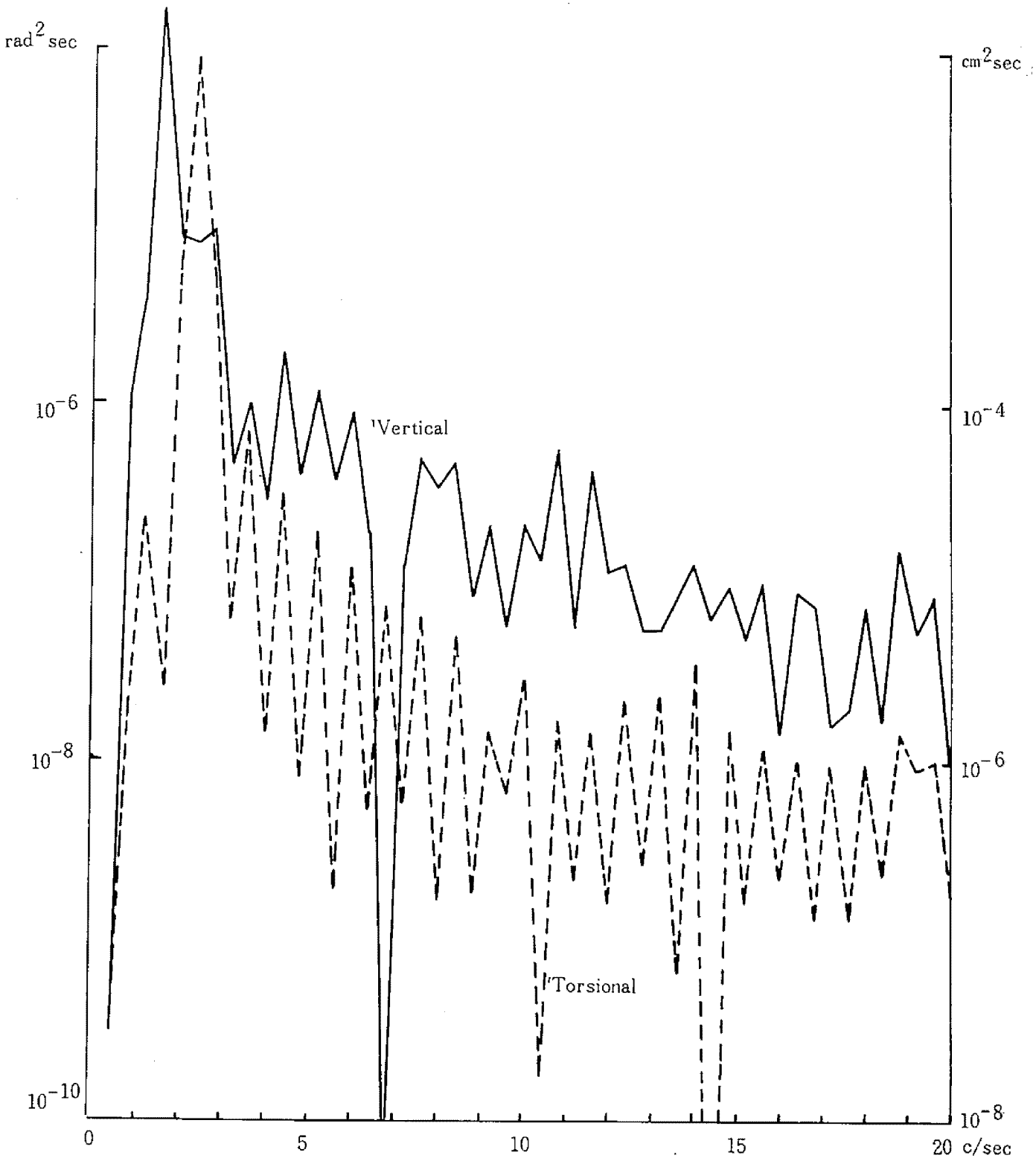

Fig. 4.20(b) Power Spectrum of Model-Response
Model ; H-section
Mesh Size ; 40cm×35cm
Mean Wind Velocity ; 3.24 m/sec

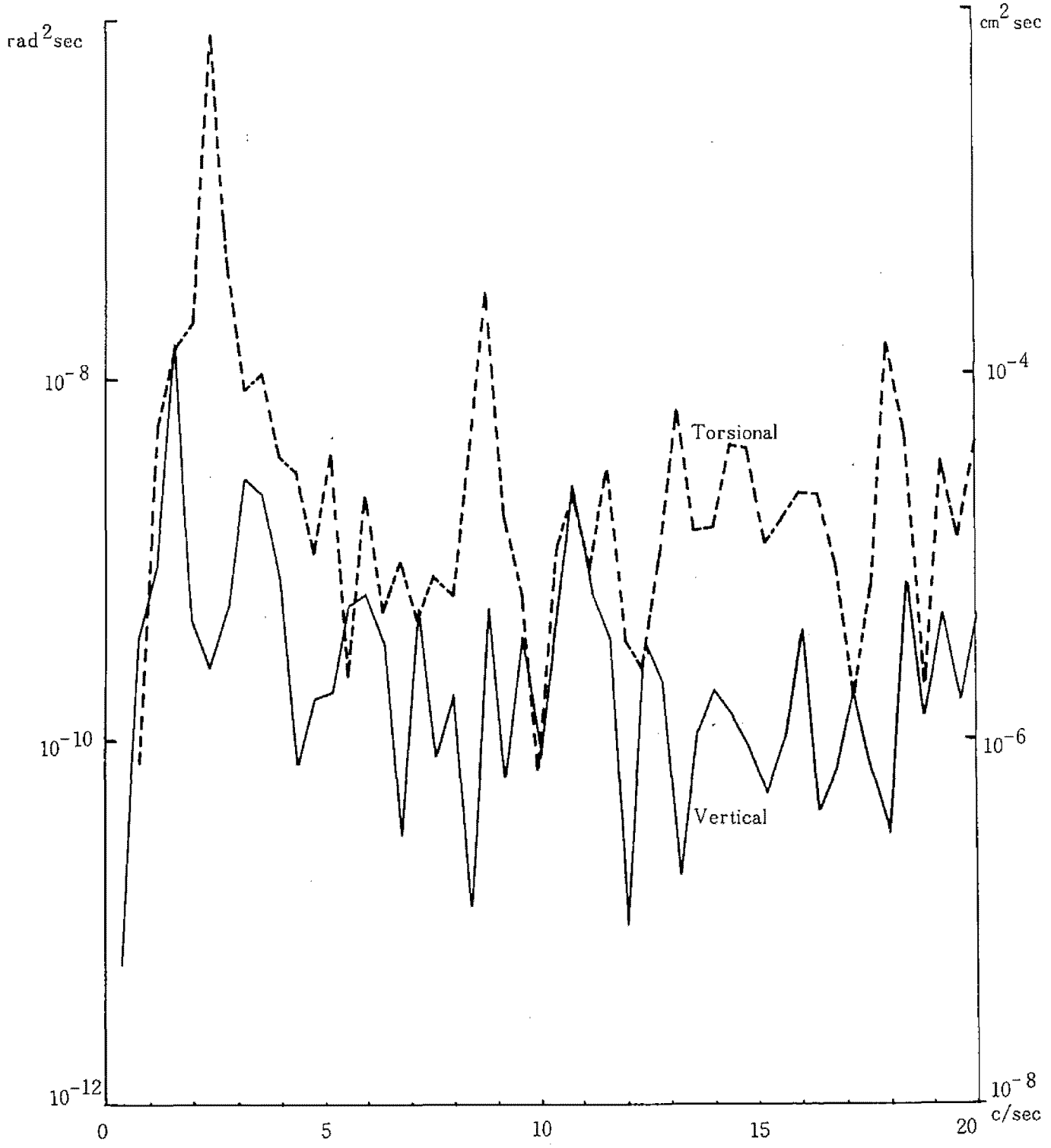

Fig. 4.21(a) Power Spectrum of Model Response
Model ; H-section
Mesh Size ; 20cm×35cm
Mean Wind Velocity ; 2.09m/sec

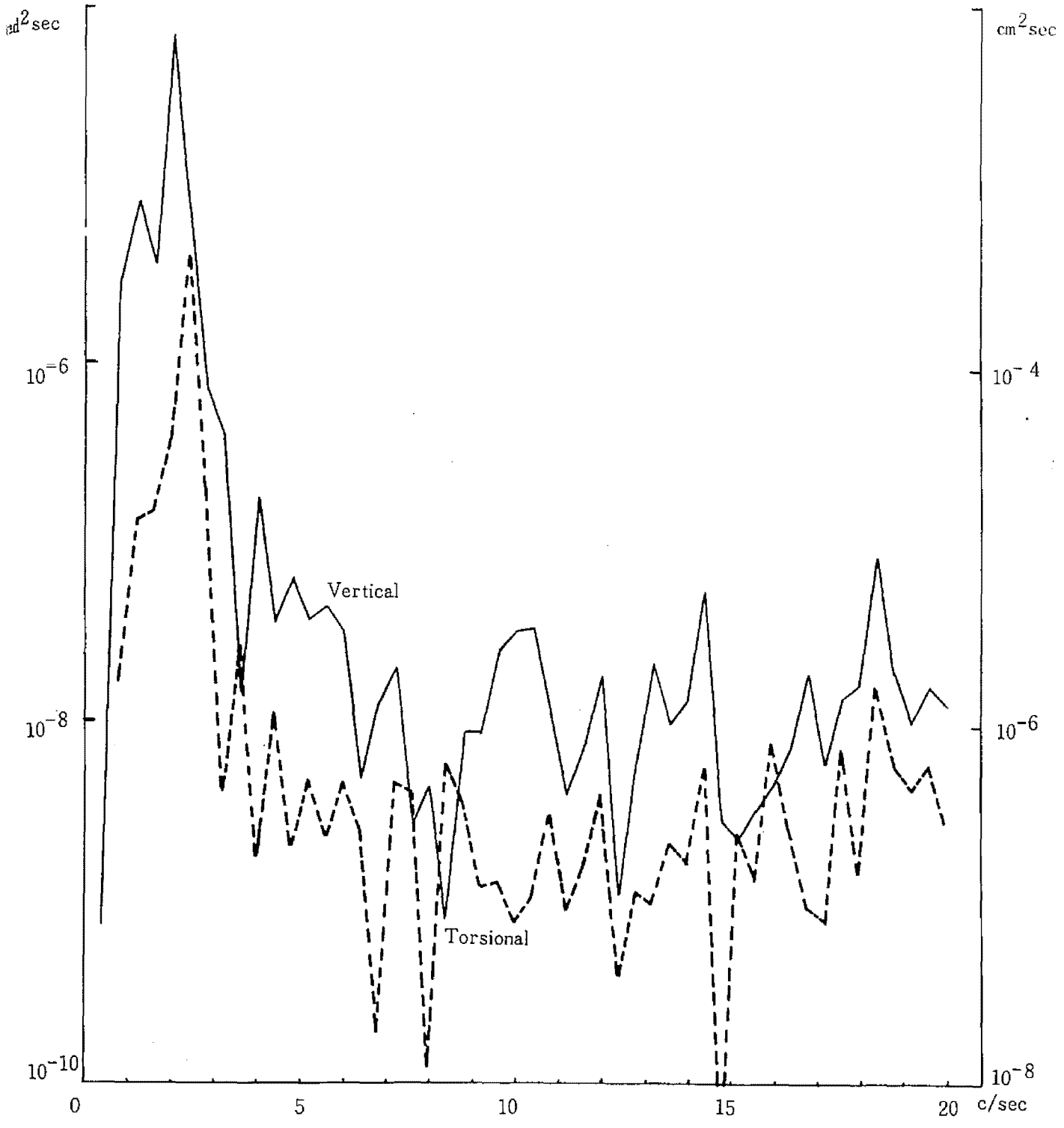

Fig. 4.21(b) Power Spectrum of Model-Response
Mocdel ; H-section
Mesh Size ; 20cm×35cm
Mean Wind velocity ; 3.24m/sec

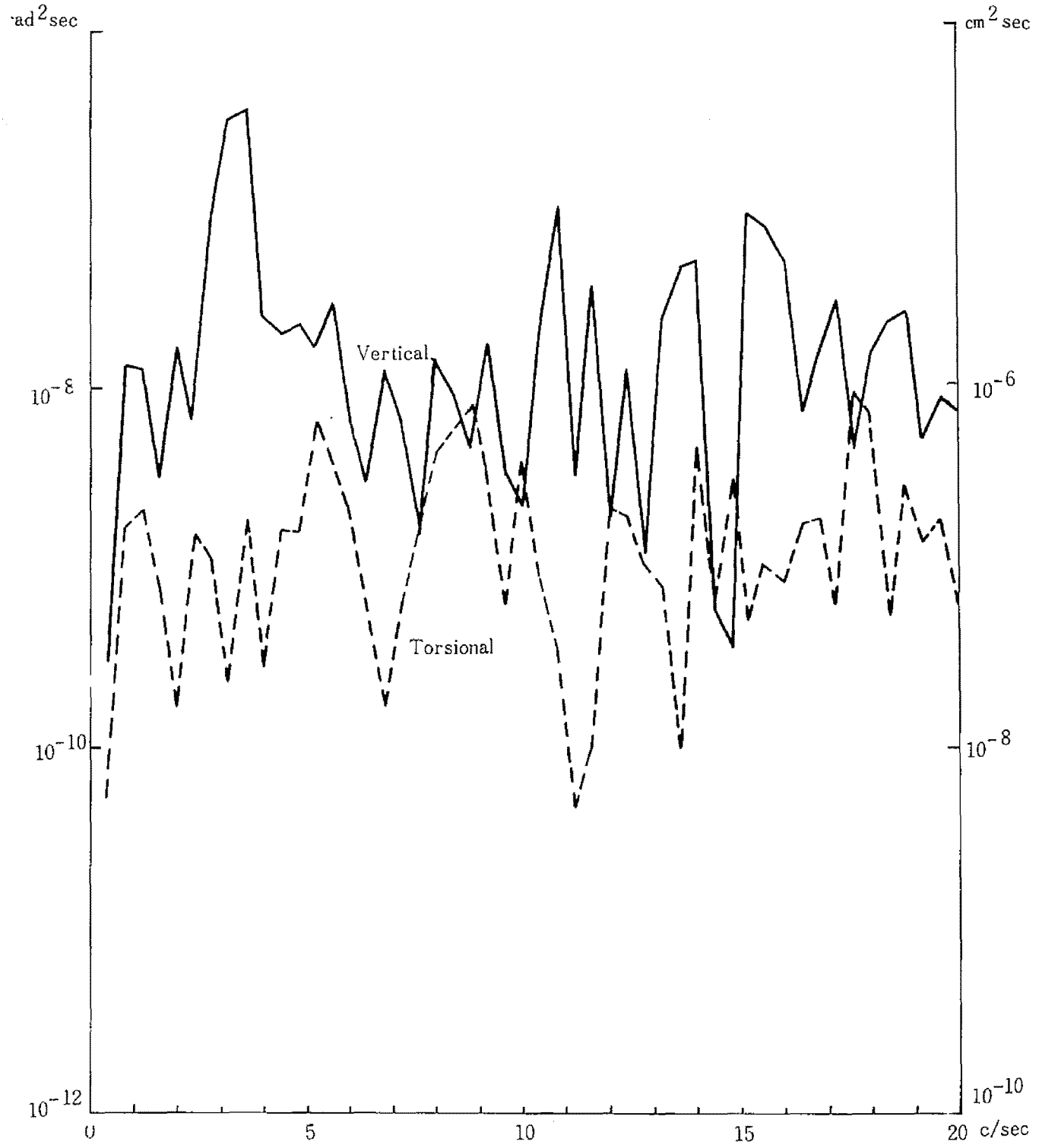

Fig. 4.22(a) Model ; H-section
Mesh Size ; 20cm×10cm
Mean Wind Velocity ; 2.01m/sec

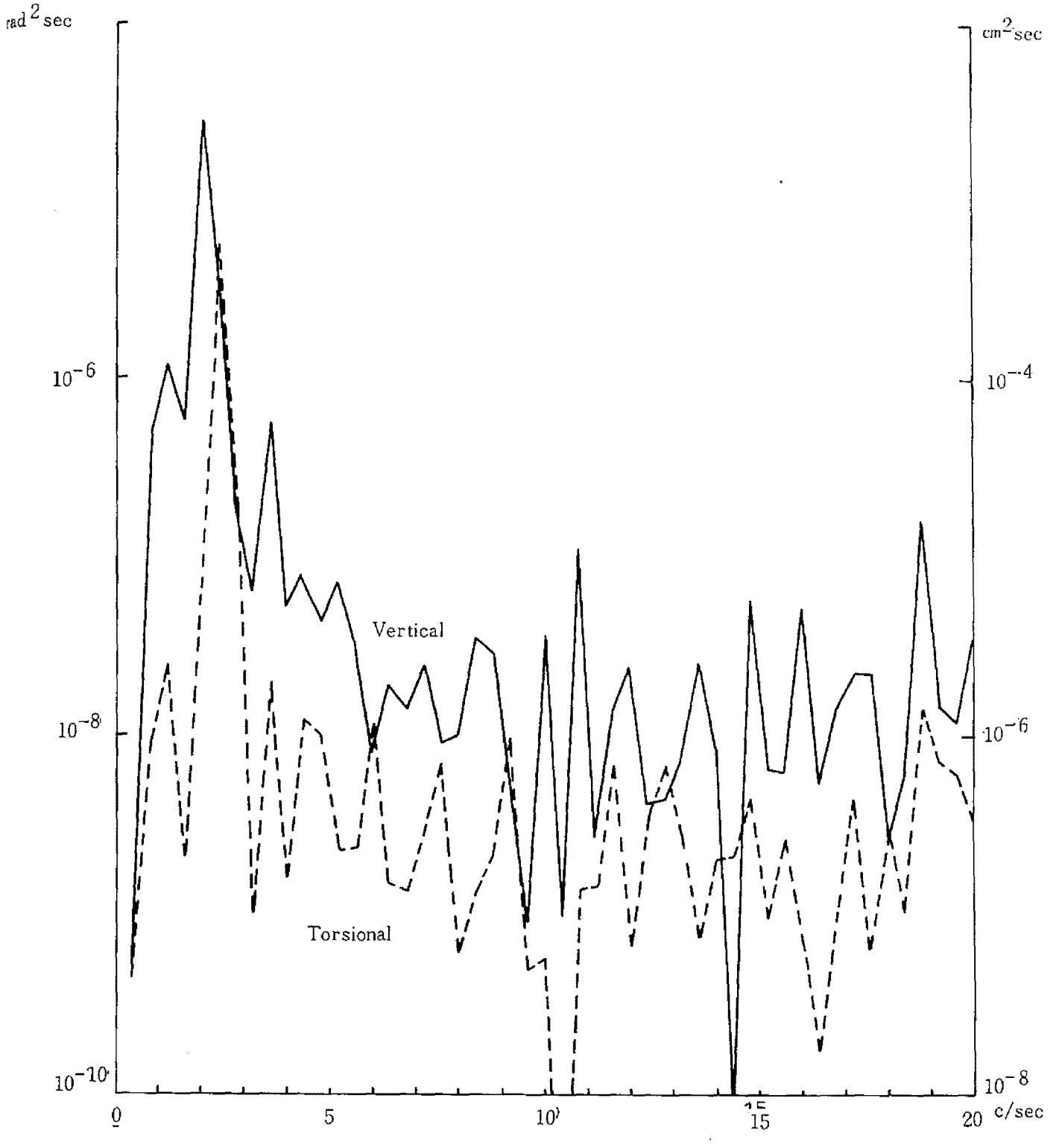

Fig. 4.22(b) Power Spectrum of Model-Respones
Model ; H-section
Mesh Size ; 20cm×10cm
Mean Wind Velocity ; 3.24m/sec

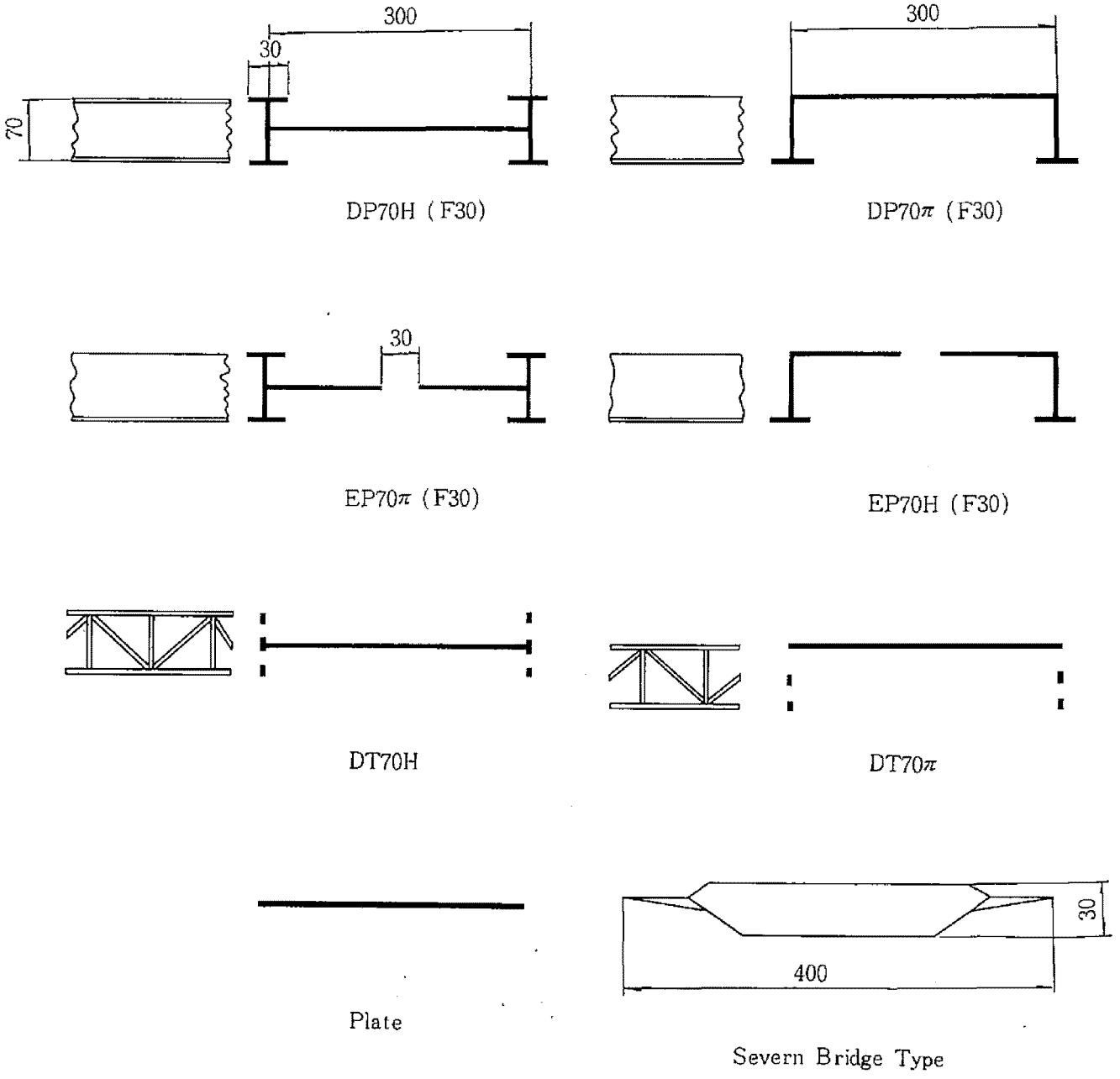

Fig. 4.23 Model Configuration

Fig. 4.24 Response-Reduced Velocity Relation
in Turbulent Flow

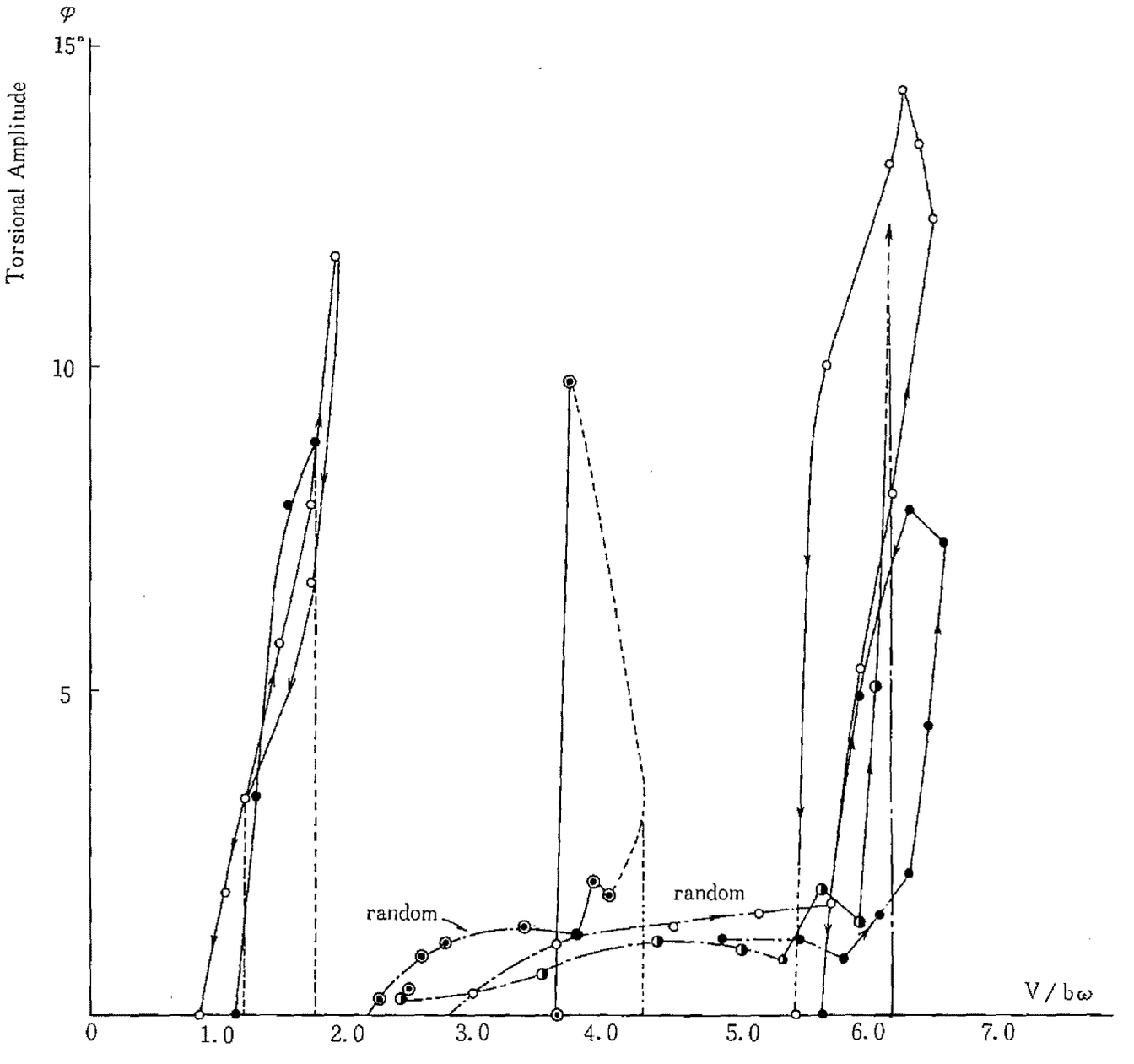

○ EP70H (F30) ($\omega_\alpha / \omega_\eta = 1.625$)

● DP70H (F30) ($\omega_\alpha / \omega_\eta = 1.636$)

◉ Severn Type ($\omega_\alpha / \omega_\eta = 1.545$)

◑ Plate ($\omega_\alpha / \omega_\eta = 1.54$)

○ DT70H (F30) ($\omega_\alpha / \omega_\eta = 1.623$)

● DT70π (F30) ($\omega_\alpha / \omega_\eta = 1.630$)

Fig. 4.25 Response-Reduced Velocity Relation in Uniform Flow

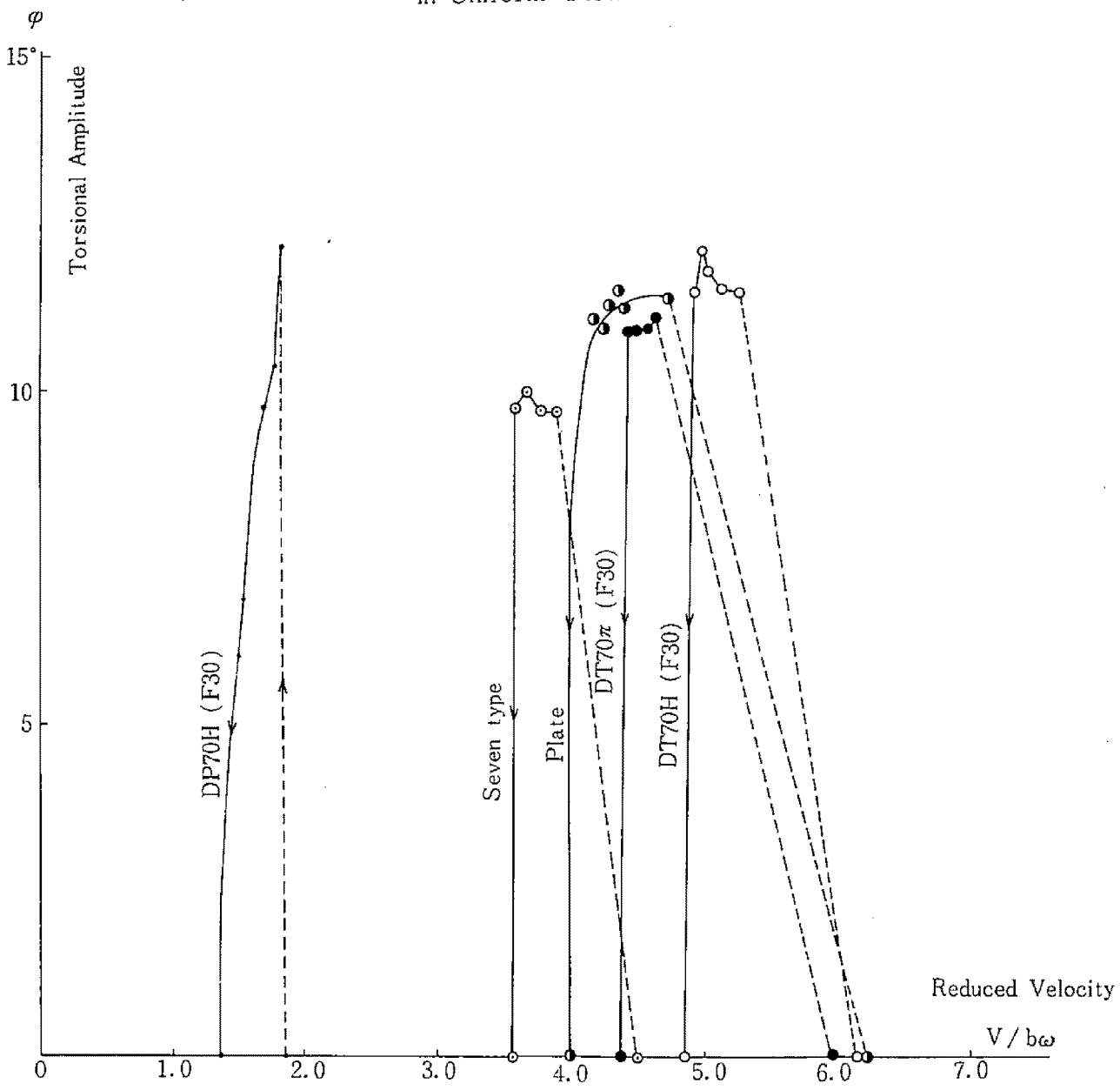

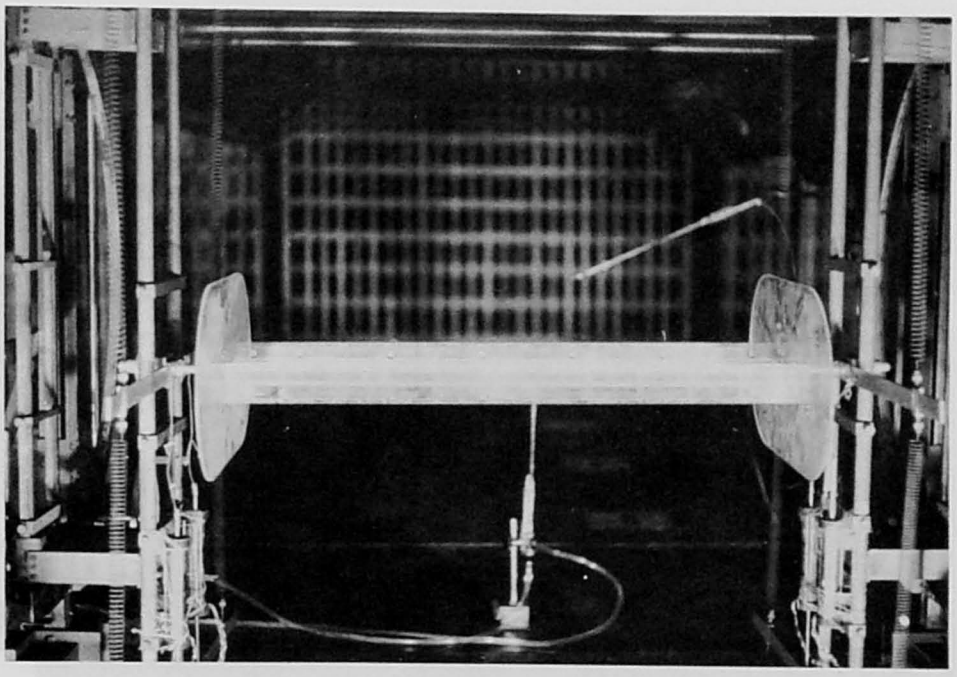

Photo 4.1 Model DP70H

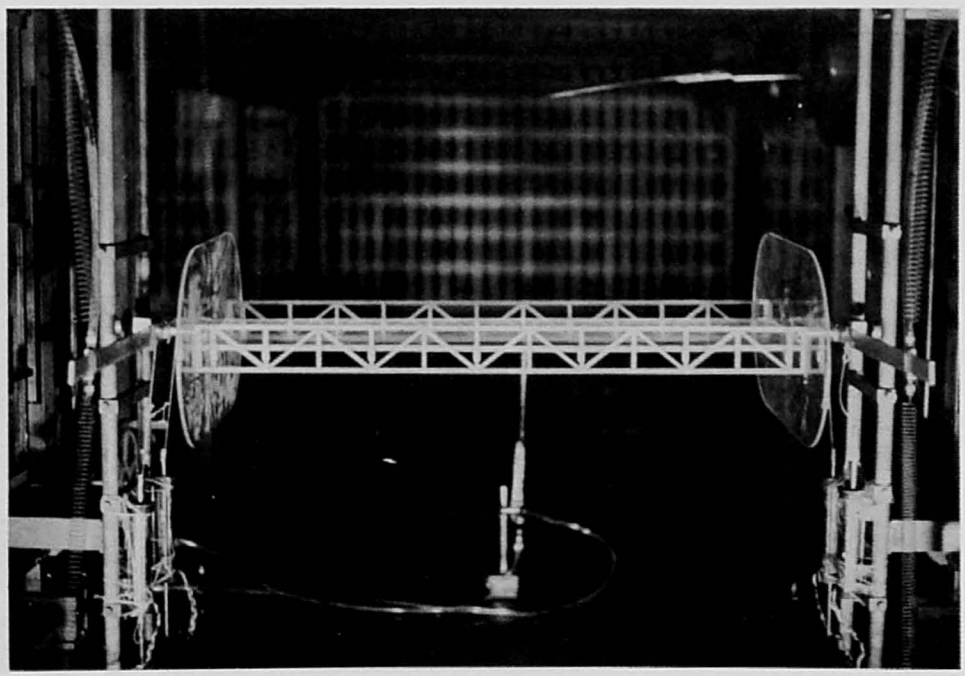

Photo 4.2 Model DT70H

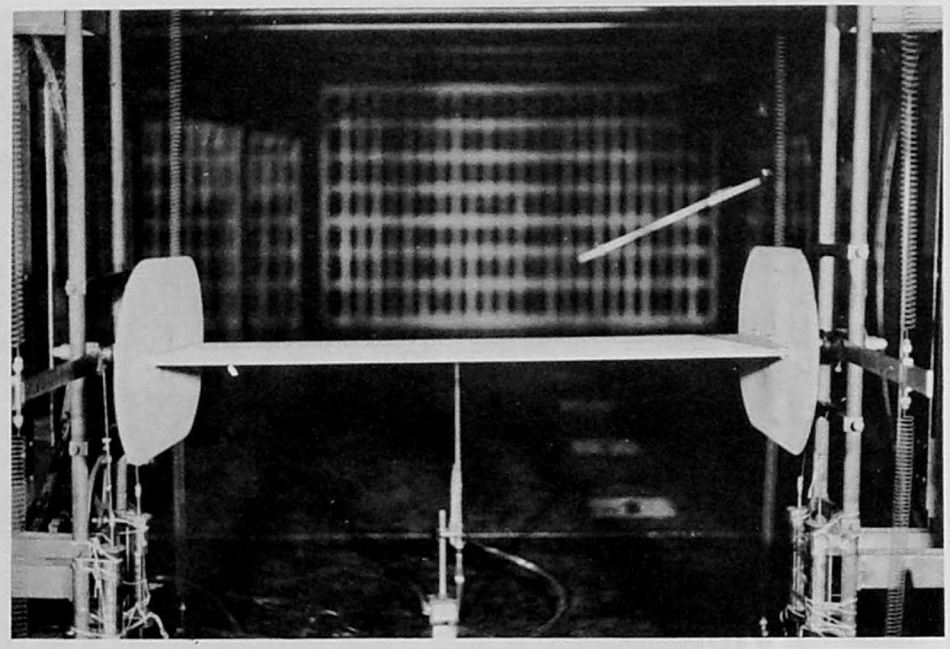

Photo 4.3 Model Plate

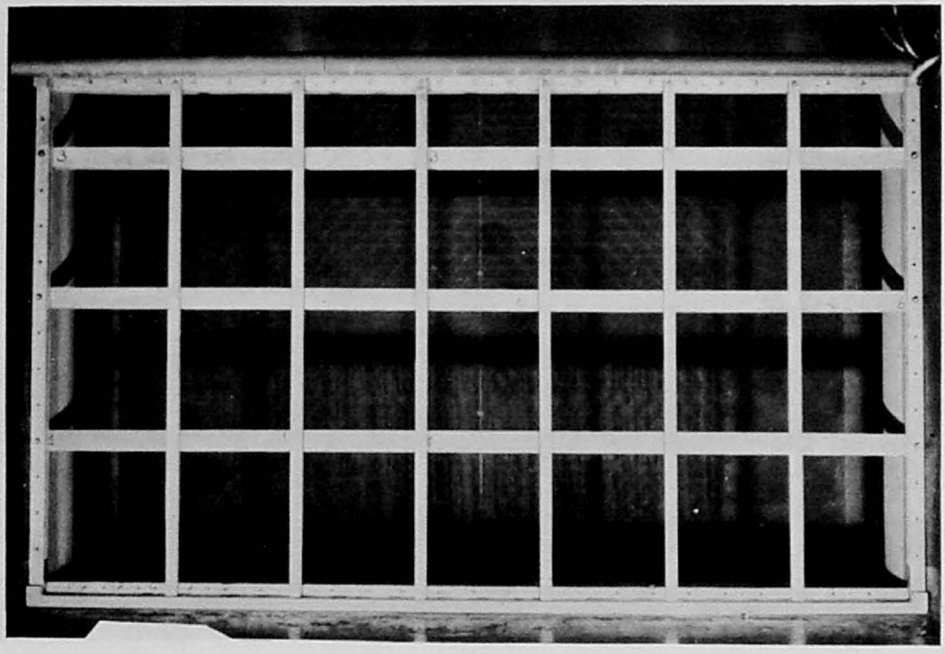

Photo 4.4 Grid A

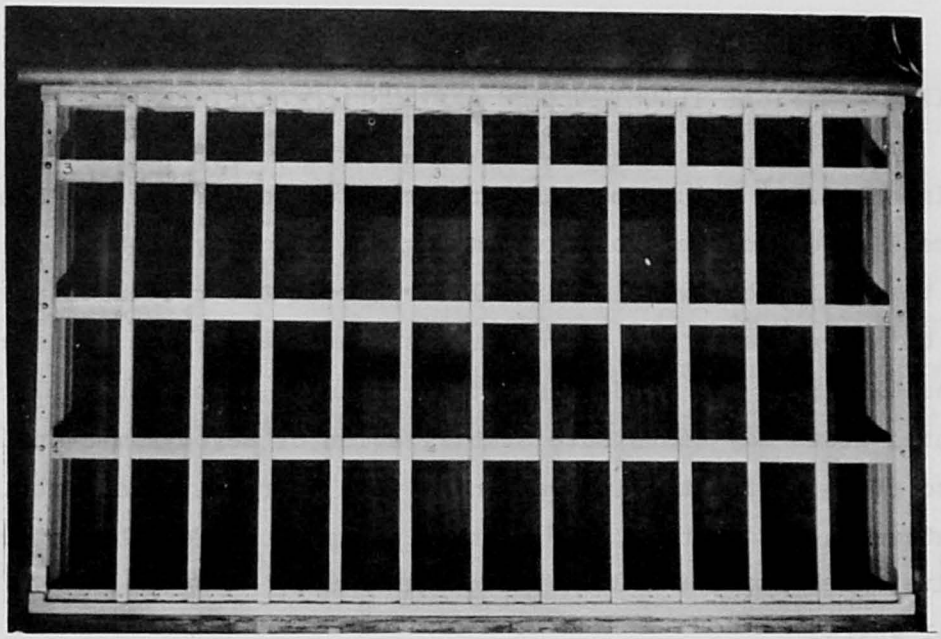

Photo 4.5 Grid `B

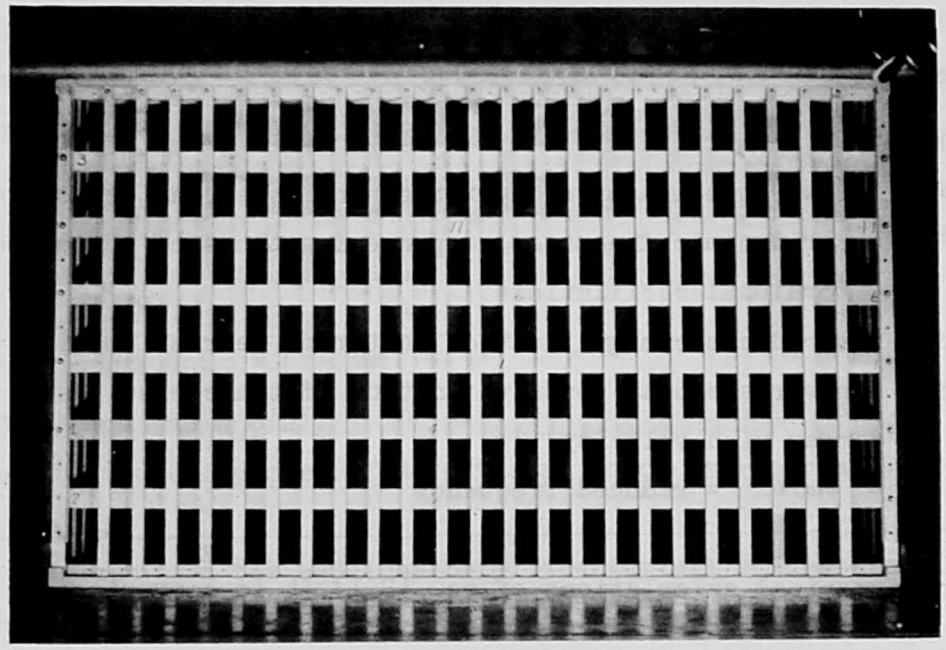

Photo 4.6 Grid C

APPENDIX NUMERICAL ILLUSTRATIONS AND SUPPLEMENTARY REMARKS

In chapter 4 a fundamental consideration on aerodynamic behaviours of plate like structures for fluctuating gusts is given based on the Karman-Sears' theory. For two dimensional air stream the responses are produced due to both transverse and chordwise gust components; the transverse gusts may possibly exert the randomness of aerodynamic responses, while the horizontal gusts may contribute stabilization of aerodynamic instability and also cause to fluctuating responses when it receives a certain amount of relative angle of attack. In this paragraph a few characteristics are illustrated for plate like structures taking into an account only the vertical gusts.

1. Power Spectra of Aerodynamic Forces

Generally the aerodynamic responses of two degrees of freedom structures are written as

$$S_{\eta\eta}(\omega) = \widetilde{Y}^2(\omega)\, U^2 \,|\, S(k) \,|^2\, S_{vv}$$

$$S_{\varphi\varphi}(\omega) = \widetilde{\Psi}^2(\omega)\, U^2 \,|\, S(k) \,|^2\, S_{vv} \qquad (B \cdot 1)$$

in which

$S_{\eta\eta}$, $S_{\varphi\varphi}$ = power spectra of deflectional and torsional responses

$\widetilde{Y}^2(\omega)$, $\widetilde{\Psi}^2(\omega)$ = aerodynamic frequency response functions of deflectional and torsional oscillations

$S(k)$ = aerodynamic magnification factor or Sear's function

S_{vv} = power spectral density function of transverse gust

U = mean wind velocity

$k = b\omega/U$ = reduced frequency

For numerical calculations of eq. (B.1) it is convenient to divide

into two parts, namely the spectral density function of aerodynamic forces and the aerodynamic frequency response functions, the former of which is therefore defined as

$$P_L(\omega) = P_M(\omega) = U^2 \,|\, S(k) \,|^2 \, S_{vv}(\omega) \qquad (B \cdot 2)$$

One of the most simple form of expressions for S_{vv} is given as eq. (4.6.21) when the associate autocorrelation function is of the form of exponential function. The normalized logarithmic power spectral function for this is thus written as

$$\frac{\omega S_{vv}(\omega)}{v^2} = \frac{1}{\pi}\left(\frac{\omega L_x}{U}\right)\frac{1}{1+\left(\frac{\omega L_x}{U}\right)^2} = \frac{s\,k}{\pi\,(s^2+k^2)}\,, \quad s=\frac{b}{L_x} \qquad (B \cdot 3)$$

where $\overline{v^2}$, L_x are the variance of transverse gust and the scale of turbulence, respectively.

An approximate expression for the squared Sear's function is given as

$$|\, S(k) \,|^2 = \frac{1}{1+2\pi k} \qquad (B \cdot 4)$$

by H. W. Liepmann* (Fig. B.3). Eq. (B.3) is shown in Fig. B.1 (Table B.1). The logarithmic power spectra of aerodynamic force for eq.(B.2) is obtained as the product of eq's (B.3) and (B.4) as follows

$$\omega P_L(\omega) = U^2 \overline{v^2}\,\frac{s\,k}{\pi\,(1+2\pi k)(s^2+k^2)} \qquad (B \cdot 5)$$

or

$$\frac{\omega P_L(\omega)}{U^2\,\overline{v^2}} = \frac{s\,k}{\pi\,(1+2\pi k)(s^2+k^2)}$$

(Fig. (B.2) and Table B.2).

Note that the power spectra of aerodynamic force is remarkably dependent on

---

* H. W. Liepmann: On the application of statistical concepts to the buffeting problem, J. Aero. Sci., Vol. 19, 1952, pp 793 - 800

the scale of turbulence as shown in Fig. B.2 and in general the larger the scale of turbulence then the larger the power spectral density of aerodynamic force. For the spectral density of aerodynamic force, the aerodynamic magnification factor $|S(k)|^2$ takes a role of the so called gust alleviation coefficient to reduce the effective amount of acting aerodynamic forces.

2. Aerodynamic Frequency Response Functions

The aerodynamic responses defined as eq. (B.1) are generally characterized by the aerodynamic frequency response functions $\tilde{y}_2$ and $\tilde{\psi}_2$ for which numerical illustrations are exemplified in this paragraph. The simplest case is the one taking into an account the uncoupled frequency functions, for which one only needs to consider

$$|H_\eta(\omega)| = \frac{1}{\sqrt{(\omega_\eta^2 - \omega^2)^2 + \omega^2(2\zeta_\eta\omega_\eta - H_1)^2}}$$

$$|\theta_\alpha(\omega)| = \frac{1}{\sqrt{(\omega_\alpha^2 - \omega^2 - A_3)^2 + \omega^2(2\zeta_\alpha\omega_\alpha - A_2)^2}} \qquad (B.6)$$

in which A_2, A_3, H_1 are aerodynamic coefficients dependent on the frequency ω and the reduced frequency $k = b\omega/U$. When one substitutes the aerodynamic coefficients given by the Theodorsen's theory for them, it is comparatively convenient to use an approximate expression for the lift reduction factor C(k) as follows

$$C(k) = 1 - \frac{0.165k^2}{k^2 + (0.041)^2} - \frac{0.335k^2}{k^2 + (0.32)^2}$$

$$- \left(\frac{0.165 \times 0.041k}{k^2 + (0.041)^2} + \frac{0.335 \times 0.32k}{k^2 + (0.32)^2} \right) i$$

The accuracy of the above approximation is shown by R. I. Jones that the maximum percentage errors based on the exact values are +10 % and - 11 % for the absolute value of the imaginary part and + 2.6 % and - 2.1 % for

the absolute value of the real part. Thus for evaluation of the frequency response functions the error can be limited to less than 6 % at most. Numerical illustrations for plate like structures are given in Fig's B.4.1 and B.4.2 (Tables B.3 and B.4) which dimensions are taken from those of the 1st symmetric modes of the Severn's Bridge. This indicates the fact that the increase in mean wind velocity the peak value of the frequency response functions are reduced on an account of the increase of the aerodynamic damping. To compare these with the case of coupled form of aerodynamic frequency functions as shown in Fig's B.5 and B.6 (Table B.5) there exists a significant difference of characteristics that the flexural responses depend on the torsional frequency at which the extreme value of spectrum appears when the mean wind velocity reaches to 40 m/sec ($\omega_\alpha b/U = 0.756$) and the peak values may be reduced first and increase secondly and then decrease again as the mean wind velocity increases. Similar aerodynamic frequency response functions are exemplified in Fig's B.7.1 through B.7.7 for the Severn type model as shown in Table B.6. For this case the flexural response $\widetilde{Y}^2$ behaves slightly differently to compare with the former case. It shows dual peak values in the neighbourhood of the natural flexural frequency and respond also significantly in the natural torsional frequency until the wind velocity reaches to about 6 m/sec ($\omega_\alpha b/U = 0.5$). As the wind velocity increases further, the spectral density at the natural flexural frequency increases remarkably and for 10 m/sec the frequency response forms one peak shape as Fig.B.7.5. For the torsional frequency response $\widetilde{\Psi}^2$ varies quite differently from $\widetilde{Y}^2$ and, when the mean wind velocity becomes more than 8 m/sec, the peak value of the spectral density function occurs at the natural flexural frequency and becomes more flat as the wind velocity increases.

An example of experimental results of the frequency responses for the Severn type model (Table B.6) is given in Fig's B.8.1 and B.8.2 for which the peak of spectral density occurs at the flutter frequency.

From the abovementioned considerations the aerodynamic responses can be characterized primarily by the aerodynamic frequency response functions which is shown in Fig. B.7.6 for this case. However at the flutter state one should take into an account not only the responses due to transverse gusts but the responses due to chordwise gusts, as schematically shown in Fig. B.9. So far there is no comparative data of theoretical and experimental results, but it can be said that there appears no satisfactory explanations for the aerodynamic responses for this case without considering the effects of simultaneous action of transverse and chordwise gusts.

3. Bounds of Critical Flexure-torsion Flutter Wind Velocity

The fluctuation of wind velocity induces the varying unsteady aerodynamic forces on plate like structure as considered in chapter 4 and it is known that horizontal gusts contribute to stabilization of aerodynamic instability, while transverse gusts to destabilization. In this paragraph numerical results are compared with experimental results for plate like structure models as Table B.7, where the minimum value of critical wind velocity due to destabilizing effect and the maximum value due to stabilizing effect are termed as the lower and upper bounds, respectively. As shown in this table the experimental results lie between upper and lower bounds and ratios of V_{cr}^{u}/V_{cr}^{l} are about 2.0 and the experimental results are slightly close to the upper bounds. Note that V_{cr}^{l}/V_{cr}^{exp} are about 0.5 to 0.6 and this indicates that the structure possibly subjects to aerodynamic instability which is restricted to an unstable mechanism, when the wind velocity exceed about half of critical wind velocity.

Table B・1 Logarithmic Power Spectra of Vertical Gust

$$\frac{\omega P_{(\omega)}}{\sigma^2} = \frac{1}{\pi}\frac{\omega L}{U}\frac{1}{1+\left(\frac{\omega L}{U}\right)^2} = \frac{s\,k}{\pi\,(s^2+k^2)}$$

$s = b/L$: *ratio of semichord to scale of turbulence*

$k = b\omega/U$: *reduced frequency*

k \ s	0.001	0.005	0.010	0.050	0.100	0.500	1.000	5.000
.001	.15916	.06121	.03152	.00636	.00318	.00064	.00032	.00006
.005	.06121	.15916	.12732	.03152	.01588	.00318	.00159	.00031
.010	.03152	.12732	.15916	.06121	.03152	.00636	.00318	.00064
.050	.00636	.03151	.06121	.15916	.12732	.03152	.01588	.00318
.100	.00318	.00636	.03152	.12732	.15916	.06121	.03152	.00636
.500	.00064	.00318	.00636	.03115	.06121	.15916	.12732	.03152
1.000	.00032	.00064	.00318	.01588	.03152	.12732	.15916	.06121
5.000	.00006	.00031	.00064	.00318	.00636	.03152	.06121	.15916
10.000	.00003	.00016	.00031	.00159	.00318	.01588	.03152	.12732

Table B・2 Logarithmic Power Spectra of Aerodynamic Forces ($|S(k)|^2 \omega P(\omega) / \sigma^2$)

k	$\|S(k)\|^2$	$s = .001$	.010	.100	1.000	10.000
.001	.9937	.15816	.03132	.00316	.00032	.00003
.002	.9876	.12574	——	——	——	——
.005	.9695	.05934	.12344	.01540	.00154	.00016
.010	.9409	.02965	.14975	.02966	.00299	.00031
.020	.8884	——	——	——	——	——
.050	.7609	.00484	.04657	.09688	.01208	.00121
.100	.6141	——	.01936	.09774	.01935	.00195
.200	.4431	——	——	——	——	——
.500	.2415	——	.00153	.01478	.03075	.00384
1.000	.1373	——	——	.00433	.02185	.00432
2.000	.0737	——	——	——	——	——
5.000	.0308	——	——	.00020	.00189	.00392

Table B·3 Frequency Response Functions of Uncoupled Deflectional Vibrations

ρ (air density) $=0.125$ kg sec²/m⁴

ζ_η (damping ration) $=0.005$

ω_η (natural frequency) $=0.8985$ rad/sec

m (mass per unit length) $=1.190\times10^3$ kg sec²/m²

b (semichord) $=12.878$ m

$k=\frac{b\omega}{U}$	$U=20$ m/sec		$U=40$ m/sec	
	ω (rad/sec)	$\lvert H_\eta(\omega)\rvert$ (sec²)	ω (rad/sec)	$\lvert H_\eta(\omega)\rvert$ (sec²)
.01	.015,53	1.239,06	.031,06	1.240,147
.025	.038,83	1.241,00	.077,65	1.247,842
.050	.077,65	1.247,97	.155,30	1.276,156
.100	.155,30	1.276,67	.310,61	1.403,669
.200	.310,61	1.406,11	.621,21	2.326,241
.300	.465,91	1.689,00	.931,82	7.555,404
.400	.621,21	2.362,57	1.242,42	1.331,612
.500	.776,52	4.766,28	1.553,04	.619,451
.600	.931,82	12.208,7	1.863,64	.374,043
.800	1.242,4	1.351,96	2.484,9	.186,088
1.00	1.553,0	.622,34	3.106,1	.113,042
1.20	1.863,6	.374,86	3.727,3	.076,389
1.50	2.329,6	.216,38	4.659,1	.047,835
2.00	3.106,1	.113,10	———	———
3.00	4.659,1	.047,84	———	———
4.00	6.212,1	.026,46	———	———
6.00	———	———	———	———
10.00	———	———	———	———

Table B・4 Frequency Response Functions of Uncoupled Torsional Vibrations

ρ (air density) $=0.125$ kg sec^2/m^4

ζ_α (damping ratio) $=0.005$

ω_α (natural frequency) $=2.3499$ rad/sec

I (moment of inertia per unit length) $=8.971\times10^4$ kg sec^2

b (semichord) $=12.878$ m

$k=\frac{b\omega}{U}$	$U=20$ m/sec		$U=40$ m/sec	
	ω (rad/sec)	$\theta_\alpha(\omega)$ (sec^2)	ω (rad/sec)	$\theta_\alpha(\omega)$ (sec^2)
.010	.015,53	.190,99	.031,06	.228,38
.025	.038,83	.190,70	.077,65	.227,14
.050	.077,65	.190,50	.155,30	.225,67
.10	.155,30	.190,43	.310,61	.225,29
.20	.310,61	.192,04	.621,21	.234,56
.30	.465,91	.195,89	.931,82	.259,44
.40	.621,21	.202,08	1.242,4	.309,64
.50	.776,52	.210,96	1.553,0	.416,94
.60	.931,82	.223,00	1.863,6	.723,27
.70	——	——	2.174	3.983
.80	1.242,4	.262,13	2.485	.748,54
1.0	1.533,0	.338,68	3.106	.209,43
1.2	1.863,6	.527,12	3.727	.111,06
1.5	2.329,6	5.945,7	4.659	.059,51
2.0	3,106,1	.233,57	6.212	.029,69
3.0	4.659,1	.062,14	9.318	.012,21
4.0	6.212,1	.030,10	——	——
6.0	——	——	——	——
10.0	——	——	——	——

Table B・5 Frequency Response Functions of Coupled Vibrations

$U = 0.1$ m/sec

k	ω	$\lvert H_\eta \rvert$	$\lvert H_\alpha \rvert$	$\lvert \theta_\eta \rvert$	$\lvert \theta_\alpha \rvert$	$\theta_{\eta\eta}$	$\theta_{\alpha\eta}$	$\theta_{\eta\alpha}$	$\theta_{\alpha\alpha}$	$\widetilde{Y}^2(\omega)$	$\widetilde{\Psi}^2(\omega)$
	0.2	1.30	.000,390	.000,002	·182	−.002,45	−1.57	−1.54	−.000,866	.000,123	.000,001,12
	0.4	1.54	.000,946	.000,004	·186	−·005,81	−1.56	−1.55	−·001,77	.000,172	.000,001,17
	0.6	2.24	.002,13	.000,009	·194	−·012,6	−1.56	−1.55	−·002,76	.000,361	.000,001,27
	0.8	5.97	.008,03	.000036	·205	−·045,0	−1.52	−1.52	−·003,89	.002,58	.000,001,42
	1.0	5.18	.009,41	.000,042	·221	·048,8	1.53	1.53	−·005,25	.001,94	.000,001,65
	1.4	.867	.002,80	.000,012	·281	·011,4	1.57	−1.57	−·009,33	.000,05	.000,002,65
	2.0	.313	.003,38	.000,015	·657	·005,89	−1.55	−1.54	−·031,2	.000,007	.000,014,5
	3.0	.122	.000,864	.000,004	·287	·003,45	1.55	1.55	·020,5	.000,001	.000,002,85
	4.0	.0658	.000,206	.000,001	·095,4	·002,48	1.56	1.56	·009,06	.000,000	.000,000,31
	6.0	.0284	.000,046	.000,000	·032,8	·001.60	1.56	1.57	·004,67	——	——

$U = 10$ m/sec

k	ω	$\lvert H_\eta \rvert$	$\lvert H_\alpha \rvert$	$\lvert \theta_\eta \rvert$	$\lvert \theta_\alpha \rvert$	$\theta_{\eta\eta}$	$\theta_{\alpha\eta}$	$\theta_{\eta\alpha}$	$\theta_{\alpha\alpha}$	$\widetilde{Y}^2(\omega)$	$\widetilde{\Psi}^2(\omega)$
.258	0.2	1.30	.157	.000,256	.184	−.018,5	−1.55	−.275	−.001,16	.000,104	.000,001,14
.515	0.4	1.54	.184	.000,521	.188	−.037,7	−1.53	−.553	−.002,85	.000,149	.000,001,19
.773	0.6	2.23	.306	.001,07	.195	−.075,8	−1.49	−.739	−.004,67	.000,309	.000,001,29
1.03	0.8	5.80	.976	.003,75	.207	−.255	−1.31	−.710	−.006,44	.0 '1,96	.000,001,43
1.29	1.0	4.98	1.05	.004,25	.222	.269	1.31	−1.34	−.012,9	.001,85	.000,001,65
1.80	1.4	.864	.304	.001,28	.283	.063,3	1.53	−1.26	−.019,0	.000,051	.000,002,71
2.58	2.0	.312	.358	.001,54	.670	.032,0	−1.54	−1.28	−.063,2	.000,009	.000,0151
3.86	3.0	.122	.087,0	.000,381	.285	.019,2	1.51	−1.46	.040,1	.000,001	.000,002,73
5.15	4.0	.065,8	.020,8	.000,091,2	.095,1	.013,6	1.54	−1.47	.017,8	.000,000	.000,000,30
7.73	6.0	.028,4	.004,61	.000,020,3	.032,8	.008,80	1.55	−1.50	.009,22	——	——

(continued)

Dimensions $\lvert H_\eta \rvert$ (sec²), $\lvert H_\alpha \rvert$ (m sec²), $\lvert \theta_\eta \rvert$ (sec²/m), $\lvert \theta_\alpha \rvert$ (sec²), $\widetilde{Y}^2$ (sec⁴/m²), $\widetilde{\Psi}^2$ (sec⁴/m⁴)

(*continued*)

$U = 20$ *m/sec*

k	ω	$\lvert H_\eta \rvert$	$\lvert H_\alpha \rvert$	$\lvert \theta_\eta \rvert$	$\lvert \theta_\alpha \rvert$	$\theta_{\eta\eta}$	$\theta_{\alpha\eta}$	$\theta_{\eta\alpha}$	$\theta_{\alpha\alpha}$	$\widetilde{Y}^2(\omega)$	$\widetilde{\Psi}^2(\omega)$
.129	0.2	1.30	.702	.000,594	.191	−.037,1	−1.53	−.103	.000,121	.000,049,1	.000,001,23
.258	0.4	1.54	.783	.001,28	.194	−.079,5	−1.49	−.212	−.000,641	.000,074,2	.000,001,27
.386	0.6	2.21	1.12	.002,59	.202	−.157	−1.41	−.286	−.001,31	.000,154	.000,001,37
.515	0.8	5.34	2.88	.008,15	.217	−.490	−1.07	−.093,6	−.000,754	.000,942	.000,001,50
.644	1.0	4.50	2.73	.008,79	.229	−.490	1.09	−1.19	−.037,0	.001,85	.000,001,68
.901	1.4	.856	.760	.002,81	.292	−.118	1.48	−.995	−.032,9	.000,044	.000,002,87
1.29	2.0	.309	.851	.003,43	.718	−.055,9	−1.53	−1.04	−.104	.000,019,4	.000,017,4
1.93	3.0	.122	.177	.000,752	.276	−.036,8	1.48	−1.33	.058,7	.000,001,7	.000,002,57
2.58	4.0	.065,9	.042,3	.000,183	.094,2	−.025,4	1.52	−1.37	.026,6	.000,000,3	.000,000,3
3.86	6.0	.028,4	.009,3	.000,041	.032,7	−.016,2	1.54	−1.43	.013,8	———	———

$U = 40$ *m/sec*

k	ω	$\lvert H_\eta \rvert$	$\lvert H_\alpha \rvert$	$\lvert \theta_\eta \rvert$	$\lvert \theta_\alpha \rvert$	$\theta_{\eta\eta}$	$\theta_{\alpha\eta}$	$\theta_{\eta\alpha}$	$\theta_{\alpha\alpha}$	$\widetilde{Y}^2(\omega)$	$\widetilde{\Psi}^2(\omega)$
.064	0.2	1.30	3.51	.001,50	.225	−.062,5	−1.57	−.004,00	.015,7	.000,087,9	.000,001,70
.129	0.4	1.54	3.95	.003,34	.230	−.141	−1.42	.004,25	.030,6	.000,103	.000,001,77
.193	0.6	2.18	5.55	.006,94	.244	−.289	−1.27	.080,4	.053,8	.000,267	.000,001,97
.258	0.8	4.43	11.5	.018,8	.293	−.821	−.736	.540	.056,6	.004,84	.000,002,54
.322	1.0	3.45	9.48	.018,9	.291	.739	.854	−1.09	−.190	.004,72	.000,002,61
.451	1.4	.816	2.90	.007,51	.345	.196	1.42	−.675	−.117	.000,182	.000,004,02
.644	2.0	.283	3.45	.011,1	1.05	.049,6	−1.38	−.531	−.315	.000,327	.000,036,8
.966	3.0	.123	.375	.001,42	.246	.083,5	1.41	−1.10	−.091,7	.000,004	.000,002,03
1.29	4.0	.066,0	.090,2	.000,364	.090,5	.052,5	1.48	−1.17	−.043,4	.000,000	.000,000,27
1.93	6.0	.028,4	.019,3	.000,082	.032,2	.031,9	1.52	−1.29	.022,8	———	———

Table B・6 Model Characteristics

	m $kgsec^2/m^2$	ζ_η	ω_η rad/sec	I $kgsec^2$	ζ_α	ω_α rad/sec	Grid Size (cm)	$\omega_\alpha/\omega_\eta$
DP70H (F30)	.5426	.003,55	8.708	.018,29	.002,60	14.137	30×25	1.623
DP70π (F30)	.5954	.003,34	8.796	.020,03	.002,40	14.399	〃	1.637
EP70H (F30)	.6339	.004,10	8.752	.017,42	.005,22	14.137	〃	1.615
EP70π (F30)	.5966	.004,82	8.836	.020,07	.002,97	14.451	〃	1.635
Plate	.4473	.005,50	10.210	.016,31	.002,21	15.904	〃	1.558
DT70H	.5426	.003,77	9.163	.021,04	.003,84	15.512	〃	1.693
DT70π	.5440	.003,75	9.163	.020,26	.003,19	15.512	〃	1.693
Severn Type	.4553	.006,37	10.210 (1.62 cps)	.014,63	.002,94	15.661 (2.492 cps)	〃	1.534

Aerodynamic Responses of Severn Type Model

Mean Wind Velocixy	Reduced Velocity	Remarks
6.516 ~ 9.764m/sec	2.239 ~ 3.355*	randomly vibrating
9.764 ~ 11.636	3.355 ~ 3.998*	almost steady
12.305	4.229*	divergent
12.695	4.409**	divergent in uniform flow

* flutter frequency = 14.923 rad/sec , chord length = 40 cm

** flutter frequency = 14.765 rad/sec

7

Table B·7 Bounds for Flexure-Torsion Flutter Critical Wind Velocity

Model	m (kgsec^2/m^2)	ζ_η	ω_η	I (kgsec^2)	ζ_α	ω_α	b (m)	ρ(kgsec^2/m^4)	V_{cr}^{l} m/sec	V_{cr}^{u} m/sec	V_{cr}^{exp} (m/sec)
Plate	0.5326	.00487	4.86	0.01406	.00005	6.89	0.10	0.1199	3.442	6.322	5.78
〃	0.5326	.00418	4.76	0.01406	.00316	7.504	0.10	0.1202	3.413	6.666	6.55
〃	0.5326	.00439	4.76	0.01406	.00364	5.467	0.10	0.1202	1.980	3.770	3.16
〃	0.4473	.00589	11.69	0.01631	.00345	17.80	0.15	0.125	5.421	12.582	10.11
DT70H	0.5426	.00584	10.60	0.01794	.00341	17.06	0.15	0.125	5.776	13.220	8.87
〃	0.5426	.00605	10.60	0.02104	.00280	18.85	0.15	0.125	6.549	15.271	11.15
〃	0.5426	.00598	10.55	0.02564	.00442	20.74	0.15	0.125	9.156	19.126	14.43
〃	0.5426	.00670	10.52	0.03180	.00307	22.44	0.15	0.125	9.646	20.887	17.55

V_{cr}^{l} : Lower bound of critical velocity of aerodynamic instability

V_{cr}^{u} : Upper bound of critical velocity of aerodynamic instability

V_{cr}^{exp} : experimentally obtained critical velocity

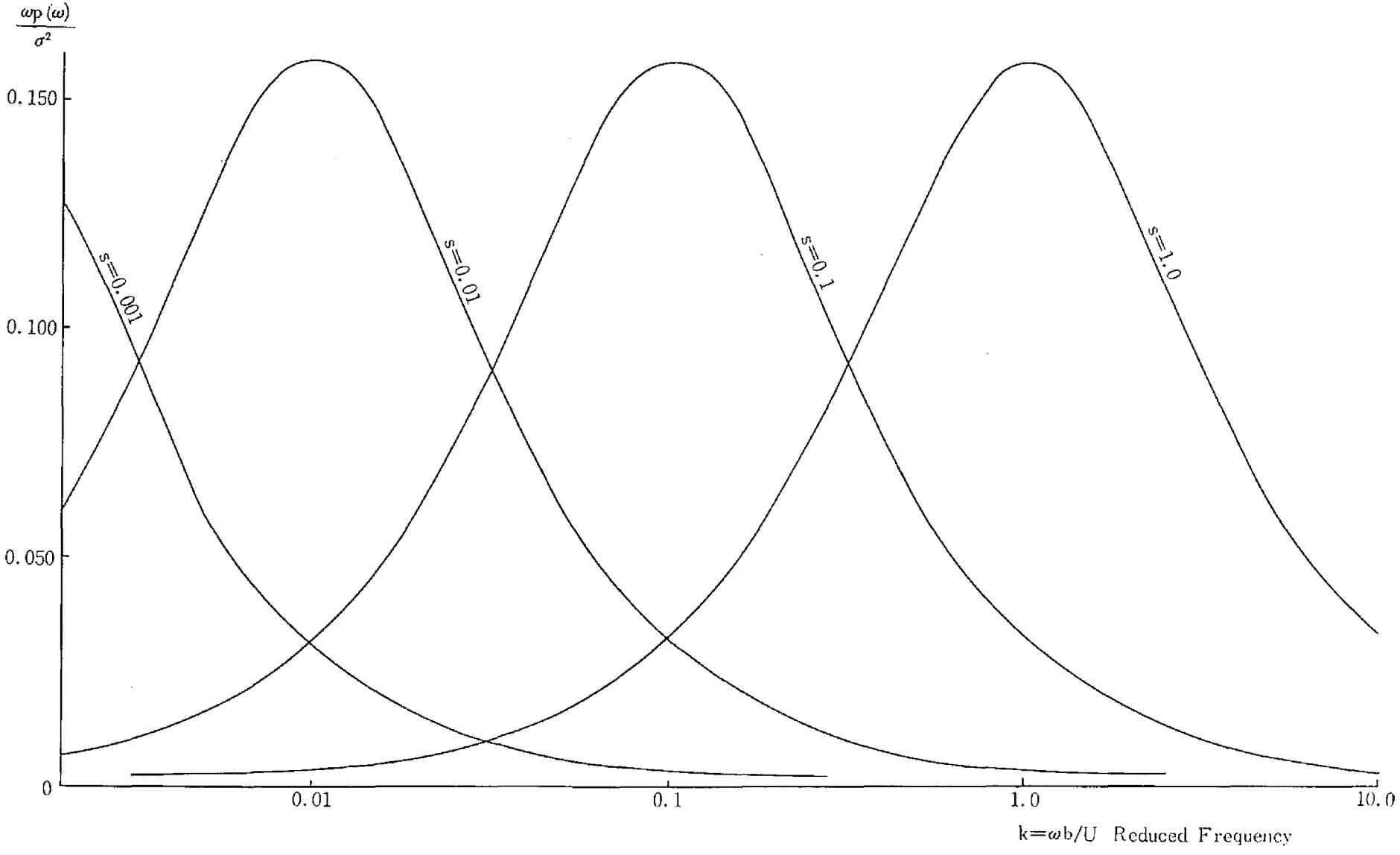

Fig. B. 1 Logarithmic Power Spectra of Wind-Reduced Frequency Relation

$$\frac{\omega P(\omega)}{\sigma^2}=\frac{1}{\pi}\frac{\omega L}{U}\frac{1}{\left\{1+\left(\frac{\omega L}{U}\right)^2\right\}},\quad s=\frac{b}{L}\ (\text{ratio of semichord to scale of turbulence})$$

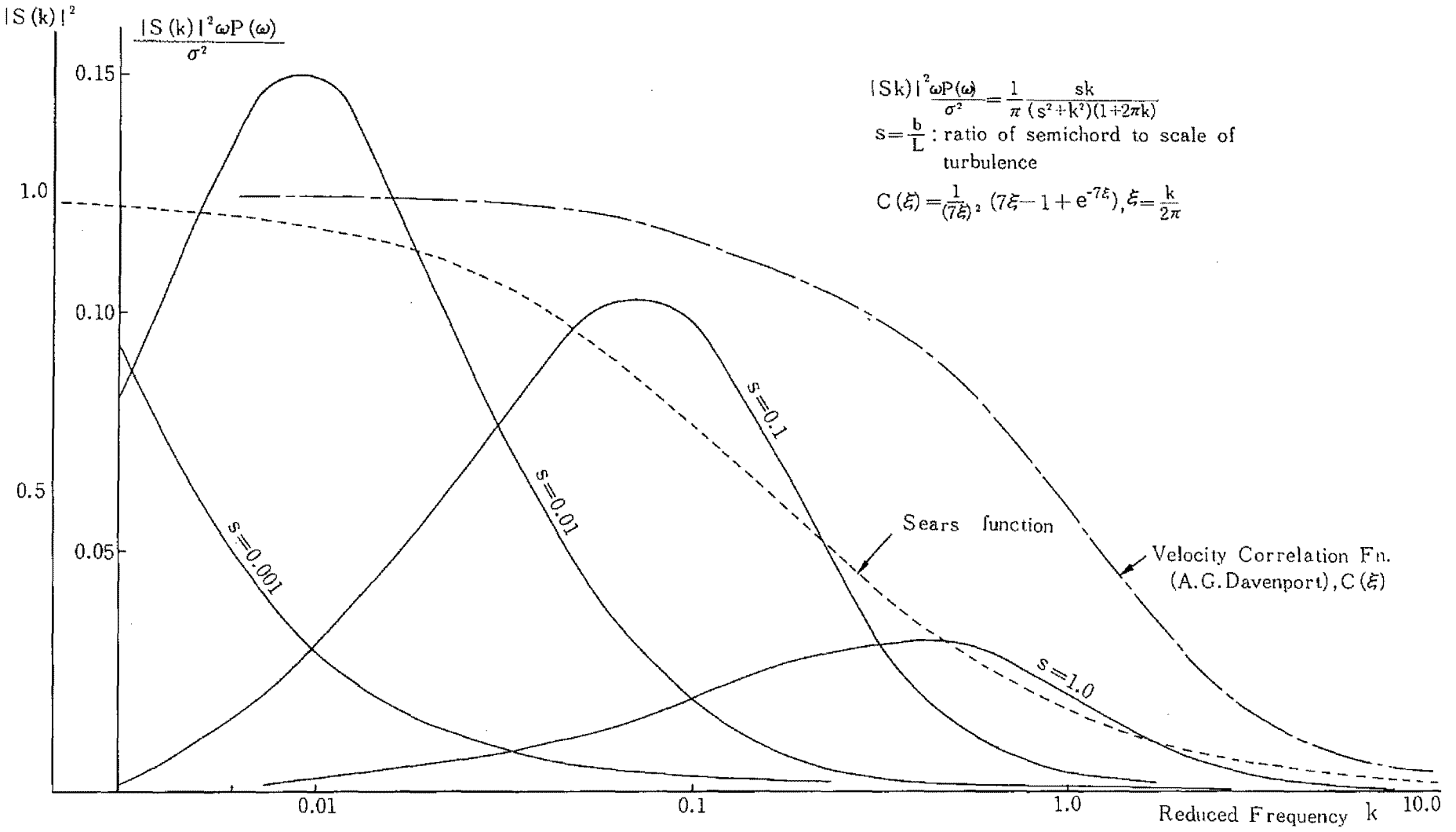

Fig. B.2 Product of Aerodynamic Magnification Factor and Logarithmic Power Spectra

(Power Spectra of Aerodynamic Force on Plate)

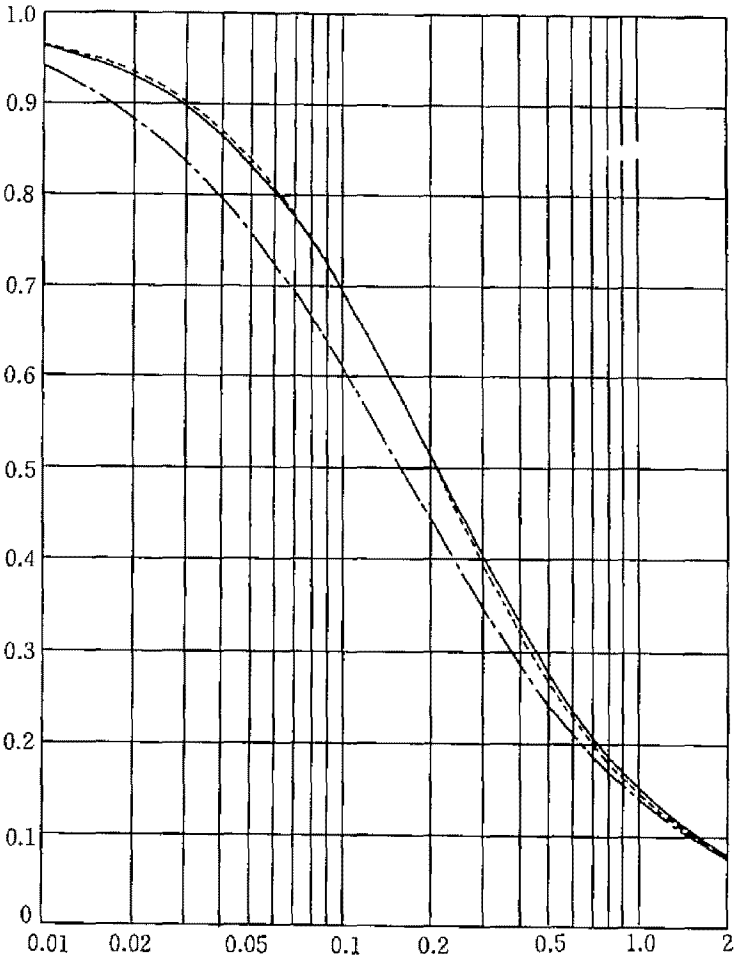

——— Sears Function $|S(k)|^2$

--------- $\dfrac{0.1811+k}{0.1811+(0.1811\pi+)k+2\pi k^2}$

—·—·— $\dfrac{1}{1+2\pi k}$ (by H.W.Liepmann)

Fig. B.3. Comparison of Approximate expressions of Sears Functions. (Y.C.Fung)

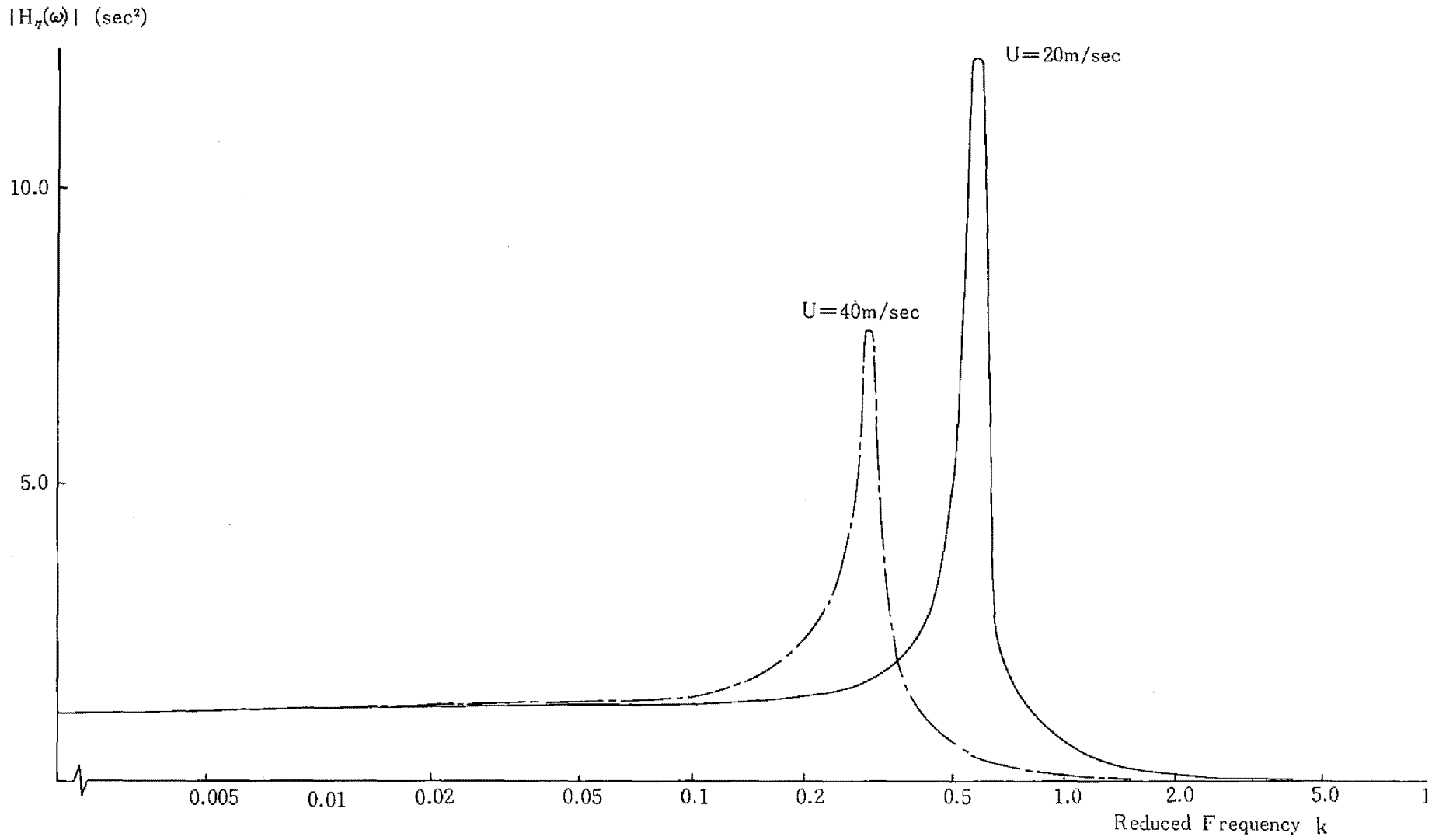

Fig. B.4.1 Frequency Response Function for Uncoupled Deflectional Mode
(ω_η=0.8985 rad/sec, ζ_η=0.005, $m/\rho b^2$=57.40)

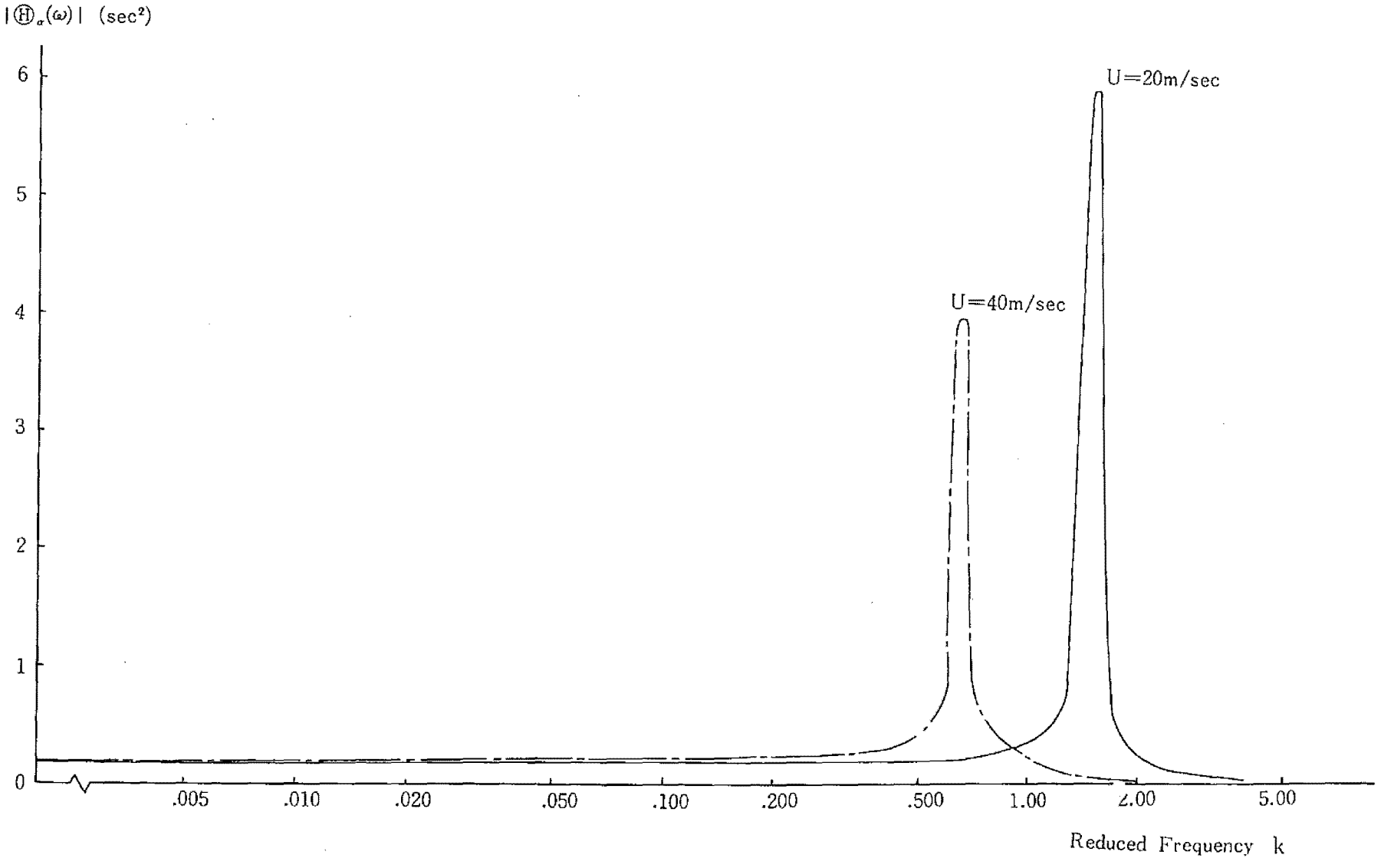

Fig. B.4.2 Frequency Response Function for Uncoupled Torsional Mode
(ω_α=2.3499, ζ_α=0.005, I/pb⁴=26.09)

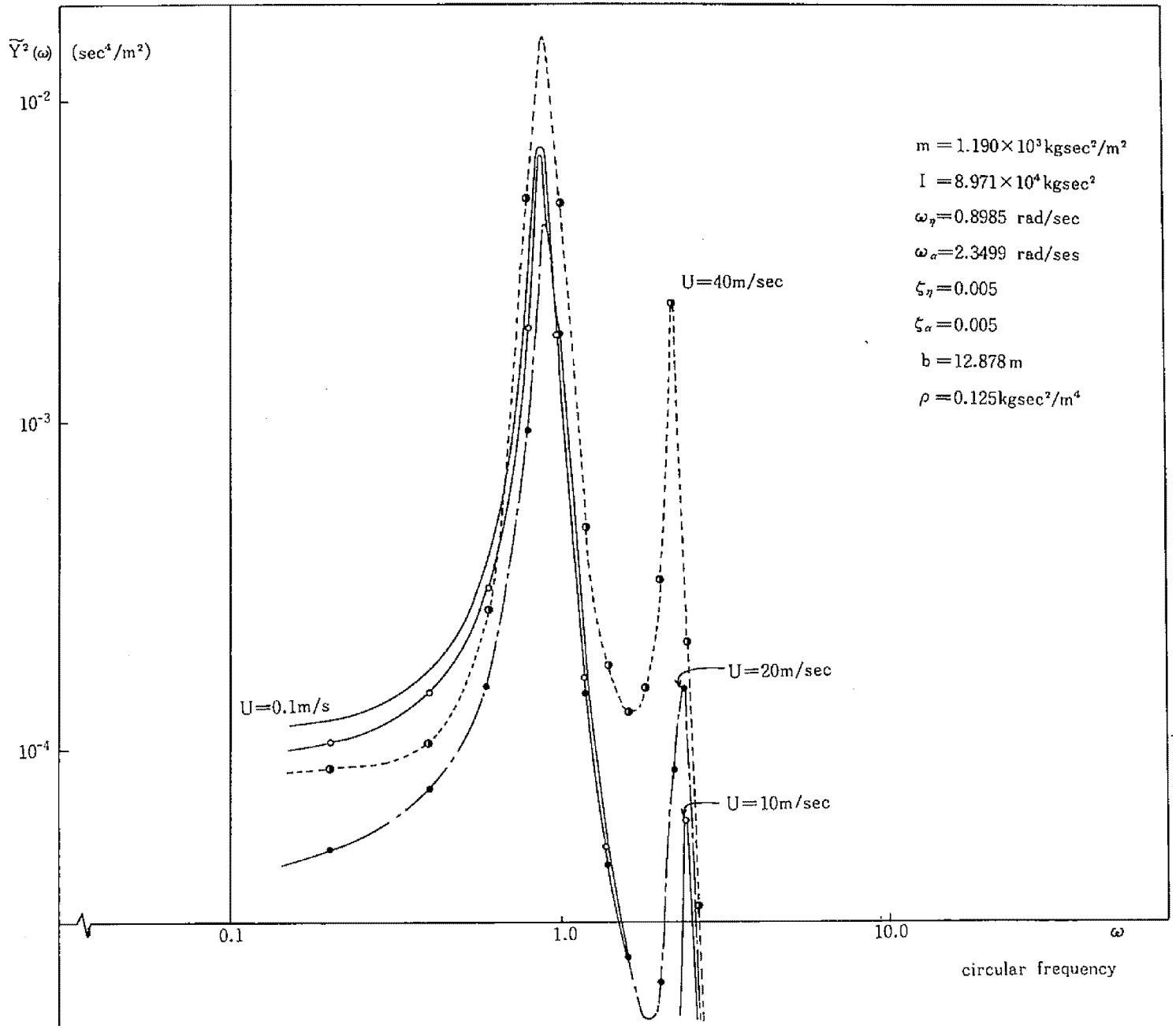

Fig. B.5 Aerodynamic Fequency Response Functions for Deflectional Oscillations

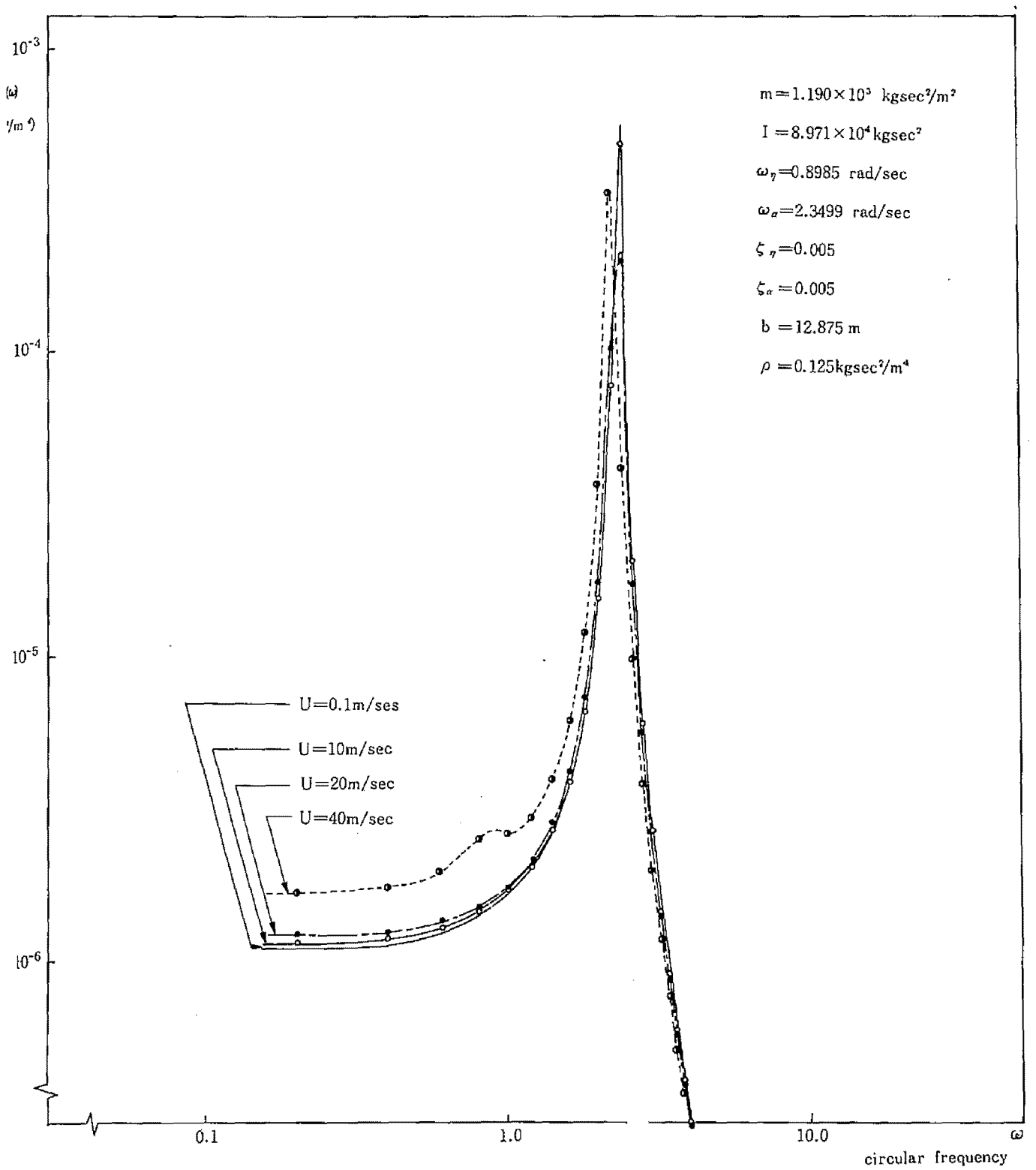

Fig. B.6 Aerodynamic Frequency Response Functions for Torsional Oscillations

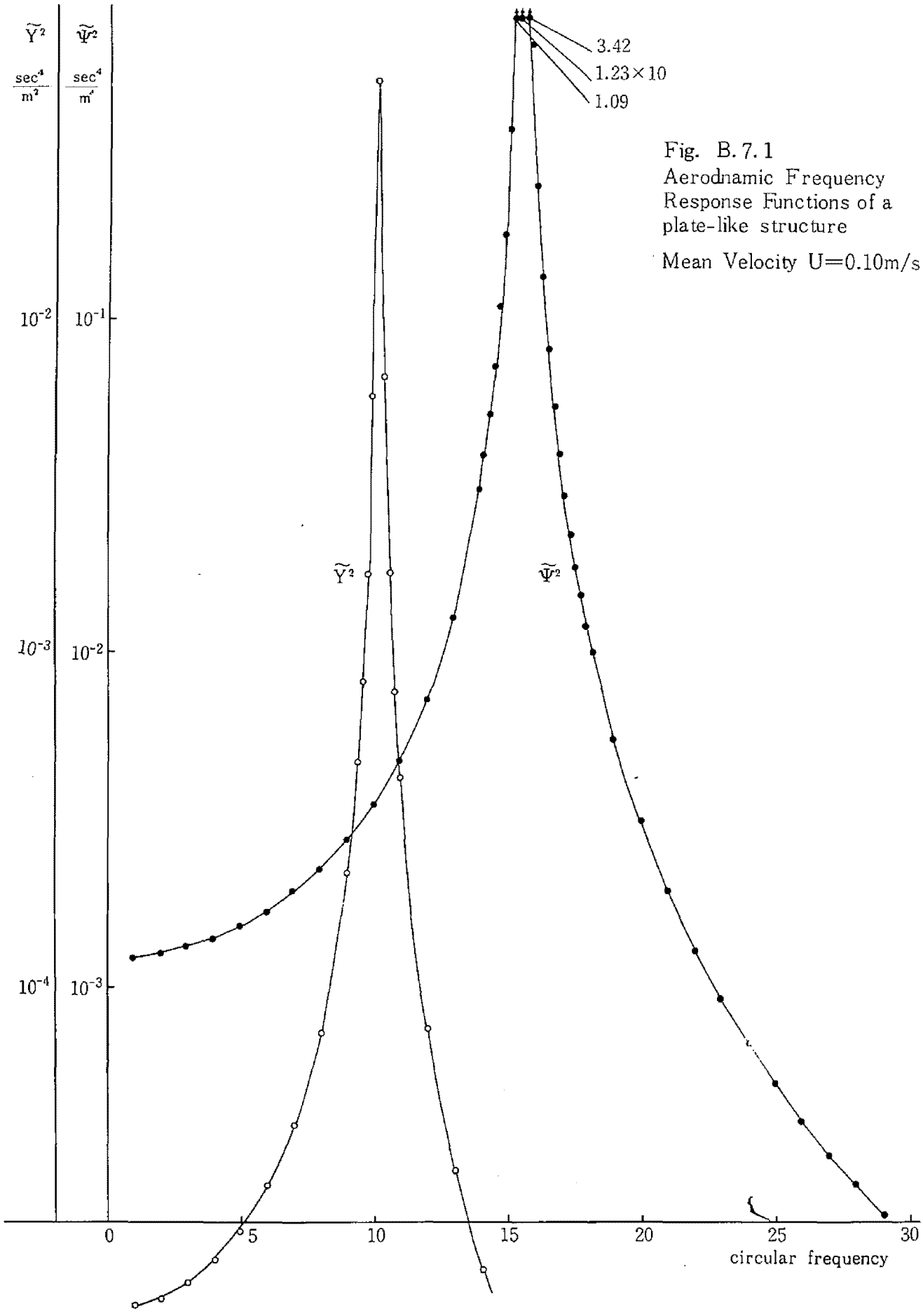

Fig. B.7.1
Aerodnamic Frequency Response Functions of a plate-like structure

Mean Velocity U=0.10m/s

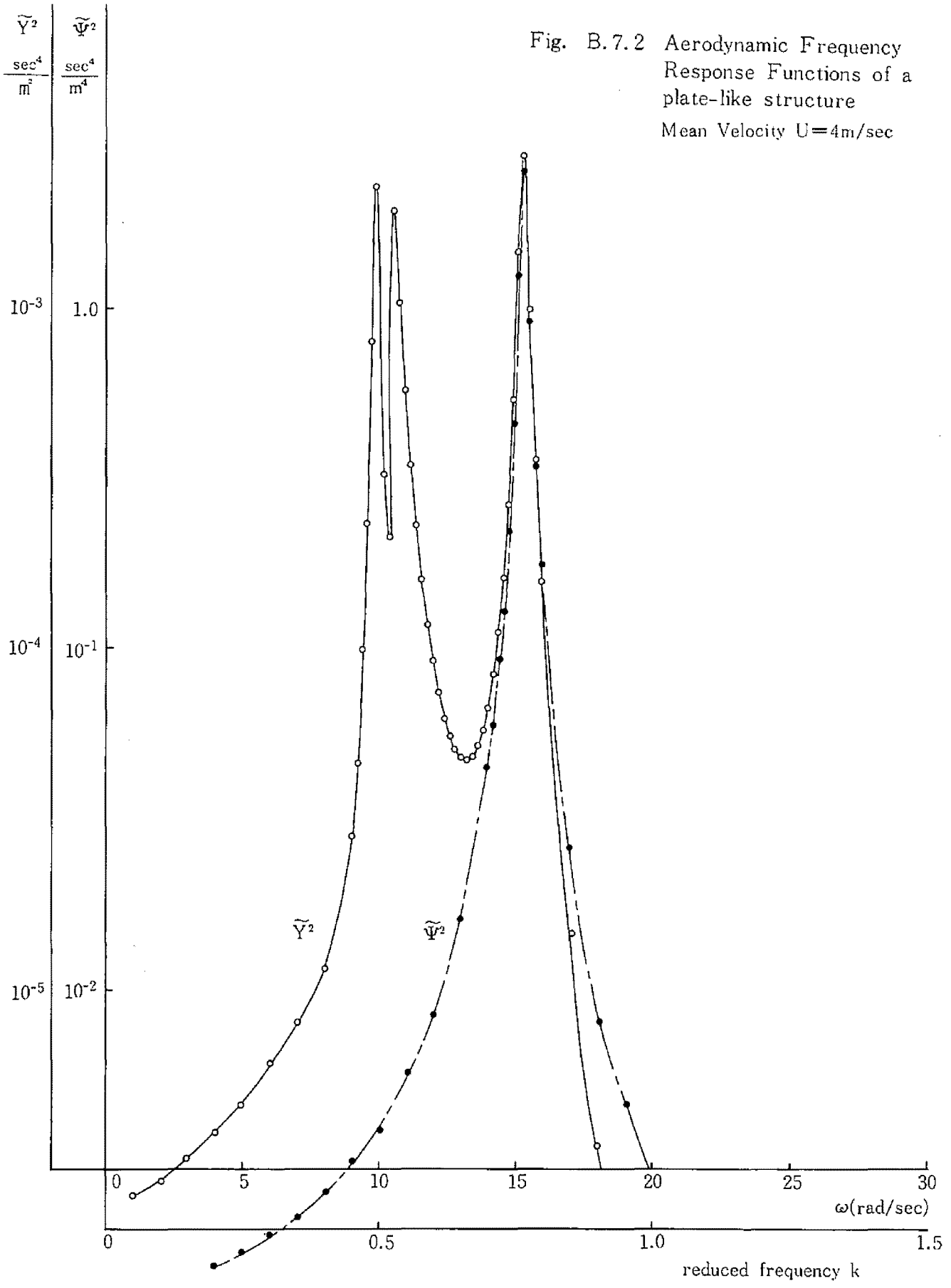

Fig. B.7.2 Aerodynamic Frequency Response Functions of a plate-like structure
Mean Velocity U=4m/sec

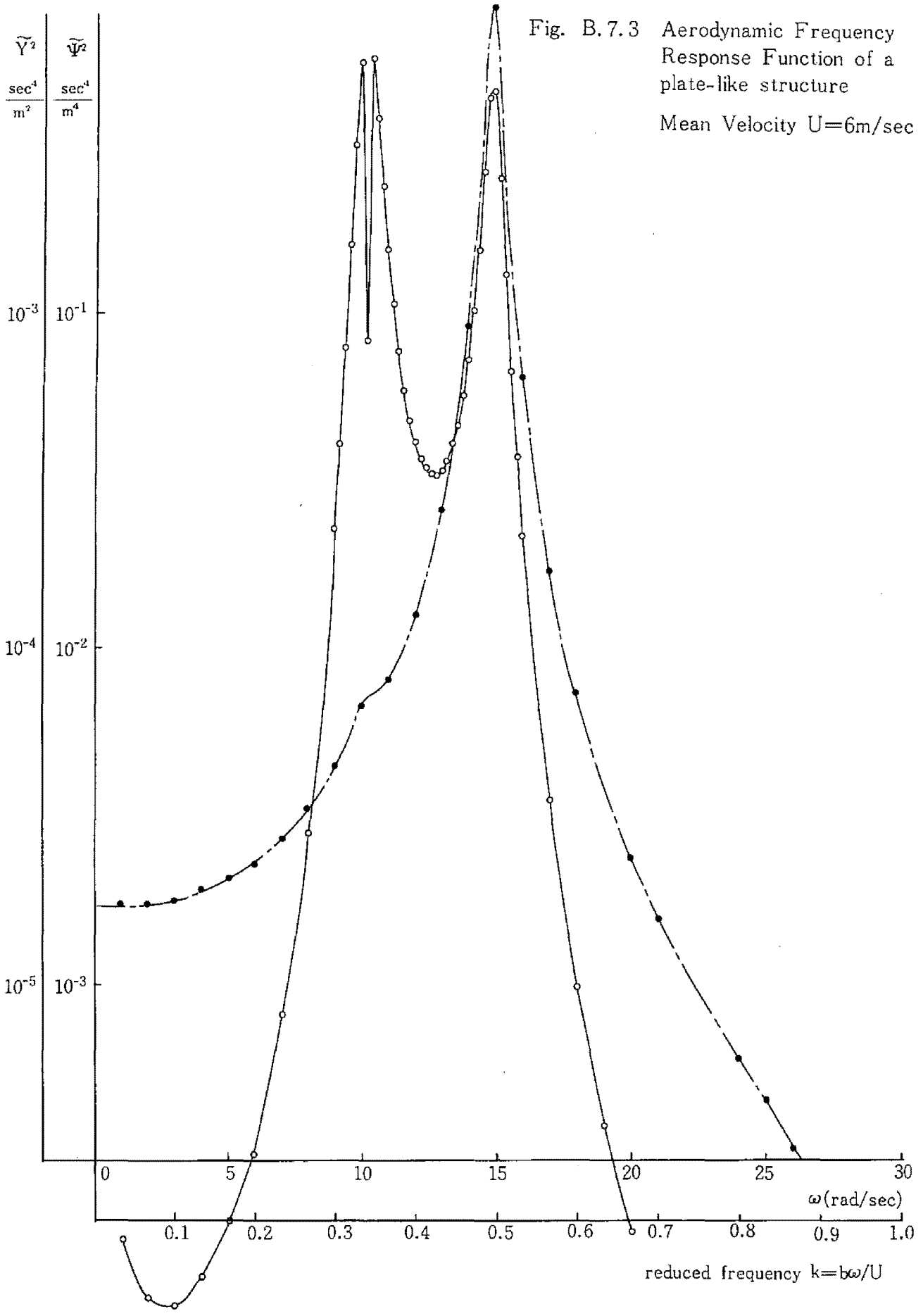

Fig. B.7.3 Aerodynamic Frequency Response Function of a plate-like structure

Mean Velocity U=6m/sec

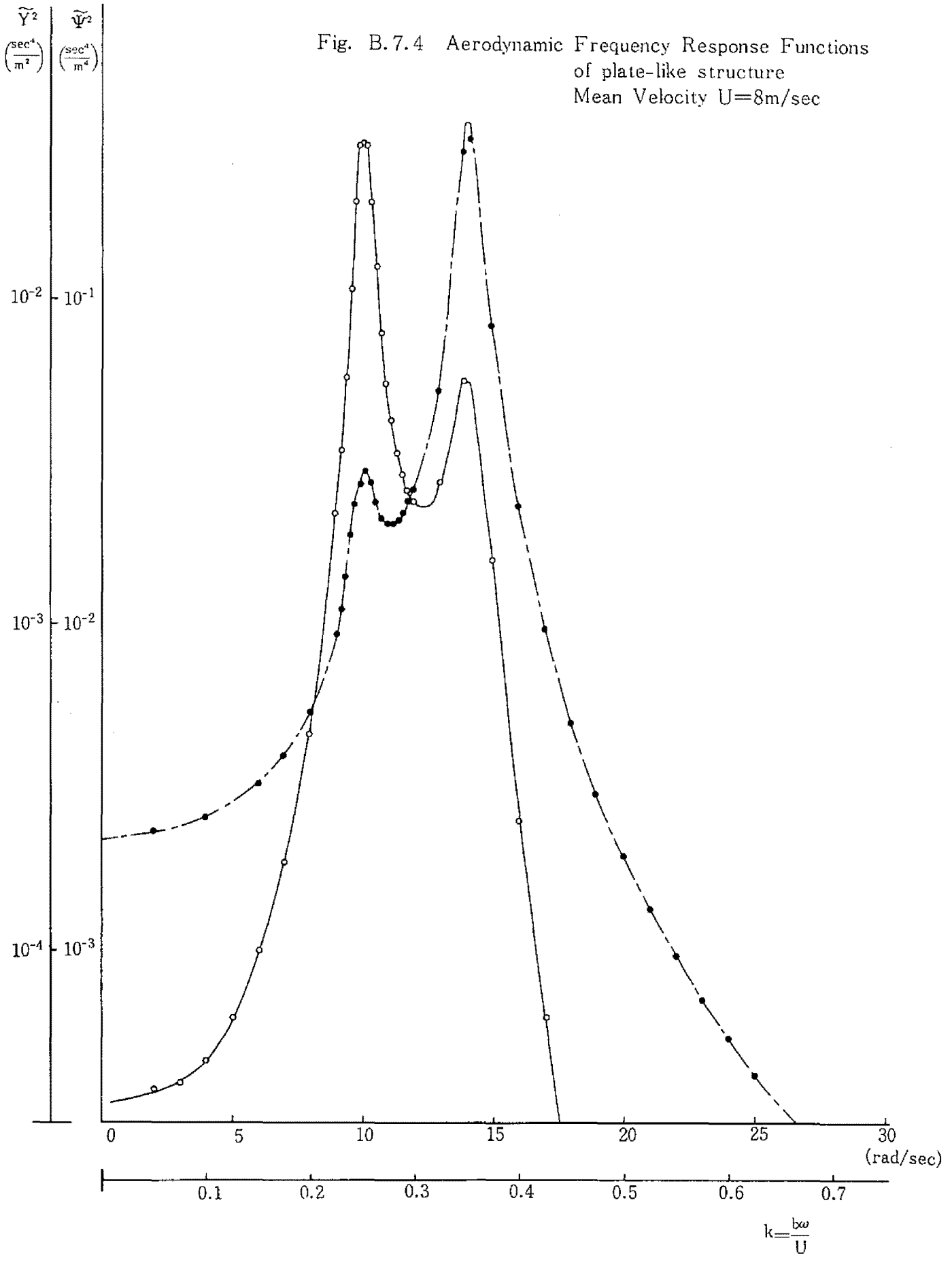

Fig. B.7.4 Aerodynamic Frequency Response Functions of plate-like structure
Mean Velocity U=8m/sec

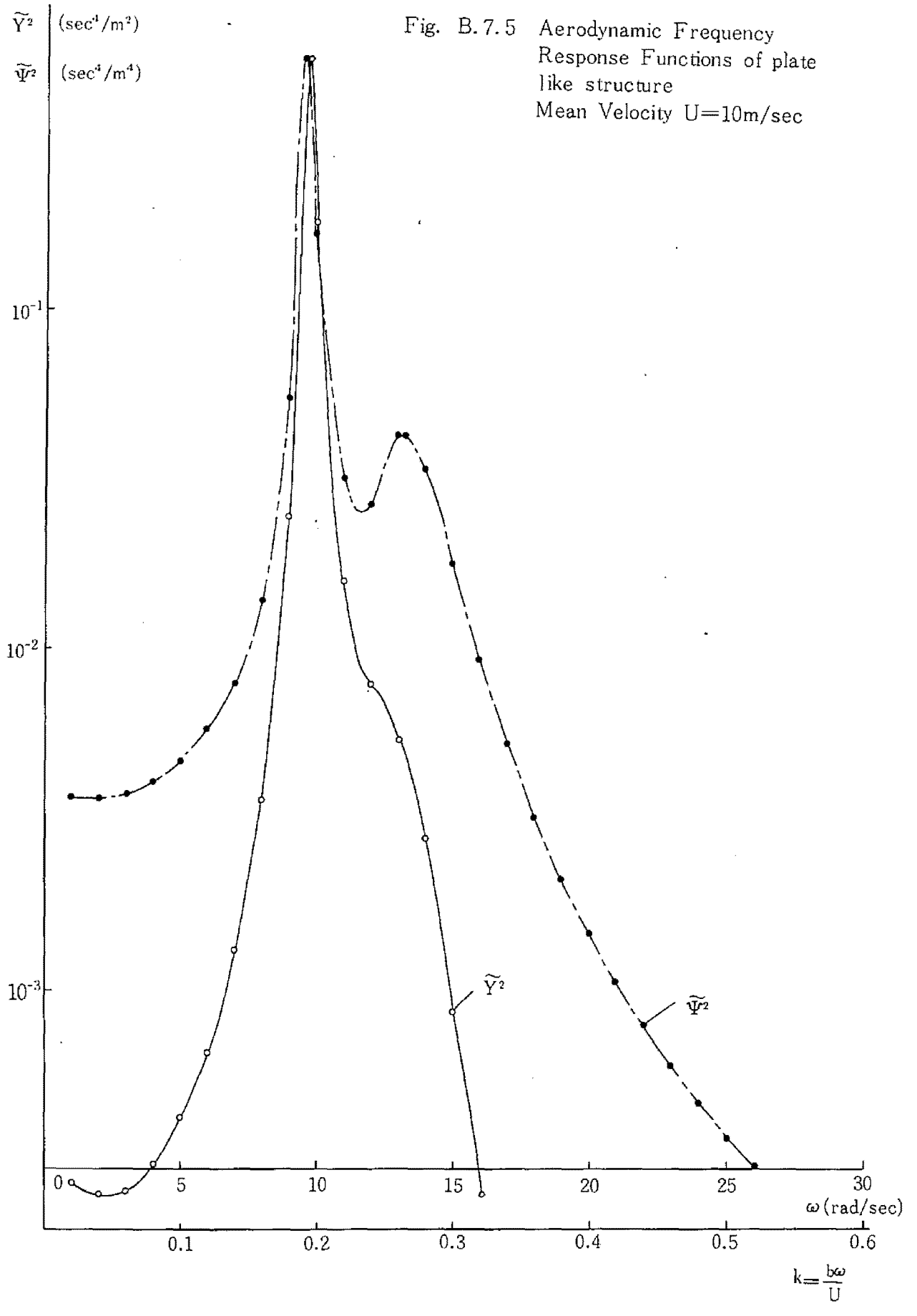

Fig. B.7.5 Aerodynamic Frequency Response Functions of plate like structure
Mean Velocity U=10m/sec

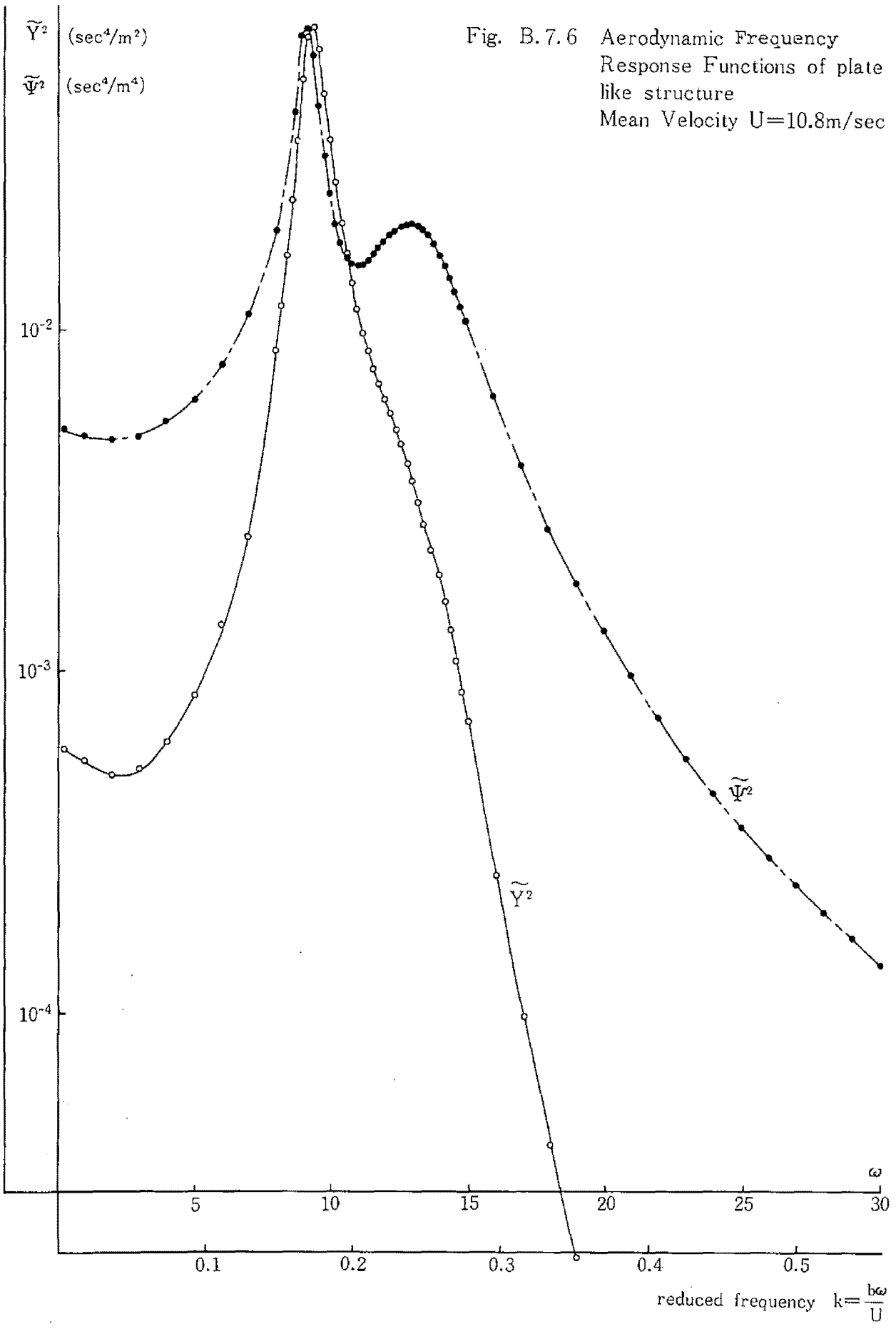

Fig. B.7.6 Aerodynamic Frequency Response Functions of plate like structure
Mean Velocity U=10.8m/sec

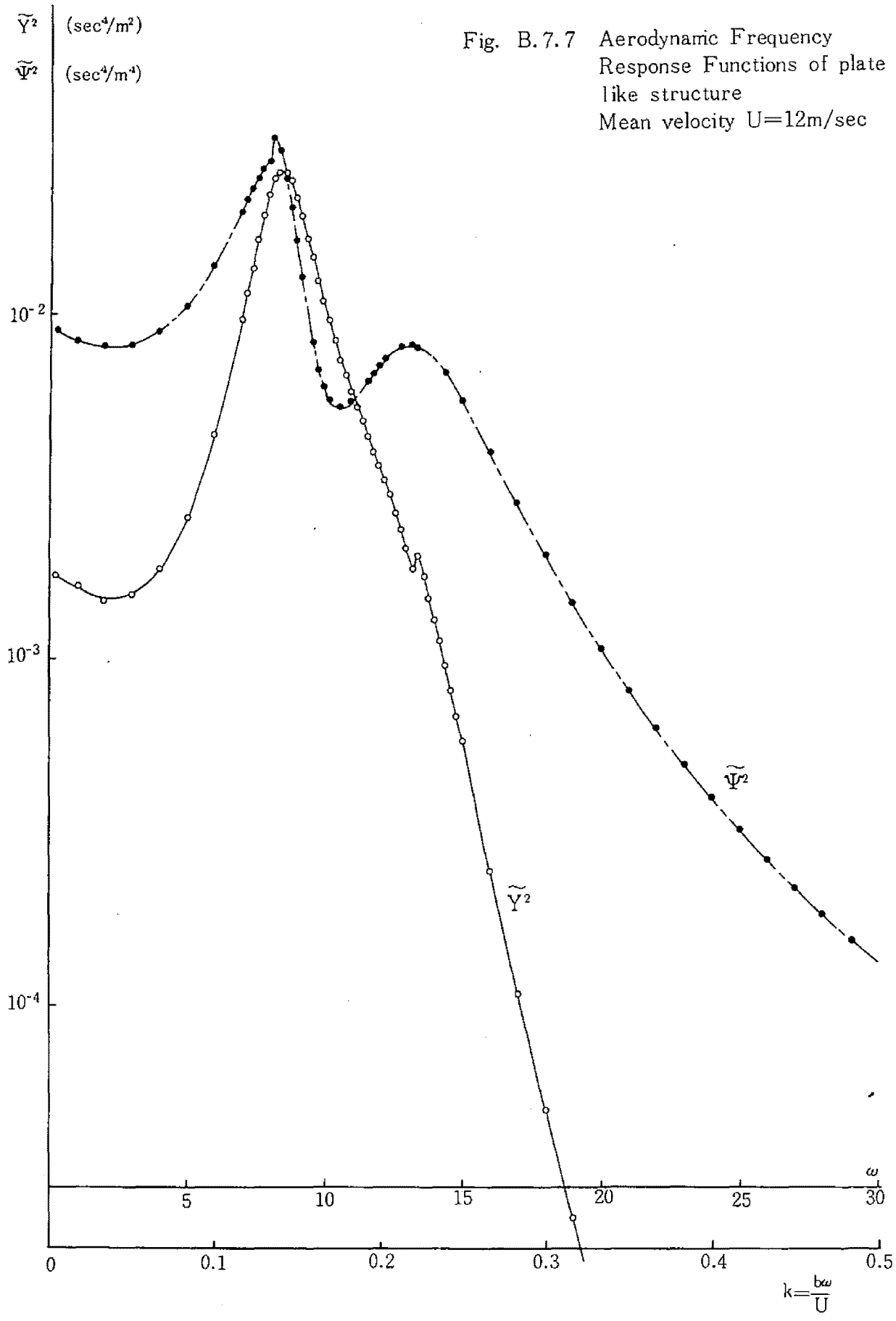

Fig. B.7.7 Aerodynamic Frequency Response Functions of plate like structure
Mean velocity U=12m/sec

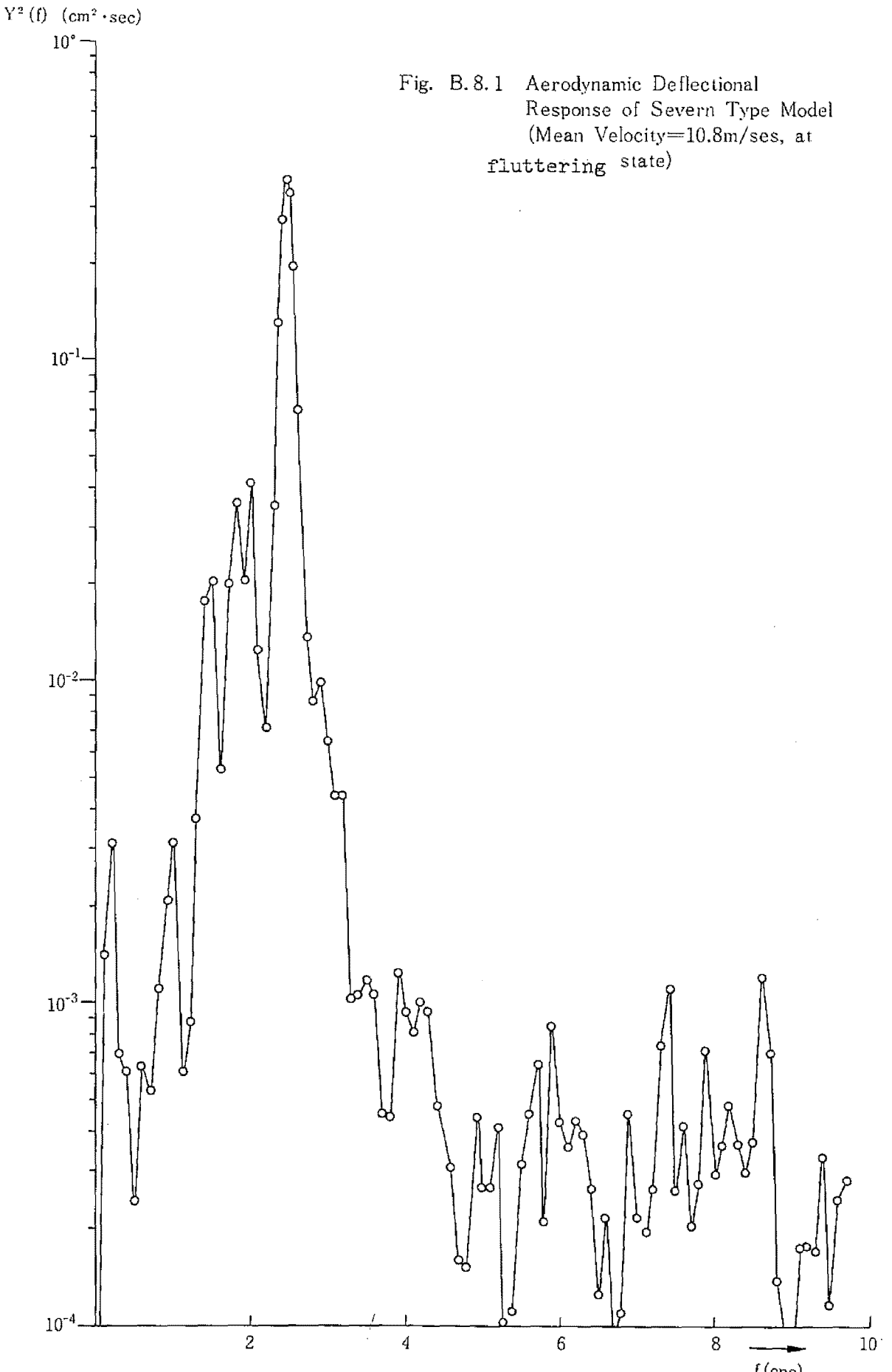

Fig. B.8.1 Aerodynamic Deflectional Response of Severn Type Model (Mean Velocity=10.8m/ses, at fluttering state)

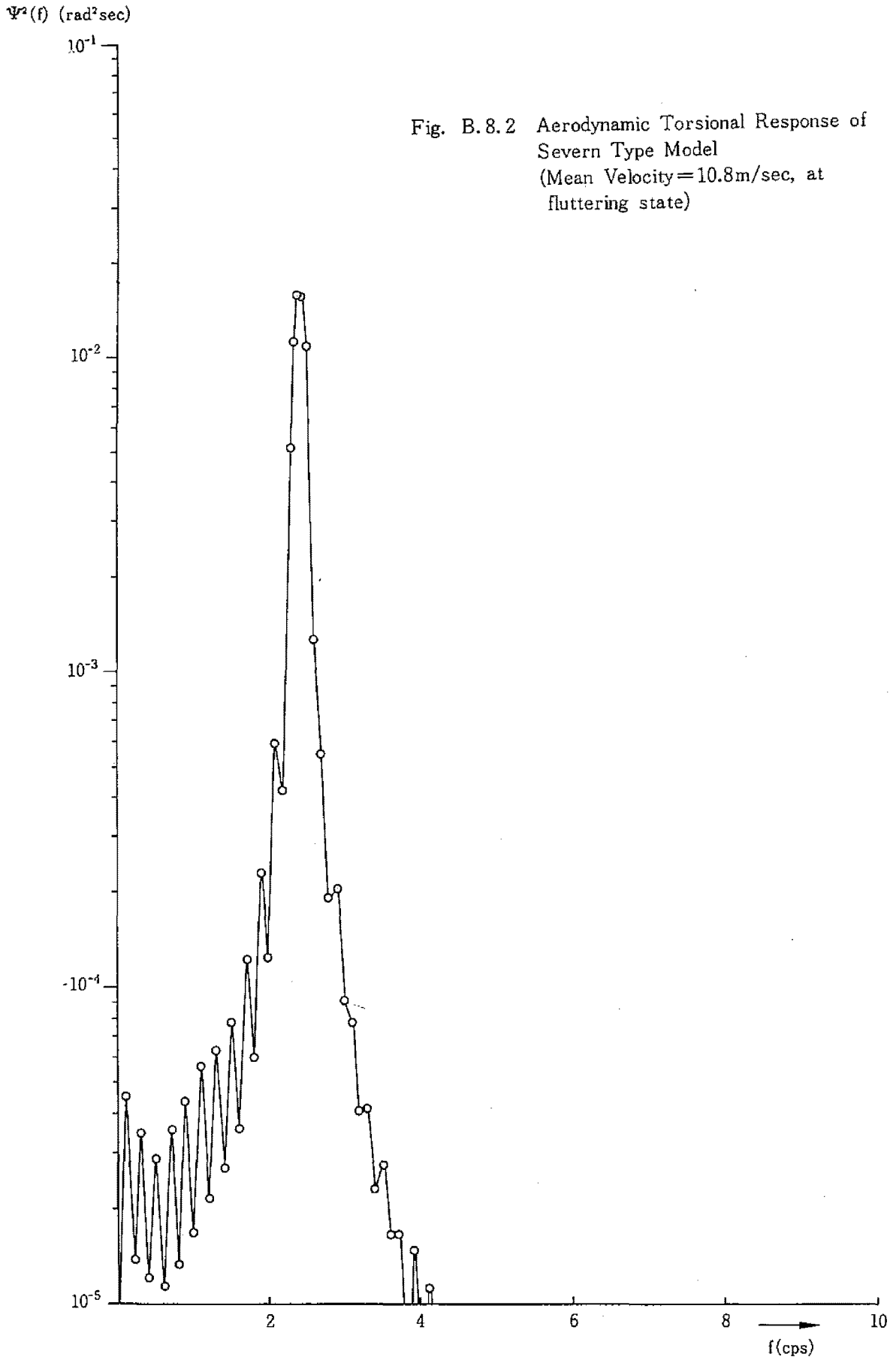

Fig. B.8.2 Aerodynamic Torsional Response of Severn Type Model
(Mean Velocity = 10.8m/sec, at fluttering state)

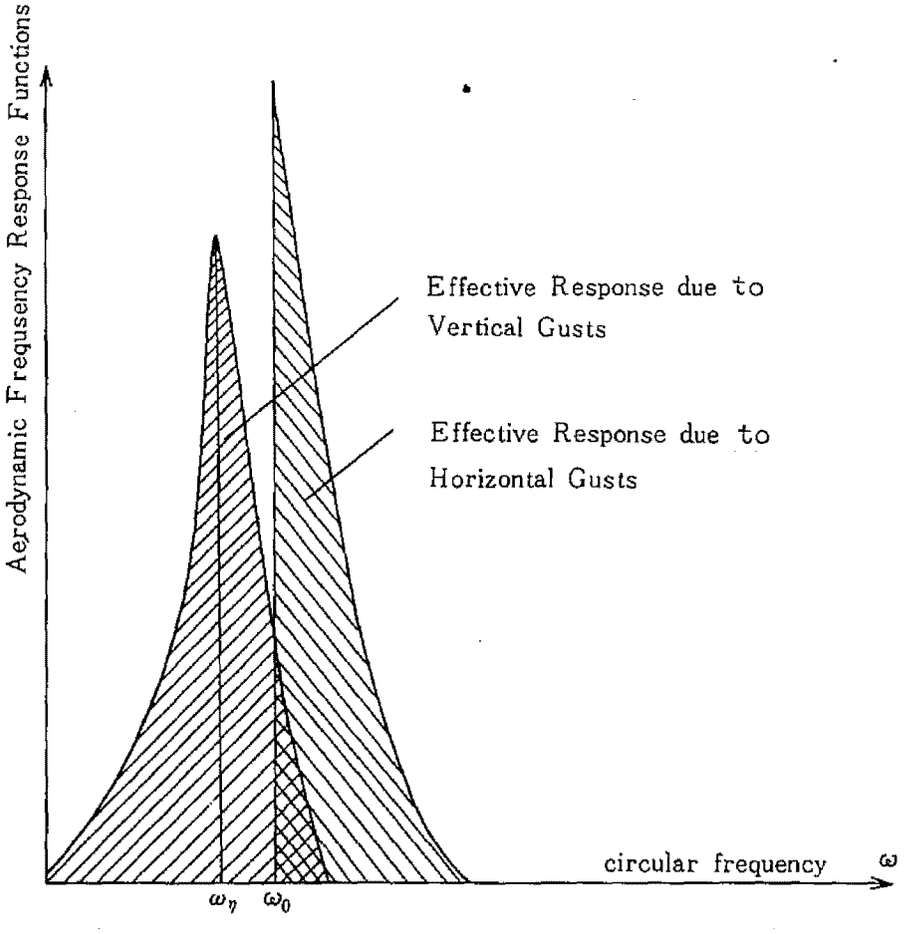

Fig. B.9. Characteristics of Aerodynamic Frequency Response Functions of structure subjected to external oscillations of frequency ω_0 (ω_η : natural flexural frequency)

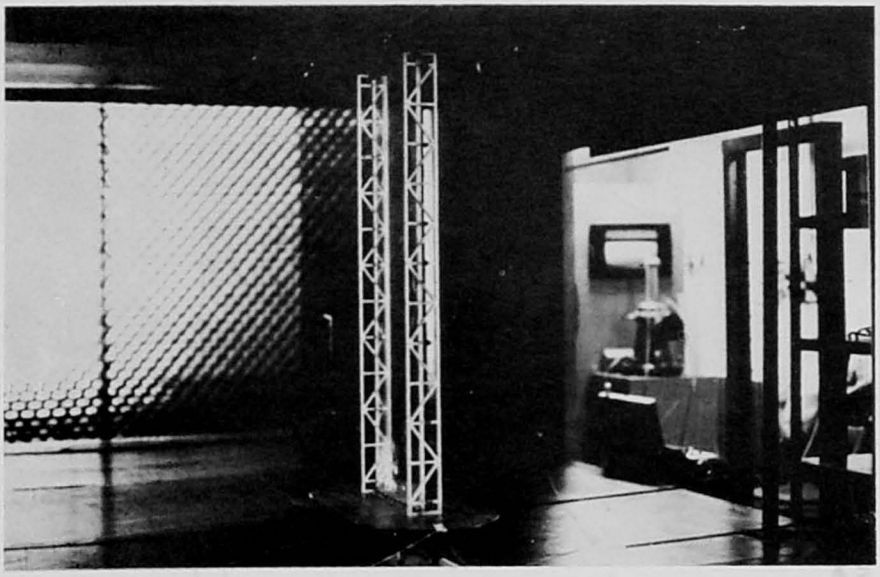

Photo A. 1 Model Mounting for Measurement of Unsteady Aerodynamic Forces (DT70H)

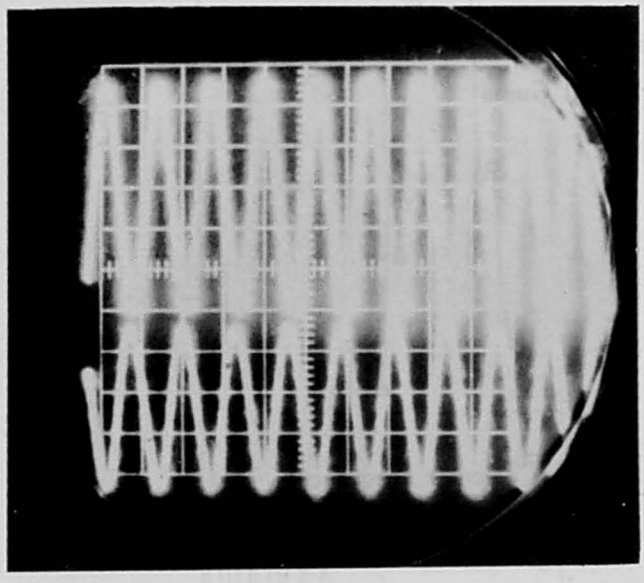

Oscillatory Record of Torsional (adove) and Flexural (below) Deformations

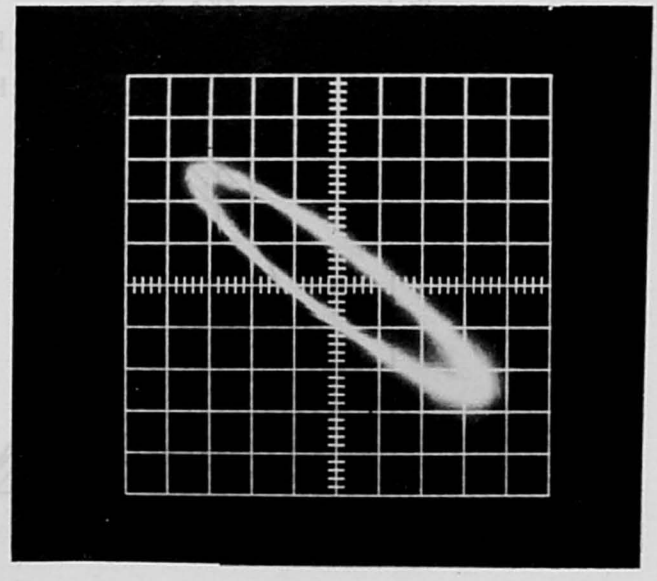

Lissajous' Diagram of Torsional (horizontal) and Flexural (vertical) Deformations

Photo A. 2 Record Example (Model, DT70H)

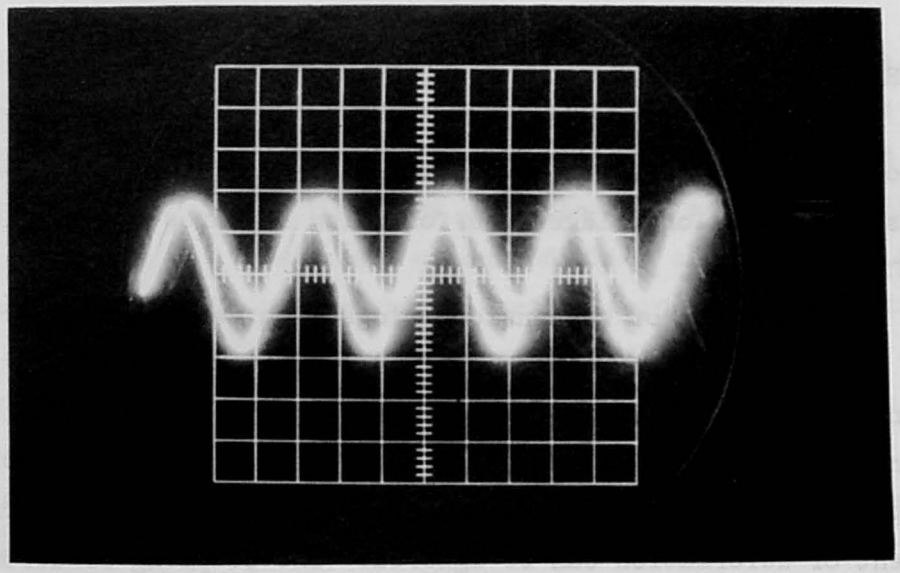

Oscillatory Record of Torsional (above)
and Flexural (below) Deformations

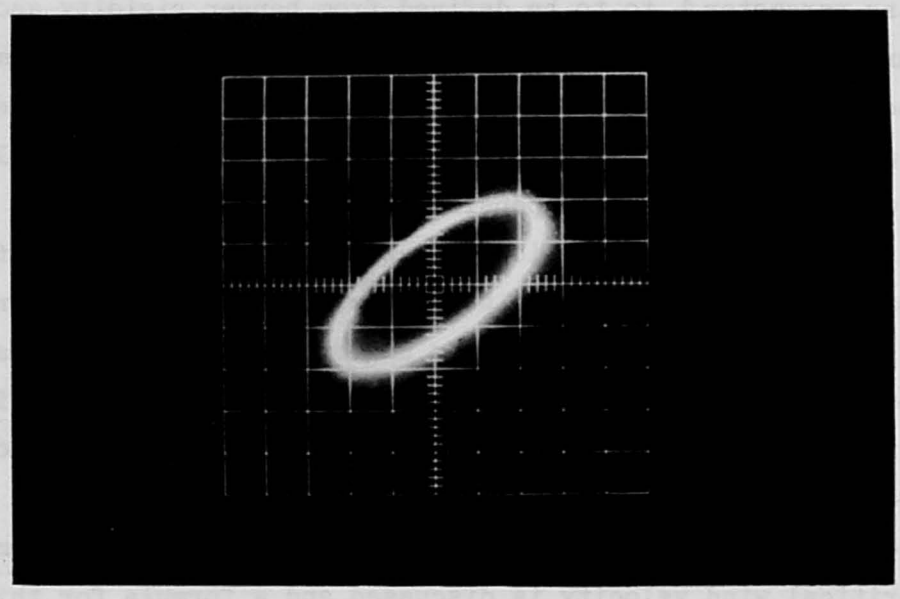

Lissajous' Diagram of Torsional (horizontal)
and Flexural (vertical) Deformations

Photo A.3 Record Example (Model, plate)

CHAPTER 5 CONCLUSIONS

Through this investigations on vibraticnal and aerodynamic characteristics of suspension bridges the following features are considered to be clarified

1. For ordinary type of suspension bridge with vertical hanger system the vibrational modes are classified into two types, namely deflectional modes and torsional modes, the former of which consists of transverse flexural components of stiffening girder and cables and longitudinal component of cables while the latter of which no component of deformation can be ignored. The coupling of deformation components is eventually of the non-linear form so that usually it may be unnecessary to take into an account for actual design calculation as long as small deformation is considered
2. The inclined hanger system is so effective to increase both damping capacity and flexural rigidity, which is characterized by a stiffening parameter Λ to to be defined from hanger rigidity and configurations. The fundamental equations form a modified form of those of the ordinary deflection theory. The theoretical results are satisfactorily in accordance with the experimental results by use of the three spans suspension bridge model.
3. The fundamental investigations of aerodynamic instability of bridge section are performed and it should be said that the flutter phenomenon are of primary importance in uniform winds. For long spanned suspension bridge the aeroelastic characteristics may contribute to the non-linear dynamic behaviours to some extent, but the non-linear aerodynamic behaviour is considered more significant, which should be continuously researched. An approximate method of determination of critical wind velocity is discussed and a formula for this is presented taking into an account the effect of slit decks. The determination of unsteady aerodynamic coefficients is investigated by the free and the forced vibration methods by which the fundamental characteristics of plate-like structures are illustrated .

4. Aerodynamic responses of plate and plate-like structures due to fluctuating gusts are discussed on the basis of Karman-Sears and Horlock theories. The aerodynamic magnification factors and the frequency response functions are characterized and the stabilizing and destabilizing effects are discussed which consideration is affirmatively assured by wind tunnel test. Aerodynamic investigations tend to increase the importance when one considers so large scale of structures as long spanned suspension bridges and tall buildings. As mentioned already there are two most important problems to be mentioned as future analysis, viz., the non-linear aerodynamic characteristics and the statistical behaviours of structures for fluctuating wind, for which the author wishes to continue his research work.